Investigating the susceptibility of foreskin myeloid cells to *ex vivo* HIV infection

By

Bokani Nleya

NLYBOK001

SUBMITTED TO THE UNIVERSITY OF CAPE TOWN

In fulfillment of the requirements for the degree

PhD in Clinical Science and Immunology

Department of Pathology

Faculty of Health Sciences

UNIVERSITY OF CAPE TOWN

Date of Submission:07th March 2023
Supervisor: Dr Nyaradzo Chigorimbo-Tsikiwa
Co-supervisors: Prof Clive Gray, Dr Sonwabile Dzanibe

University of Cape Town

The copyright of this thesis vests in the author. No quotation from it or information derived from it is to be published without full acknowledgement of the source. The thesis is to be used for private study or non-commercial research purposes only.

Published by the University of Cape Town (UCT) in terms of the non-exclusive license granted to UCT by the author.

University of Cape Town

Table of Contents

Acknowledgements

First and foremost, I would like to thank the God Almighty whose grace and unmerited favor carried me from the beginning to the very end of this journey.

I would also like to extend heartfelt gratitude to my supervisor Dr. Nyaradzo-Chigorimbo-Tsikiwa for her patience, tireless guidance, the willingness to teach and for mentorship. Dr Nyaradzo Chigorimbo-Tsikiwa went over and above the call of duty in ensuring that I had all the support I ever needed, in both her professional and personal capacity. I'd also like to thank Steve, Ati and Ngoni for the many nights and weekends that Dr Chigorimbo-Tsikiwa sacrificed in training and equipping me with the necessary skills to evolve into a better scientist. For being family away from family, I am eternally grateful.

I'd also like to extend gratitude to my co-supervisor Professor Clive Gray for the invaluable guidance, impartation of knowledge and the constructive criticism that helped train me into a better scientist. I am also grateful to Dr Sonwabile Dzanibe for the willingness to teach and guide whenever needed, and for coaching me through FlowJo and R. I'd also like to thank Dr Melissa Rose-Abrahams for her support and the induction into Virology. I'd also like to thank Gadisi Nthambeleni, Michael Mndini, Toni Wiggins, and Berenice Alinde for all the lab and technical support. To my lab mates and fellow students, Yamkela Qumbelo, Christen Da Costa, Shorouk Sebaa and Dr Cosnet Lerato Rametse, I am thankful to have shared parts of this journey with you.

To my best-friend, Dr Silindile Maphosa, thank for being a listening ear, for the unconditional love and the support. You held my hand, even at times when yours wasn't as steady. I could never thank you enough! Thank you for being my light since day one. We surely are a long way from where we began. Yay! Sindy Claire Ndlovu, what a beacon of light you are. Thank you for picking me up & holding me there. For cranking and reminding me of the strength that I sometimes felt I didn't have. You shone the light on me more times than I could ever recount, thank you Mamsoni. Thembekani "Ntie" Phida, what would I have been without you? You brought ease into my writing process by ensuring I was always fed, nursed me back to life when I ailed, all with a wide smile. Yours is a heart of gold and your empathy knows no bounds. I am ever so grateful. Thank you for always reminding me to go back to the source whenever I found myself on shaky grounds & to go back to give gratitude for the wins. To Dr Nyaradzo Chigorimbo-Tsikiwa, again, for the laughs amidst the craziness, for putting on your mommy hat when I was falling apart, seeing me through hospitalization, surgeries, loss, and sickness. Thank you for all the fancy home-cooked meals, and the real MVP, sadza and maguru :). For holding my hand in prayer and keeping me grounded, thank you. You're a Rockstar! Dr Tafadzwa Dube, day one since teenage hood, thank you for making me laugh through the tears and for always being there to listen.

I am deeply thankful to my mom, Mary Nleya, for all the sacrifices that lead us here. I have yet to see another like you. Thank you for your immeasurable love! The lessons you instilled in me when I was a little girl became the armor and bravery, I needed to face the world and to conquer this specific mountain. You taught me that we finish all that we start, nomatter the circumstances! Uyimbokodo ma, ngiyabonga! I'd also like to thank my siblings; Methuli Nleya, Mbiganyi Nleya, Tjebukani Nleya for being there, always! To Lulama Nleya, Rosemary Nleya & Loreen Gugulethu Nleya (Mandazi), you are superstars. To Aaron, thank you for the unwavering support and encouragement, I could write a book! To my nieces and nephews (the whole lot of them), with special mention to Skittles, Ashley and Andile; the world is yours for the taking. You absolutely CAN be anything you want to be.

Finally, I hope you're proud and looking down on me smiling from heaven dad, Agrippa Nleya, who saw greatness in me before I ever had any aspirations of my own. I know you'd have been stoked! This work is in honor of our matriarch, my Granma (MaMoyo), whose strength and resilience was something to behold, & the reason for it all, Sis'Du!

Plagiarism Declaration

I, Bokani Nleya, hereby declare that the work on which this thesis is based is my original work (except where acknowledgements indicate otherwise) and that neither the whole work or any part of it has been, is being, or is to be submitted for any other degree in this or any other university.

I empower the university to reproduce for the purpose of research either the whole or any portion of the contents in any manner whatsoever.

Signature : **REDACTED**

Date 07th March 2023

Abstract

Background: HIV/AIDS remains a global concern that, although manageable using anti-retroviral therapy (ART), is still eluded by a cure with paucity of knowledge regarding its acquisition and spread especially through the male genital tract (MGT)[1–4] . Several authors have shown the human foreskin to be an effective mucosal effector site with heterogenous populations of innate and adaptive immune cells, that are permissive to HIV infection[5–8]. In support of this, medical male circumcision (MMC), has been reported to confer up to 60 % risk reduction in HIV acquisition[9–17]. Most studies have focused on investigating blood lymphoid immune cells and their interaction with HIV-1, this study sought to elucidate the myeloid cell composition of the inner and outer foreskin, and to investigate the susceptibility of these cells to *ex vivo* HIV infection by **(i)** Isolating migratory and non-migratory Langerhans cells (LCs) and "macrophage-like" cells from the foreskin epidermis **(ii)** Immunophenotyping and characterising foreskin LCs and "macrophage-like" cells using CD4+CCR5+ as proxy for HIV susceptibility, HLA-DR+CD80/86+ for maturation, and the mannose receptor, DC-SIGN and Siglec-1 as HIV attachment factors and **(iii)** Investigating the HIV susceptibility of foreskin epidermal cells using an optimised *ex vivo* pluricellular foreskin infection model of suspension cells.

Methodology: Foreskin specimen were obtained from 60 seronegative adult South African men (aged 18-35 years) undergoing voluntary medical male circumcision (vMMC). Migratory and non-migratory foreskin cells were isolated from the inner and outer foreskin using spontaneous migration and enzymatic digestion of remnant epidermal tissue respectively, and subsequently immunophenotyped using multiparameter flow cytometry (n=31). The optimal HIV infection model was determined through assessment of different infection models inclusive of i) epidermal sheets, ii) foreskin explants and iii) pluricellular suspension cells (n=5). Using the *ex vivo* pluricellular foreskin infection model of suspension cells (n=17), Subtype C transmitted founder (T/F) and chronic infection derived (CC) infectious molecular clones (IMCs) were used alongside Subtype B NL4-3 IMCs with CCR5, CXCR4 and BaL envelopes. The extent of HIV infection was quantified by measurement of p24 in different immune cell subsets over a time-course. The different HIV infected cell subsets were characterized using CD45, CD207, CD1a, CD11c, CD14, CD3, HLA-DR, CD80/86, CD209, CD206, CD169, CD4 and CCR5.

Results: Foreskin myeloid cells contained a rare population of LCs (1.11 % ± 1.02 %;) that was predominantly migratory ($p = 0.0084$) and "macrophage-like" cells (9.87 % ± 9.64 %) that, in addition to being 8-fold more abundant ($p<0.0001$), were non-migratory ($p = 0.0002$). While the LC component was 53 % conventional LCs (0.59 % ± 0.11 %; $p<0.0001$), non-conventional LC subsets inclusive of i) CD3+ LCs (12 %), ii) CD11c+CD14+ LCs (7% %), iii) CD14+ LCs (18.6 %) and iv) CD11c+ LCs (9 %) were also identified. Compared to all the other LC subsets, the frequency of CD4+CCR5+ cells was higher in CD11c+CD14+ LCs (62.99 % ± 23.81; $p<0.0001$). Similarly, CD11c+CD14+ LCs had more HLA-DR+CD80/86+ co-expressing cells (42.69 % ± 23.34 %; $p<0.0001$) and CD206+ cells (29.79 % ± 24.62 %; $p = 0.0172$) than other LC subsets. The expression of other attachment factors such as DC-SIGN (23.75 % ± 17.02 %) and Siglec-1 (12.37 % ± 11.38 %) was also observed in CD14+ LCs ($p<0.0001$). CD11c+CD14+ LCs and CD14+LCs thus, displayed HIV susceptible phenotypes and were corroboratively the only LC subsets to be productively infected with HIV ($p = 0.0144$). Although there were no differences in the infectivity of the different HIV strains, NL4-3 X4 infected CD14+ LCs decreased 0.23-fold with time progression, while Subtype C CH198 (TF) infected CD14+ LCs increased 79-fold. Meanwhile, foreskin "Mϕ-like" cells were predominated by the "M2-like" Mϕ (5.60 % ± 4.13 %; $p<0.0001$) and the unconventional CD3+ Mϕ (2.90 % ± 2.73 %; $p<0.0001$). "M1-like" Mϕ (0.60% ± 1.49 %), "M1/M2" intermediates (0.27 % ± 0.55 %) and CD169+ Mϕ (0.15 % ± 0.18 %) were the least frequent "Mϕ-like" subsets. However, CD4+CCR5+ was more highly co-expressed in "M1-like" Mϕ (54.15 % ± 26.12 %; $p<0.0001$), and M1/M2 intermediates (59.35 % ± 27.49 %; <0.0001). Although the co-expression of CD4+CCR5+ was lower in "M2-like" Mϕ (28.38 % ± 13.99 %) and CD3+ Mϕ (32.77 % ± 18.57 %), these were the only two "Mϕ-like" subsets to be productively infected with HIV ($p=0.0352$).

Conclusion: This study elucidated the foreskin epidermis to harbour subsets of LCs and Mϕ capable of supporting HIV infection. Foreskin LCs that were infectable with HIV exhibited a "Mϕ-like" phenotype owing to the co-expression of CD14 and predominance in non-migratory cells[18]. These were identified as CD14+ LCs and the CD14+CD11c+ LCs, described as non-conventional LCs. HIV infectable Mϕ were "M2-like" Mϕ and the unconventional CD3+ Mϕ. The location of these cells in the foreskin epidermis offers an opportunity for early intervention against HIV entry and therefore calls for further characterisation to better design anti-HIV small molecules. Restriction mechanisms governing the non-infectability of conventional LCs could also be further investigated and capitalised on.

Abbreviations

AGM	Fetal organs (aorta, gonada, mesonephros)
AIDS	Acquired Immune Deficiency Syndrome
ANOVA	Analysis of Variance
APC	Antigen Presenting Cell
APOBEC3G	Apolipoprotein B mRNA editing enzyme, catalytic polypeptide-like 3G
ART	Anti-retroviral therapy
ARVs	Anti-retroviral drugs
AS-DCs	Axl+ and Siglec6+ Dendritic cells
AXL DCs	Axl+ Dendritic cells
BG	Birbeck granules
BM	Bone marrow
BSA	Bovine Serum Albumin
CC	Chronic Control
CCR1	Chemokine receptor 1
CCR2b	Chemokine receptor 2b
CCR3	Chemokine receptor 3
CCR5	Chemokine receptor 5
CCR8	Chemokine receptor 8
CD-	Cluster of differentiation
cDC	Conventional Dendritic cells
cDNA	Complementary DNA
CDP	Common DC precursor
CLP	Common-lymphoid progenitor
CLRs	C-type lectin receptors
CMAF	Transcription factor c-musculoaponeurotic fibrosarcoma
CMP	Common-myeloid-erythroid progenitor
CRD	Carbohydrate recognition domain
CRF	circulating recombinant form
CTL	cytotoxic T lymphocyte
CX3CR1	C-X-C chemokine receptor 1
CXCR4	C-X-C chemokine receptor 4
CXCR6	C-X-C chemokine receptor 6
DC	Dendritic cells
DC-SIGN	Dendritic cell-specific intercellular adhesion molecules
DCIR	Dendritic Cell immunoreceptor
DEC-2	C-type lectin receptor Dectin-2
DMEM	Dulbecco's Modified Eagle Medium
DMSO	Dimethyl sulfoxide
DNA	Deoxyribonucleic acid
DNGR-1	Dendritic cell specific sensor of tissue damage
EDTA	Ethylenediamine tetra acetic acid
EMP	Erythromyeloid progenitors
Env	Viral gene encoding the Envelope protein
Env	Viral envelope protein
FACS buffer	Flow cytometry Staining Buffer
FBS	Fetal Bovine Serum
Fc	Fragment crystallizable region of the Immunoglobulin
FCS	Fetal Calf Serum
FGT	Female genital tract
Flt3	FMS-like tyrosine kinase-3-ligand
FMO	Fluorescence minus one
Gag	Viral gene encoding the capsid, matrix and nucleoproteins
GFP	Green fluorescent protein
GIT	Gastro intestinal tract
GM-CSF	Granulocyte-macrophage colony-stimulating factor
GP120	120kDa Envelope glycoprotein
Gp160	160kDa Envelope glycoprotein

Gp41	41kDa Envelope glycoprotein
HEK-293Ts	Human Embryonic Kidney
HEPES	4-(2-hydroxyethyl)-1-piperazineethanesulfonic acid
HIV	Human Immune Virus
HLA-DR	Human Leukocyte Antigen – DR isotype
HSC	Haematopoietic stem cells
IC50	Half-maximal inhibitory concentration
ICAM-2	Intercellular adhesion molecule 2
ICAM-3	Intercellular adhesion molecule 3
IDECs	Inflammatory Dendritic Epidermal Cells
IFITM	Interferon-induced transmembrane
IFN	Interferon
Ig	Immunoglobulin
IL	Interleukin
IMCs	Infectious Molecular Clones
iNKT	Invariant natural killer cells
IP-10	Gamma induced protein10
IRF	Interferon regulatory factor
Kb	Kilobases
kDa	Kilodaltons
LB	Luria Bertani Broth
LCMV	Lymphocytic choriomeningitis virus
LCs	Langerhans Cells
LFA-1	Lymphocyte Function Associated Antigen 1
LN	Lymph node
LPS	Lipopolysaccharide
LTR	Long terminal Repeats
M1	Type 1 macrophage phenotype
M2	Type 2 macrophage phenotype
MDMs	Monocyte Derived Macrophages
MDP	Macrophage-DC progenitor
MDSCs	Myeloid derived suppressor cells
MGCs	Multi-nucleated giant cells
MGT	Male genital tract
MHC	Major histocompatibility complex
MMC	Medical Male Circumcision
MNPs	Mononuclear phagocytes
Mo-DCs	Monocyte derived Dendritic cells
MOI	Multiplicity of Infection
MR	Mannose receptor
mRNA	Messenger RNA
MSM	Men who have sex with men
MVBs	Multi vesicular bodies
Nef	Viral negative regulatory factor
NFkB	Nuclear factor kappa-light-chain-enhancer of activated B cells
NK	Natural killer cells
NNRTI	Non-nucleoside reverse transcriptase inhibitors
NRTI	Nucleoside reverse transcriptase inhibitors
P24	Viral capsid protein
PAMP	Pathogen Associated Molecular Patterns
PBMCs	Peripheral blood mononuclear cells
PBS	Phosphate Buffered Saline
PCA	Principal component analysis
PCR	Polymerase Chain Reaction
pDC	Plasmacytoid Dendritic cells
PFA	Paraformaldehyde
PHA	Phytohemagglutinin
PRR	Pattern Recognition Receptor
PWB	Perm Wash Buffer
RANK	Receptor activator of NFkB

RANTES	Regulated upon activation, normal T cell expressed and secreted
Rev	Regulator of virion protein
RIA	Residual Immune Activation
RLU	Relative light units
RNA	Ribonucleic acid
ROS	Reactive oxygen species
Rpm	Revolutions per minute
RSV	Respiratory syncytial virus
RT	Reverse transcriptase
SAMHD1	SAM domain- and HD domain-containing protein 1
SCID	Severe combined immunodeficiency
SD	Standard Deviation
Siglec	Sialic acid-binding immunoglobulin-like lectins
SIV	Simian immune virus
SOC	Super Optimal Catabolite
STIs	Sexually transmitted Infections
T/F	Transmitted founder
Tat	Trans-activator
TCID	Tissue culture infectious dose
TCR	T cell receptor
TGFβ	Transforming growth factor beta-1
Th-	T-helper cells
TLRs	Toll-like receptors
TNF	Tumor necrosis factor
TNTs	Tunneling nanotubes
Tregs	T regulatory cells
TRIM5α	Tripartite motif-containing protein 5
TSLP	Thymic stromal lymphopoietin
VCCs	Virus containing compartments
Vif	Virion infectivity factor
vMMC	Voluntary medical male circumcision
Vpr	Viral protein R
Vpu	Viral protein U
VS	Virological Synapse
VSV	Vesicular Stomatitis virus
WHO	World Health Organization

List of Tables and Figures

I. INTRODUCTION

The human foreskin has been shown to play an important role in HIV infection as its complete removal during medical male circumcision (MMC) has been shown to reduce the risk of HIV acquisition by up to 60% [12–16,19]. This is thought to be due to the removal of HIV target cells of both the lymphoid and myeloid origins, that reside in the foreskin[12–16,19]. Several studies have reported the foreskin to harbour CD3+CD4+ T cells, CD1a+CD207+ Langerhans cells, CD68+ or CD14+ macrophages, as well as CD11c+DC-SIGN+ dendritic cells[15,20]. In addition to the co-expression of CD4 and CCR5, the foreskin myeloid cells have been shown to express high levels of C-type lectin receptors (CLRs) inclusive of DC-SIGN, langerin and the mannose receptor [21]. C-type lectin receptors reportedly augment HIV infection and facilitate HIV spread through various cell-cell transmission mechanisms[22–25]. Myeloid cell CLRs have been shown an indispensable part of the infectious synapse, a structure that resembles the immunological synapse and concentrates HIV virions on the surface of the target cell[20,26,27]. DC-SIGN has particularly been shown to recognise and bind HIV using conserved sugar structures and to subsequently sequester HIV into protective endocytic structures for effective dissemination later[27]. HIV uptake in this manner has been referred to as *trans* infection, a well-documented role of myeloid cells in HIV pathology[20,26,27].

However, myeloid cells, as innate immune effectors also confer several host restrictions mechanisms against HIV infection, inclusive of IFN-1 inducible genes and CLR based abrogation pathways[28,29]. CLR abrogation pathways are autophagy based mechanisms that concomitantly utilise CLRs and host restriction factors such as TRIM5α [28–32]. Langerhans cells have particularly been shown to successfully abrogate CXCR4 HIV infection (X4-tropic viruses) using a langerin based degradation mechanism[28,30,32]. However, restriction against CCR5 using HIV (R5-tropic viruses) was deemed insufficient and ineffective, therefore rendering Langerhans cells permissive to R5 tropic HIV[28,30,32]. Dendritic cells and macrophages have also been shown to support HIV replication, and thus *cis*-infection[20,26,33,34]. HIV infected macrophages have been shown to persist over extended periods of time, thereby contributing to the viral reservoir, residual immune activation, and perpetual inflammation[35]. Therefore, the foreskin is an important mucosal effector site, enamoured with diverse innate immune myeloid cells that pose a double edged sword in HIV pathology and antiretroviral therapy (ART).

However, the full repertoire and sub-population plasticity of DCs and macrophages of the male genital tract (MGT) remain uncharacterised. During infection, both innate and adaptive immune responses are prompted but they seem to be insufficient or too late to eliminate the virus. The precise mechanisms underlying the *in vivo* myeloid cell-HIV interactions that occur in relation to HIV dissemination and immune response are still unknown and is partly a focus of this PhD.

II. LITERATURE REVIEW

Epidemiological data on HIV

The etiological cause of the Acquired Immune Deficiency Syndrome (AIDS) is HIV (human immunodeficiency virus), that although identified in 1984, has been globally spreading before then, resulting in a devastating pandemic[1]. There is still no cure for HIV infection, although progress has been made in the past years, rendering it a more manageable chronic condition and thus, improving the quality of life among HIV infected people[2,3]. However, there has been a surge of new HIV infections due to Covid-19 related disruptions in health service delivery and faltering urgency in public health response to HIV[4]. As such 1.5 million new infections were recorded in 2021 with 650 000 (510 000 – 860 000) AIDS related deaths being recorded in the same year, and thus bringing the global mortality of AIDS to an estimate of 40.1 million deaths (33.6 million – 48.6 million)[4]. As at year end 2021, 38.4 million people were reported to be living with HIV[4], two-thirds (25.6 million) of whom were reported to be from the WHO African Region, within which South Africa was identified as the epicentre[2–4].

The HIV epidemic in South Africa has therefore been described the biggest in the globe, characterised by an 18.9 % prevalence in the country[2,3]. This has been attributed to complex socio-economic, behavioural, contextual and biological factors inclusive of unsafe sex practices, sexual violence, alcohol and substance abuse[3]. Age-disparate relationships due to either cultural practices or poverty have also been implicated in the increased risk of HIV acquisition among vulnerable adolescent girls and young women aged 15-24 years[3]. Compared to their male counterparts, young females have been reported as 8-fold more prone to acquiring HIV[3]. Owing to the complexity of factors at play, the HIV/AIDS pandemic remains a global threat and crisis despite worldwide concerted efforts to manage, prevent and eliminate the retrovirus[2–4].

HIV nomenclature and geotropism

It is widely accepted that globally circulating strains of HIV are highly polymorphic and exhibit an extra-ordinary degree of genetic diversity with a direct bearing on infectivity, transmissibility as well as immunogenicity[36–39]. As such, it was deemed important to come up with a globally consented to nomenclature[40]. Historically, HIV-1 sequences have been classified according to their phylogenetic relationships into groups and subtypes thereby giving rise to distinct groups: M, N, O and P (Main, Outlier and Not M nor N), with Group M being the most globally widespread[40,41]. Using envelope sequencing, Group M was further distinguishable into clades referred to as sub-types; A, B, C, D, F, G, H, J and K[40]. Lineages closely related to any of these main subtypes but not genetically distinct enough to be assigned a unique subtype, were classified as sub-subtype[40,41]. Lastly, viruses descending from the same recombination event with an identical mosaic structure or hybrids of two or more subtypes, with

high significance in the global pandemic, were designated the circulating recombinant form (CRF) class[40,41].

Among the main subtypes, Subtype C has been reported responsible for 47 % of global HIV infections, while Subtypes B and A were attributable to 12 % and 10 % of infections respectively[2,36,37,40]. CRF strains were reported responsible for <10 % of infections, and these were particularly CRF02_AG (8 %) and CRF01_AE (5 %)[2,36–39]. In addition to the different degrees of penetration, geo-location was also influential on the spread of the different subtypes [40]. For instance, Subtype C was most prevalent in Southern Africa and India where it accounted for 99 % and 95 % of HIV infections respectively. Subtype B, on the other hand, was more rife in Western and Eastern Europe, North and Latin America, the Caribbean, and Oceania where it was responsible for > 75 % of infections[2,40]. Interestingly, Central Africa was the hub of all the different subtypes, thus the region with the greatest diversity of subtypes and CRFs[2].

Importantly, differences within subtypes, were also driven by the infection stage at which the viruses were isolated[42–44]. Isolates from Fiebig stages I-VI were designated transmitted founder viruses (T/F) while those isolated from chronically infected individuals were designated chronic controls (CC)[42–44], described in more detail later.

HIV structure and replication cycle

The HIV genome consists of typical retroviral genes that can be classified as structural, functional, regulatory as well as accessory[45–47]. These genes are flanked on either side by the long terminal repeats (LTRs) that contain the promoter. *Gag (group antigen)* and *env (envelope)* are the structural genes that encode the capsid (CA), matrix (MA), nucleocapsid (NC) and the envelope glycoproteins (gp120 and gp41) as shown in Figure 1 below [48]. *Pol (polymerase)* is the functional gene that mainly encodes retroviral enzymes, reverse transcriptase (RT), protease (PR) and integrase (IN)[45–47]. Additionally, regulatory genes; *tat (trans-activator)* and *rev (regulator of virion protein)* are essential for proviral transcription[46]. Accessory genes include *nef (negative regulatory factor)*, *vif (virion infectivity factor)*, *vpr (viral protein R)* and *vpu (viral protein U)* which, while not completely required to aid viral replication, encode multiple elements that all work together towards the common goal of host immune evasion and silencing of host restriction factors in favor of its own proliferation[46,49].

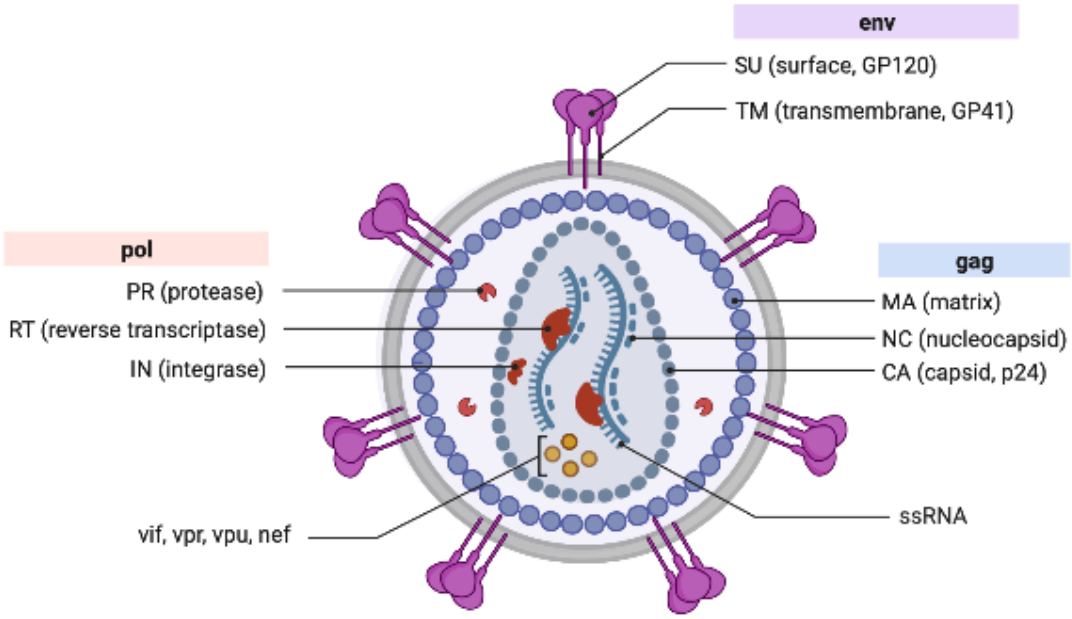

Figure 1. ***Structure of the HIV-1 virus.*** *The HIV genome is encased in a host derived lipid bi-layer envelope (grey), embedded with viral gp120 and trans-membranal gp41 protein spikes (lilac). Inward, the viral RNA, enzymes, accessory genes, and the nucleocapsid, are encased in an oval p24 capsid (green) within a spherical matrix (purple). Image edited on BioRender.com*[48]

The replication cycle of HIV is a very complicated, sequential process that employs both host machinery and retroviral components as illustrated in Figure 2 below [46,48,49]. Put simply, this occurs in a series of consecutive steps stratified into; entry, reverse transcription, uncoating, nuclear import, integration, transcription, RNA export, translation, assembly and budding, and lastly release and maturation as shown in Figure 2 [46,49]. The cycle time lapse is characteristically very short and is liable to high mutation rates leading to the generation of a myriad of quasispecies thereby rendering HIV extremely adaptable and hard to eradicate[44,50]. Each stage of the cycle provides an opportunity for interruption and introduction of intervention strategies [49].

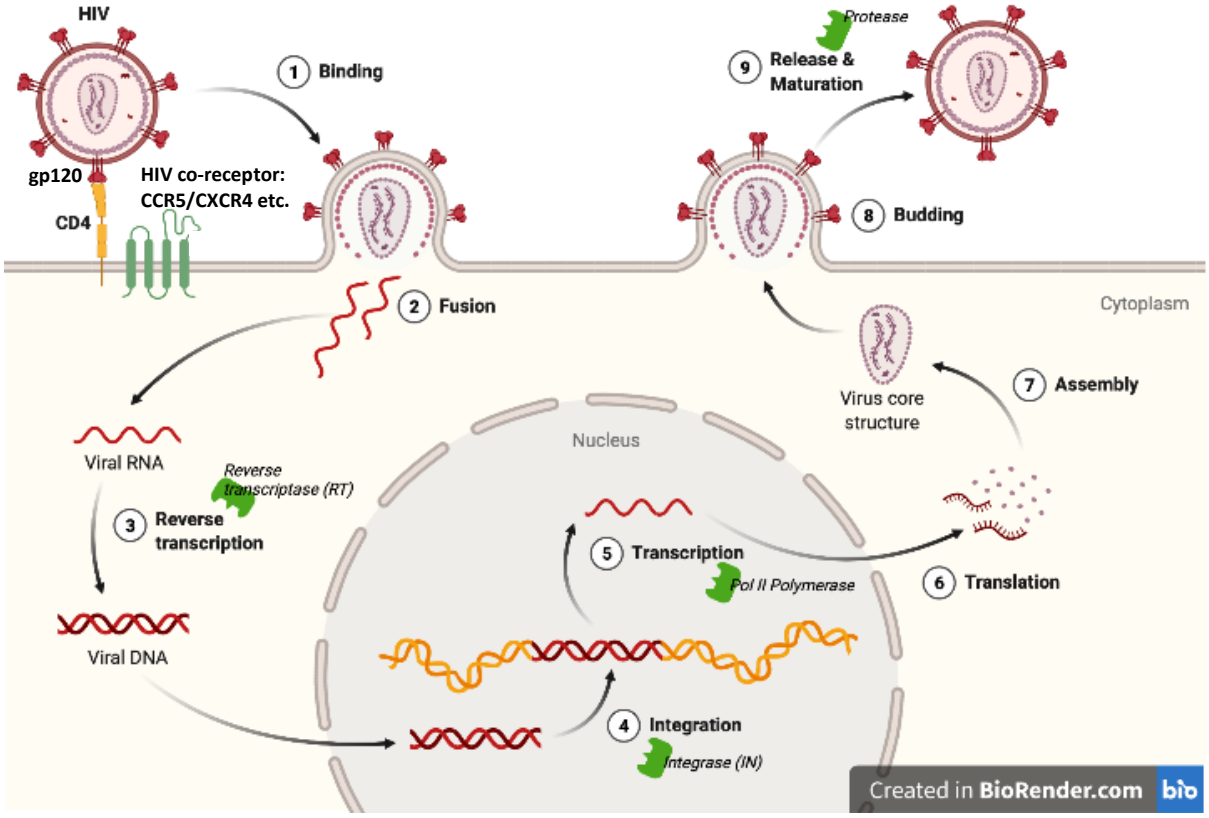

Figure 2. ***HIV replication cycle.*** *1. Binding of the HIV envelope protein, gp120 to the host cell through the aid of the HIV receptor, CD4 and co-receptor i.e CCR5 or others 2. Fusion of the virion into the cell membrane of the host 3. Reverse transcription of viral RNA through the reverse transcriptase enzyme 4. Integration of the viral DNA into host's DNA 5-7 Transcription, Translation and Assembly of viral proteins 8-9. Budding and release of mature virions. Image edited on BioRender.com*[48]

Briefly, viral attachment is prerequisite to viral entry and is dependent on the expression of CD4 on the cell surface of the target cell[45]. Attachment of CD4 to envelope reorganizes the cytoskeleton and consequently attributes to envelope conformational changes on the variable loops on the glycoprotein, gp120 subsequently leading to its exposure[45,51,52]. Consequently, gp120 interacts with either one of the extensively studied co-receptors (CCR5 and CXCR4) or other chemokine receptors such as CCR3, CXCR6, CCR1, CCR2b, CCR8, CX3CR1 [51,53]. This leads to the exposure of gp41 and the ultimate insertion of the fusion peptide into the cell membrane of the host[51,53].

Viral attachment and entry have been targeted for intervention strategies currently employed in anti-retroviral therapy (ART)[54–56]. Co-receptor and fusion inhibitors such as maraviroc and enfuvirtide, have been successfully developed and implemented for the inhibition of virus entry at the stages of co-receptor binding and membrane fusion, respectively[54,55,57].

Post-entry is the reverse transcription stage that is catalyzed by reverse transcriptase against which nucleos(t)ide reverse transcriptase inhibitors (NRTIs- tenofovir, disoproxil fumarate) and non-nucleoside reverse transcriptase inhibitors (NNRT1s- efavirenz) work, to impede DNA elongation and inactivate reverse transcriptase (RT) respectively[58]. Furthermore, the resultant cDNA goes through a series of uncoating and nuclear entry steps prior to being integrated into the host's DNA catalyzed by Integrase as shown in Figure 2[58].

The activation status of the host cell and the presence or absence of exogenous stimuli determine if integration and the resultant proviral DNA culminate in productive or latent infection[59]. Resting memory cells and other quiescent immune cells as well as macrophages can harbour proviral DNA, post the integration stage, a phenomenon that promotes viral latency and contributes to the viral reservoir which has posed major challenges for intervention strategies in terms of viral clearance[59–61]. Integrase inhibitors , such as raltegravir are currently being used to impede integration[62,63].

Productively infected cells transcribe the proviral DNA through Pol II polymerase to yield viral proteins[49,60]. The viral promoter is ubiquitously active, hence a myriad of host cells can support viral transcription if not prematurely abrogated[60,64]. Viral proteins Tat and Rev mediate much of the transcription, and constitute the initial viral transcripts alongside Nef[60,64]. Nef is essential for concealing the visibility of the infected host cell from the immune system by down-regulating class 1 MHC as well as CD4 while increasing the productivity of progeny virions[65–68].These newly formed progeny virions are then released from the host cell through budding as shown in Figure 2 and the host cell may then lyse[46].

In summary, the virus essentially enters the host cell through engagement of the HIV receptor, CD4 and an HIV co-receptor, which could be one of the extensively reported CCR5 and CXCR4 or the less common CCR3, CXCR6, CCR1, CCR2b, CCR8 and CX3CR4[51,53]. Cells that express these receptors are inadvertently permissive to HIV infection, hence described as HIV target cells[5,69,70]. Post-entry, HIV integrates into the host's DNA in a series of steps that yield viral proteins, support replication, and consequently generate progeny virions as illustrated in Figure 2[46]. In some instances, HIV integrates and lies dormant for years, thereby establishing latent infection[60,61].

HIV acquisition

There are several ways through which HIV can be transmitted from people living with HIV (PLWH)[47,71]. HIV is transmissible through certain bodily fluids in mucosal membranes such as blood, semen, pre-seminal fluid, rectal fluids, vaginal fluids as well as breast milk[47]. Such mucosal membranes include the foreskin, urethra, cervix, vagina, anus, and the rectum[72]. In addition, HIV transmission and

acquisition can also be driven by parenteral exposure in intravenous drug users and less commonly, through mother to child transmission[73]. In extremely rare cases, HIV has been reported to transmit through blood transfusions and organ donors[73].

Notably, successful infection in a new host is attributable to only a single HIV variant following HIV exposure in 80% of heterosexual transmissions, 75% of MSM transmissions, 70% of mother to child transmissions and in 40-80% of intravenous drug user transmissions[47]. Factors governing the selective advantage of the single HIV variant are poorly understood and have been collectively described under the HIV transmission bottleneck[42,44,47,74]. However, mucosal membranes are known to confer a physical and immunological protective barrier against microbial invasions[75]. As such, only the most fit variant, termed the transmitted founder (T/F) virus, can by-pass these barriers and successfully establish systemic infection[42,74]. Increased risk of breakthrough of multiple HIV variants in heterosexual transmissions is linked to factors that both compromise barrier integrity and attract HIV target cells to mucosal epithelia[39,43,44,50]. There is evidence of an association between the presence of sexually transmitted infections (STIs) and initial infection with multiple HIV variants[50]. Genital ulcerations have also been linked to the incidence of multiple variants. This suggests that physical aberrations to the mucosal epithelia increase the risk of HIV acquisition[50].

The male genital tract (MGT)

In heterosexual males, approximately 70% of HIV acquisitions are established through vaginal sexual intercourse[6,73]. The penis is therefore a predominant site of HIV entry[9,10]. The penis is distinguishable into “dry” and “wet” compartments comprising the penile shaft, glans (corona), urethral introitus, frenulum and of particular interest, the prepuce (foreskin), which comprises the inner and the outer foreskin[6,7]. The “dry” compartments of the penis are reportedly covered by a “dry” keratinized squamous epithelium that is impenetrable by HIV unless inflamed or breached, particularly in circumcised men [9,10]. The sub preputial epithelia covering the inner foreskin and glans/corona are mucosal “wet” epithelia that may be more susceptible to HIV, with reports indicating less keratinization and target cell enrichment at these sites [6,11,17,76].

The foreskin is attached to the glans by the frenulum. In a flaccid penis, the foreskin folds around the penis as shown in Figure 3(a), whereas in an erect penis, it retracts as illustrated in Figure 3(b)[6].

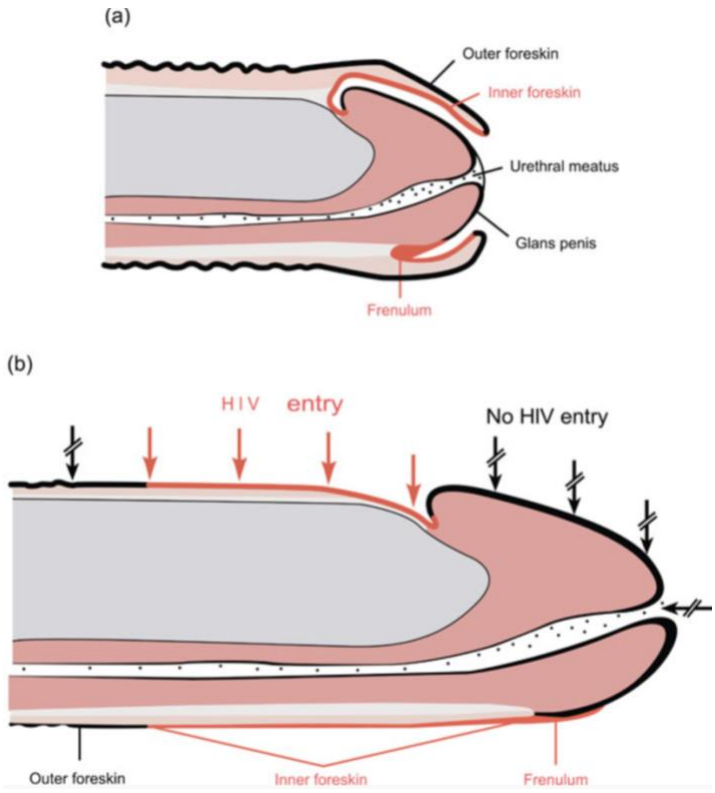

Figure 3. ***The inner foreskin is a likely site of HIV entry in an erect penis.*** ***(a)*** *Flaccid uncircumcised penis* ***(b)*** *The foreskin retracts in an erect penis exposing the HIV target cell enriched inner foreskin to vaginal mucosal fluids during heterosexual intercourse. Figure adapted from McCoombe SG, Short RV. Potential HIV-1 target cells in the human penis. Aids 2006; 20(11): 1491-5*

Foreskin retraction increases the likelihood of exposure to vaginal mucosal fluids that may carry HIV virions and is some instances, induce micro-tears that break the protective barrier as shown in Figure 3 above[6,7]. Furthermore, a sub-preputial space exists between the glans and the foreskin[6,11,17,76]. The sub-preputial space offers a warm and moist micro-environment that is conducive to pro-inflammatory anaerobic bacteria [76]. Consequently, this alters the MGT microbiome and triggers penile microbial dysbiosis which is pre-disposing to HIV susceptibility and acquisitions[76].

HIV target cells in the MGT

Various immunohistochemistry studies have reported on the presence of HIV target cells in varied regions of penile tissue including the foreskin and urethral introitus[5–8]. Langerhans cells have been identified to span the stratified squamous epithelia (shaft, glans, meatus), while macrophages and αEβ7^{+}CD4+ T cells have been reported to reside in the columnar urethral mucosa[6,7]. The inner foreskin has particularly been purported to harbour higher proportions of Langerhans cells compared to the outer foreskin [5–8]. Increased susceptibility to HIV infection, using cell-cell transmission, has therefore been purported to culminate in the spread and dissemination of HIV to CD4+ T cells and DCs as illustrated in Figure 4 below[77,78].

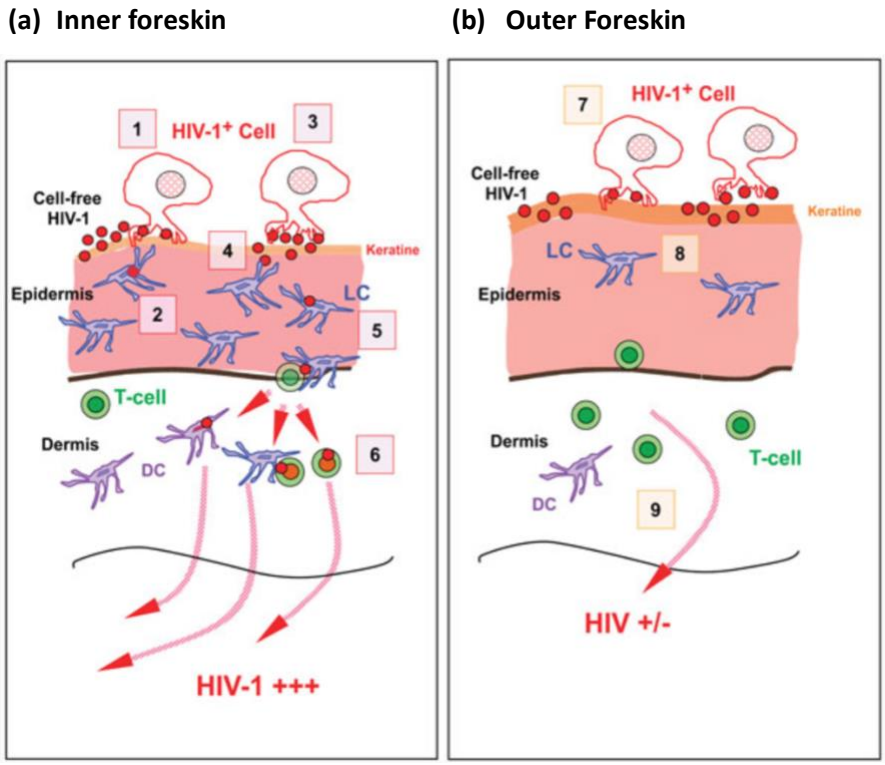

Figure 4. ***Likely initial events during HIV acquisition in the inner and outer foreskin****.* ***(a) Inner foreskin****: Langerhans cells succumb to infection through heavily infected cells and less likely to be infected by cell-free virus or lightly infected cells*[11] ***(b) Outer foreskin.*** *The keratinized epithelium likely traps lightly and highly infected cells as well as cell-free virus thereby limiting virus entry*[11]*. Figure Adapted from Jayathunge P.H.M et al., Male Circumcision and HIV Transmission; What do we know?. Aids 2014; 8:31-44*[11]

The presence of asymptomatic STIs has been shown to significantly elevate the presence of HIV target cells at mucosal sites such as the foreskin[9,19,79,80]. More to this, it has been previously demonstrated that foreskin CD4+ T cells are predominantly CCR5+, portraying approximately 90% of expression[5,8]. Other authors substantiating these findings, additionally reported that this is significantly higher than is witnessed in CD4+ T cells from the blood [8]. Various scholars have purported that removal of the foreskin eliminates all these pre-disposing attributes, thereby contributing to the 60% risk reduction associated with medical male circumcision (MMC), although the mechanism is not fully understood [9–17].

Innate and adaptive immunity in the male genital tract

The innate immune system forms the immediate and first line of defense against invading pathogens, implemented by two main strategies[81,82]. These include, i) use of ubiquitous pattern recognition receptors (PRRs) to recognize and destroy pathogens and ii) secretion of non-specific molecules and cytokines that simulate other components and cells of the immune system to act against invading

pathogens[21,34,81,83]. Notably, PRRs recognize and bind a myriad of pathogen associated molecular patterns (PAMPs)[21,84,85]. To these effects, mucosal epithelia are lined with innate immune cells of the myeloid origin, that illicit an immune response and recruit players of the more specific arm of immunity, adaptive immunity [86–88].

Confirmatory to this, various PRRs have been identified through foreskin tissue immunohistochemistry, thereby affirming the presence of innate immunocompetent cell [78,89–92]. Likewise, various scholars have identified the presence of resident memory immune cells in the foreskin, identified by their expression of CD45RO[8]. The human penis is therefore an efficient mucosal effector site with the capability to illicit both non-specific innate and specific adaptive immune responses against invading mucosal pathogens[5,7,70,77,79,89].

Substantiating evidence of immune activation and modulation has been described in the sub-preputial space[76]. Increased secretion of pro-inflammatory cytokines, such as IL-8 have been observed and shown to recruit CD4+CCR5+ cells[6,8,9,13,78]. More to this, a wider repertoire of interferon inducible cytokines, such as the granulocyte-macrophage colony-stimulating factor (GM-CSF), interferon γ-induced protein (IP-10/CXCL10) and RANTES have been identified in *ex vivo* foreskin tissue models[72]. These cytokine combinations have been shown to increase HIV susceptibility and acquisition in pre-infection studies using cervico-vaginal explants[93,94]. Additionally, they were also shown to increase the permissiveness of HIV target cells to HIV variants that normally exhibit diminished viral fitness and infectivity[93,94].

Noteworthy, the presence of myeloid cells in foreskin epithelia serves as a double edged sword[95]. While myeloid cells may illicit restrictive immune responses that link innate and adaptive immunity; they also act as trojan horses that shield and cargo infectious virus from entry sites to lymphoid organs[95–98]. Myeloid cells may also promote and induce an inflammatory environment conducive to HIV proliferation and spread[95–98]. This, alongside with their positioning at entry sites and contribution to the viral reservoir, makes them an interesting component in HIV pathology that's worth further elucidation and understanding[95–98].

III. BRIEF OVERVIEW OF CHAPTERS

This study was sectioned into two chapters i) Immunophenotyping and ii) HIV challenge assays. In Chapter one (Immunophenotyping), optimization of antibody titre and fluorescence minus one (FMO) controls were shown and the foreskin primary cells quantified (n=31). The different myeloid cells, inclusive of LCs and "Mϕ" like cells were also identified and quantified. This was subsequently followed by sectioning the two cell groups into the different subsets within each group. Traditional LCs,

also referred to as conventional LCs, were identified by the simultaneous lack of CD11c and CD14 while unconventional LCs were identified by the differentially co-expression of CD11c and CD14 into the following subsets : i) **CD11c+**CD14- LCs, ii) CD11c-**CD14+** LCs and the iii) **CD11c+CD14+** LCs. Likewise "Mϕ" like cells were also characterised into different subsets inclusive of i) "M1" Mϕ, ii) "M2" Mϕ, iii) CD169 Mϕ and iv-v) "M1/M2" intermediates. Interestingly, in both LCs and "Mϕ" like cells, unconventional CD3+ subsets were also identified. All subsets were further assessed for the co-expression of HIV susceptibility markers (CD4+CCR5+), HIV attachment factors (DC-SIGN, Siglec-1, mannose receptor) and maturation markers (HLA-DR+CD80/86+) using both manual gating and unsupervised clustering.

In Chapter two (HIV challenge assays), method development and optimization assays were shown. The stepwise process of virion generation from the different IMCs was sectioned into transformation, restriction digestion, transfection, virus concentration, titre determination and reporter gene detection (GFP/mCherry). Optimization of titres was conducted in different cell lines (TZM-GFPs, CEM-GFPs, JLTR-5 and CEM-REVs) and PBMCs prior to being optimized in the pluricellular cell suspension foreskin model that was also optimized and selected after comparisons of the infection signal in different infection models (n=5). The optimal inhibitory concentration of maraviroc (IC_{50}) was also optimized using the TZM-bl assay for use against HIV infection in the foreskin model (n=5). HIV challenge assays were subsequently conducted using optimized virus titres from 6 different viruses, at the optimized time-points and using the pluricellular cell suspension foreskin model (n=17). HIV infected foreskin myeloid and lymphoid cells were identified and analysed seperately. HIV infected myeloid cells were further identified and characterised into the different LC and "Mϕ" subsets, using both manual and unsupervised clustering similarly to the Immunophenotyping chapter.

CHAPTER 1: Immunophenotyping and Characterization of foreskin myeloid cells

1.0 BACKGROUND INFORMATION : Myeloid Cells

Myeloid cells are a heterogenous group of cells that constitute much of the leukocytes in the body and originate from either hematopoietic stem cells (HSCs) from the bone marrow or embryonic stem cells from the yolk sac or fetal liver[88,99,100]. There have been many arguments over how best to classify myeloid cells due to i) shared ambiguous morphology among sub-groups, ii) contextual differentiation, iii) subjective naming preferences in varied research groups, and lastly iv) cellular origin[88,99,100]. A consensus was, however, reached whereby myeloid cells were eventually hierarchically classified according to ontogeny, function and lastly, location and morphology[18].

1.01 Ontogeny

Myeloid cells originate from progenitors that are derived from either bone marrow (BM) derived haematopoietic stem cell precursors (HSCs) or self-renewing embryonic precursors [101]. Mechanisms yielding both precursors are similar and are distinguished by transitioning through the BM or lack thereof as shown in Figures 5 and 6[101]. The fetal liver is seeded in three waves by i) yolk sac precursors, ii) erythromyeloid-specific yolk sac precursors and iii) precursors from other fetal organs including the aorta, gonada and mesonephros (AGM) as illustrated in Figure 5 below[101].

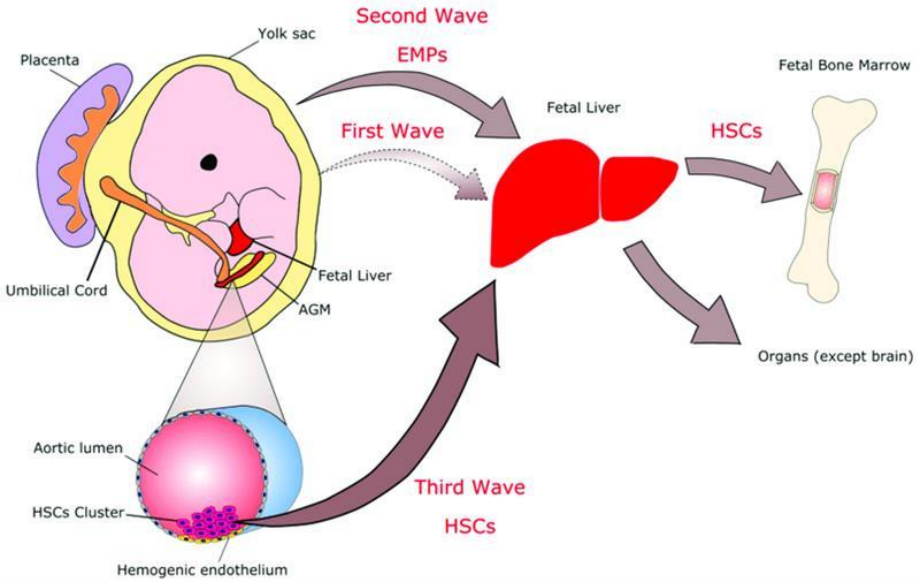

Figure 5. ***The origins of myeloid cell progenitors****. Fetal liver is seeded in 3 waves i) First wave and ii) Second wave HSCs arise from the yolk sac and iii) Third wave HSCs from other fetal organs (AGMs). Fetal liver embryonic precursors subsequently seed the bone marrow and other organs (i.e skin). Figure adapted from Freitas-Lopes et al., 2017. Differential Location and Distribution of Hepatic Immune Cells.* Cells ***6****, 48*[101]

In the first wave, the yolk sac seeds the fetal liver at week 7 of gestation, although these cells are transitory and have been shown to also seed the epidermis where they later serve as self-renewing precursors of epidermal cells. In the second wave, erythromyeloid progenitors (EMPs) seed the fetal liver from the yolk sac[101,102]. HSCs arising from the AGM region of the embryo, seed the fetal liver in wave three, thereby rendering it the main source of haematopoiesis[101]. The fetal liver subsequently seeds the BM, which takes over as the main source of HSCs at the end of gestation[101].

From the bone marrow, the hematopoietic stem cell, gives rise to two distinct progenitors namely the common-myeloid-erythroid progenitor (CMP) and the common-lymphoid-progenitor (CLP) as illustrated in Figure 6 below[88,103]. CMP then further yields either the myeloid lineage or

erythroid/megakaryotic lineage while on the other hand, CLP derives the NK, T or B lineage as shown in Figure 6[88].

In myelopoiesis, the common-myeloid-erythroid progenitor (CMP), differentiates according to ubiquitous transcription factors, such as PU.I[88,101,102]. This ultimately yields the macrophage-DC progenitor (MDP)[101]. Under the tight regulation of distinct transcription factors, MDP then differentiates into either the common DC precursor (CDP) or into monocytes as shown in Figure 6[101].

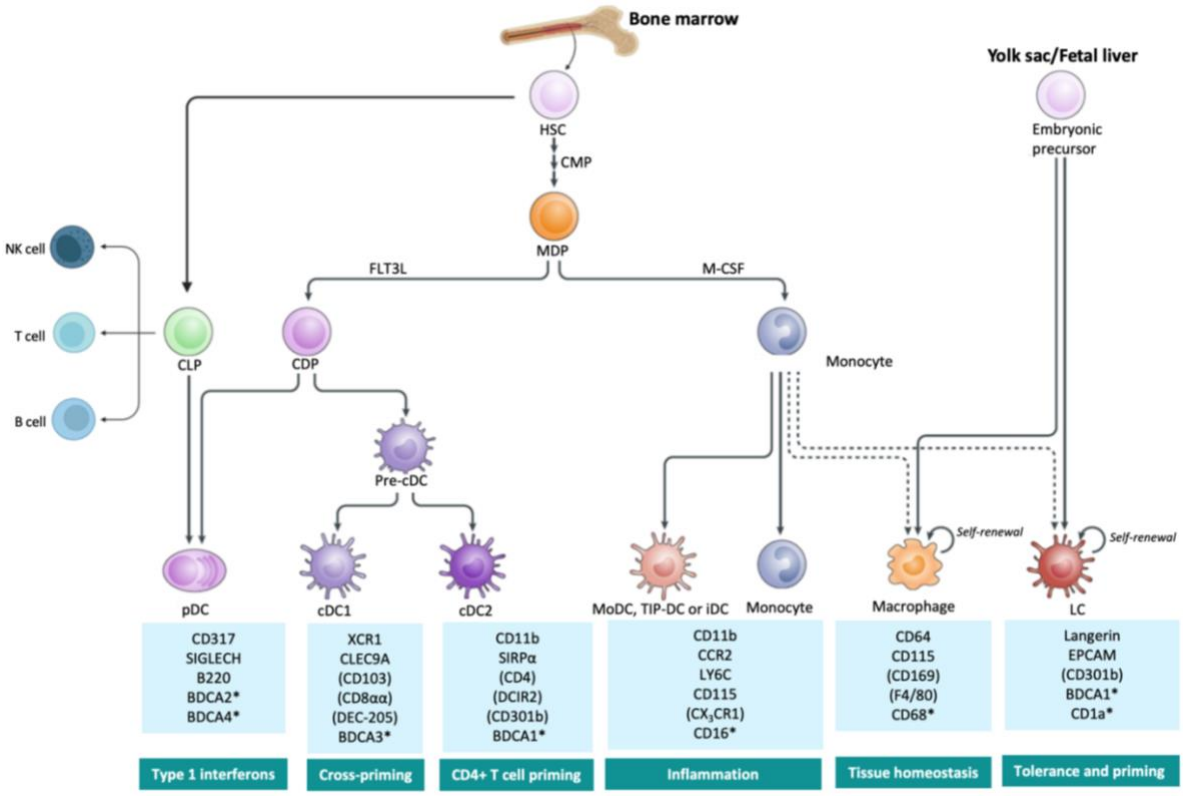

Figure 6. ***Ontogeny of DCs, LCs and macrophages****. Bone marrow derived HSCs give rise to lymphoid and myeloid cells through a series of intermediary precursors. The lymphoid progenitor CLP yields NK cells, T cells, B cells and pDCs. The myeloid progenitor, MDP gives rise to either the DC precursor or monocytes from which different myeloid cells originate through transcription factor prompted maturation. The yolk sac/fetal liver embryonic precursors give rise to LCs and macrophages with self-renewal properties. Surface markers are listed in the light blue boxes for each cell type and the roles of the cell types are defined in the green boxes. Image edited in Biorender.com*[48].

Common DC precursor (CDP)

The common DC precursor (CDP) is an intermediary precursor for the transcriptionally dissimilar; conventional dendritic cells (cDCs) and plasmacytoid DCs (pDCs)[104,105]. Plasmacytoid DCs may also originate from the lymphoid progenitor (CLP) as shown in Figure 6. In the cDC route, CDP is transcriptionally programmed by the FMS-like tyrosine kinase-3-ligand (Flt3), to differentiate into pre-cDCs that ultimately egress from the bone marrow to colonize lymphoid and non-lymphoid organs

[104,105]. In peripheral tissues, pre-cDC precursors differentiate into cDCs that function as resting immune sentinels which are activatable by PAMP. In lymph nodes, they give rise to resident, steady state cDCs[104,105].

Monocytes & monocyte-derived myeloid cells

Bone marrow derived HSCs yield myeloid progenitors that differentiate into circulatory monocytes[106]. Under inflammatory conditions, leading to severe DC depletion, monocytes are seeded into ubiquitous adult tissue where they give rise to monocyte derived DCs (Mo-DCs) and macrophages (MDMs)[107]. Consistent to this, monocytes have been shown as capable of acquiring an LC-like phenotype[107,108]. However, it is postulated that MDMs do not become part of the tissue resident population although they establish well in organs like the gut where they completely replace the tissue resident population [107,109–111]. MDMs are unique from the tissue resident yolk-sac and fetal derived macrophages, as shown by the different set of surface markers as shown in Figure 6 above[109–111].

Embryonic precursors

The yolk sac myeloid progenitor releases primitive macrophages into the circulatory system which are seeded into the embryonic brain, liver, skin, and lungs[110,112]. Subsequently, these primitive macrophages differentiate into tissue resident macrophages with self-renewal properties[108,113]. In privileged tissues such as the liver and the brain, macrophages are postulated to exclusively derive in this manner[18,111]. The ability to self-renew has raised interests as to whether there is a subset of tissue resident macrophages with stem cell properties[87,113]. Similarly, LCs are postulated to distinctly arise from a heterogenous population of proliferative and self-renewing precursors that are seeded into the epidermis from the yolk sac or fetal liver at only week 7 of gestation, as described earlier and shown in Figure 5 [113]. Noteworthy, yolk sac derived LCs only constitute approximately 10% of the total LC pool while the majority derive from the fetal liver[101,113].

1.02 General Functions of Myeloid Cells

Pathogen recognition

Myeloid cells are ubiquitously distributed in secondary lymphoid organs such as mucosal epithelia, lymph nodes and the spleen, where they act as immune sentinels[88]. They capture antigens through several complementary mechanisms such as pattern recognition receptors (PRRs) and Fcγ receptor processing[21]. Captured antigens are subsequently processed and presented as antigenic peptides to cognate CD4+ T cells in the lymph nodes [114,115]. PRRs recognize pathogen associated molecular patterns (PAMPs) that are associated with most pathogens[114,115]. Myeloid cells express a wide repertoire of PRRs

that fall into varied classes such as C-type lectin receptors (CLRs), Immunoglobulin-like lectin receptors (Siglecs), toll like receptors (TLRs) and Rig-I-receptors [114–118].

C-Type Lectin Receptors

C-type lectin receptors (CLRs) are a group of critical PRRs in pathogen recognition and capture that can independently illicit immunity and engage in cross-talks with signals from other PRRs[21]. CLRs are proteins that bind conserved carbohydrate structures (lectin), in a Ca^{2+} dependant manner[21]. There are 17 groups of CLRs, although only 3 groups are restricted to myeloid cells[21]. These include type II, IV and V[21,114,116–118]. Langerin and dendritic cell-specific intercellular adhesion molecule-3-Grabbing non-integrin (DC-SIGN), are type II CLRs which have one carbohydrate recognition domain (CRD) and they form oligomers in the cell surface[21,114,116–118]. They recognize conserved sugar structures present on pathogens including HIV-1, such as monosaccharides, mannose, fucose, N-acetylglucosamines and mannan[21]. Additionally, CLRs bind self-ligands such as ICAM-2 and 3, thereby facilitating crosstalk among immune cells[21]. The mannose receptor (MR) is a type IV CLR with multiple CRDs and does not form oligomers. C-type lectin receptors are the main HIV attachment factors in mucosal cells, although the most studied have been the mannose receptor, DC-SIGN, langerin, DC-immunoreceptor (DC1R) and an unidentified trypsin resistant CLR[116–11820,21,26,33,89,119]. Although CLRs confer a protective anti-viral role, HIV has been shown to hijack and subvert CLRs for viral transmission as shown in Figure 7[20,21,26,33,89,119].

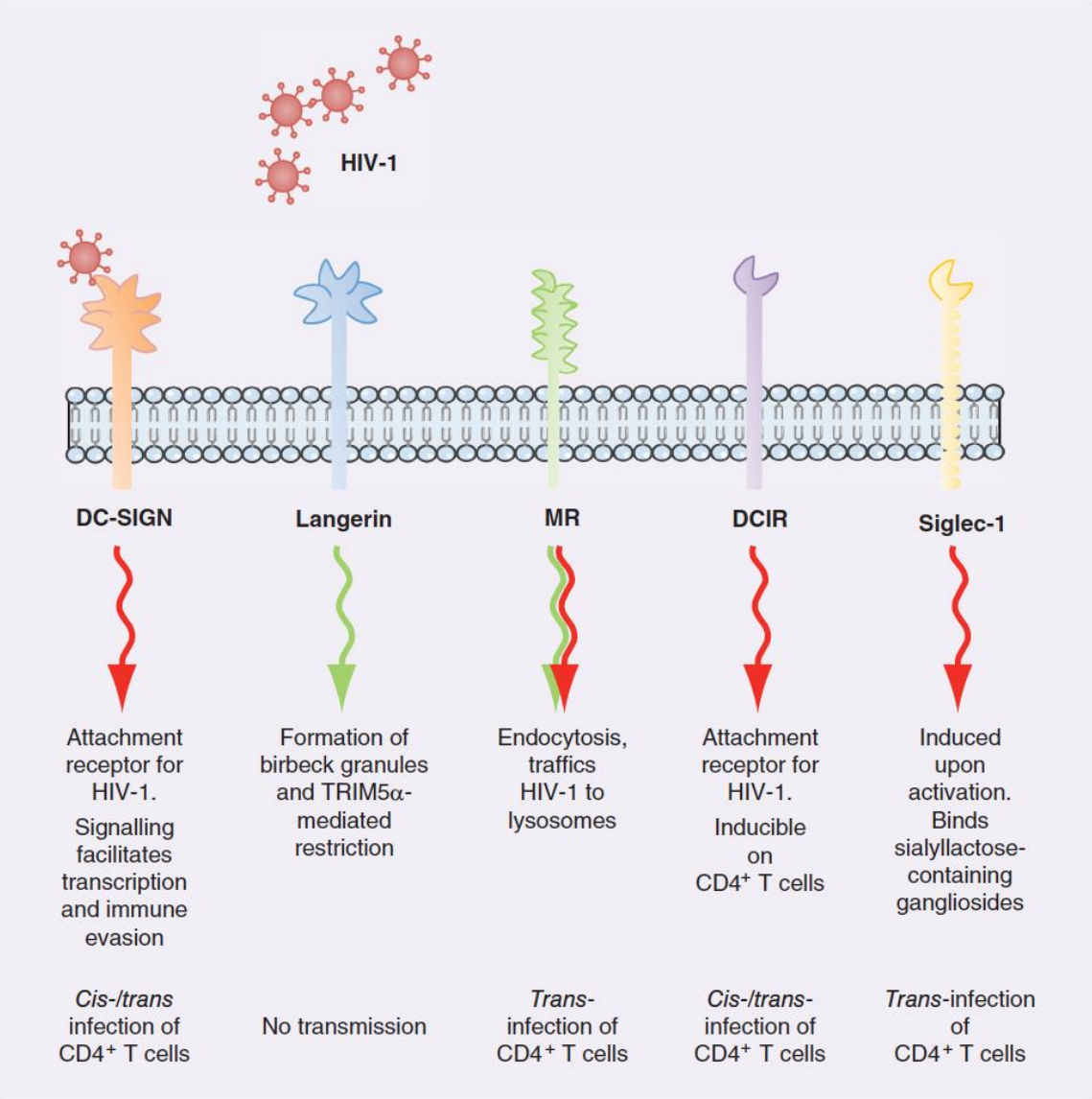

Figure 7. ***Myeloid cell surface expressed C-type lectin receptors****. Myeloid cell membranes are laden with different HIV attachment factors: i) DC-SIGN (CD209), ii) Langerin (CD207) iii) Mannose Receptor (MR – CD206), iv) DCIR and Siglec-1 (CD619) that augment cis-and trans- infection of myeloid HIV targets.. Image adapted from Nina Hertoghs et al., 2017 : Mucosal dendritic cells in HIV-1susceptibility: a critical role for C-type lectin receptors*[34]

The most implicated and reported on CLR, regarding subversion by HIV is DC-SIGN[20,26,33,72,120]. Both DCs (mature and immature) and macrophages have been shown to efficiently bind HIV using DC-SIGN with subsequent dissemination to CD4+ T cells[20,26,33]. Langerin, on the other hand has been shown to confer a protective role in which CXCR4 using HIV is sequestered for degradation as shown in Figure 8 below[34].

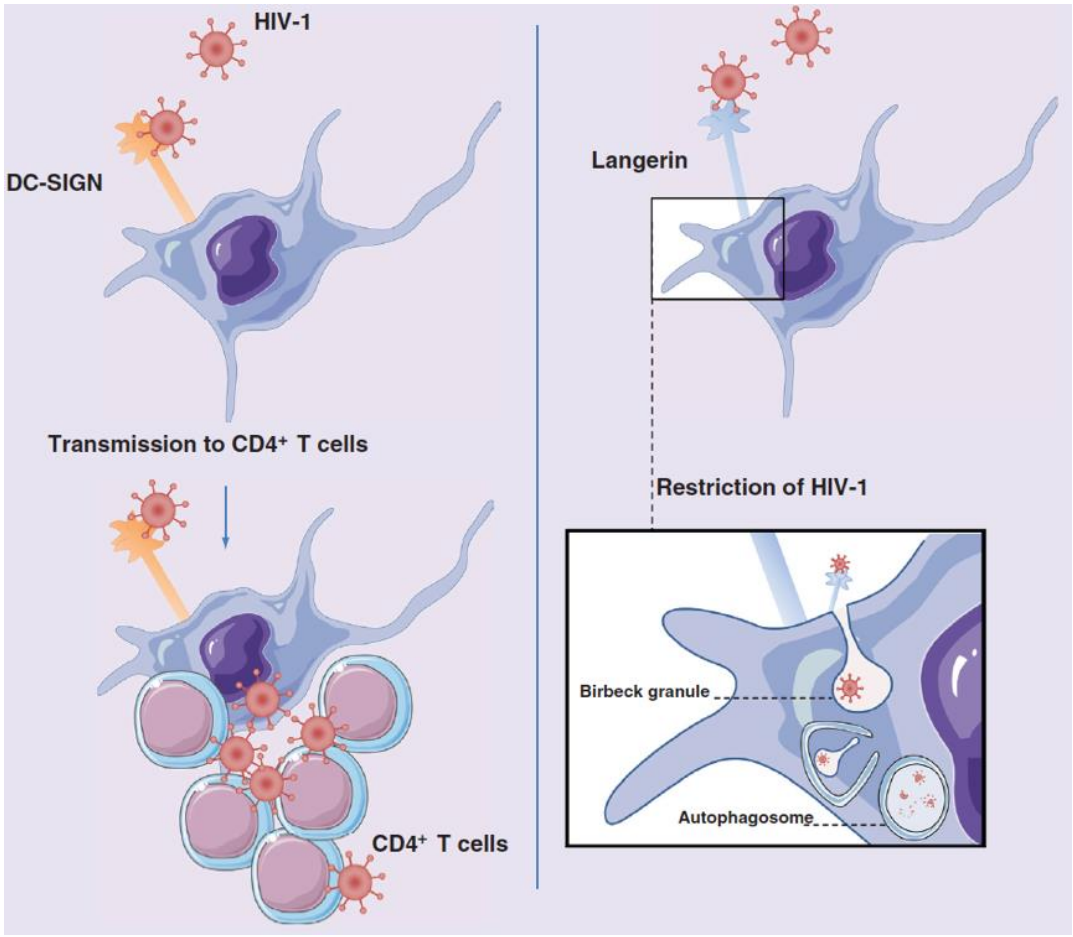

Figure 8. ***Differential roles of myeloid cell CLRs in HIV transmission****. HIV-DC-SIGN interaction aids HIV dissemination and transmission to CD4+ T cells while Langerin-HIV interaction leads to HIV abrogation. Image Adapted from Nina Hertoghs et al., 2017 : Mucosal dendritic cells in HIV-1susceptibility: a critical role for C-type lectin receptors*[34]

Ig-type lectin receptors i.e Siglecs

Sialic acid-binding immunoglobulin-like lectins (siglecs) are another group of proteins that specifically recognize terminal sialic acids associated with N and O linked glycosylation, such as the N-terminal sialic acid of HIV gp120[34]. Eleven human siglecs have been cloned and characterized and are inclusive of; siglec-1 (CD169/sialoadhesion), siglec-2 (CD22), siglec-3 (CD33), siglec-4a (myelin associated glycoprotein) and siglec-5 to 11, all of which can recognize and interact with HIV[34]. Sialic mutations have been shown to correlate with reduced infectivity and increased sensitivity to neutralization[121,122]. More specifically, Siglec-1, has been shown to bind HIV independently of CD4 and to additionally get upregulated in response to inflammation and HIV exposure[121,123,124]. Furthermore, Siglec-7 (CD328) has been shown to bind gp120 in a sialic acid-dependent manner, and it's blockade shown to markedly reduce the degree of HIV infection in Siglec-7+ MDMs[119]. Cells that do not constitutively express Siglec-7, such as CD4+ T cells were shown to display increased infectivity when enhanced with Siglec-7 *in vitro*[119].

Toll Like Receptors

There are 10 known TLRs expressed by humans that differ and stratify according to location within the cell and cognate PAMP. TLRs recognize a plethora of microbial molecules such as lipids, proteins, nucleic acids, and carbohydrates, leading to the secretion of type 1 IFNs (IFN-a and IFN-B). Specifically, plasma membrane bound TLR10 can sense gp41 in a synergized manner with TLR1 and TLR2[125]. On the other hand, endosomal TLR7,8 and 9, recognize methylated dsDNA from bacteria and viruses. TLR3 detects viral dsRNA in dead cell debris[125]. Myeloid cells generally express the full repertoire of TLRs, although this may be immunomodulated by pathogen encounter and activation[125]. For instance, under steady state conditions, macrophages do not express TLR3. However, in response to virus infection, TLR3 expression is induced by Type 1 IFNs (αβ)[59,126]. Likewise, TLR1, 2 and 7. Therefore, Type 1 IFNs mediate virus-induced activation of innate immunity through the modulation of TLR expression[59,126].

While pathogen recognition by PRRs is a branch of non-specific innate immunity, cells of the myeloid lineage including granulocytes, macrophages and DCs also co-express several classes of Fcγ receptors on their surface at all stages of their differentiation[88,97,127]. This broadens antigen recognition to unlimited diversity by linking adaptive immune antibodies with innate immunity[98]. Myeloid cells express high levels of Fc receptors that recognize and bind antibody Fc domains, subsequently mediating cellular activation, cytotoxicity as well as phagocytosis of Ig-G opsonized targets[98].

Antigen processing and presentation

DCs and macrophages are professional antigen presenting cells (APCs) due to their ability to prime naïve T cells[51,120]. DCs particularly have an intrinsic migratory pattern that renders them able to capture antigens from affected areas and migrate to draining lymph nodes where antigens are presented to T cells that are subsequently primed for an immune response[114,128–130]. Both DCs and macrophages present protein antigens on the major histocompatibility complex I and II (MHC I and II), analogous to HLA-A, B, C and HLA-DR, DP, DQ respectively and co-stimulatory molecules CD80 and CD86 as shown in Figure 9 below[97,129,130]. Antigenic peptides presented on MHCI and MHCII molecules are presented to CD4+ and CD8+ T cells respectively as shown in Figure 9[131]. Meanwhile, lipid and other non-protein antigens are presented on the non-classical CD1 family of proteins comprised of CD1a, b, c, d, which allow the selection of rare antigen-specific T lymphocytes. CD1 molecules are all differentially expressed in the varied myeloid cell subsets[97,129,132].

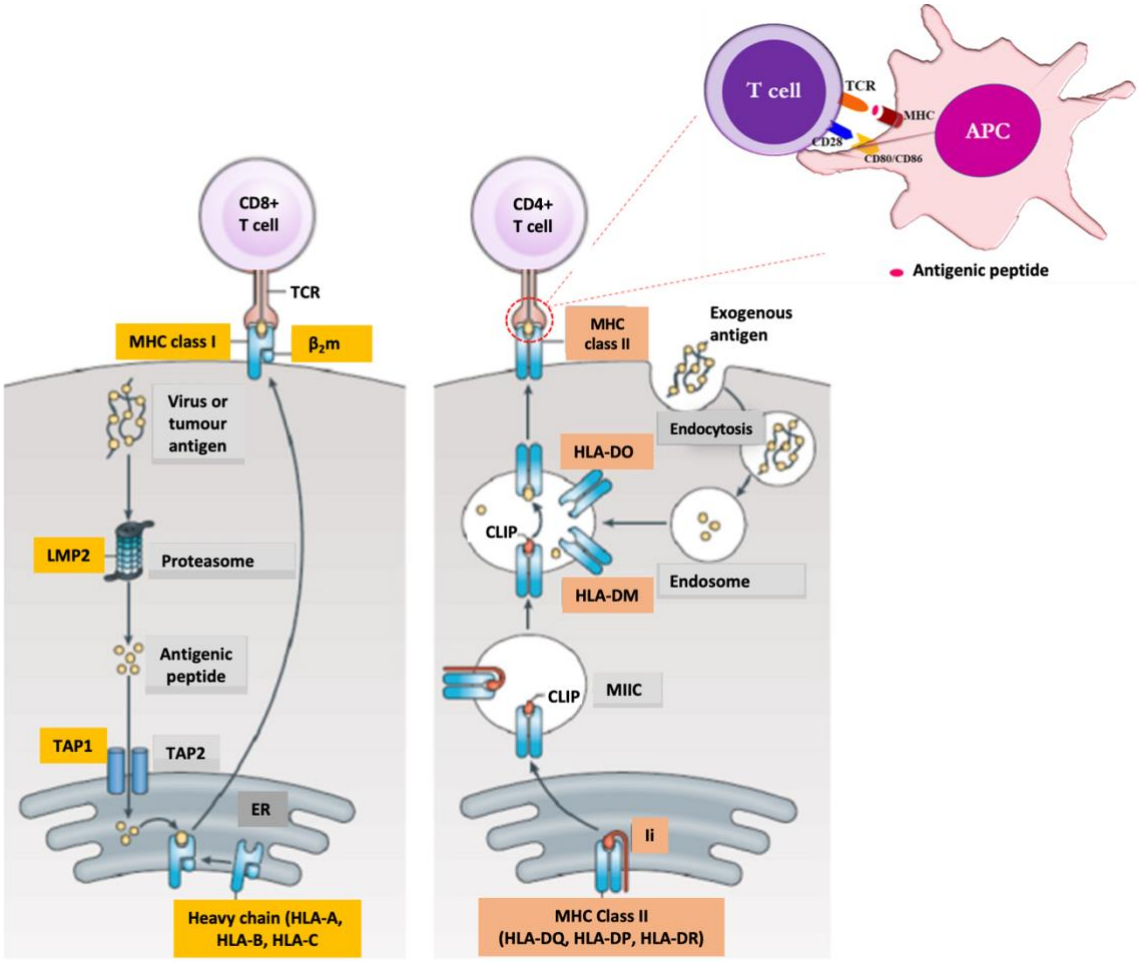

Figure 9. ***Myeloid cells as professional antigen presenting cells.*** *Myeloid cells are antigen presenting cells (APCs) that use MHCI and MHCII to present antigenic peptides, with the aid of co-stimulatory CD80.CD86 to CD8+ and CD4+ T cells respectively. Image adapted from Macmillan Publishers Ltd: Nature Reviews Immunology. 12, 813-820, copyright 2012*[131]

Under steady-state conditions, defined as quiescent bodily conditions that precede acute infection and inflammation, tissue resident DCs and LCs are typically immature and not fully differentiated into their roles as immune effectors[131]. They are, however, highly adaptable to efficiently capture antigens as evidenced by the high surface expression of PRRs, especially CLRs [113,133,134]. Immature DCs accumulate MHC II molecules in the late endosome-lysosomal compartment as shown in Figure 10 below. However, upon antigen encounter, immature DCs are activated and upregulate the expression of surface MHC II molecules[28,135]. Activated, antigen laden DCs are induced to migrate into the afferent lymph node (LN) through signaling by the chemokine receptor, CCR7 and sphingonsine-1-phosphate (SIP)[97,98]. Meanwhile, they process antigenic proteins into peptides that bind in the appropriate antigenic context, on either MHC or CD1 molecules as described above[97,129,132]. Subsequently, T cells are activated and drive DCs to terminal maturation thereby inducing further expansion and differentiation of T cells into effector T cells[114,115,136]. Without maturation signals, immature DCs remain inactivated

and alternatively induce tolerogenecity (immune suppression or regulation) characterized by the expansion of regulatory T cells[131].

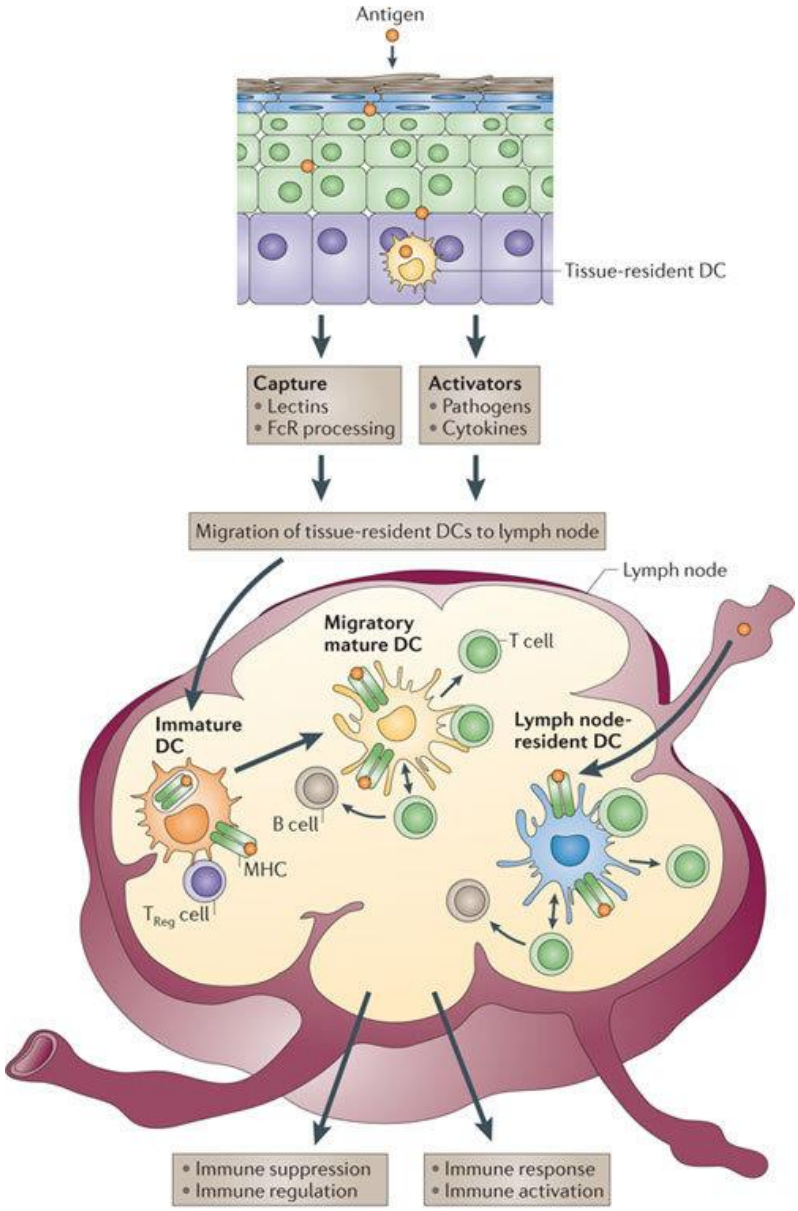

Figure 10.. ***Summary – Role of myeloid cells in antigen presentation****. Tissue resident DCs capture antigens through CLRs and FcR processing with subsequent activation and migration to lymph nodes for antigen presentation. MHC is internalized in Immature DCs, and surface expressed in migratory/mature DCs. Image Adapted from Palucka & Banchereau., (2012) Cancer immunotherapy via dendritic cells*[98]

1.03 Dendritic Cells

DCs constitute a small population of hematopoietic APCs with stellate morphology[97]. They closely resemble macrophages as well as LCs as evidenced by some of the shared phenotypic and transcriptional characteristics[97]. DCs express multiple CLRs such as DC-SIGN (CD209) and DEC-205 as described above. Although DC-SIGN was initially purported to be exclusively expressed in DCs, various studies have since shown it common to other myeloid cell types such as macrophages[137].

Similarly, some DC subsets have also been reported to express the mannose receptor (MR/CD206), Siglec-1 (CD169) and scavenger receptor (CD163) all previously thought as exclusive to macrophages as well as Langerin (CD207) common to LCs, all of which recognize and bind unique PAMPs[138]. Therefore, DCs and macrophages converge on several cell surface markers, including the antigen presentation machinery (MHC II, CD80 and CD86) and additionally the β_2 integrins, CD11c (integrin-α_x) and CD11b (integrin- α_M) as shown in Figure 11 below[137]. However, markers such as CD14 (glycosyl-phosphatidyl-inositol-anchored co-receptor), CD68 (lysosomal-associated membrane protein) and CD64 (Fc γ receptor I) are more commonly expressed in macrophages[103], while DCs more exclusively express CD1c (cDC2) and CD141 (cDC1) and thus enabling distinction between the two myeloid cell groups as shown in Figure 11 below. As such, DCs are broadly heterogenous and plastic, differing in the expression of markers, origin, tissue localization and maturation. Consequently, there has been a lot of debate regarding which cells are bona fide DC subsets or modified versions of the same cell type[137].

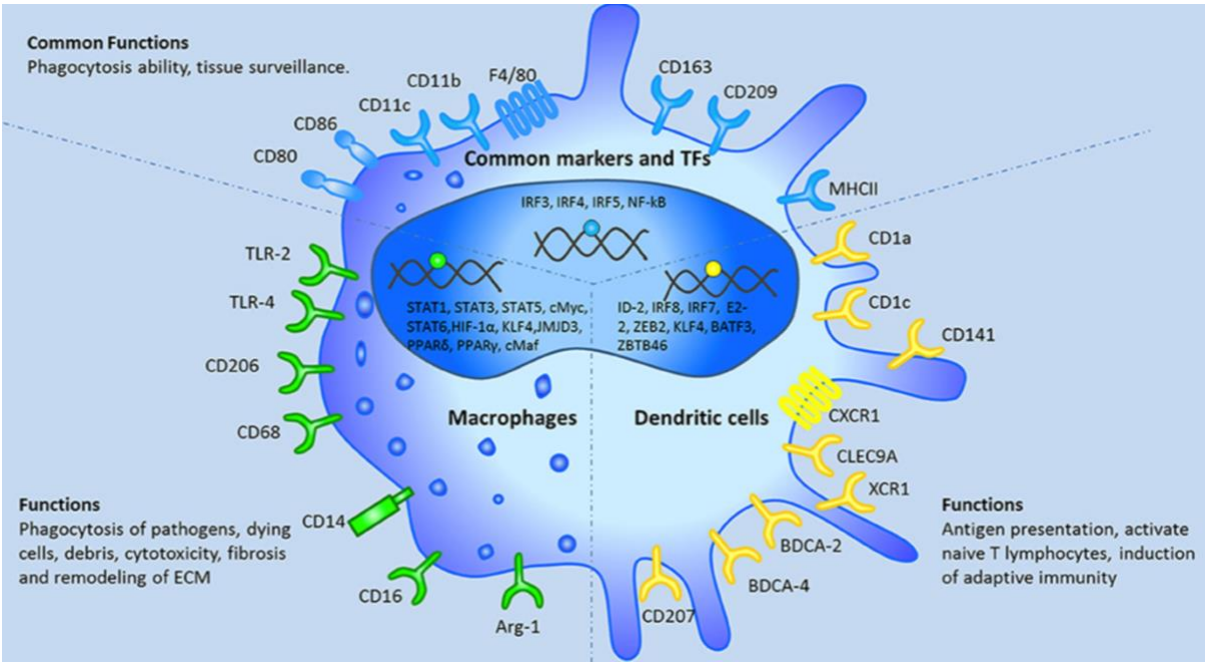

Figure 11. ***Delineating phenotypes of macrophage and DCs***. *Markers common to DCs/LCs and macrophages include CD80, CD86, MHCII, CD11c, CD11b, CD163 and CD209 (blue). Macrophages constitutively express TL2-4,4, CD206, CD68, CD14 (green) while DCs are distinguishable by the expression of CD1a-c, CD141, CXCR1, CLEC9A, BDCAA-2/4 (yellow). Langerin is also more constitutively expressed in LCs and in lower levels in some DC subsets. Figure adapted from Yao Yongli et al., 2019. Macrophage Polarization in Physiological and Pathological Pregnancy. Frontiers in Immunology*[137]

DC maturation

As DCs mature, the expression of PRRs is grossly downregulated, particularly of CLRs and TLRs. For instance, mature DCs have been shown to comparatively express lower levels of TLR1, 2, 4, and 5, thereby reducing the capacity of mature DCs to take up antigens. Conversely, mature DCs upregulate

the expression of co-stimulatory molecules such as CD80, CD86 and CD40[139]. This renders mature DCs more efficient in stimulating T cells by enhancing the stabilization of MHC I and MHC II at the cell surface. Interestingly, Siglec-1(CD169) is also upregulated upon DC maturation in positive co-relation with both co-stimulatory molecules CD80/CD86 and HLA-DR[139]. It is however, unclear as to how CD169 influences antigen presentation.

DC immunogenicity and tolerogenecity

While DC maturation and activation characteristically precede immunogenicity, tolerogenecity may be alternatively induced depending on the nature of PRR stimuli and signaling[32,140]. Naïve T cells may be primed to differentiate to varied T helper subsets or memory T cells may be stimulated to launch effector molecules[138]. Fully mature DCs are reported to be the drivers of immunogenicity. In contrast, tissue resident, semi-mature DCs can elicit both recessive and dominant tolerance[138]. Recessive tolerance is whereby self-antigens are presented to induce negative selection for autoreactive T cells while dominant tolerance is established when naïve T cells are primed via TGFβ to T regs which enhances DC-induced secretion of IL-10 in a positive feedback mechanism[138]. Similarly, to ontogeny-based plasticity, DCs exhibit functional plasticity and conventional DCs are delineated into two main groups exhibiting distinct transcriptional programs namely, type 1 and type 2 cDCs[138].

DC plasticity and subsets

Conventional DCs

Type 1 cDCs (cDC1) are a minor DC subset that is found in the epidermis. cDC1s characteristically express high levels of TLR3 with a signaling cascade that culminates in IFN-β expression and CD8+ T cell priming[141]. They also express the DC-specific sensor of tissue damage (DNGR-1/CLEC9A) which mediates cross presentation of viruses and allografts. cDC1s can be distinguished from cDC2s, the most abundant and heterogenous of the two subsets, by lack of CD1c, CLEC4a, CLEC10a, Langerin, Sirpa, CD163 and Siglec-1 expression [141]. cDC2s are confined in the dermis and lamina propia and characterized by the differential expression of CLRs that are shared across varied myeloid cells such as the mannose receptor, langerin and Siglec-1[97]. Specifically, cDC2b, a subtype of cDC2s uniquely expresses CD163 which is also found on macrophages. In addition, cDC2s uniquely exhibit differential expression of CD11c, CD11b and CD13. Importantly, cDC2s uniquely express TLR7 which senses ssRNA and are therefore important in HIV pathogenesis. Owing to the plasticity of cDCs in response to inflammatory stimuli, tissue localization and function; various other tentative populations exist as illustrated in Figure 12[141].

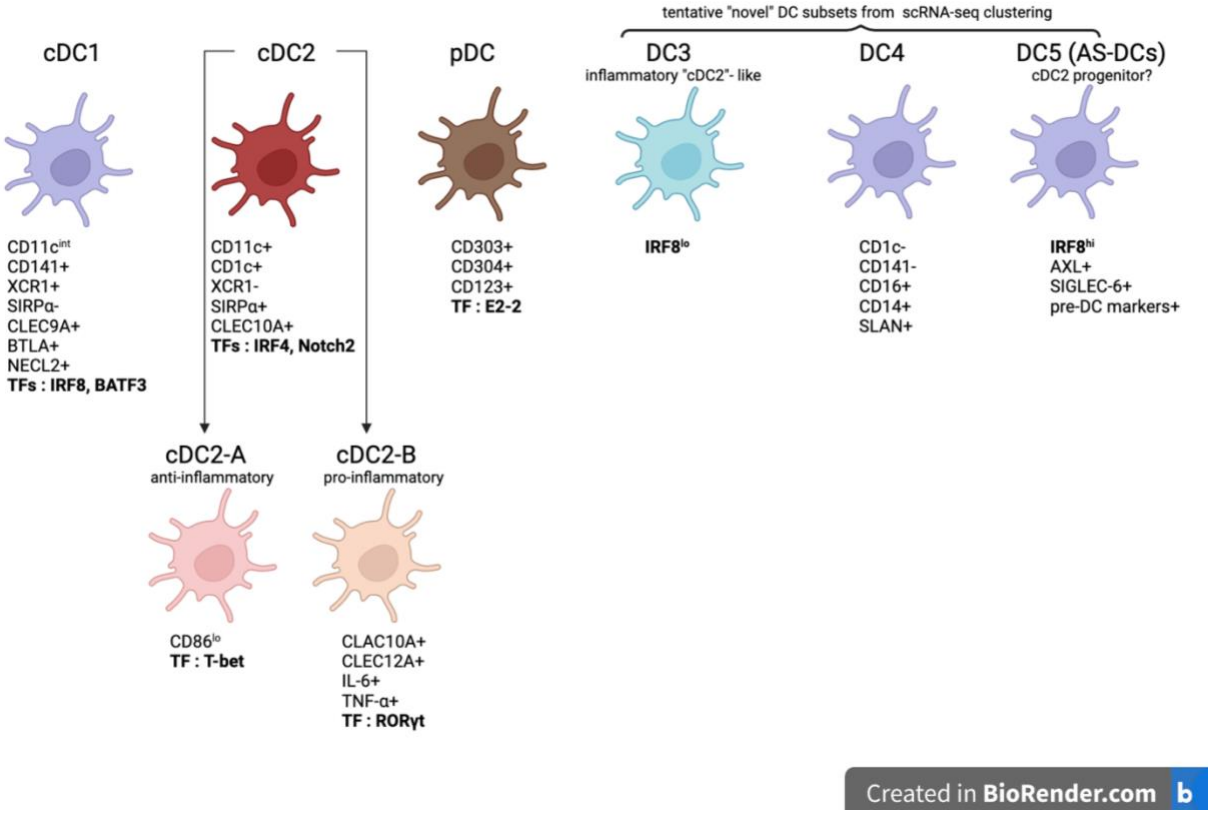

Figure 12. ***Classes of Dendritic Cells***. *Conventional DCs are classified into the homogenous Type 1 DCs (cDC1) and the heterogenous Type 2 DCs (cDC2) that comprise cDC2-A and cDC2-B subtypes. Other DC subtypes that are neither cDC1nor cDC2 are inclusive of DC3-DC5. DC5s (AS-DCs) are postulated to be resemble cDC2 precursors.* ***TFs =*** *transcription factors &* ***IRF*** *= Interferon Regulatory Factor. Image created in Biorender.com*[48]

Notwithstanding that these could possibly be precursors or modified versions of existent classes, single cell RNA sequencing has shown them quite distinct and unable to fit in either of the two existent cDC classes. Inflamed tissue has been shown to harbor cDC2-like cells, uncharacteristically expressing low 1RF8, and these have been classified as DC3[142,143]. Furthermore, another peculiar subset, named DC4 has been described that resembles MoDCs and likely arises due to the inflammation-mediated tissue influx by monocytes [141]. This is further cemented by the co-expression of CD16 and CD14, which is usually descriptive of intermediate monocytes as illustrated in Figure 10 above. In addition, DC4s characteristically lack the expression of definitive cDC markers previously shown to delineate the main cDC subsets; CD1c and CD141. Lastly, DC5s, alternatively referred to as AS-DCs uniquely express AXL and Siglec-6 also augmented by inflammation [141]. However, it's been strongly argued that DC5 is in-fact a subset of cDC2 precursors.

pDCs

Other than conventional DCs and associated subtypes, there are plasmacytoid DCs (pDCs) in peripheral blood, that have been described to sense bacterial and viral pathogens, enabled by the exclusive expression of TLR7 and TLR9[104]. Various authors have purported pDCs to specialize in initiating antiviral cytotoxic T cells and secrete high amounts of type 1 interferons[104].

CD11c+ Epidermal DCs

Historically, Langerhans cells were reported to be the only mononuclear phagocyte (MNP) resident in the skin epidermis. However, a novel epidermal CD11c+ cDC population was recently described in human abdominal and anogenital epidermis[29,72]. Epidermal CD11c+ DCs were shown to lack langerin expression, hence, delineated from LCs but were transcriptionally and morphologically similar to cDC2. Dissimilarities with cDC2s were based on location and the comparatively lower expression of CLRs and other surface receptors inclusive of the mannose receptor, Siglecs: 1, 6 and 16, and CLEC8A[72]. More importantly, epidermal CD11c+ DCs demonstrated higher levels of CCR5 in comparison to cDC2s and LCs with correspondingly more permissiveness to both lab adapted and transmitted founder HIV strains[72].

Inflammatory Dendritic Epidermal Cells (IDECs)

In the inflamed epidermis, a unique DC population termed inflammatory dendritic epidermal cells (IDECs), has been elucidated co-localizing with LCs. IDECs resemble mature DCs, but are distinguishable by higher mannose receptor, CD11c and CD1c expression while completely lacking langerin expression[98]. Furthermore, IDECs express lower levels of CD1a and are CD11b+, unlike LCs. Another delineating characteristic of IDECs is lack of CD14 expression, which separates them from monocyte derived CD1c+CD1a+ DCs that flood inflamed tissues. Moreover, IDECs are skewed towards IL-10 secretion to quench the inflammatory response[82]. In summary, DC subset identity and function is malleable to the micro-environment and inflammatory status.

1.04 Langerhans Cells (LCs)

Human LCs, often termed skin DCs, are resident in the *stratum spinosum* in the epidermis, where they make up 3-8% of epidermal cells. LCs were originally classified as DCs although later resolved to share ontogeny with macrophages with which they also share self-renewal properties while still overlapping on a lot of functions with DCs. Similarly to cDCs, LCs use their dendritic processes and surface PRRs to regularly sample the extracellular space for invading pathogens[34,144]. This renders LCs, the first immune cells to encounter pathogens, including HIV at mucosal epithelia of the vagina and the foreskin. Consistent with this, LCs have been described at high densities in foreskin epithelia. In a study on uncircumcised human penile tissue from cadavers, the mean frequency of LCs was highest in the outer (85.5 cells/mm^2) and inner foreskin (61.3 cells/mm^2) in comparison to other sites of the MGT such as the frenulum (56 cells/mm^2), glans (41 cells/mm^2) and urethral meatus (14 cells/mm^2) with none being observed in the penile urethra[70]. The foreskin therefore harbours a superficial epithelial population of LCs proximal to the epithelial surface where the extracellular environment is easily accessible. However, epithelial cell distribution and composition has been purported to also vary based on immune

status, and compromised epithelial integrity due to ulcerative STIs, physical aberrations during intercourse or inflammation[70].

LCs abundantly express the CLR, langerin (CD207) and exclusively express langerin-positive intracellular structures called Birbeck granules[30,145]. Langerin has been postulated to grab and sequester CXCR4 HIV viruses for TRIM5α-mediated autophagic degradation in Birbeck granules (BGs) in immature, steady state LCs[28,30,32,145]. Furthermore, LCs express intracellular sensors such as caveolins which have been shown to co-localize with langerin at the cell membranes and within Birbeck granules, where they are capable of mediating CD4-independent caveolar-endocytosis of HIV for degradation[30,146].

LC activation and maturation

Under steady state conditions, described above as quiescent conditions that precede immunogenicity, the transcriptomic profiles of tissue resident, immature LCs hierarchically cluster away from other myeloid cells such as macrophages and cDCs as previously alluded to[144]. However, upon antigen encounter, TLR signaling induces LC maturation and activation[32]. Activated LCs conserve the steady state transcriptome and additionally acquire new transcriptional programs that are shared between certain cDC subsets and macrophages[144]. They acquire migratory properties evidenced by increased expression of activation markers such as CCR7, tumor necrosis factor alpha (TNFα), IL-6 as well as the induction and proliferation of CD4+ T cells[5,144]. This transcriptional shift from tissue resident LCs to migratory LCs has been shown to significantly bring migratory LCs closer to migratory DCs, although migratory LCs induce more profound cytotoxic T lymphocyte (CTL) effector functions[144]. In addition, migratory LCs upregulate surface MHC molecules and T cell co-stimulatory molecules such as CD80, CD86, CD70 and CD40. Furthermore, migratory LCs are purported to upregulate Flt3, and become more cDC-like, subsequently clustering midway between macrophages and cDCs[147].

One of the crucial regulatory pathways in myelopoiesis is the interferon regulatory factor (IRF) gene regulatory pathway, particularly IRF4/8[116,147]. Deletion of IR4/8 has been observed to completely wipe-out monocyte and DC populations with no effect on LC development. However, high levels of TNFα have been observed to depict a positive correlation with IFR4/8. This further corroborates that LCs are distinct from other myeloid cells, although activation seems to bridge this gap.

Noteworthy, tissue resident DC subpopulations from similar sites have been shown to cluster away from blood DC subtypes irrespective of ontogeny. For instance, dermal CD14- DCs cluster with LCs in genital sites and exhibit similar transcriptional programs that are inseparable by principal component analysis (PCA)[142]. The microenvironment plays a major role in shaping the terminal phenotype.

Therefore, LC maturation and differentiation are driven by cumulative signals associated with tissue localization, activation status and function. More to this, during skin inflammation, the LC compartment comprises cells with two distinct origins: i) resident LCs which originate from the fetal liver, and ii) monocyte derived LCs which originate from the bone marrow and typically prominent in skin lesions. This has made elucidating the role of bona fide resident LCs an arduous task[113].

LC immunogenicity and tolerogenecity

Due to the constant exposure to external stimuli, LCs are engraved with strict gene regulatory pathways that are constantly shifting between tolerogenecity and immunogenicity[134,144,147]. Similarly to cDCs, LCs capture, process and present antigenic peptides either in the context of MHC1 or MHC II to CD4+ T cells or CD8+ T cells respectively as shown in Figure 13 below[134]. LCs have been described to effectively engage in antigen cross-presentation.

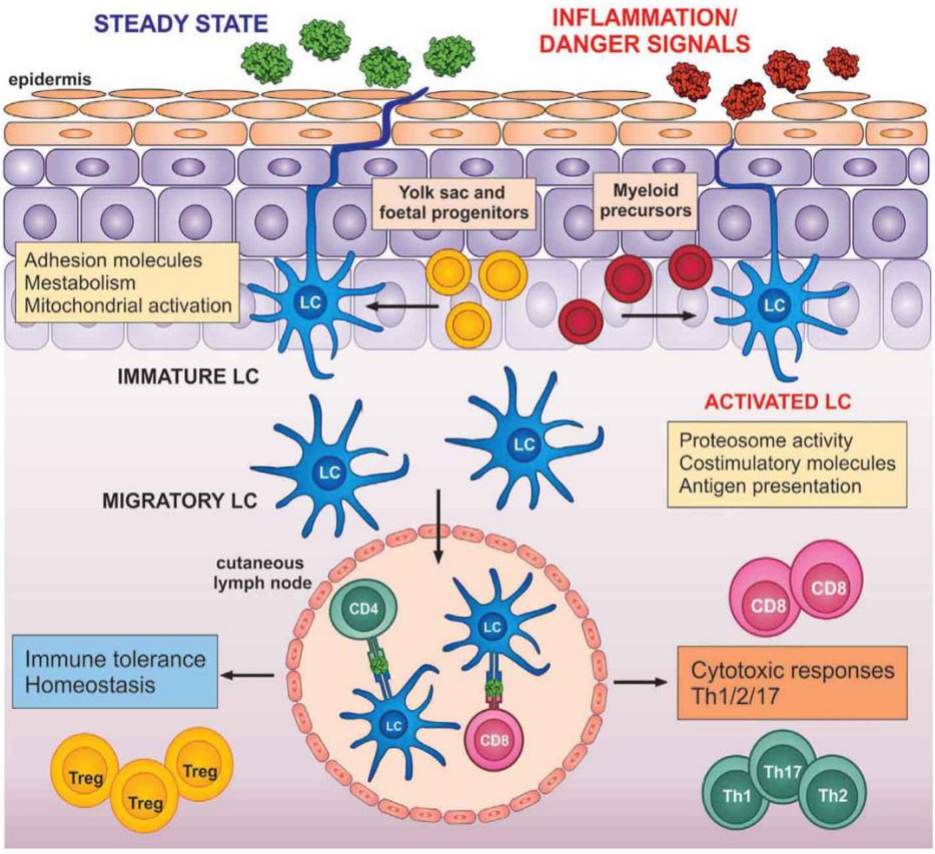

Figure 13. ***Langerhans Cells under steady state (tolerogenic) and inflammatory setting (immunogenic).*** *Langerhans cells derive from the yolk sac/fetal progenitors (yellow) in steady state and from the myeloid precursors (monocytes/red) under inflammatory conditions. Steady state LCs are anchored in the epithelium and express high levels of adhesion molecules while activated LCs are migratory and upregulate co-stimulatory molecules. Depending on the nature of stimuli, LC immune response can be homeostatic/tolerant or cytotoxic. Image adapted from K. Clayton et al. Langerhans cells—programmed by the epidermis, Front. Immunol., 8, 1676 (2017)*[134]

Viral or endogenous peptides such as those of HIV are loaded via MHCI and elicit a cytotoxic response while MHC II presents exogenous antigenic peptides and recruits T helper cells and other specific

effector molecules[88,96,138]. MHC I and MHC II molecules are cell-surface expressed although they may be internalized in endocytic vesicles during antigen processing, loading and transit to cognate lymphoid organs for antigen presentation prior to being re-cycled to the cell surface as shown earlier in Figure 9[129,136].

In quiescent conditions and immunosuppressive environmental perturbations such as radiation, LCs are regulatory[144]. They reside alongside heterogenous structural cells in the epidermis, such as keratinocytes. The neighbouring keratinocytes act as immune sentinels that may instruct LC immunity. LC tolerogenecity is regulated by PU-1 and nuclear factor kappa-light-chain-enhancer of activated B cells (NFkB) pathways which are induced by cytokines such as thymic stromal lymphopoietin (TSLP) and transforming growth factor beta-1(TGFβ) secreted by keratinocytes in response to environmental signals. PU.1, similarly to other myeloid progenitors, also facilitates steady state LC maturation and development[148]. The NFkB pathway is key in regulating both tolerogenecity and immunogenicity, it encourages the proliferation of steady state LCs through the engagement of metabolites derived from the adaptive immune system[149]. Steady state LCs predominantly express Receptor activator of NFkB (RANK) which is used to engage with keratinocytes via the RANK ligand. RANK-RANK-L interactions trigger LCs to induce the expansion of CD4+CD25+ regulatory T cells (Tregs), Foxp3+ Tregs and modulate the secretion of the cytokine CCL27 which is constitutively expressed by keratinocytes[149].

1.05 Macrophages

Macrophages are cells of the myeloid lineage that exhibit unique, tissue-dependant morphology and pleiotropic functions. They are professional phagocytes capable of mounting an immune response against invading pathogens and are integral in tissue homeostasis and architecture[87,111]. Similarly to DCs and LCs, Mϕ are also APCs and therefore express varied PRRs, multiple chemokine and cytokine receptors that enable them respond to other immune cells and effector molecules[87].

Mϕ proliferation and specialization in different tissues is driven by specific signals that enable adaptability to unique tissue requirements. For example, precursors differentiate to alveolar Mϕ in the lungs where they are adaptable to promote barrier immunity and surfactant clearance[88]. Other examples include Kupffer cells in the liver and microglia in the central nervous system. Noteworthy, Mϕ from different sites portray differential susceptibility to HIV infection. Viral reservoir studies, using both HIV and SIV, have shown that different tissues contribute differently to the viral reservoir [35,61,84]. Vaginal Mϕ, positioned at the initial point of HIV contact during sexual intercourse, express high levels of surface CD4 and CCR5 and are reportedly the major cell type that's permissive to CCR5 tropic viruses and susceptible to early HIV-1 infection[120]. In stark contrast, the gastro-intestinal tract (GIT),

harbours intestinal Mϕ that do not express innate immune receptors such as the LPS receptor CD14, CD16, CD32 and CD64. Moreover, they are downregulated for co-stimulatory molecules such as CD80 and lack the secretion of pro-inflammatory cytokines[150]. More importantly, they express markedly reduced levels of cell surface CD4, CXCR4 and CCR5, as well as their cognate mRNAs. This phenotype renders intestinal Mϕ less susceptible to HIV infection while purported to support low-level receptor virus entry with no evidence of viral replication[150].

Macrophage polarization

Macrophages also exhibit unique functions imprinted by site-specific signals, that can modulate macrophages to either pro-inflammatory or regulatory states through polarization. Polarization yields two distinct Mϕ phenotypes/states, namely classical (M1) and pro-inflammatory (M2) Mϕ[111,151]. Notably, although shared among DCs, LCs and both Mϕ polarized phenotypes, markers such as CD80, 86 and MHC11 are more highly expressed in M1 Mϕ and thus, used to distinguish these pro-inflammatory Mϕ from the restorative/regulatory M2 Mϕ as shown in Figure 14[137]. Noteworthy, macrophage polarization is a continuum within which exists intermediary Mϕ states, whereby M1 and M2 markers are co-expressed. These intermediate populations have additionally been shown to harbour replication competent HIV in the urethra of ART patients[35].

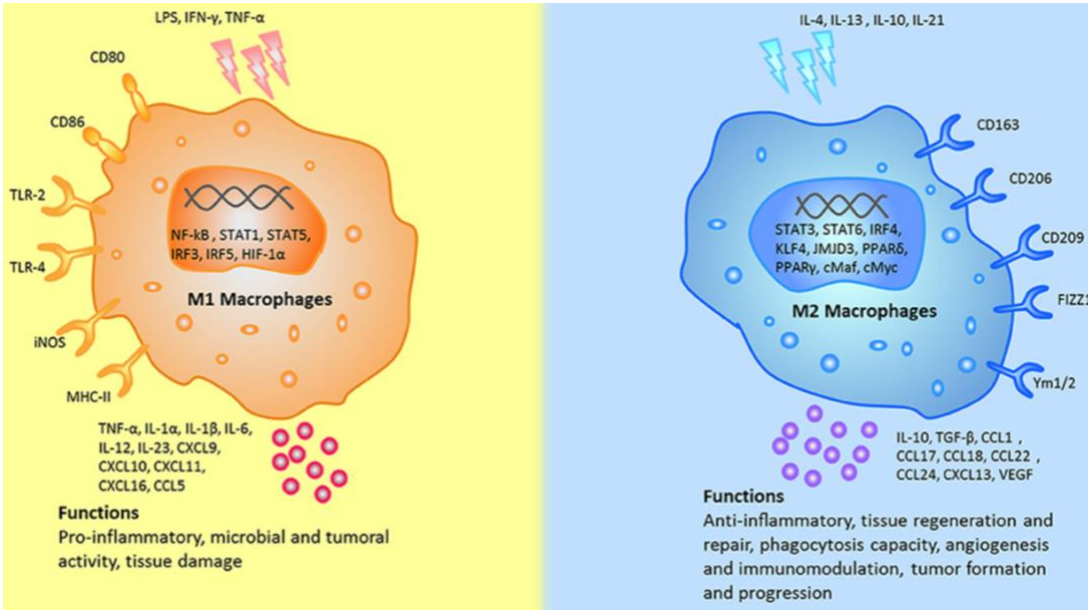

Figure 14. ***Macrophage polarization****. Macrophages polarize towards the M1 macrophage phenotype in response to pro-inflammatory cytokines (IFN-γ and TNF-α) under the strict regulation of transcription factors : NF-KB, STAT1,STA expressSTAT5,IRF3, IRF5 and HIF-1α. M1 macrophages are distinguishable from M2 macrophages by the higher cell surface expression of CD80/86, MHC II, TLR2, TLR4 and iNOS coupled with the secretion of pro-inflammatory cytokines inclusive of IL-6 and TNF-α. M2 macrophages polarize in response to anti-inflammatory cytokines (IL-4, IL-13, IL-10, IL-21) and are characterised by the high cell surface expression of CLRs (CD206 and CD209) and C163, as well as secretion of anti-inflammatory cytokines such as IL-10 and TGF-β. Figure adapted from Yao Yongli et al., 2019. Macrophage Polarization in Physiological and Pathological Pregnancy. Frontiers in Immunology*[137]

Classical macrophages (M1)

As illustrated above, classically activated Mϕ express a broad range of receptors that detect i)PAMPs from variable pathogens, ii) tissue damage and iii) signalling cytokines from other cell types. M1 Mϕ express TLR-2 and TLR-4 which they synergistically use, TLR-4 in particular, with CD14 to bind lipopolysaccharide (LPS), a PAMP common in pathogenic bacteria. CD14, although constitutively expressed in Mϕ, has been shown to upregulate in M1 Mϕ in like-manner to CD64 upregulation, whose blockage has been shown to negatively impact M1-polarization while retaining the M2 Mϕ population[152]. CD14 also recognizes other PAMPs such as lipoteichoic acid whose soluble form is secreted by pro-inflammatory monocytes into the circulatory system[88,138]. During infection, LPS or Th-1 cytokines such as IFN-γ and TNF-α,stimulate Mϕ to polarize to the M1 phenotype. M1 Mϕ are thus distinguishable from other myeloid cell-subsets and M2 Mϕ by the comparatively higher, but not exclusive expression of opsonic receptors (CD64, CD16 and CD32), antigen presentation molecules (MHC II, CD80, CD86) and CD14[152]. CD11c, with its pro-inflammatory ability to bind complement molecules and mediate phagocytosis for antigen presentation has also been reported more highly expressed in M1 Mϕ compared to M2 Mϕ[153]. M1 Mϕ respond to pro-inflammatory stimuli by the secretion of copious amounts of pro-inflammatory cytokines such as IL-12, TNF-α, reactive oxygen species (ROS), IL-23 and IL-6[120]. MI Mϕ are therefore characterized by enhanced microbicidal, pro-inflammatory, antigen presentation and anti-tumoral properties[153].

Alternatively activated macrophages (M2)

M2 Mϕ are characterized by anti-inflammatory properties. They are inducible by anti-inflammatory molecules such as glucocorticoid hormones and Th2-derived cytokines such as IL-4, IL-13, IL-10 and IL-21 that trigger a distinct activation program that polarizes M2 Mϕ as shown in Figure 13 above[154]. In contrast to M1 Mϕ, M2 Mϕ express abundant levels of non-opsonic receptors and CLRs such as the mannose receptor (MR) CD206 and CD163. However, some authors have argued that M1 and M2 Mϕ exhibit comparable CD206 expression[154].The upregulation of CD200 receptor is purported to be more specific to M2 Mϕ than CD206[151,154]. More to this, CD163 has also been suggested to be more acceptable as an M2 marker when used in combination with the transcription factor CMAF. Tissue resident M2 Mϕ additionally express DC-SIGN[151]. The mannose receptor (MR) identifies and binds mannose N acetylglucosamines and fucose on viruses, bacteria and parasites. Bound antigens are endocytosed and sequestered for lysosomal degradation or alternatively routed to MHCI or II molecules for subsequent antigen presentation and cross-presentation respectively[138]. Similarly to MHC molecules illustrated earlier, the MR recycles back to the surface[138].

Furthermore, M2 Mϕ secrete high levels of immunosuppressive cytokines such as IL-10 and TGFβ which subsequently inhibit IFN-γ production thereby modulating inflammatory responses[103]. Interestingly, TGFβ has also been reported to downregulate the expression of the mannose receptor in a negative feedback mechanism. During the induction of the M1 phenotype, Th1 cytokines also downregulate MR expression and thus negatively select against M2 Mϕ. In summary, M2 Mϕ tune inflammatory responses and adaptive Th1 immunity, scavenge debris, promote angiogenesis, as well as tissue remodelling and repair[103,137,155,156]. Depending on the nature of external stimuli, the continuum of M2 polarization is characterised by varied subgroups inclusive of M2a, M2b, M2c and M2d as shown in Figure 15[154]. While it is broadly accepted that M2 Mϕ polarize in response to Th2 cytokines as described above, this is particularly in reference to the M2a Mϕ as shown in Figure 15. M2b Mϕ are activated by immune complexes, while M2c and M2d Mϕ are activated by glucocorticoids and TLR antagonists respectively[137].

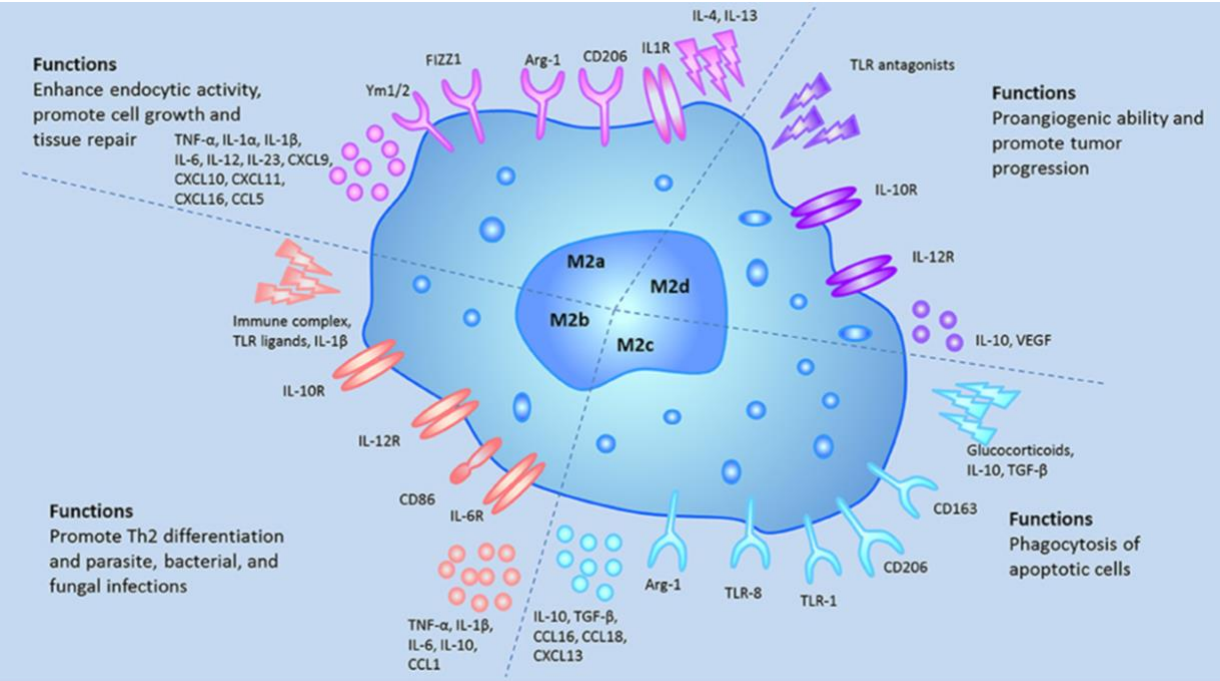

Figure 15. ***M2 macrophage sub-groups****. M2-macrophages are sub-grouped into M2 (a)-(d) based on different stimuli, surface markers, secreted cytokines and biological functions. Figure adapted from Yao Yongli et al., 2019. Macrophage Polarization in Physiological and Pathological Pregnancy. Frontiers in Immunology* [137]

M1/M2 macrophages during HIV infection

As illustrated earlier, Mϕ originate from embryonic precursors that imprint self-renewal properties and a long half-life while inflammatory settings induce monocyte infiltration into tissues[99]. This is of utmost importance in HIV pathology as it reportedly provides a route for the spread of HIV to privileged tissues

such as the spleen, lung, heart, colon, brain and adipose tissue[157]. The infiltration of circulatory HIV infected monocytes in varied tissues gives rise to long-lived HIV infected MDMs[157].

Of the two polarized states, M1 Mϕ reportedly accelerate the formation of viral reservoirs in early HIV infection after which a shift is prompted towards the M2 phenotype[155]. Briefly, M1 Mϕ suppress the expression of CD4 and CCR5 during acute HIV infection using a two-step TNFα mediated process. TNFα induces TNFR2, which subsequently triggers GM-CSF to downregulate CCR5[138] while also synergizing with IFN-β and IFN-γ to enhance the secretion of MIP1-α, MIP1-β and RANTES which downregulate and reduce transcription of both CD4 and CCR5[155]. In addition, RANTES inhibits HIV fusion in Mϕ, which, together with the low level of surface HIV receptors, consequently prevents Mϕ superinfection while retaining steady viral replication and persistent inflammation[59]. Persistent inflammation triggers a shift in the cytokine milieu and launches M2 polarization. IL-10 specifically induces MHC II downregulation and accelerated uptake of apoptotic cells generating an anti-inflammatory response[60].

Beyond the M1/M2 paradigm

While the concept of M1/M2 is widely accepted to delineate pro-inflammatory and regulatory Mϕ, the combinatorial spectrum of Mϕ populations is quite fluid and dependent on timeframe, tissue, several intrinsic, extrinsic and tissue-environmental stimuli. Therefore, macrophage phenotypes represent a continuum of activation status beyond M1/M2 phenotypes[151], that include CD169+ macrophages, TCR+/CD3+ macrophages and tumor associated macrophages (TAM) as shown in Figure 16 below.

CD169+ macrophages

CD169+ Mϕ are ubiquitously distributed *in vivo* where they reportedly serve an immuno-regulatory role similarly to LCs described above. Phenotypically, CD169+ Mϕ have been described to simultaneously co-express markers of M1 and M2 Mϕ inclusive of CD11c, CD11b, MHC-II, CD68 and CD206 [158,159]. Therefore, as a subset within the Mϕ group, CD169+ Mϕ also possess self-renewal properties when derived from the yolk sac progenitors and also derive from monocytes in diseased or inflamed tissue[160].

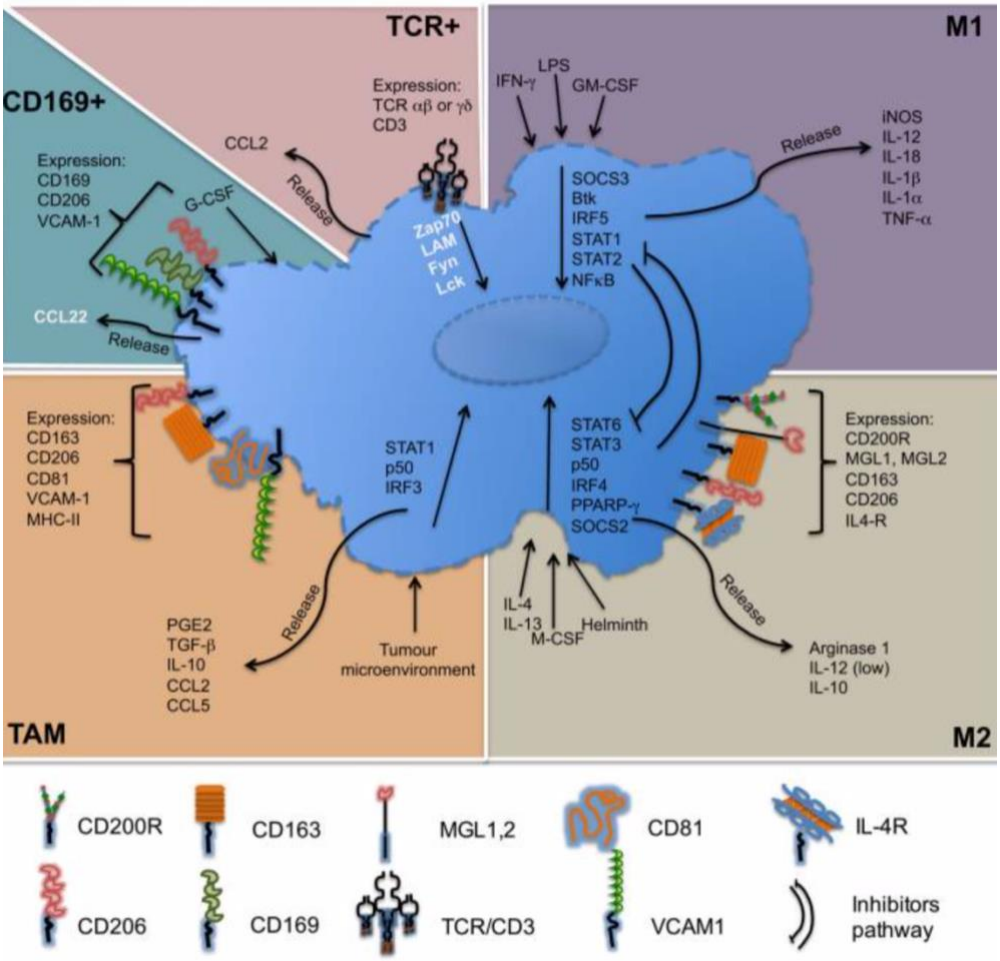

Figure 16. ***Other macrophage subsets beyond the M1/M2 phenotypes****. CD169+ macrophages, TCR+ macrophages and TAM are macrophage subsets with immunoregulatory roles that are distinguishable from the M1/M2 macrophage phenotypes. Image adapted from ChÃ¡vez-GalÃ¡n, Much More than M1 and M2 Macrophages, There are also CD169+ and TCR+ Macrophages.* Front Immunol ***6****, (2015)*[158]

Although the signaling and activation pathways as well as the biological roles of CD169+ Mϕ have yet to be fully deciphered, they have been implicated in immune tolerance, viral infection, autoimmune diseases and tumours[159]. They interestingly play a dual role in viral infection, whereby the CD169 molecule, similarly to CLRs, recognizes and binds sialic acid on viral pathogens including HIV. Consequently, this leads to antigen presentation and activation of invariant natural killer cells (iNKT) leading to an influx of DCs, NK, B and T cells [158–160]. In immune tolerance, CD169+ Mϕ bind α2,3- and α2,6-sialic acid on apoptotic cells resulting in either direct or cross-presentation of apoptotic antigens to CD8+ T cells via CD8α+ DCs (cross-presentation) whilst also secreting CCL22 and recruiting Tregs[158].

TCR+ myeloid cells

Although a growing area of research, there is evidence of the T cell receptor (TCR) and CD3 expression on the cell surface of non-lymphoid cells including neutrophils, eosinophils and myeloid cells, especially in inflammatory conditions[161–163]. Earlier studies have reported the presence of unusual markers on myeloid cells that were suggested to derive from cross-dressing, whereby APCs transfer preformed functional MHC peptide complexes to recipient cells[115] .Other authors have attributed it to "passive receptor expression", arising from the phagocytosis of T-lymphocytes. However, more recent findings have disproved these suggestions by describing TCR+ neutrophils in T cell deficient individuals diagnosed with severe combined immunodeficiency (SCID) and acute graft deficiency[164,165]. Likewise, in athymic mice, 5-8% of the neutrophil population was shown to be TCRαβ+ and to secrete IL-8 upon stimulation[164].

A separate study reported that 15% of an MDM population co-expressed CD3 and the MR with differential TCR expression yielding two sub-classes namely, CD3+TCRαβ+and CD3+TCRαβ-. The CD3+TCRαβ+ MDMs, expressed high levels of the CD1 family (CD1a,b,c) and resembled M1 Mϕ regarding the opsonic receptor CD16 and MHC-II expression[162]. Pro-inflammatory CD3+TCRαβ+ MDMs have been shown to characteristically proliferate in pathogenic conditions such as tuberculosis (TB) and may be pathologically relevant in multiple other infections[162,163].

In splenic and lymphoid DCs, 7-8% of the cells were described to express TCRαβ with intermediate expression of cDC markers; CD11c, CD11b, MHC II, F4/80 and FcγR[166,167]. These were named T-DCs as they were observed to possess both innate and adaptive immune properties, such as antigen presentation and TLR signalling while simultaneously expressing conventional T cell markers[166,167]. T-DCs were distinguishable from cDCs and conventional T cells by a distinct gene profile. Further to this, T-DCs were observed to resemble T lymphocytes in size while displaying an association with the FLT3 ligand, typically characteristic of DCs. They were therefore concluded to be a subset of T cells with DC characteristics[166,167]. Consistent to this, different authors also elucidated a subset of CD11c expressing T cells that were proliferative in symptomatic bacterial vaginosis in women[166]. Notably, it has been reported that conventional T cells express CD11c in inflammatory settings[166]. However this subset was described to additionally display high innate immune capacity and a mucosal homing potential due to an increased expression of adhesion surface molecules, and therefore not truly T-lymphocytic[166,167]. Importantly, these studies depict these cells to be associated with inflammation and pathological conditions[158,162,164–166,168]. Elucidation of their immunological role in such settings may be integral in further understanding and strategizing intervention technologies, especially in HIV.

1.06 CONCLUSION

The human foreskin is an immunological site laden with lymphoid and myeloid cells that are potentially susceptible to HIV infection. Lymphoid cells, particularly CD4+ T cells are the proven and more extensively studied targets of HIV infection. However, myeloid cells, although a rare population, also offer an interesting group of long-lived HIV targets capable of hoarding the virus and to persist over extended periods of time in a manner that's contributory to the viral reservoir. The role of DCs, LCs and Mϕ has been reported in cervico-vaginal studies and while knowledge of their role in the male genital tract is on the rise, it remains rudimentary. It is therefore important to understand the composition and identity of these cells in an "obvious" HIV entry site such as the foreskin. Myeloid cell plasticity is a known and appreciated aspect of this cell group, contributed to, by varied factors inclusive of ontogeny, function, and the micro-environment. Myeloid cells perform a myriad of immuno-regulatory functions, most of which are shared by the different myeloid cell subsets such as the antigen presentation role of DCs, LCs and Mϕ. It is therefore, nearly impossible to tackle myeloid cell diversity based on function alone. In-depth immunophenotyping requires a component of ancestry and ontogeny although recent studies have begun showing ambiguity in markers previously thought as indelible such as the TCR. It is however, common consensus that myeloid cells, like all haematopoietic cells, are vastly derived from the bone marrow HSCs (DCs, monocytes and monocyte derived myeloid cells) although there are subsets of LCs and Mϕ (self-renewing) that derive from the embryonic precursors arising from the yolk sac and/or fetal liver. Self-renewal properties of Mϕ and LCs contribute to the longevity of these cells, and thus, further characterisation and elucidation of their role in HIV infection is paramount.

1.2. PURPOSE OF THE STUDY

The broad aim of this study was to identify primary foreskin myeloid subsets and cell states in order to assess their susceptibility to *ex vivo* HIV-1 infection.

To do this, we firstly characterized and immunophenotyped migratory and non-migratory myeloid cells as potential HIV target cells from *ex vivo* foreskin tissue obtained from men undergoing voluntary medical male circumcision (vMMC). Migratory and non-migratory foreskin cells were isolated using optimized cell-isolation techniques identified as spontaneous migration and enzymatic digestion of remnant tissue post-migration. Using an optimized antibody panel and unsupervised clustering, multi-parameter flow cytometry was used for the quantification and immunophenotyping of foreskin Langerhans' Cells and "Mϕ-like" cells, with particular focus on the co-expression of HIV susceptibility markers (CD4+CCR5+), attachment factors (CD206,CD209,CD169) and part of the antigen presentation machinery was used to assess maturity (HLA-DR+CD80/86+).

Secondly, an optimised *ex vivo* pluricellular cell suspension foreskin model was used to conduct HIV challenge assays against foreskin primary cells inclusive of both myeloid and lymphoid HIV targets. This was conducted using Subtype C infectious molecular clones (IMCs) that comprised of transmitted founder (ZM246F-10 and CH198), and chronic control (CH167) strains. These were used alongside NL4-3 IMCs (NL4-3-BaL, NL4-3 92TH14-12 and NL4-3-X4) and were all obtained by Dr. Chigorimbo-Tsikiwa from Dr. Frank Kirchhoff and Dr. David Russell. Clonal virions from the IMC's were used to were used to establish infection using the optimized infection model. HIV infected foreskin myeloid cell subsets were identified and quantified using multi-parameter flow cytometry and unsupervised clustering over a time-course. The expression of p24 was used to determine infection and an optimized minimum inhibitory concentration (IC_{50}) of maraviroc was used as an entry inhibitor to evaluate HIV infection.

1.3 STUDY RATIONALE

The first hypothesis of this study was based on the observations that the foreskin is populated with heterogenous populations of differentially activated, HIV susceptible cells and was thus, "*the foreskin has diverse innate immune cells that are susceptible to HIV infection"*. While HIV susceptibility was measured using the co-expression of CD4 and CCR5; cell activation was assessed using CD80/86 and HLA-DR. During antigen exposure, antigen presenting cells (APCs), such as DCs, have been shown to upregulate the expression of co-stimulatory molecules including CD80, CD86 and CD40[139]. Additionally, APCs have been shown to acquire migratory properties, thus differentiating into an activated state preceding an immune response [32,140]. The migration assay therefore capitalizes on the innate ability of DCs to migrate to and from the lymph nodes for antigen presentation and T cell activation. The characterisation of macrophages as tissue-resident cells [169], was also the basis upon which enzymatic cell isolation from remnant tissue post-migration, was employed. Migratory and non-migratory myeloid cell populations were thus, independently assessed and characterised in order to determine the different activation states, decipher the impact of activation on HIV susceptibility and identify macrophages.

The myeloid cell focus of this study was inspired by the high impact of myeloid cells in HIV pathology despite being rare, a phenomenon that's earned them the term, "quality over quantity HIV substrates" [127]. Although the question of productive infection in myeloid cells has posed a longstanding argument in the HIV field, various studies have since shown that myeloid cells are unique targets from the extensively studied lymphoid targets, capable of supporting HIV replication over extended periods of time[60,72,120,170]. However, unlike activated T cell targets that rapidly get infected, myeloid cells are not as effective in the short term although their comparatively longer half-life offers viral persistence[171]. As

evidence of this, the CD4+ T cell: macrophage ratio is reportedly 1:10 at advanced AIDS stages[35,127,172]. Moreover, HIV infected macrophages have also been shown to effectively transmit to CD4+ T cells, thus eliminating the requirement for excessive infection to qualify as potent targets in HIV pathology [127]. HIV infected macrophages have been shown to possess intracellular structures (VCCs and filopodia) that harbour infectious virions, transmissible to other targets and with the ability to evade neutralizing antibodies[173,174].

Macrophages are therefore long-lived, HIV susceptible cells that perpetually contribute to the viral reservoir[35,61] and worth exploring in the context of the male genital tract given that the majority of *ex vivo* and *in vitro* HIV transmission studies have been conducted in cervico-vaginal explant models, monolayers of macrophages, homologous cell cultures of CD4+ T cells, and reconstructed epithelia[35,91,92] that do not provide the heterogeneity and complexity that is present *in vivo* [36,175]. SIV-Macaque transmission models, have also been extensively used and considered the gold standard although not fully and accurately translating to neither HIV pathology nor *in vivo* human events. Using an *ex vivo* foreskin pluricellular model was therefore key in attempting to mimick and capture the interplay of adaptive and innate immune cells that has been reported during HIV infection [20,27,149,176]. Elucidating such interactions of foreskin myeloid cells with HIV could also help inform the mechanisms through which medical male circumcision confers protection against HIV infection, as this, despite being effective, is still not completely understood[12,13]. The second hypothesis was therefore derived from these assumptions and reports as, "*foreskin derived cells can be infected in vitro and used as an ex vivo HIV infection model to interrogate the susceptibility of different myeloid cells to HIV-1 infection*".

Viral tropism is also an important determinant of infection, therefore, geographically relevant (Subtype C) virus strains, homologous to *in vivo* isolates [36,37,40,44,74] , were used with the lab-adapted R5 and X4 using NL4-3 IMCs. This was in corroboration with previous studies whereby foreskin lymphocytes and Langerhans cells were reportedly predominantly CCR5+[5,77]. NL4-3 X4 was incorporated to compare and explore CXCR4 co-receptor usage, especially in Langerhans cells that have been shown to efficiently abrogate CXCR4 infection when in an immature state[28,32].

Use of flow cytometry was chosen particularly for its unique ability to simultaneously analyse mixed populations of cells and assay for multiple parameters [177–179] thereby enabling the elucidation of the composition of foreskin epithelia, identification of potential HIV target cells and assessment of their susceptibility to HIV. However, analyzing such high dimensional data is arduous, prone to bias and occasionally lacks reproducibility, further augmented by the rarity and complexity of myeloid cells, thus making it to harder to capture all possible marker combinations[88]. Owing to this, we opted to use

both manual gating and unsupervised clustering to eliminate expert bias and to also capture novel myeloid cell subsets that succumb to HIV infection[180].

The allosteric inhibitory mechanism of maraviroc was used to validate infection and determine co-receptor usage, particularly of CCR5[28]. This was the basis of our third hypothesis, "*foreskin primary cells are infectable with HIV and can support viral replication which can be blocked using anti-retroviral drugs such as maraviroc and small molecules (IFN agonists)*".

1.4 MATERIALS AND METHODS

1.4.1 Ethics Statement

Informed consent was attained from all participants whose foreskins were collected to be used in this study after performing voluntary medical male circumcision (vMMC). This sub-study, including laboratory protocols and the use of the human foreskins, was reviewed and approved by the University of Cape Town's (UCT) Faculty of Health Sciences Human REC (HREC REF number 568/2020).

1.4.2 Sample/specimen collection

HIV seronegative males between the ages of 18-35 were recruited through the Western Cape Department of Health at selected clinics including TC Newman, Mitchells Plain, Delft and Elsies rivier. Men with symptomatic STIs were excluded from the study and the presence of asymptomatic STIs in urine samples was assayed for by real-time multiplex PCR (M-PCR) to detect *Neisseria gonorrhea* (NG), *Mycoplasma genitalium* (MG), *Trichomonas vaginalis* (TV) and *Chlamydia trachomatis* (CT). MMC was performed by clinic staff using standardized techniques. Foreskin specimens collected from newly circumcised participants were immediately collected into RPMI1640 (Gibco®) BRL Life Technologies, Paisley, UK) collection media containing 10% heat-inactivated fetal calf serum (FCS) (Gibco®) BRL Life Technologies, Paisley, UK), 100 IU/ml penicillin and 100 mg/ml streptomycin (Gibco®) BRL Life Technologies, Paisley, UK) and transported to the BSL2 laboratory in the Division of Immunology at UCT. 60 foreskin specimens were collected for use in this sub-study.

1.4.3 Cell isolation, culture, and maintenance

Primary foreskin cells

Spontaneously migrating cells

Foreskin specimens were rinsed in Phosphate Buffered Saline (PBS) containing100 IU/ml penicillin and 100 mg/ml streptomycin (Gibco®) BRL Life Technologies, Paisley, UK) and subsequently sectioned and separated into inner and outer compartments using disposable surgical scalpels as shown in Figure 17 (a). These were treated separately throughout the study. Excess hypodermis and adipose tissue were trimmed beneath the dermal layer of the tissue, cut into 0.25 cm^2 pieces and added to 25 mg/ml dispase II protease solution (Gibco® BRL Life Technologies, Paisley, UK) on either side of a split 10 cm bacteriological petri-dish (Corning®) as shown in Figures 17 (b)-(c). These were incubated at 4°C for a maximum of 18 hrs. Thereafter, foreskin epidermal sheets were stripped using forceps and tweezers and washed in PBS with 10% FCS to wash off the dispase that was used to hydrolyse the

bonds between the epidermal and dermal layers as shown in Figure 17 (d). Epidermal sheets were carefully placed in 10cm tissue culture dishes (Corning Star®) containing 10 ml of RPMI 1640 supplemented with 2mM L-glutamine (Gibco®) and 25 mM HEPES (4-(2-hydroxyethyl)-1-piperazineethanesulfonic acid) (Gibco®), 100 IU/ml penicillin, 100 mg/ml streptomycin, 0.25 μg/ml Amphotericin B/fungizone (Lonza Bioscience) and 10% FCS and filter sterilised using the 500 ml Filter bottle system (0.1μm) (Corning®). Hereon, this medium will be referred to as complete R10. Caution was exercised to ensure that the extracellular side of the epidermal sheets was facing the air-interface and subsequently incubated for 48 hrs at 37°C with 5% CO_2 and 95% humidity as shown in Figure 17 (e). Unless specified otherwise, all incubations were carried out under these conditions. Cells spontaneously migrating out of the epidermal sheets were harvested using a 3 ml Pasteur pipette (Corning®) to gently draw out the migratory cell suspension that was subsequently filtered through a 70-μm cell strainer as illustrated in Figure 17 (f) below. Suspension cells in a 50 ml conical flask were centrifuged at 400 g for 5 mins, after which the supernatant was discarded, and the resultant cell pellet was resuspended in R10 media. Thereafter, 2 ul of cells were diluted four-fold with trypan blue (Invitrogen™) to assess viability by dye exclusion and for cell enumeration using the Countess counting slide (Invitrogen™) and the Countess counter (Invitrogen™) as shown in Figure 17 (h).

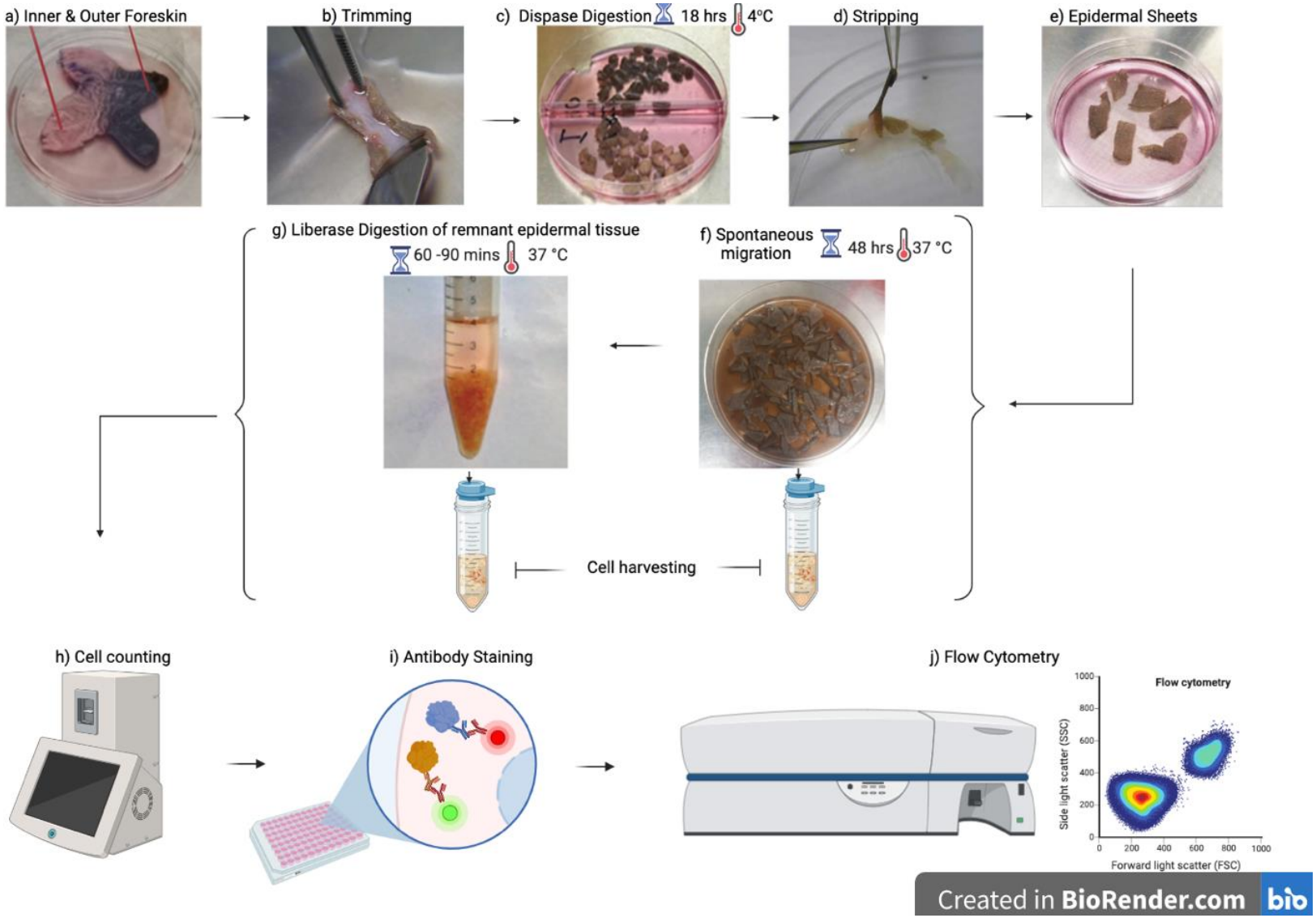

Figure 17. ***The collection of spontaneously heterogenous foreskin cells migrating out of the foreskin epidermis:*** ***(a)*** *Dissected foreskin tissue from circumcision showing Inner and outer FS compartments* ***(b)*** *FS tissue after removal of adipose* ***(c)*** *0.25 cm^2 x 0.25 cm^2 FS pieces submerged and incubated in dispase for 18 hrs at 4°C* ***(d)*** *forceps guided stripping of* ***e****pidermal layer from FS dermal layer* ***(e)*** *Epidermal sheets suspended in R10 medium* ***(f)*** *Migratory foreskin cells and remnant epidermal tissue after 48 hrs followed by cell filtration and harvesting through a 70-µm cell strainer* ***(g)*** *Liberase enzymatic digestion of remnant epidermal sheets after the migration in* ***(f)*** *using liberase enzyme and subsequent harvesting through a 70-µm cell strainer* ***(h)*** *Cell counting and viability assessment* ***(i)*** *Antibody staining* ***(j)*** *Flow cytometry on BDLSRII and analysis using FlowJo. All images captured in the lab except* ***(b)*** *and* ***(d)*** *adapted from Aasen et al., 2010* [181] *and* ***(e)*** *from Choi et al., 2017*[182] *Workflow illustrated using Biorender.com*[48]

Liberase enzyme digestion of epidermal sheets

Liberase enzyme (Roche, UK) was used to isolate, non-migratory tissue resident cells in remnant foreskin tissue after the crawl assay. Foreskin tissue was partially minced using a surgical scalpel and added to 5-8 ml of 5 mg/ml liberase (Roche, UK) in a 15 ml or 50 ml conical tube for enzymatic digestion as shown in Figure 17 (g). The 50 ml conical tube was placed in a shaking incubator (Labnet, Labnet International, Inc.) for 90-120mins at 37°C, after-which the cells were harvested by using a 3ml pasteur pipette to gently draw out the partially homogenized tissue alongside the cell suspension and filtered through a 70-µm cell strainer. Suspension cells in a 50 ml conical tube were centrifuged at 450 g for 5 mins, after which the supernatant was discarded, and the pelleted cells resuspended in R10 media. Thereafter, cells were counted and assessed for viability as previously described and shown in Figure 17 (h).

1.4.4 Flow cytometry

Flow Cytometry is one of the extensively used methods of immunophenotyping whereby the unique ability of flow cytometry to simultaneously analyse mixed populations of single cells, for multiple parameters is utilized[177–179]. It is a technology that utilizes lasers as light sources to give scattered and fluorescent light signals that are read by detectors and subsequently converted to electronic signals that are analysed by a computer and given out in a standardized ".fcs" format [177]. Samples are prepared for fluorescence measurement through i) transfection and expression of reporter, fluorescent proteins such as GFP and mCherry ii) staining with nucleic acid fluorescent dyes such as propium iodide or iii) staining with fluorescently conjugated antibodies such as PE p24[177–179]. An immunophenotyping panel inclusive of markers of lineage, maturation (antigen presentation), C-type lectin receptors (CLRs), HIV reporter proteins, receptors and co-receptors ; was designed for this study. Antibodies were purchased from Biocom Africa (Biolegend) : ***AF700*** CD4 (Clone RPA-T4), ***BV785*** CD45 (Clone H130), ***APC*** CD1a (Clone HII49), ***PE-Cy5*** CD206 (Clone 15-2), ***BV421*** CD209 (Clone 9E9A8), ***APC-Cy7*** CD3 (UCHTI), ***BV750*** CD14 (Clone63D3), ***BV650*** CD11c (CloneBu15), ***FITC*** CD80/CD86, ***BV711*** CCR5 (J418FI), ***PercP-Cy5-5*** HLA-DR (Clone L243), ***BV605*** CD169 (Clone7-239) and ***BV510*** live/dead zombie-aqua. ***PE-Cy7*** CD207 and ***PE*** p24 (Clone KC57) were purchased from Miltenyi and Beckman Coulter respectively.

Optimization of antibody titres

Antibody titrations were used to determine optimal antibody titres for staining cells. Optimal stain index (SI), defined as the ratio of the separation between the positive and negative population divided by two

times the standard deviation of the negative population, were used as a guide[177]. The stain index was calculated for a range of antibody titres (5 µl, 2.5 µl, 1.25 µl and 0.625 µl) derived through two-fold serial dilutions, starting from 5 µl and using FACs buffer, that was prepared by supplementing PBS with 2% FBS and 2mM EDTA.

Cell surface staining

Isolated spontaneously migrating and digested foreskin cells were washed in FACS buffer and resuspended at $4x10^6$ per 100 ul of FACS buffer for each antibody titre. 100 µl aliquots of foreskin cells were pipetted into a non-tissue culture treated 96 well plate (Corning) and were washed twice with plain PBS to remove the viability stain inhibitors. To prepare the viability stain, 1 µl of thawed Zombie Aqua™ (Biolegend) was added to 39 µl of plain PBS, from which 4 µl was drawn and diluted with 96 µl of plain PBS. For each well of foreskin cells, 50 µl of the viability stain working solution was added and the cells were incubated for 20 minutes, in the dark at RT. After incubation, cells well were then washed with FACS buffer twice and were resuspended in 40 µl of FACS buffer in preparation for antibody staining. Thereafter, 10 ul of the serially diluted antibody solutions was added and the cells were gently mixed with using a pipette and incubated in the dark for 20 mins at RT. Thereafter, cells were washed twice with 100 µl of FACS buffer and centrifuged at 450 g for 5 mins between washes. 100 µl of 1% paraformaldehyde (PFA) (BD Pharmingen™) was then added and mixed with the cells by pipetting followed by a 20 min incubation at RT. This was done to fix the cells. The washing step was repeated twice with FACS buffer to remove the fixative after incubation. Finally, the cells were resuspended in 300 µl of FACS buffer in FACS tubes and were acquired using the BD LSR II flow cytometer or alternatively kept in the dark at 4°C until acquisition time. FlowJo Software (version 10.7.2 ; Treestar) and Graph pad prism (version 7.0a) were used to analyse flow cytometry data. After titre optimization and FMO determination, the full antibody panel was used to stain and immunophenotype foreskin samples collected from 30 participants using this cell surface staining protocol. Notably, this cell-surface staining protocol was also used to determine Fluorescence Minus One Controls (FMOs). For each FMO control, foreskin cells were stained using all other antibodies except one (the control) to determine any spillage into the particular channel.

1.4.5 Immunophenotyping Data Analysis

Cell subsets of interest, defined as live, singlet, LCs (CD1a+CD207+) and "Mϕ-like" cells (CD11c+/-CD14+/-) were identified and gated on using FlowJo (version 10.7.2; Treestar). Statistical analyses were conducted using two approaches. The "manual" gating approach was used in conjunction with Graph pad prism (version 7.0a) while the unsupervised cell clustering approach was conducted using the open source statistical software, R (https://www.r-project.org/, version 3.6.3).

1.4.6 Statistical Analysis

Using the manual gating approach, the cell frequencies described in this study were all reported as mean ± standard deviation (SD). All manual gating box plots show mean with standard deviation (SD), where each participant is represented as a dot to show sample variance/distribution. The Shapiro Wilk test was used to test for Gaussian Distribution, and the FSK data was not normally distributed [183,184]. Therefore, a t-test was used to compared difference between 2 groups while the Wilcoxon test was used to compute *p* values. ANOVA was used to compare differences across multiple groups and post-hoc analysis performed using Tukey's multiple comparisons test [185,186]. (Y=Log(Y) was used to log-transform Y values for visualization purposes[183]. *P* values are only shown for comparison that had statistically significant differences and $p<0.05$ was used for significance.

Analysis limitations

Due to limitations on the number of colours that could be assessed at a time on the BDLSRII cytometer, the immunophenotyping panel could not exceed 14 different fluorochromes. As such, the panel was insufficient for the full characterisation of Mϕ hence use of the term "Mϕ-like" cells.

1.5 RESULTS

Section 1: Isolation of migratory and non-migratory myeloid cells of the foreskin

1.5.1. Introduction

Using previously optimized enzymatic and spontaneous migration protocols, non-migratory and migratory primary cells were isolated from the inner and outer compartments of adult foreskin epithelia. Migratory cells were defined as cells that spontaneously migrated out of foreskin epithelia into media while non-migratory cells were defined as remnant, tissue bound cells that were enzymatically digested out of FS epithelia after migration as shown in Methods Figure 16. We employed flow cytometry (FC) to characterise myeloid cells residing in the foreskin, using the FC antibody panel shown in Table 1 below. The use of a single panel was used in conjunction with unsupervised clustering to identify novel populations expressing "unconventional" markers, that would otherwise be missed in two separate panels. This was further necessitated by myeloid cell heterogeneity that makes it difficult to define explicit populations. The number of samples per study participant was also insufficient to split between two separate panels.

Table 1: Antibody panel for immunophenotyping foreskin myeloid cells

MARKER	CLONE	SPECIES/ISOTYPE	FLUOR	SIGNIFICANCE	USE IN THIS STUDY
CD45	H130	Mouse IgG1, κ	BV785	Leukocyte Common Ag	Immune Cells
CD3	UCHT1	Mouse BALB/c IgG1, κ	APC-Cy7	T cell lineage	Lineage exclusion & T-DCs
CD4	RPA-T4	Mouse IgG1, κ	AF700	TCR co-receptor	HIV susceptibility
CCR5	J418F1	Rat IgG2b, κ	BV711	Chemokine co-receptor	HIV susceptibility
CD1a	HI149	Mouse IgG1, κ	APC	Lipid Ag presentation	Langerhans Cells
CD207	MB22-9F5	Mouse IgG1	PE-Cy7	Langerin	Langerhans Cells
CD14	63D3	Mouse IgG1, κ	BV750	Pan myeloid	Macrophages & Ontogeny
CD11c	Bu15	Mouse BALB/c IgG1, κ	PE	Pan myeloid	Macrophages & LC sub-setting
CD80	BB1	Mouse IgM, κ	FITC	Co-stimulation	M1 macrophages / maturation
CD86	BU63	Mouse BALB/c IgG1, κ	FITC	Co-stimulation	M1 macrophages / maturation
HLA-DR	L243	Mouse IgG2a, κ	PercP Cy5.5	Peptide Ag presentation	M1 macrophages / maturation
CD206	15-2	Mouse IgG1, κ	PE-Cy5	Mannose receptor	M2 Macrophages / HIV susceptibility
CD209	9E9A8	Mouse IgG2a, κ	BV421	DC-SIGN	M2 macrophages / HIV susceptibility
CD169	7-239	Mouse BALB/c IgG1, κ	BV605	Sialoadhesion/Siglec-1	CD169+ macrophages / HIV susceptibility
Zombie-Aqua	-	-	BV510	Live/Dead	Dead cell exclusion

The panel was designed to identify two main groups of myeloid cells, i) Langerhans cells (LCs) and ii) "Mϕ-like" cells. Foreskin LCs and "Mϕ-like" cells were further characterised into different subsets and cell states using either the manual gating approach or unsupervised cell clustering. Langerhans Cells were identified as CD1a+CD207+ cells that were further characterised into different subsets according

to the expression of pan-myeloid markers (CD11c and CD14). CD1a+CD207+CD11c-CD14- cells were identified as conventional LCs and referred to, in this study, as **traditional LCs**. Non-conventional LC subsets were identified as i) CD1a+CD207+CD11c+CD14- (**CD11c+LCs**), ii) CD1a+CD207+CD11c+CD14+ (**CD11c+CD14+LCs**) and iii) CD1a+CD207+CD11c-CD14+ (**CD14+ LCs**). Owing to the advent of T-DCs and other TCR+/CD3+ myeloid cells[187] described in the Literature Review Section, foreskin LCs that co-expressed CD3 were also identified as the CD1a+CD207+CD3+ cells (**CD3+ LCs**).

"Mϕ-like" subsets were also distinguished and characterised into the classically activated "M1-like" Mϕ, alternatively activated "M2-like" Mϕ, CD169+ Mϕ and CD3+ Mϕ[161,163,187,188]. These heterogenous foreskin LCs, and "Mϕ-like" populations were subsequently interrogated for HIV susceptibility (those co-expressing CD4+CCR5+), attachment factors (C-type lectin receptors) and maturation markers (HLA-DR and CD80/86) [161,187,189]. Except for CD169 macrophages, where CD169 expression was the benchmark marker, all the other LC and "Mϕ-like" subsets were also assessed for the expression of CD169 (Siglec-1) as an attachment factor.

1.5.1.1 Yields of primary, migratory, and non-migratory cells from foreskin epithelia

Proportions and viability

Migratory and non-migratory foreskin cells from the inner (I) and outer (O) foreskin were harvested, counted and assessed for viability. Migratory cells were denoted as "Crawl" in all Figures, while non-migratory cells were shown as "Lib". Migratory foreskin cells were 1.9-fold more frequent in the outer foreskin ($102.8 \times 10^6 \pm 124.8 \times 10^6$) than in the inner foreskin ($53.91 \times 10^6 \pm 55.99 \times 10^6$; $p = 0.0004$). Although non-migratory cells also 2-fold less frequent than migratory cells, they displayed similar distribution patterns in the inner and outer foreskin whereby the outer foreskin ($48.65 \times 10^6 \pm 43.05 \times 10^6$) harboured more cells than the inner foreskin ($19.02 \times 10^6 \pm 17.53 \times 10^6$; $p < 0.0001$) as shown in Figure 18 (a).

Similarly, viability was generally higher in migratory compared to non-migratory cells although not differed between the inner and outer foreskin compartments. Therefore, migratory cells exhibited a similar range in the inner (51.35 % ± 19.03 %) and outer foreskin (50.26 % ± 17.75 %) and likewise, non-migratory cells (28.32 % ± 9.3 %; 27 % ± 11.51 %) as shown in Figure 18 (b).

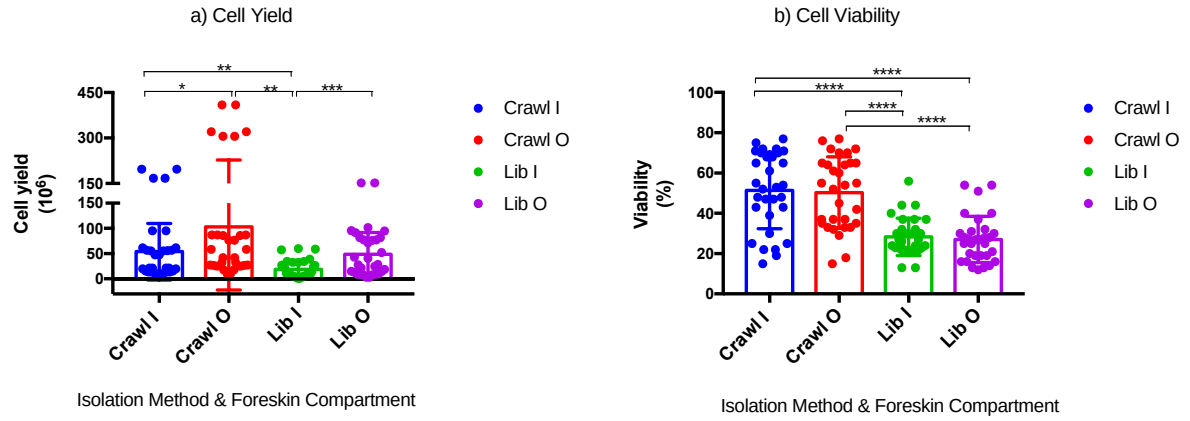

Figure 18. ***Cell isolation of migratory and non-migratory cells from the inner (I) and outer (O) compartments of adult foreskin epidermal tissue by spontaneous migration (Crawl) and liberase digestion of remnant tissue (Lib).*** ***(a)*** *The total numbers of cells isolated using spontaneous migration and enzymatic digestion were counted using an automated cell counter, up to 450 x10^6 cells were isolated* ***(b)*** *Viability was calculated using trypan blue exclusion and an automated cell counter (n=31). Statistics were generated using one-way ANOVA with the Tukey's multiple comparisons test and adjusted p values. *p <0.05; **p < 0.01; ***p < 0.001; ****p < 0.0001.*

Proportions and viability - Assay

To assess for the general impact of cell isolation techniques on foreskin cell yields, the proportions and viability of migratory and non-migratory cells were assessed without separation by foreskin compartment. Therefore, using the averages of inner and outer foreskin for each assay, migratory cells were 2.3-fold more frequent (78.38 x 10^6 ± 87.12 x 10^6) than non-migratory cells (33.84 x 10^6 ± 27.75; *p =0.0334*) as illustrated in Figure 19 (a). Additionally, migratory cells were more viable (50.81 % ± 16.13 %) than non-migratory cells (27.66 % ± 8.77 %; *p<0.0001*) as shown in Figure 19 (b).

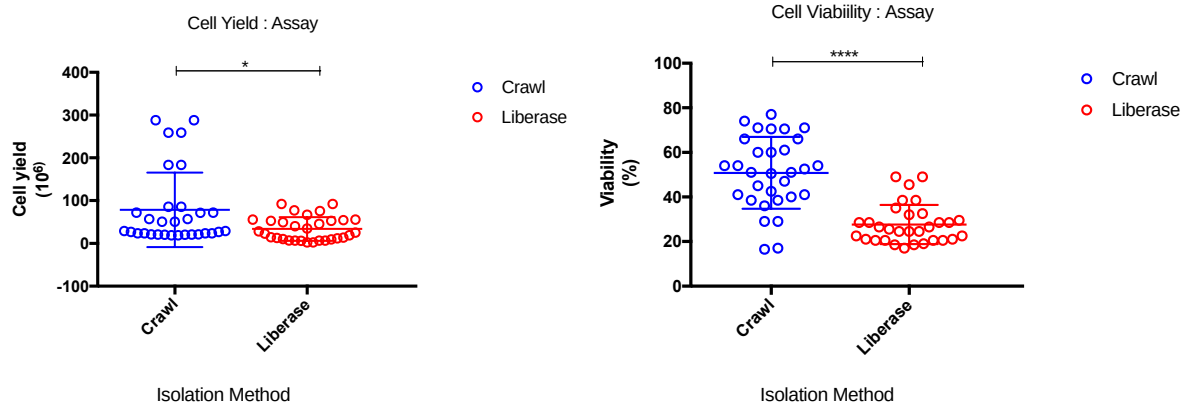

Figure 19. ***Cell yields and viability of migratory and non-migratory cells from the spontaneous migration assay and the post-migration digestion of remnant foreskin tissue assay.*** ***(a)*** *Total cell yields from the migratory assay (Crawl) and enzymatic digestion (Liberase)* ***(b)*** *Viability of total cell yields isolated using the migratory assay and enzymatic digestion (n=31). The Wilcoxon test was used to calculate p values. *p <0.05; **p < 0.01; ***p < 0.001; ****p < 0.0001*

Proportions and viability – Compartment

The inner and outer foreskin compartments were also assessed for resultant cell yields and viability, regardless of cell isolation techniques. Although outer foreskin cells were 2.1-fold more abundant ($75.75 \times 10^6 \pm 62.95 \times 10^6$) than the inner foreskin ($36.47 \times 10^6 \pm 30.43 \times 10^6$; $p<0.0001$) as shown in Figure 20 (a), there were no differences in cell viability between the two compartments (39.84 % ± 10.55 %; 38.63 % ± 10.29 %) as shown in Figure 20 (b).

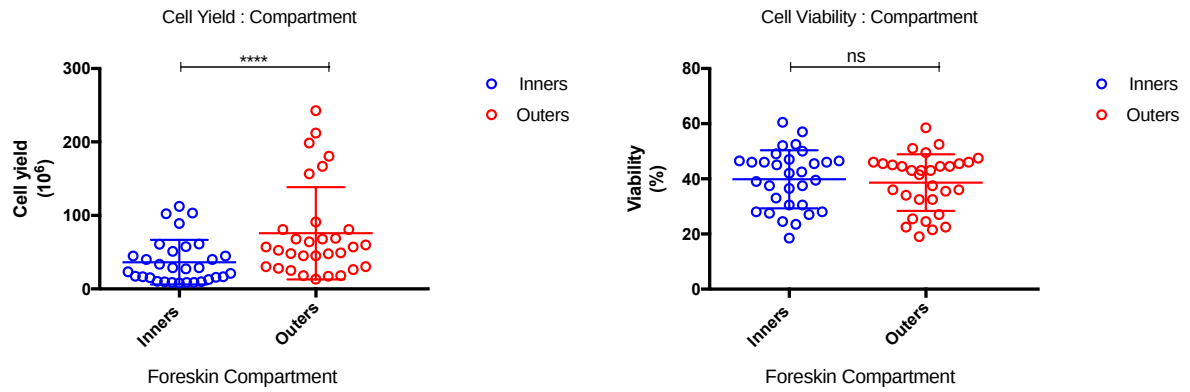

Figure 20. ***Cell yields and viability of migratory and non-migratory cells in the inner and outer foreskin. (a)*** *Total cell yields in the inner and outer foreskin* ***(b)*** *Viability of total cell yields isolated from the inner and outer foreskin (n=31). The Wilcoxon test was used to calculate p values. *p <0.05; **p < 0.01; ***p < 0.001; ****p < 0.0001*

Summary

Migratory foreskin cells were more abundant and viable than non-migratory cells that remained tissue bound and thus, enzymatically isolated. Foreskin cells were additionally more abundant in the outer, in comparison to the inner foreskin, although this was in corroboration with tissue size. The data was, however, normalized by measuring frequencies of specific populations.

1.5.1.2 Flow cytometry antibody titrations and FMO's

Optimal antibody titres for the subsequent characterisation and immunophenotyping of FS cells were determined. A FC antibody panel was designed for the characterisation of foreskin LCs and "Mϕ-like" cells as shown in Table 1 above. Foreskin primary cells were stained using antibody titres that were attained through 2-fold serial dilutions ranging from 5 µl to 0.625 µl as described in Methods. Subsequent analysis of multi-parameter flow cytometry data was performed using FlowJo as seen in Figure 21 below. Optimal antibody titres (circled in red), were selected based on the separation between the negative and positive populations, also taking into account the stain index.

Titrations

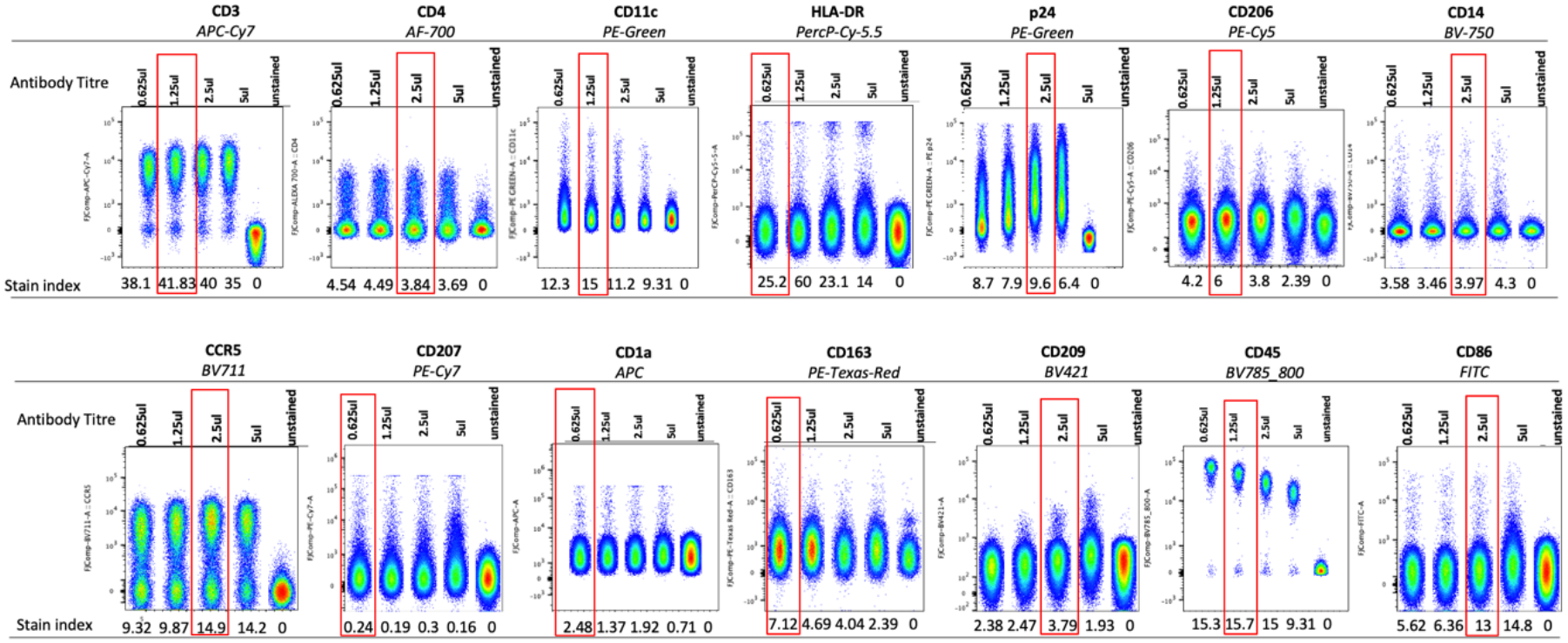

Figure 21. ***Titrations of the antibody panel used to stain foreskin cells in multi-parameter flow cytometry for immunophenotyping and HIV Infection Assays.*** *Serially diluted antibody titres; 0 µl (Unstained), 0.625 µl, 1.25 µl, 2.5 µl and 5 µl; were used to satin foreskin cells with each of the following antibodies- CD3, CD4, CD11c, HLA-DR, p24, CD206, CD14, CCR5, CD207, CD1a, CD163, CD209, CD45 and CD80/86. High stain indices and corresponding titres shown and marked in red.*

To further optimise the immunophenotyping protocol, fluorescence minus one (FMO) controls were also designed and determined for gating. Unstained cells were used as controls alongside FMOs. There were interestingly, no differences observed between unstained and FMO controls for all antibodies such as, CD45, CD11c, CD206, CCR5, CD209, CD169, CD1a, HLA-DR and CD207. However, apparent dissimilarities were observed with gate placements using FMOs and unstained controls in CD4 and p24 as shown in Figure 22 below.

FMOs

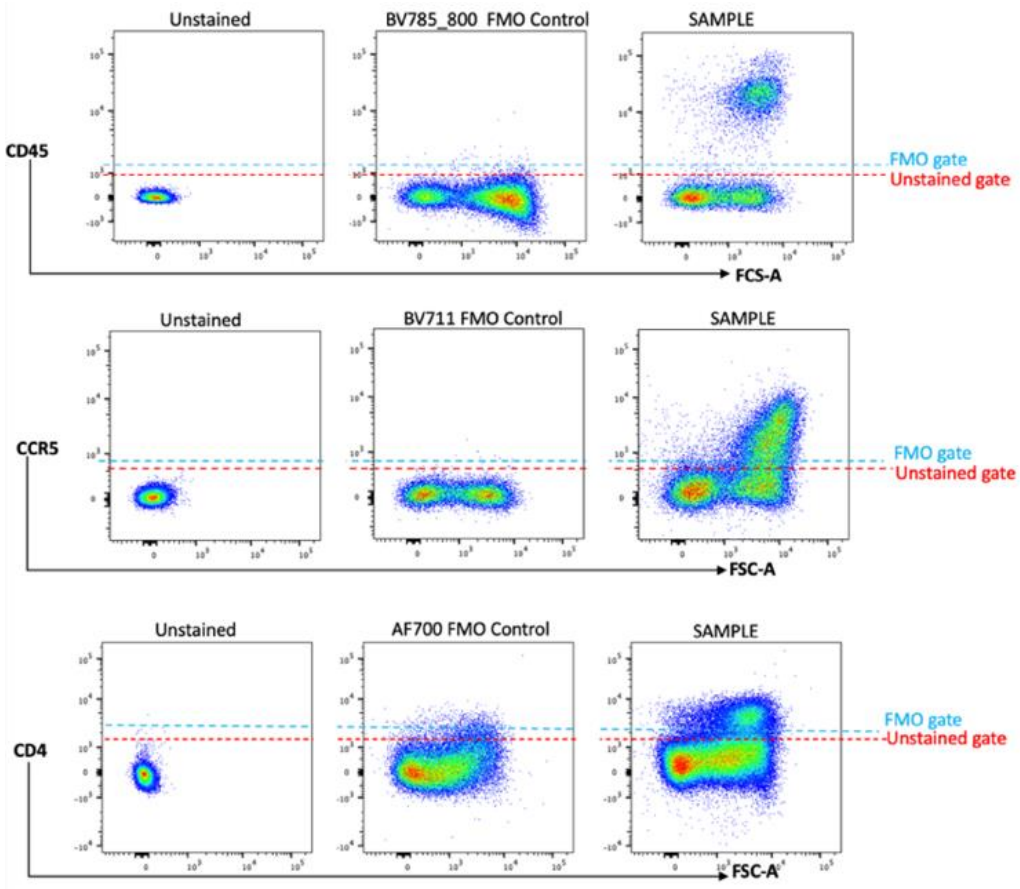
Unstained
BV785_800 FMO Control
SAMPLE
CD45
FMO gate
Unstained gate
FCS-A
Unstained
BV711 FMO Control
SAMPLE
CCR5
FMO gate
Unstained gate
FSC-A
Unstained
AF700 FMO Control
SAMPLE
CD4
FMO gate
Unstained gate
FSC-A

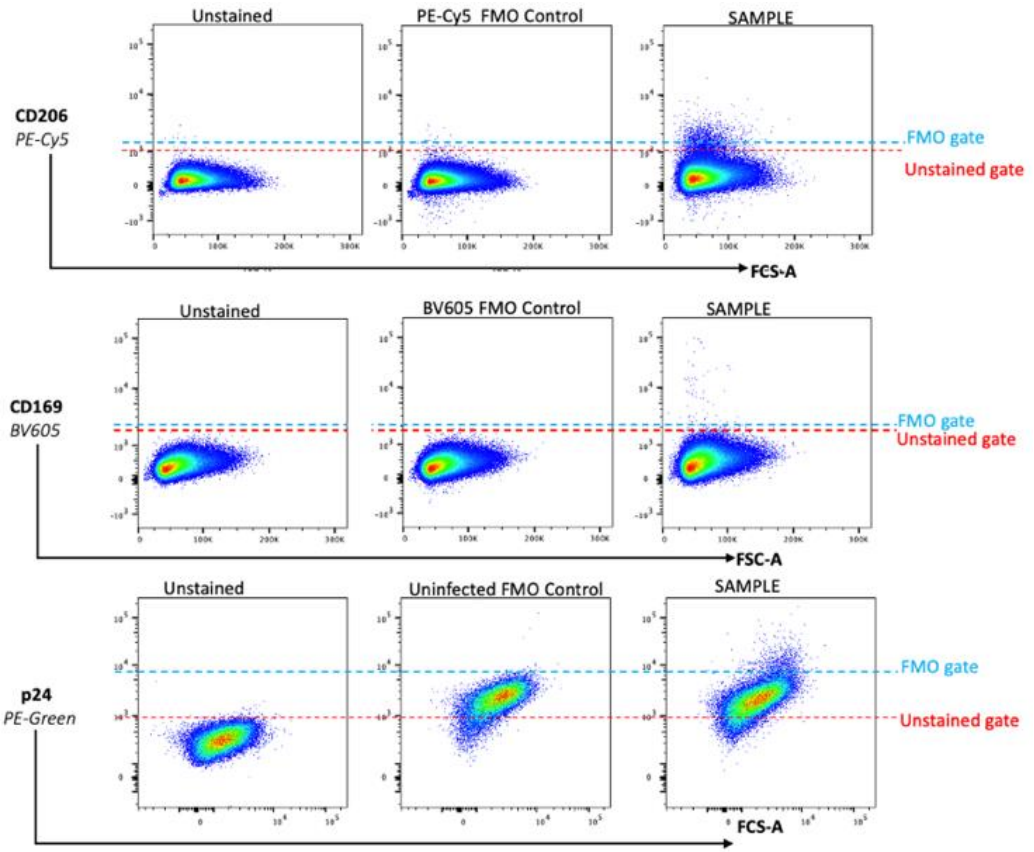
Unstained
PE-Cy5 FMO Control
SAMPLE
CD206
PE-Cy5
FMO gate
Unstained gate
FCS-A
Unstained
BV605 FMO Control
SAMPLE
CD169
BV605
FMO gate
Unstained gate
FSC-A
Unstained
Uninfected FMO Control
SAMPLE
p24
PE-Green
FMO gate
Unstained gate
FCS-A

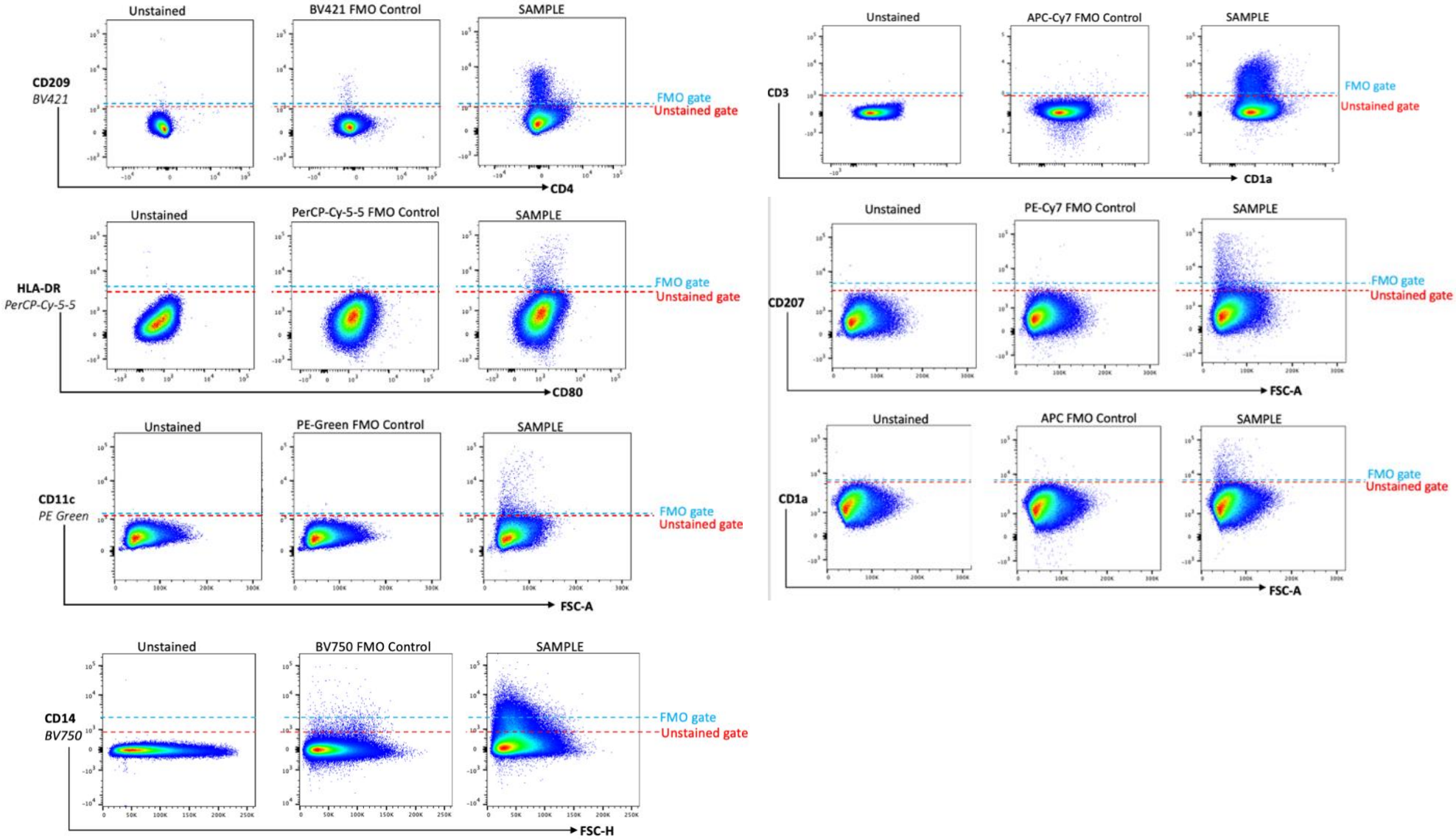

Figure 22. ***Fluorescence minus one (FMO) and unstained controls used for gate determination.*** *Gate determination according to FMOs in conjunction with unstained controls. Myeloid cell antibody panel:CD3, CD4, CD11c, HLA-DR, p24, CD206, CD14, CCR5, CD207, CD1a, CD163, CD209, CD45 and CD80/86, gates were selected with the guide of FMOs (blue) and Unstained Controls (red)*

1.5.1.3 Quantification and Identification of FS myeloid cells using pan myeloid markers:

General delineation of foreskin myeloid groups using CD11c and CD14

Using pan-myeloid markers, CD11c and CD14 and the gating strategy shown in Appendix Figure A1; foreskin myeloid cells were delineated into three groups. These were identified as: i) CD14+CD11c- ii) CD14-CD11c+ and iii) CD11c+CD14+. Of the three, CD14+CD11c- myeloid cells were the most frequent (8.50 % ± 6.19 %) with proportions 42.5-fold and 21.3-fold more than the CD11c+CD14- (0.20 % ± 0.23 %; *p< 0.0001*) and CD11c+CD14+ (0.40 % ± 0.37 %; *p<0.0001*) myeloid cells respectively as illustrated in Figure 23 (a) below. Non-myeloid cells, CD11c-CD14-, were 56.7 % ± 17.63 % of the total live granulocytes as shown in Figure 23 (b).

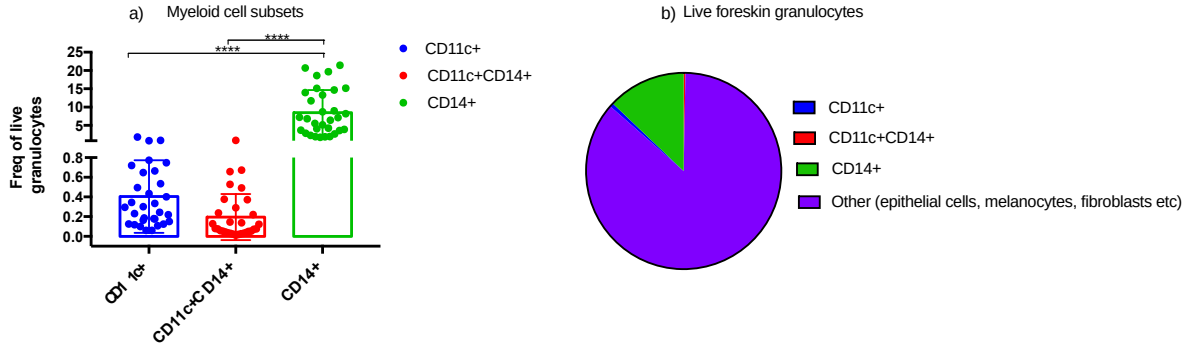

Figure 23. ***Quantification and Identification of the different myeloid cell groups in migratory and non-migratory foreskin primary cells isolated from the inner and outer foreskin compartments.*** *CD11c and CD14 were gated on live granulocytes after lymphocyte exclusion (Figure A1 in the Appendix) for the identification and quantification of* ***(a)*** *different myeloid cell groups and* ***(b)*** *myeloid and non-myeloid cells. Data was acquired and analysed using flow cytometry (n=31). Statistics were generated 2-way ANOVA using the Tukey's multiple comparisons test and adjusted p values. *p <0.05; **p < 0.01; ***p < 0.001; ****p < 0.0001.*

Proportions of migratory and non-migratory myeloid cell groups in I and O foreskin

The three myeloid cell groups were further assessed according to migration and non-migration as well as distribution in the inner and outer foreskin compartments. While CD11c+CD14+ myeloid cells were overall the least abundant of the three myeloid cell groups, the population of migratory CD11c+CD14+ myeloid cells was 2-fold higher in the inner foreskin (0.24 % ± 0.33 %) compared to the outer foreskin (0.10% ± 0.15%; *p = 0.0002*) as illustrated in Figure 24 (i). Similarly, migratory CD11c+CD14- myeloid cells were also 2-times more frequent in the inner foreskin (0.81 % ± 0.81 %) compared to the outer foreskin (0.41 % ± 0.62 %; *p = 0.0001*) as shown in Figure 24 (ii).

Contrary to both the CD11c+CD14+ and the CD11c+CD14- myeloid cell groups that had higher proportions of migratory cells, the CD14+CD11c- myeloid cells comprised higher proportions of non-

migratory cells that additionally portrayed equal distribution in the inner and outer foreskin as illustrated in Figure 24 (iii). However, the mean frequency of non-migratory CD14+CD11c- myeloid cells from the outer foreskin (12.33 % ± 11.37 %) was higher than that of migratory CD14+CD11c- myeloid cells in the inner (5.32 % ± 7.66 %; $p = 0.0150$) and outer foreskin (5.19 % ± 6.67 %; $p = 0.0276$) as shown in Figure 24 (iii).

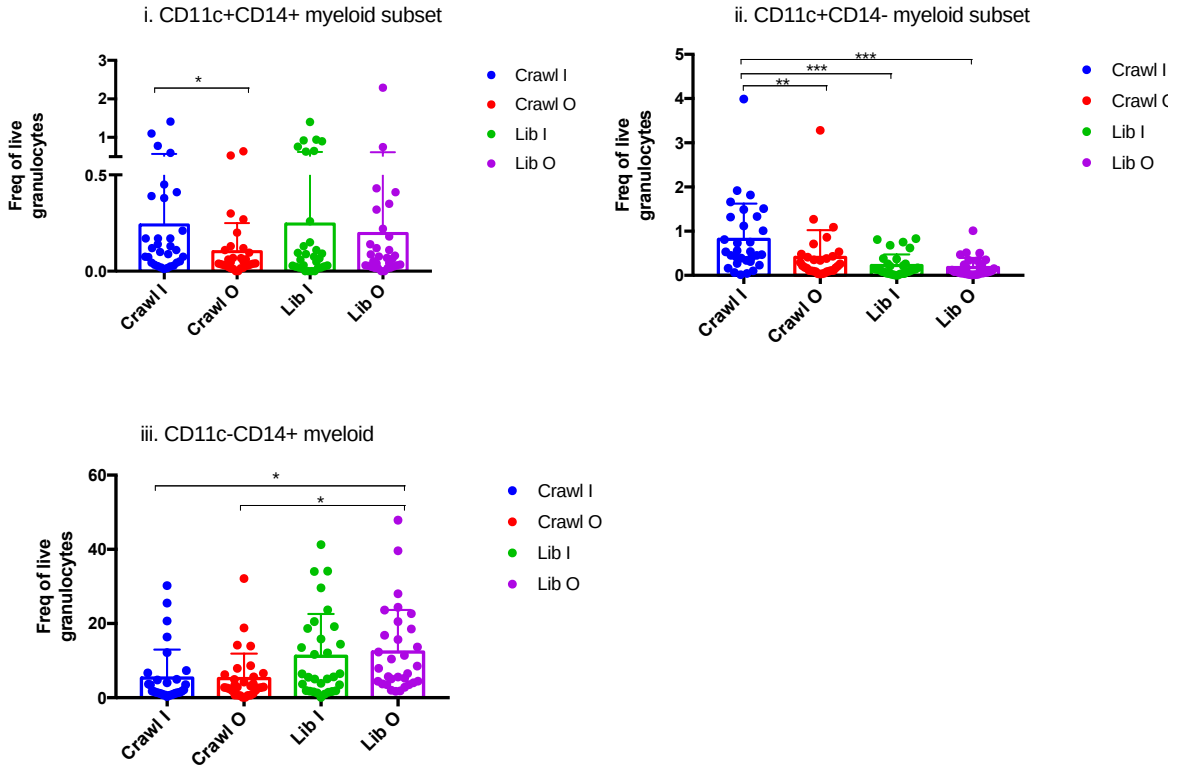

Figure 24. ***Quantification of migratory (Crawl) and non-migratory (Lib) myeloid cell subsets in the inner and outer adult foreskin epidermal compartments*** *Flow cytometry identification and quantification of different myeloid cell subsets* ***(a)*** *Proportions of CD11c+CD14+ myeloid cells* ***(b)*** *Proportions of CD11c+CD14- myeloid cells* ***(c)*** *Proportions of CD11c-CD14+ myeloid cells (n=31). Statistics were generated using one-way ANOVA using the Tukey's multiple comparisons test and adjusted p values. *p <0.05; **p < 0.01; ***p < 0.001; ****p < 0.0001.*

Proportions of migrating and non-migrating myeloid cell groups

Similar to Figures 17-18, we measured and compared cell recovery of the two cell isolation techniques for the myeloid cell subsets. Migratory CD11c+CD14- myeloid cells (0.61 % ± 0.67 %) were more abundant compared to non-migratory CD11c+CD14- myeloid cells (0.20 % ± 0.20 %; $p = 0.0015$) as shown in Figure 25 (a). Conversely, non-migratory CD11c-CD14+ myeloid cells (11.75 % ± 10.09) were 2-fold more frequent than migratory CD11c-CD14+ cells (5.25 % ± 6.73 %) %; $p = 0.0047$) as shown in Figure 25 (b). Interestingly, similar cell recovery rates were observed for the isolation of migratory (0.17 % ± 0.22 %) and non-migratory (0.22 % ± 0.34 %) CD11c+CD14+ myeloid cells (data not shown).

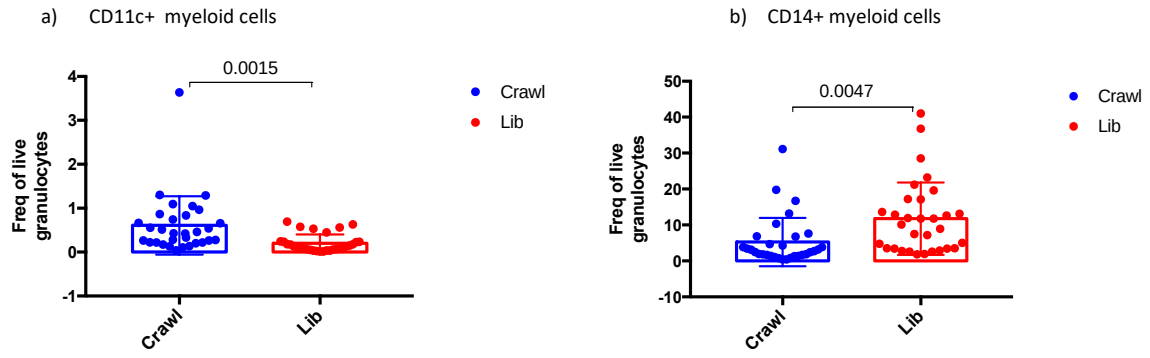

Figure 25. ***Myeloid cell composition of migratory and non-migratory foreskin primary cells. (a)*** *Proportions of migratory and non-migratory CD11c+CD14- myeloid cells* ***(b)*** *Proportions of migratory and non-migratory CD11c-CD14+ myeloid cells (n=31). The Wilcoxon test were used to generate p values.*

Compartment

Consistent to the findings shown in Figure 23 (i-ii); the mean frequency of both CD11c+CD14+ and CD11c+CD14-myeloid cells was higher in the inner compared to the outer foreskin as shown in Figure 26 (i-ii). This was however without statistical significance in the CD11c+CD14+ myeloid cell group, although a trend was observed whereby the mean frequency was higher in the inner foreskin (0.24 % ± 0.30 %) compared to the outer foreskin (0.15 % ± 0.23 %; $p = 0.0517$) as shown in Figure 26 (i). Similarly, CD11c+CD14- myeloid cells were more in the inner foreskin (0.52 % ± 0.46 %) compared to the outer foreskin (0.29 % ± 0.33 %; $p = 0.0003$) as shown in Figure 11 (ii). However, there were no differences in the proportions of CD11c-CD14+ myeloid cells in the inner (8.25 % ± 6.74 %) and outer foreskin (8.76 % ± 6.51 %) (data not shown).

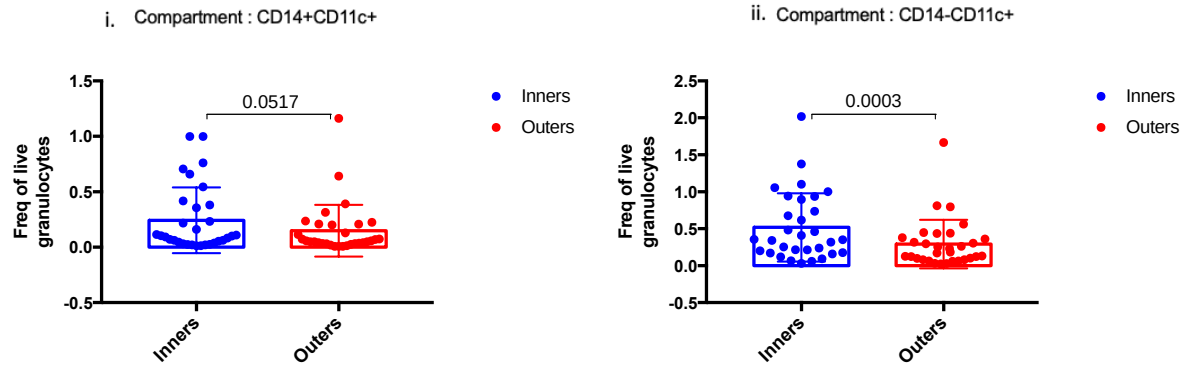

Figure 26. ***The composition of Myeloid cell derived from migratory and non-migratory foreskin primary cells.*** *Proportions of myeloid cell subsets in migratory (Crawl) and non-migratory (Lib) foreskin primary cells (n=31). The Wilcoxon test was used to compute p values.*

Summary

Foreskin myeloid cells could be classified as either i) CD11c+CD14-, ii) CD11c-CD14+ or iii) CD11c+CD14+. Among these myeloid subsets, CD11c+CD14- myeloid cells were more frequent in migratory inner foreskin cells while CD14+CD11c- myeloid cells were more frequent in non-migratory cells, with equal distribution in the inner and outer foreskin. Lastly, there were no differences in the proportions of migratory and non-migratory CD11c+CD14+ myeloid cells although they were more enriched in the inner compared to the outer foreskin.

Section 2: Identification and characterization of specific foreskin myeloid cell subsets by multiparameter flow cytometry

Langerhans Cells and "Macrophage-like" populations

Overall Gating Strategy

Foreskin Langerhans cells were identified as the CD1a+CD207+ population derived from the live singlet granulocytes (big cell gate) as illustrated in Figure 27 (i-iii) below[113]. The LC cell population was further investigated for the expression of CD11c and CD14 and thus further classified into four subsets: i) traditional LCs, ii) CD11c+ LCs , iii) CD14+ LCs and iv) CD11c+CD14+ LCs also shown in the gating strategy in Figure 27 (A) and briefly described in the Introduction[177,178,181,182]. In addition, CD3+ LCs were also identified from the overall LC gate as shown in Figure 27 (A)[160,178].

Subsequently, "Mϕ-like" cells were derived from the LC exclusionary gate (without CD1a+CD207+ but with CD1a+CD207- and/or CD1a-CD207+) shown in Figure 27 (B). The Mϕ-like population was also characterised based on the expression of CD11c and CD14 as shown in the gating strategy as an "L gate" ; within which were different CD11c+CD14-, CD11c+CD14+ and CD11c-CD14+ "Mϕ-like" populations Figure 27 (B). This CD11c/CD14 gate (L gate), was used to identify and derive the different "Mϕ-like" populations including i) "M1-like" Mϕ (CD80/86+HLA-DR+) and ii) "M2-like" Mϕ, (CD206+CD209+, CD206-CD209+, CD206+CD209-) as shown in the gating strategy in Figure 27 (B)[179].

The "M1-like" and "M2-like" Mϕ populations were each, subsequently used to identify transitionary "M1/M2-like" intermediate populations. Furthermore, the CD11c/CD14 gate was investigated for the presence of cells expressing CD169 and CD3, which led to the characterisation and identification of CD169+ Mϕ and CD3+ Mϕ respectively**,** as illustrated in the gating strategy in Figure 27 (B) [60,158–160,163,187].

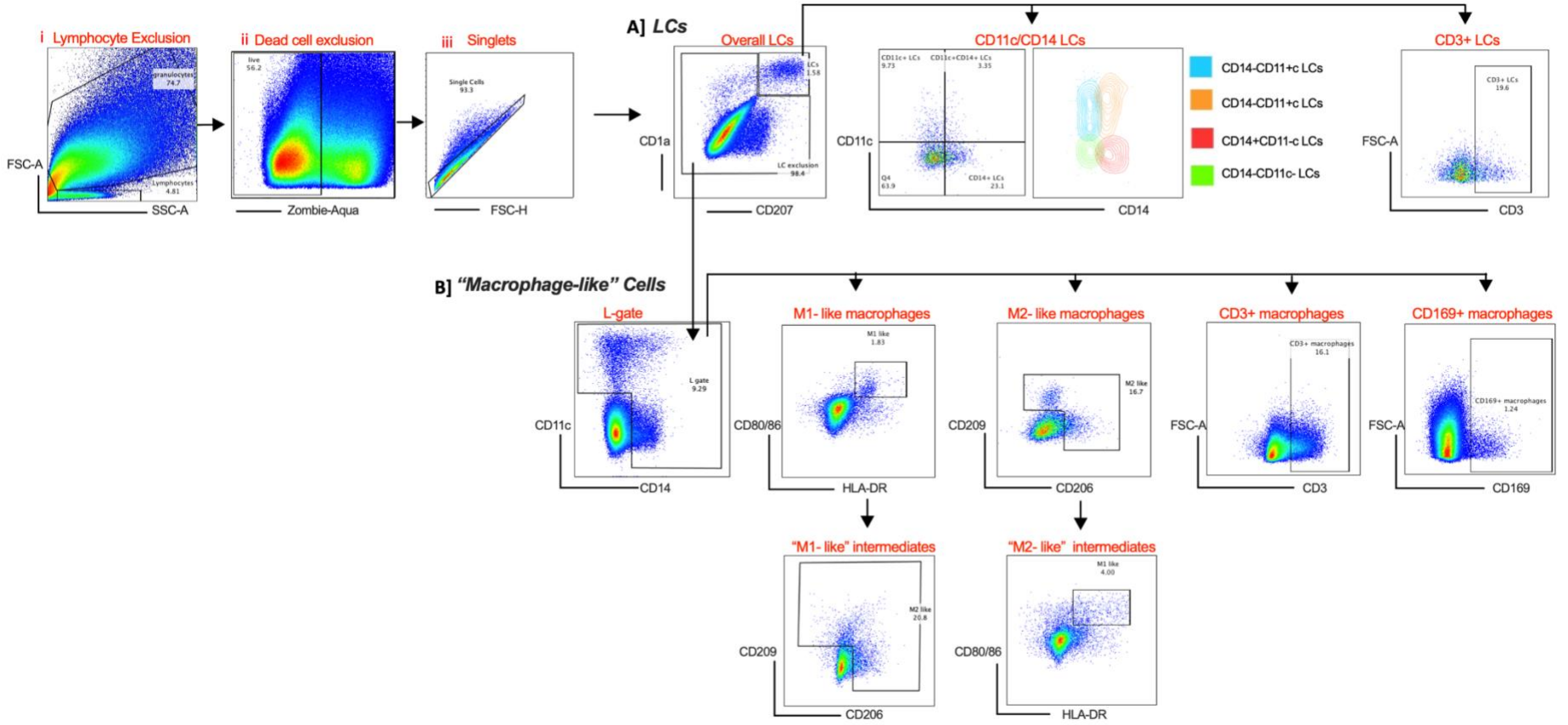

Figure 27. ***Identification of migratory and non-migratory foreskin Langerhans cells and "Macrophage-like" cell subsets using multiparameter flow cytometry***. ***(A)*** *Identification of the different Langerhans cells' subsets; CD11c-CD14- traditional LCs, CD11c+ LCs, CD14+ LCs, CD11c+CD14+ LCs and the CD3+ LCs* ***(B)*** *Identification of the "macrophage-like" cells from the LC exclusionary CD11c/CD14 gate into; "M1-like" macrophages, "M2-like" macrophages, CD169+ macrophages, CD3+ macrophages and the. M1/M2 intermediate "macrophage-like" cells*

1.5.2 Langerhans cells

1.5.2.1 Quantification of overall foreskin LCs using manual gating

The foreskin epidermal CD1a+CD207+ LCs were a rare population, constitutive of 1.11 % ± 1.02 % of the total foreskin epidermal myeloid cell population. Foreskin LCs were further distinguished and quantified according to migration/non-migration (crawl/liberase) and distribution in the 2 foreskin compartments (inner and outer FS). The inner foreskin had 2-times higher, the proportions of migratory LCs (0.36 % ± 0.32 %) than non-migratory LCs (0.17 % ± 0.13 %; *p = 0.0084, n =31*) as shown in Figure 28 below. Contrary to this, the outer foreskin had similar proportions of both migratory (0.30 % ± 0.24 %) and non-migratory LCs (0.28 % ± 0.33 %) also shown in Figure 28.

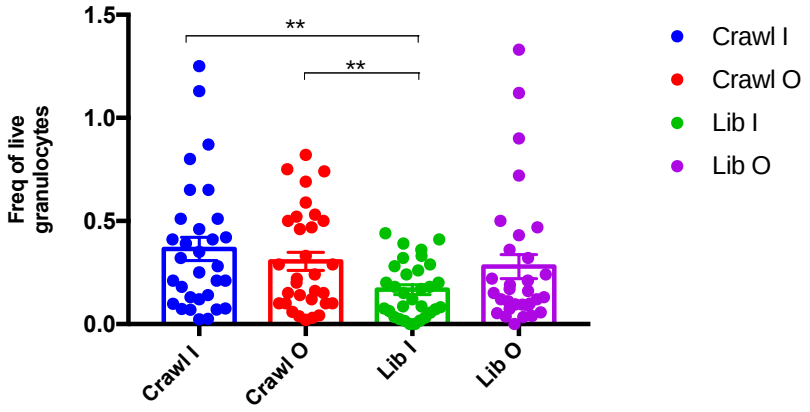

Figure 28. ***Quantification and distributions of migratory and non-migratory LC subsets in the inner and outer foreskin compartments.*** *Flow cytometry quantification of overall migratory and non-migratory foreskin Langerhans Cells in the inner and outer foreskin compartments (n=31). Statistics were generated using one-way ANOVA with the Tukey's multiple comparisons test at 95 % CI of difference and adjusted p values. *p <0.05; **p < 0.01; ***p < 0.001; ****p < 0.0001*

Following the quantification and determination of the distribution of foreskin LCs in the inner and outer foreskin, foreskin LCs were further characterised into different subsets using the gating strategy shown

below in Figure 29 below. As described earlier, traditional LCs were distinguishable from the rest of the CD1a+CD207+ cells as CD11c-CD14- cells, while non-conventional LC subsets were identified as;

CD11c+ LCs, CD14+ LCs and CD11c+CD14+ LCs shown in Figure 29 (a) (i). Additionally, CD3+ LCs were identified as illustrated in Figure 29 (a) (ii). Subsequently, each LC subset was assessed and analysed for the co-expression of HLA-DR+CD80/86+, HIV susceptibility markers (CD4+CCR5+) as well as attachment factors (CD206, CD209, CD169) as illustrated in Figure 29 (b) - (d).

LC Gating Strategy

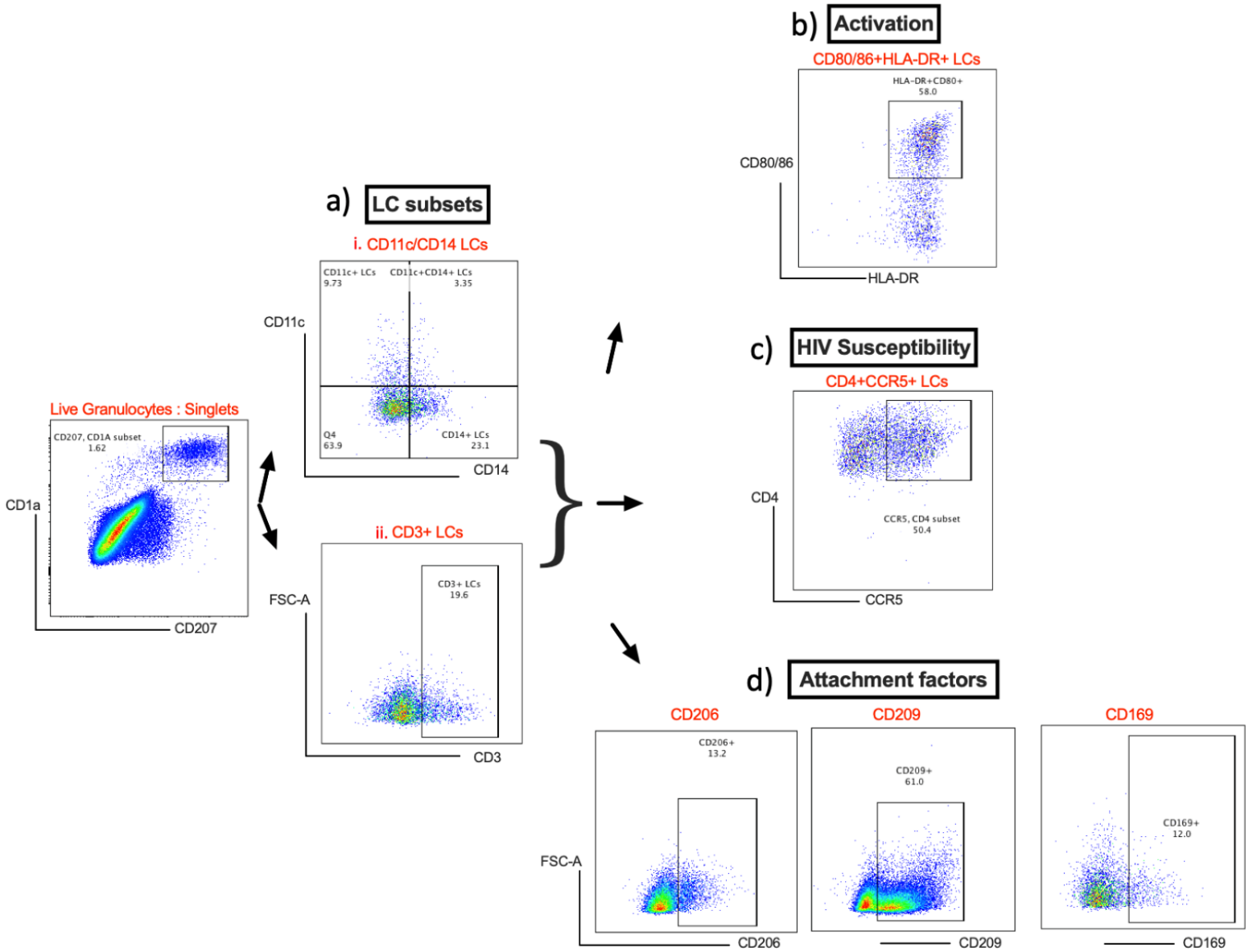

Figure 29. ***Identification and Characterisation of foreskin Langerhans cells and LC subsets using multiparameter flow cytometry****. Single, live foreskin granulocytes were used to derive foreskin LCs (CD1a+CD207+) and LC subsets : i) traditional LCs, ii) CD11c+, iii) CD11c+CD14+, iv) CD14+ and v) CD3+ LCs that were further characterised by activation status, HIV susceptibility and the expression of attachment factors*

Identification of LC subsets using manual gating

Traditional LCs were identified as the most abundant LC subset, with a frequency of 0.59 % ± 0.11 % of the foreskin granulocyte population that represented 53.4 % of the overall LC population. The other half was constitutive of the non-conventional LC subsets and distributed as follows: i) 18.6 % CD14+ LCs, ii) 11.6 % CD3+ LCs, iii) 9.3 % CD11c+ LCs and iv) 7 % CD11c+CD14+ LCs as illustrated in Figure 30 below.

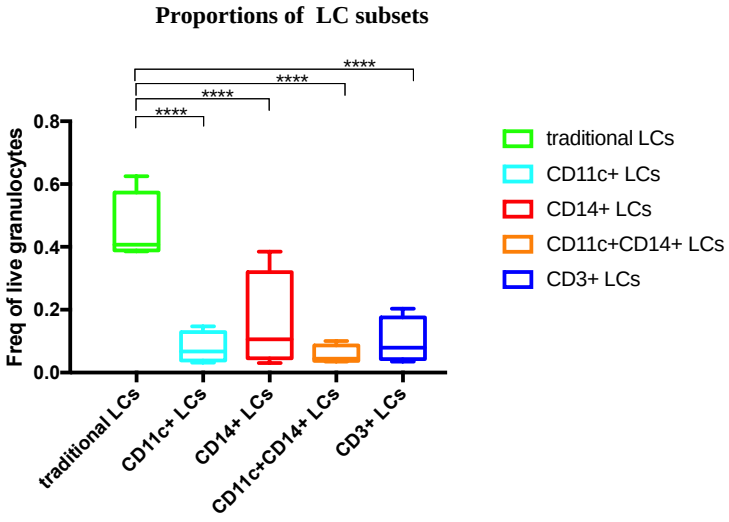

Figure 30. ***Quantification of foreskin traditional Langerhans cells and LC subsets using multiparameter flow cytometry.*** *Proportions of: i) traditional LCs, ii) CD11c+, iii) CD11c+CD14+, iv) CD14+ and v) CD3+ LCs . Statistics were generated using 2-way ANOVA and the Tukey's multiple comparisons test with adjusted p values. *p <0.05; **p < 0.01; ***p < 0.001; ****p < 0.0001*

Proportions and distributions of LC subsets in the inner and outer foreskin

Similarly, to the previous sections, the different LC subsets were further quantified according to migration and non-migration alongside compartmental distribution in the inner and outer foreskin. Interestingly, traditional LCs were similarly distributed in the inner and outer foreskin with no differences in the proportions of migratory and non-migratory cells as shown in Figure 31 (i). However, the inner foreskin harboured higher proportions of migratory CD11c+ LCs (0.15 % ± 0.20 %) and CD11c+CD14+ LCs (0.10 % ± 0.16 %) compared to the outer foreskin where they were both 2-times less frequent and constituted 0.08 % ± 0.08 %; $p = 0.0003$ and 0.04 % ± 0.06 %; $p = 0.0028$ respectively as illustrated in Figures 31 (ii) - (iii). Contrary to these two subsets that were migratory, CD14+ LCs and CD3+ LCs were more frequent in non-migratory cells. In addition, non-migratory CD3+ LCs were 6-times more abundant in the outer foreskin (0.20 % ± 0.45 %) compared to the inner foreskin (0.04 % ± 0.07 %; $p = 0.0327$) as illustrated in Figure 31 (v).

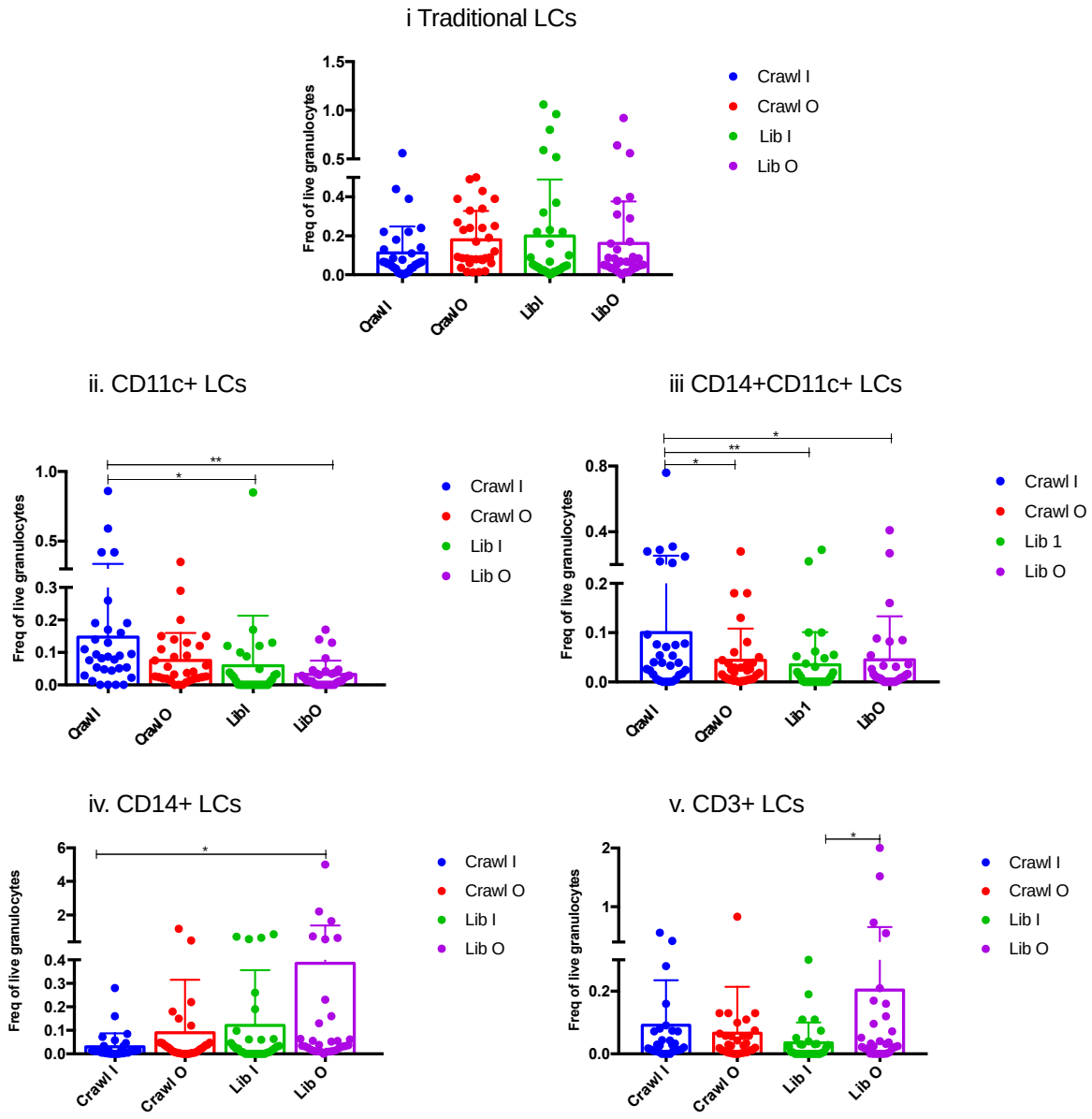

Figure 31. ***Quantification and distributions of migratory and non-migratory LC subsets in the inner and outer foreskin compartments.*** *Flow cytometry quantification of migratory and non-migratory foreskin LCs and LC subsets from the inner and outer foreskin;* ***(i)*** *Traditional LCs* ***(ii)*** *CD11c+ LCs* ***(iii)*** *CD14+CD11c+ LCs,* ***(iv)*** *CD14+CD11c+ LCs and* ***(v)*** *CD3+ LCs (n=31). LC frequencies were log-transformed (Y=Log(Y) for visualization. Statistics were generated using one-way ANOVA using the Tukey's multiple comparisons test and adjusted p values. *p <0.05; **p < 0.01; ***p < 0.001; ****p < 0.0001*

Quantification of markers associated with susceptibility to HIV-1 infection in foreskin LC subsets

CD4 is an HIV receptor, that facilitates HIV entry alongside the co-receptor CCR5 as described earlier. The co-expression of these markers (CD4+CCR5+) was used as a proxy for HIV susceptibility in migratory and non-migratory LC subsets as shown in the gating strategy in Figure 29 (c) above.

The mean frequency of CD4+CCR5+ cells was the highest in CD11c+CD14+ LCs (62.99 % ± 23.81 %) compared to all other LC subsets inclusive of CD11c+ LCs (41.34 % ± 26.35 %; $p < 0.0001$), CD14+ LCs (47.77 % ± 19.18 %; $p = 0.0007$) and traditional LCs (48.54 % ± 20.65 %; $p = 0.0015$) as illustrated in Figure 32 (a) below. Although both comparatively lower than CD11c+CD14+ LCs, the mean frequency of CD4+CCR5+ cells was additionally lower in CD11c+ LCs compared to CD3+ LCs (56.93 % ± 25.17 %; $p = 0.0005$) as shown in Figure 32 (a).

Furthermore, migratory LC subsets collectively displayed higher mean frequencies of CD4+CCR5+ cells (55 % ± 18.75 %) compared to non-migratory cells (48.03 % ± 25.27 %; $p = 0.0198$) as shown in Figure 32 (b). However, there were no differences in the mean frequency of CD4+CCR5+ LCs in the inner (55.39 % ± 23.62 %) and outer foreskin (54.61 % ± 20.11 %) (data not shown).

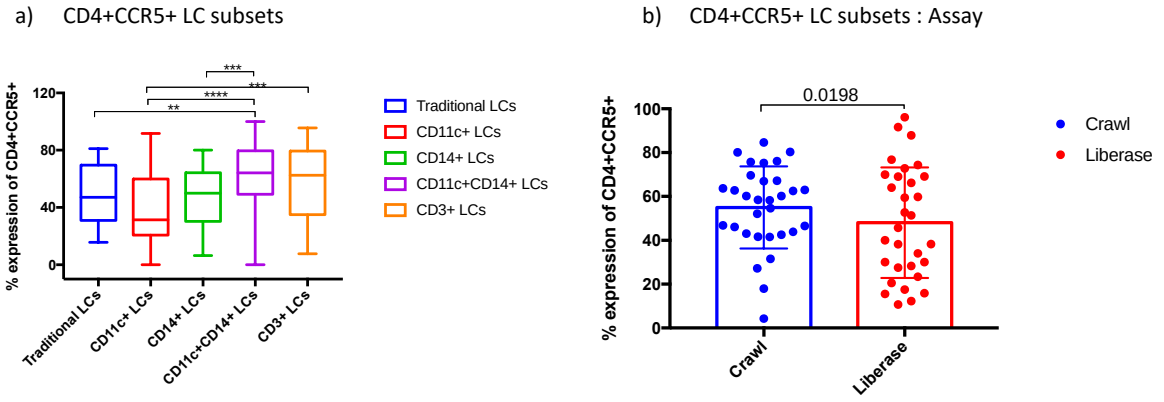

Figure 32. ***Proportions of markers of HIV susceptibility in migratory and non-migratory foreskin Langerhans Cells in the inner and outer foreskin.*** *Flow Cytometry quantification and measurement of HIV susceptibility in foreskin LCs* ***(a)*** *Proportions of CD4+CCR5+ in different foreskin LC subsets* ***(b)*** *Proportions of CD4+CCR5+ in migratory and non-migratory foreskin LCs (n=31). Statistics were generated using two-way ANOVA using the Tukey's multiple comparisons test and adjusted p values. *p <0.05; **p < 0.01; ***p < 0.001; ****p < 0.000. The Wilcoxon test was used to compute p values in (b).*

Summary

The mean frequency of CD4+CCR5+ cells was generally high in all foreskin LC subsets with an average of 51.51 % ± 23.03 %. However, CD11c+CD14+ LCs and CD3+ LCs displayed higher proportions of CD4+CCR5+ than all the other subsets whose mean frequency was similar except CD11c+ LCs that displayed the least. Although higher in migratory cells compared to non-migratory cells, the mean frequency of CD4+CCR5+ LCs did not differ by foreskin compartment.

Quantification of C-lectin receptors:(CD206 & CD209) and Siglec-1 (CD169) in foreskin LC subsets

LC subsets were also assessed for the expression of attachment factors (CLRs and Siglec-1) as shown in the LC gating strategy in Figure 29 (c) above. In addition to portrayal of the highest mean frequency

of CD4+CCR5+ cells, CD11c+CD14+ LCs and CD3+ LC subsets additionally portrayed the highest mean frequency CD206+ cells among all the other LC subsets, although only significantly differed from the CD14+ LCs. Specifically, the proportions of CD206+ cells averaged 19.83 % ± 15.08 % in CD14+ LCs while both CD3+ LCs and CD11c+CD14+ LCs displayed similar CD206+ cell proportions of 30.14 % ± 20.37%; $p = 0.0109$ and 29.79 % ± 24.62 %; $p = 0.0172$ respectively.

Interestingly, CD14+ LCs conversely potrayed the highest mean frequency of CD209+ cells (23.75 % ± 17.02 %) and although not the least, this significantly differed from the mean frequency of CD209+ cells observed in both CD3+ LCs (13.94 % ± 10.99 %; $p = 0.0002$) and CD11c+CD14+ LCs (11.90 % ± 10.95 %; $p = 0.0001$) as shown in Figure 33 (b). However, CD11c+ LCs were identified as the subset with the least proportions of CD209+ cells (2.28 % ± 5.41 %), 10-times less than observed in CD14+ LCs ($p<0.0001$) as illustrated in Figure 33 (b).

Similarly to CD209, the mean frequency of CD169+ cells was the highest in CD14+ LCs (12.37 % ± 11.38 %) and CD3+ LCs (12.73 % ± 14.43 %) in comparison to CD11c+CD14+ LCs (5.53 % ± 7.86 %; $p = 0.02000$), traditional LCs (4.42 % ± 5.92 %; $p = 0.0039$) and CD11c+ LCs (4.11 % ± 8.15 %; $p = 0.0024$) as shown in Figure 33 (c).

Therefore, with the exception of CD14+ LCs, CD206 was the most abundant attachemnet factor in all LC subsets followed by CD209 and CD169, that were more frequent in CD14+ LCs and CD3+ LCs than in other subsets as illustrated in Figure 33 (d). Notably, CD11c+ LCs persistently portrayed low mean frequency of all the three attachment factors as shown in Figure 33 (d).

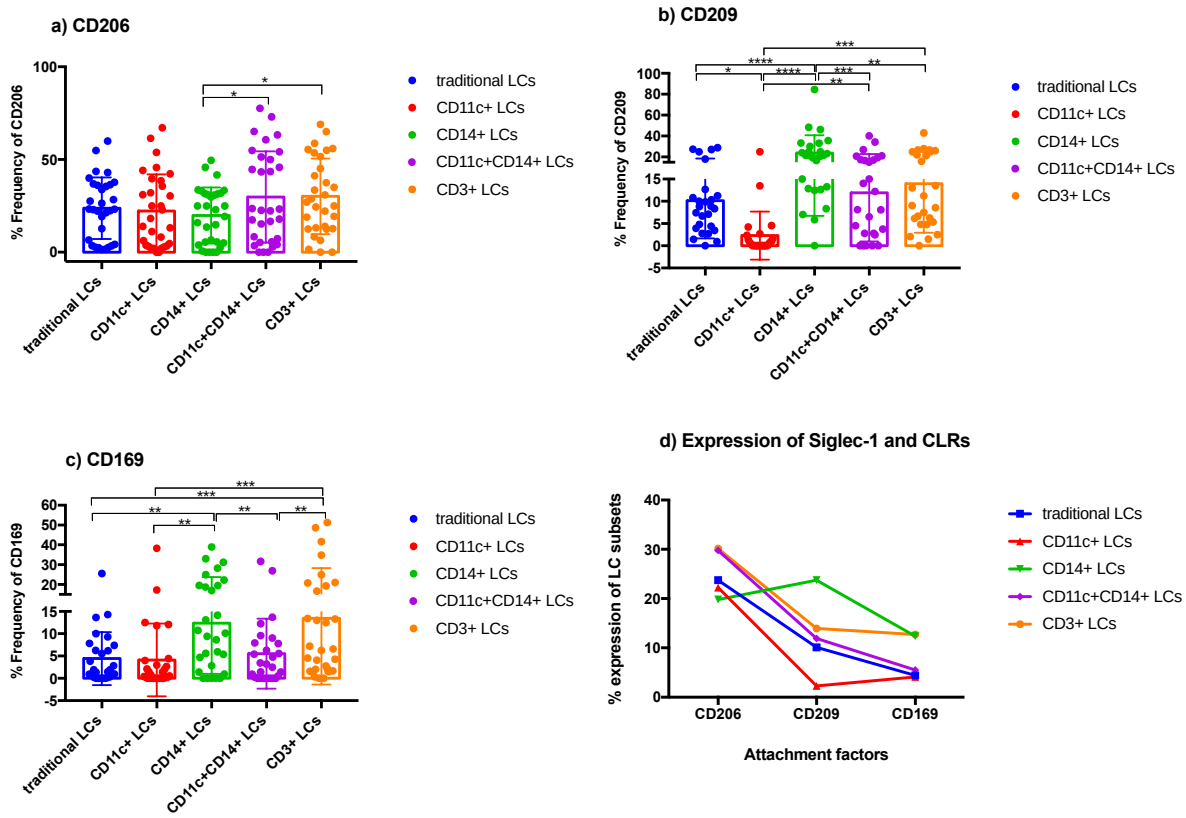

Figure 33. ***Assessment of HIV attachment factors; C-type lectin receptors (CD206 & CD209) and Siglec-1 (CD169), in migratory and non-migratory traditional LCs and LC subsets from the inner and outer foreskin.*** *Flow cytometry quantification of the proportions of CD206, CD169 and CD209 in traditional LCs and LC subsets (n=31). Statistics were generated using two-way ANOVA using the Tukey's multiple comparisons test and adjusted p values. *p <0.05; **p < 0.01; ***p < 0.001; ****p < 0.0001*

Impact of cell isolation methods on CLRs and Siglec-1

Similarly to previous sections, CLR and Siglec-1 expression was additionally compared and assessed between migratory and non-migratory LCs. While a trend was established whereby attachment factors were more frequent in non-migratory cells compared to migratory cells, this was only statistically significant for DC-SIGN (CD209). The mean frequency of CD209+ cells was 52 % higher in non-migratory (16.48 % ± 13.19 %) compared to migratory LCs (7.90 % ± 5.15 %; $p = 0.0022$) as shown in Figure 34 below. Likewise, Siglec-1 (CD169) and the mannose receptor (CD206) retained the trend and were 40.5 % and 11.2 % more frequent in non-migratory than migratory cells (data not shown).

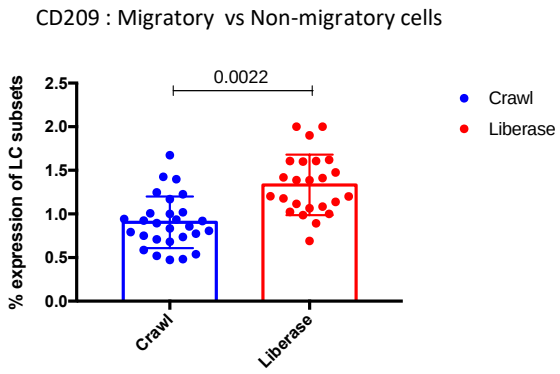

Figure 34. ***Assessment of HIV attachment factors; C-type lectin receptors (CD206 & CD209) and Siglec-1 (CD169), in migratory vs non-migratory traditional LCs and LC subsets from the inner and outer foreskin.*** *Flow cytometry quantification of the proportions of CD206, CD169 and CD209 in migratory vs non-migratory traditional LCs and LC subsets (n=31). The Wilcoxon test was used to compute p values. Y values were transformed using Y = Log(Y).*

Impact of inner and outer foreskin compartmentalization on CLRs and Siglec-1

The proportions of the different attachment factors were further assessed and compared between the inner and outer foreskin compartments. The mean frequencies of CD169+ and CD209+ cells were higher in the outer foreskin LCs (9.70 % ± 8.91 % and 14.59 % ± 0.6 %) compared to the inner foreskin (5.87 % ± 7.00 %; $p = 0.0308$ and 7.94 % ± 8.67 %; $p = 0.0099$) as shown in Figures 35 (a)-(b). There were no differences in the frequencies of CD206+ LCs in the inner and outer foreskin (data not shown).

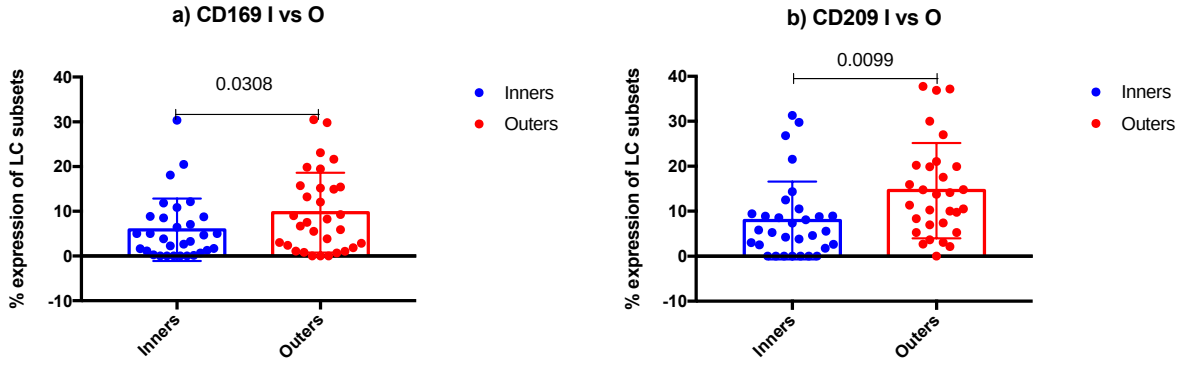

Figure 35. ***Assessment of HIV attachment factors; C-type lectin receptors (CD206 & CD209) and Siglec-1 (CD169), in traditional LCs and LC subsets from the inner and outer foreskin.*** *Flow cytometry quantification of the proportions of* ***(a)*** *CD169 and* ***(b)*** *CD209 in LC subsets in the inner vs outer foreskin (n=31). The Wilcoxon test was used to compute the p values.*

Summary

CD206 was the most frequently expressed CLR in all the different LC subsets. All attachment factors were more abundant in non-migratory cells in comparison to migratory cells. In addition, CD169 and

CD209 were more frequent in the outer foreskin compared to the inner foreskin, while CD206 was similarly distributed in both foreskin compartments.

Quantification of LC cell maturation markers

Lastly, migratory and non-migratory LC subsets, in the inner and outer foreskin were collectively assessed for the co-expression of HLA-DR and CD80/86 as illustrated in the gating strategy in Figure 29 (b) above. Both migratory and non-migratory LC subsets were HLA-DR+ and differentially expressed CD80/86 (data not shown). Among the different LC subsets, the mean frequency of HLA-DR+CD80/86+ cells was highest in CD3+ LCs and CD11c+CD14+ LCs where it averaged 50.2 % ± 19.54 % and 42.69 % ± 23.34 % respectively. This was significantly differed from the proportions of HLA-DR+CD80/86+ witnessed in traditional LCs (31.56 % ± 18.87 %; *p<0.0001*) and CD14+ LCs (31.91 % ± 17.13 %; *p<0.0001*) as shown in Figure 36 (a) below.

When assessed collectively, the mean frequency of HLA-DR+CD80/86+ cells, was higher in migratory LCs (43.28 % ± 18.89 %) compared to non-migratory LCs (36.57 % ± 18.08 %; *p = 0.0157*) as shown in Figure 36 (b) below. HLA-DR+CD80/86+ cells were also more enriched in the inner foreskin (43.46 % ± 18.84 %) compared to the outer foreskin (34.87 % ± 27.01 %), although without statistical significance (data not shown).

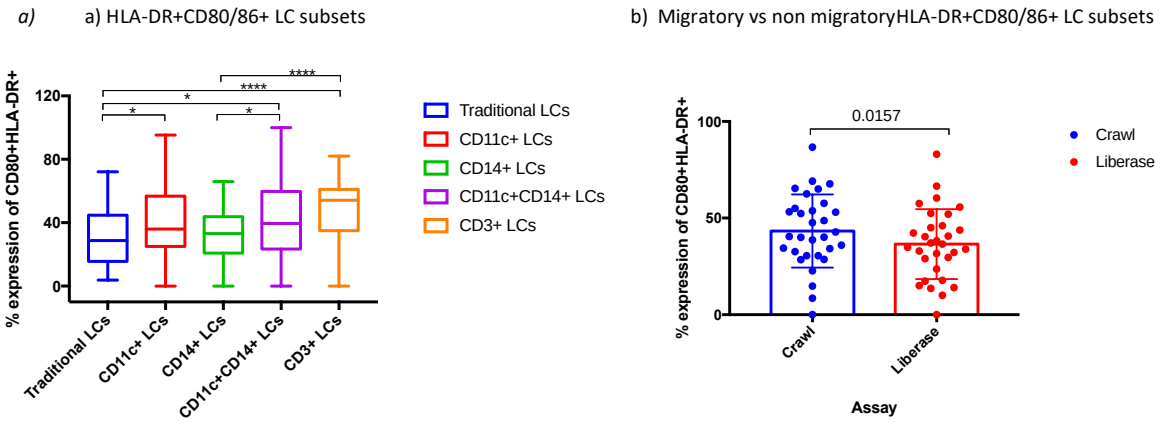

Figure 36. ***Assessment of the activation states (HLA-DR+CD80/86+) of migratory and non-migratory foreskin Langerhans Cells in the inner and outer foreskin.*** *Flow Cytometry quantification and measurement of activation states in foreskin LCs.* ***(a)*** *Proportions of HLA-DR+CD80/86+ in different foreskin LC subsets* ***(b)*** *Proportions of HLA-DR+CD80/86 + in migratory and non-migratory foreskin LCs. Statistics were generated using two-way ANOVA using the Tukey's multiple comparisons test and adjusted p values. *p <0.05; **p < 0.01; ***p < 0.001; ****p < 0.0001 in* ***(a).*** *The Wilcoxon test was used to compute p values in* ***(b)****.*

Manual gating summary and conclusions

Two methods were used for isolating migratory and non-migratory foreskin cells from the inner and outer foreskin compartments. Migratory foreskin cells were more abundant, and more viable in comparison to the non-migratory foreskin cells possibly due to enzymatic treatment and mechanical digestion. Moreover, outer foreskin cell recovery was 2-fold higher than the inner foreskin although the outer foreskin was often bigger than the inner foreskin tissue, thus, cell yields were proportional to tissue size. There were no significant differences in cell viability between the 2 foreskin compartments. Further assessment on these cells was subsequently performed using flow cytometry, prior to which, optimal staining antibody titres were determined by staining the harvested foreskin cells with 2-fold serially diluted antibodies. FMOs controls were included to account for the effects of other fluorochrome markers included in the antibody panel and thus improve our gating accuracy.

Foreskin myeloid cells, defined as those derived from the "big cells" in our FC gating, were generally classified into i) CD11c+, ii) CD14+ and iii) CD11c+CD14+ myeloid cells. These different myeloid cell populations were differentially distributed in the inner and outer foreskin compartments. Migratory, CD11c+ myeloid cells were more frequent in the inner foreskin, while non-migratory CD14+ myeloid cells were not differed in the inner and outer foreskin. Specific myeloid cell populations were subsequently identified and characterised from the general myeloid cell population. Foreskin Langerhans cells (CD1a+CD207+) were identified and classified into traditional LCs, CD11c+ LCs, CD14+ LCs, CD11c+CD14+ LCs and the CD3+ LCs. Of these, traditional LCs constituted half the LC population, while the rest were minor populations accounting for <1% of the myeloid cells. Similar to the general myeloid cell populations, specific LC subsets such as the CD11c+ LCs and the CD11c+CD14+ LCs were migratory and more frequent in the inner foreskin, while CD14+ LCs and CD3+ LCs were non-migratory.

Further to this, CD11c+CD14+ LCs and CD3+ LCs were identified as potentially, the most HIV susceptible LC subsets owing to the comparatively higher frequencies of cells co-expressing HIV susceptibility markers (CD4+CCR5+), HLA-DR+CD80/86+ and the CLR, CD206 in comparison to other LC subsets.

Interestingly CD14+ LCs, in addition to non-migration, also portrayed the least mean frequency of maturation markers, HLA-DR+CD80/86+, while conversely displaying the highest mean frequency of attachment factors, DC-SIGN and Siglec-1. In contrast, migratory CD11c+ LCs had a higher mean frequency of HLA-DR+CD80/86+ cells and the least proportions of DC-SIGN, Siglec-1, and the mannose receptor.

1.5.2.2. Identification of traditional LC subsets and "novel" LC states using unsupervised cell clustering approach

Although foreskin LCs were identified as a rare population as described above, various subsets were shown to exist that differed in the co-expression of pan myeloid markers (CD11c+CD14+), HIV susceptibility markers (CD4+CCR5+), antigen presentation and co-stimulatory markers (HLA-DR+CD80/86+) as well as attachment factors (CD206+CD169+CD209+). While it was not elaborative if these different LC phenotypes were static populations, we sought to further define LC heterogeneity using an unbiased approach through FlowSOM and hierarchical clustering taking into account the expression of all the markers in the panel shown in Table 1 above[180]. Using this unbiased approach was important in elucidating the complexities of LC heterogeneity and identification of novel LC clusters without expert bias, in a manner that could not be captured through manual gating[180]. To do this, migratory and non-migratory foreskin LCs from the inner and outer foreskin, were analysed using the R software as mentioned in the Methods section.

Marker expression profile of migratory and non-migratory foreskin LCs in I and O FS

High dimensional flow cytometry data was reduced in R to a lower two-dimensional space computed tSNE, in order to better visualise the expression of all markers in manually pre-gated foreskin LCs (CD1a+CD207+)[178–180]. A color gradient was used to illustrate marker expression intensities whereby, green denoted low or no expression and red denoted high or intense expression as shown in Figure 38 below. On this basis, foreskin LCs were predominantly CD45+CD4+ and differentially co-expressed other markers as shown in Figure 37 below.

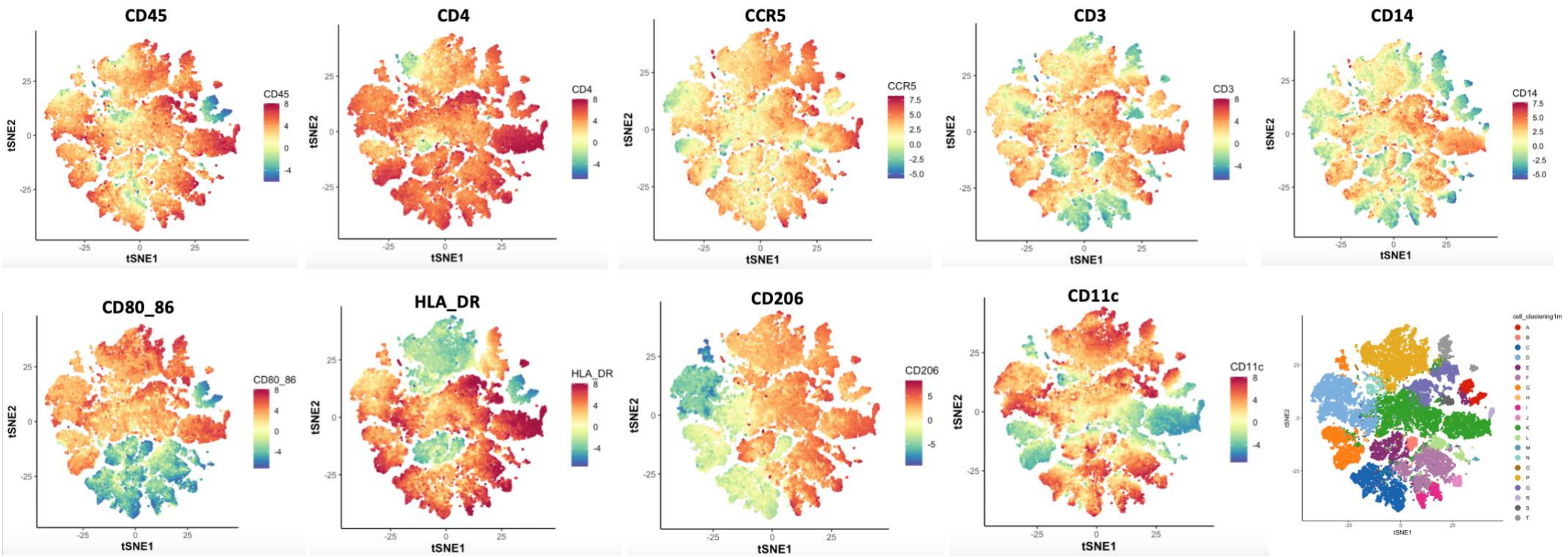

Figure 37. ***Assessment of the marker expression profiles of migratory and non-migratory Langerhans cells of the inner and outer foreskin using tSNE plots generated by non-biased, unsupervised clustering.*** *tSNE plots based on the arcsinh-transformed expression of the 9 markers in foreskin LCs: CD3, CD4, CD11c, HLA-DR, CD80/86, CD206, CD14, CCR5 and CD45.The color spectrum denotes increasing intensities of marker expression, ranging from green which represents no to low marker expression while red is high marker expression*

Determining the optimal number of LC clusters

The delta area plot was used to determine the number of optimal clusters for fitting the LC clusters using the elbow criterion strategy, whereby the last k preceding the plateau was considered the best fit [178–180]. Therefore, using the point of minimum relative change in cumulative distribution function (CDF), the optimal k for clustering LCs was 8-10 as shown in Figure 38 below.

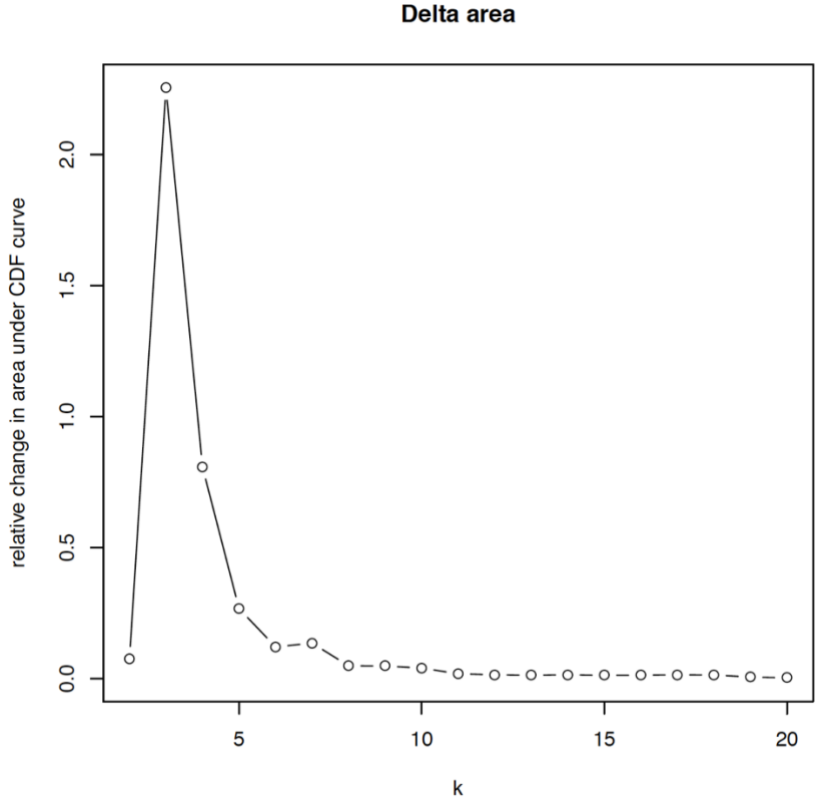

Figure 38. ***Determination of the optimal number of LC clusters****. The elbow criterion strategy was used to determine the optimal k for LC clustering. The point of relative minimum change was k = 10.*

However, using lower k=10, did not fully resolve the LC populations as shown in Figure 39 (a) below. We opted to "over-cluster" and select k=20 in order to detect subtle populations such as Clusters, Q (*purple*), G (*orange*) and N (*turquoise*) in Figure 39 (b), that were otherwise coalesced into the circled clusters in Figure 39 (a) as shown with the aid of yellow arrows.

a) LC clusters when k = 10

b) LC clusters when k = 20

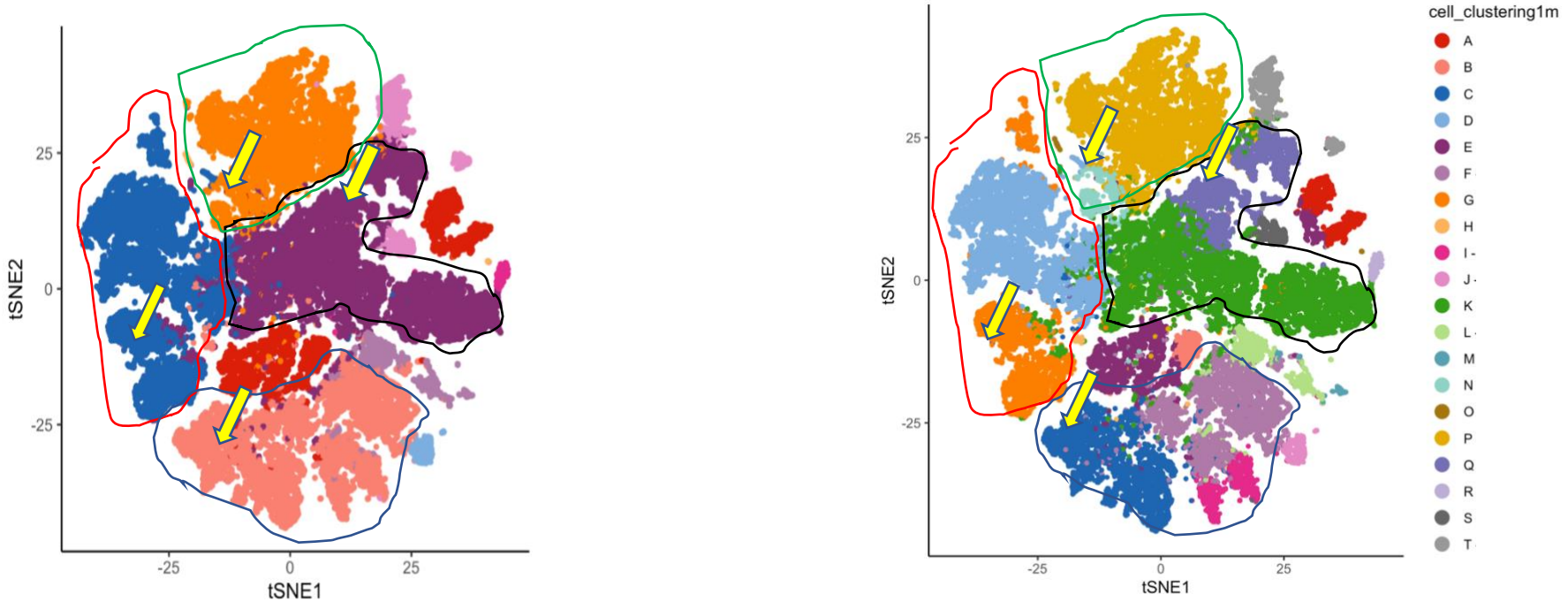

Figure 39. ***tSNE plot demonstrating the different LC clusters using different k means****.* ***(a)*** *LC clusters at k = 10 and* ***(b)*** *LC clusters at k = 10. Each cluster is represented by a different color denoted on the right.*

Identification of the different LC clusters using unsupervised clustering

Twenty LC clusters of varying proportions were therefore identified using FlowSOM and were mapped out on the coloured tSNE plots as shown in Figure 39 (b) above. Of these 20 clusters, only 3 were identified as main due to relatively higher proportions in comparison to other clusters as shown in parentheses on Figure 40 below. Thus, the main clusters were identified as Cluster K (*green;* 20.06 %), Cluster P (*tan;* 15.01 %) and Cluster D (*blue;* 14.06 %) that amounted to 49.13 % as shown by green arrows in Figure 40. Cell cluster relatedness was shown using hierarchical cluster dendrograms on the left of the heatmap in Figure 40, and also through Principal Component Analysis in the Appendix. The main LC clusters (Cluster D, K, and P) were thus, closely related to Cluster Q (*purple;* 6.22 %), Cluster G (*orange;* 7.21 %) and Cluster N (*turquoise*; 1.54 %) (shown in yellow arrows in Figure 40). The relatedness of these main clusters, DKP, with clusters QCN was mainly driven by the shared co-expression of CD80/86+CD3+CD45+CD4+ as illustrated in Figure 40 below.

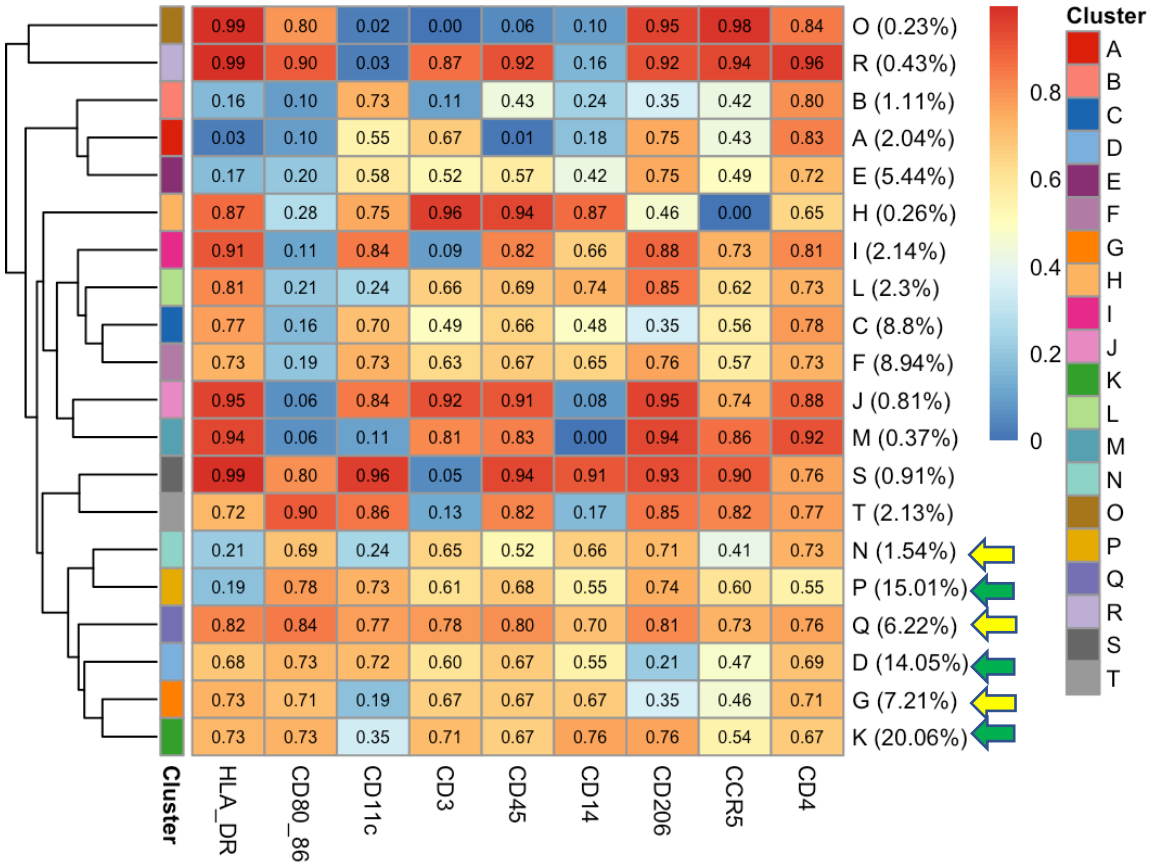

Figure 40. ***Heatmap of the median marker intensities across the 20 LC populations obtained with FlowSOM after metaclustering with ConsensusClusterPlus****. Heatmap colour represents the median of the arcsinh, 0-1 transformed marker expression calculated over cells from all the LC samples. The heat varies from blue (low expression) to red (high expression) and 0.60 was used as the cut-off. Dendrogram represents hierarchical similarity according to consensus clustering. Annotation bar is colored according to the LC clusters. The relative Cluster size is shown in parenthesis next to the different populations .The green arrows are highlighting the main clusters while the yellow arrows are pointed at the closely related, but less frequent clusters.*

Except for Cluster P, the other two main LC clusters (Cluster K and Cluster D) accounting for 34.11 % of the foreskin LCs were CD45+HLA-DR+CD80/86+ suggestive of co-stimulatory and antigen presentation capabilities. They additionally co-expressed CD4 although with low CCR5 co-expression while differed in the expression of pan myeloid markers CD11c and CD14 as well as the CLR, CD206. While Cluster K was CD11c-CD14+CD206+, Cluster D was CD11c+CD14-CD206-. Meanwhile, Cluster P differed from both Cluster K and Cluster D, by the lack of HLA-DR, low CD4 and higher CCR5 co-expression. However, similarly to Cluster D, Cluster P was also CD11c+CD14- as shown in Figure 40 above and Table 2 below.

Table 2. Phenotypes of the different LC clusters

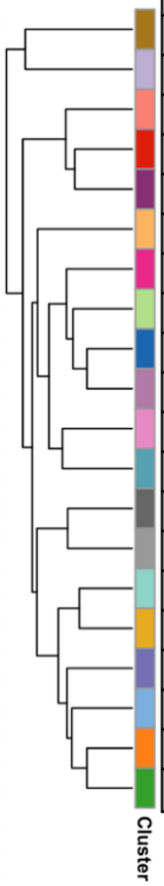

Cluster	Phenotype	%
O	CD1a+CD207+HLA_DR+CD80_86+CD11c-CD3-CD45-CD14-CD206+CCR5+CD4+	0.23 %
R	CD1a+CD207+HLA_DR+CD80_86+CD11c-CD3+CD45+CD14-CD206+CCR5+CD4+	0.43 %
B	CD1a+CD207+HLA_DR-CD80_86-CD11c+CD3-CD45-CD14-CD206-CCR5-CD4+	1.11 %
A	CD1a+CD207+HLA_DR-CD80_86-CD11c-CD3+CD45-CD14-CD206+CCR5-CD4+	2.04 %
E	CD1a+CD207+HLA_DR-CD80_86-CD11c-CD3-CD45-CD14-CD206+CCR5-CD4+	5.44 %
H	CD1a+CD207+HLA_DR+CD80_86-CD11c+CD3+CD45+CD14+CD206-CCR5-CD4+	0.26 %
I	CD1a+CD207+HLA_DR+CD80_86-CD11c+CD3-CD45+CD14+CD206+CCR5+CD4+	2.14 %
L	CD1a+CD207+HLA_DR+CD80_86-CD11c-CD3+CD45+CD14+CD206+CCR5+CD4+	2.3 %
C	CD1a+CD207+HLA_DR+CD80_86-CD11c+CD3-CD45+CD14-CD206-CCR5-CD4+	8.8 %
F	CD1a+CD207+HLA_DR+CD80_86-CD11c+CD3+CD45+CD14+CD206+CCR5-CD4+	8.94 %
J	CD1a+CD207+HLA_DR+CD80_86-CD11c+CD3+CD45+CD14-CD206+CCR5+CD4+	0.81 %
M	CD1a+CD207+HLA_DR+CD80_86-CD11c-CD3+CD45+CD14-CD206+CCR5+CD4+	0.37 %
S	CD1a+CD207+HLA_DR+CD80_86+CD11c+CD3-CD45+CD14+CD206+CCR5+CD4+	0.91 %
T	CD1a+CD207+HLA_DR+CD80_86+CD11c+CD3-CD45+CD14-CD206+CCR5+CD4+	2.13 %
N	CD1a+CD207+HLA_DR-CD80_86+CD11c-CD3+CD45-CD14+CD206+CCR5-CD4+	1.54 %
P	CD1a+CD207+HLA_DR-CD80_86+CD11c+CD3+CD45+CD14-CD206+CCR5+CD4-	15.01 %
Q	CD1a+CD207+HLA_DR+CD80_86+CD11c+CD3+CD45+CD14+CD206+CCR5+CD4+	6.22 %
D	CD1a+CD207+HLA_DR+CD80_86+CD11c+CD3+CD45+CD14-CD206-CCR5-CD4+	14.05 %
G	CD1a+CD207+HLA_DR+CD80_86+CD11c-CD3+CD45+CD14+CD206-CCR5-CD4+	7.21 %
K	CD1a+CD207+HLA_DR+CD80_86+CD11c-CD3+CD45+CD14+CD206+CCR5-CD4+	20.06 %

1Table 2 shows marker expression per LC cluster. Dendrogram on the right shows cluster relatedness according to marker expression intensities. 1st column is cluster name derived from the corresponding heatmap in Figure 40. Phenotype column shows cluster phenotype as per the 0.6 cut-off from the heatmap. The frequencies of each cluster are shown in the last column denoted as %.

As described above, the main clusters (D, K, and P) displayed phenotypic relatedness with the more subtle populations (Cluster G, N and Q), with which they clustered using hierarchical dendrograms and also coalesced with, when lower k=10 was used as illustrated earlier in Figures 39 (a) – (b). Cluster K

1

was nearly identical to Cluster G and differed only by CD206 expression as shown in Table 2. However, Cluster N and Cluster Q were more distinguishable as unique populations, separate from the main populations (Cluster P and Cluster D) with which they coalesced at k=10, hence the need to "over-fit" the LC data. In particular, Cluster N differed from Cluster P by the lack of CCR5, CD11c, CD3 and CD206 expression as shown in Table 2. Although similar to Cluster D, Cluster Q co-expressed CD11c and CD14 unlike all the other clusters in the main branch, that were either CD11c+CD14- or CD11c-CD14+. More importantly, Cluster Q was also CD4+CCR5+CD206+ and therefore, potentially susceptible to HIV infection.

The remainder of the LC clusters were less frequent, and thus identified as minor and constituted the following: Clusters; A (*red*; 2.04 %), B (*coral*; 1.11 %), E (*purple*; 5.44 %), C *(blue*; 8.8 %), F (*violet*; 8.94 %), I (*hot pink*; 2.14 %), L (*lime*; 2.3 %), and T (*light grey*; 2.13 %). In total, these minor LC clusters accounted for 32.9 % of the LC population as show in Table 2 above. Similarly to the main clusters, Cluster A (*red*), Cluster B (*coral*) and Cluster E (*purple*) also displayed phenotypic relatedness using dendrograms from hierarchical clustering as displayed on the table above. Clusters: A, B and E were all CD4+CCR5-HLA-DR-CD80/86-CD14-CD45- and differed in the expression of CD11c and CD206 as shown in Table 2. The lack of CCR5 expression in Cluster A, B and E suggested that these clusters would not be infectable with HIV. A similar phenomenon was observed with Cluster C (*blue*) and Cluster F (*violet*) that were both HLA-DR+CD80/86-CD11c+CD45+CD4+CCR5- with differential expression of CD14 and CD206 as shown in Table 2.

Other minor, but potentially HIV susceptible clusters were inclusive of Cluster L (*lime;* 2.3 %) that, unlike all the other clusters described above, was a natural population since it resolved using both low k=10 and "over-fitted" k=20 data as shown in Figures 39 (a)-(b). Phenotypically, Cluster L (*lime*) was a CD14+CD11c- LC cluster, that co-expressed HIV susceptibility markers (CD4+CCR5+) and the mannose receptor (CD206+) alongside CD45, HLA-DR and CD3 as shown in Table 2. Cluster I (*hot pink*; 2.14 %) was also a CD4+CCR5+ cluster that, although similar to Cluster L, was CD14-CD11c+.

CD4+CCR5+ clusters were also identified among the least frequent CD11c-CD14- LC clusters (<1 %), that consisted of : Cluster M (*teal*; 0.37 %), Cluster O (*brown*; 0.23 %), and Cluster R (*lavender*; 0.43 %). Cluster O and Cluster R both co-expressed co-stimulatory markers (HLA-DR+CD80/86+) and the mannose receptor (CD206+) while differing in CD3 and CD45 expression as shown in Table 2. Cluster M (*teal*) and Cluster R (*lavender*) were similar and both portrayed bright CD3 co-expression while displaying lack of CD80/86. Lastly, Cluster H (*light orange;* 0.26 %) and Cluster J (*light pink;* 0.81 %) were also CD80/86- clusters, that additionally co-expressed CD3 at higher intensity than observed in all the other LC clusters where it was dimly expressed (Clusters : A, L, F, N, P, Q, D,G and K) as

shown in the heatmap in Figure 40 above. Cluster H (*light orange*) was however CD11c+CD14+ CD4+CCR5-, while Cluster J (*light pink*) was CD11c+CD14-CD4+CCR5+ as shown in Table 2.

Migratory and non-migratory LC clusters in the inner and outer foreskin

Coloured tSNE plots were stratified according to assay (crawl and liberase) and compartment (inner and outer foreskin) in order to identify and distinguish migratory and non-migratory LC clusters in the inner and outer foreskin compartments as shown in Figure 41 below. Clusters that were more frequent in migratory than in non-migratory cells, were Cluster A (*red*), Cluster B (*coral*), Cluster C(*light blue*), Cluster D (*blue*), and Cluster P(*tan*). Except for Cluster A, identified as CD11c-CD14-, all the other migratory LC clusters were CD11c+CD14- (circled in green) as described above. Cluster B (*coral*) was particularly diminished in non-migratory cells as shown in Figure 41. Although less apparent in Figure 41, the CD11c-CD14+ clusters; Cluster K (*green*) and Cluster L (*lime*) (circled in red), were conversely more frequent in non-migratory cells as shown with more clarity in Figure 42 (a) below. However, no differences were observed between the inner and outer foreskin, as was also observed using manual gating earlier.

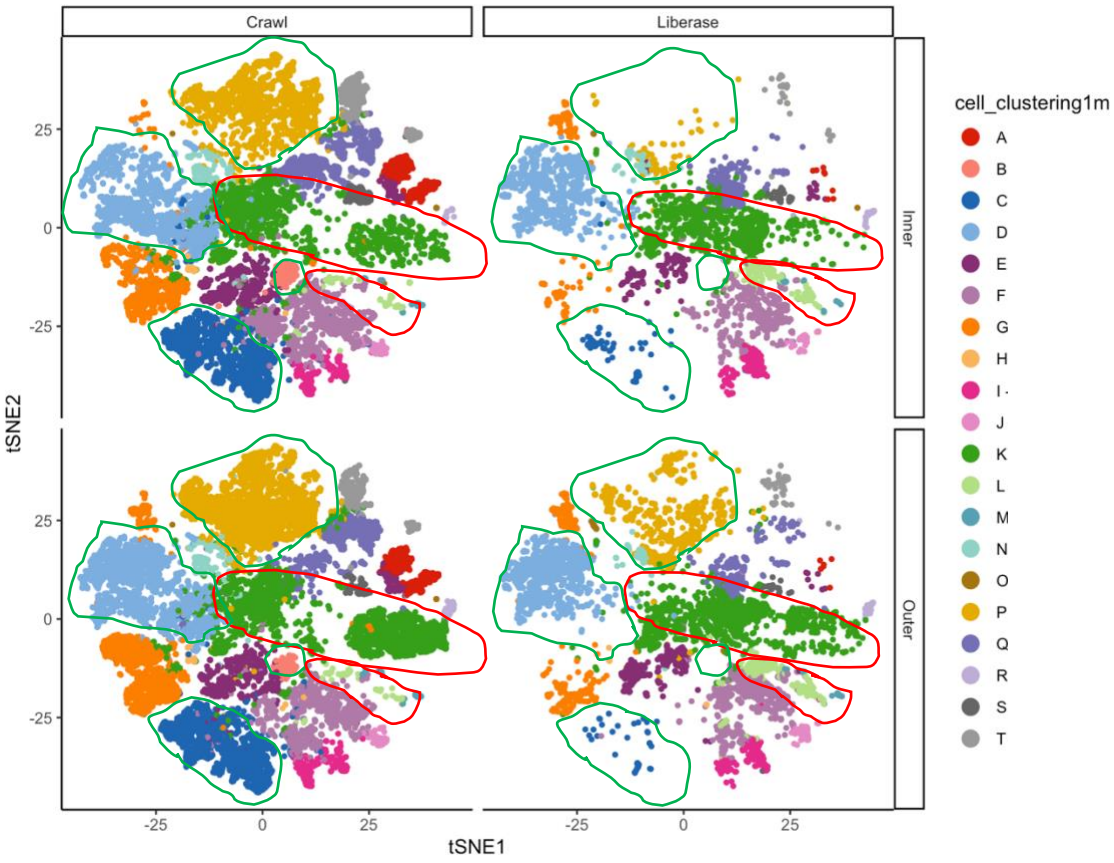

Figure 41. ***Determination of the different LC clusters within the migratory (Crawl) and non-migratory (Liberase) Langerhans cells of the inner (I) and outer (O) foreskin, using colored tSNE plots generated by non-biased, computerised clustering.*** *Colored tSNE plots demonstrating the different LC subsets (clusters) shown in the plot as different colours and demarcated by migration and non-migration(Crawl/Lib) and compartment (Inner/Outer).*

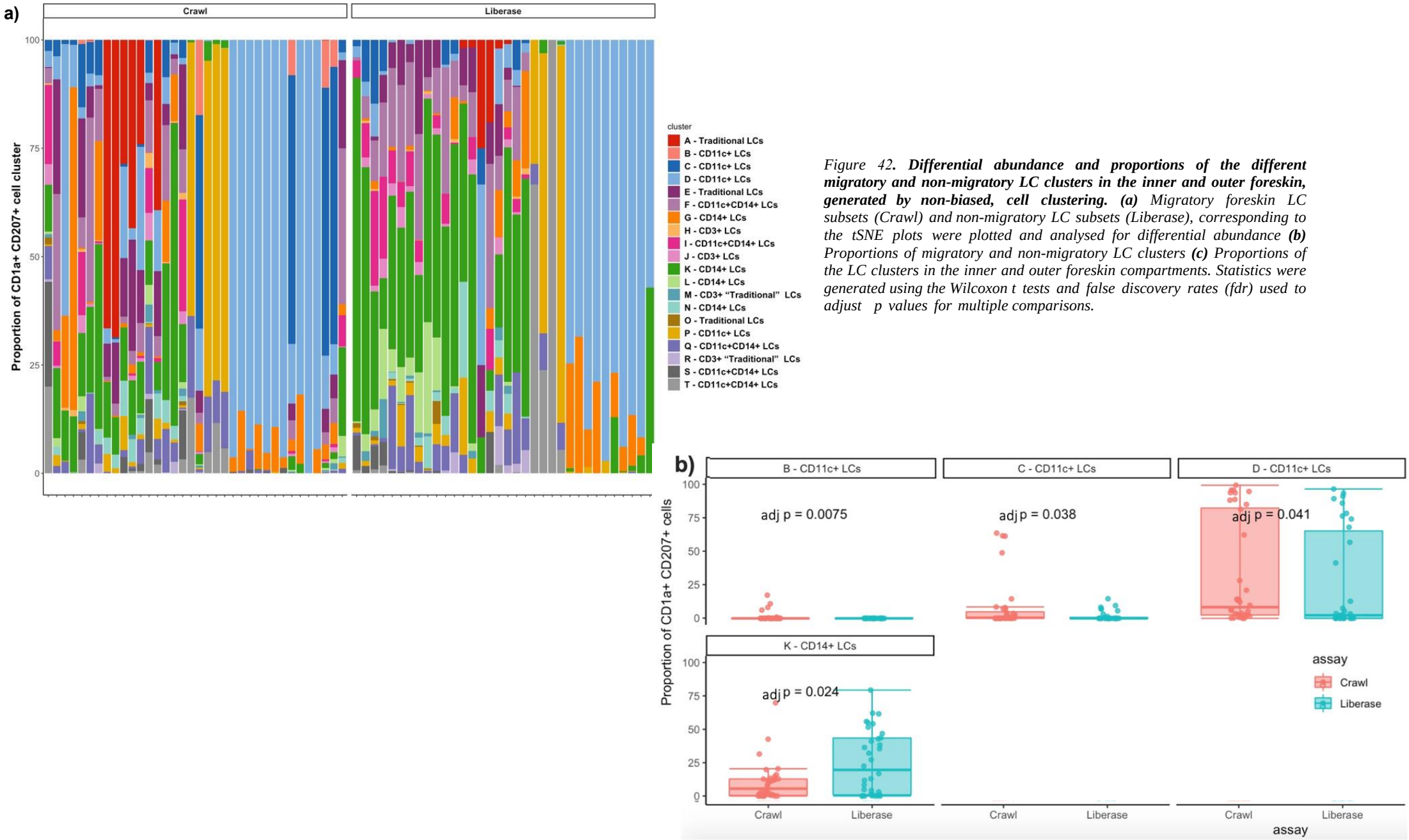

Figure 42. ***Differential abundance and proportions of the different migratory and non-migratory LC clusters in the inner and outer foreskin, generated by non-biased, cell clustering.*** ***(a)*** *Migratory foreskin LC subsets (Crawl) and non-migratory LC subsets (Liberase), corresponding to the tSNE plots were plotted and analysed for differential abundance* ***(b)*** *Proportions of migratory and non-migratory LC clusters* ***(c)*** *Proportions of the LC clusters in the inner and outer foreskin compartments. Statistics were generated using the Wilcoxon t tests and false discovery rates (fdr) used to adjust p values for multiple comparisons.*

Proportions of Migratory vs Non-migratory LC subsets

Corroborative to Figure 41 and manual gating findings, the CD11c+ LC clusters were more frequent in migratory cells in comparison to non-migratory cells as seen for Cluster B *(coral; adj p = 0.0075)*, Cluster C *(blue; adj p = 0.038)* and Cluster D *(sky-blue; adj p = 0.041)* in Figures 42 (a)-(b) above.

The CD11c-CD14- LC cluster that was identified as traditional LCs, (Cluster A*; red)* was also visibly more abundant in migratory LCs compared to non-migratory LCs, although without statistical significance after adjusting for multiple comparisons, as shown in Figure 42 (a).

In contrast, CD14+ LCs were more frequent in non-migratory cells compared to migratory cells, particularly for Cluster K *(green; adj p = 0.024)* as shown in Figures 42 (a)-(b). Other minor CD14+ LC clusters such as Cluster L (*lime*), and Cluster G (orange) also exhibited similar trends, and were more frequent in non-migratory cells, although not statistically different after adjustment of multiple comparisons as shown in Figure 42 (a). Similarly, CD11c+CD14+ LC clusters, such as Cluster F (*purple*) and Cluster T (*grey*) were also more enriched in the non-migratory LCs in comparison to migratory LCs as shown in Figure 42 (a). This suggests that CD14 expression was associated with tissue residency and non-migration in foreskin LCs.

There were no clear distinctions in the proportions of migratory and non-migratory cells among the remaining of the LC clusters (E, H, I, J, M, N, O, P, Q, R and S) as illustrated in Figure 42 (a) above. There were also statistically significant differences in the proportions of all clusters in the inner and outer foreskin (data not shown).

Summary

Similarly to manual gating, the proportions of migratory cells were comparatively higher than non-migratory cells, although without any notable differences between the inner and outer foreskin compartments. Although not significantly differed, an observable trend was also established with unsupervised clustering whereby CD11c+ clusters were more frequent in migratory cells from the inner foreskin while CD14+ LC clusters were more frequent in non-migratory cells. Moreover, the mannose receptor (CD206), identified earlier as the main attachment factor in foreskin LCs, was also more frequent in the non-migratory Cluster (Cluster K) as shown above in Table 2.

Except for Cluster P (CD11c+ LCs), where CD4 expression was low, all LC clusters were CD4+, with differential CCR5 co-expression. CD4+CCR5+ co-expression was more observable in CD11c+CD14+ LC clusters inclusive of Clusters I, Cluster Q, Cluster S and Cluster T) that accounted for 11.4 % of the

foreskin LCs. CD4+CCR5+ co-expression was also most notable in CD11c+CD14+ LCs when manual gating was used. High CD3 co-expressing clusters; Cluster J and the CD3+ "traditional LCs" (Cluster M and Cluster R), also co-expressed CD4+CCR5+, although only constituted 1.61% of the foreskin LCs. Only one of the CD11c-CD14- clusters (Cluster O), was CD4+CCR5+, likewise CD14+ LCs (Cluster L) as shown in Table 2. Overall, 15.54 % of the foreskin LC clusters were CD4+CCR5+.

Similarly to CD4, foreskin LCs were HLA-DR+, except for a few minor clusters (A, B and N) as well as one of the main clusters, Cluster P, that was also identified above as CD4lo. CD80/86 was differentially co-expressed among the clusters and HLA-DR+CD80/86+ LC clusters were distinguishable into; 27.27 % CD14+ LCs (Cluster G and Cluster K), 14.05 % CD11c+ LCs (Cluster D), 9.26 % CD11c+CD14+ LCs (Cluster Q, S, T), 0.23 % traditional LCs (Cluster O) and 0.43 % CD3+ "traditional LCs" (Cluster R).

1.5.3 "Macrophage-like" cells

"Mϕ-like" cells were defined as non-LC cells heterogeneously expressing CD11c and CD14 (CD11c-CD14+, CD11c+CD14+ and CD11c+CD14-) as shown in the gating strategy below in Figure 43 (a). These Mϕ-like subsets were collectively referred to as the "L-gate" from which the following subsets were derived: (i) "M1-like" Mϕ, (ii) "M2-like" Mϕ, (iii) CD169+ Mϕ and (iv) unconventional CD3+ Mϕ as illustrated in Figure 43 (b). Transitionary and intermediary cells expressing markers common to "M1-like" and "M2 like" Mϕ were also identified as (v-vi) "M1" and "M2" intermediates respectively. "M2-like" Mϕ were defined as CD206+CD209+/- cells while "M1-like" Mϕ were defined as CD80/86+HLA-DR+ cells. "Mϕ-like" cells expressing CD169 or CD3, were simply defined as CD169+ Mϕ and CD3+ Mϕ respectively shown in Figure 43 (b) iii-iv.

Furthermore, HLA-DR and CD80/86 were used to assess the maturation states of these subsets shown in Figure 43 (c). However, in "M2 like" Mϕ, these markers were used to identify transitionary "M1/M2" intermediates, while used to characterise "M1-like" Mϕ as part of the gating strategy in b (ii). The use of HLA-DR and CD80/86 to assess the activation states of "Mϕ-like" subsets was therefore only limited, and applicable to CD3+ Mϕ and CD169+ Mϕ.

Additionally, all the different "Mϕ-like" subsets were analysed for HIV susceptibility using the co-expression of CD4 and CCR5 as shown in Figure 43 (d). Lastly, "Mϕ-like" subsets were assessed for the expression of attachment factors, the C-type lectin receptors (CD206 and CD029) and Siglec 1 (CD169) as shown in Figure 43 (e). However, similarly to the activation markers, CLRs were used to

identify “M2-like” Mϕ while Siglec-1 was used to identify CD169+ Mϕ and could therefore not be assessed in a similar manner as the expression of HIV susceptibility markers.

“Macrophage” specific gating strategy

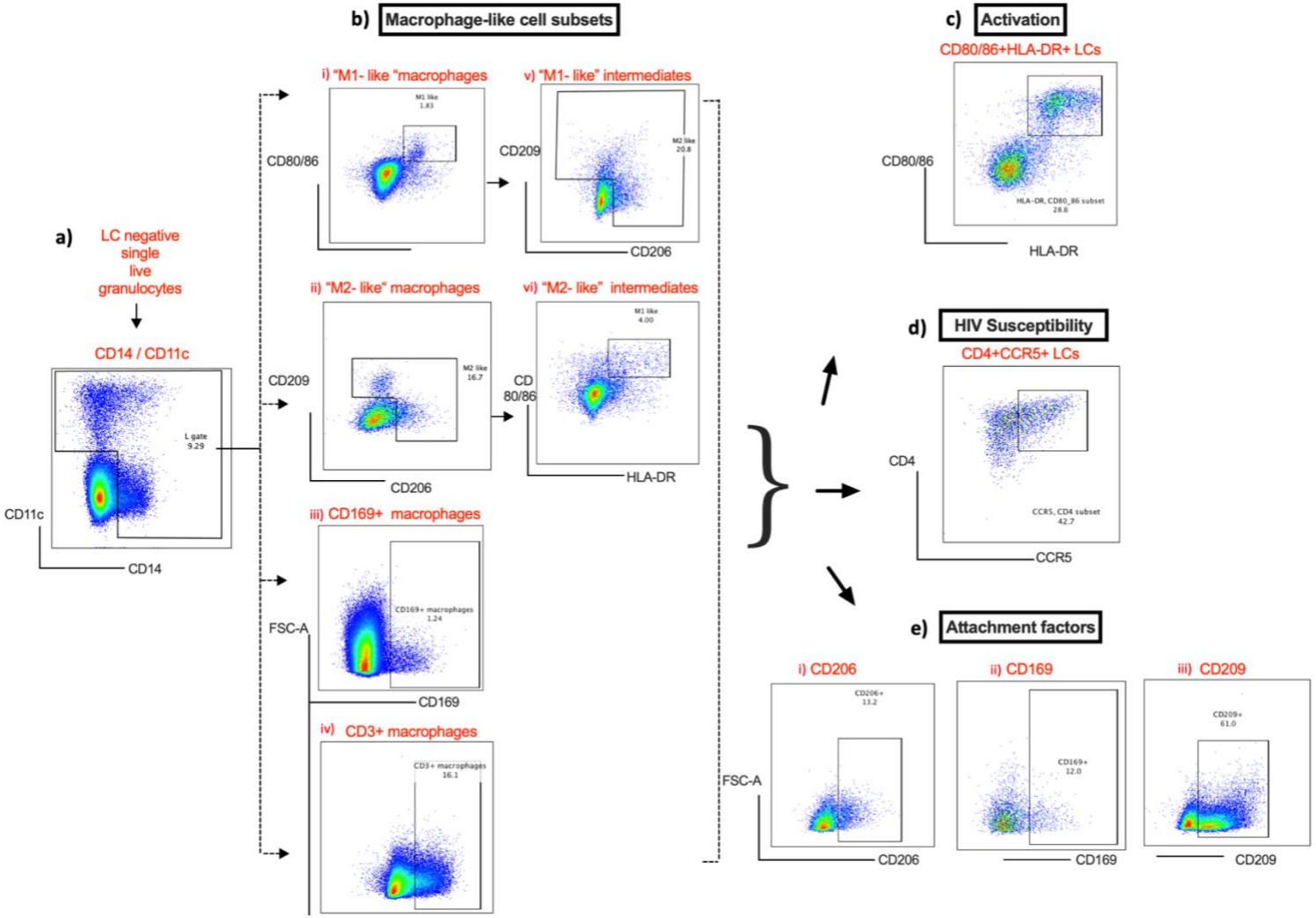

Figure 43. ***Identification of foreskin “Macrophage-like” cell subsets using multiparameter flow cytometry****. “Macrophage-like” cells derived from the LC exclusionary, CD11c/CD14 gate; “ M1-like” macrophages, “M2-like” macrophages, CD169+ macrophages, CD3+ macrophages “M1” and “M2”intermediates.*

1.5.3.1 Quantification of foreskin "Macrophage-like" subsets using manual gating

Following the identification of the different "Mϕ-like" populations, they were subsequently compared as shown in Figure 44 below. The most abundant "Mϕ-like" population, in relation to the other subsets, were the "M2-like Mϕ " that made up 5.60 % ± 4.13 % of the foreskin epidermal granulocytes (big cell gate). These were 1.93-fold more frequent than the CD3+ Mϕ whose mean frequency was the second highest (2.90 % ± 2.73 %; *p<0.0001*). Meanwhile, "M1-like" Mϕ and CD169+ Mϕ were the least frequent "Mϕ-like" subsets with mean frequencies 9.3-fold and 37.3-fold less than "M2-like" Mϕ (*p<0.0.0001*) respectively. Thus, "M1-like" Mϕ constituted 0.60 % ± 1.49 % of the foreskin granulocytes whereas CD169+ Mϕ only constituted 0.15 % ± 0.18 % as shown in Figure 44. Notably, "M1" (0.27 % ± 0.55 %) and "M2" intermediates (0.27 % ± 0.56 %) were also identified as rare "Mϕ-like" populations, of similar proportions (data not shown).

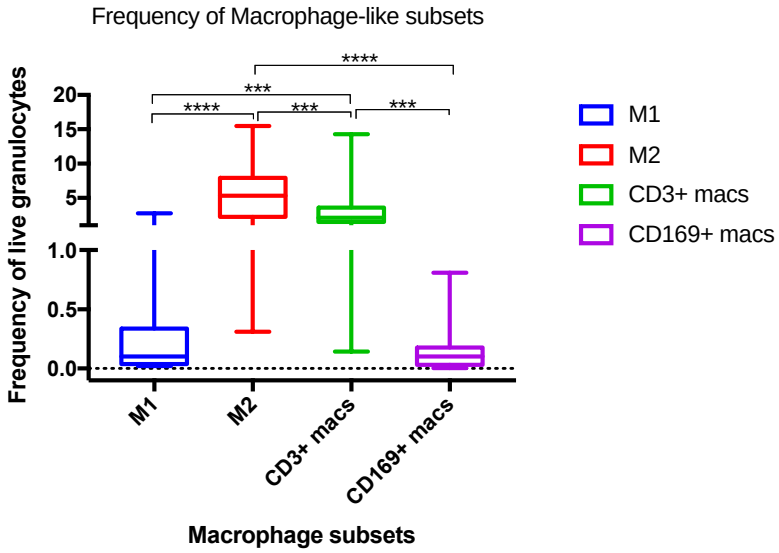

Figure 44. ***Proportions and distributions of migratory and non-migratory "Macrophage-like" cell subsets isolated from the inner and outer compartments of adult foreskin epidermal tissue.*** *Proportions of "Macrophage-like" populations in the foreskin: "M1-like" macrophages, "M2-like" macrophages, "M1" intermediates, "M2" intermediates, CD169+ macrophages and CD3+ macrophages. Statistics were generated using two-way ANOVA using the Tukey's multiple and adjusted p values. *p <0.05; **p < 0.01; ***p < 0.001; ****p < 0.0001 (n=31).*

Similarly to LCs, "Mϕ-like" subsets were further characterised according to migration and non-migration as well as distribution in the inner and outer foreskin. Rare "Mϕ-like" subsets, inclusive of "M1-like" Mϕ, "M1/M2" intermediates and the CD169+ Mϕ were more frequent in migratory cells while "M2" like Mϕ and the CD3+ Mϕ were more frequent in non-migratory cells.

As shown in Figure 45 (a) below, the mean frequency of "M1-like" Mϕ was higher in the inner foreskin, although with comparatively higher proportions of migratory cells (0.65 % ± 1.23 %) in comparison to

non-migratory cells (0.43 % ± 1.33 %; *p = 0.09*). A similar trend was observed in "M2" intermediate Mϕ as shown in Figure 45 (b). The inner foreskin harboured higher frequencies of both migratory (0.40 % ± 0.94 %) and non-migratory "M2" intermediates (0.38 % ± 1.27 %) in comparison to the outer foreskin where they constituted (0.13 % ± 0.34 %; *p = 0.4023*) and (0.17 % ± 0.32 %; *p = 0.6615*) respectively as illustrated in Figure 45 (b). CD169+ Mϕ portrayed the same trend whereby the mean frequency was higher in inner foreskin compared to outer foreskin albeit not statistically significant (data not shown).

In contrast, there were no differences in the distribution of "M2-like" Mϕ in the inner and outer foreskin compartments, although they were more enriched in non-migratory cells compared to migratory cells. In particular, non-migratory "M2-like" Mϕ were 1.5 fold more frequent in the inner (6.78 % ± 10.43 %) and outer foreskin (7.71 % ± 7.47 %), compared to migratory "M2-like" Mϕ in the inner (4.55 % ± 5.05 %;) and outer foreskin (3.32 % ± 3.78 %; *p = 0.00570*) as illustrated in Figure 45 (c). Similarly, CD3+ Mϕ were more frequent in non-migratory cells than in migratory cells. This was however, more apparent in the outer foreskin where CD3+ Mϕ were 3.8 fold more frequent in non-migratory cells (5.33 % ± 8.82 %) compared to migratory cells (1.40 % ± 1.50 %; *p = 0.0083*) as shown in Figure 45 (d).

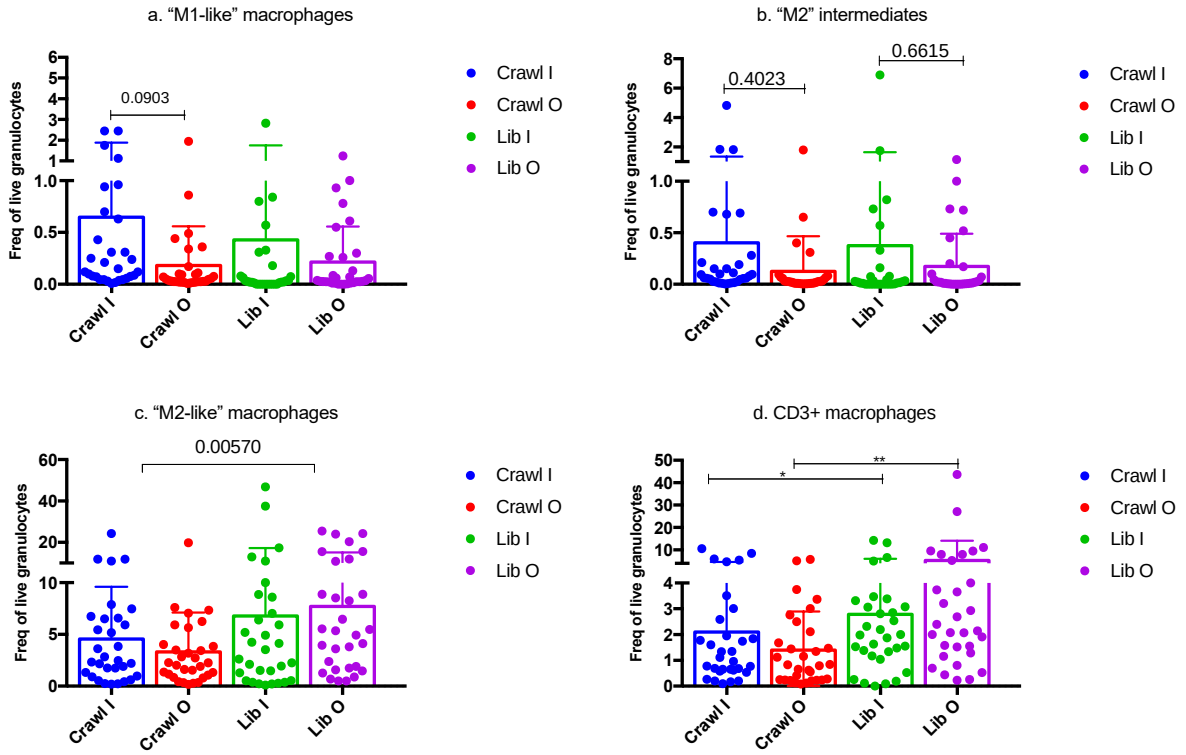

Figure 45. ***Proportions and distributions of migratory and non-migratory "Macrophage-like" cell subsets isolated from the inner (I) and outer (O) compartments of adult foreskin epidermal tissue by spontaneous migration (Crawl) and liberase digestion of remnant tissue (Lib).*** *Compartmental proportions and distributions of non-migratory and migratory:* ***(a)*** *"M1-like" macrophages* ***(b)*** *"M2-like" intermediates* ***(c)*** *"M2-like" macrophages* ***(d)*** *CD3+ macrophages in the inner and outer foreskin. Statistics were generated using one-way ANOVA using the Tukey's multiple comparisons test and adjusted p values. *p <0.05; **p < 0.01; ***p < 0.001; ****p < 0.0001 (n=31).*

Summary

Except for "M1-like" Mϕ and the intermediates, foreskin "Mϕ-like" subsets were less frequent in spontaneously migrating cells compared to cells that were enzymatically digested out of the epidermis after collecting those that were spontaneously migrating. "M1-like" Mϕ and the "M2" intermediates additionally portrayed a trend, whereby the inner foreskin had a higher frequency of cells than the outer foreskin.

Quantification of HIV target markers

Migratory and non-migratory "Mϕ-like" subsets from the inner and outer foreskin were collectively assessed for HIV susceptibility using the co-expression of CD4 and CCR5 as a proxy, as shown in LCs earlier. The mean frequency of CD4+CCR5+ cells was similar and highest in "M1-like" Mϕ (54.15 % ± 26.12 %), "M1" intermediates (59.35 % ± 27.49 %) and "M2" intermediates (59.24 % ± 27.52 %). Meanwhile, "M2-like" Mϕ (28.38 % ± 13.99 %), CD169+ Mϕ (30.96 % ± 20.93 %) and CD3+ Mϕ (32.77 % ± 18.57 %) potrayed comparatively lower mean frequencies of CD4+CCR5+ cells, all 2-fold less than was observed in "M1-like" Mϕ and the "M1/M2" intermediates ($p < 0.0001$) as shown in Figure 46 below.

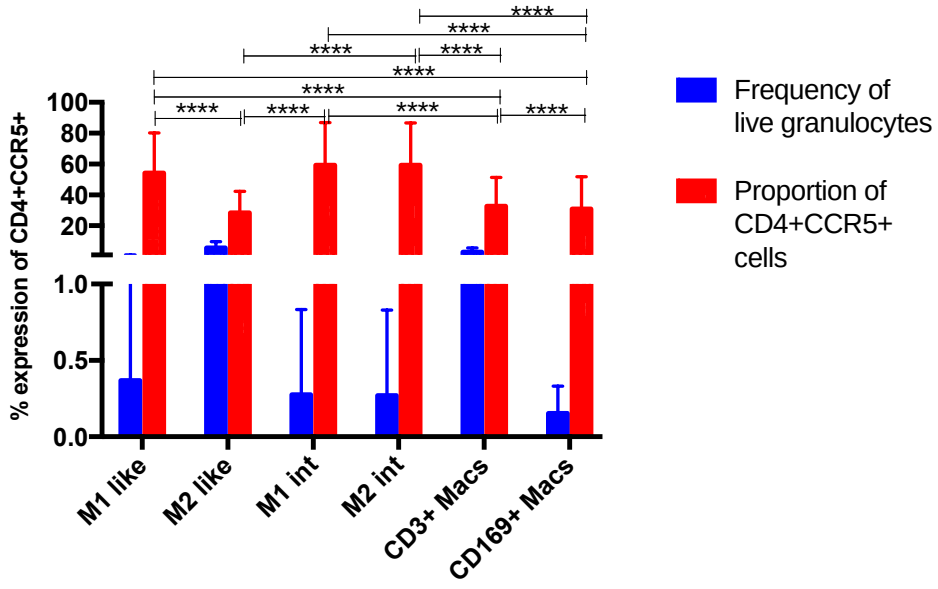

Figure 46. ***Proportions of markers of HIV susceptibility (CD4+CCR5) in "Macrophage-like" populations.*** *Different "Macrophage-like" populations displaying differential proportions ofCD4+CCR5+ cells (n=31). Statistics were generated using two-way ANOVA using the Tukey's multiple comparisons test and adjusted p values. *p <0.05; **p < 0.01; ***p < 0.001; ****p < 0.0001*

Quantification of markers of HIV susceptibility in migratory and non-migratory "macrophage-like" sub-sets in the inner and outer foreskin

The impact of cell isolation technique and foreskin compartment, was additionally assessed on the co-expression CD4+CCR5+ cells in the different "Mϕ-like" subsets as follows;

"M1-like" macrophages

Based on earlier sections, "M1-like" Mϕ, were migratory and enriched in the inner foreskin. Furthermore, the "M-like" Mϕ had the highest frequency of CD4+CCR5+ cells. There were, however, no significant differences in the proportions of CD4+CCR5+ cells among migratory and non-migratory "M1-like" Mϕ in the inner and outer foreskin compartments (data not shown).

"M2-like" macrophages

"M2-like" Mϕ had the least mean frequency of CD4+CCR5+ cells compared to other Mϕ subsets as shown in Figure 46. Unlike "M1-like" Mϕ, described above, CD4+CCR5+ "M2-like" Mϕ were 1.6-fold more frequent in non-migratory cells (31.95 % ± 20.39 %), compared to migratory cells (19.56 % ± 14.04 %; $p = 0.0002$) as shown in Figure 47 below. There were, however no differences in the proportions of CD4+CCR5+ cells in "M2-like" Mϕ by FS compartment (data not shown).

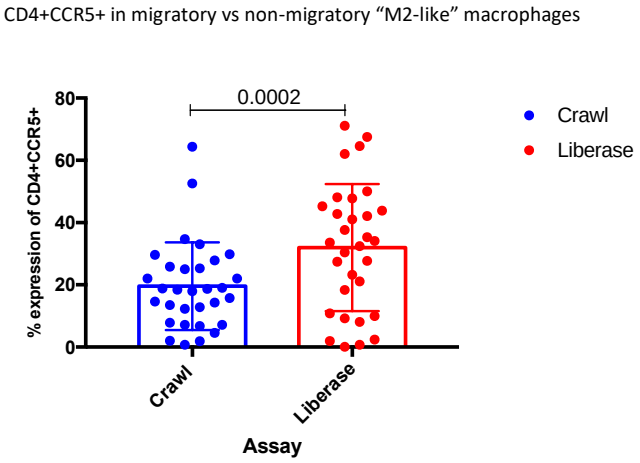

Figure 47. ***Proportions of markers of HIV susceptibility (CD4+CCR5+) in migratory and non-migratory "M2-like" macrophages from the inner and outer foreskin*** *Proportions of CD4+CCR5+ in migratory and non-migratory "M2-like" macrophages using multi-parameter flow ((n=31). The Wilcoxon test was used to compute p values.*

"M1/M2" Intermediate states

Although "M1" and "M2" intermediates constituted the least of "Mϕ-like" subsets while conversely portraying a high frequency of CD4+CCR5+ co-expression (Figure 47), it was not significantly differed by migration (58.3 % ± 32.48 %) and non-migration (49.34 % ± 36.56 %) (data not shown). However,

disparities were noted between the inner and outer foreskin compartments. In particular, the outer foreskin was 1.2-fold more constitutive of CD4+CCR5+ cells (59.77 % ± 34.13) than the inner foreskin (48.08 % ± 33.62 %; *p = 0.0174*) as shown in Figure 48 (a). Similarly, the mean frequency of CD4+CCR5+"M2" intermediates was 1.7-fold higher in the outer (59.73 % ± 34.18 %) compared to the inner foreskin (47.92 % ± 33.45 %; *p = 0.0249*) as shown in Figure 48 (b).

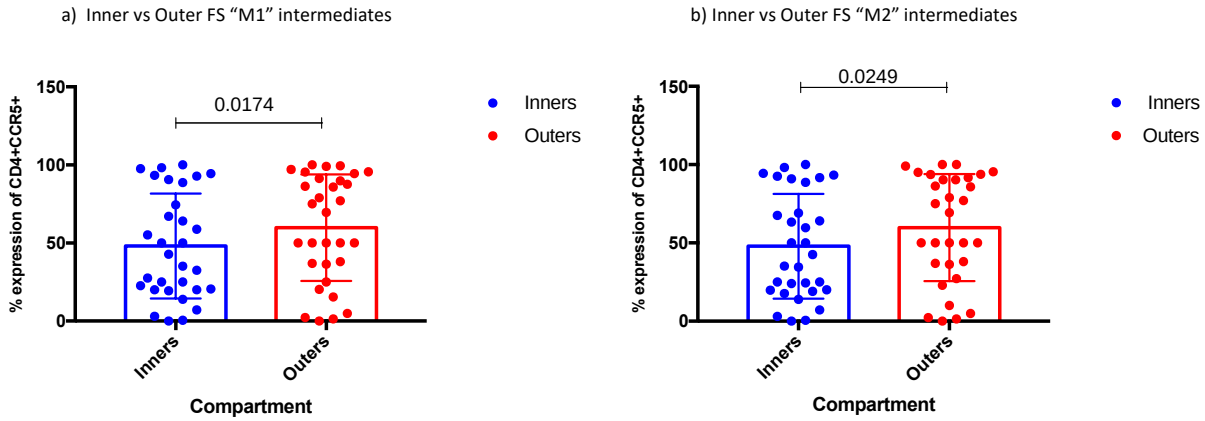

Figure 48. ***Proportions of CD4+CCR5+ cells in migratory and non-migratory "M1/2" intermediate macrophages from the inner and outer foreskin*** *Proportions of CD4+CCR5+ in M1/2 intermediates in the inner and outer foreskin, using multi-parameter flow cytometry* ***(a)*** *"M1" intermediates* ***(b)*** *"M2" intermediates (n=31). The Wilcoxon test was used to generate p values.*

CD169+ Macrophages

Although also a minor population as shown in Figure 46 above, CD169+ Mϕ portrayed a higher mean frequency of CD4+CCR5+ cells in non-migratory cells (34.81 % ± 28.44 %) compared to migratory cells (27.11 % ± 19.3 %), although without statistical significance (*p= 0.0842*) (data not shown).

CD3+ Macrophages

Similarly to "M1-like" Mϕ described above, there were no differences in the proportions of CD4+CCR5+ cells in migratory and non-migratory CD3+ Mϕ (data not shown). However, a trend similar to "M1/M2" intermediates described above was observed for CD3+ Mϕ, whereby CD4+CCR5 + cells were more enriched in the inner foreskin compared to the outer foreskin (data not shown).

Summary

There were higher proportions of CD4+CCR5+ cells in "M1-like" Mϕ and the "M1/M2" intermediates compared to "M2-like" Mϕ, CD169+ Mϕ and the CD3+ Mϕ.

Quantification of C lectin receptors:(CD206, CD209) and Siglec-1 (CD169)

The different "Mϕ-like" subsets were also assessed for the expression of attachment factors as shown in the gating strategy in Figure 43 (e) above. While a common trait was shared among "M2-like" Mϕ, CD3+ Mϕ and CD169+ Mϕ, where they were all more frequent in non-migratory compared to migratory cells; CLR expression also exhibited a pattern that was shared among the three Mϕ groups. Likewise, the intermediary "M1" and "M2" populations also exhibited identical attachment factor expression profiles that were additionally similar to "M1-like" Mϕ, as shown in Figure 49 below.

Although siglec-1 (CD169) was used to identify the CD169+ Mϕ subset as shown in Figure 43 (b) above, it was also expressed in lower proportions in other Mϕ subsets as shown in Figure 49 below. Among these low CD169 expressing subsets, the mean frequency of CD169+ cells was higher in "M2" intermediates (9.75 % ± 12.12 %), "M1" intermediates (8.70 % ± 9.92 %) and "M1-like" Mϕ (6.66 % ± 8.02 %) in comparison to "M2-like" Mϕ (3.98 % ± 4.66 %) and CD3+ Mϕ (2.67 % ± 4.45 %) albeit not statistically significant.

Similarly to CD169+ cells, the mean frequency of CD206+ cells was also higher in "M1" (56.64 % ± 28.40 %) , "M2" intermediates (56.14 % ± 28.13 %) and "M1-like" macrophages (40.22 % ± 25.71 %) compared to CD169+ Mϕ (35.32 % ± 21.52 %), "M2-like" Mϕ (31.3 % ± 29.16 %) as well as CD3+ Mϕ (18.85 % ± 18.63 %) as shown in Figure 49. However, these differences were trends that did show statistical significance.

Contrary to the mean frequencies of CD169+ and CD206+ cells being higher in "M1" like Mϕ and the "M1/M2" intermediates, the mean frequency of CD209+ cells was conversely higher in "M2-like" Mϕ (63.68 % ± 20.98 %), CD3+ Mϕ (34 % ± 19 %) and CD169+ Mϕ (54 % ± 20 %), among which were no significant differences.

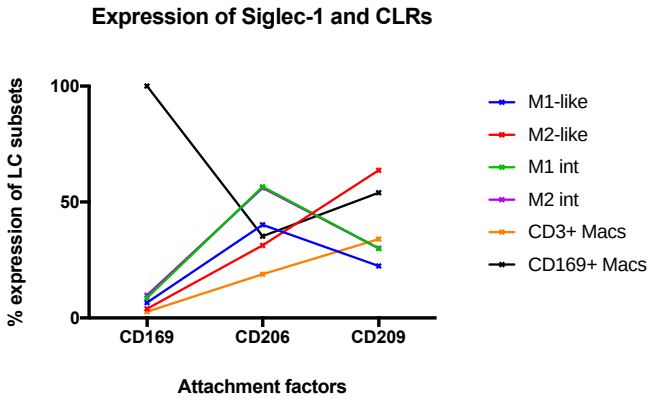

Figure 49. ***Proportions of HIV attachment factors in migratory and non-migratory foreskin "Macrophage-like" cells from the inner and outer foreskin.*** *Proportions of CD169 (Siglec-1), CD206 (Mannose Receptor) and CD209 (DC-SIGN) in "M1-like" macrophages, "M2-like" macrophages, "M1/2" intermediates, CD3+ macrophages and CD169+ macrophages. (n=31). Statistics were generated using two-way ANOVA using the Tukey's multiple comparisons test and adjusted p values.*

Impact of cell isolation technique on CLRs and Siglec-1 in "macrophage-like" cells

As shown above, the mean frequency of CD209+ cells was the highest in "M2-like "Mϕ, CD3+ Mϕ, and CD169+ Mϕ, all previously descibed as predominantly non-migratory. Corroborative to this, the overall mean frequecy of CD209+ cells was 1.4-fold higher in non-migratory cells (44.8 % ± 23.51%) compared to migartory cells (32.21 % ± 15.02 %; $p = 0.0020$) as shown in Figure 50 below.

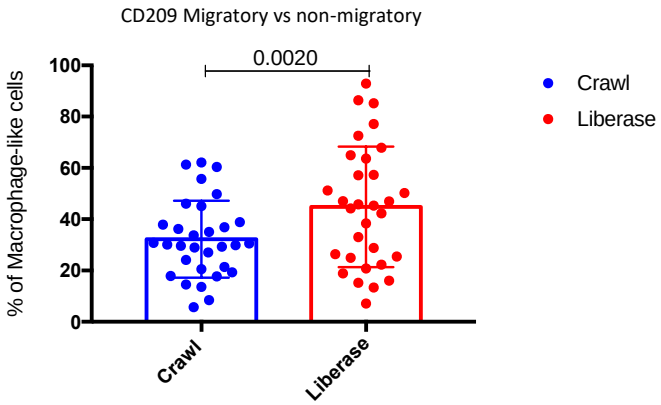

Figure 50. ***Proportions of DC-SIGN in migratory and non-migratory macrophage-like subsets.****, Proportions of CD209+ cells in migratory and non-migratory "macrophage-like" cell subsets (n =31). The Wilcoxon test was used to compute p values.*

Impact of foreskin compartment on CLRs and Siglec-1 in "macrophage-like" cells

There were no differences in the expression of attachment factors by the different "Mϕ-like" subsets, in the inner and outer foreskin except for CD209 that was more abundant in the outer forekin (41. 66 % ± 16.13 %) compared to the inner forekin (35.4 % ± 20.54 %; $p = 0.0374$) as shown in Figure 51 below.

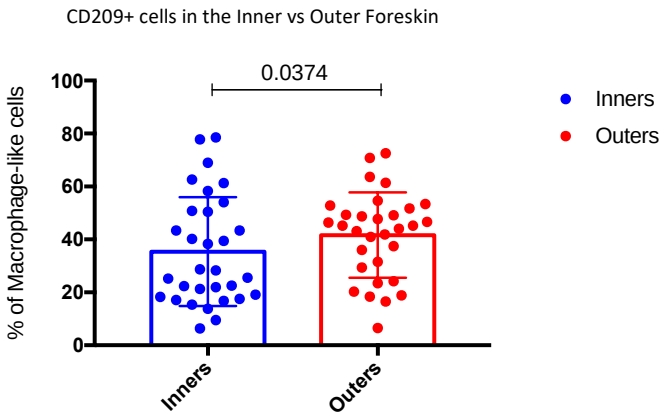

Figure 51. ***Proportions of DC-SIGN in migratory and non-migratory macrophage-like subsets from the inner and outer foreskin.*** *Proportions of CD209 in migratory and non-migratory "macrophage-like" subsets (n =31). The Wilcoxon test was used to compute the p value.*

Quantification of markers of Maturation

While the co-expression of HLA-DR and CD80/86 was used as a proxy for the identity of "M1-like" Mϕ and "M1"intermediates as described above and shown in Figure 43 (c); it was additionally used to assess maturity in CD3+ Mϕ and CD169+ Mϕ.

Similarly to LCs described above, the mean frequency of migratory HLA-DR+CD80/86+CD3+ Mϕ was higher (7.92 % ± 8.19 %) than non-migratory HLA-DR+CD80/86+CD3+ Mϕ (4.79 % ± 8.27 %; $p = 0.0066$) as shown in Figure 52 (a) below. In addition, the inner foreskin exhibited higher frequencies
of these HLA-DR+CD80/86+CD3+ Mϕ (8.45 % ± 11.26 %) compared to the outer foreskin, where they were 2-times less frequent (4.25 % ± 4.78 %; $p = 0.0177$) as shown in Figure 52 (b). In like-manner, migratory HLA-DR+CD80/86+CD169+ Mϕ were more frequent (24.46 % ± 31.56 %) than non-
migratory HLA-DR+CD80/86+CD169+ Mϕ (15.72 % ± 25.92 %) although without statistically significant differences (data not shown) and without any disparities in the inner and outer foreskin.

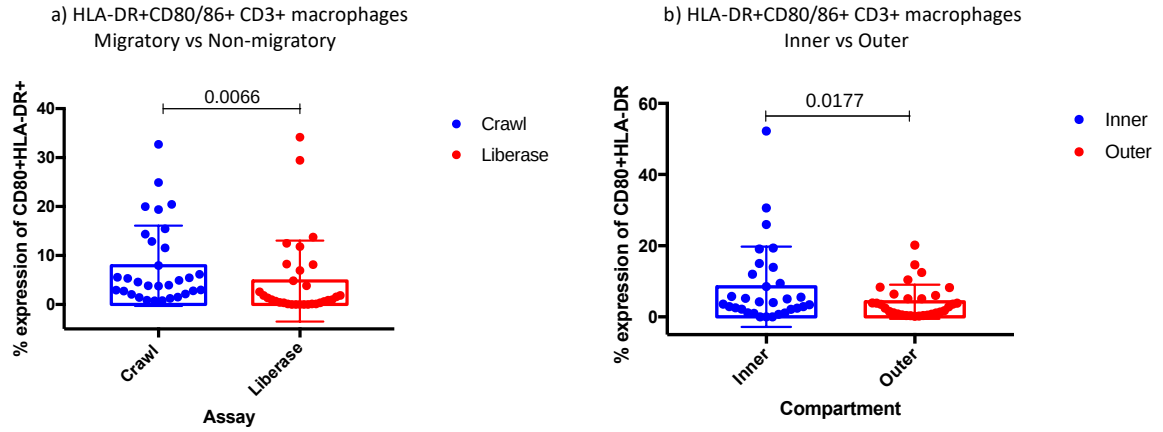

Figure 52. ***Assessment of the activation states of migratory and non-migratory foreskin CD3+ macrophages from the inner and outer foreskin*** ***(a)*** *Proportions of HLA-DR+CD80/86+ in migratory vs non-migratory CD3+ macrophages* ***(b)*** *Proportions of HLA-DR+CD80/86+ in CD3+ macrophages in the inner vs outer foreskin (n=31). The Wilcoxon test was used to generate p values.*

Summary

HLA-DR+CD80/86+ "Mϕ-like" subsets were more frequent cells migrating from the inner foreskin.

1.5.3.2 Identification of “macrophage” states using unsupervised cell clustering

As described in the Introduction, the Mϕ component of myeloid cells is comprised of non-static heterogenous populations that differ based on a myriad of factors inclusive of external stimuli and tissue specificity. Using manual gating, we were also able to identify heterogenous foreskin Mϕ in different states, although this may have not fully captured the complexity and fluidity of these cells. As such, we sought to further elucidate Mϕ heterogeneity, through an unbiased approach using FlowSOM and hierarchical clustering as described in the LC section above.

Marker expression profile of migratory and non-migratory foreskin “Mϕ” in the I and O FS

Dimensionality reduction (tSNE) was also used to visualise the expression of all markers in the manually pre-gated cells from the LC-exclusionary, CD14+/-CD11c+/- gate, whereby marker expression intensities transitioned from low (green) to high (red) as shown in Figure 53 below. The different Mϕ-like clusters portrayed differential expression of all markers except CD206 that was uniformly expressed and CD207 that was not expressed as shown in Figure 53.

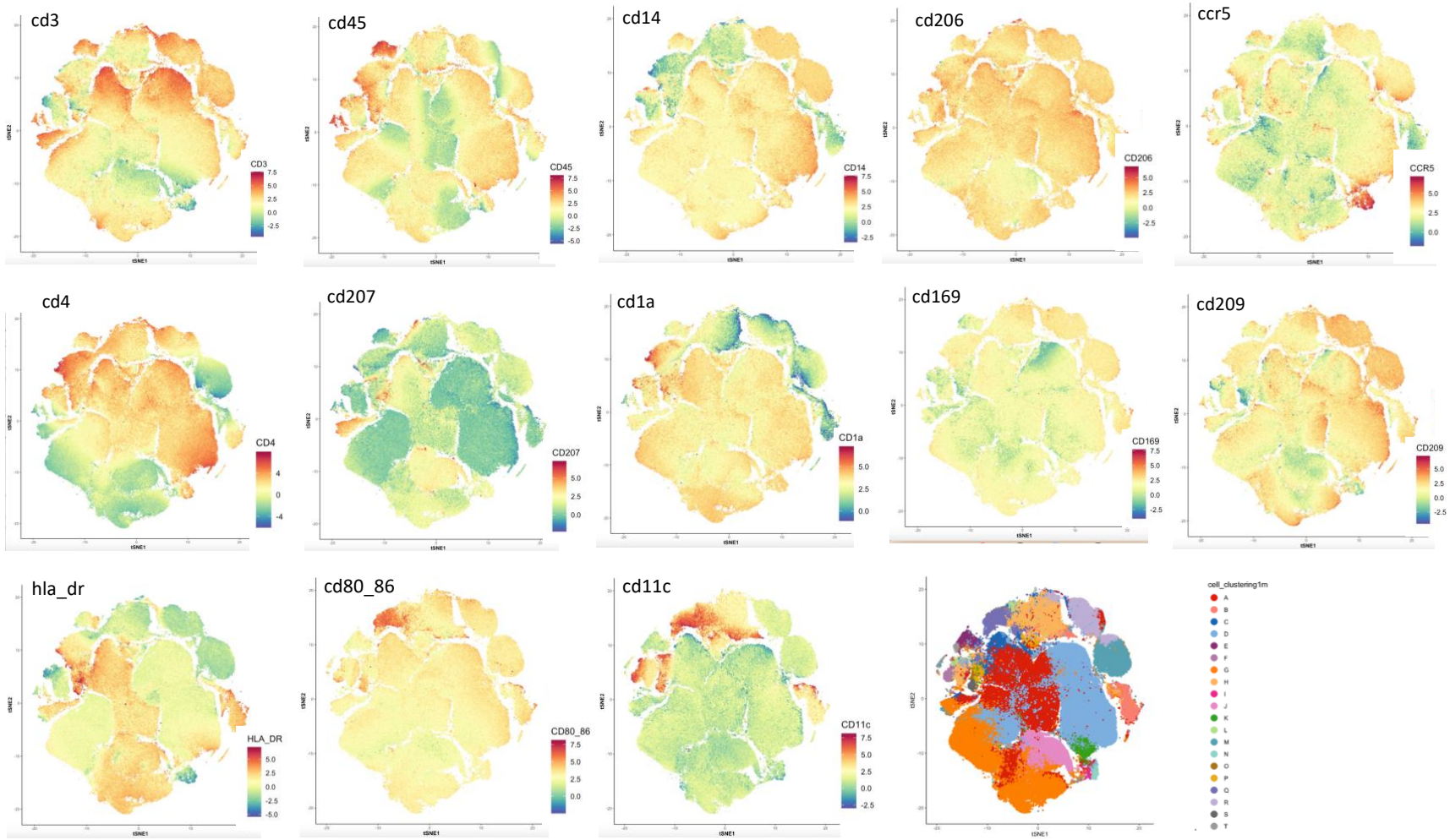

Figure 53. ***Assessment of the marker expression profiles of migratory and non-migratory "Macrophage-like" cells of the inner and outer foreskin using tSNE plots generated by non-biased, computerised clustering.*** *tSNE plots displaying the differential expression of : CD1a, CD3, CD4, CD11c, HLA-DR, CD80/86, CD206, CD14, CCR5, CD207, CD45, C169 and CD209.The color spectrum denotes increasing intensities of marker expression, ranging from green which represents no to low marker expression while red is high marker expression*

Optimization of Mϕ cluster numbers

Using the elbow criterion strategy, the point of minimum relative change in CDF (k=20), was considered the optimal k for clustering Mϕ as shown in Figure 54 below.

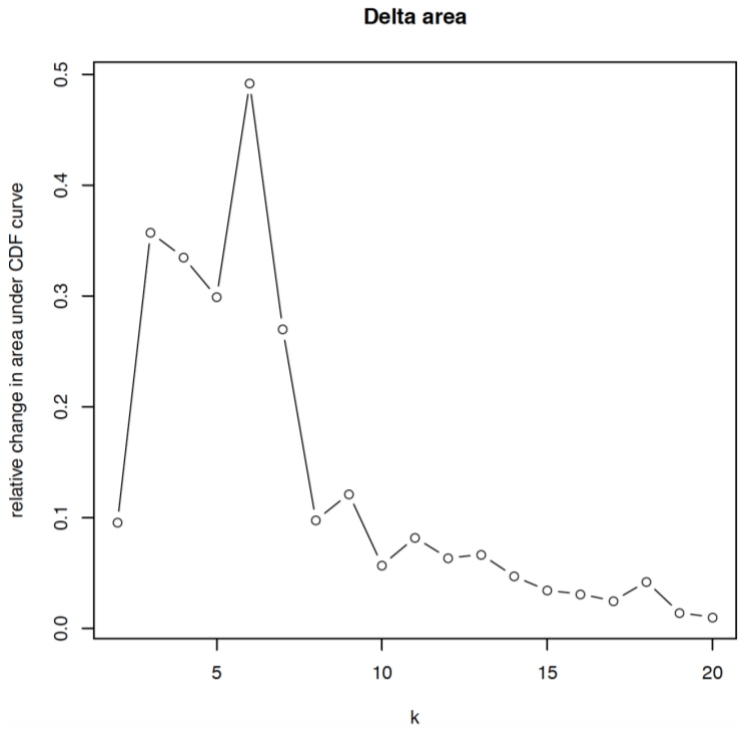

Figure 54. ***Determination of the optimal number of clusters****. Number of clusters optimal for unsupervised clustering of macrophage-like cells using k means*

Therefore, 20 “macrophage-like” clusters were identified and mapped onto tSNE as shown in Figure 55 below.

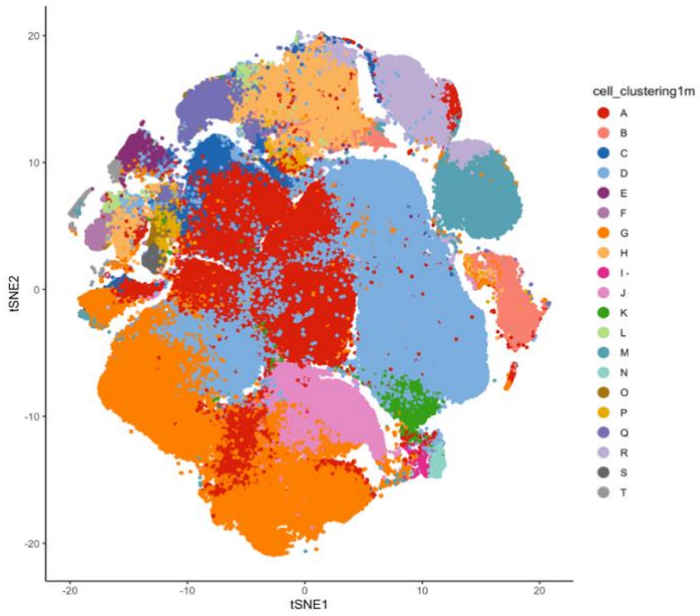

Figure 55. ***Determination of the different clusters within the migratory (Crawl) and non-migratory (Liberase) CD14/ CD11c cells of the inner (I) and outer (O) foreskin, using colored tSNE plot generated by non-biased, computerised clustering.*** *tSNE plot demonstrating the different "Macrophage-like" clusters shown in the plot as different colours and demarcated by migration potential (Crawl/Lib) and compartment (Inner/Outer)*

Identification of "macrophage-like" clusters

Of the 20 "Mϕ-like" clusters, the most frequent were identified as core clusters and were inclusive of Cluster G (*orange;* 14.96 %), Cluster A (*red;* 22.34 %) as well as Cluster D (*sky blue;* 45.68 %) that constituted 82.98 % in total. Core clusters were observed to display phenotypic relatedness using dendrograms from hierarchical clustering as shown on the left of Figure 56. Cluster D was CD14+CD1a+CD4+, and additionally co-expressed "M2-like" Mϕ markers, CD206+CD209+CD11c- with dim Siglec-1 (CD169) co-expression as illustrated in Figure 56 below. Cluster A, although similarly a CD14+CD1a+CD4+CD169^{dim}CD11c- Mϕ cluster, had lower expression intensities of CD206 and CD209 compared to Cluster D as shown in Figure 56. Notably, both clusters were devoid of the peptide antigen presentation and co-stimulatory markers (HLA-DR-CD80/86-). Also phenotypically related to these two clusters, was Cluster G; a similarly CD14+CD1a+CD11c- M ϕ cluster that co-expressed the same set of markers as Cluster A although without CD4 co-expression as

shown in Table 3 below. The core Mϕ clusters were therefore either CD4+CCR5- (Cluster A and Cluster D) or CD4-CCR5- (Cluster G) and thus, less susceptible to HIV infection with R5 using HIV strains.

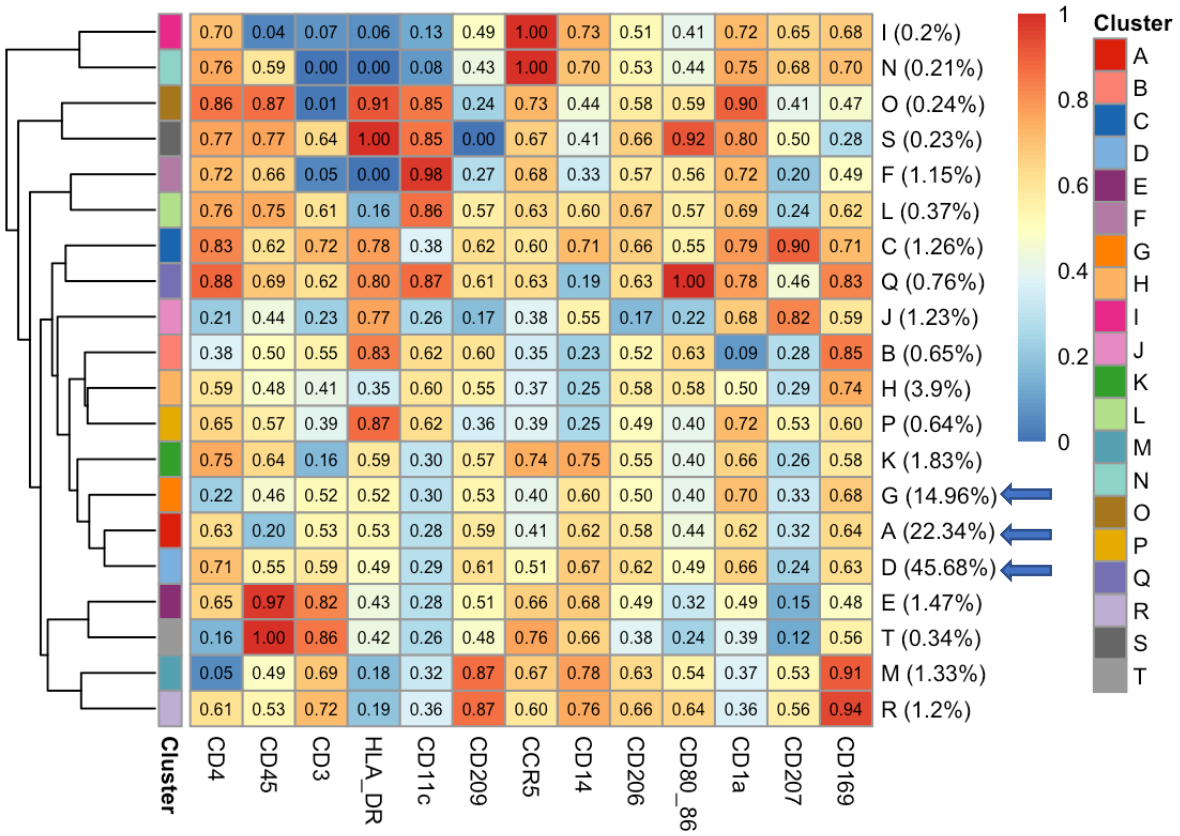

Figure 56. ***Heatmap of the median marker intensities across the 20 "Mϕ-like" clusters obtained with FlowSOM****. Heatmap colour represents the median of the arcsinh, 0-1 transformed marker expression calculated over cells from all the "Mϕ-like" cells. The heat varies from blue (low expression) to red (high expression) and 0.60 was used as the cut-off. Dendrogram represents hierarchical similarity according to consensus clustering. Annotation bar is colored according to the "Mϕ-like" clusters. The relative Cluster size is shown in next to the different populations*

Meanwhile, CD4+CCR5+ co-expression was observed in the less frequent, sparsely distributed clusters constitutive of; Cluster R (*violet;* 1.2 %), Cluster E (*dark purple*;1.47 %), Cluster K (*green*; 1.83 %),

Cluster I (*hot pink*; 0.2 %), Cluster N (*turquoise*; 0.21 %), Cluster O (*brown*; 0.24 %), Cluster S (*grey*; 0.23 %), Cluster F (*mauve*; 1.15 %), Cluster L (*lime*; 0.37 %), Cluster C (*blue*; 1.26 %) and Cluster Q (*lavender*; 0.76 %). Overall, the CD4+CCR5+ clusters accounted for 8.92 % of the Mϕ population as shown in Table 3 below.

Table 3. Phenotypes of the different "macrophage-like" clusters

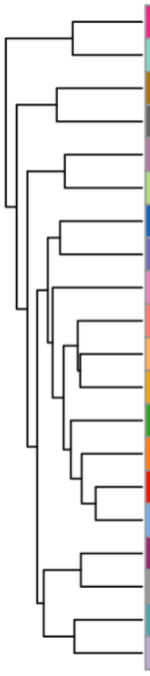

Cluster	Phenotype	%
I	CD4+CD45-CD3-HLA_DR-CD11c-CD209-CCR5+CD14+CD206-CD80_86-CD1a+CD207+CD169+	0.20 %
N	CD4+CD45-CD3-HLA_DR-CD11c-CD209-CCR5+CD14+CD206-CD80_86-CD1a+CD207+CD169+	0.21 %
O	CD4+CD45+CD3-HLA_DR+CD11c+CD209-CCR5+CD14-CD206-CD80_86-CD1a+CD207-CD169-	0.24 %
S	CD4+CD45+CD3+HLA_DR+CD11c+CD209-CCR5+CD14-CD206+CD80_86+CD1a+CD207-CD169-	0.23 %
F	CD4+CD45+CD3-HLA_DR-CD11c+CD209-CCR5+CD14-CD206-CD80_86-CD1a+CD207-CD169-	1.15 %
L	CD4+CD45+CD3+HLA_DR-CD11c+CD209-CCR5+CD14+CD206+CD80_86-CD1a+CD207-CD169+	0.37 %
C	CD4+CD45+CD3+HLA_DR+CD11c-CD209+CCR5+CD14+CD206+CD80_86-CD1a+CD207+CD169+	1.26 %
Q	CD4+CD45+CD3+HLA_DR+CD11c+CD209+CCR5+CD14-CD206+CD80_86+CD1a+CD207-CD169+	0.76 %
J	CD4-CD45-CD3-HLA_DR+CD11c-CD209-CCR5-CD14-CD206-CD80_86-CD1a+CD207++CD169-	1.23 %
B	CD4-CD45-CD3-HLA_DR+CD11c+CD209+CCR5-CD14-CD206-CD80_86+CD1a-CD207-CD169+	0.65 %
H	CD4-CD45-CD3-HLA_DR-CD11c+CD209-CCR5-CD14-CD206-CD80_86-CD1a-CD207-CD169+	3.90 %
P	CD4+CD45-CD3-HLA_DR+CD11c+CD209-CCR5-CD14-CD206-CD80_86-CD1a+CD207-CD169+	0.64 %
K	CD4+CD45+CD3-HLA_DR-CD11c-CD209-CCR5+CD14+CD206-CD80_86-CD1a+CD207-CD169-	1.83 %
G	CD4-CD45-CD3-HLA_DR-CD11c-CD209-CCR5-CD14+CD206-CD80_86-CD1a+CD207-CD169+	14.96 %
A	CD4+CD45-CD3-HLA_DR-CD11c-CD209-CCR5-CD14+CD206-CD80_86-CD1a+CD207-CD169+	22.34 %
D	CD4+CD45-CD3-HLA_DR-CD11c-CD209+CCR5-CD14+CD206+CD80_86-CD1a+CD207-CD169+	45.68 %
E	CD4+CD45+CD3+HLA_DR-CD11c-CD209-CCR5+CD14+CD206-CD80_86-CD1a-CD207-CD169-	1.47 %
T	CD4-CD45+CD3+HLA_DR-CD11c-CD209-CCR5+CD14+CD206-CD80_86-CD1a-CD207-CD169-	0.34 %
M	CD4-CD45-CD3+HLA_DR-CD11c-CD209+CCR5+CD14+CD206+CD80_86-CD1a-CD207-CD169+	1.33 %
R	CD4+CD45-CD3+HLA_DR-CD11c-CD209+CCR5+CD14+CD206+CD80_86+CD1a-CD207-CD169+	1.20 %

2 *Table 3 showing marker expression per "macrophage-like" cluster. Dendrogram on the right shows cluster relatedness according to marker expression intensities. 1st column is cluster name derived from the corresponding heatmap in Figure 56. Phenotype column shows cluster phenotype as per the 0.6 cut-off from the heatmap. The frequencies of each cluster are shown in the last column denoted as %.*

Interestingly, the CD4+CCR5+ Clusters, S and Q, also intensely co-expressed HLA-DR, CD80/86 and CD11c (markers typically used to identify inflammatory M1 Mϕ) as shown in Figure 56 above . They were additionally CD45+CD206+CD1a+, dimly co-expressed CD3 and differed in the expression of CD209 and CD169. Although ubiquitously distributed among the different Mϕ clusters, CD169, CD14 and C209 were more intensely co-expressed in Cluster M (*teal*; 1.33 %) and Cluster R (*violet;* 1.2 %). Cluster M was however, CD4-CCR5+ as shown in Table 3.

Cluster E (*dark purple;*1.47 %) and Cluster T (*light grey;* 0.34 %) were also of interest due to the intense co-expression of CD45+CD3+ relative to all the other clusters, although Cluster T was CD4-CCR5+. Other than the shared CD45+CD3+CCR5+CD4+/- phenotype, these two clusters only co-expressed CD14, and were therefore unique from all other "Mϕ-like" subsets as shown in Table 3.

Langerin+ Mϕ clusters, Cluster C (*blue;* 1.26 %) and Cluster J (*light pink;* 1.23 %), were also identified as shown in Table 3. While both clusters co-expressed CD1a+CD207+HLA-DR+, similarly to LCs, Cluster C additionally co-expressed M2 Mϕ markers (CD14+CD209+CD206+) as shown in Table 3

2

above. Cluster I (*hot pink;* 0.2 %) and Cluster N (*turquoise;* 0.l2 %), were also identified as Langerin+ clusters that could not fit any of the conventional Mϕ profiles.

Migratory and non-migratory "macrophage-like" cell clusters in the inner and outer foreskin

Macrophage clusters were further stratified according to assay and compartment in order to identify migratory and non-migratory clusters in the inner and outer foreskin as shown in Figure 57 below. With the exception of Cluster Q (*lavender*) and Cluster M (*teal*), that were diminished in cells migrating from the inner foreskin (blue arrows), migratory Mϕ clusters were more abundant than non-migratory Mϕ clusters as shown in Figure 57 below. Noteworthy, all the CD4+CCR5+ clusters (R, E, K, I, N, O, S, F, L, C and Q) were minor (circled in black), closely proximal to each other and more frequent in cells migrating from the inner and outer foreskin compared to non-migratory cells. However, this was in exception of the CD169hi Cluster R(*violet*) that was alternatively closer to the other CD169hi cluster, M (*teal*). The miscellaneous CCR5hi clusters (Cluster I and Cluster N), also clustered away from the other CD4+CCR5+ clusters, and were more proximal to Cluster K (*green*).

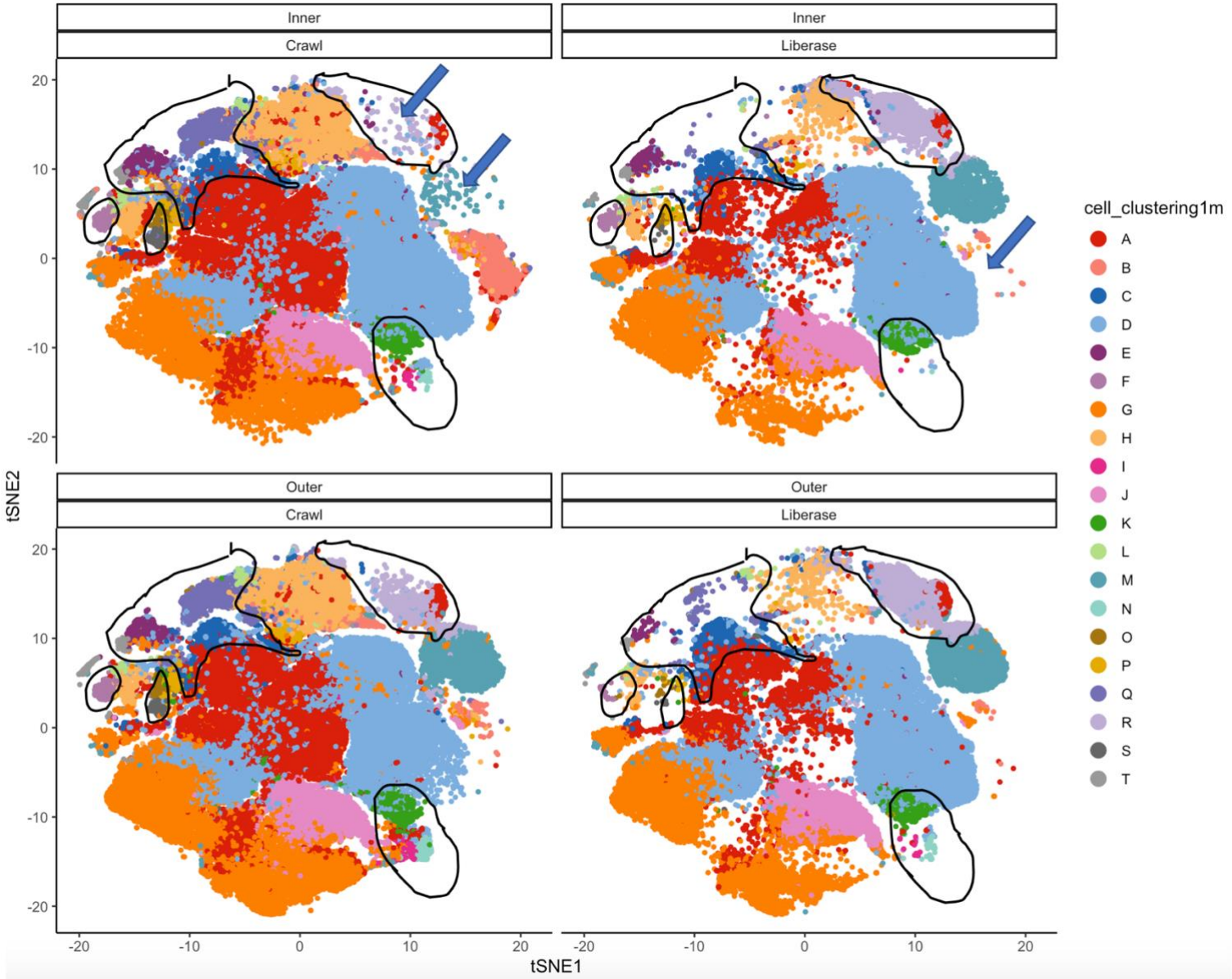

Figure 57. ***Determination of the different clusters within the migratory (Crawl) and non-migratory (Liberase) "macrophage-like" cells of the inner (I) and outer (O) foreskin, using colored tSNE plots generated by non-biased, computerised clustering.*** *tSNE plots demonstrating the different "Macrophage-like" clusters shown in the plot as different colours and demarcated by migration potential (Crawl/Lib) and compartment (Inner/Outer)*

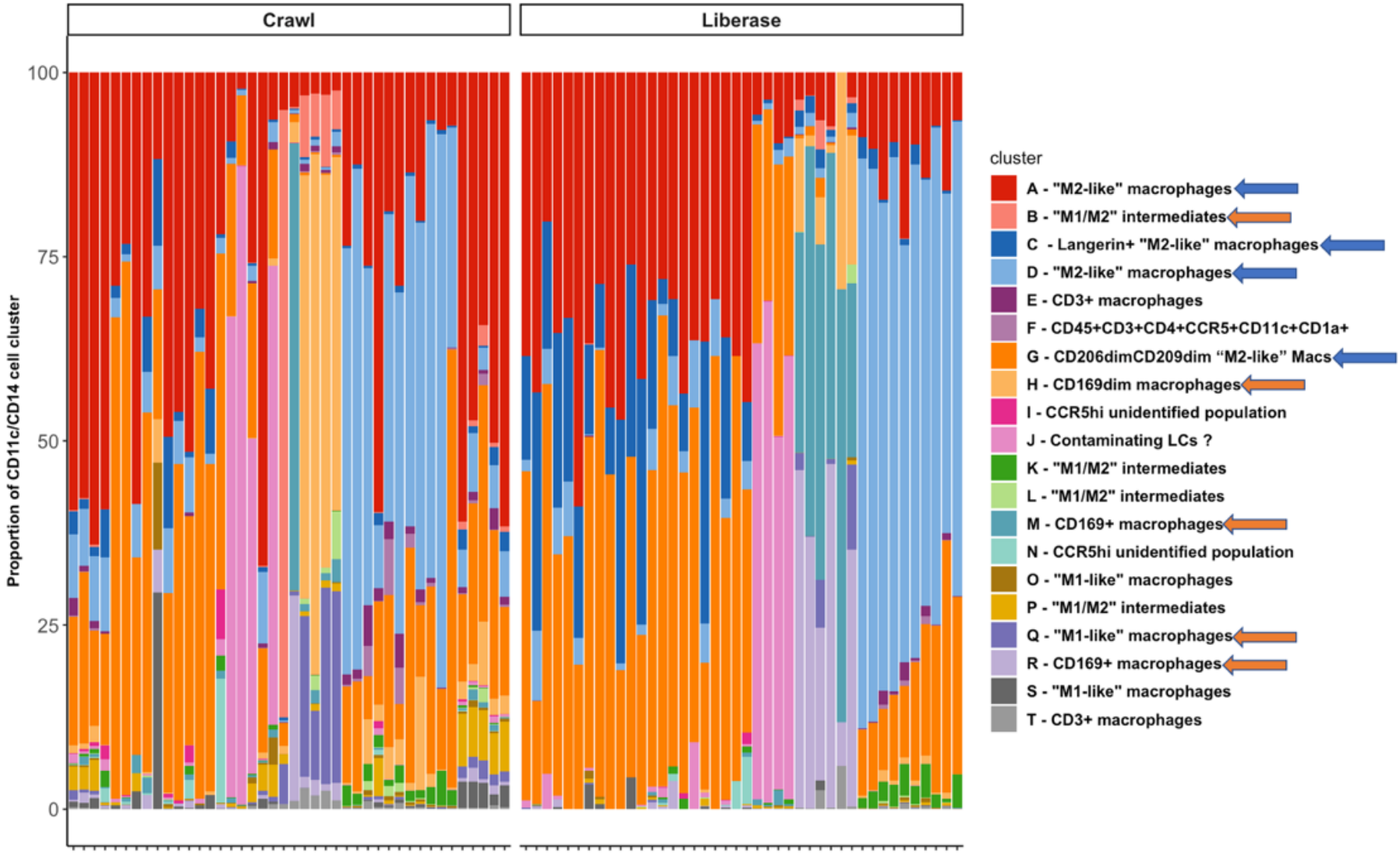

Figure 58. ***Proportions of the different migratory and non-migratory "macrophage-like" clusters in the inner (I) and outer (O) foreskin, generated by non-biased, computerised clustering.*** ***(a)*** *Migratory foreskin "macrophage-like" subsets (Crawl) and non-migratory "macrophage-like" subsets (Liberase), corresponding to the tSNE plots were plotted and analysed for differential abundance.* ***(b)*** *Proportions of migratory and non-migratory LC clusters* ***(c)*** *Proportions of "macrophage-like" clusters in the inner and outer foreskin. Statistics were generated using the Wilcoxon t tests and false discovery rates (fdr) used to adjust p values for multiple comparisons*

Interestingly, the core clusters did not differ by both migration (blue arrows in Figure 58, or with compartment. In particular, Cluster A (*red*), although more frequent in migratory cells as shown in Figures 58, the difference was not statistically significant and additionally portrayed similar distribution in the inner and outer foreskin (Appendix Figure A16). Similarly, Cluster D (*light blue*) was more frequent in non-migratory cells as shown in Figures 58, albeit statistically insignificant. Lastly, Cluster G (*orange*), was more frequent in cells in non-migratory inner foreskin cells, although non-significantly so (data not shown). However, Cluster C (*blue*), although comparatively less frequent than the three core clusters, was more frequent in non-migratory cells compared to migratory cells (*adj p = 0.0041*) (Appendix Figure A16).

Only the minor clusters (orange arrows in Figure 58), were significantly more frequent in migratory cells in comparison to non-migratory cells : Cluster B (*adj p<0.0001*), Cluster E (*adj p<0.0001*), Cluster F (a*dj p=0.00017*), Cluster H (*adj p=0.00036*), Cluster I (*adj p=0.00098*), Cluster L (*adj p=0.0021*), Cluster M (*adj p=0.018*), Cluster N (*adj p=0.0093*), Cluster O (*adj p<0.0001*), Cluster P (*adj p<0.0001*), Cluster Q (*adj p=0.00038*), Cluster S (*adj p<0.0001*) and Cluster T (*adj p=0.0024*) (data in Appendix A16). However, the proportions of these minor clusters did not portray any disparities in the inner and outer foreskin (data not shown).

1.6 IMMUNOPHEOTYPING SUB-CONCLUSION

The foreskin was observed to harbor heterogenous myeloid cell subsets. These were immunophenotyped and classified into i) Langerhans Cells and ii) "Mϕ -like" cells, using manual gating and unsupervised clustering of flow cytometry data. LCs were identified as a rare population while "Mϕ -like" cells were comparatively more frequent as shown in Figure 59 below. Therefore, the foreskin epidermal myeloid cells were predominated by "Mϕ -like" cells, particularly the non-migratory "M2-like" Mϕ from the inner foreskin as shown in Figure 59 below (Lib I) as well as through unsupervised clustering above.

"M1-like" Mϕ and "M1/M2" intermediates were less frequent, although with comparatively higher frequencies of CD4+CCR5+ cells, than "M2-like" Mϕ. Moreover, "M1-like" Mϕ and the "M1/M2" intermediates were enriched migratory cells isolated from the inner foreskin as shown in Figure 59 below. Non-conventional CD3 expressing cells were also observed in both LCs and macrophages, although more highly frequent in macrophages.

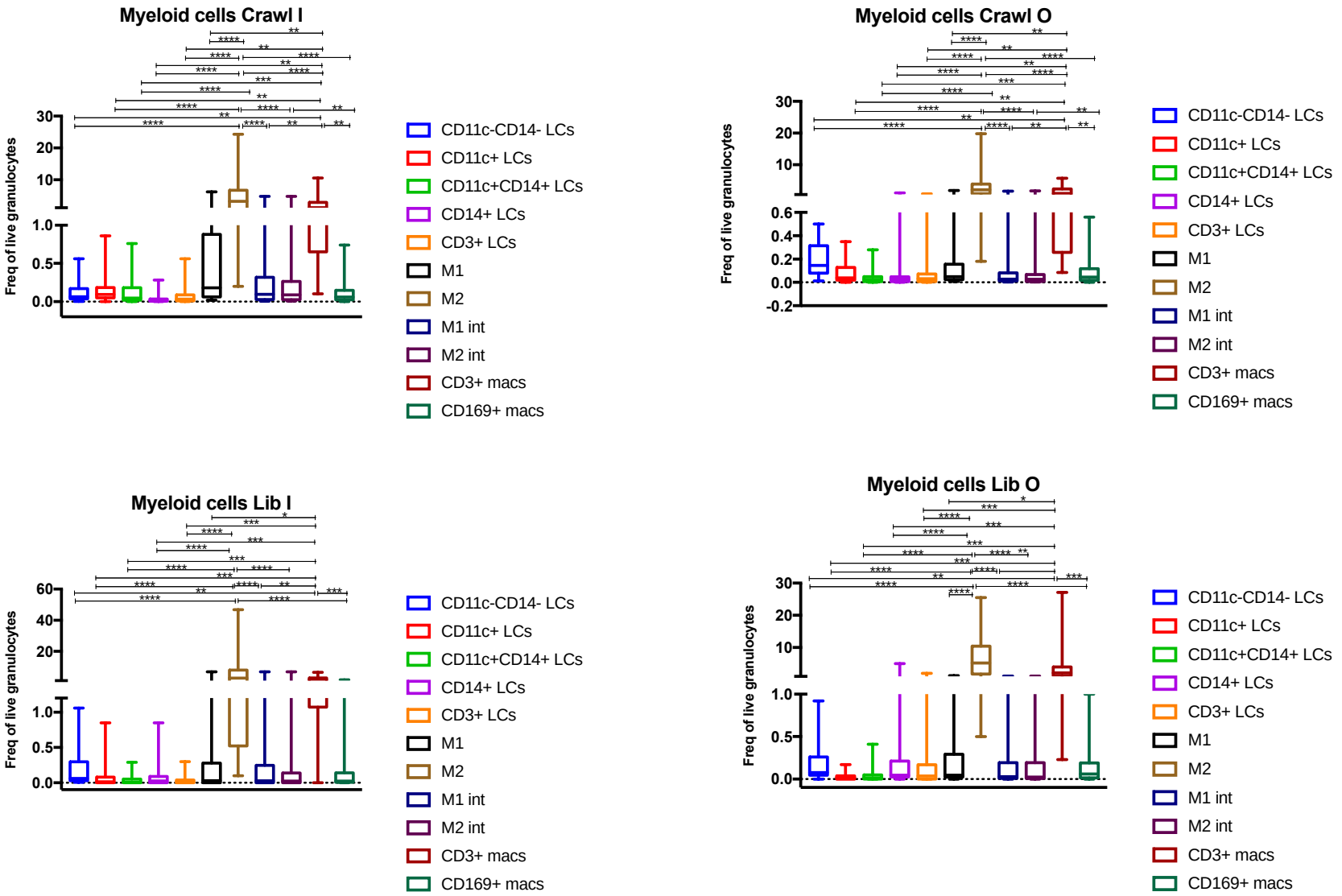

Figure 59. ***A summary of proportions and distributions of overall migratory and non-migratory LCs and "macrophage-like" subsets isolated from the inner and outer foreskin.*** *Migratory and non-migratory foreskin myeloid cells present in different compartments were identified and analysed as follows:* ***(i)*** *Inner foreskin migratory myeloid cells (Crawl I)* ***(ii)*** *Outer foreskin migratory myeloid cells (Crawl O)* ***(iii)*** *Inner foreskin non-migratory myeloid cells (Lib I) and* ***(iv)*** *Outer foreskin non-migratory myeloid cells (Lib O) (n=31). Statistics were generated using two-way ANOVA using the Tukey's multiple comparisons test and adjusted p values. *p <0.05; **p < 0.01; ***p < 0.001; ****p < 0.0001*

Notably, foreskin LCs were HLA-DR+CD4+, with differential co-expression of CD80/86 and CCR5 that varied according to migration and non-migration. There were higher proportions of HLA-DR+CD80/86+ cells in migratory LCs compared to non-migratory LCs, particularly in the inner foreskin. However, CD11c+CD14+ LCs that migrated from the inner foreskin were of particular interest owing to the highest mean frequency of CD4+CCR5+, HLA-DR+CD80/86+ and CD206+, in comparison to all the other LC subsets. Note, HLA-DR+CD80/86+ co-expression was also high CD3+ LCs and CD11c+ LCs. However, in contrast to HLA-DR and CD80/86 that were comparatively less frequent in non-migratory cells; CLRs, especially DC-SIGN, were more frequent in non-migratory foreskin LCs. In particular, CD14+ LCs displayed the highest proportions of CLR enamored cells, although with a lower mean frequency of CD206+ cells. This was corroborative with the non-migration status of CD14+ LCs. Furthermore, DC-SIGN was least observed in CD11c+ LCs, identified as a highly migratory LC subset.

The foreskin, therefore harbours heterogenous populations of myeloid cells differentially expressing HIV susceptibility markers and attachment factors and of different maturation states. CD11c+CD14+ LCs, CD14+ LCs, CD3+ LCs, "M1-like" Mϕ and the "M1/M2" intermediates through their displayed high CD4+CCR5+ co-expression were thus identified as potential HIV targets in the foreskin.

CHAPTER 2 – Ex Vivo HIV-1 INFECTION OF FORESKIN MYELOID CELLS

2.0 BACKGROUND INFORMATION

2.0.1 Relevance of LCs, DCs and macrophages in HIV pathology

Owing to their phenotypic features, immunological roles and epithelial location; myeloid cells are reportedly the initial cells with which HIV establishes contact[170] . Although these interactions have been extensively studied, the question of productive HIV infection, remains an ongoing bone of contention. Productive infection (*cis* infection) is defined as the ability of HIV to engage with the CD4 receptor and co-receptor on the host cell's surface, using the virus's glycoproteins in a process that culminates in HIV replication, generation of progeny virions and in some instances, host cell lysis[60]. Many authors have argued that myeloid cells do not support *cis* infection and only serve as cargo that disseminates HIV to CD4+ T cells, in a mechanism referred to as *trans* infection [20,23,25,26,190].

However, there is over two-decades of data showing that myeloid cells support *cis* infection and persist over extended periods of time while evading immune clearance and causing chronic inflammation coupled with immune exhaustion [28,29,32,60,72,120,133]. Although still controversial, earlier reports were also suggestive of HIV replication in LCs whereby developmental forms of HIV were shown to bud off the cell surface and mature virions detected in intracytoplasmic LC vacuoles alongside viral proteins[41,133]. In more recent studies, replication competent HIV has also been isolated from co-culture experiments of uninfected monocytes with LCs isolated from HIV+ skin biopsies[112]. However, it has been argued that HIV infected LCs witnessed during chronic infection were previous circulatory monocytes that were infected in blood prior to being seeded in skin epithelia and differentiating to CD14+ "LC like" cells[112]. Other authors have argued adult epidermal LCs to mainly derive from self-renewing precursors that seed the epidermis in infancy, arising from monocytes only as temporal replenishment following inflammation induced ablation, thus affirming LC infection[41]. More recently, DC subsets have also been reported to support productive infection by both lab-adapted R5 and X4 HIV strains including the recently described epidermal CD11c+ DCs[29,72] and vaginal epithelial dendritic cells (VEDCs)[120].

However, only 1-3 % of DCs have been shown to support productive infection due to impediments inclusive of host restriction factors, lower HIV receptor densities (compared to CD4+ T cells) and CLR-mediated abrogation[22,25,28]. Despite the low infectivity, DC infection is impactful with less than 0.1% of productively infected DCs being required to infect CD4+ T cells. Moreover, DC *trans* infection, has been shown to account for over 90% of HIV dissemination to CD4+ T cells, even in the absence of productive infection, in cervico-vaginal samples[20,26,69]. Likewise, Mϕ and LCs have also been shown to

endocytose virions and to subsequently disseminate to CD4+ T cells through varied cell-cell transmission mechanisms (described below). In LCs, this is reportedly relevant to CCR5 using HIV, since it has been shown that LCs can effectively restrict CXCR4 using HIV through langerin mediated abrogation and the restriction factor, TRIM5a[24,28,191].

Myeloid cells therefore play critical roles in HIV pathology, inclusive of both *cis* and *trans* infection as well as host restriction [24,28]. Understanding molecular markers that govern the relationship between HIV and the myeloid cell would therefore be key for the design of myeloid cell based therapy. Further to this, "Mϕ-like" cells were shown to constitute the bulk of foreskin epithelial myeloid cells as shown and described in Chapter 1 above. Understanding the relationship of these cells with HIV is therefore important, particularly due to the hypothesis that Mϕ are contributors of the HIV reservoir, a stumbling block in anti-retroviral therapy (ART).

2.0.2 HIV transmission mechanisms

The transmission and spread of HIV is largely orchestrated by the virion's ability to override much of the immuno-modulatory components of the immune system. While this has been documented in CD4+ T cells, myeloid cells have been implied to facilitate the spread of HIV using similar strategies. HIV manipulates the immunological and structural components of the host cells such as i) immunological synapses that establish between APCs and T lymphocytes during antigen presentation, membranal protrusions such as the tunneling nanotubal filaments (TNTs) that facilitate cellular cross talks as well as immunological processes such as phagocytosis[20,21,119,192]. Integral to all these immunological and structural components, is the wide repertoire of myeloid cell surface attachment factors that HIV hijacks and, through its own fusogenic properties, use to establish attachment and entry[22]. As described in Chapter 1, such attachment factors are inclusive of C-type lectin receptors (CD206 and CD209) as well as Siglec-1 (CD169), shown as abundantly co-expressed in foreskin LCs and Mϕ in Figures 37 and 53 above. Although not assayed for in this study, integrins such as α4β7[22,25] and those from the immunological synapse (LFA-1α/β) including dis-integrins ICAM-1/3 are all similarly important in the context of HIV attachment. While the level of cell surface CLRs is grossly important in HIV attachment and dissemination, the maturation and activation states of myeloid cells are of equal importance (more fully described later). Figure 60 illustrates some of the proposed mechanisms through which HIV hijacks physiologic and immunologic structures to establish infection and the subsequent dissemination to other HIV target cells[22,24,25].

Subversion of myeloid cell structural components to establish HIV infection

Filopodia and nanotubules

Myeloid and lymphoid cells all utilize membranal protrusions for intercellular communication between cells from different physiological systems such as the neurological and immunological systems. Open-ended nanotubes (TNTs), have been reported key in these intercellular communications[190]. TNTs are characterised as 100 μm long and 50-200 nm wide, F-actin containing membranal protrusions through which cytoplasmic and plasma membrane components are transferred between cell-types [190]. Owing to the wide diameter and ability to extend through lengthy distances, TNTs also mediate and facilitate the transfer of various vesicles inclusive of lysosomes, early endosomes, endoplasmic reticulum and Golgi derived vesicles, as well as organelles and pathogens (bacteria)[190]. While TNTs may be very instrumental in cell-cell communication as described, they also provide a platform through which HIV gains direct access into target cells as shown in Figure 60 (A) below[190,193]. The nature of initial HIV interaction with the cell governs the mechanism through which filopodia are manipulated. In HIV infected Mϕ, CD9+CD53+CD81+HLA-DR+ virus containing vesicles (VCCs) have been deciphered in the cytoplasm. VCCs, through their formation as continuity of the intracellular domain of the plasma membrane, enable the accumulation, assembly and budding of progeny virions post *de-novo* viral replication[190]. They subsequently transmit intact replication competent virions to target cells as shown in Figure 60 (B). Meanwhile, DC-SIGN/HIV interactions in DCs reportedly activate filopodia extension to allow HIV budding from the tip of the filopodia while concomitantly tethering and disseminating to several target cells as illustrated in Figure 60 (C). Interestingly, nef has been purported to upregulate DC-SIGN in HIV infected DCs in order to recruit and cluster CD4+ T cells around the infected DC in a manner similar to the illustration in Figure 60 (C)[22].

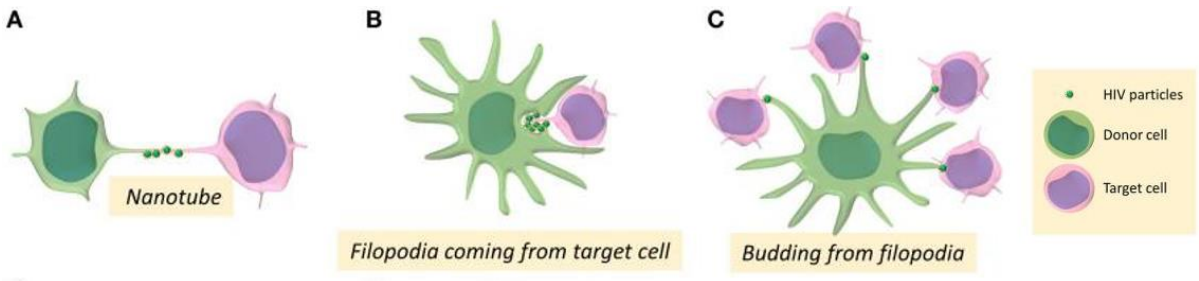

Figure 60. ***HIV cell-cell contact transmission mechanisms in T-cells, macrophages and DCs. (A)*** *HIV hijacks host's cell transport structures (filopodia) that form tunneling nanotubes (TNTs) and offer direct passage of HIV virions from infected to uninfected cells* ***(B)*** *TNTs also facilitate the passage of HIV virions from endocytic vesicles* ***(C)*** *DC-SIGN-HIV interactions activate filopodia extension to allow concomitant tethering and disseminate to several target cells. Image Adapted from Lucie Bracq et al., 2018. Mechanisms for Cell-Cell Transmission of HIV-1*[22]

TNTs have additionally been reported to express surface DC-SIGN and Siglec-1 that also attach to HIV as shown in Figure 61 **(1)** below. While viral transmission through VCCs directly engages the HIV

receptor (CD4) and co-receptors (CCR5 or others), with HIV's gp120 as shown in Figure 61 **(4)**; it has also been shown to capitalise on the formation of TNTs as described above[22,190]. The role of TNTs in Mϕ infection and transmission of HIV has been substantiated by reports of Nef induced upregulation of nanotubes and filopodia in HIV infected MDMs and ThP1 derived Mϕ[190].

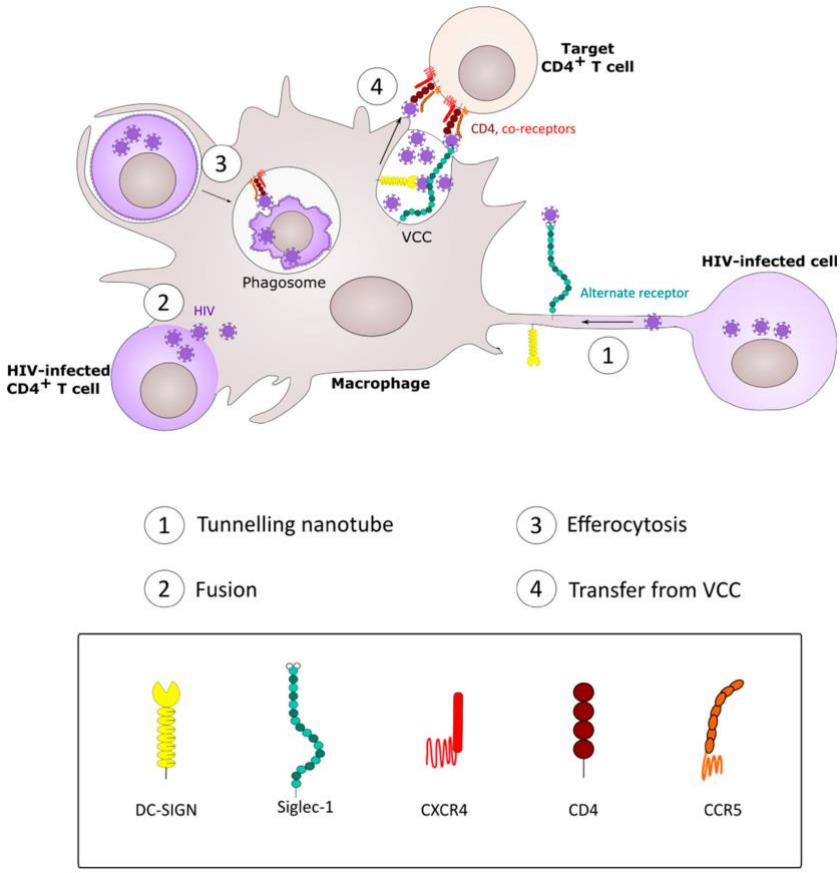

Figure 61. ***HIV transmission mechanisms in myeloid cells.*** ***(1)*** *CD169/CD209 rich tunnelling nanotubules (TNTs) showing) HIV virions surfing through from infected cells to uninfected cells* ***(2)*** *Fusion of HIV infected cells with uninfected cells* ***(3)*** *Phagocytic uptake of an infected CD4+ T cell inadvertently harbouring high MOI* ***(4)*** *HIV Infection of neighbouring CD4+ T cells through VCCs. Image adapted from Dupont and Sattentau. Macrophage Cell-Cell Interactions Promoting HIV-1 Infection. Viruses. 2020*[194]

The virological synapse (VS)

Other than TNTs and filopodia, HIV has also been reported to transmit through the virological synapse, a structure homologous to the immunological synapse. By definition, the virological synapse (VS) is a closed, organized, dynamic structure that forms between an infected donor cell and an HIV target cell enabling the transfer of virions between the two as shown in Figure 62 (A) below[192,193].

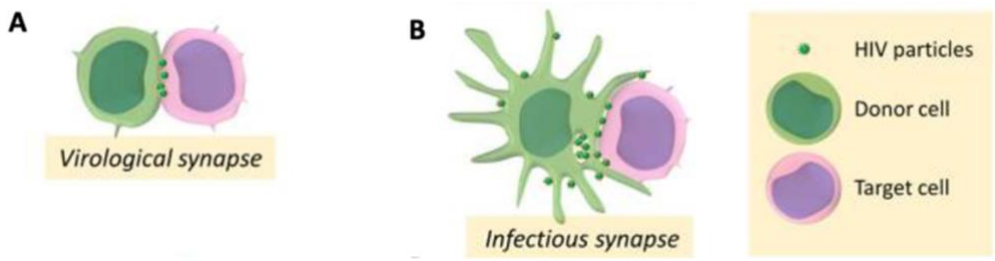

Figure 62. ***HIV transmission through the virological and infectious synapses (A)*** *gp120/CD4 interaction triggers recruitment of adhesion molecules (LFA-1/ICAM-1) and actin filaments that form and stabilize the virological synapse for HIV transfer* ***(B)*** *Dissemination of endocytosed virions from DCs to target cells through trans-infection using the infectious synapse formed by hijacking the immunological synapse (TCR/MHCII). Image Adapted from Lucie Bracq et al., 2018. Mechanisms for Cell-Cell Transmission of HIV-1*[22]

Despite the extensive elucidation of the VS in cell-cell transmission between CD4+ T cells, there is fragmentary knowledge on the mechanisms through which the VS is assembled and functions. It has been postulated that engagement of gp120 with CD4 as illustrated earlier in Figure 1, induces structural changes and recruits adhesion molecules; LFA-1α/β, ICAM-1/3 as well as tetraspanins that are required for assembly and stabilisation[22]. While this implies the indispensability of the HIV receptor in viral transmission through the VS, other authors have reported transmission to proceed independently of CD4 although culminating in poor replication in the target cell[192].

Notably, HIV transmission through the VS, in not only restricted to CD4+ T cells. DCs and Mϕ have also been shown to transmit HIV to CD4+ T cells using a related virological synapse, termed the infectious synapse as shown in Figure 60 (B) above[22]. While the outcome is productive (*cis* infection) in CD4+ T cells, HIV transmission through the infectious synapse has been shown to yield either one of two outcomes : i) *cis* infection or ii) *trans* infection in DCs and Mϕ[23,192,194].

During *trans* infection, DCs reportedly endocytose HIV using attachment factors such as DC-SIGN, MR, Langerin and Siglec-1 that have all been shown to recognize and bind HIV, through conserved sugar structures. HIV is internalized in a way that retains its infectivity inside endocytic vesicles and protective, tetraspanin enriched membranal structures (MVBs) that are synonymous with the Mϕ VCCs [51,192]. While exhibiting similarities in structure, size and complexity, VCCs have been suggested to carry progeny virions in Mϕ while MVBs carry endocytosed virions. In addition, they are distinguishable by unique marker profiles whereby VCCs are CD9+CD53+CD81+HLA-DR+ while MVBs are CD63+CD9+CD1b+HLA-DR+[192].

Internalization of HIV in such protective vesicles renders it transmissible and replicative when eventually trafficked to CD4+ T cells in the lymph nodes and to uninfected target cells in the vicinity. HIV harnesses the migratory potential of mature DCs to reach the more HIV prone CD4+ T cells in the lymph nodes[95]. Noteworthy, both MVBs and VCCs are HLA-DR+, suggesting these to be the

compartments where antigenic viral peptides are also loaded and thus packed with T cell activators. T cell activators induce HIV retro-transcription and infection of non-activated T cells that would be normally less permissive to HIV infection[192].

HIV containing endosomes follow either the exosome release pathway into the virological/infectious synapse as shown in Figure 63 (A) or the lysosomal degradation pathway shown in Figure 63 (B). The exosome release pathway is induced by the interaction of CD4 from the target cell, with the HIV-harbouring-DC, which triggers MVBs to migrate to the cell surface[192]. At the cell surface, MVBs fuse with the plasma membrane and generate HIV containing exosomes (small 50-200 nm structures) that release virions into the infectious synapse as illustrated in Figure 62 (B) above and Figure 63 (A) below. Virions that escape the lysosomal degradation pathway and those that are surface-bound are also capable of infecting neighbouring target cells as shown in Figure 62 (B)[192]. Interestingly, membranal invagination also accumulates infectious HIV inside non-endocytic vesicles that disseminate HIV to CD4+ T cells or other target cells using a mechanism referred to as "pocket-transfer" as shown in Figure 63 (C). HIV remains accessible to the infectious synapse or extra-cellular milieu and thus, delivered back for infection as illustrated in Figure 63 (C)[192].

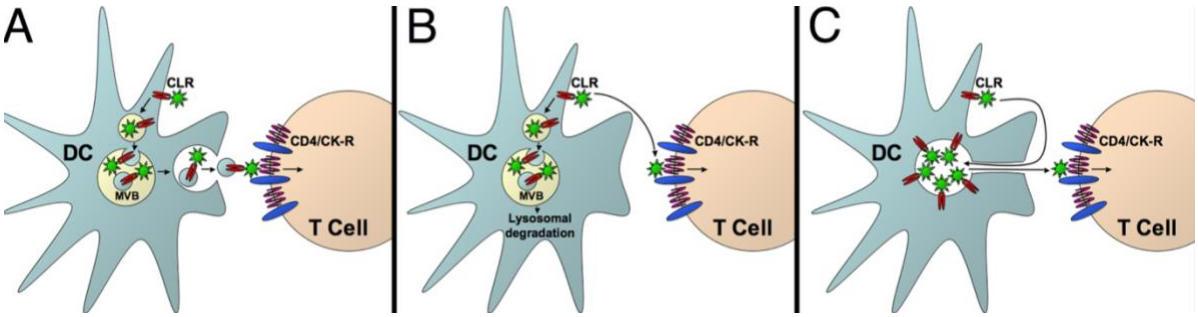

Figure 63. ***Trans-infection mechanism in the infectious synapse****.* ***(A)*** *Exosome release pathway. HIV is endocytosed using CLRs (DC-SIGN/MR) into protective MVB compartments followed by migration to the cell surface and the ultimate release* ***(B)*** *DCs bind HIV on the surface and disseminate without internalization* ***(C)*** *Pocket transfer. HIV delivery into the infectious synapse from membranal invaginations****.*** *Image adapted from Hyun Jae Yu et al., 2008 HIV Traffics through a Specialized, Surface-Accessible Intracellular Compartment during trans-Infection of T Cells by Mature Dendritic Cells*[192]

Other than the use of structural components, such as TNTs and virological/infectious synapses described above, HIV can also transmit through phagocytosis, endocytosis, macropinocytosis or entosis as illustrated in Figures 64 (A) and (B) below[22].

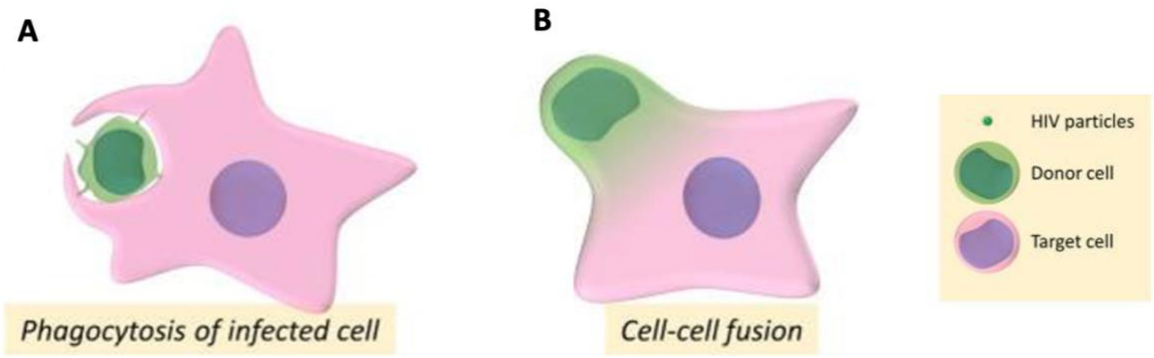

Figure 64. ***Other myeloid cell HIV uptake mechanisms (A)*** *Productive infection via the engulfment of infected CD4+ T cells by myeloid cells through entosis* ***(B)*** *Multinucleated giant cells (MGCs) from cell-cell fusion. Image Adapted from Lucie Bracq et al., 2018. Mechanisms for Cell-Cell Transmission of HIV-1*[228]

In particular, Mϕ, have been reported to phagocytose infected apoptotic T cells with consequent productive infection. This was particularly reported with CCR5 using viruses[21,119,190,192]. Furthermore, Mϕ have also been shown to engulf non-apoptotic T cells, in a mechanism named *entosis* which induces the formation of cell in cell structures capable of replication[22,190,192]. In colon explants, epithelial cells were reported to engulf HIV infected T cells this way[190]. Entosis has been postulated to yield multi-nucleated giant cells (MGCs) seen in infected tissues[119]. Specifically, MGCs have been witnessed in DCs and Mϕ from HIV patients and shown to productively infect neighboring HIV target cells[119,190]. HIV transmission through MGCs is evidenced by the presence of specific T cell markers in the cytoplasm and cell surface of the macrophage targets[119,190]. Importantly, MGCs are highly replicative and display longevity in host tissues[22,119,190]. In summary, Mϕ and DCs support productive infection, although with comparatively lower replication rates when compared to CD4+ T cells. They influence viral transmission and HIV dissemination to target cells through varied cell free and cell-cell contact mechanisms post *cis* infection or through *trans* infection [22,119,190].

2.0.3 HIV restriction mechanisms in myeloid cells

As briefly suggested above, the lower HIV replication capacities in myeloid cells are not only attributable to low receptor densities but have also been shown as due to the C-type lectin receptor (CLR) mediated degradation as well as host restriction factors [145,191].

To effect viral degradation, myeloid cells must first bind and engulf HIV virions using mechanisms that engage CLRs. DC-SIGN particularly mediates much of the endocytosis in cDCs while, langerin and caveolin-1 are specialized for LCs [145,191]. In DCs, endocytosed virions are enveloped inside multi-vesicular bodies (MVBs) that, although protective and hijacked by HIV to enable immune evasion and viral transmission, enter the lysosomal degradation pathway[23,195]. The fusion of MVBs or other virus containing endocytic vesicles with the autophagosome generates an amphisome that, when fused with

lysosomes, leads to viral degradation. Owing to this, autophagy enhancing drugs such as everolimus and rapamycin, that augment lysosomal degradation, have been reported to prevent HIV infection of vaginal LCs and epidermal CD11c+ DCs[29,72,120].

Steady state LCs, characterised by an abundance of langerin in the endosomal recycling compartment as well as in Birbeck granules (BG) where langerin co-localizes with caveolin-1, also sequester HIV for degradation[21,30,34,195]. Inhibition of caveolar endocytosis has been shown to abrogate HIV sequestration to BG and enhance LC infection. Langerin binds HIV through mannan recognition and directs it to the TRIM5-α degradation pathway whereby autophagy is orchestrated by a TRIM5-α complex formed with scaffolding proteins, Atg161 and Ag5[195,196].

Steady state LCs have therefore, been demonstrated to successfully abrogate CXCR4 infection. However, a couple of factors have been shown to enhance HIV fitness in the face of TRIM5-α lysosomal degradation and these are inclusive of inflammation, STI co-infections, high multiplicity of infection (MOI) and IFN resistance such as that displayed by transmitted founder (T/F) viruses [170,197,198]. The T/F virus is defined as an HIV variant depicting high virulence and transmission fitness, against which host restriction is insufficient [170,197,198]. It is postulated that 60-80% of mucosal infections can be traced back to one single virus, hence the term[47]. HSV-2 co-infections have also been reported to dampen HIV restriction by LCs, through increased TNF-α secretion, consequently leading to impaired langerin internalization and the concomitant depletion of Birbeck granules[38,80,199]. Consequently, LCs have been suggested to become susceptible to HIV infection and also disseminate to CD4+ T cells.

While it has been purported that maturation negates CLR mediated restrictions thereby rendering mature DCs and LCs more susceptible to HIV infection, it has also been shown that a level of post-integration blockade is mounted against HIV infection and replication. This is attributable to host restriction factors such as SAM domain- and HD domain-containing protein 1 (SAMHD1), the interferon-induced transmembrane (IFITM) proteins, tetherin and apolipoprotein B mRNA editing enzyme, catalytic polypeptide-like 3G (APOBEC3G)[28,30,195,196]. Host restriction factors are capable of implementing anti-viral activity at varied stages of the HIV life cycle, ranging from viral fusion up to assembly and budding. However, in like-manner to CLR-mediated abrogation pathways, HIV has evolved to by-pass and replicate despite the host-restriction factor mediated antiviral state.

2.0.4 Implications of insufficient restriction and myeloid cell infection in HIV pathology

Chronic inflammation and contribution to the viral reservoir

Viral reservoirs are cells or anatomical sites that harbor replication competent virus that persists over long periods of time with more stable kinetic properties in comparison to the main pool of actively replicating virus[35,61,84,196]. Cellular reservoirs are additionally stable against cytolysis and other immune effectors. They have also been reported to integrate viral nuclei acid over extended periods of time thereby promoting viral latency[200]. HIV is maintained in a state of non-productive infection during latency while contributing to the viral reservoir. In HIV infected macrophages, HIV has been suggested to modulate apoptotic pathways, provoke changes in polarization, downregulate the expression of cell surface receptors as well as shift the cytokine milieu to ensure immune evasion while retaining persistent viral replication[96]. It has also been shown that macrophage VCCs, DC MVBs and MCGs all "hide" and harbor replication competent virions[192]. Furthermore, HIV infected circulatory monocytes have also been shown to cross the blood brain barrier and to infiltrate privileged sites such as the CNS (concealed from drug delivery and immune response) where they terminally differentiate into long lived macrophages[157]. Viral reservoirs are, therefore, the principal culprit for chronic inflammation and residual immune activation (RIA) that is witnessed even during anti-retroviral therapy[35].

Intervention strategies - Understanding *in vivo* events leading to HIV acquisition

The elucidation of *in vivo* events leading up to productive infection, has the potential to inform the design of intervention strategies that effectively augment HIV restriction mechanisms in order to eliminate and abrogate HIV infection. Therefore, it is important to devise infection models that best mirror *in vivo* events, including the use of biologically relevant HIV strains. Earlier studies of HIV infection heavily relied on laboratory adapted strains encoding all known HIV gene products, initially distinguished by cellular tropism into lymphotropic and macrophage-trophic, analogous to CXCR4 and CCR5 tropic strains inclusive of NL4-3, SF2, SG3.1, BaL, YU2 and SF162[44]. To date, lab adapted strains are routinely used in infection assays and drug screening protocols as they are easily accessible and highly amenable to recombinant DNA technology. Although useful, using transmitted founder viruses and primary isolates is deemed more impactful, especially due to their potency, as well as the perceived specificity for the CCR5 co-receptor and macrophages. As described above, the ability of T/F viruses to overcome IFN restriction has been suggested as one of the mechanisms through which T/F potency is achieved[42,44].

2.0.5 Infectious molecular clones (IMCs)

Therefore, to allow a closer look into the factors that govern the vigor of transmitted founder viruses, advances in science have made it possible to elucidate the nucleotide sequences of the T/F HIV genomes and translate them to routine laboratory use[42,44]. To achieve this, a group of scientists designed a mathematical model that reliably inferred T/F virus genomes from the genomic sequences of plasma derived viral RNA (vRNA). The IMCs that were sourced from Dr Frank Kirchoff and used in this study, were generated through cloning of single genome (SG) amplicons from PCR amplified proviral DNA (gDNA) isolated during acute infection from the lab of Beatrice Hahn[74]. Compared to cloning and sequencing SG amplicons directly from plasma vRNA, this approach was less prone to polymerase induced errors while enabling the generation of IMCs without the patients' samples and retainment of the complete LTR[44,74].

2.0.6 Infection models

Much like IMCs, infection models provide a biologically relevant platform to carry out research that would be otherwise deemed impractical and unethical *in vivo*. Therefore, an ideal infection model is one that can recapitulate *in vivo* events, and using this basis, several models have been developed over the years, dating as far back as the late 19th century. Some of these are inclusive of animal models, reconstructed 3D epithelial models, *in vitro* cell cultures and PBMCs[91,201–203].

Animal models

Animal models represent some of the earliest platforms through which science was historically conducted. These were inclusive of murine, porcine, and non-human primates. Of these, murine models were the most popular although there were concerns around species incompatibility, lack of crucial components of the human immune system and restricted pathogen tropism[201]. Similar concerns were raised regarding the translation of SIV infection in non-human primates such as Macaques, to HIV pathology. Although still widely used, one of the major drawbacks of using animal models such as Macaques, is that there are significant genetic and biological differences among lentiviruses and some HIV specific interventions are not effective against other lentiviruses in non-human hosts[201–203]. More recently, humanized mice (MoMs) with the capability to support HIV replication and recapitulate its key aspects have been developed either by transplanting immunodeficient mice with the CD34+ hematopoietic progenitor cell or transplanting mice with human thymus or liver that subsequently develops into a functional human immune system[203]. This has been a major stride in HIV research, providing a rapid and reliable platform to conduct reproducible experiments. Moreover, humanized mice enable multiple cohorts from the same donor thereby limiting challenges associated with

individual variability[203]. However, these mice have only been used to conduct rectal and vaginal HIV transmission studies, the feasibility of elucidating penile HIV transmission in such models remains to be seen.

Despite the attractiveness and the systemic context, they provide, there are several logistics that interfere with use of animal models. They are expensive and labor intensive to maintain and breed, and in addition, ethical guidelines and applications tend to slow down research. Moreover, animal models do not always recapitulate the human context, in particular macrophages isolated from humanized mice (MoMs), have been shown to slightly differ in marker expression, from human macrophages[203]. Therefore, relevant human models are still needed to fully understand pathogenesis as much of the human studies have been conducted in cell cultures as described below.

In vitro and *ex vivo* infection models

Several strategies have been employed to develop optimal human models that best fit varied hypotheses and best suited to address the researcher's questions and these include:

i. Cell monolayers and suspension cells

Cell monolayers have been extensively used to elucidate pathogenesis and, in some cases, as infallible positive controls. Cell monolayers are generally easy to propagate, maintain and manipulate using standard tissue culture techniques and by this virtue, are the most attractive of infection models[200,204–206]. Most 2D models are commercially available from the American Type Culture Collection (ATCC) in the form of cell lines, derived from either biopsies or tissue explants. Moreover, the ATCC has a myriad selection of HIV relevant cell lines and interestingly, foreskin derived neonatal epithelial keratinocytes. Some of the HIV-relevant cell lines were used in this study and will be described in later sections. However, it is crucial that data generated from these cell lines, be carefully interpreted due to differences between normal and oncogenic cells. Another drawback would be that these cells lack the ability to acquire the native 3D architecture, despite their desirable high serial growth status[200,204,205]. On the other hand, tissue explant derived, immortalized cell lines also present with unique challenges associated with a considerably low serial growth status, hence cannot be passaged multiple times. This suggests that, with this type of a model, routine use would require more resources[200,204,205].

ii. Tissue Explants

Tissue explants have been extensively used in the pathogenesis of variable human viruses[202]. They have a high degree of biological relevance and may be in the form of an organ or as explants such as cadaver penile samples, or skin from varied surgeries[70]. Foreskin explants are routinely used in HIV studies,

whereby small pieces from either the inner or outer foreskin are oriented and sealed in apical chambers and sometimes, treated with thrombin and fibrinogen to stimulate coagulation [7,70,91]. Owing to minimal morphological obtrusions, tissue explants closely mimick physiological processes that enable tracking cytokine release and HIV replication without the bias of preselecting for HIV target cells nor the need for exogenous stimulation. Time and dose dependant HIV infection has been remarkably elucidated in tonsilitis explants whereby a direct correlation between MOI (multiplicity of infection) and p24 expression was observed[202]. Moreover, tissue explants have been purported to demonstrate permissiveness to both lab adapted and patient isolates hence their malleability in HIV research[201]. Intact explant specimen is cultured over time while maintaining an accurate 3D architecture, stratification and more importantly, differentiation status[7,70,91,202,207]. However, differentiation status may succumb to stimulation induced by handling techniques and media components. In addition, this may induce macrophage polarization, shift differentiation and activation statuses of DCs and LCs, ultimately failing at recapitulation[207].

In comparison to cell monolayers, tissue explants may be time consuming, require readily available tissue and may exhibit tissue variability leading to lack of reproducibility. Moreover, down-stream processing must be carefully executed to preserve status[201]. Ideally, models should enable long term culture to monitor progression over time. However, tissue explants degenerate over time and viability may be subsequently affected[201]. Furthermore, overgrowth of undesired, more resilient epithelial cells may be witnessed. Consistent to this, it's postulated that some cell loss may be incurred in organ cultures due to death and interestingly, migration. Lastly, disintegration and loss of structural integrity may contribute to contamination of cells from different compartments[201]. Alternatively, and to circumvent much of these challenges, scientists are opting to mimic tissue in a more controlled set-up, hence the growing popularity of 3D models.

iii. 3D models

The advancement of tissue engineering has made it possible to develop complex tissue and organ models using primary cells in the form of 3D models. 3D models are widely used in immune-oncology studies where they reflect the architecture and cellular composition while allowing for re-modelling of the micro-environment[201,208]. Assessment of tumor cells in engineered varied environments is suggested to help in the identification and stratification of patients likely to respond to immunotherapy.

Similar approaches are being explored for immuno-therapy in several, varied pathological conditions such as HIV[91,208]. Several scholars have reported on recapitulated foreskin epithelia whereby primary structural cells; keratinocytes and fibroblasts, are enzymatically isolated from the foreskin epidermis and dermis respectively. Cell isolation techniques are very critical, especially if downstream processing

will involve immunophenotyping[72,207]. Certain enzymatic preparations, such as trypsin and collagenase have been shown to cleave markers of interest which may alter biological interactions, described in more detail below[72,207]. These cells are subsequently seeded in a curated manner, with LCs and DCs that were differentiated *in vitro* from blood monocytes. Critically, special media is required to reconstruct dermis/epidermis-like structures[208].

Notwithstanding the advantages that come with using 3D models such as having the option to pre-select cells of interest and facilitate cross talk; they lack cellular immune response and the systemic host background since the primary cells have been purified and are blood derived, MDDCs and MDMs[201]. Additionally, in reference to the previous section on ontogeny, epithelial LCs are rarely monocyte derived, and differ in morphology and function from those that are monocyte derived. Therefore, 3D models may not adequately recapitulate *in vivo* systems and are very labor intensive[207].

iv. Are pluricellular models the answer?

Primary cell cultures isolated from specific tissues offer an unbiased approach that could be manipulated to recapitulate cell heterogeneity that lacks from 3D models. Monocellular *ex vivo* models of isolated primary cells have been used successfully in oral HIV transmission studies using human palatine tonsil tissue.

Furthermore, isolation of tissue resident mononuclear phagocytes is characteristically hard, owing to multiple factors such as tissue inaccessibility and more importantly, the rarity of these populations[207]. For this reason, a lot of *in vitro* studies base on monocyte derived macrophages (MDMs). Also, of paramount importance, would be the technique used for isolation as it has direct consequences on downstream processes[207]. It has been argued that different isolation methods affect i) phenotype, ii) activation status and lastly, iii) the cell surface expression of various markers including PRRs and CD4[207].

Enzymatic cell isolation, which typically involves mechanical tissue disruption, is one of the most used techniques. However, enzyme choice and subsequent culture media, have a direct bearing on the expression of markers that may be indispensable in evaluating pathogen interactions and on cell survival post isolation[207]. In a study conducted on myeloid cell isolation techniques from abdominal tissue, it was reported that trypsin, while optimal for LC isolation, negatively affects other lineage markers by cleaving CD11c, CD1c, CD141 and CD14[72]. This consequently renders immunophenotyping impossible, particularly true for cDCs and macrophage populations. Similarly, and of dire consequence especially for HIV studies, trypsin cleaves CLRs, siglec-1, CD4 and CCR5[72]. Likewise, variable collagenase preparations differentially cleave cell surface markers inclusive of CD80, CD86, CXCR4

and CD1c. Therefore, enzyme selection must be expedited cautiously, bearing in mind the intended use of the isolated cells[72].

Spontaneous migration from epidermal explants, initially observed in the 90's, has become increasingly popular as a cell isolation technique and is currently in routine use for the characterization of migrated cells[29]. The inherent capability of mature LCs and DCs to migrate to cognate lymphoid organs is exploited while ensuring minimal morphological aberrations. However, profound differences have been reported to exist between enzymatically isolated and migratory cells. Enzymatic digestion yields immature cells whereas spontaneous migration yields mature cells, although it has also been postulated that when rested, enzymatically isolated cells start expressing co-stimulatory molecules such as CD80 and CD86 as early as 1-hour post-harvest [144,147,209].

It is therefore important to conduct experiments soon after harvest as this suggests that there is possible exposure to activation signals during cell isolation[207]. Furthermore, there may be collateral downregulation of CLRs on enzymatically isolated cells during this time, for instance, the mannose receptor. It's also been purported that spontaneous migration yields pluricellular cultures which may prove arduous to characterize, particularly cDC subsets. Consistent to this, cDC2s have been purported to start expressing CD141 while cDC1s upregulate CD1a thereby requiring confirmatory techniques beyond flow cytometry such as transcriptomics. Additionally, tissue resident non-migratory cells may lack representation in the pluricellular culture as they remain tissue bound post-migration[143].

Tissue explants provide the ideal architecture by way of maintaining the impenetrable stratum corneum which corroborates with *in vivo* morphology whereby target cells reside underneath a protective mucosal surface. On the other hand, primary foreskin cells enable direct virus or drug contact with the heterogenous target cells without the intervention of the epithelial barrier. It has also been argued that epithelial cells facilitate HIV transmission by transcytosis[202] . In support of this, studies on reconstructed epithelia have reported the presence of multi-nucleated gigantic cells expressing high levels of p24. Such interactions could be a prelude to transfer of HIV infectivity across an otherwise intact mucosal barrier. There is fragmentary information on the nature of interactions between epithelial cells and myeloid or lymphoid cells which could be elucidated by a cell culture model that enables direct interaction of these cells[209].

Therefore, epidermal sheets and pluricellular models complement each other and may be used in parallel to provide robust and minimally disruptive platforms to assess and evaluate HIV target cells. While tissue explants, 3D-models and the unicellular primary cell model have been used and reported on in numerous HIV studies, the use of a multicellular suspension model would be a unique 2D, way to assess HIV interactions[29]. Notably, each of the models provide useful information and none is

superior to the other although care must be implemented in selecting an infection model that best suits the study hypothesis.

Immortalized cell lines

While the detection of HIV capsid proteins, particularly p24, is one of the most widely used methods for the determination of HIV infectivity *in vitro*, immortalized cell lines with reporter gene assays have also gained popularity as determinants of HIV infection. They are particularly attractive because they are simple, rapid, and accurate to use. They also enable use of different readouts inclusive of i) fluorescence microscopy, ii) cytofluorimeter and iii) flow cytometry. A wide range of cell-lines have been manipulated for this purpose, among which are the modified versions of Jurkats, CEM-GFP cells, Rev CEMs and the TZM-GFPs[204].

The Jurkat cell line is an immortalized T lymphocyte cell line that was originally isolated from the peripheral blood of a 14-year-old boy with T cell leukemia. Much of what is currently known about T cell immunity and molecular events of the HIV life cycle, was deciphered using Jurkats and its sub-clones. Jurkats have been very instrumental in identifying key players in HIV pathogenesis, such as the HIV receptor, CD4 and co-receptors CCR5 and CXCR4 as well as in unraveling underlying mechanisms responsible for HIV latency, signaling pathways and induction of T cell activation. Over the years, multiple sub-clones have been derived from Jurkats to serve varied purposes; among which is the Jurkat LTR-GFP CCR5+ cells (JLTR5-G) used in this study. The JLTRG-R5 cell line expresses CD4 (95%), CCR5 (77%) and CXCR4[205] and through the expression of Tat-induced GFP, offers a direct and quantitative marker of HIV infection[205,206].

CEM-GFP cells are engineered to express GFP in a time and dose dependent manner that is directly proportional to p24 expression. CEM-GFPs have however, been reported to lack the expression of CCR5, thereby rendering them selectively permissive. Overall, CEM-GFPs are most valuable for their unique features of visualization, direct counting, and the possibility of sorting fluorescent cells without the addition of external substrate or markers [205,206]. Meanwhile, Rev-CEMs carry a reporter gene that's coupled to a Rev response element in order to eliminate background noise that's usually associated with LTR based reporters. This is particularly instrumental in cases, whereby the infection signal is low. Using Rev-CEMs is also advantageous due to the wide range of HIV strains that it's permissive to. Rev-CEMs are susceptible to a wide range of lab adapted and primary virion strains belonging to Subtypes A, B, C, D E and G [205,206].

2.1 METHODOLOGY

2.1.1 Brief overview

While the main aim of Chapter 2 was to assess the susceptibility of foreskin myeloid cells to HIV infection, various optimization steps were conducted as a prerequisite. Thus, one of the first steps was virion generation. To do this, IMCs were transformed in *E. coli*, and subsequently assessed for integrity using gel electrophoresis and sequencing. Upon successfully expanding IMC stocks, the resultant IMCs were subsequently used to generate virus stocks using transfection. Virus stocks were assessed for titre determination using the TZM-bl assay to infer MOIs for infection assays. Prior to conducting infection assays, optimal infectious titres (MOIs) were determined and optimized using PBMCs and various cell lines (TZM-GFPs, CEM-GFPs, JLTR5Gs and CEM-REVs). The same models were simultaneously used to quantify signal detection (reporter genes – GFP/mCherry or p24), used as determinants of HIV infection and to also determine optimal incubation times. HIV infection was validated with maraviroc controls, using concentrations derived from IC_{50} determination. Subsequently, optimized infectious titres ($TCID_{50}$), timeframes and optimized drug concentrations (Maraviroc IC_{50}), were used against foreskin epidermal cells, epi-sheets, and explants to design the optimal infection model. The *ex vivo* pluricellular infection model was thus, the model of choice through which primary foreskin cells could be, identified, quantified, and assessed for HIV infection using Flow Cytometry. Statistical analyses were conducted using GraphPad Prism and R.

2.1.2 CELL CULTURE AND MAINTENANCE

Primary foreskin cells

Primary foreskin cells were isolated using spontaneous migration and liberase enzyme digestion of epidermal sheets illustrated in Figure 15 and described in Chapter 1.

Cell lines

While HEK-293T cells and HeLa-TZM-bls used for titre determination and infection assays (TZM-GFPs) were all adherent cell lines sharing similar cell culture and maintenance methods, all the other cell lines used for infection assays were suspension cells requiring different culture methods:

i. Adherent cell lines

Source

HEK293T cells are a derivative human cell line that expresses a mutant version of the SV40 large T antigen rendering them very useful in generating HIV virions [210,211]. For this study, **HEK293Ts (CRL-11268)** were obtained from the American Type Culture Collection (ATCC®). The ***HeLa -TZM-bl cell line (ARP-1829)*** was obtained from the National Institute of Health (NIH) AIDS Reagent Program-Division of AIDS, National Institute of Allergy and Infectious Disease (NIAID) contributed by Dr. John C. Kappes and Dr. Xiaoyun Wu. It is a HeLa cell line that was engineered to express high levels of CD4 , CCR5 and CXCR4[200]. In addition, TZM-bls have integrated Tat-regulated reporter genes for firefly luciferase (Luc) and B-galactosidase under the control of the HIV long terminal repeat (LTR) [200]. The reporter system permits quantification of viral infectivity by measuring chemiluminescence.

Thawing, Cell Culture and Maintenance

Both HEK293Ts and TZM-bls were cultured and maintained in Dulbecco's Modified Eagle Medium (DMEM) supplemented with 2mM L-glutamine, sodium pyruvate, glucose, pyridoxine and 25mM HEPES (Gibco® BRL Life Technologies, Paisley, UK) containing 10% FBS, 0.25 μg/ml Amphotericin B, 100 IU/ml penicillin and 100mg/ml streptomycin, and filter sterilised. Hereon, this complete medium is referred to as D10. Frozen cells were quickly thawed by suspending the cryovial (Corning®) in a 37 °C water-bath (Memmert WNB14), using plastic tweezers (Labnet) to prevent water from seeping through the lid into the tube. Thawed cells were pipetted into a 15 ml conical tube (Falcon) to dilute the cryopreservative dimethyl sulfoxide (DMSO) (Sigma-Aldrich) that exhibits room temperature (RT) toxicity. The cell suspension was centrifuged at 450 g for 5 minutes after which, the supernatant was discarded and the pellet resuspended in 10 ml pre-warmed D10. The 10 ml cell suspension was subsequently pipetted into a T 75 ventilated tissue culture flask (Corning®) that was horizontally incubated to allow the cells to adhere and grow in monolayers at 37°C with 5% CO_2 and 95% humidity, until the monolayers were 60%-80% confluent.

Splitting/Passaging

Monolayer cells were passaged every 2-4 days at approximately 60% - 80% confluency. The media was removed using a serological pipette and rinsed with sterile PBS supplemented with 100 IU/ml penicillin and 100 mg/ml streptomycin (P/S) (Gibco®) BRL Life Technologies, Paisley, UK), to remove FBS that inhibits enzyme activity. Thereafter, 1 x trypsin-EDTA (0.25% trypsin, 1 mM Ethylenediamine tetra acetic acid (EDTA) was added to dissociate the adherent cells from the flask and

from each other, 1 ml was used for HEK293Ts and 2.5 ml for TZM-bls. The culture flask was incubated horizontally, at 37°C for a 2-3 minutes to dissociate HEK293Ts and up to 7 minutes for TZM-bls or until the cells were suspended and assumed a rounded up, refractile form when viewed under the phase contrast microscope (Zeiss). An equal volume of D10 was added to inactivate trypsin and the cells were gently triturated and transferred to a 15 ml conical for centrifugation at 450 g for 5 minutes. The supernatant was discarded and the cell pellet was resuspended in D10 followed by viability and enumeration assessments using trypan blue exclusion. Cells were seeded in new T 75 culture flasks at a concentration of $2x10^6$ cells in 12 ml of D10 to be passaged again in 2-4 days.

Freezing

Excess cells were centrifuged at 450g for 5 minutes and resuspended in cold FBS and aliquoted into 2 ml cold cryovials which were slowly topped up with an equal volume of cold freezing medium, in a drop-wise manner with gentle 'swirls' in between. The freezing medium was prepared by supplementing FBS with 20% DMSO, such that the final concentration was 10% DMSO. The cryovials were stored in a pre-cooled Mr. Frosty (Nalgene®, ThermoScientific™) dipped in 100 % isopropanol (generic), that was routinely changed after every 5th use and refrigerated at -80°C (Snijders Scientific) overnight where the cells would freeze at -1°C per minute. Cryovials were transferred the next day to liquid nitrogen for long term storage. This freezing protocol was maintained across all cell lines, inclusive of primary foreskin cells.

ii. Suspension Cell lines

Sources

All cell lines, except the TZM-GFPs were obtained through the NIH HIV Reagent Program, Division of AIDS, NIAID, NIH : contributed by various scholars. ***Jurkat LTR-GFP CCR5+ Cells ARP-11856 (JLTRG-R5)*** were contributed by Dr. Olaf Kutsch, the ***CEM-Green Fluorescent Protein (GFP) ARP-3655*** cell line contributed by Dr. Jacques Corbeil while the ***RevCEM-D4 Cells, ARP-13437 (Uninfected)*** were contributed by Dr Alex Sigal. The TZM-GFP cell-line, was a modification of the HeLa TZMBL cell line, obtained as a gift from Dr. David Russel[200].

Cell culture and Maintenance

All suspension cell lines were thawed and cultured using the same protocol. Briefly, cells were quickly thawed and transferred to a 15 ml conical tube (Falcon) containing 10 ml of pre-warmed R10 medium. The cell suspension was centrifuged at 450 g for 5 mins, and the supernatant was cautiously drawn out

by a pipette. The resultant cell pellet was resuspended in warm R10 to a final concentration of $2x10^6$ /ml in a T 25 culture flask (Corning) that was vertically incubated at 37°C with 5% CO_2 and 95% humidity for 24 hours. Cells were passaged the following day by pelleting and resuspending the cells in warm R10 at a final concentration of $1x10^6$ /ml and incubated at 37°C with 5% CO_2 and 95% humidity. Thereafter, cells were passaged after every 2-4 days. CEM-GFPs, Rev-CEMs and JLTRG-R5 cell line all had a doubling time of 24 hours, as described by the NIH HIV Reagent Program.

PBMCs

PBMC Isolation

Buffy coats were obtained from healthy, HIV seronegative donors through the Western Cape Blood Service (WCBS). Peripheral blood mononuclear cells (PBMCs) were isolated by density gradient centrifugation using the Leucosep method (Greiner bio-one). Briefly, the density gradient medium, Ficoll-Paque™ and the wash buffer, prepared by supplementing PBS with 1% FBS, were equated at RT and 15 ml of the Ficoll-Paque™ reagent added into a 50 ml sterile Leucosep tube (Falcon). The Leucosep tube was centrifuged for 1 minute at 2 200 rpm to force the Ficoll-Paque™ reagent below the Leucosep barrier and any residual fluid above the barrier was discarded. Whole blood was diluted eight-fold with Ca^{2+} and Mg^{2+} free PBS and subsequently added in the Leucosep tube containing the Ficoll-Paque™ reagent, above the barrier at a 25 ml volume. The Leucosep tube was then centrifuged at RT, 2 200 rpm for 18 minutes with ascending brake 5 and descending brake 0. After centrifugation, the tubes were carefully lifted to avoid disturbance of the PBMC layer which was subsequently harvested into a new 50 ml conical tube. The harvested PBMCs were washed twice by adding the wash buffer (RT) and spinning in the centrifuge at 1 500 rpm for 10 minutes. The supernatant was carefully discarded, and the pellet was resuspended in 10 ml of the wash buffer. The cell suspension was assessed for viability and cell numbers by trypan blue exclusion as described above. The freezing protocol described above was also used for long term PBMC storage.

PBMC Stimulation

PBMCs isolated from at least 3 different donors were stimulated in separate by tubes by resuspending the PBMCs in stimulation media prepared by supplementing R10 with 200 UI/ml IL-2 and 0.5 µg /ml PHA. PBMCs were resuspended at a concentration of 1 $x10^6$ cells/ml in a T-25 culture flask and were vertically incubated for 72 hours at 37°C with 5% CO_2 and 95% humidity. The stimulated cells were pipetted into a 50 ml conical tube and centrifuged to remove the supernatant. The remaining pellet of stimulated cells was resuspended in an isolation buffer (described below) for CD8 depletion at 1 x 10^7 cells/ ml.

PBMC CD8 depletion

CD8+ T cells were depleted from stimulated PBMCs by immunomagnetic bead separation, using a CD8 Positive Isolation Dynabeads® Kit (Invitrogen™) and an EasySep™ magnetic column (STEMCELL® Technologies). Briefly, the isolation buffer was prepared by supplementing Ca^{2+} and Mg^{2+} free PBS with 0.1% bovine serum albumin (BSA) (Gibco®) BRL Life Technologies, Paisley, UK) and adjusting the pH to 7.4 using 2mM EDTA as per kit's guidelines. The isolation buffer was subsequently used to wash the CD8 Dynabeads® and $1x10^7$ PBMCs. Using the magnetic column, the wash buffer was subsequently discarded and both beads and cells resuspended in fresh isolation buffer prior to being mixed together. The cell/bead mixture was incubated at 4°C with gentle rotations at 5 minute intervals, for 30 mins. After incubation, the CD8- cells' supernatant was drawn out using the magnetic column, onto which the bead-bound CD8+ cells attached. The CD8- cells in the supernatant were pooled for at least 3 different donors and were centrifuged at 450 g for 5 mins, after which the isolation buffer was discarded. The resulting cell pellet was resuspended in the isolation buffer and assessed for cell viability and cell numbers by using trypan blue.

2.1.3 Transformation

Infectious molecular clones containing GFP and mCherry reporter genes were kindly received from Dr Frank Kirchhoff (University of Ulm) and Dr David Russell (Cornel University) respectively. Bacterial plasmid transfections were carried out using Stbl3™ *E.coli* competent cells using the manufacture's protocol. Briefly, 5 µg of DNA (1-12 µl) were thawed on ice and added to 50 µl of the cells in a clean 1.5 ml Eppendorf tube. These were incubated for 30 mins on ice and then transferred to a 42°C water bath where the cells were heat-shocked for 45 seconds followed by incubation on ice for 5 minutes. Thereafter, 200 µl of Super Optimal Catabolite (SOC) medium (Invitrogen) was added and cells incubated for 2 hours at 30°C whilst shaking at 300 revolutions per minute (rpm). Afterwards, the mixture was plated on the Luria Bertani (LB) agar plates for 20 hours at 30°C. Single colonies were subsequently picked and inoculated by streaking on new LB agar plates followed by an overnight incubation at 30°C for 20 hours. Single colonies were picked and inoculated in 5 ml Luria Bertani broth supplemented with 100 mg/ml of carbenicillin (Sigma-Aldrich) for positive isolation of the transformants, the bacterial cultures were put in the shaking incubator set at the rotation speed of 300 rpm, at 30°C for 6 hrs. The mini-culture was then transferred to a 100 ml LB-broth supplemented with 100 mg/ml of carbenicillin and incubated overnight at 300 rpm and 30°C.

2.1.4 DNA Extraction and Quantification

Plasmid DNA was extracted from the overnight cultures described above, using the QIAGEN® Plasmid Plus Midi Kit. Briefly, the bacterial culture was pelleted in 50 ml falcon tubes as per manufacturer's instructions. The resultant pellet was resuspended in an RNA degrading suspension buffer, followed by the addition of a LyseBlue® infused lysis buffer to ensure efficient cell lysis and complete precipitation of SDS, cell debris as well as genomic DNA. The subsequent viscous mixture was incubated at RT for 3 mins, prior to being neutralised (blue to clear). The lysate was then filtered using the QIAfilter Cartridge QIAGEN® and plunger. Thereafter, the cleared lysate was then added with a binding buffer and transferred to the QIAGEN® Plasmid Plus spin columns on the QIAvac 24 Plus through which a -300 mbar vacuum was used to draw out the liquid. The remnant, column bound DNA was then washed twice using ETR and PE buffers that, also through the vacuum, were subsequently drawn out. Residual buffer was removed by centrifugation of the column at 10 000 g (9 700 rpm) for 1 min in a Heraeus™ Pico™ 21 table microcentrifuge (Thermo Scientific). Finally, the DNA was eluted by placing the QIAGEN® Plasmid Plus column into a clean 1.5 ml tube, into which was added 200 µl of DNase free molecular grade water (Sigma).

DNA Quantification

A NanoDrop™ 2000/2000c Spectrophotometer (Thermo Scientific, MA, USA) was then used to quantify the DNA according to manufacturer's protocol. Plasmid DNA purity level was quantified by measuring their spectral readings at 260 nm and 280nm. Samples whose 260/280 ratio was greater than 1.8 were deemed impure and were not used.

Restriction Digestion

The extracted, pure plasmid DNA was further assessed for quality using control restriction digestion and the subsequent gel electrophoresis. Owing to the variable restriction enzymes required for the different plasmid DNA clones as well as buffer incompatibilities, Fast Digest Enzymes (ThermoFisher Scientific, MA, USA) were used as they enabled the use of a universal FastDigest buffer and eliminated the need for sequential digestion. Four pairs of enzymes were used namely; i) *HpaI* and *MluI* for NL4-3 (R5) and NL4-3 (X4), ii) *NotI* and *HpaI* for Bal Env-NL4-3 iii) *NotI* and *MluI* for subtype C ZM246-10 TF (CS596) and iv) *AscI* and *AsiSI* for subtype C CH167 CC (CS642) and subtype C CH198 TF (CS769). All constructs had eGFP cassettes except for Bal-Env NL4-3 that had mCherry. A standard protocol was used for all enzyme combinations, whereby 1µg of DNA was diluted in 2.5 µl of the FastDigest Buffer, followed by 1µl of each of the unique pair of enzymes. The reaction mixture was topped up with dH_20 to a final volume of 25 µl and incubated for 1 hour at 37 ^oC.

Gel electrophoresis

The expected band sizes for the constructs were i) ~850 bp for NL4-3 92TH14-12 (R5) and NL4-3 (X4) ii) ~1 300 bp for NL4-3 BaL and all the subtype C strains; ZM246-10 TF, CH198 TF and CH167 CC. To confirm these sizes and plasmid DNA integrity, 2 µl, constitutive of 1 µg of the restriction digestion products, was diluted with 8 µl of the 6x loading dye containing GelRed and loaded onto a 1% agarose gel in TEA buffer. The restriction digests were gel electrophoresed at 100 volts for 1 hour in TEA. Bands were visualized with a UVIPro Silver gel documentation system (UVItec, Cambridge, UK).

2.1.5 Generation of Virus Stocks

2.1.5.1 Transfection

0.6 x10^5/ml and 1.2 x 10^6/ml HEK293T cells were transfected using the $CaCl_2$ and lipofectamine method respectively. Cells were seeded in 6 well plates and transfected with DNA co-precipitates from each of the protocols:

i. $CaCl_2$

The calcium chloride transfection protocol was optimal for **R5 NL4-3**, **X4 NL4-3** and **subtype C CH167 CC.** Reagents used were either from the Calphos mammalian transfection kit (BD Clontech) or were prepared manually. For the manual protocol, 10x HEPES buffered saline (HBS) was prepared by dissolving 8.18 g sodium chloride (NaCl) (Sigma Aldrich), 5.94 g HEPES, 0.25 g natriumhydrogenphosphat ($NA_2HPO_4x2H_2O$) (Sigma Aldrich) in 100 ml dH_2O. 2x HBS was made by a five-fold dilution of 10x HBS in dH_2O. Finally, 2 M calcium chloride ($CaCl_2$) was prepared by dissolving 22.2 g calcium chloride dihydrate in 100 ml H_2O. All reagents were filter sterilized and the HBS pH was maintained at 7.21. In tube 1, 5µg of the plasmid DNA was directly mixed with 13 µl of 1M $CaCl_2$ and topped up with H_2O to a final volume of 100 µl. In a separate tube 2, 100 µl of 2 x HBS was diluted with 100 µl of H_2O. Thereafter, the DNA complex from tube 1 was mixed by pipetting and dropped into the diluted HBS solution in tube 2. The mixture was vortexed for at least 10 seconds, after which it was dropped into a well that was pre-seeded with 0.6 x10^5 HEK293Ts in a drop-wise manner, D10 was added to ensure the final well volume was 2 ml. The 6 well plate was gently agitated to ensure that the DNA precipitate was well dispensed. The culture was then incubated for 48 hrs at 37°C with 5% CO_2 and 95% humidity.

ii. Lipofectamine

The lipofectamine protocol was optimal for **Bal-Env NL4-3** and the **subtype C strains; ZM246-10 TF** and **CH198 TF**. R5 NL4-3 transfection was equally optimal in both protocols. In one tube, 5 µg of the plasmid DNA was diluted in 250 µl Opti-MEM™-Reduced Serum Media (Gibco®) BRL Life Technologies, Paisley, UK) and 10 µl of lipofectamine P3000 reagent (Invitrogen). In a separate tube, 7.5 µl of lipofectamine (Invitrogen) was diluted in 125 µl Opti-MEM™. The lipofectamine mixture was then added to the DNA plasmid mixture, mixed by vortexing and incubated at room temperature for 15 minutes to allow for lipofectamine/DNA complexes to form. Subsequently, the lipofectamine/plasmid mixtures were then directly added to the pre-seeded 1.2 $x10^6$ cells to a final volume of 2ml. Plates were incubated for 48 hours at 37°C with 5% CO_2 and 95% humidity.

2.1.5.2 Virus Harvesting and Concentration

Infectious virus stocks were harvested by centrifugation of culture supernatants at 887 g for 8 minutes to remove cells and debris. The supernatants were transferred to new clean 50 ml conical tubes and were diluted four-fold with 5x PEG-it™ Virus Concentration Reagent (System Biosciences, CA, USA). PEG-it™. PEG-it™ is a polyethylene glycol optimized for the precipitation of all lentiviral-based particles. It concentrates the virus by over 100-fold and also acts as a cryo-preservative, thereby allowing multiple freeze/thaw cycles. The supernatant/PEG-it™ mixture was incubated at 4˚C for 24 hrs. Thereafter, the mixture was centrifuged at 1 500 g for 30 minutes at 4˚C. After centrifugation, the virus particles could be observed as a beige pellet at the bottom of the falcon tube. The supernatant was discarded, and the tube was centrifuged again at 1 500 g for 5 minutes to remove residual fluid that was carefully aspirated by a pipette. The pellet was resuspended in 1/10 of the initial culture medium volume using cold D10 and 200 µl aliquots were transferred to cryovials and stored at -80˚C until titre determination and the subsequent infection assays.

2.1.5.3 Virus expansion in PBMCs

Stimulated, CD8 depleted PBMCs were used as controls for HIV infection assays but were also instrumental in expanding virus stocks that were generated through transfection. Stimulated and CD8 depleted PBMCs that were pooled from 3 different donors were resuspended at 5$x10^6$ cells in 1.5 ml R10 supplemented with 200 UI/ml IL-2 (IL-2 medium). Cells were seeded into a 6 well tissue culture plate and inoculated with low titre virus with a 50 % tissue culture infectious dose ($TCID_{50}$) of at least 1$x10^3$/ml, without spinoculation. The inoculated cell suspension was then topped up with IL2 medium to a final volume of 3 ml and incubated overnight at 37°C with 5% CO_2 and 95% humidity. The cell culture was topped up with IL-2 medium to 5 ml and transferred to a T25 culture flask. On day 4, cells

were pelleted and the virus containing supernatant was gently removed, taking care not to disturb the cell pellet and was transferred to a new tube for harvesting. A small volume of the supernatant was left in the tube with the pellet to which 10 ml of fresh IL-2 medium was added for resuspension. On day 7, cells were pelleted and resuspended in 15 ml IL-2 medium, similarly to day 4 and a small volume of the virus containing supernatant was left in the tube. This was repeated on day 11, whereby 20 ml IL-2 medium was used to resuspend the remaining cell pellet. The final harvest was on day 14, cells were pelleted and the supernatant was centrifuged to remove cells and cell-debris. 500 µl aliquots of the supernatants were then transferred to -80˚C freezer for storage until further use.

2.1.5.4 Titre determination (TZMBL ASSAY)

The number of infectious virus particles present in viral preparations can be quantified using the $TCID_{50}$ assay. Virus stocks are serially diluted in a 96 well plate, by a factor of 4. The dilution at which 50% of the wells either show a cytopathic effect or result in positive detection of infection, is used to approximately quantify the infectious virus particles. Infection is measured by a chemiluminescence readout (relative luminescence units) upon addition of the firefly luciferase substrate to the cells[200]. The relative luminescence units (RLUs) are proportional to infected cells[200]. 80% confluent TZM-bl cells were split and resuspended at $1x10^5$/ml in D10 containing 40 µg/ml diethylaminoethyl (DEAE)-dextran (Sigma Aldrich). 100 µl aliquots of the TZM-bl cell suspension were dispensed into the 96 well tissue culture plate containing serially diluted virus stocks and incubated at 37°C with 5% CO_2 and 95% humidity for 48 hours. After incubation, 75 µl of the culture supernatant was pipetted from all the wells using a multi-channel pipette (BioPette[PLUS]) and replaced with 100 µl of the reconstituted BrightGlo reagent (BrightGlo™ Luminescence Reporter Gene Assay System-Promega E2650). BrightGlo permeates infected TZM-bls and contains Beetle luciferin, which is excited by luciferase to yield oxyluciferin and photons of light that are translated to RLUs by a luminometer as illustrated in Figures 65-66 below:

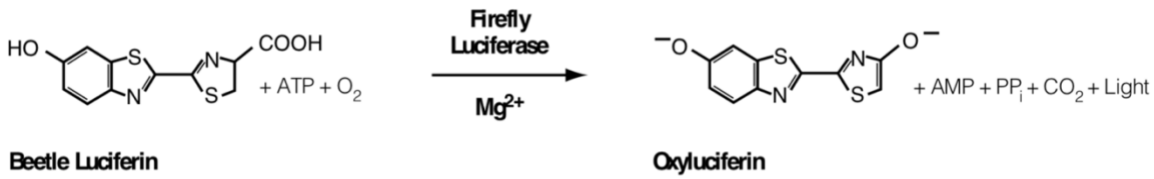

Figure 65. ***A schematic diagram showing the BrightGlo Luminescence Reporter Gene Assay System reaction.*** *Figure adopted from https://www.med.upenn.edu/robertsonlab/assets/user-content/documents/tb281.pdf med.upenn.edu*

Plates were incubated in the dark at RT, for 2 minutes after which the contents of each well were mixed well, by pipetting up and down multiple times. 150 µl was transferred to a black 96-well microtiter plates (Corning) that was read on a Glomax 96 Microplate Luminometer (Lumin2 Promega), to

determine the RLUs. Wells with RLUs that were higher than the average background from the negative control well, were considered positive. The Reed Muench method was used to infer the $TCID_{50}$ values for each virus strain.

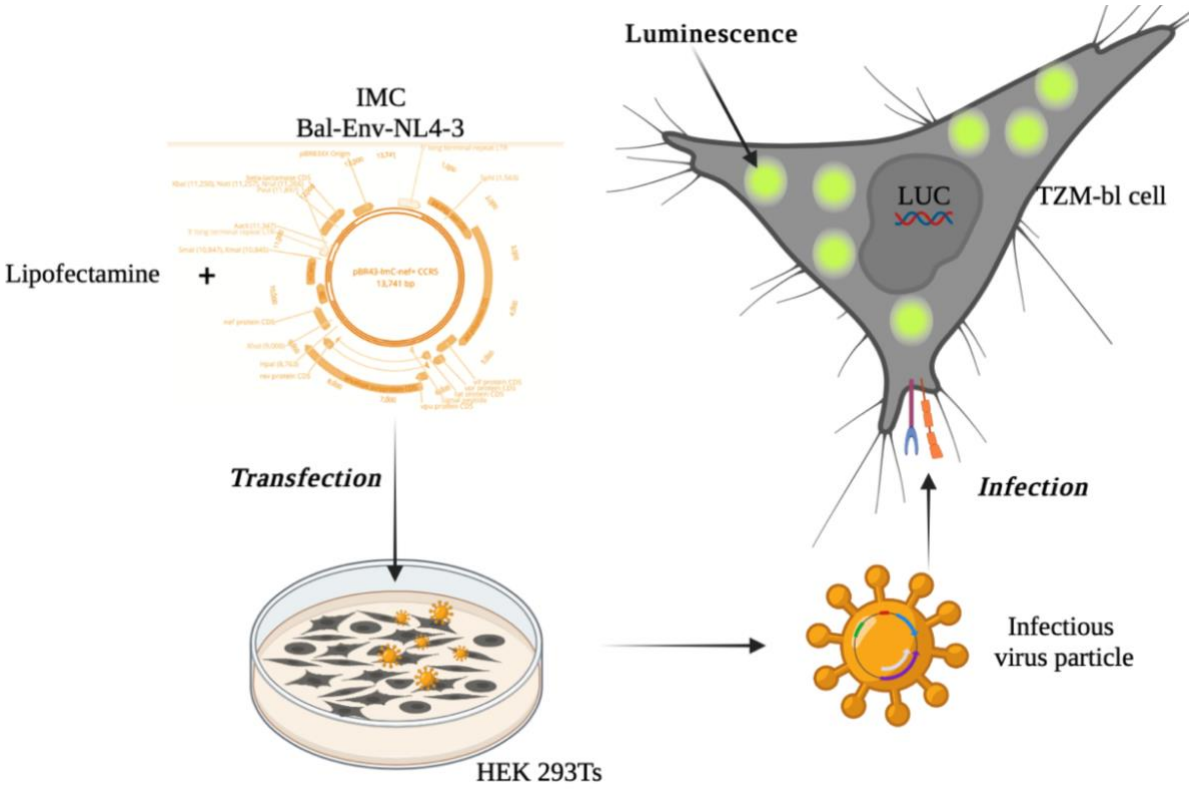

Figure 66. ***Flow diagram demonstrating the virus production in HEK293Ts, and titre determination in TZM-bl cells****. HEK293Ts are transfected in culture over 48 hours when they are harvested. Infectious supernatant bearing virions is used to infect TZM-bl cells using the TZM-bl assay. The LUC gene is HIV-tat activatable and expresses the luciferase excites the luciferin substrate in BrightGlo resulting in light emission that is used to quantify the number of infectious particles.*

2.1.6 HIV infection optimisation

Multiplicity of Infection (MOI)

After determining the infectious titre, the desired multiplicities of infection (MOIs), were calculated for each virus. The MOI is defined as the ratio between the number of infectious units (IU) as calculated by the Reed Muench method and the number of HIV target cells; 1000 infectious units :100 000 cells, will yield an MOI of 1000/100 000 = 0.01, translating to one infectious particle per 100 HIV target cells[39,212].

Maraviroc IC_{50} Determination

The minimum inhibitor concentration causing 50% reduction in viral infectivity (IC_{50}) was determined through five-fold serial dilutions of maraviroc starting from 40 nM up to 0.000512 nM. TZM-bl cells were split and seeded in a 96 well tissue culture treated plate as described in the TZM-bl assay and incubated with the varying dilutions of maraviroc for 30 minutes at 37°C with 5% CO_2 and 95% humidity to allow drug interaction with the cells. Thereafter, the TZM-bl cells were inoculated with a pre-determined MOI of 0.01. A positive control was set up, whereby TZM-bls were inoculated with the virus in the absence of maraviroc. Two negative controls were also set up by i) incubating TZM-bl cells with maraviroc only and ii) TZM-bls only. The tissue culture plate was incubated at 37°C with 5% CO_2 and 95% humidity for 48 hours. The inhibitor concentrations causing 50% reduction in viral infectivity (IC_{50}) were calculated by fitting pooled data from four independent experiments to sigmoid dose response curves using GraphPad prism.

HIV infection of PBMCs

To determine the optimal MOI for each virus, the virus was serially diluted into varying MOIs ranging from 0.1, 0.01 and 0.001. These were then used to infected PBMCs and assayed for infectivity at two separate time-points (24 and 72 hrs). Stimulated and CD8-depleted PBMCs were thawed according to the protocol described above and resuspended at $1x10^6$ cells/ml in IL-2 medium. For each well of the 6 well tissue culture plate, $2x10^6$ cells were seeded and inoculated with viral preparations at the different MOIs to a final volume of 2 ml. Negative control wells were also set up, whereby the $2x10^6$ PBMCs were cultured in 2 ml IL-2 medium without viral inocula. Thereafter, the plate was spinoculated at 1 200 g for 2 hours, at 25 ˚C followed by incubation at 37°C with 5% CO_2 and 95% humidity.

HIV Infection of Cell lines

All cell line cultures were spun in the centrifuge to remove the culture medium and subsequently resuspended in fresh IL2 medium for enumeration and assessment of viability by trypan blue exclusion prior to HIV infection. Similar to PBMCs, $2x10^6$ cells were seeded in 6 well tissue culture plates and inoculated with the different viral preparations at an MOI of 0.01. All cultures were incubated at 37°C with 5% CO_2 and 95% humidity for 72 hours. This was the pre-determined optimal time-point for reporter gene detection and p24 expression in cell lines.

2.1.7 HIV infection of foreskin primary cells

Using optimized virus titres, incubation timeframes and infection determinants, foreskin tissue was used to set up different infection models (method development). Thereafter, only one model was selected for all HIV infection assays. Foreskin specimens were partitioned into 3 parts for each participant (n=5): i) foreskin explants ii) foreskin epidermal sheets (epi-sheets) and iii) epidermal sheets for migration as shown in Figures 67 (a) - (c) respectively. The inner and outer compartments were pooled across all *ex vivo* models. To set up the explants, intact foreskin tissue was sectioned into small 0.25cm^2 cm x 0.25cm^2 cm blocks that were either used as the explant model shown in Figure 67 (a) or incubated in dispase overnight as described earlier in Figure 17, to attain epidermal sheets and set up the epi-sheet and pluricellular infection models shown in Figures 17 (b)-(c).

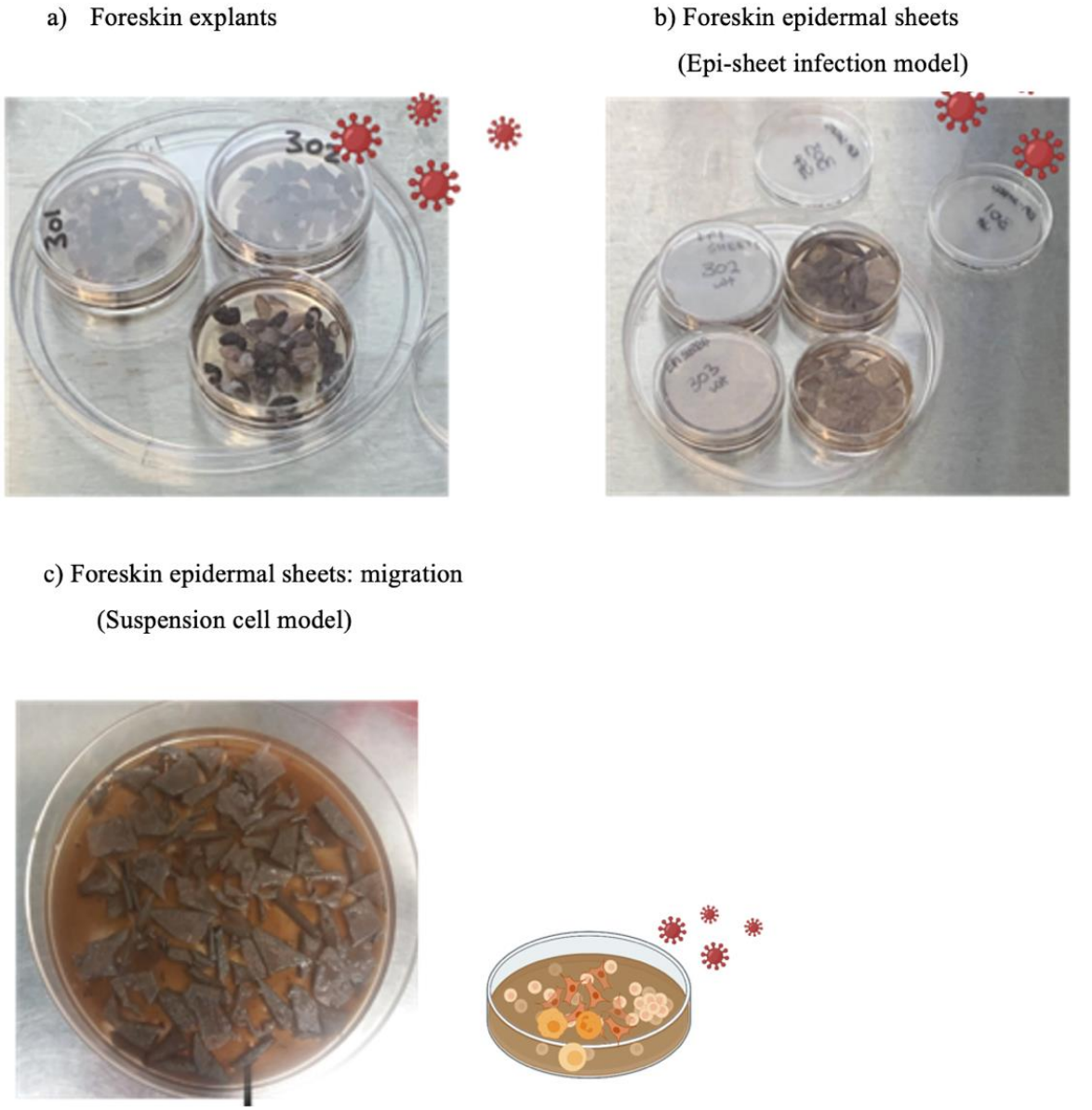

Figure 67. ***Foreskin infection models.*** *Foreskin tissue was sectioned into* ***(a)*** *explants,* ***(b)*** *epidermal sheets and* ***(c)*** *epidermal sheet derived pluricellular infection model and inoculated with the different HIV strains. Cell migrating from infected explants in* ***(a)*** *and epidermal sheets in* ***(b)*** *were assessed for infection using p24 expression. Cell migrating from the epidermal sheets in (c) were used to set up the pluricellular cell suspension model, that after inoculation and incubation were also assessed for HIV infection using p24 expression.*

The intact tissue explants and epidermal sheets were placed on their basal side, onto droplets of virus containing media at an MOI of 0.1 and incubated at 37°C with 5% CO_2 and 95% humidity for 5 hours. Thereafter, explants and epi-sheets were washed in PBS to remove the virus and were cultured and incubated in R10 at 37°C with 5% CO_2 and 95% for up to 5 days. Migratory cells from both models were harvested and remnant epi-sheets were digested with liberase to release non-migratory, tissue resident cells.

In Figure 67 (c), the other half of the epidermal sheets were incubated in R10 medium for 48 hours to allow foreskin cells to migrate out. Migratory cells were harvested and resuspended at $1x10^6$ / ml in R10 medium. Cells were seeded in 35 mm tissue culture treated petri dishes and inoculated with viral preparations at an MOI of 0.01 after which they were spinoculated at 1 200 g, 25°C for 2 hrs. Thereafter, cell cultures were incubated at 37°C with 5% CO_2 and 95% humidity for up to 5 days.

2.1.8 Intracellular Staining

At 5hrs, 18 hrs, 48 hrs and 120 hrs;, cell suspensions of HIV inoculated cells and negative controls were pipetted into 15 ml conical tubes and centrifuged at 2 100 rpm for 3 mins, after which the supernatant was gently aspirated without disturbing the pellet. The cell pellet was resuspended in plain PBS for enumeration and the assessment of cell viability by trypan blue exclusion, on the Countess Counter. Thereafter, $4x10^6$ cells/100 µl in plain PBS were stained with the viability stain according to the standard protocol described in Chapter 1 and subsequently intracellularly stained to assay for reporter gene expression and p24. Following the viability stain, cells were resuspended in 150 µl FACS buffer. The plate was then centrifuged at 2100 rpm for 3 mins after which the supernatant was gently discarded, and the pellet was resuspended and washed twice in 150 µl of 1 x perm wash buffer (PWB) prepared by a four-fold dilution of perm wash buffer (BD Pharmingen™ Transcription Factor Buffer Set) in RO water. A working solution of 1 x cytofix buffer, was prepared by a 3-fold dilution of cytofix buffer (Pharmingen™) in diluent buffer (Pharmingen™), the cells were then resuspended in 100 µl of 1 x cytofix buffer and incubated at RT for 20 minutes. Afterward, the cells were was washed in 100 µl of PWB, centrifuged at 2 100 rpm for 3 mins and the supernatant was discarded. This was done twice after which, the cells were resuspended in 50 µl of the intracellular antibody cocktail prepared in PWB and incubated in the dark at 4C for 45 mins. Thereafter, cells were topped with 100 µl of PWB, centrifuged at 2 100 rpm for 3 mins and the supernatant was discarded. Finally, the cells were resuspended in 300 µl of FACS buffer in FACS tubes and were acquired using the BD LSR II or alternatively kept in the dark at 4^{o}C until acquisition time.

2.1.9 Statistical Analysis

Graphs were generated using GraphPad Prism and R, similarly to Chapter 1. The data was also tested for normality using the Shapiro-Wilk test (data not shown)[184]. While comparisons using cell lines were normally distributed, foreskin samples were not normally distributed[184]. Thus, for all pair-wise comparisons, the *p*-values were calculated using two-sample t-tests. Where multiple comparisons were made, the Kruskal Wallis test was used, and the *p*-value cut-offs adjusted using a Benjamin Hochberg correction[185,186]. Due to the small sample size all correlations on infection optimisation using the cell lines were performed using a Spearman correlation coefficient (CI = 95%)[183].

2.2 RESULTS

Differential susceptibility of foreskin myeloid subsets and lymphoid cells to ex vivo HIV-1 infection

Section 1 : Method Development

HIV challenge assays were sequentially derived and optimized from several method development experiments. Initial optimization experiments were for the clonal expansion of infectious molecular clones (IMCs) and subsequent virus production as well as titre determination required for infection assays. Figure 68 illustrates the sequential steps through which this was achieved.

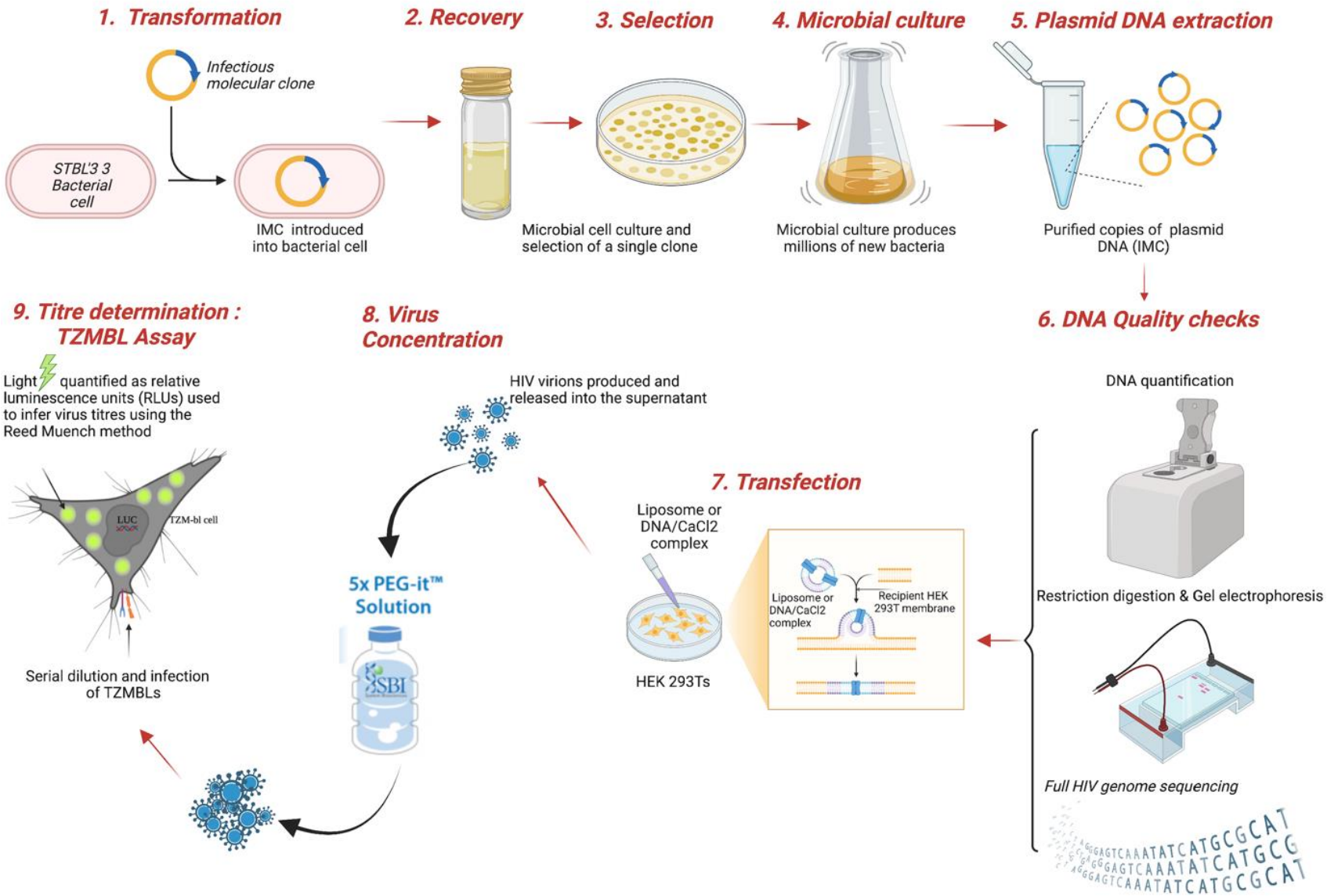

Figure 68. ***Flow chart of infection optimisation steps.*** *An illustration of IMC transformation, transfection, virus concentration and titre determination. IMCs were transformed in E.coli cells (STBL'3) and subsequently extracted and analysed for purity and size prior to being used for virus production through transfection. Resultant virus supernatants were harvested and concentrated followed by titre determination using the TZMBL assay and analysed using the Reed Muench method.*

2.2.1.1 Generation of infectious molecular clones (IMCs)

Transformation

DNA quantity

IMCs obtained were a kind gift from Dr Frank Kirchoff and Dr David G. Russel as previously mentioned. DNA was expanded through transformation of Stbl'3 *E coli*. Transformed bacterial colonies were selected and prepared for DNA extraction using the DNA midi-prep kit (Figure 68, Steps 1-5). The amount of extracted DNA was quantified using a Nano-Drop 2000 spectrophotometer as illustrated in Step 6, on Figure 68. The average concentration of extracted plasmid DNA was 1 46 µg/µl ± 57.98 µg/ as shown in Figure 69 below.

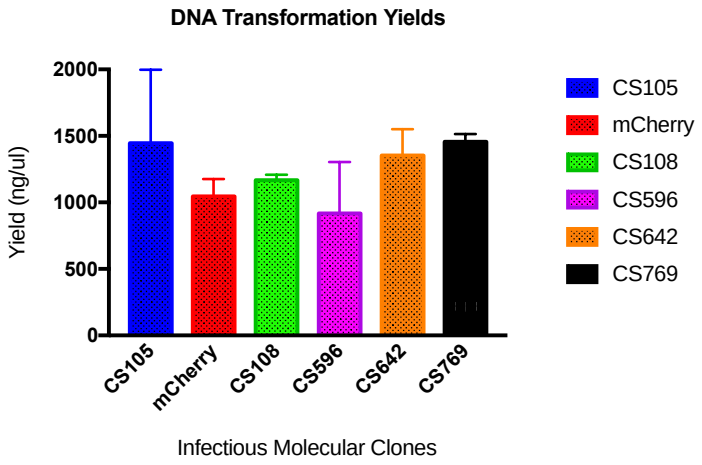

Figure 69. ***Quantification of DNA yields.*** *Proportions of DNA yields after transformation and DNA extraction. Statistics were generated using two-way ANOVA with Tukey's multiple comparisons test.. There were no significant different differences in DNA quantities measured using the Nano-Drop spectrophotometer*

DNA size and integrity

Enzymatic restriction digestion were used to confirm the identity and integrity of amplified plasmids as shown in Figure 68, Step 6 above. To do this, specific restriction digestion enzymes were used to cut the extracted DNA at specific restriction sites. In particular, HpaI/MluI were used to cut the GFP tagged NL4-3 IMCs, [NL4-3 X4 and NL4-3 92TH14-12 (R5)]. Meanwhile, Subtype B IMCs [CH058.c, CH077.t (TF), CH077.t (6 mo.) and RHGA (CC)] were cut using NotI/MluI and Subtype C IMCs [CH167, ZM246F-10, and CH198)] were cut using AscI/AsiSI. The size and integrity of the resultant restriction digests was performed using gel-electrophoresis on a 1 % agarose gel, and was confirmed as ~ 850 bp for the two NL4-3 IMCs as shown in Figure 70, Lanes 4 and 9. Subtype B IMCs were confirmed as ~3 200 bp (Figure 3, Lanes 1-3) while the Subtype C IMCs were confirmed as ~1 300 bp as shown in Figure 70, Lanes 5-8 below.

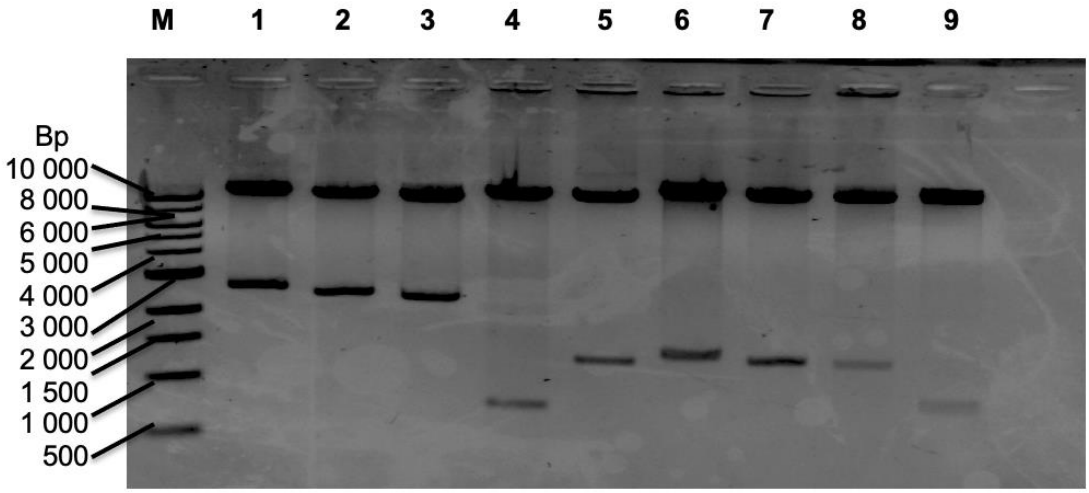

Figure 70. ***Determination of DNA size and purity using gel electrophoresis. Restriction digestion products of the extracted GFP tagged DNA plasmids were run on 1% agarose. Lane M: Molecular weight marker, Lanes 1-3: Subtype Cs', 1:CH167, 2: ZM246F-10, 3: CH198 Lane 4: NL4-3 X4, Lanes 5-8: Subtype Bs', 5: CH058.c, 6: RHGA, 7: CH077.t, 8: CH077.t (6 mo.) Lane 9: NL4-3 92TH14-12 (R5)***

Other than the GFP tagged NL4-3s' described above, an mCherry tagged NL4-3-BaL IMC was similarly transformed, extracted, cut and run on 1 % agarose gel through electrophoresis. There were three variations of this IMC namely; i) full genome (NL4-3-BaL), ii) backbone (NL4-3-Δ-Env) and iii) envelope (Bal-Env). While the full genome NL4-3 BaL was used to identify and infect CCR5 expressing HIV target cells, the backbone NL4-3-Δ-Env was used to assess the infectivity of NL4-3 using different envelopes, such as the BaL-Env and VSV-Env. NL4-3-Δ-Env was integrated with the VSV envelope for pseudo-typing, whereby VSV-G-NL4-3-Δ-Env was used for single round, non-replicative infection. This was used to promote the expression of reporter genes, to assess the expression and detection of mCherry.

Clones carrying the correct band sizes were digested and cut using HpaI/NotI. Subsequently, gel electrophoresis was used to visualize the confirmatory bands of ~3 000 bp for NL4-3-BaL and NL4-3-Δ-Env shown in Lanes 2 and 4 respectively, on Figure 71. The confirmatory band size for VSV-Env and BaL-Env, was ~ 5 500 kb as shown in Lane 6 and Lane 8 as illustrated in Figure 71 below.

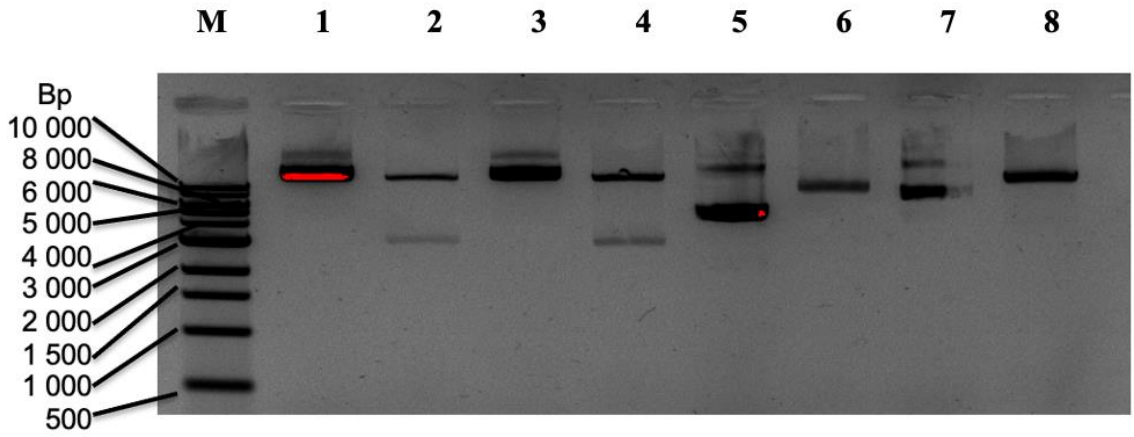

Figure 71. ***Determination of DNA size and purity of mCherry tagged IMCs.*** *Restriction digestion products of mCherry tagged IMCs were assessed and visualised using gel electrophoresis. Lane* ***M****: Molecular weight marker,* ***1****: uncut NL4-3-BaL,* ***2****: cut NL4-3-BaL,* ***3****: uncut NL4-3-Δ-Env,* ***4****: cut NL4-3-Δ-Env,,* ***5****: uncut pVSV-G,* ***6****: cut pVSV-G,* ***7****: uncut pBAL,* ***8****: cut pBAL*

Transfection and titre determination (TCID50)

After transformation and quality assessment checks, HEK 293Ts were transfected using the different IMCs in order to generate replication competent virus stocks as illustrated in Figure 68, Step 7, above. Transfected HEK 293Ts' were analysed for reporter gene expression using flow cytometry as shown in Figure 72 (a) below. Meanwhile, subsequent virus supernatants were concentrated using PEG-it and subsequently assayed for titre determination using the TZMBL-assay as shown in Figure 68, Steps 8-9. Proportions of GFP+ HEK 29Ts and the corresponding virus titres were different among the different viruses, as illustrated in Table 4, and Figure 72 (b) below.

Table 4. Proportions of GFP+ HEK 293T's and corresponding virus titres

Virus	Frequency of GFP+ HEK293Ts (Mean ± SD)	Titre (TCID50)
NL4-3 92TH14-12 (R5)	24.05 ± 13.51	91 376
Subtype B CH058.c (TF)	32.15 ± 17.04	54 437
NL4-3 X4	15.95 ± 9.83	13 975
Subtype C ZM246F-10 (TF)	15.63 ± 8.87	9 767
Subtype C CH167 (CC)	9.94 ± 4.75	16 275
Subtype B CH077.t (TF)	7.47 ± 5.42	2 795
Subtype C CH198 (TF)	6.65 ± 4.72	3 655
Subtype B (CH077.t (6 month)	5.23 ± 3.85	6 250
Subtype B RHGA (CC)	4.28 ± 3.42	559

Regression analysis was used to assess if there was any correlation between the frequency of transfected HEK 293Ts and virus titres as shown in Figure 72 (c). The frequency of transfected HEK 293Ts cells,

measured as the proportions of cells that were GFP+ or mCherry+, positively corelated with the corresponding virus titres. High titre viruses, identified as NL4-3 92TH14-12 (R5) and CH058.c (TF), simultaneously portrayed higher proportions of GFP+ HEK 293T cells, while lower titre viruses displayed lower proportions of GFP+ HEK293Ts as shown in Figure 72 (c).

a) Representative flow cytometry plots showing GFP expression in transfected HEK 293 Ts'

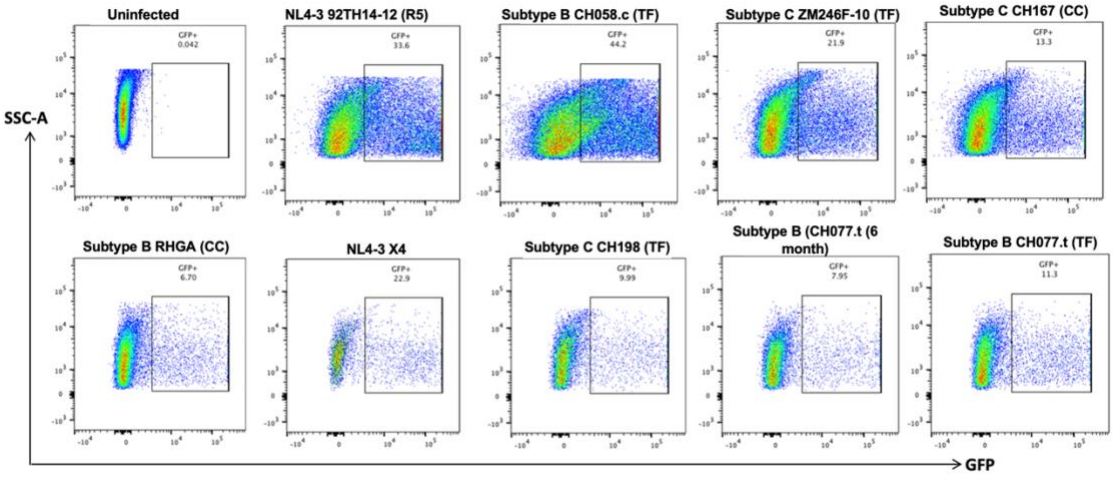

b) Proportions of GFP+ cells and virus titres

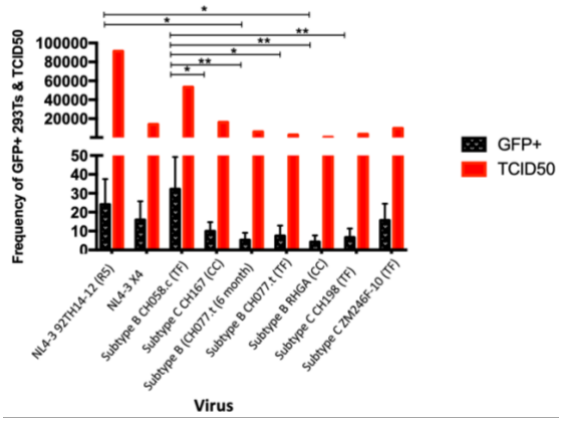

c) Corelation of GFP signal with corresponding virus titres

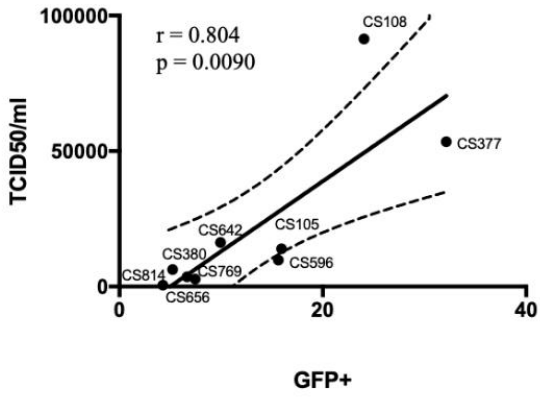

Figure 72. ***Proportions of GFP+ transfected HEK293Ts and corresponding virus titres.*** *Proportions of the GFP+ transfected HEK-293Ts alongside titres of the subsequent virus supernatants from the different GFP-tagged IMCs).* ***(a)*** *Representative flow cytometry plots showing GFP expression in transfected HEK 293Ts'.* ***(b)*** *Proportions of GFP+ HEK 29Ts and corresponding virus titres.* ***(c)*** *Corelation of the proportions of GFP+ HEK 293Ts' and the resultant virus titres. "CS" annotations correspond to the different viruses as follows; CS108=NL4-3-92TH14-12 (R5), CS377=CH058.c (TF), CS596=ZM246F-10 (TF), CS642=CH167 (CC), CS656=RHGA (CC), CS105=NL4-3X4, CS769=CH198 (TF), CS814=CH077.t (6 mo.), and CS380=CH077.t (TF). Statistics were generated using Pearson's Corelation-n Coefficient at 95 % Confidence Interval to assess the corelation between GFP signal and virus titres. One way Anova was used with Tukey's multiple comparisons test to compute differences among proportions of GFP+ 293Ts infected using different viruses.*

2.2.1.2 Infection – PBMCs and Cell lines

Having produced infectious virions and consequential determination of virus titres and the infection signal; selected viruses were then used to optimize and determine optimal titres for HIV infection and sampling time-points in PBMCs. Subsequently, different cell lines were used for validation and to further determine and compare the use of p24 and GFP/mCherry as infection signals.

PBMCs

Optimal M.O.I and incubation time-point for PBMC HIV Infection

In order to determine the optimal MOI/titre of the virus to use for infections, CD8 depleted and PHA stimulated PBMCs were used as described in the methods. Therefore, stimulated and CD8 depleted PBMCs were exposed to varying titres of GFP and mCherry tagged viruses and subsequently sampled at two different time points; i) 24 hours and ii) 72 hours. MOIs 0.01 and 0.001 were used for all the selected viruses except NL4-3 92TH14-12 (R5), that was additionally used at MOI 0.1 as a positive control, as shown in Figure 73 (a) below. HIV infection was measured as the expression of the reporter genes; GFP and mCherry *whereby, the proportions of GFP+ and mCherry+ PBMCs were quantified and identified as infected* as illustrated in Figures 73 (a) - (c).

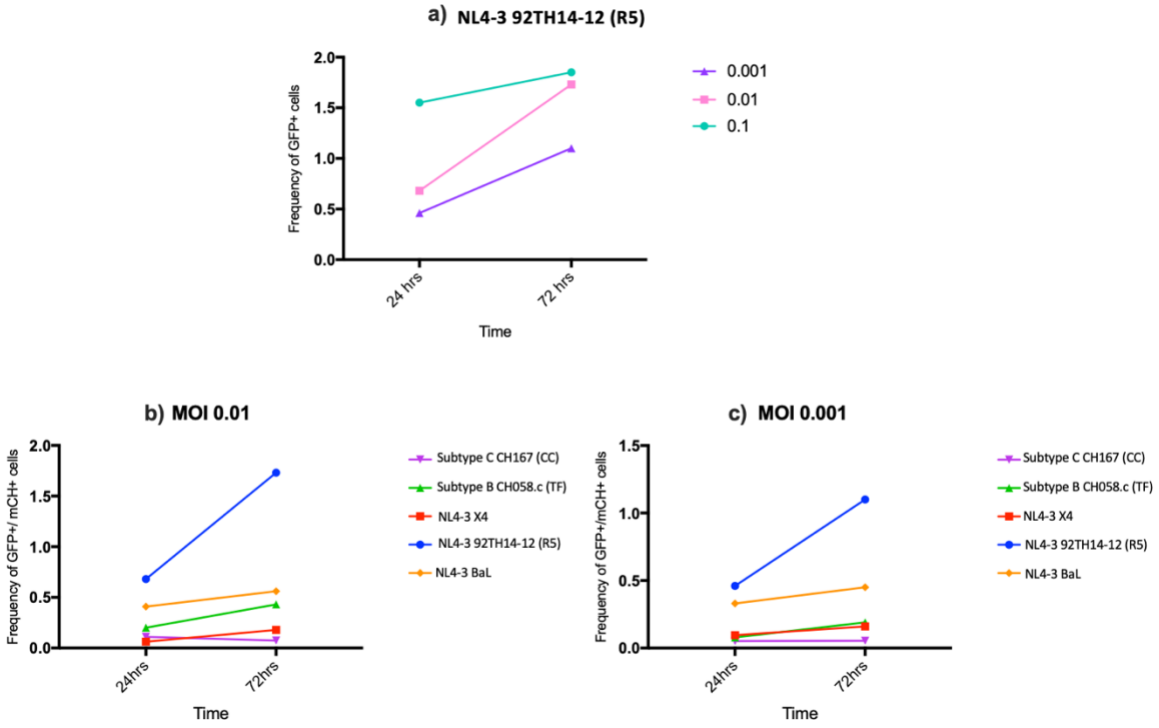

Figure 73. ***Assessment of optimal M.O.I and time-point for PBMC HIV Infection. (a)*** *Proportions of GFP+ PBMCs, infected using NL4-3 92TH14-12 (R5), at MOIs; 0,1, 0.01 and 0.001, at 24 and 72 hours. Representative flow cytometry plots showing proportions of HIV infected GFP+ and mCherry+ (b) Proportions of GFP+ PBMCs, infected using CH167 (CC), CH058.c (TF), NL4-3 X4, NL4-3 92TH14-12(R5) and NL4-3 BaL at MOI 0.01 and (c) 0.001, at 24 and 72 hours. The Wilcoxon test was used to compute p values.*

Figure 73 (a) illustrates that higher virus titres and longer incubation times were synonymous with high infection signal. The mean frequency of GFP+ cells, was highest (1.70 % ± 0.21 %) when NL4-3 92TH14-12 (R5) was used at an MOI of 0.1. This reduced 28.82 % when the virus was diluted to MO1 of 0.01, and the resultant mean frequency of GFP+ PBMCs was consequently 1.21 % ± 0.74 %. Further dilution to MOI 0.001 reduced the infection signal by 35.5 %. In like form, the mean frequency of GFP+ cells increased with time progression and this was witnessed using both high and low infectious titres. At MOI 0.01 the average frequency of GFP+ PBMCs, across all viruses, was 2-times more at 48 hours (0.59 % ± 0.66 %) compared to the 24 hour time-point (0.29 % ± 0.25 %).

Overall, PBMCs were more permissive to NL4-3 R5 viruses*;* NL4-3 92TH14-12 (R5) and NL4-3 BaL compared to NL4-3 X4 and Subtype B/C viruses at the different MOIs and incubation times as shown in Figures 73 (b) - (c) above. Although both NL4-3 92TH14-12 (R5) and NL4-3 BaL were comparatively more infective than other viruses, the mean frequency of NL4-3 92TH14-12 (R5) infected PBMCs (1.21 % ± 0.74 %) was 1.47-fold higher than that of NL4-3 BaL infected PBMCs (0.49 % ± 0.11 %) at MOI 0.01 and differed less when virus inocula was more dilute (MOI = 0.001) as shown in Table 5. However, infection with NL4-3 92TH14-12 (R5) was more significantly differed from the other viruses. In particular, at MOI 0.01, the mean frequency of NL4-3 X4 infected PBMCs was 9.08-fold lesser (0.12 % ± 0.01 %), while infection with CH167 (CC) was more profoundly differed and was 120-fold less than achieved with NL4-3 92TH14-12 (R5) as shown in Table 5.

Table 2.Fold change & % decrease from high to low MOIs in HIV infected PBMCs

Virus	MO1 0.01 (initial)	MO1 0.001 (final)	Fold CHANGE	% Decrease
NL4-3 X4	0.12 % ± 0.01 %	0.13 % ± 0.05 %	**0.08**	**-**
NL4-3 92TH14-12 (R5)	1.21 % ± 0.74 %	0.78 % ± 0.45 %	**- 0.36**	**35.54**
CH058.c (TF)	0.32 % ± 0.16 %	0.13 % ± 0.01 %	**- 0.59**	**59.38**
CH167 (CC)	0.01 % ± 0.03 %	0.05 % ± 0.01 %	**4.00**	**-**
NL4-3 BaL	0.49 % ± 0.11 %	0.39 % ± 0.08 %	**- 0.20**	**20.41**
Mean ± SD	0.44 % ± 0.45 %	0.30 % ± 0.30 %	**- 0.32**	**31.82**

Cell lines

Using the most infectious virus, as pre-determined in PBMCs above; various reporter based cell lines were exposed to varying titres of NL4-3 92TH14-12 (R5). These were inclusive of TZM-GFPs, CEM-GFPs, JLTR5Gs and CEM-REVs. TZM-GFPs and CEM-GFPs were engineered to express GFP upon HIV infection as described earlier, thereby enabling the simultaneous use of both p24 and GFP as HIV

infection signals. Infected cells were therefore identified by the detection of p24 and/or GFP using flow cytometry, as described below. This was done over an incubation period of 9 days (216 hours), during which sampling was carried out at 18 hours, 72 hours, 6 days (144 hours) and 9 days for all cell lines as follows:

TZM-GFP

TZM-GFPs were exposed to NL4-3 92TH14-12 (R5) at MOIs; 0.01, 0.001, 0.002 and 0.0005 for up to 9 days. Using GFP as measures of infection, TZM-GFPs were least infected at 18 hours where the proportions of GFP+ cells averaged 0.80 % ± 0.60 % as shown in Figure 74 (a). However, this increased 18.04-fold with time-progression and thus, averaged 15. 23 % ± 20.62 % at the 72 hour time-point, additionally identified as peak infection. This was especially observed using high titre virus (MOI 0.01) as shown in Figure 74. Meanwhile, infection with lower virus titres only peaked at the 144 hours' time-point, with the proportions of GFP+ cells amounting to 19.28 % ± 15.91 % as shown in Figure 74 (a). Further incubation resulted in declined proportions of GFP+ cells across all virus titres at the 216 hours' time point (11.26 % ± 5.37 %) in Figure 74 (a).

In contrast, using p24 as an infection determinant positively corelated with time. Therefore, the mean frequency of p24+ cells was highest at the furthest incubation time-point at 216 hours' as shown in Figure 74 (b). Notably, this was only assessed with MOI 0.01. The frequency of p24+ TZM-GFPs increased 2.3-fold between 18 and 216 hours as shown in Figure 74 (b). The positive corelation between the frequency of p24+ TZM-GFPs with time is depicted in Figure 74 (c). However, there was no corelation between the proportions of GFP+ and p24+ cells in HIV infected TZM-GFPs as illustrated in Figure 74 (d). With the exception of the 72 hour time point, the frequency of p24+ cells (37. 65 % ± 21. 59 %) was 1.2-fold higher than the frequency of GFP+ cells (17.09 % ± 19.88 %) shown in Figure 74 (d).

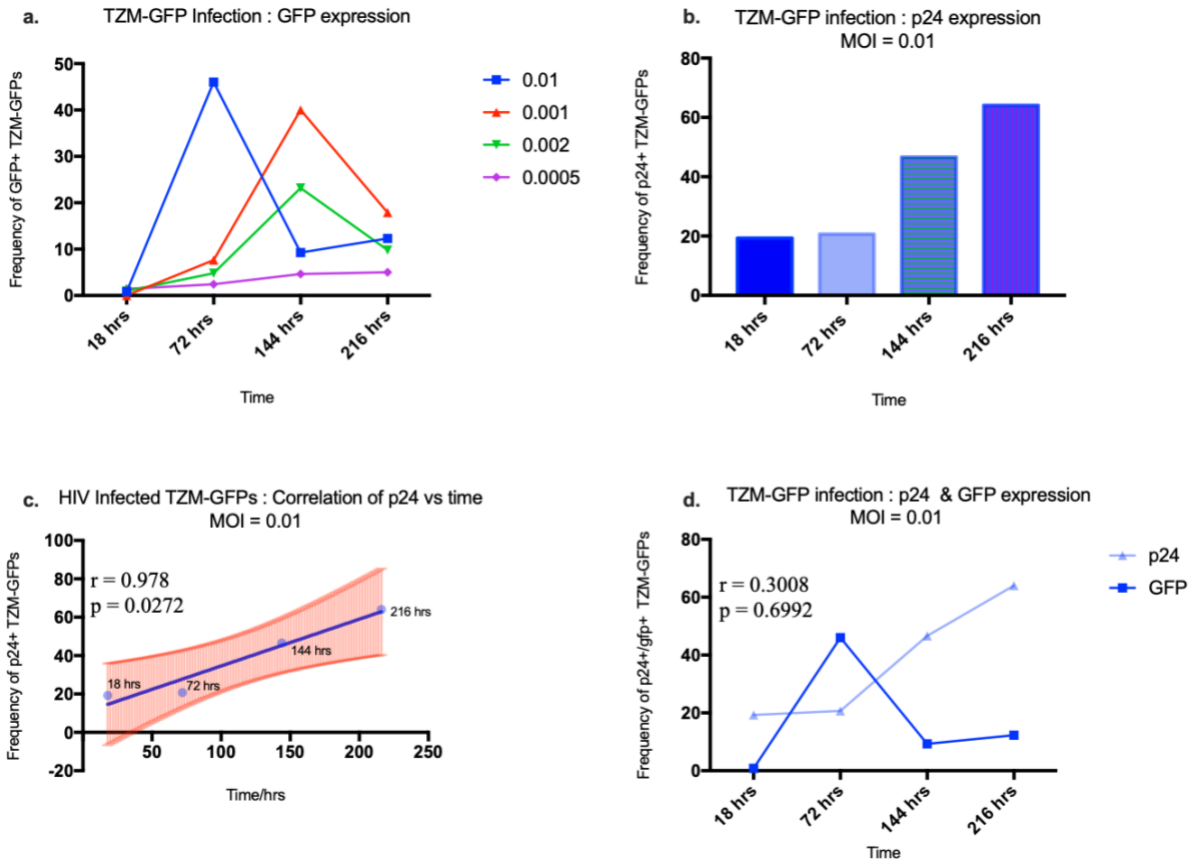

Figure 74. ***Optimisation and Determination of the HIV infection signal and optimal MOIs in TZM-GFPs. (a)*** *Proportions of GFP+ TZM-GFP cells infected using different MOIs of CS108; 0.01, 0.001, 0.002 and 0.0005 over 9 days* ***(b)*** *Proportions of p24+ TZM-GFP cells infected using CS108 at an MOI of 0.01over 9 days* ***(c)*** *Corelation of p24+ TZM-GFP with time* ***(d)*** *Proportions of GFP+ and p24+ TZM-GFPs over time. Statistics were calculated using Pearson's Corelation Coefficient at 95 % Confidence Interval and t tests. Two way Anova, with Tukey's multiple comparisons test was used to compute differences among proportions of GFP+ and p24+ 293Ts.*

JLTR5G

Similarly to TZM-GFPs above, different titres of NL4-3 92TH14-12 (R5), MOIs; 0.01, 0.001, 0.002 and 0.0005; were used to infect the JLTRG5 cell line with subsequent assessment of GFP and p24 to measure HIV infection, over 9 days. In like-manner to TZM-GFPs, GFP expression was dose dependent as shown in Figure 75 (a). Peak infection was at 72 hours (11.57 % ± 11.45 %), followed by a 22 % decline upon further progression with time. Expression of p24 was also measured as an infection indicator in JLTR5Gs'at MO1 0.01, similarly to TZM-GFPs above in Figure 75 (b). The peak infection time-point for p24 use was 144 hours, beyond which, the proportions of p24+ JLTRG5's declined by 51 % as shown in Figure 75 (b).

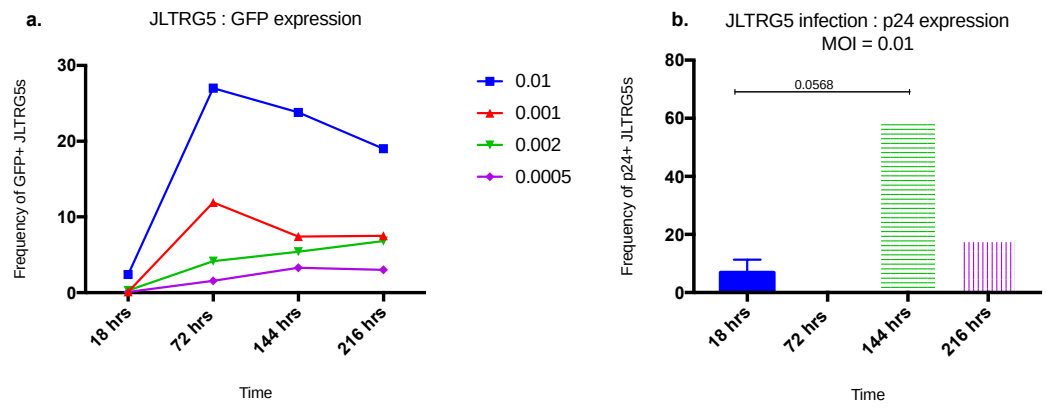

Figure 75. ***Optimisation and Determination of the HIV infection signal and optimal MOIs in modified Jurkats (JLTR5Gs).*** *Proportions of GFP+ and p24+ JLTR5Gs.* ***(a)*** *Proportions of GFP+ JLTRG5 cells infected using different MOIs of NL4-3 R5 (CS108) and NL4-3 Bal (mCherry); 0.01, 0.001, 0.002 and 0.0005 over 9 days* ***(b)*** *Proportions of p24+ JLTR5G cells infected using CS108 at an MOI of 0.01over 9 days Statistics were calculated using Pearson's Corelation Coefficient at 95 % Confidence Interval and t tests. Two way Anova, with Tukey's multiple comparisons test was used to compute differences among proportions of GFP+ and p24+ 293Ts.*

CEM-GFP and CEM-REV

CEM-GFPs were also infected under the same conditions as infection of TZM-GFPs and JLTRG5's, as described above. Similarly, infection was dose dependent. At an MOI of 0.01, the mean frequency of GFP+ CEM-GFPs was 10.59 % ± 10.01 %, 22 % more than achieved with lower MOI 0.001 (8.67 % ± 6.7 %). Furthermore, the peak infection time point was also at 144 hours using p24 while GFP peaked at 72 hours. On average p24+ CEM-GFPs (35.95 % ± 40.98) were 2.4-fold more frequent than GFP+ CEM-GFPs (10.59 % ± 10.01 %) under the same experimental conditions as shown above. However, infection of CEM-REVs was similar across all the different titres used and not dose dependent (data not shown).

Summary

Use of GFP as an infection signal resulted in comparatively lower frequencies of HIV infected cells than when p24 was used as a measure of infection. This was true for all cell lines, except for TZM-GFPs whereby a positive corelation was observed between the frequency of p24+ and GFP+ cells when the same virus titre was used to establish HIV infection. The MOI of 0.01 at 72 hours and at 144 hours yielded more HIV infected cells than other virus titres and time-points, for both GFP and p24 use as determinants of HIV infection. This was also observed in PBMCs. Based on these findings, p24 was therefore used as a measure of HIV infection.

2.2.1.3 Evaluation of foreskin infection models: suspension cells & epidermal sheets

Having pre-determined optimal virus titres and optimal incubation periods in PBMCs shown in Figures 73 (a) - (c) as well as in cell lines shown in Figures 74 - 75 above; the different viruses were then used to optimize and design infection models against foreskin cells. To do this, two modes of *ex vivo* HIV infection of primary foreskin tissue cells, were assessed as illustrated in Figure 76 below. These were the a) the epidermal sheet model and b) the pluricellular cell suspension model shown in Figure 76 (i-ii).

Using 5 participants, foreskin epidermal sheets were stripped off the rest of the foreskin dermis at the basal layer as previously described in Methods, using dispase enzyme. Resultant epidermal sheets were treated in two different ways. In one experiment, shown in Figure 76 as (A), epidermal sheets were inoculated with virus by placing them on media with virus on the basal layer for 5 hours as described in the methods, after which they were washed and cells allowed to migrate out of the virus exposed epidermal sheets (labelled in red). Following migration, remnant tissue was digested using Liberase enzyme to yield non-migratory infected cells (*Epi-sheets: Lib)* shown in Figure 76 (i) while migratory infected cells (*Epi-sheets: Crawl)* are shown in (ii).In parallel, shown in Figure 76 (B), epidermal sheets were directly incubated for cells to migrate out, as described earlier. Cells spontaneously migrating out of foreskin epithelia were harvested and exposed to NL4-3 BaL at an MOI of 0.01, according to the optimisation findings in cell lines and PBMCs described above (Figures 73-75*)*. NL4-3 BaL was used for optimisation owing to its CCR5 usage, and thus expected to infect myeloid cells such as Mϕ and LCs. Due to the suspension of heterogenous primary cells in tissue culture media, this mode of HIV infection was referred to as the pluricellular cell suspension model, shown in Figure 76 (iii). These, alongside migratory (Epi-sheets: Crawl) and non-migratory (Epi-sheets: Lib) cells from HIV infected epidermal sheets where assessed for p24 expression at 18 and 48 hours as illustrated in Figure 76 (C).

To assess HIV infection in these different infection models, foreskin lymphocytes (*purple*) were analysed seperately from foreskin granulocytes (big cells – *multi-color*) which were infected within the same experimental well as demonstrated in Figure 76 (C) below. Cells from the granulocyte gate were further characterized into Langerhans Cells (*yellow*) and "Mϕ-like" populations (*blue*), that were additionally sub-sectioned into different subsets and analysed for HIV infection (Figure 76 (C). However, the expression of CD80/86 was omitted in HIV infected cells due to panel limitations. GFP (a measure of HIV infection) and CD80/86 were both on the same FITC fluorochrome and there was no additional space in the panel to introduce a new fluorochrome for either one of the markers. Owing to this, "M1-like" Mϕ and the transitionary "M1/M2" intermediates could not be classified, although highly HLA-DR expressing subsets were still identifiable. "M2-like" Mϕ, identified as CD206+CD209+/- from the CD11c/CD14 gate could also still be identified.

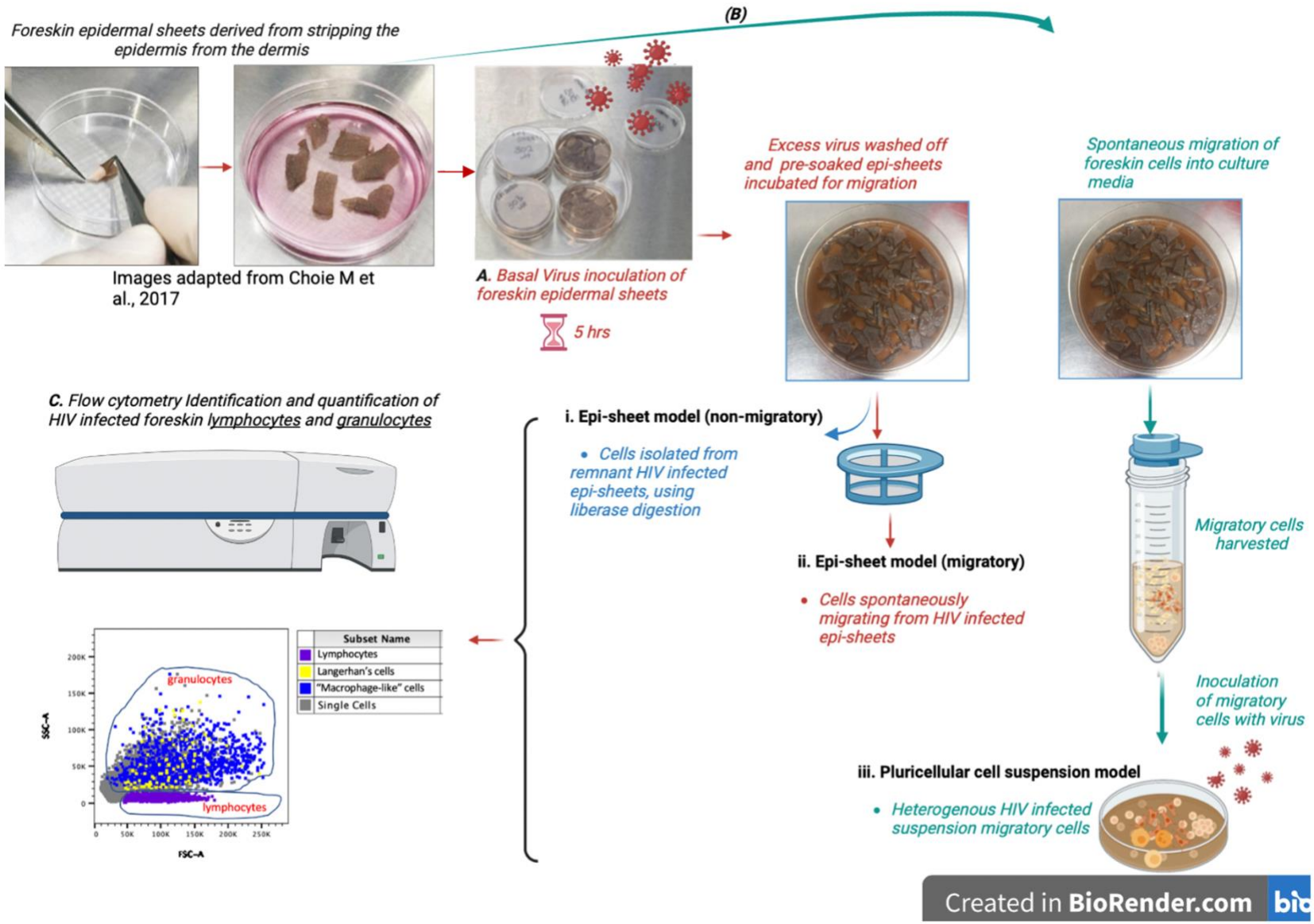

Figure 76. ***Infection of foreskin cells using different infection models****; i) non-migratory and ii) migratory epi-sheet models and iii) pluricellular suspension cell model. Foreskin epidermal sheets were stripped from the rest of the foreskin tissue and treated as follows;* ***(A-cell suspension model)*** *Inoculated and incubated with virus for 5 hours. (ii) Infected migratory cells were harvested from infected epi-sheets (i) Non migratory infected cells were harvested from remnant epi-sheets* ***(B-epidermal sheet model)*** *.Cells spontaneously migrating from non-infected epi-sheets were inoculated with virus to set up the pluricellular cell suspension infection model in (iii). (C) Infected foreskin cells from the different models were analysed for p24 expression using flow cytometry, where granulocytes (big cell gate-multi-color) and lymphocytes (small cell gate-purple), were analysed seperately.*

HIV-1 infection of FS Lymphocytes

As shown in Figure 77 (C) above, foreskin lymphocytes were also analysed for HIV infection using p24 expression and the different infection models. Therefore, at 18 hours, the mean frequency of p24+ lymphocytes was higher in the pluricellular suspension infection model compared to the epidermal sheet infection model. In particular, the mean frequency of p24+ lymphocytes was 13.54 % ± 3.59 in the pluricellular suspension infection model, 14.9-fold higher than the epidermal sheet infection model where p24+ lymphocytes were only 0.91 % ± 0.62 % (*p = 0.0017*) as shown in Figure 77 (i) below. Consistent to this, the expression levels of p24 in HIV infected lymphocytes, measured as mean fluorescence intensities of p24 (p24 MFIs), were also correspondingly higher (3-fold) in the suspension model (11 274 ± 1 961) in comparison to the epidermal sheet model (3 713 ± 302.2; *p = 0.01*) as illustrated in Figure 77 (ii) below.

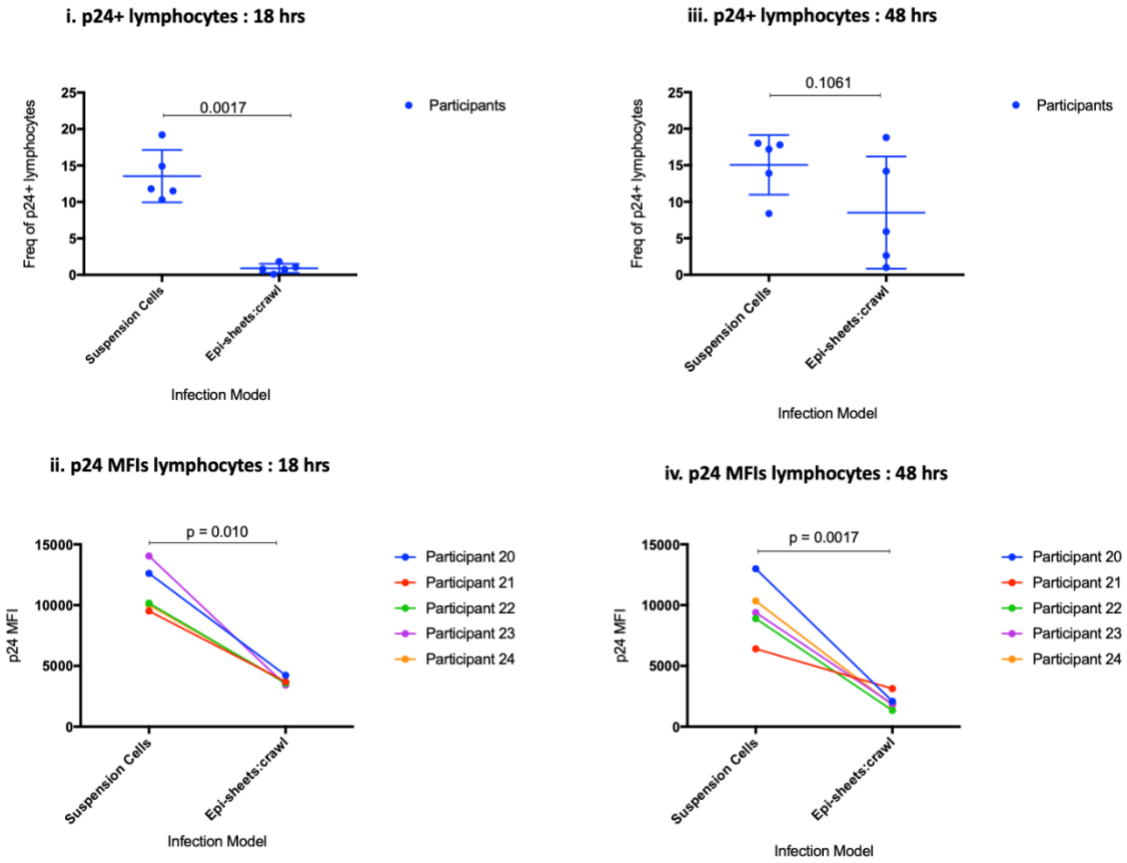

Figure 77. ***Proportions of p24+ lymphocytes and p24 MFIs in different foreskin infection models at two different time points.*** *(i). Frequency of p24 in foreskin lymphocytes infected using the cell suspension infection model and epidermal sheet infection models at 18 hours (ii) p24 MFIs in foreskin lymphocytes infected using the cell suspension infection model and epidermal sheet infection models at 18 hours (iii). Frequency of p24 in foreskin lymphocytes infected using the cell suspension infection model and epidermal sheet infection models at 48 hours (iv) p24 MFIs in foreskin lymphocytes infected using the cell suspension infection model and epidermal sheet infection models at 48 hours (n=5). The Wilcoxon test was used to compute p values.*

Similarly to PBMCs above, HIV infected foreskin lymphocytes were seen to increase with time in both infection models although more profoundly in the epidermal sheet infection model, where HIV infected lymphocytes increased 8.4-fold between 18 (0.91 % ± 0.62 %) and 48 hours (8.51 % ± 7.68 %; *p = 0.0020*) as demonstrated in Figures 77 (i-ii). Similarly to the 18 hr time point, p24 expression levels as measured by p24 MFIs, were 4.7-fold higher in the suspension model (9 608 ± 2 390) compared to the epidermal sheet model (2 043 ± 662.9; *p = 0.0017*) as shown in Figure 77 (iv).

HIV infection of Granulocytes (big cells)

Although without statistical significance, the mean frequency of p24+ granulocytes was 3.69-fold higher in the pluricellular suspension cell model (9.37 % ± 7.88 %) in comparison to the epidermal sheet model (2.54 % ± 1.95 %; *p = 0.0762*) at 18 hours, as shown in Figure 78 (i) below. Correspondingly, foreskin granulocytes from the pluricellular suspension cell model portrayed 2.08-fold higher, the levels of p24 expression (MFI =6 893 ± 4141), in comparison to the epidermal sheet model (MFI =3 316 ± 288.6; *p = 0.1167*) as shown in Figure 78 (ii).

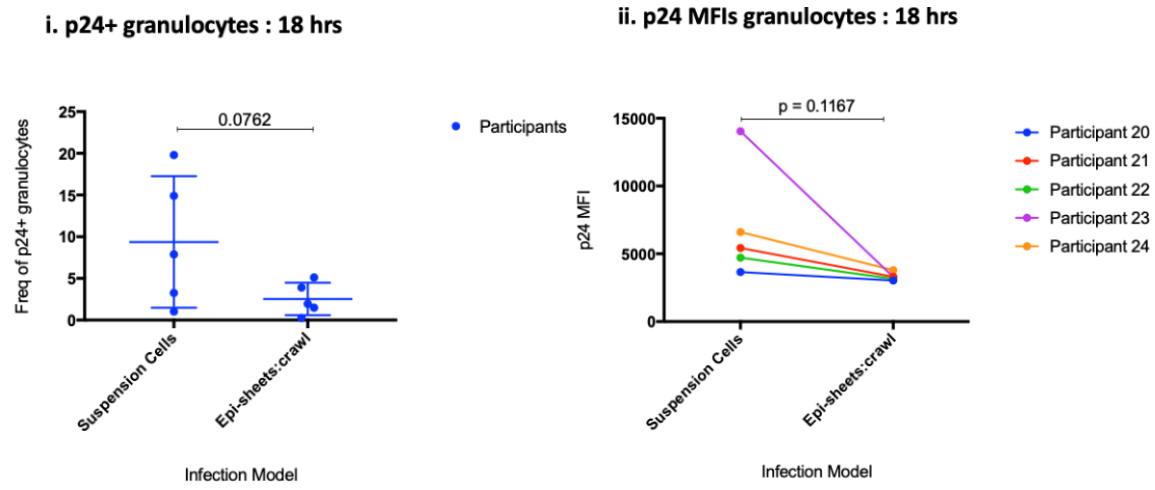

Figure 78. ***Proportions of p24+ granulocytes and p24 MFIs in different foreskin infection models at two different time points.*** *(i). Frequency of p24 in foreskin granulocytes infected using the cell suspension infection model and epidermal sheet infection models at 18 hours (ii). MFI of p24 in foreskin granulocytes infected using the cell suspension infection model and epidermal sheet infection models at 18 hours (iii) Frequency of p24 in foreskin granulocytes infected using the cell suspension infection model and epidermal sheet infection models at 18 hours (iv). MFI of p24 in foreskin granulocytes infected using the cell suspension infection model and epidermal sheet infection models at 18 hours (n=5). The Wilcoxon test was used to compute p values.*

Impact of time on the infection of FS lymphocytes and granulocytes

Using the same infection model illustrated in Figure 76, the foreskin epidermal sheet model (Epi-Crawl) was used to monitor the progression of HIV infection over a 5-day period in 3 participants. Only one of the three participants, was infected with HIV (data not shown), and displayed similar trends as those described above when more participants were infected (Figures 77-78). Although the mean frequency

of p24+ lymphocytes (24.72 % ± 24.72 %) was 8.8-fold higher than that of p24+ granulocytes (2.82 % ± 2.72 %) at all time-points, similar trends were exhibited in both cell types. The proportions of HIV infected lymphocytes and granulocytes were the highest at earlier time points: 5 hours (50.7 %; 3.09 %) and 18 hours (50.2 %; 6.35 %) followed by a steep decline at 48 hours (1.41 %; 0.26 %). Interestingly, this steep decline preceded a sharp 14.1-fold and 16-fold increase in the proportions of HIV infected lymphocytes and granulocytes (respectively) upon a further 120-hr incubation period (21.3 %; 4.42 %) as shown in Figure 79 (a) below. The expression levels of p24 as measured by mean fluorescence intensities per cell, also depicted a similar trend and were highest at 120 hours where MFI/cell equated 5.5 and 1.05 respectively as shown in Figure 79 (b).

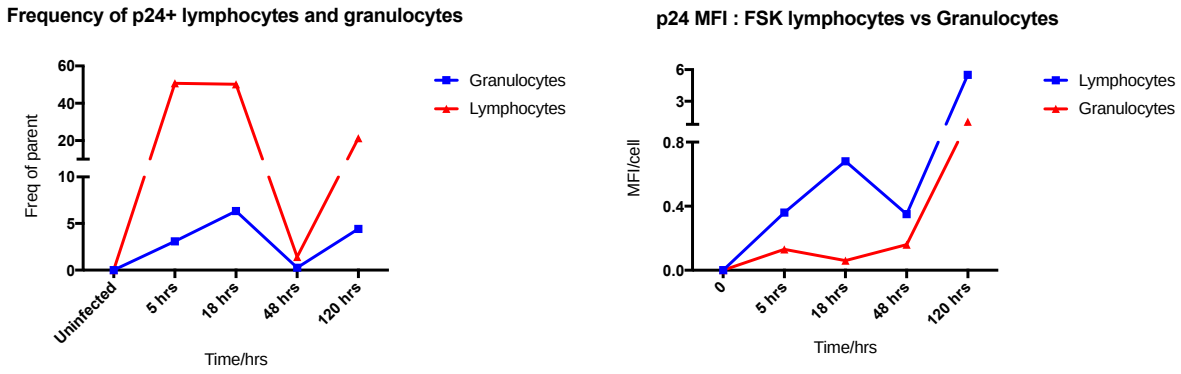

Figure 79. ***HIV infection of FS lymphocytes and granulocytes over 120 hours (participant 303).***

Specific granulocyte populations

After establishing the differences in the infection of foreskin lymphocytes and granulocytes using different models and incubation times, the cells derived from the granulocyte gate (big cell gate) were further categorized into specific cell types. These cell types were LCs and "Mϕ-like" cells, denoted as yellow and blue inside the granulocyte gate in Figure 76 (C) above. This was done to assess the infectability of foreskin LCs and "Mϕ-like" cells and cell recovery in the different infection models. Note, both migratory (Epi-crawl) and non-migratory (Epi-Lib) cells from the epidermal sheet models were analysed alongside the pluricellular suspension cell model.

Langerhans Cells

Proportions of HIV infected Langerhans cells in the different infection models

LC recovery was not differed when isolated using the pluricellular cell suspension and epidermal sheet models, as evidenced by similar uninfected LC proportions of 0.18 % ± 0.08 % and 0.22 % ± 0.09 % respectively, as shown in Figure 80 (a) below. However, when assessed as fraction of the p24+ granulocyte population, HIV infected LCs were 2-times more enriched in the epidermal-sheet model (0.8 % ± 0.76 %) compared to the pluricellular cell suspension infection model (0.4 % ± 0.23 %; $p = 0.6250$), although without statistical significance as shown in Figure 80 (b).

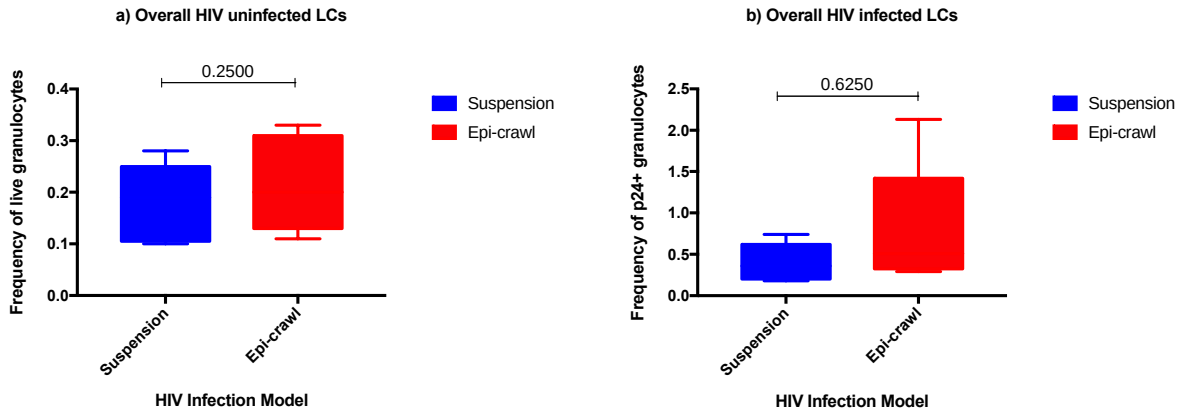

Figure 80. ***Proportions of HIV infected Langerhans Cells from the different infection models. (a)*** *Proportions of uninfected LCs in the pluricellular cell suspension model and the epidermal sheet model* ***(b)*** *Proportions of infected LCs in the pluricellular cell suspension model and the epidermal sheet (n=5). Statistics were calculated with t-tests, using the Wilcoxon test to compute p values.*

Different LC subsets were subsequently gated from the overall LC population and assessed for distribution in the different infection models. These were i) traditional LCs, ii) CD11c+ LCs, iii) CD14+ LCs, iv) CD11c+CD14+ LCs as well v) non-conventional CD3+ LCs shown in Figure 81 below and described in the Immunophenotyping Chapter.

Different HIV infection models resulted in different proportions of LC subsets as shown in Figures 81 (a) – (d). Traditional LCs were described in the Immunophenotyping to constitute ~50 % of the foreskin CD1a+CD207+ cells. In corroboration, the epidermal sheet and pluricellular cell suspension models also portrayed higher proportions of traditional LCs in relation to other LC subsets. Specifically, traditional LCs constituted 44.53 % and 29.22 % of the uninfected LC subsets in the pluricellular and epidermal-sheet models respectively (Figures 81 a-b). In accordance with the rarity of LCs as a myeloid subset, these proportions were only representative of 0.09 % ± 0.04 % and 0.07 % ± 0.03 % of the

overall foreskin granulocyte (big cell gate) population from the pluricellular cell suspension model and the epidermal sheet model respectively.

Interestingly, this traditional LC subset was further under-represented in HIV infected LC subsets from the pluricellular suspension cell model where it only constituted 0.25 % of the infected LCs, an equivalent of 0.0008 % ± 0.001 % of the p24+ foreskin granulocytes (Figure 81c). Similarly, HIV infected traditional LCs from the epidermal sheet model only constituted 0.06 % of the HIV infected LC subsets, representative of a small, 0.0004 % ± 0.0005 %, fraction of the overall p24+ foreskin granulocytes (Figure 81d). Traditional LCs were therefore poorly infectable using both infection models.

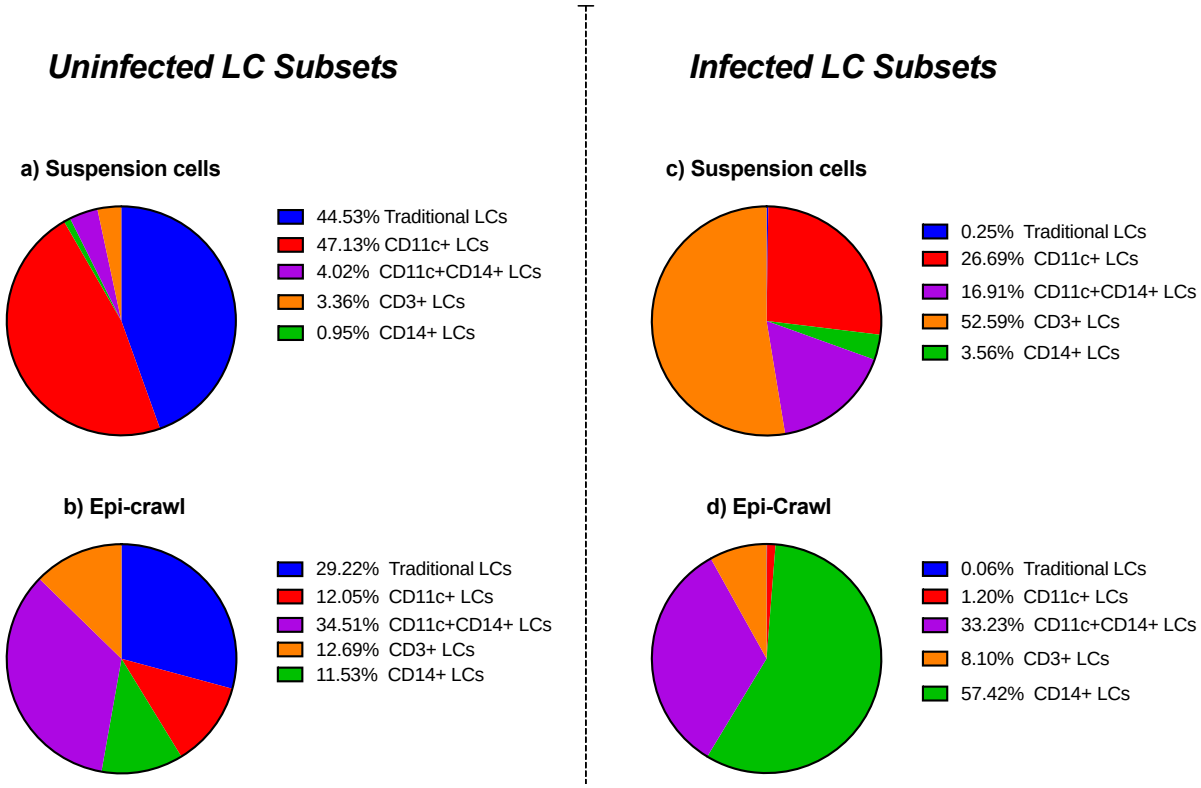

Figure 81. ***Evaluation of HIV infection models for the HIV infection of foreskin Langerhans Cells' Subsets.*** *Proportions of Uninfected and p24+ LC subsets; Traditional LCs (blue), (ii) CD3+LCs, (orange) CD11c+ LCs (red), (iv) CD11c+CD14+ LCs (purple) and (v) CD14+ LCs (green) from different infection models;* ***(a)- (b)*** *Uninfected LC subsets from the pluricellular suspension cell model and the epidermal sheet model* ***(c)-(d)*** *Infected cells from the pluricellular cell suspension model and the epidermal-sheet model (n=5). Statistics were calculated with two-way ANOVA using the Tukey's multiple comparisons test at 95 % CI of difference and adjusted p values. *p <0.05; **p < 0.01; ***p < 0.001; ****p < 0.0001*

Contrary to uninfected traditional LCs whose proportions were similar in the two infection models, the mean frequency of uninfected CD11c+ LCs was 3-fold higher in the pluricellular suspension model (0.09 % ± 0.05 %) compared to the epidermal sheet model (0.03 % ± 0.01 %; $p = 0.0020$). These constituted 47.13 % and 12.05 % of the LC subsets respectively, as shown in Figures 81 (a) - (b). However, unlike traditional cells, CD11c+ LCs remained disproportionately high in the HIV infected

LCs from the pluricellular suspension cell model (0.09 % ± 0.1 %) which was constitutive of 26.69 % of p24+ LC subsets as shown in Figure 81 (c).

Notably, CD3+ LCs were among the least frequent uninfected LC subsets (3.36 %) in the pluricellular suspension cell model, amounting to 0.008 % ± 0.008 % of the granulocyte population. However, CD3+ LCs were over-represented in HIV infected LCs, where they increased 20-fold to 0.17 % ± 0.21 %, thus attributing to 52.69 % of the HIV infected LC subsets as shown in Figure 81 (c). This was suggestive of a model based response, since it was only observed in the pluricellular cell suspension model.

Contrary to the over-representation of HIV infected CD11c+ LCs in the pluricellular suspension cell model; HIV infected CD11c+ LCs from the pre-soaked epidermal sheets were under-represented (0.008 % ± 0.02 %) and only constituted 1.2 % of the HIV infected LC subsets as shown in Figure 81 (d). HIV infected CD11c+ LCs from the epidermal sheet model were thus, 11.25-fold lesser in comparison to those from the pluricellular suspension cell model. Instead, the HIV pre-soaked epidermal sheets were more populated with CD14+ LCs (0.4 % ± 0.61 %) and CD11c+CD14+ LCs (0.23 % ± 0.16 %) that constituted 57.42 % and 33.23 % of the HIV infected LC subsets respectively as shown in Figure 81 (d).

"Macrophage-like" Cells

Proportions of HIV infected "Mϕ-like" in different infection models

Different HIV infected "Mϕ-like" populations were also determined in the different HIV infection models. These were inclusive of: i) "M2-like" Mϕ , ii) CD3+ Mϕ iii) CD169+ Mϕ and iv) HLA-DR+ cells (potential "M1" Mϕ phenotype) as shown in Figure 82 below.

According to the Immunophenotyping data, the foreskin Mϕ population was constitutive of M2-like" Mϕ and CD3+ Mϕ, while CD169+ Mϕ, "M1-like" Mϕ and M1/M2 intermediates were the least frequent subsets. As mentioned above, without CD80/86, the characterisation of "M1-like" Mϕ and the intermediates was not feasible and therefore HLA-DRhi cells, were identified instead. Corroboratively to immunophenotyping, "M2-like" Mϕ constituted 43 % of the uninfected macrophages isolated using the pluricellular suspension cell model as shown Figure 82 (a), although this was only representative of 0.72 % ± 0.30 % of the foreskin granulocytes. The epidermal sheet model was conversely more populated with CD3+ Mϕ, whose mean frequency was 3.89 % ± 4.42 % and constituted 63.43 % of the uninfected Mϕ population while "M2-like" Mϕ (1.5 % ± 0.76 %) constituted a lower proportion of

24.09 % as shown in Figure 82 (b). Although differed in these aspects, both the pluricellular suspension cell model and the epi-sheet model comprised lower proportions (<10 %) of uninfected CD169+ Mϕ (0.13% ± 0.09 %; 0.28 % ± 0.11 %) and HLA-DR+ cells (0.16 % ± 0.16 %; 0.49 % ± 0.23 %) respectively (Figures 82 a-b).

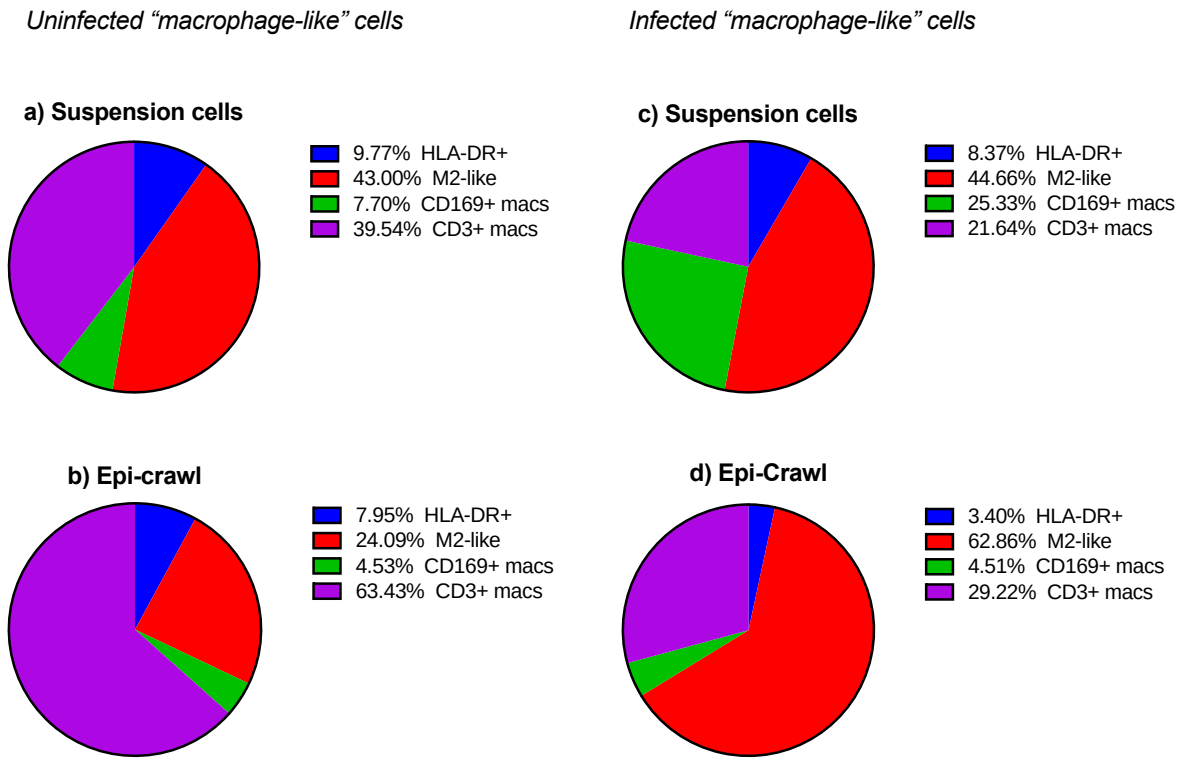

Figure 82. ***Evaluation of HIV infection models for the HIV infection of foreskin "Macrophage-like" Subsets.*** *Proportions of p24+ "macrophage-like" cell subsets; (i) "M2-like" macrophages (red), (ii)) CD3+ macrophages (purple) and (iii) CD169+ macrophages (green) from the different infection models;* ***(a)- (b)****Uninfected pluricellular suspension cell model, and migratory epi-sheet model* ***(c)-(d)*** *Infected pluricellular suspension model and migratory epidermal-sheet model (n=5). Statistics were calculated with two-way ANOVA using the Tukey's multiple comparisons test.*

Interestingly, the mean frequency of CD169+ Mϕ increased 12.3-fold (1.73 % ± 1.60 %) upon HIV infection using the pluricellular suspension cell model, resulting in an increased proportion of 25.33 % within the infected Mϕ population as shown in Figure 82 (c). While the proportions of HIV infected "M2-like" Mϕ predominated both infection models; a more profound, 5.26-fold increase (1.5 % ± 0.76 %)**,** was noticeable in the epidermal sheet model where "M2-like" Mϕ constituted 62.86 % of the HIV

infected Mϕ. Owing to the bulk of the HIV infected Mϕ being "M2-like"; HLA-DR+ cells (0.51 % ± 0.63 %) and CD169+ Mϕ (0.67 % ± 0.31 %) were the least represented subsets in the epidermal sheet infection model where they comprised 3.4 % and 4.5 % respectively, as shown in Figure 82 (d).

Summary

"Mϕ-like" subsets were more abundant compared to the proportions of LC subsets in both infected and uninfected models as illustrated in Figures 81 (a)-(b). Traditional LCs, although more frequent in uninfected cells were least frequent in HIV infected cells, while CD11c+ LCs and CD11c+CD14+ LCs were more enriched in the HIV infected cells as shown in Figures 83 (a) – (b). Except for the comparatively lower cell recovery of uninfected LC subsets such as CD14+ LCs, CD11c+CD14+ LCs and the CD3+ LCs in the pluricellular suspension cell model, the two infection displayed similar proportions of all the other myeloid cell subsets.

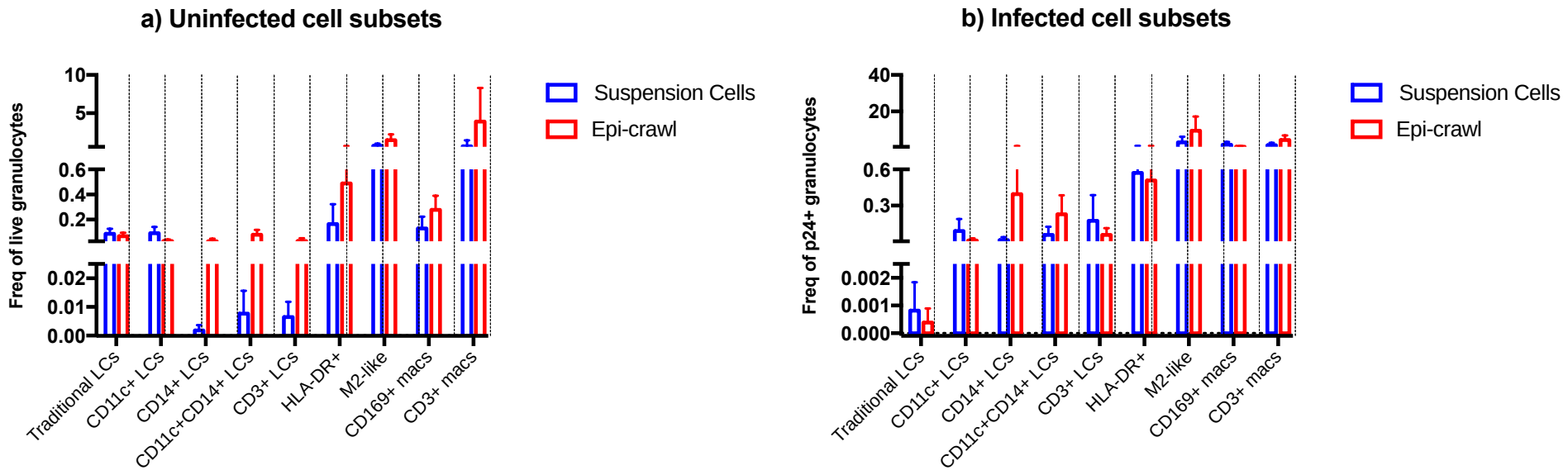

Figure 83. ***Proportions of HIV infected Langerhans Cells and "Macrophage-like" Cells from different infection models.*** *HIV infected LCs and "macrophage-like" subsets in the suspension cells, migratory epi-sheet (Epi-crawl) infection models (n=5). Statistics were calculated with two-way ANOVA using the Tukey's multiple comparisons test at 95 % CI of difference and adjusted p values. *p <0.05; **p < 0.01; ***p < 0.001; ****p < 0.0001*

2.2.1.4 *Ex vivo* HIV Infection of isolated pluricellular foreskin primary cell suspensions

Due to small sample requirement, minimal manipulation associated with spontaneous migration and the heterogeneity of infectable myeloid cell types, the pluricellular suspension cell model was selected as the HIV infection model going forward. The anti-HIV entry drug, maraviroc, was used to validate the *ex vivo* infection.

Optimization of the drug titre

TZM-bl cells were used to determine the optimal drug concentration by comparing the different levels of HIV inhibition using a range of drug concentrations from 40 nM to 0.000512 nM as described the Methods. A dose dependant inhibition of HIV infection was observed, as shown in Figure 84. Maraviroc dosage was inversely proportional to HIV infection, with an IC50 of 0.3551 nM ± 0.2158 nM.

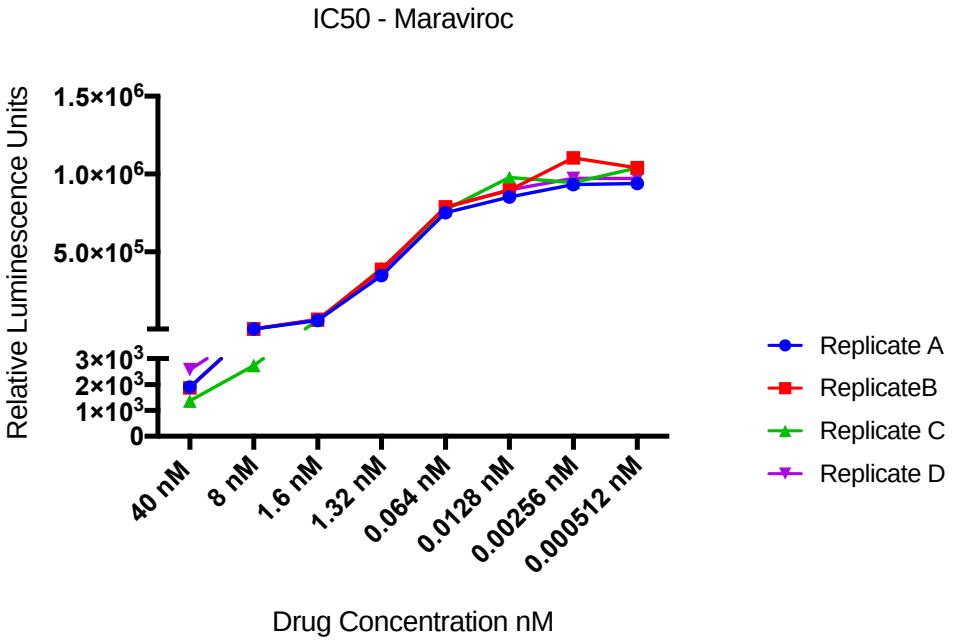

Figure 84. ***Determination of the minimum inhibitory concentration (IC_{50}) of the control anti-retroviral drug (Maraviroc)***. *Using four replicates (A-D), the TZMBL assay was used to determine the IC_{50} of Maraviroc in HIV inhibition. Statistics were calculated using non-linear regression (curve fit) analysis using inhibitor vs normalized response – Variable slope (four parameters) and the least squares ordinary fitting method*

In vitro/Ex vivo Foreskin cell Infection by HIV

Subsequently, HIV entry inhibition was used to validate the HIV infection of primary foreskin cells. Primary foreskin cells were isolated from 5 participants, and challenged using the optimized pluricellular cell suspension HIV infection model that was shown in Figure 76 (iii) and the optimized virus titre MOI of 0.01 alongside control experiments in which HIV entry was blocked by using the entry inhibitor, maraviroc at the optimised IC50 of 0.36 nM as determined above.

Virions derived from different IMCs' as described earlier, were used for this. Various NL4-3 Subtype B viruses were used; i) NL4-3 (X4), ii) NL4-3-BaL (R5) and NL4-3 92TH14-12 (R5). Two types of Subtype C viruses were used; i) transmitted founder (TF) and ii) chronic infection (CC) derived viruses. Namely, the transmitted founder viruses were ZM246F-10 (TF) and CH198 (TF). Lastly, the chronic infection derived virus was CH167 (CC).

The pluricellular model enabled different cell types to be infected simultaneously within the same culture, however, lymphocytes were analysed seperately from cells in the big cell gate, referred to here, as the granulocytes as shown in Figure 76 (C) above and in the gating strategy below in Figure 86. HIV infection was measured using the expression and detection of p24 in the foreskin lymphocytes and granulocytes as illustrated in the gating strategy below (Figure 85).

Gating strategies

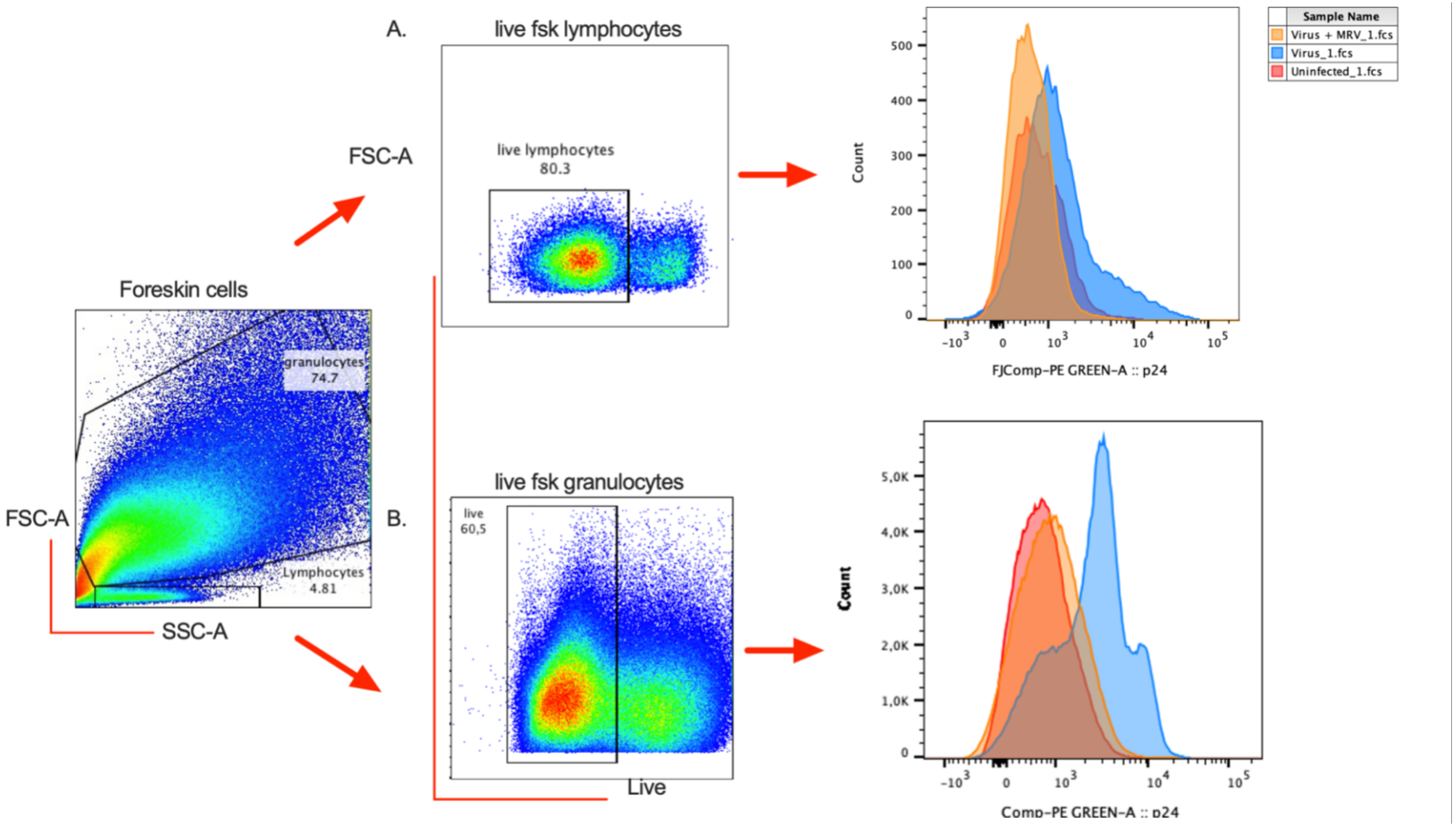

Figure 85. ***Representative flow plots demonstrating the gating strategies used to determine the HIV infection of foreskin lymphocytes and granulocytes, using HIV inhibition by maraviroc as a control***. *Representative flow cytometry plots illustrating the expression of p24 that was used as a measure of HIV infection in CD45+CD3+ lymphocytes and the live granulocyte population (blue peak) Maraviroc was used to inhibit and confirm HIV infection in these populations (orange). Uninfected cells are shown as the red peaks*

Evidence of foreskin HIV Infection - HIV inhibition by maraviroc

Maraviroc inhibited foreskin lymphocyte infection by 70.33 % as evidenced by the reduced mean frequency of p24+ lymphocytes from 8.73 % ± 4.74 % to 2.59 % ± 0.80 % upon the introduction of the drug (*p = 0.0142*) as shown in Figure 86 (a) below. Notably, the extent to which maraviroc inhibited HIV entry was variable among the different viruses, similarly to how virus infectivity differed among the different viruses as shown in Figure 86 (b). In particular, infection with NL4-3 92TH14-12 (R5) was 2.8-fold more impactful (17.76 % ± 5.85 %) than infection with Subtype C CH167 (CC) (6.26 % ± 3.15 %; *p<0.0001*). The impact of maraviroc inhibition was similarly highest against NL4-3 92TH14-12 (R5) infection whereby the mean frequency of HIV infected lymphocytes (2.28 % ± 0.49 %) decreased by 87.16 % as shown in Figure 86 (b). Meanwhile minimal inhibition was displayed against CH167 (CC) infection reduced, whereby the mean frequency of p24+ lymphocytes only declined by 41.50 %.

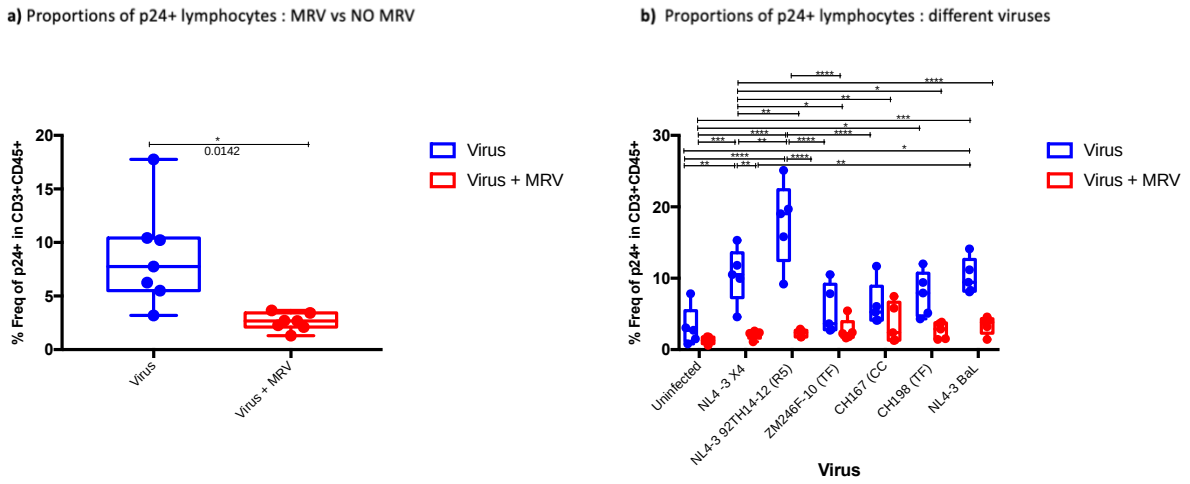

Figure 86. ***Inhibition of HIV infection of foreskin lymphocytes using different viruses by entry inhibitor maraviroc.*** *Foreskin lymphocytes were infected using the pluricellular cell suspension model using different viruses; NL4-3 X4, NL4-3 92TH14-12 (R5), ZM246F-10 (TF),CH167 (CC), CH198 (TF) and NL4-3-BaL over an 18 hr incubation period. Flow cytometry was used to determine p24 expression which was used as a measure of HIV infection (n = 5). The Wilcoxon test was used to compute the p value in* ***(a)*** *while statistics were generated using two-way ANOVA and the Tukey's multiple comparisons test with adjusted p values. *p <0.05; **p < 0.01; ***p < 0.001; ****p < 0.0001*

Although without statistical significance, the mean frequency of HIV infected granulocytes (1.25 % ± 1.43 %) also reduced 48.8 % in the presence of maraviroc (0.64 % ± 0.20 %; *p = 0.3061*) as shown in Figure 87 (a) below. However, unlike foreskin lymphocytes above, there were no significant differences among the different virus strains in granulocytes. Infection with Subtype C CH198 (TF) resulted in an average of 4.43 % ± 8.71 % HIV infected granulocytes, against which maraviroc was 87.58 % inhibitory as shown in Figure 87 (b). Compared to Subtype C CH198 (TF), infection with NL4-3 92TH14-12 (R5) (1.25 % ± 1.49 %), was 2.5-fold less impactful and only reduced 20 % in the presence of maraviroc as shown in Figure 87 (b). These trends were, however, driven by a single participant.

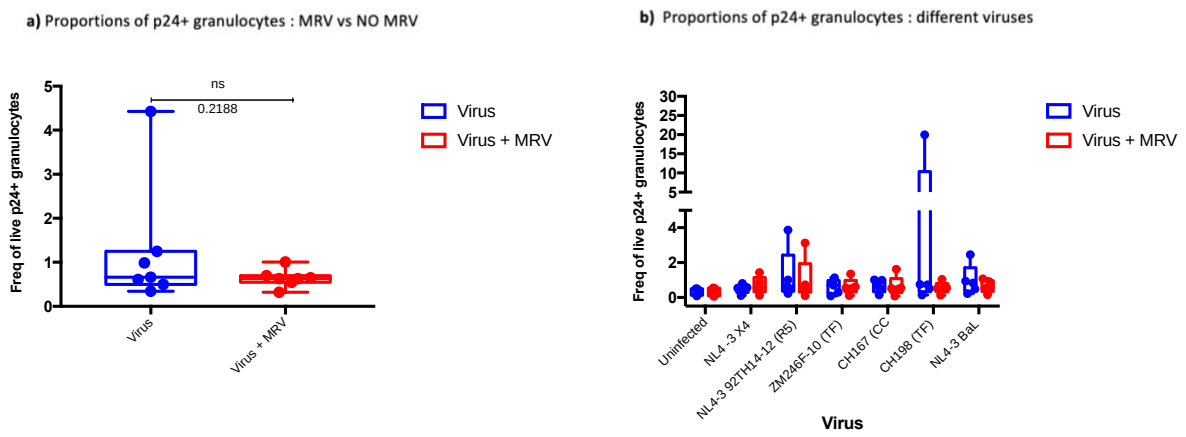

Figure 87. ***Inhibition of HIV infection of foreskin granulocytes using different viruses by maraviroc.*** *Foreskin granulocytes were infected using the pluricellular cell suspension model using different viruses; NL4-3 X4, NL4-3 92TH14-12 (R5), ZM246F-10 (TF), CH167 (CC), CH198 (TF) and NL4-3-BaL over an 18 hr incubation period. Flow cytometry was used to determine p24 expression which was used as a measure of HIV infection (n = 5).). The Wilcoxon test was used to compute the p value in* ***(a)*** *while statistics were generated using two-way ANOVA and the Tukey's multiple comparisons test with adjusted p values in* ***(b).*** *There were no significant differences.*

Infection of foreskin lymphocytes and granulocytes

After the above validation, foreskins from 17 participants were infected using the pluricellular suspension cell model as described in Figure 76 (iii) using the same NL4-3 and Subtype C viruses described above. The subsequent analysis of HIV infected lymphocytes and granulocytes was also performed seperately as shown in Figure 18 (C) and in the gating strategy above (Figure 85). Both lymphocytes and granulocytes were assessed for HIV infection after 18 and 48 hours as shown in the representative flow cytometry plots in Figure 88 below.

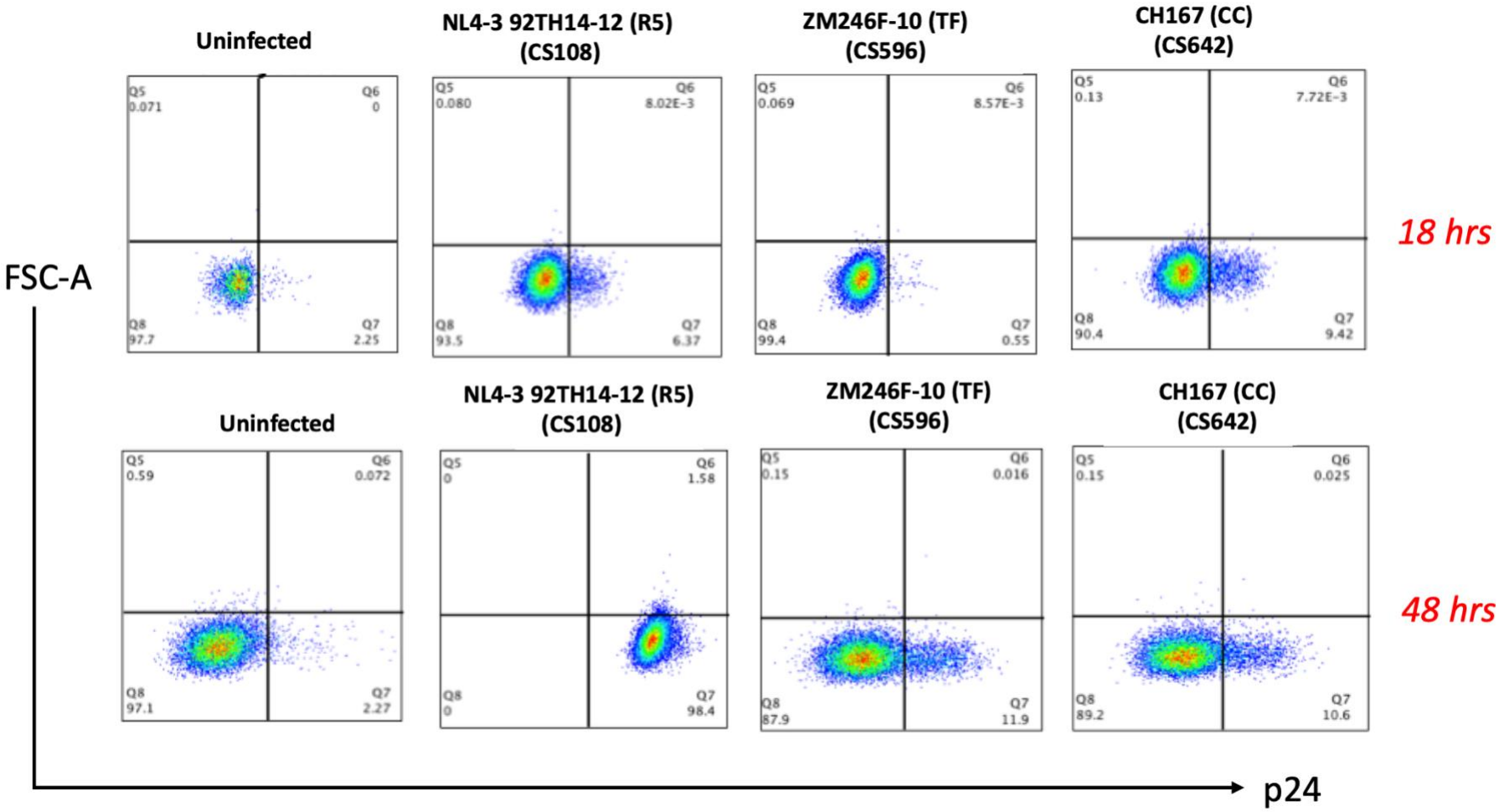

Figure 88. ***Differential infection of foreskin lymphocytes by different HIV strains at 18 and 48 hours. (i)*** *Representative flow cytometry plots of live CD45+CD3+ lymphocytes displaying differential foreskin lymphocytes infection by different viruses at two time points, 18 and 48 hours*

HIV infection of foreskin Lymphocytes

The mean frequency of HIV infected FS lymphocytes ranged from 3.91 % ± 3.06 % to 15.6 % ± 22.96 % for 17 participants infected using various viruses. The distribution of these frequencies by different viral IMC is shown is Figure 89 below. As can be observed in Figure 90, there was an increase in the frequency of infection over time although not statistically significant. This infection was variable between different participants, as can be seen by the Standard Deviation in particularly NL4-3 92TH14-12 (R5) infected cells (shown in more detail in Appendix).

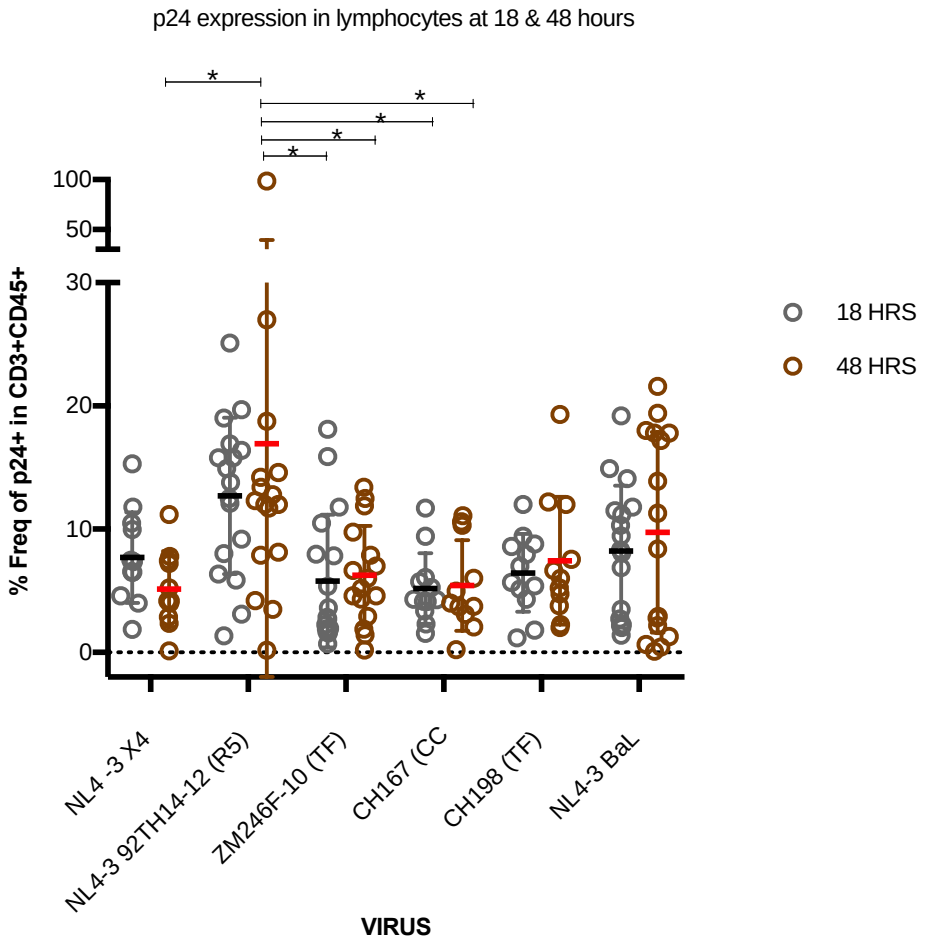

Figure 89. ***Differential infection of foreskin lymphocytes by different HIV strains at 18 and 48 hours. (a)*** *Proportions of p24+ foreskin lymphocytes infected using NL4 -3 X4, NL4-3 92TH14-12 (R5), ZM246F-10 (TF), CH167 (CC),CH198 (TF) and NL4-3 BaL among different participants at 18 and 48 hours (n=17).. Statistics were calculated with two-way ANOVA using the Tukey's multiple comparisons test at 95 % CI of difference and adjusted p values. *p <0.05*

Foreskin lymphocytes were infectable with NL4-3 92TH14-12 (R5) and NL4-3 BaL compared to transmitted founder and chronic infection derived Subtype C viruses when participant size increased (n=17), as shown in Figure 90 above. At 18 hours, the mean frequency of NL4-3 92TH14-12 (R5)

infected cells was 11. 56 % ± 5.46 , which was 76.22 % and 86.15 % more impactful than infection with NL4-3-BaL and NL4-3 X4 that were averages of 6.56 % ± 5.61 % and 6.21 % ± 3.34 % respectively, as shown in Figure 90. While the trend was retained with time progression, the mean frequency of NL4-3 92TH14-12 (R5) infected lymphocytes additionally increased 34.95 % at 48 hours as shown in Table 5. Productive infection was also observed upon infection with NL4-3-BaL as shown in Table 5, although only with a 21.95 % increment in the mean frequency of infected cells with time progression also shown in Table 5.

Although with comparatively lower infectivity, infection with the Subtype C, transmitted founder; CH198 (TF) and chronic infection derived; CH167 (CC), also depicted a time-dependent increase in the proportions of infected lymphocytes. CH198 (TF) was particularly the most infectious of the Subtype C viruses, shown to increase by 21.63 %. A similar increase was noted with CH167 (CC), whereby HIV infected lymphocytes increased 20.57 % between 18 and 48 hours as shown in Table 5.

Table 5. Proportions of HIV infected lymphocytes at 18 and 48 hours

VIRUS	**% CHANGE 18 vs 48 hrs**
Uninfected	0
NL4-3 X4	- 37.04
NL4-3 92TH14-12 (R5)	34.95
ZM246F-10 (TF)	- 3.66
CH167 (CC)	20.57
CH198 (TF)	21.63
NL4-3 BaL (R5)	21.95

Impact of viral tropism in the infection of foreskin lymphocytes

Statistical analysis was performed to assess the impact of viral tropism on viral infection of FS lymphocytes. However, this was only carried out on the basis of IMC envelopes, further mechanisms that govern viral tropism were not explored in this study and remain to be elucidated. R5 tropic NL4-3 viruses identified as NL4-3-BaL and NL4-3 92TH14-12 (R5) were grouped together and annotated in the figures below as **NL4-3 R5** while the X4 tropic virus, **NL4-3 (X4)** was analysed seperately. The Subtype C viruses were separated according to the transmission stage at which they were initially isolated. Transmitted founder viruses, ZM246F-10 (TF) and CH198 (TF) were grouped together and annotated in the figures as **TF** while the chronic infection derived virus, CH167 (CC), was analysed seperately and annotated as **CC**.

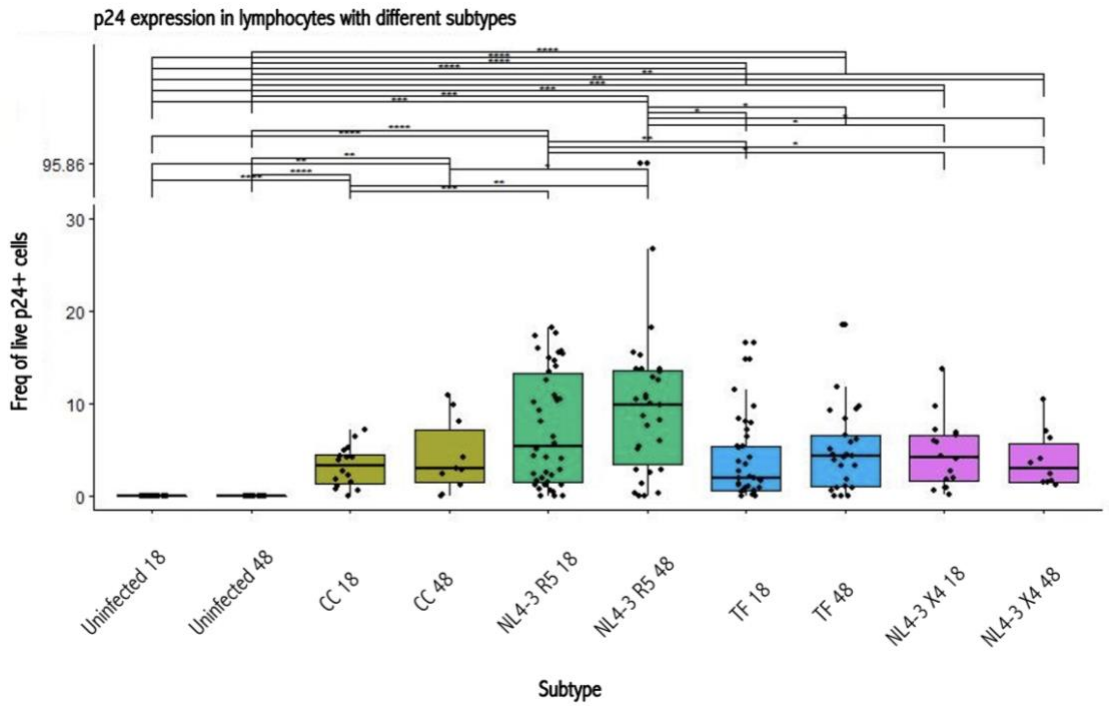

Figure 90. ***Differential infection of foreskin lymphocytes by different HIV strains at 18 and 48 hours.*** *Proportions of foreskin lymphocytes infected with NL4 -3 X4, NL4-3 R5, Subtype C (TF) and Subtype C (CC) at 18 and 49 hours. Flow cytometry was used to determine p24 expression which was used as a measure of HIV infection. Statistics were generated in collaboration with the UCT Statistics Department using Kruskal Wallis with the Bonferroni test to adjust for multiple comparisons. *p <0.05; **p < 0.01; ***p < 0.001; ****p < 0.0001*

At 18 and 48 hours, the mean frequency of p24+ lymphocytes was higher upon infection with NL4-3 R5 viruses compared to NL4-3-X4 and both Subtype C viruses; TF and CC as shown in Figure 90 above and Table 6 below. With time progression, NL4-3 R5 infected lymphocytes increased by 30.24 %, from 18 hours to 48 hours as shown in Table 6. CC infected lymphocytes also increased 20.57 % with time progression as shown in Table 6 and Figure 90.

Table 6. Proportions of HIV infected lymphocytes according to receptor usage

	18 hrs p24 frequency	**48 hrs p24 frequency**	**% change 18 hrs vs 48 hrs**
NL4-3 R5	9.06 ± 4.59	11.8 % ± 12.87 %	30.24
NL4-3 X4	6.21 % ± 3.34 %	3.91 % ± 3.06 %	- 37.03
TF	5.43 % ± 5.02 %	5.11 % ± 3.24 %	- 5.89
CC	3.50 % ± 1.89 %	4.22 % ± 3.98 %	20.57

HIV Infection of foreskin Granulocytes

Unlike, the frequencies of HIV infected lymphocytes above, the proportions of HIV infected granulocytes were comparatively lower and ranged between 0.21 % ± 0.24 % and 6.24 % ± 22.22 % for 17 participants infected with different viruses as shown in Figure 91 (a). Although without significant differences, trends were observed among the different virus strains, by assessing both the frequency of infected p24+ cells and respective p24 MFIs, as shown in Figures 91 (a) - (b). Similarly to lymphocytes, the same participant portrayed a significantly higher frequency of p24+ cells at 48 hours and thus, increased the standard deviation in NL4-3 92TH14-12 (R5) infected granulocytes as shown in Figure 91 (a) and Table 9.

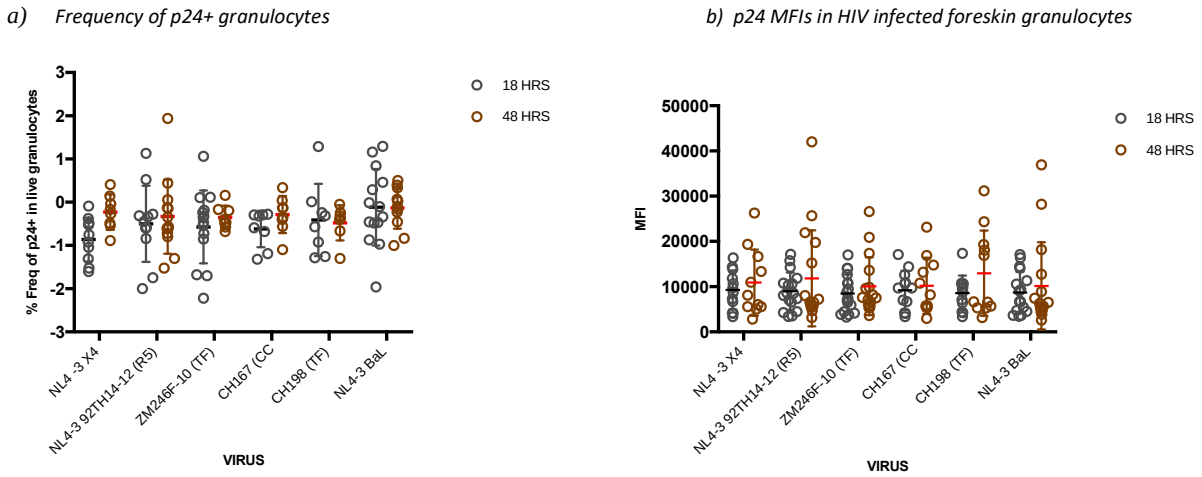

Figure 91. ***Differential infection of foreskin granulocytes by different HIV strains at 18 and 48 hours. (a)*** *Proportions of p24+ foreskin granulocytes infected using NL4 -3 X4 (CS105), NL4-3 92TH14-12 (R5), ZM246F-10 (TF), CH167 (CC), CH198 (TF) and NL4-3 BaL* ***(b)****p24 MFIs in infected foreskin granulocytes .(n =17) Statistics were calculated with two-way ANOVA using the Tukey's multiple comparisons test at 95 % CI of difference and adjusted p values. There were no significant differences.*

Contrary to foreskin lymphocytes that were less permissive to Subtype C viruses, the mean frequency of CH198 (TF) infected granulocytes was 2.01 % ± 5.82 %, and was 66.12 % higher than infection with NL4-3 92TH14-12 (R5) whose mean frequency of infected granulocytes was 1.21 % ± 3.38 % at 18 hours, as shown in Figure 91 (a). However, NL4-3 92TH14-12 (R5) infection increased 4.16-fold, with time progression as shown in Figures 91 (a) and (b) below. Similarly to this, productive infection was also established in CH167 (CC) and NL4-3 X4 infected foreskin granulocytes that increased 1.5-fold and 2.24-fold with time, respectively (Table 8). Correspondingly, p24 MFIs also increased with time progression in all the different viruses, although more profoundly in CH198 (TF) and NL4-3 92TH14-12 (R5) that increased the highest by 50.83 % and 31.72 % respectively (*Table 7).*

Table 7 . ***HIV infected foreskin granulocytes at 18 hrs and 48 hrs***

Frequency of p24+ granulocytes		
Virus	Fold change	% Change
Uninfected	**0**	**0**
NL4-3 X4	**2.24**	**223.81**
NL4-3 92TH14-12 (R5)	**4.16**	**415.70**
ZM246F-10 (TF)	**-0.73**	**- 73.15**
CH167 (CC)	**1.50**	**150.00**
CH198 (TF)	**- 0.85**	**- 85.07**
NL4-3 BaL (R5)	**- 0.72**	**- 72.49**
p24 Mean FLUORESCENCE INTENSITIES		
Virus	Fold change	% Change
NL4-3 X4	**0.18**	**17.61**
NL4-3 92TH14-12 (R5)	**0.32**	**31.72**
ZM246F-10 (TF)	**0.19**	**19.07**
CH167 (CC)	**0.11**	**10.82**
CH198 (TF)	**0.51**	**50.83**
NL4-3 BaL (R5)	**0.17**	**16.96**

Tropism

Similarly to lymphocytes, the different viruses were grouped into; NL4-3-R5, NL4-3-X4, Subtype C transmitted founder (TF) and Subtype C chronic infection derived (CC) viruses for subsequent assessment against granulocytes' infection. Foreskin granulocytes were most permissible to NL4-3-R5 (2.15 % ± 4.02 %) and Subtype C TF (1.67 % ± 3.59 %) viruses at 18 hours. NL4-3 R5 infected foreskin granulocytes were additionally seen to increase 64.65 % with time progression as shown in *Table 8* and Figure 92 below. Both CC and NL4-X4 viruses also noticeably increased with time, 1.5- and 2.24-fold respectively (*Table 8* & *Figure 92*).

Table 8. HIV infected foreskin granulocytes at 18 hrs and 48 hrs – tropism

	Fold change 18 hrs vs 48 hrs	**% Increase 18 hrs vs 48 hrs**
NL4-3 R5	0.65	64.65
NL4-3 X4	2.24	223.81
TF	-0.84	- 84.43
CC	1.50	150.00

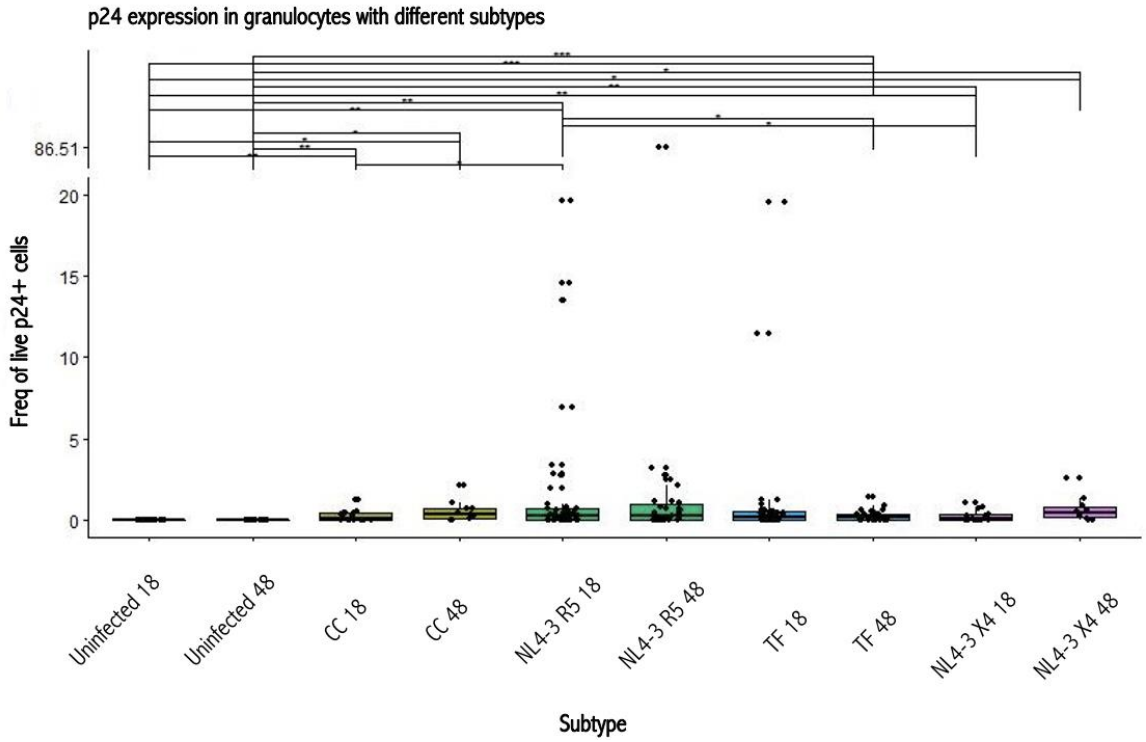

Figure 92. ***Differential infection of foreskin granulocytes by different HIV strains at 18 and 48 hours.*** *Proportions of HIV infected foreskin granulocytes infected using ; NL4 -3 X4, NL4-3 R5, Subtype C (TF) and Subtype C (CC).Flow cytometry was used to determine p24 expression which was used as a measure of HIV infection. Statistics were generated Kruskal Wallis using the Bonferroni test and adjusted p values *p <0.05; **p < 0.01; ***p < 0.001; ****p < 0.0001.*

Summary

Overall, the mean frequency of HIV infected foreskin lymphocytes (6.58 % ± 3.62 %) was 3.7-fold higher than the mean frequency of HIV infected foreskin granulocytes (1.40 % ± 1.74 %). Moreover, different viruses infected the two cell types differently, although NL4-3 92TH14-12 (R5) was the most infectious virus in both lymphocytes (13.58 % ± 2.86 %) and granulocytes (3.72 % ± 3.55 %) as shown in Figure 93 below.

However, without the outlier in NL4-3 92TH14-12 (R5) infected cells, the mean frequency of NL4-3 BaL infected cells was the highest (1.97 % ± 1.59 %), and was not significantly differed from CH198 (TF) (1.16 % ± 1.21 %) and NL4-3 92TH14-12 (R5) (0.90 % ± 0.50 %) infected cells (shown in *Appendix).* The mean frequency of foreskin lymphocytes was however, still the highest in NL4-3 R5 viruses, NL4-3 92TH14-12 (R5) (10.71 % ± 1.20 %) and NL4-3 Bal (7.3 % ± 1.02 %) in comparison to Subtype C viruses and NL4-3 X4 as shown in Figure 93 below. Although non-significantly differed, foreskin granulocytes exhibited a trend where there was 20 % less infectability with the NL4-3 X4 virus and the Subtype C chronic infection isolate (black arrows) compared to the Subtype C transmitted founder viruses (red arrows) as shown in Figure 93.

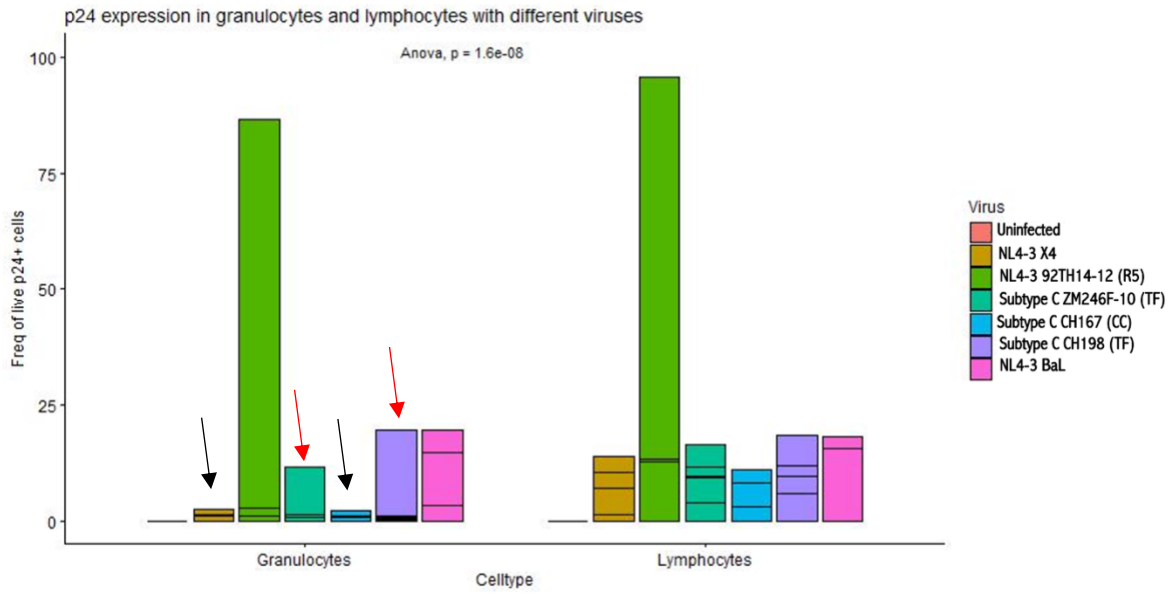

Figure 93. ***Proportions of p24+ lymphocytes and granulocytes infected using different HIV strains.*** *Foreskin lymphocytes and granulocytes were infected using the cell suspension model with different viruses; ; NL4 -3 X4, NL4-3 92TH14-12 (R5), ZM246F-10 (TF), CH167 (CC),CH198 (TF) and NL4-3 BaL (n = 17). Statistics were calculated using ANOVA to compare HIV infection in foreskin lymphocytes against foreskin granulocytes. Differences were observed in cell type i.e. lymphocytes vs granulocytes. There were no significant differences among the different viruses.*

Section 2: Infection of specific granulocyte populations

2.2.2.1 HIV Infection of Langerhans Cells

Proportions of HIV infected LCs and LC subsets

Overall LCs

Uninfected LCs constituted a small portion of the uninfected granulocyte population (0.08 % ± 0.04 %), and decreased 3-fold with time progression (0.02 % ± 0.01 %; $p = 0.0001$) as shown in Figure 94 (a). Upon HIV infection, the mean frequency of LCs was constitutive of 3.10 % ± 0.85 % of the HIV infected (by all the 6 different virus strains) granulocyte population, although depicting a 0.93-fold decrease at 48 hours (1.61 % ± 0.35 %; $p = 0.0312$) as shown in Figure 94 (b). Noteworthy, initial virus inocula was not washed off as shown in the HIV Section 1 in Figure 76, and was therefore possibly contributory to the higher p24 detection at earlier time-points.

Although the mean frequency of HIV infected LCs also declined with time in all viruses in Figure (c), as observed in Figure (b), the median frequency alternately increased with time progression for NL4-3 X4 and CH198 (TF) (circled in the figure). This was in part due to trends observed in the differential

permissibility to the different virus strains as shown by the aid of circles in Figure 94 (c). more-so, the centrality of the median. Such trends were not observable in Figure (b), where granulocyte infection was summarised for all the different participants, and analysed as composite viruses. In particular, the median frequency of CH198 (TF) infected LCs was 2-times higher at 48 hours where it was 1.97 (0.12) (shown with IQR) compared to 18 hours 0.84 (2.13). However, these changes were not significantly differed using both mean and median frequency.

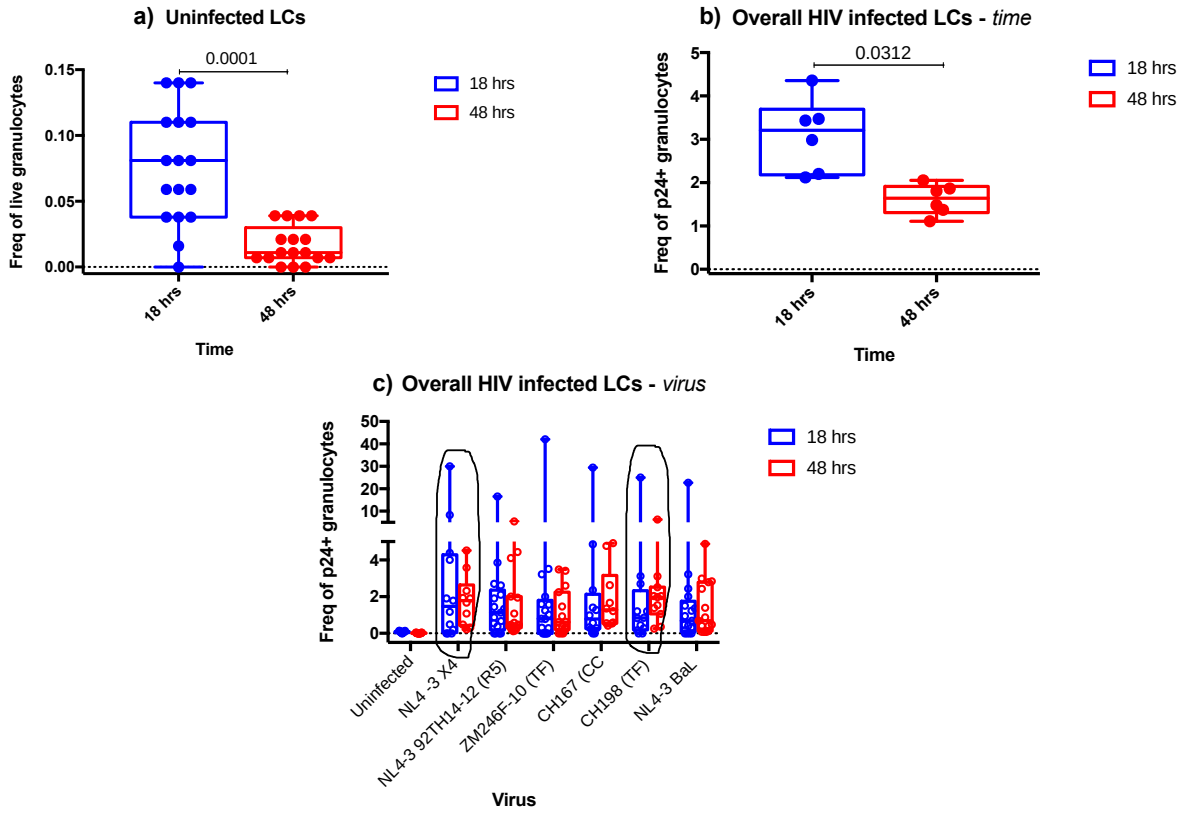

Figure 94. ***Proportions of HIV infected LCs at 18 and 48 hours***. *Foreskin LCs were infected using NL4-3 (X4), NL4-3 92TH14-12 (R5), ZM246F-10 (TF), CH167 (CC), CH198 (TF) and NL4-3 BaL over 18 and 48 hr incubation periods* ***(a)*** *Proportions of HIV infected LCs, using 6 different viruses at 18 and 48 hours* ***(b)*** *Proportions of overall HIV infected LC subsets at 18 and 48 hours (n = 17). Statistics were generated with one-way ANOVA using the Tukey's multiple comparisons test with adjusted p values. There were no significant differences in (c).*

Overall LCs – Tropism

Further analysis was done to assess the infection of foreskin Langerhans cells according to virus tropism as was done to assess the broad granulocyte population in HIV Infection Section Part 1. Although without significant differences, the mean frequency of HIV infected LCs was the highest upon infection with NL4-3 X4 viruses (4.35 % ± 8.50 %) compared to NL4-3 R5 (2.16 % ± 4.57 %), TF (2.93 % ± 7.84 %) and CC viruses (3.47 % ± 8.28 %) as shown in Figure 95. Consistent to the observations above, infection of foreskin LCs was negatively impacted by time progression, although the median frequency NL4-3 X4 and CC infected LCs conversely increased with time as shown in Table 9.

Table 9. HIV infected LCs : Tropism

	18 hrs Mean ± SD	48 hrs Mean ± SD	% Change (Mean ± SD)	18 hrs Median (IQR)	48 hrs Median (IQR)	% Change Median (IQR)
NL4-3 X4	4.35 % ± 8.50 %	1.80 % ± 1.41 %	**- 58.62**	1.48 % (4.24)	1.79 % (2.20)	**20.95**
NL4-3 R5	2.16 % ± 4.57 %	1.42 % ± 1.51 %	**- 34.26**	1.22 % (0.95)	0.58 % (2.07)	**- 52.46**
TF	2.93 % ± 7.94 %	1.31 % ± 1.33 %	**- 55.29**	1.11 % (1.42)	0.76 % (1.75)	**- 31.53**
CC	3.47 % ± 8.28 %	1.86 % ± 1.71 %	**- 46.40**	0.78 % (1.86)	1.28 % (2.62)	**64.10**

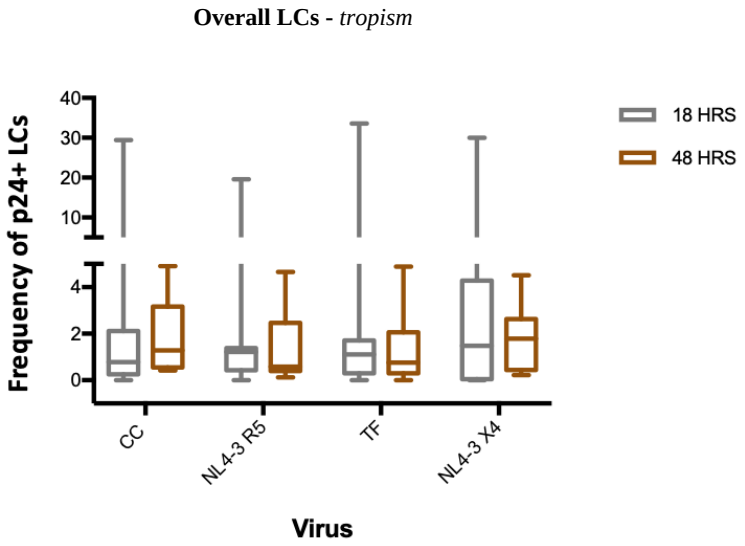

Figure 95. ***Proportions of HIV infected LCs at 18 and 48 hours, according to tropism .*** *HIV infected LCs were assessed according to different groups of viruses; NL4 -3 X4, NL4-3 R5, transmitted founder (TF) and chronic infection derived (CC) Subtype C viruses, at 18 and 48 hrs (n = 17). Statistics were generated with one-way ANOVA using the Tukey's multiple comparisons test. There were no significant differences.*

HIV infected LC subsets

As described in the Immunophenotyping Section, using both manual and unsupervised clustering; foreskin LCs were distinguishable into different subsets, namely; i) traditional LCs, ii) CD11c+ LCs, iii) CD11c+CD14+ LCs and v) CD3+ LCs. Using the same approach, overall HIV infected LCs were characterised into the different subsets and quantified, using manual and unsupervised clustering. Different subsets were differentially infected by the different viruses. However, only the CD14 expressing LC subsets; i) CD14+ LCs and the ii) CD11c+CD14+ LCs were productively infected with HIV as shown in Figure 97 below. CD14+ LCs increased 3.14-fold from 18 hours (0.07 % ± 0.08 %) to 48 hours (0.29 % ± 0.10 %; $p = 0.0144$). Although with a smaller margin, HIV infected CD11c+CD14+ LCs also increased by 24.14 % between 18 hours (0.29 % ± 0.13 %) and 48 hours (0.36 % ± 0.38 %; $p = 0.0153$) as shown in Figure 96.

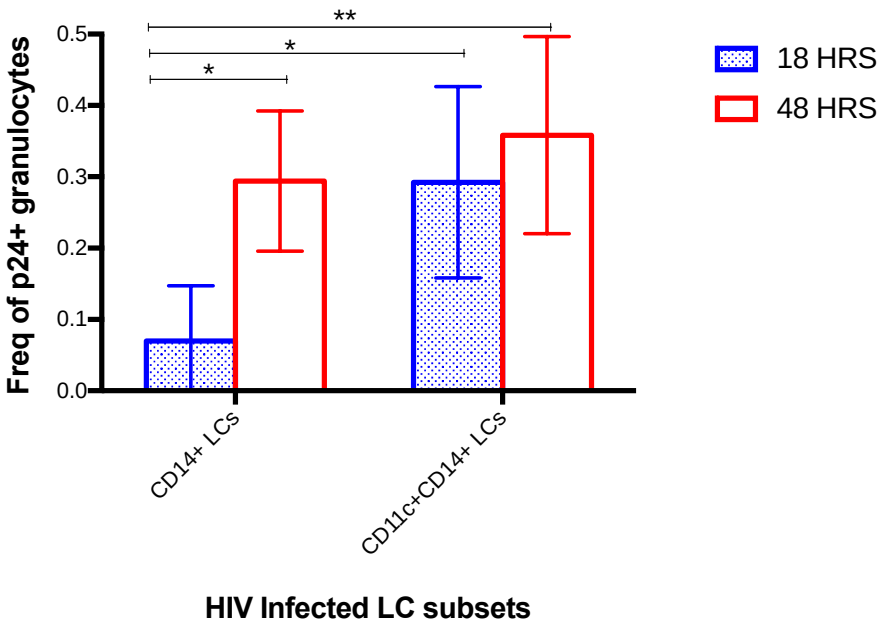

Figure 96. ***Proportions of productively HIV infected LC subsets, CD14+ LCs and the CD11c+CD14+ LCs at 18 and 48 hours****. HIV infected LCs were analysed and compared in their different subsets; CD14+ LCs and CD11c+CD14+ LCs (n= 17). HIV infected LC subsets were derived from the p24+ granulocyte gate. Statistics were calculated with one-way ANOVA using the Tukey's multiple comparisons test at 95 % CI of difference and adjusted p values. *p <0.05; **p < 0.01; ***p < 0.001; ****p < 0.0001*

LC subsets – impact of virus type

Having established the proportions of the different HIV infected LC subsets, these cells were further analysed for the impact of virus type on the level of HIV infection that was achieved. Similarly, to overall HIV infected LCs in Figures 94 and 95 above; there were also no statistically significant differences in the infectivity of the different viruses on the different LC subsets, although trends were observed as displayed in Table 10 below and Figure 97.

Table 10. HIV infected LCs : Different viruses & time-points

Virus	CD14+ LCs		CD11c+CD14+ LCs	
	Fold Change	% Change	Fold Change	% Change
Uninfected	- 0.86	**- 86.30**	- 0.60	**- 60.00**
NL4-3 (X4)	- 0.23	**- 22.73**	- 0.13	**- 13.04**
NL4-3 92TH14-12 (R5)	3.50	**350.00**	1.36	**135.70**
ZM246F-10 (TF)	8.50	**850.00**	- 0.36	**- 35.56**
CH167 (CC)	3.86	**385.71**	- 0.07	**- 7.41**
CH198 (TF)	79.00	**7 900.00**	1.08	**107.69**
NL4-3 BaL	8.50	**850.00**	0.22	**22.22**

The mean frequency of p24+CD14+ LCs decreased by 22.73 % with time, when infected using the NL4-3 X4 strain compared to the 79-fold increase observed in infection using the Subtype C transmitted

founder virus, CH198 (TF) as shown by black circles in Figure 97 (a). Similarly, p24+CD11c+CD14+ LCs decreased 13.04 % on infection with NL4-3 X4 (red circle) as shown in Figure 97 (b). The mean frequency of CD11c+CD14+ LCs increased the most (1.36-fold) upon infection NL4-3 92TH14-12 (R5) and only 1.08-fold with CH198 (TF) as shown in Table 11 as well as Figure 97 (a) - (b).

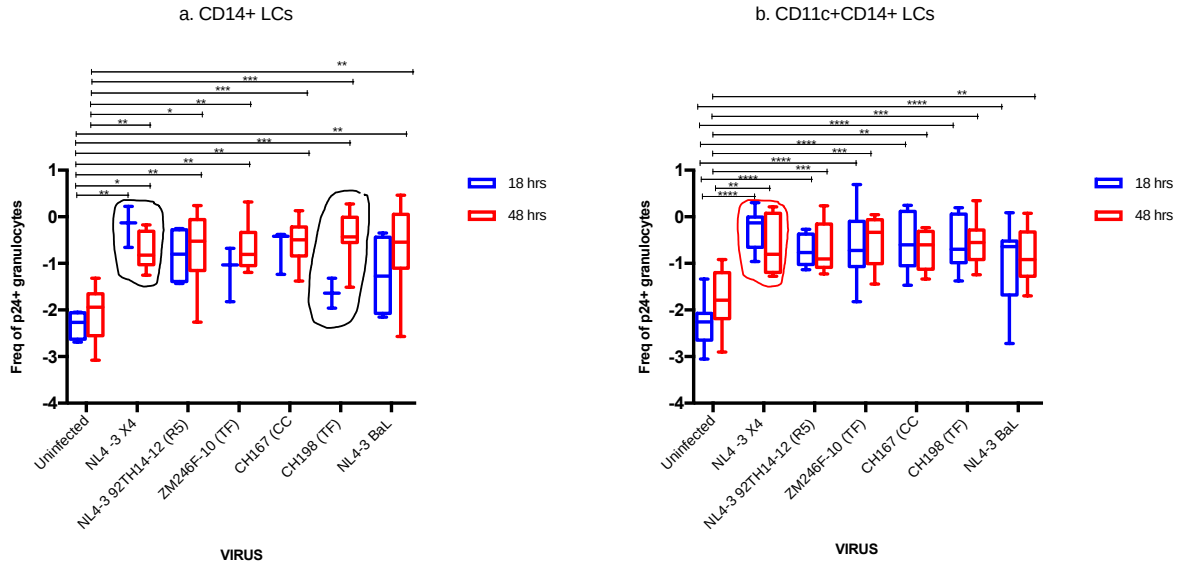

Figure 97. ***Comparison of uninfected and p24+ foreskin LC subsets from HIV infection with different viruses, at 18 and 48 hours.*** *Foreskin LCs were infected using NL4-3 (X4), NL4-3 92TH14-12 (R5), ZM246F-10 (TF), CH167 (CC), CH198 (TF) and NL4-3 BaL over 18 and 48 hr incubation periods* ***(a)*** *Traditional LCs* ***(b)*** *CD11c+ LCs* ***(c)*** *CD14+ LCs (n = 17). Statistics were calculated with one-way ANOVA using the Tukey's multiple comparisons test at 95 % CI of difference. There were no significant differences.*

LC subsets – Tropism

Although non-productive and non-statistically significant; the mean frequency of NL4-3 X4 infected CD14+ LCs (0.22 % ± 0.50 %), was the highest among all the other virus groups at the 18 hour time-point. It differed the most against Subtype C TF viruses whose mean frequency of infected CD14+ LCs (0.01% ± 0.01 %), was 21-fold lower as shown in Figure 98. However, this high mean frequency of NL4-3 X4 infected CD14+ LCs decreased 23 % at 48 hours and was an average of 0.17 % ± 0.23 %, while all the other viruses were productively infective. Infection with NL4-3 R5 viruses increased 5.6-fold (0.33 % ± 0.62 %) while Subtype C viruses; CC (0.34 % ± 0.41 %) and TF (0.25 % ± 0.37 %) increased 3.6-fold and 24-fold respectively (Figure 98).

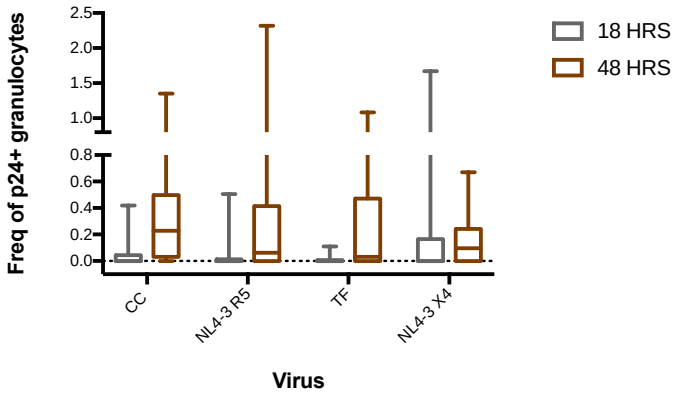

Figure 98. ***Proportions of HIV infected LC subsets using viruses with different tropisms at 18 and 48 hours.*** *Box and whisker plots showing proportions of p24+ LC subsets infected with i) NL4 -3 X4, ii) NL4-3 R5), Subtype C transmitted founder viruses (TF) and , Subtype C chronic infection derived viruses (CC) over an 18 hr and 48 hr incubation period (n = 17). Statistics were generated with one-way ANOVA using the Tukey's multiple comparisons test and adjusted p values. There were no significant differences among the different virus groups.*

Summary

The mean frequency of foreskin LCs reduced over time, under normal culture conditions without virus inoculation. Although this was similarly observed in the different LC subsets, HIV infected CD14+ LCs and CD11c+CD14+ LCs were not negatively impacted by time progression, and thus productively infected. Both subsets were more infectable using Subtype C transmitted founder viruses, especially CH198 (TF) and the NL4-3 R5 viruses, NL4-3 92TH14-12 (R5) and NL4-3 BaL, although NL4-3 BaL was infective in CD14+ LCs.

Unsupervised clustering: LC marker expression profile

Pre-gated HIV infected (p24+) and uninfected (p24-) CD1a+CD207+ cells were visualized through the dimensional reduction approach using tSNE as described earlier. A color gradient was used to illustrate marker expression intensities in each cluster whereby, green was used to denote low or no expression and red to show high or intense expression. All LC clusters portrayed high HLA-DR expression and differentially expressed all the other markers as shown in Figure 99 below.

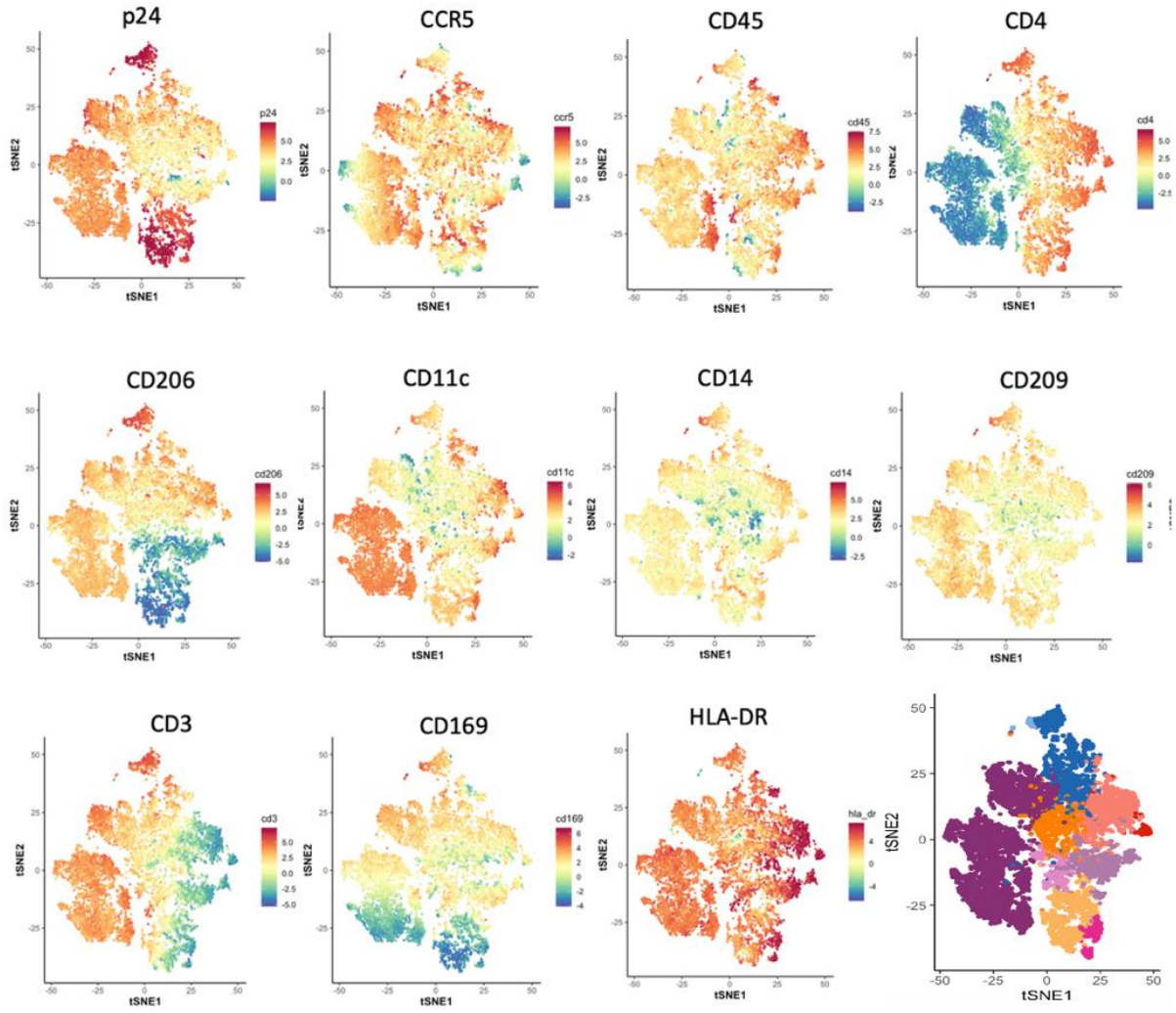

Figure 99. ***Assessment of the marker expression profiles of HIV infected and Uninfected foreskin Langerhans cells using tSNE plots generated by non-biased, computerised clustering.*** *tSNE plots displaying the LCs' differential expression of : p24, CCR5, CD45, CD4, CD3, HLA-DR, CD206, CD11c, CD14, CD209, and CD169.The color spectrum denotes increasing intensities of marker expression, ranging from green which represents no to low marker expression while red is high marker expression*

Identification and characterisation of LC clusters

Using the k means and the CDF plots as described in the Immunophenotyping Chapter, k=10 was selected as the best fit to identify the different HIV infected and uninfected LC clusters. Thus, 10 clusters of varying proportions were identified using FlowSOM and were mapped out on the coloured tSNE plots as shown in Figures 100 (a) - (c) below. Of these, the most abundant clusters, hence identified as main, were Cluster E (41.77 %; *dark purple*) and Cluster C (33.04 %; *blue*) that attributed 74.81 % of the LC population as shown in Figures 100 (a)-(b). Interestingly, both Clusters were p24+, and thus identified as the HIV infected clusters as shown in Figure 100 (c).

The two clusters additionally portrayed close phenotypic relatedness as shown in dendrograms on the left of Figures 100 (a) and (b). In addition to p24 expression, both subsets co-expressed the following markers with similar expression intensities: CD3, CD206, CCR5, HLA-DR, CD14, and CD209 as shown in Figure 100 (b). However, Cluster C and Cluster E differed by the expression of CD4, CD169 and CD11c. While Cluster C was CD4+CD11c^{lo}CD169+, Cluster E was conversely CD4-CD11c+CD169^{lo} as displayed in Figure 100 (b). Therefore, Cluster E portrayed resemblance with the CD14+ LC population, identified through manual gating above, as productively infected. Similarly, Cluster C resembled the CD11c+CD14+ LCs that were described above. Sub-clustering was additionally observed within Cluster C whereby a brightly p24 sub-cluster could be identified, differing from the rest of the cluster by bright co-expression of CD206 and CD3.

a)

Cluster	%	Marker Expression
D	0.77 %	CD4+CD3+CD206+CCR5+HLA-DR-CD45+CD11c+CD169+CD14+p24+CD209+
H	10.38 %	CD4+CD3-CD206-CCR5+HLA-DR-CD45-CD11c+CD169-CD14+p24+CD209+
I	2.25 %	CD4+CD3-CD206-CCR5-HLA-DR+CD45+CD11c+CD169-CD14+p24+CD209+
F	8.3 %	CD4+CD3-CD206-CCR5-HLA-DR+CD45+CD11c+CD169+CD14+p24-CD209-
J	3.28 %	CD4+CD3+CD206-CCR5+HLA-DR+CD45+CD11c+CD169+CD14+p24+CD209+
A	1.1 %	CD4+CD3-CD206CCR5-HLA-DR+CD45+CD11c+CD169+CD14+p24-CD209-
B	11.62 %	CD4+CD3-CD2+CCR5+HLA-DR+CD45+CD11c+CD169+CD14+p24-CD209-
E	41.77 %	CD4-CD3+CD206+CCR5+HLA-DR+CD45+CD11c+CD169+CD14+p24+CD209+
C	33.04 %	CD4+CD3+CD206+CCR5+HLA-DR+CD45-CD11c-CD169+CD14+p24+CD209+
G	7.48 %	CD4-CD3-CD206+CCR5+HLA-DR-CD45-CD11c-CD169-CD14-p24-CD209-

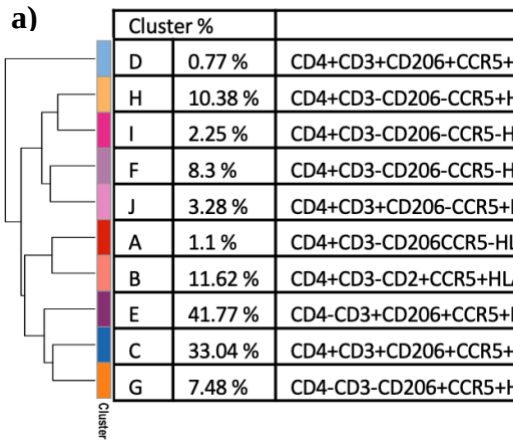

b)

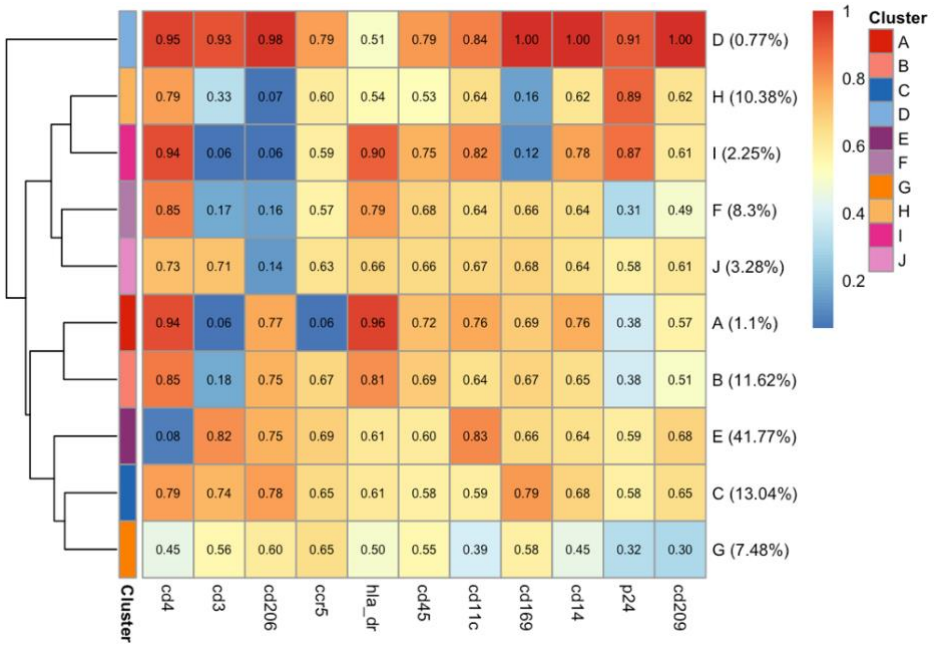

c)

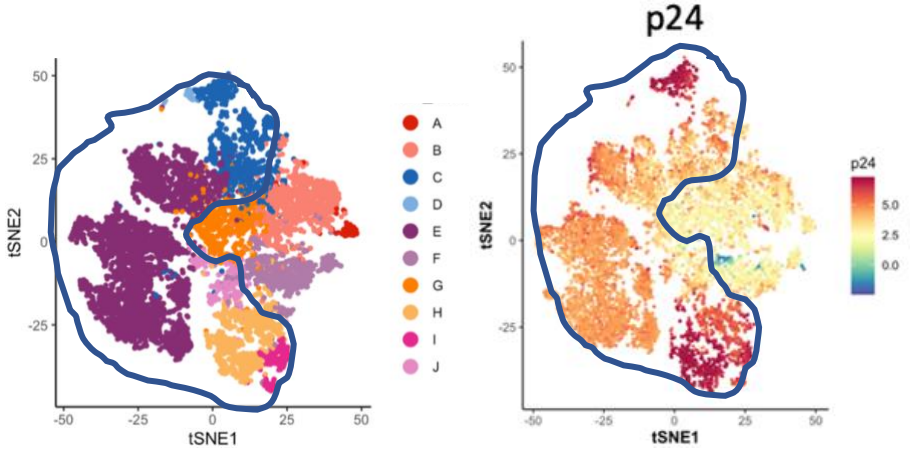

Figure 100. ***Determination of the overall different foreskin LC subsets in HIV uninfected foreskin LCs and LCs infected with different viruses;*** *; NL4 -3 X4, NL4-3 92TH14-12 (R5), ZM246F-10 (TF), CH167 (CC), CH198 (TF) and NL4-3 BaL at 18 and 48 hours. tSNE plots were generated using non-biased, computerised clustering*

Other HIV infected clusters were less abundant (minor) and were identified as Cluster D (0.77 %; *light-blue)*; Cluster H (10.38 %; *pale orange*) Cluster I (2.25 %; *fuchsia*) and Cluster J (3.26 %; *pink*) that constituted 16.66 % in total as shown in Figures 100 (a) and (b). Figure 102 (c) shows both main and minor HIV infected clusters circled in blue. However, p24 was more intensely expressed in the minor clusters; Cluster D, Cluster H and Cluster I as shown in Figures 100 (b) and (c). Cluster D, while the least abundant, also more brightly co-expressed all markers in the panel except HLA-DR. Cluster D was therefore unique from the other p24hi Clusters (H and I), that were phenotypically similar and therefore, proximal on the hierarchical dendrogram. While both Cluster H and Cluster I displayed high CD4 expression, CCR5 was more dimly expressed. More interestingly, Cluster H and I were both devoid of attachment factors, CD206 and CD169, while additionally dim for CD209. Therefore, an inverse relationship was established between bright p24 expression and attachment factors. Meanwhile, both clusters were CD3-CD11c+CD14+ although pan myeloid marker expression was brighter in Cluster I and additionally, HLA-DR (Figure 100b).

The rest of the clusters were HIV uninfected (p24-), and were identified as Cluster F (8.3 %; *purple*) Cluster A (1.1 %; *red*); Cluster B (11.62 %; *coral*) and Cluster G (*orange*; 7.48 %) with a constitution of 28.5 % as shown in Figures 100 (a) - (c). Except for Cluster G, a CD11c-CD14- cluster that only co-expressed CD206 and CCR5: all other uninfected clusters (A, B, F) were CD11c+CD14+ and were unique from the HIV infected clusters by lack of CD209 as shown in Figure 100 (b). This suggests that DC-SIGN is an important determinant of LC infection.

LC clusters according to different viruses and time-points

The different HIV infected and uninfected clusters were further stratified and visualised using tSNE plots, according to the different viruses and time-points as shown in Figure 101 (a) below. Cluster E (*purple*), identified above as a CD11c+CD14+ cluster, was more frequent in HIV infected cells in all the different viruses with less representation in uninfected cells ($p = 0.00039; adj\ p = 0.00099$) as shown in Figures 101 (a) – (c). However, Cluster E was negatively impacted by time progression (Appendix A33-34). Conversely, Cluster C (*blue*), while also with more representation in infected cells as shown in Figures 101 (a) – (b), was productively infected with all the different viruses, albeit non significantly varied among the different virus groups (Appendix A33-34). Therefore, Cluster C, a CD14+CD11c- cluster, portrayed a time-dependant increase (Appendix 34). Meanwhile, uninfected cells were more constitutive of Cluster G (*orange*), Cluster B (*coral*) and Cluster F (*lavender*) as shown in Figure 101 (a). Among these, Cluster G, a CD11c-CD14- cluster, was more frequent as shown in Figure 101 (b). This was in corroboration with manual gating whereby CD11c-CD14- LCs (traditional LCs) constituted the bulk of foreskin LCs but remained uninfected.

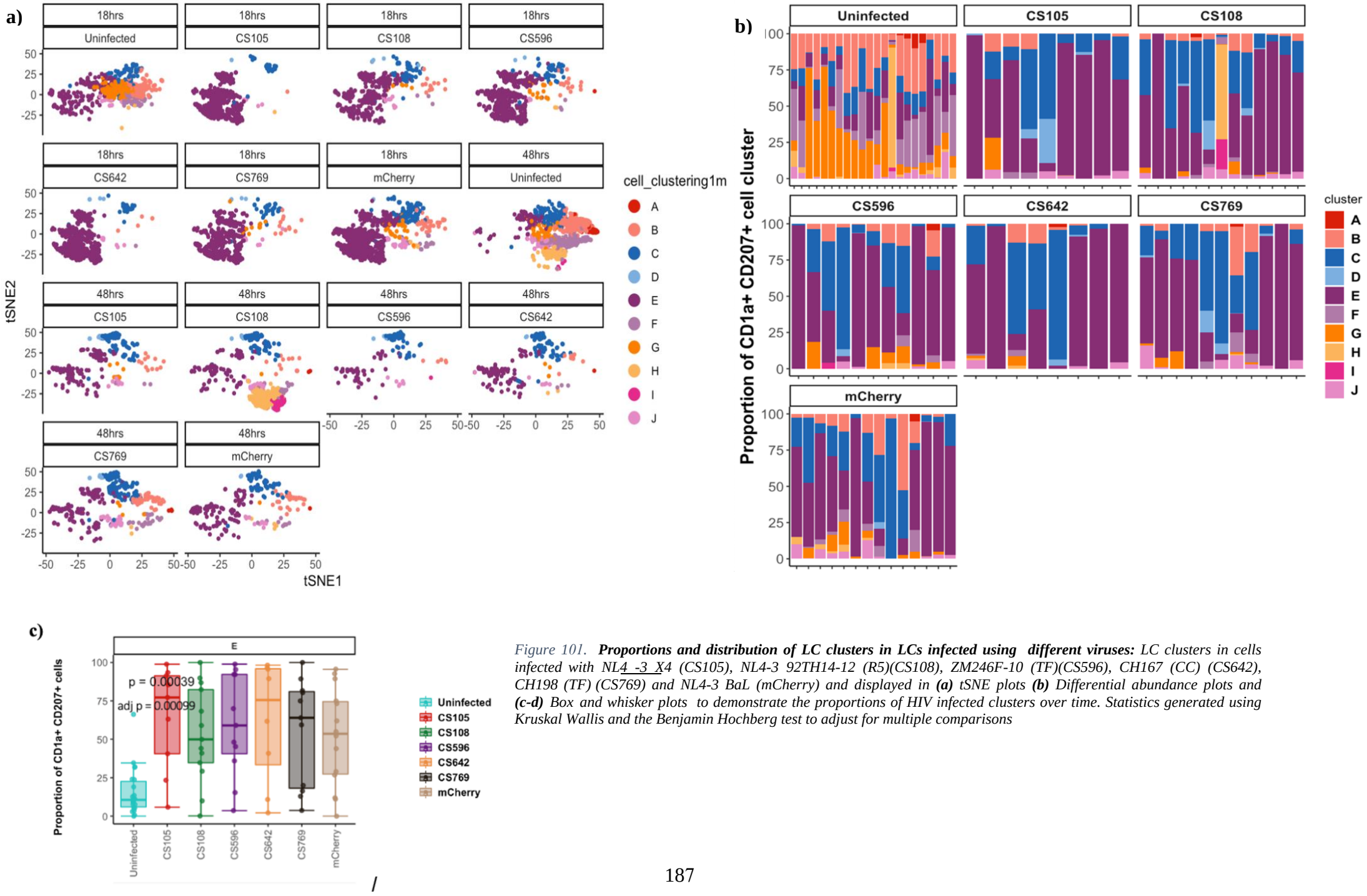

Figure 101. ***Proportions and distribution of LC clusters in LCs infected using different viruses:*** *LC clusters in cells infected with NL4 -3 X4 (CS105), NL4-3 92TH14-12 (R5)(CS108), ZM246F-10 (TF)(CS596), CH167 (CC) (CS642), CH198 (TF) (CS769) and NL4-3 BaL (mCherry) and displayed in* ***(a)*** *tSNE plots* ***(b)*** *Differential abundance plots and* ***(c-d)*** *Box and whisker plots to demonstrate the proportions of HIV infected clusters over time. Statistics generated using Kruskal Wallis and the Benjamin Hochberg test to adjust for multiple comparisons*

Summary and Conclusion

CD14 expressing LC clusters, inclusive of CD14+CD11c- and CD14+CD11c+ clusters were enriched in HIV infected LCs similarly to manual gating findings. However, only the CD14+CD11c- LC cluster enriched with time progression and was thus, productively infected. Attachment factors were differentially expressed among the different LC clusters, although DC-SIGN was more highly expressed in the HIV infected LC clusters compared to those that remained uninfected, especially Cluster G (least infectable). Therefore, DC-SIGN expression seemingly increased HIV susceptibility in the CD14+ LC clusters. Interestingly, the mannose receptor and Siglec-1 but not DC-SIGN, were completely lacking in the minor CD11c+CD14+ clusters that portrayed high p24 expression suggestive of the dispensability of these attachment factors in LC HIV infection. Unlike DC-SIGN, infection was established in both the presence and absence of Siglec-1 and the mannose receptor, although the productively infected cluster, Cluster C displayed high expression of all three.

2.2.2.2 HIV infection of "Mϕ -like" cell subsets

As illustrated in the Immunophenotyping Section; the foreskin harbours different "Mϕ-like" subsets namely, i) "M1-like" Mϕ , ii) "M2-like" Mϕ , iii) "M1" intermediates, iv) "M2" intermediates, v) CD169+ Mϕ as well as vi) CD3+ Mϕ . These heterogenous Mϕ subsets were subsequently assessed for HIV infection using the same viruses described above. However, CD80/86 was omitted in the HIV infection panel as described during optimisation in HIV infection Part 1. Therefore, "M1-like" Mϕ, previously defined as an HLA-DR+CD80/86+ population from the CD11c/CD14 Mϕ gate could not be defined within the HIV infected Mϕ population and HLA-DRhi cells were assessed instead. Overall, the mean frequency of HIV infected Mϕ-like cells increased with time progression, although non-significant as shown in Figure 102 below.

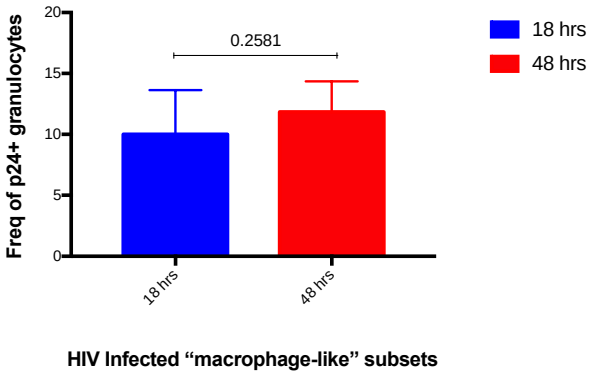

Figure 102. ***Proportions of overall HIV infected "macrophage-like" cells over time****. Statistics were generated with non-parametric paired t-tests using the Wilcoxon test and adjusted p values.*

Among the HIV infected foreskin granulocytes, "M2-like" Mϕ were the most frequent and constituted 12.58 % ± 1.59 % that increased 8.27 % as time progressed. However, owing to the small magnitude with which this change was effected, there was no statistical significance as displayed in Figure 103. A higher 34.9 % increase was displayed in the mean frequency of p24+CD3+ Mϕ between 18 and 48 hours (*p=0.0352*) also shown in Figure 103 and Table 11. Meanwhile the proportions of p24 +HLA-DRhi cells and p24+CD169+ macrophages declined with time progressed and were therefore not productively infected as shown in Table 11.

Table 11. HIV infected "macrophage-like" cells over time

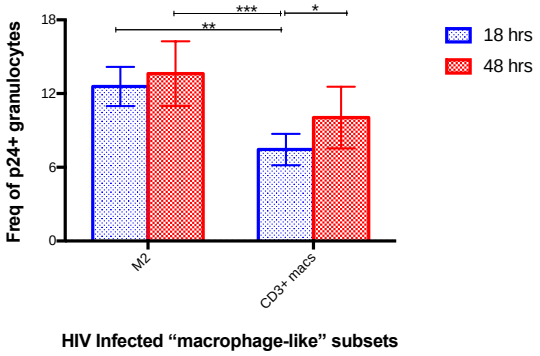

	Fold Change	*% Increase*
"HLA-DRhi" Mϕ	*- 0.40*	*- 39.57*
"M2-like" Mϕ	*0.08*	*8.27*
CD169+ Mϕ	*- 0.46*	*- 45.74*
CD3+ Mϕ	*0.35*	*34.90*

Figure 103. ***Identification and Quantification of p24+ foreskin "Macrophage-like" Cells from HIV infection with different viruses, at 18 and 48 hours.*** *Proportions of HIV infected "macrophage-like" subsets at 18 and 48 hrs. Statistics were generated with one-way ANOVA using the Tukey's multiple comparisons test at 95 % CI of difference and adjusted p values. *p <0.05; **p < 0.01; ***p < 0.001; ****p < 0.0001*

HIV infected "Mϕ-like" subsets: Different viruses & time-points

Although only "M2-like" Mϕ and CD3+ Mϕ were productively infected, different viruses resulted in different outcomes for each Mϕ subset as displayed in Table 12 below. While both CD169+ Mϕ and HLA-DR hi Mϕ were shown to decline with time progression in Table 11 above, the trend was retained across all the different viruses (data not shown).

Table 12. HIV Infected "macrophage-like" subsets : Different viruses & time-points

Virus	**M2-like Mϕ**		**CD3+ Mϕ**	
	Fold Change	**% Increase**	Fold Change	**% Increase**
Uninfected	- 0.08	**- 7.69**	- 0.30	**- 30.00**
NL4-3 X4	- 0.07	**- 6.82**	0.14	**14.27**
NL4-3 92TH14-12 (R5)	0.33	**32.59**	0.08	**7.74**
ZM246F-10 (TF)	0.01	**1.21**	0.37	**37.31**
CH167 (CC)	0.17	**16.86**	0.71	**70.50**
CH198 (TF)	0.30	**30.38**	0.74	**73.56**
NL4-3 Bal	- 0.22	**- 21.66**	0.11	**11.33**

Unlike the HIV infected CD14+ LCs, there were no apparent differences in the differential impact of time among the different virus strains in "M2-like" and CD3+ macrophages as shown in Figure 104 (a)-(b). The mean frequency of "M2-like" Mϕ increased the most when infected using CH198 (TF) and NL4-3 92TH14-12 (R5) that only increased 30.38 % and 32.59 % respectively, although without statistical significance as shown in Table 12 above. However, infection using NL4-3 X4 and NL4-3 BaL was non-productively infective and decreased 6.82 % and 21.66 % respectively as shown in Table 12 and Figure 104 (a) below. Meanwhile, the mean frequency of HIV infected CD3+ Mϕ enriched with time when infected with all the different viruses as shown in Figure 104 (b).

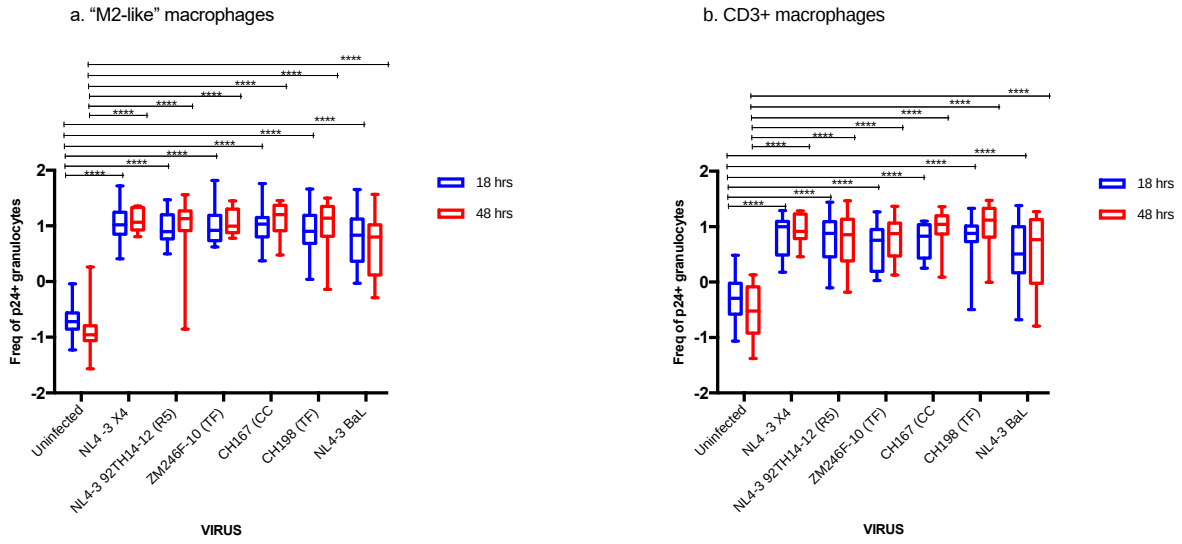

Figure 104. ***Proportions of uninfected and p24+ foreskin "macrophage-like" cells infected with different viruses at 18 and 48 hours.*** *Different subsets of "Macrophage-like" cells were infected with NL4 -3 X4, NL4-3 92TH14-12 (R5), ZM246F-10 (TF), CH167 (CC), CH198 (TF) and NL4-3 BaL at18 hrs and 48 hrs. Box and whisker plots demonstrating proportions of HIV infected "macrophage-like" cell subsets :* ***(a)*** *"M2-like macrophages"* ***(b)*** *CD3+ macrophages at 18 and 48 hours. Statistics were generated with two-way ANOVA using the Tukey's multiple comparisons test at 95 % CI of difference and adjusted p values. *p <0.05; **p < 0.01; ***p < 0.001; ****p < 0.0001*

HIV infected "Mϕ-like" subsets: Tropism

The different viruses were further grouped according to receptor usage and assessed for infectivity among the different Mϕ like subsets. Although "M2-like" Mϕ increased with time, the % increase was much lower compared to CD3+ Mϕ, as shown in Table 6. Contrary to both "M2-like" Mϕ and CD3+ Mϕ; the HLA-DRhi Mϕ and CD169+ Mϕ decreased with time in all virus groups as shown in Table 13.

Table 13. HIV Infected "macrophage-like" subsets : Tropism

VIRUS	M2-like Mϕ		CD3+ Mϕ	
	Fold Change	% Increase	Fold Change	% Increase
CC	0.17	**16.86**	0.71	**70.50**
NL4-3 R5	0.06	**5.79**	0.09	**9.36**
TF	0.17	**17.40**	0.58	**57.96**
NL4-3 X4	- 0.07	**- 6.82**	0.14	**14.38**

The mean frequency of HIV infected "M2-like" Mϕ, increased the most upon infection with Subtype C, chronic infection derived (CC) and transmitted founder (TF) viruses that increased 16.86 % and 17.4 % respectively, while NL4-3 R5 only increased 5.7 % (Table 13). Interestingly, the mean frequency of NL4-3 X4 infected "M2-like" Mϕ decreased with time (6.82 %) as described above and shown in Figure 105 (a). While all infection was productive in CD3+ Mϕ, there was particularly more enrichment upon infection with transmitted founder (TF) and chronic infection (CC) derived Subtype C viruses that increased 57.96 % and 70.5 % with time progression respectively, as displayed in Table 13 and Figure 105 (b).

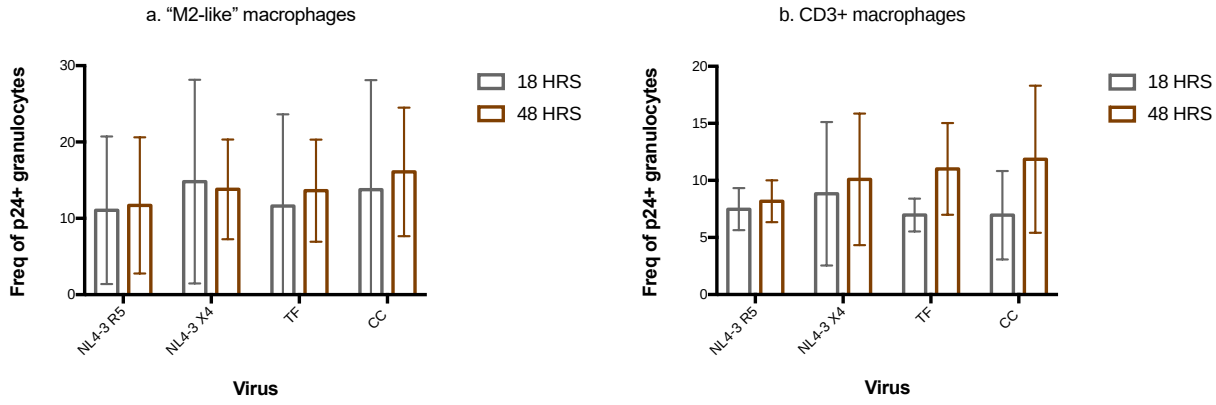

Figure 105. ***Proportions of p24+ foreskin "Macrophage-like" Cells from HIV infection with different viruses, at 18 and 48 hours.*** *Proportions of macrophage-like subsets infected using NL43-X4, NL4-3 R5, and Subtype C viruses: CC and TF viruses at 18 and 48 hours (a) "M2-like" macrophages (b) CD3+ macrophages (n=17). Statistics were generated with two-way ANOVA using the Tukey's multiple comparisons test at 95 % CI of difference and adjusted p values. There were no significant differences among the different virus groups.*

Summary

"M2-like" Mϕ and CD3+ Mϕ were the only productively infected macrophage subsets. This was however, in exception of infection using NL4-3 X4 that, similarly to CD14+ LC subsets, was non-productive in "Mϕ-like" cells . Both "M2-like" Mϕ and CD3+ Mϕ were more productively infected

using transmitted founder and chronic infection derived Subtype C viruses compared to NL4-3 viruses (X4 and R5).

Unsupervised clustering: Identification of HIV infected "Mϕ-like" subsets

Similarly to HIV infected LCs above, HIV infected "Mϕ-like" cells were further analysed using unsupervised clustering in order to identify, in an unbiased FlowSOM approach, the different HIV infected "Mϕ-like" subsets by different viruses at 18 and 48 hours.

Marker expression profile of HIV infected foreskin "Mϕ-like" cells

Using tSNE plots, the manually gated p24+ and uninfected "Mϕ-like" cells, were visualized and assessed for marker expression as shown in Figure 106 below. The color gradient, as explained above, was indicative of marker expression intensity levels (green = low/no expression; red = high/intense expression). CCR5, CD14 and CD1a were the predominantly expressed markers among these "Mϕ-like" cells, CD206 and HLA-DR were also dominant although with some regions of lower expression as shown in Figure 108. All the other markers (CD4, CD45, CD11c, CD3, CD207, CD169 and CD209) were differentially expressed.

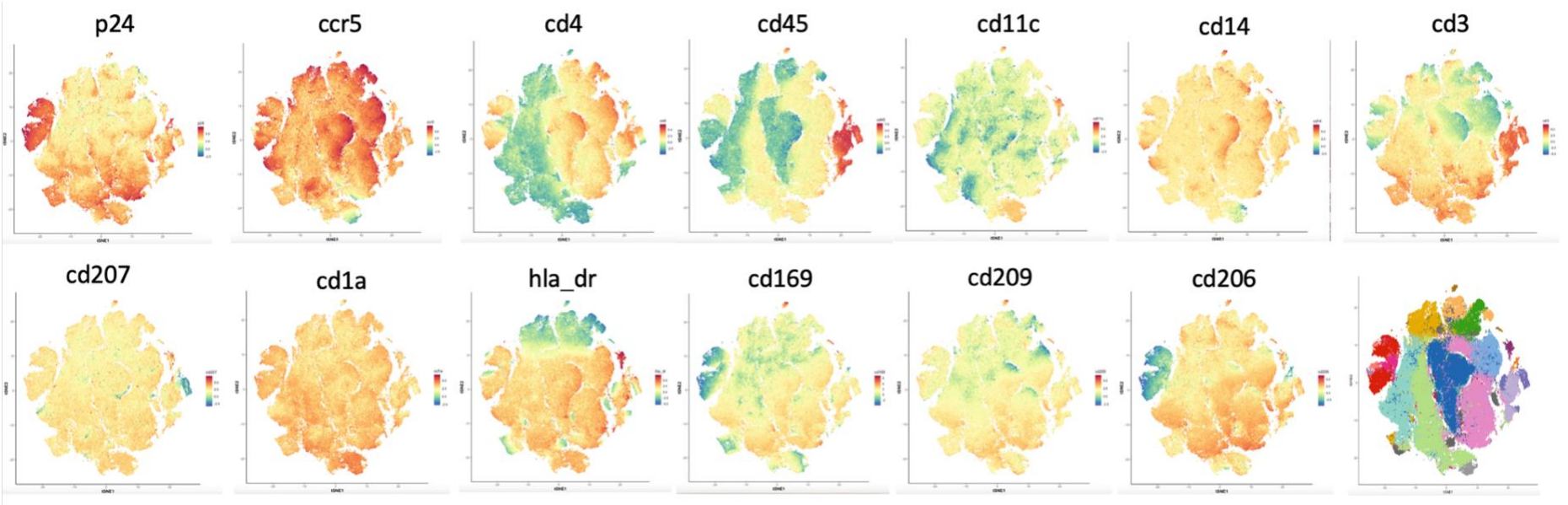

Figure 106. ***Assessment of the marker expression profiles of HIV infected and Uninfected "macrophage-like" foreskin cells from the CD11c/CD14 gate using tSNE plots generated by non-biased, computerised clustering.*** *tSNE plots displaying the differential expression of : p24, CCR5, CD45, CD4, CD3, HLA-DR, CD206, CD11c, CD14, CD209, and CD169.The color spectrum denotes increasing intensities of marker expression, ranging from green which represents no to low marker expression while red is high marker expression*

Identification of "Mϕ-like" subsets using unsupervised clustering

Using k=20, as described in Chapter 1, 20 "Mϕ-like" clusters were identified and mapped out onto the colored tSNE plot as shown in Figure 108.

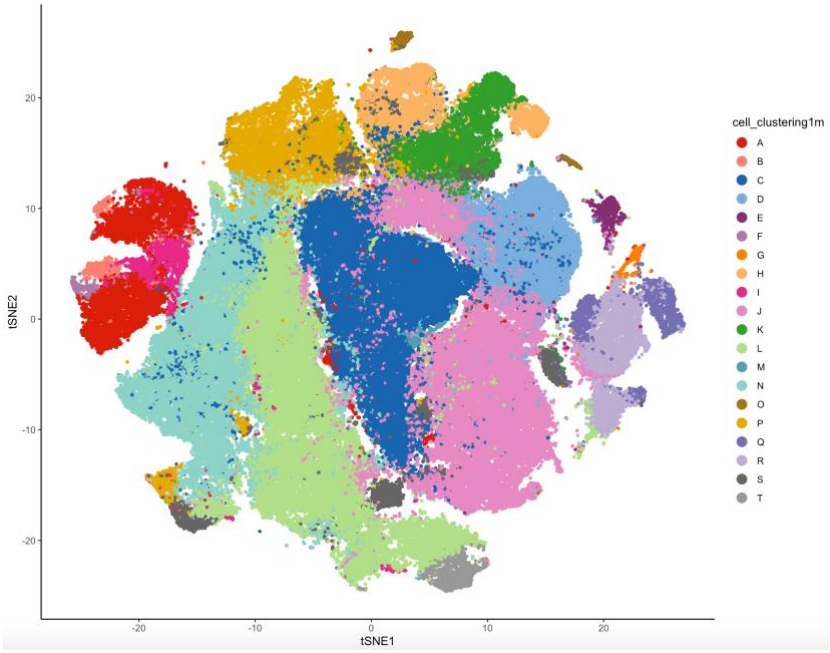

Figure 107. ***HIV infected "macrophage-like" clusters.****. Foreskin "macrophage-like" cells were infected using NL4 -3 X4, NL4-3 92TH14-12 (R5), ZM246F-10 (TF), CH167 (CC), CH198 (TF) and NL4-3 BaL; at 18 and 48 hours and tSNE plots were generated by overlaying FLOWSOM data generated using non-biased, computerised clustering to display the different "macrophage-like" clusters when k =20.*

Of these, Cluster C (*blue*; 17.21 %), Cluster A (*red*; 16.69 %), Cluster J (*pink*; 13.92 %), Cluster L (*lime*; 11.92 %), Cluster N (*turquoise*; 9.19 %) and Cluster D (*sky-blue*; 6.31 %) were the most frequent

and constituted the bulk of the foreskin "Mϕ-like" population (72.24%) as illustrated in Figure 108 (a) below. Noteworthy, all these clusters portrayed high HLA-DR expression which, if co-expressed with CD80/86 (missing from panel), would have had them characterised as the "M1" phenotype, although the immunophenotyping data identified the "M2" phenotype as predominant among all foreskin "Mϕ-like" cells. Moreover, HLA-DR was comparatively more intensely expressed in minor clusters, Cluster M (*turquoise*; 0.31 %) and Cluster E *(purple*; 0.43 %) that additionally co-expressed, with high

intensity, CD4 and CCR5 (Figure 108b) and thus more closely resembled the "M1-phenotype" than the core clusters did.

Except for Cluster A, all the other dominant clusters (C, J, L, N and D) additionally co-expressed high levels of C-type lectin receptors (CD206, CD209 and CD207) as well as Siglec-1 (CD169) and, thus clustered together while differing in the expression of CD45, CD3, CD4 and CCR5 as shown in Figure

108 (b).

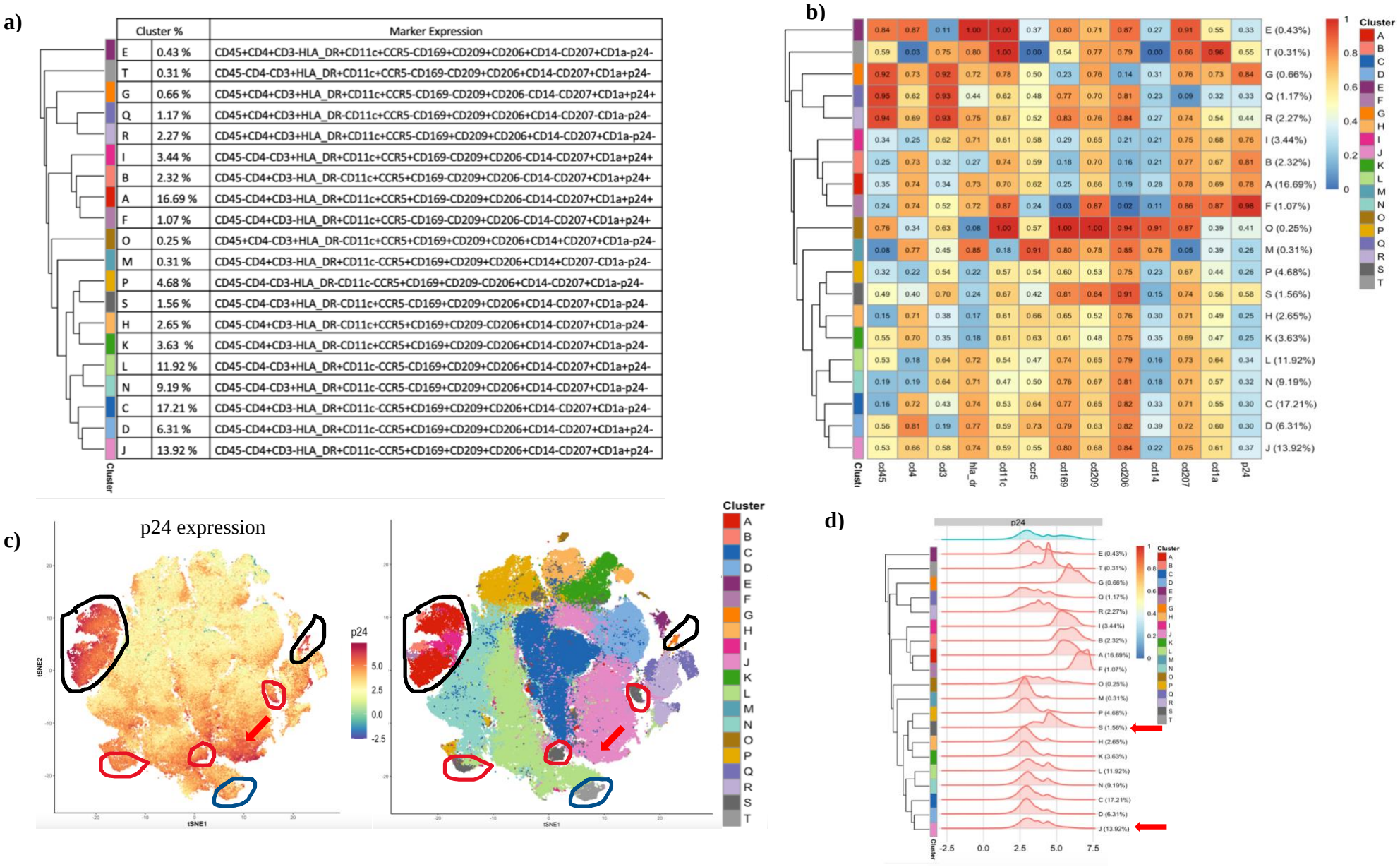

Figure 108. ***HIV infected (p24+) "macrophage-like" clusters.*** *Foreskin "macrophage-like" cells were infected using ; NL4 -3 X4, NL4-3 92TH14-12 (R5), ZM246F-10 (TF), CH167 (CC), CH198 (TF) and NL4-3 BaL at 18 and 48 hours & analysed using unsupervised clustering :* ***(a)*** *Table showing marker expression profiles of the 20 "macrophage-like" clusters* ***(b)*** *Heatmap showing marker expression intensities of the 20" macrophage-like" clusters* ***(c)*** *tSNE plots illustrating p24 expression and the different "macrophage-like" clusters* ***(d)*** *Histogram showing p24 expression in the different "macrophage-like" clusters*

Cluster A also exhibited high expression levels of the CLRs; CD209 and CD207 but was CD206-CD169-. Interestingly, this was also the only HIV infected (p24+) cluster among the most frequent "Mϕ-like" clusters according to Figures 108 (a)-(c). Note, however, that Cluster J displayed p24 expression to an extent, and was thus p24+/- according to the variable p24 intensities within the pink cluster (red arrows) shown in Figure 108 (c) further substantiated by the double peak in Figure 108 (d).

All the other p24+ clusters were minor and inclusive of Cluster G (*orange*; 0.66 %), Cluster I (*hot pink*; 3.44 %), B (*coral*; 2.32 %), and F (*purple*; 1.07 %) as shown in Figure 108 (c) (circled in black). Thus, HIV infected "Mϕ-like" clusters constituted 24.18 % of the overall foreskin "Mϕ-like" cells and all, except for Cluster G, were phenotypically related and clustered together as shown in Figures 108 (a)-(c). Noteworthy, p24 expression was the brightest in Cluster F (*purple*; 1.07 %) along with CD11c, CD209, CD207 and CD1a that were also more brightly co-expressed than in other p24+ "Mϕ-like" clusters, while CD169 and CD206 were at their most dim in this cluster as shown in Figure 108 (b).

Interestingly, Cluster S (*grey*; 1.56 %) and Cluster O (brown; 0.25 %) uniquely and simultaneously co-expressed all attachment factors (CD169, CD206 and CD209) with the brightest intensity whilst constituting one of the few HLA-DR- clusters as shown in Figure 108 (b). This was in corroboration with the hypothesised inverse co-relation between attachment factors and maturation markers although HLA-DR expression alone was insufficient to affirmatively conclude this. Cluster S, similarly to Cluster J, was also p24+/-as shown in Figures 108 **(c)** (circled in red) and **(d)** (red arrows) above.

"Mϕ-like" Clusters: Different viruses and time-points

Similarly to LCs above, "Mϕ-like" clusters were further stratified according to the different viruses and time-points. At 18 hours, Cluster A (*red*;16.69 %) was in NL4-3 BaL infected cells when compared to all the other viruses and uninfected cells as shown in Figure 109 below. However, as time progressed, Cluster A was more pronounced in NL4-3 92TH14-12 (R5) infected cells and unexpectedly, in uninfected cells as shown in Figure 109.

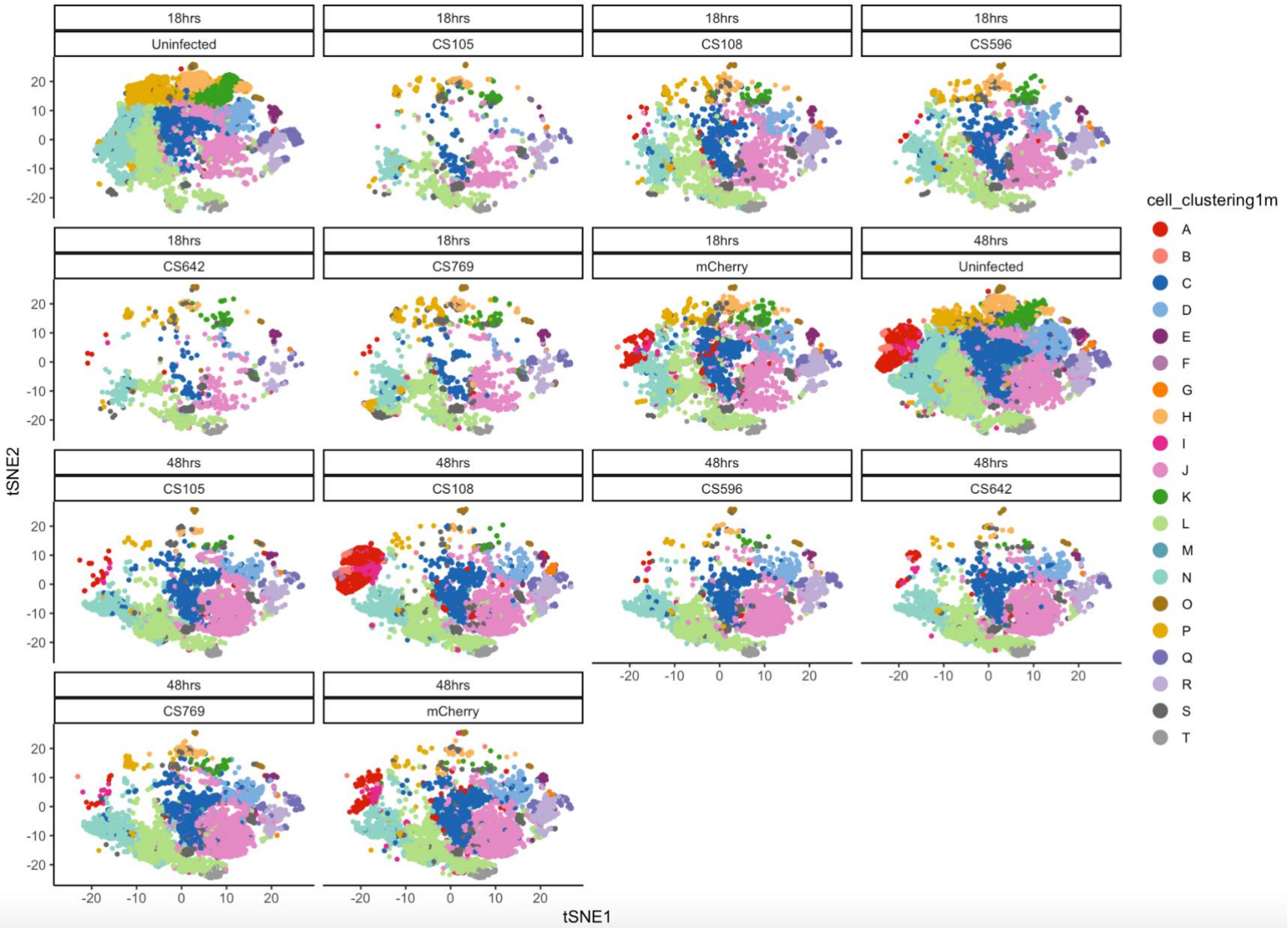

Figure 109. tSNE plots displaying ***HIV infected Mϕ-like clusters according to the different viruses and time-points****. Mϕ-like cells were infected using different viruses at 18 and 48 hours. Mϕ-like cells infected with NL4 -3 X4 (CS105), NL4-3 92TH14-12 (R5) (CS108), ZM246F-10 (TF)(CS596), CH167 (CC)(CS642), CH198 (TF)(CS769) and NL4-3 BaL (mCherry) and analysed at 18 and 48 hours (n = 17).*

While Figure 110 (a) below further corroborates Cluster A as more detectable in NL4-3 BaL, NL4-3 92TH14-12 (R5) and uninfected cells; this was without any statistical significance (*p = 0.51, adj p = 0.126*) as shown in Figure 110 (b) below. When assessed at the different time-points, Cluster A was more outstanding in NL4-3 BaL infected cells at 18 hours (*p = 0.052; adj p = 0.130*) and less-so at 48 hours where there were no notable differences among the different virus groups (*p = 0.455; adj p = 0.53*) as shown in Figure 110 (c).

Cluster J (*pink*; 13.92 %) portrayed differential infectivity among the different viruses and was more noticeable in cells infected with ZM246F-10 (TF), NL4-3 92TH14-12 (R5) and NL4-3 BaL while also increasing with time progression, including in cells infected with NL4-3 X4, CH167 (CC) and CH198 (TF) as shown in tSNE plots in Figure 109 above and in Figures 110 (a) – (b) below (*p = 0.00042; adj p = 0.0016*). While differential infectivity among the different viruses was more apparent at 48 hours (*p = 0.001; adj p = 0.0052*) compared to 18 hours (*p = 0.021; adj p = 0.071*); Cluster J additionally portrayed a time-dependant increase in all viruses and was thus productively infected as shown in Figure 110 (c).

Although less conspicuous in the tSNE plots above, Cluster R (*purple*; 2.27 %) and Cluster S (*grey*; 1.56 %) were also more frequent in infected cells in all virus groups compared to uninfected cells (*p = 0.0049, adj p = 0.0089; p = 0.0022, adj p = 0.0000009*) as illustrated in Figures 110 (a) - (b) below. However, in Cluster R, these differences were only noticeable with time progression, although without productive infection. The proportions of Cluster R were thus, different among the different viruses and uninfected cells at 48 hours (*p = 0.021, adj p = 0.071*) while no differences were noted at 18 hours (*p = 0.176, adj p = 0.29*) as shown in Figure 110 (c).

Contrary to Cluster J that portrayed productive infection, a time-dependant decline was observed in Cluster S although the differences among the different virus groups were retained at both 18 hours (*p = 0.00085, adj p = 0.0048*) and 48 hours (*p = 0.00058, adj p = 0.0048*) as illustrated in Figure 110 (c). Interestingly, both the non-productively infected cluster (Cluster S) and the productively infected cluster (Cluster J) portrayed high expression levels of the CLRs (CD206, CD209, CD207, CD169) as shown earlier in Figure 108. Other than the differential impact of time, Cluster J additionally differed by the expression of HLA-DR, CD4 and CCR5, which were all lacking in Cluster S and thus, possibly linked to the productive infectivity of Cluster J. While CD4 and CCR5 corroborate the susceptibility of Cluster J to infection, analyzing HLA-DR in conjunction with CD80/86, would have been instrumental in elucidating the association between cell maturity and/or Mϕ polarization with HIV susceptibility.

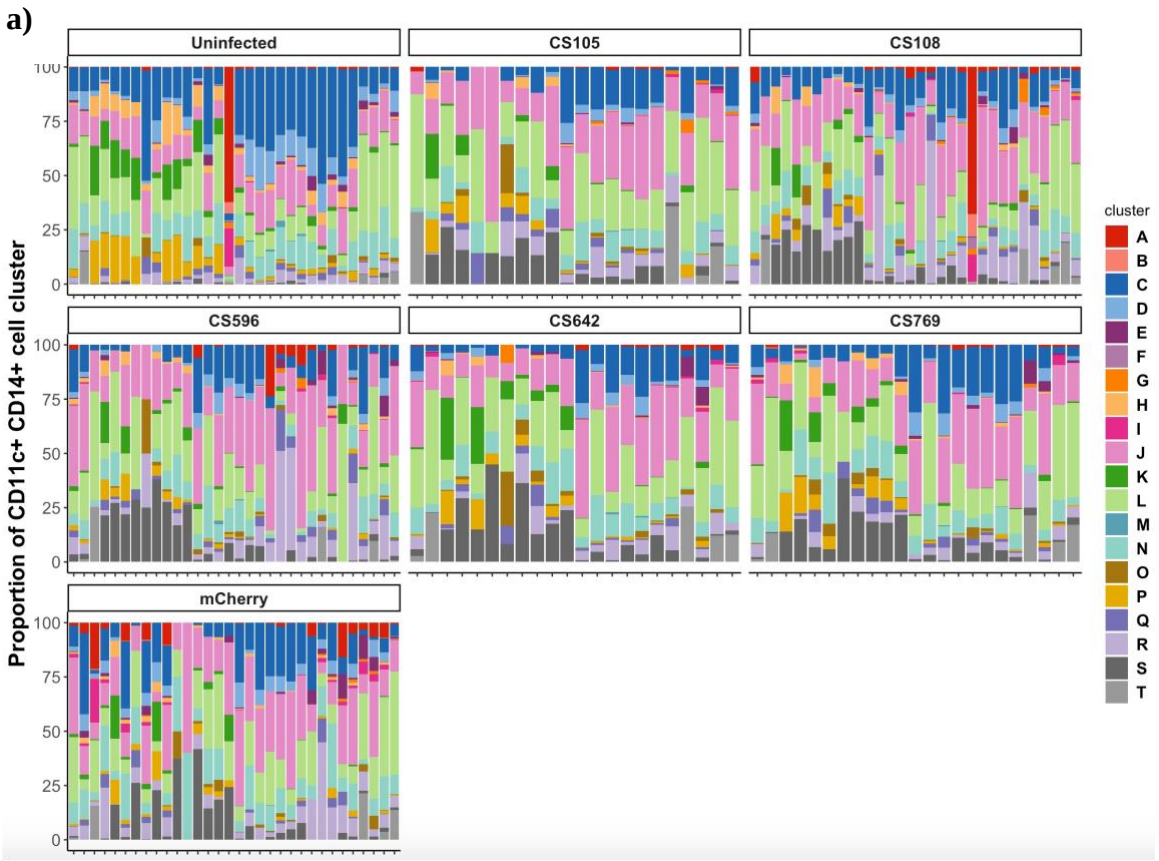

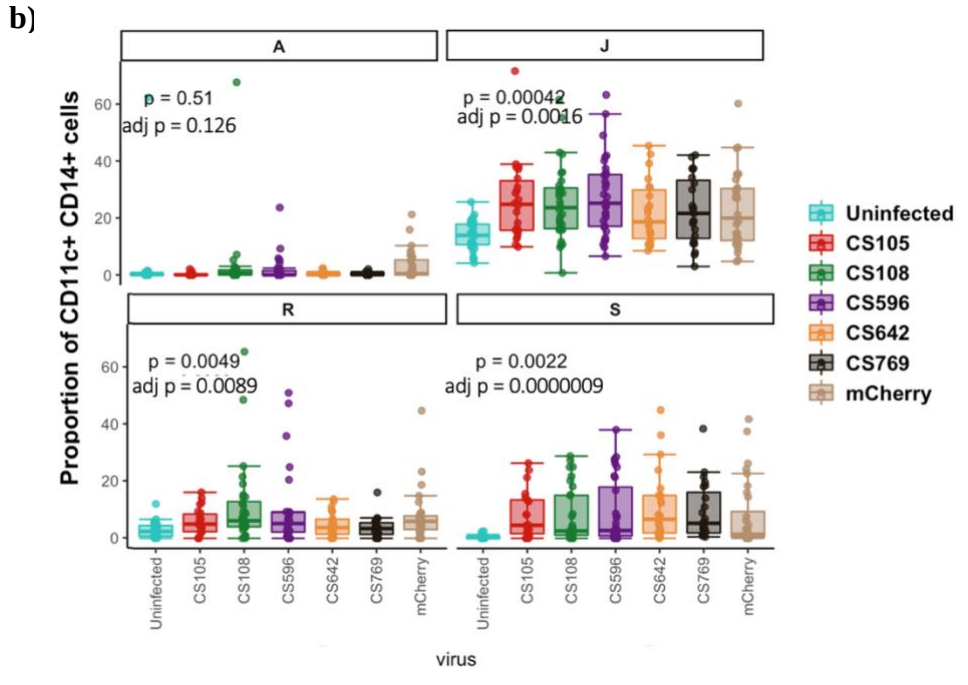

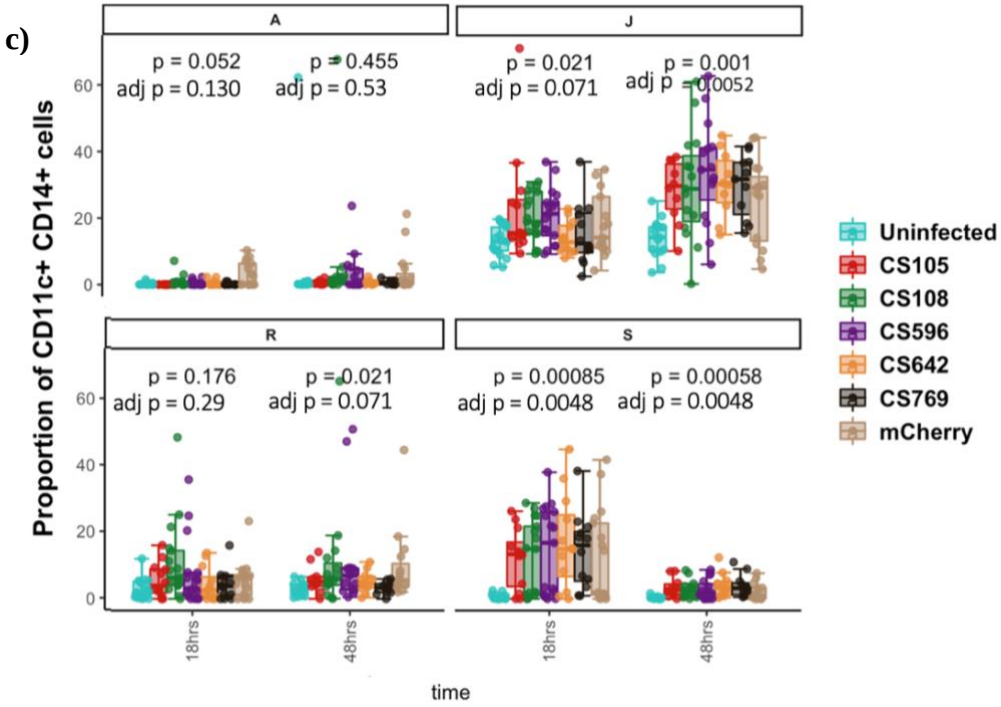

Figure 110. ***Determination of the different foreskin "macrophage-like" subsets in HIV uninfected and infected foreskin "macrophage-like" cells infected with different viruses;*** *NL4 -3 X4(CS105), NL4-3 92TH14-12 (R5)(CS108), ZM246F-10 (TF)(CS596), CH167 (CC)(CS642), CH198 (TF) (CS769) and NL4-3 BaL (mCherry); at 18 and 48 hours. tSNE plots were generated using non-biased, computerised clustering. Statistics were generated using Kruskal Wallis and the Benjamin Hochberg test to adjust for multiple comparisons.*

All the other minor p24+ clusters, Cluster B (*coral*; 2.32 %), Cluster G (*orange*; 0.66 %), Cluster I (*hot pink*; 3.44 %) and Cluster F (*purple*; 1.07 %) including the p24dim, Cluster T (light-grey; 0.31 %), did not portray any statistically significant differences among the different virus groups at both 18 and 48 hours (data shown in Appendix).

Meanwhile, uninfected "Mϕ-like" clusters comprised of Cluster C (*blue*;17.21 %) (*p = 1.1e-06, adj p = 0.0027*) and Cluster D (*sky-blue*;6.31 %) (*p = 2.3e-06, adj p = 0.0027*) that were interestingly shown above, to cluster with the productively infected cells (Cluster J). While the three clusters had similar marker expression profiles, Cluster J differed by CD3 co-expression and comparatively lower expression intensities of CD4+CCR5+ possibly due to infection induced down-regulation. Uninfected "Mϕ-like" cells were also constitutive of Cluster H (*light-orange*;2.65 %) (*p = 2.3e-07, adj p = 0.0000009*) and Cluster P (*tan*;4.68 %) (*p = 0.0019, adj p = 0.0048*) as shown in Figure 110 (a) and Appendix. These trends were retained at both 18 and 48 hours. Note, there were no statistical differences in the proportions of all the other clusters (E, K, L, M, N, O and Q) among the infected and uninfected cells (data not shown).

Summary: Infection of foreskin "Mϕ-like" cells

Cluster J was the only productively infected "Mϕ-like" cluster among the "Mϕ-like" cells, when unsupervised clustering was used. The identification of Cluster J as one of the core "Mϕ-like" clusters and also portraying high co-expression of CD206 and CD209, was in sync with manual gating findings whereby, "M2-like" Mϕ (CD206+CD209+) were identified as the most frequent and productively infected Mϕ phenotype. Also identified alongside the "M2-like" Mϕ, as the most frequent and productively infected phenotype, were the CD3+ Mϕ. While this may not have been the case with unsupervised clustering, where the non-productively infected Cluster G (0.66 %) was the only p24+ cluster intensely co-expressing CD3; Cluster J also portrayed CD3 co-expression although with dim intensity. Thus, the "M2-like" Mϕ phenotype or the expression of CLRs and CD3 co-expression are favourable to the HIV infection of foreskin "Mϕ-like" cells.

2.3 INFECTION SUB-CONCLUSION

The foreskin therefore harbours heterogenous myeloid cell populations that are differentially susceptible to *ex vivo* HIV infection using lab-adapted Subtype B (NL4-3s) and Subtype C viruses (transmitted/founder and chronic infection derived HIV strains). Using the pluricellular cell suspension infection model, HIV infected myeloid cells were distinguishable into LC subsets and "Mϕ-like" cells, along with foreskin lymphocytes. Among these, HIV infected "Mϕ-like" cells predominated the myeloid cell component of HIV infected myeloid cells while LCs were fewer at both 18 and 48 hours

as shown in Figures 111 (a) – (b) below. In particular, traditional LCs did not support infection, while CD14+ LCs and CD11c+CD14+ LCs were the only productively infected LC subsets. Furthermore, LC infection was only productive with Subtype C transmitted founder viruses and NL4-3 R5 viruses while restrictive to NL4-3 X4. Although other CD11c+ LCs and the CD3+ LCs also portrayed p24 expression at 18 hours and constituted the bulk of HIV infected LCs as shown in Figure 111 (a), this decreased with time and was therefore non-productive as shown in Figure 111 (b).

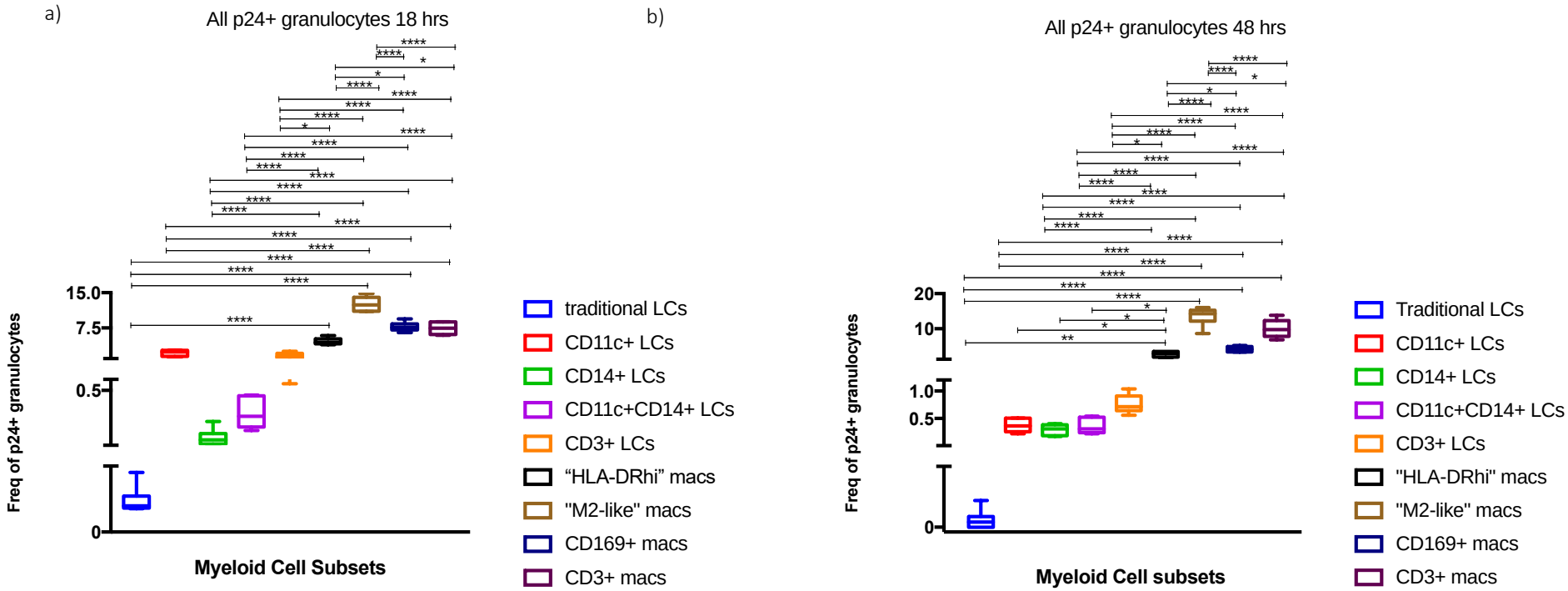

Figure 111. ***Proportions of HIV infected foreskin LC subsets and “Macrophage-like” subsets at 18 and 48 hours***. *Foreskin myeloid cells were infected with NL4 -3 X4, NL4-3 92TH14-12 (R5), ZM246F-10 (TF), CH167 (CC), CH198 (TF) and NL4-3 BaL and analysed at 18 and 48 hours (n = 17). Statistics were generated with two-way ANOVA using the Tukey’s multiple comparisons test at 95 % CI of difference and adjusted p values. *p <0.05; **p < 0.01; ***p < 0.001; ****p < 0.0001*

Meanwhile, HIV infected "Mϕ-like" cells were dominated by the "M2-like" Mϕ, CD3+ Mϕ and the CD169+ Mϕ although with a diminishing frequency of CD169 Mϕ as time progressed as shown in Figure 111 (a) – (b). Thus, CD3+ Mϕ and the "M2-like" Mϕ were the only two, productively infected subsets. While this was a manual gating paradigm, the most frequent and productively HIV infected cluster identified using unsupervised clustering, also displayed "M2-like" characteristics while also dimly co-expressing CD3 as described above. The Mϕ panel was however limited and the lack of CD80/86 in the HIV infection panel restricted the characterisation of the "M1-like" Mϕ phenotype and the transitionary intermediate "Mϕ-like" phenotypes that were characterised in Chapter 1. High HLA-DR expressing cells were thus simply identified as the "HLA-DRhi" phenotype, and when assessed for the co-expression of CD4, CCR5 and CD11c, these cells constituted the least abundant phenotype similarly to the "M1-like" Mϕ in Chapter 1. While there were no profound differences in the infectivity of the different viruses, trends were noted whereby "M2-like" Mϕ were more frequent Subtype C transmitted founder infected cells compared to the NL4-3 R5 infection.

Although the dissemination of HIV from infected LCs and "Mϕ-like" cells to CD4+ T cells was not measured, foreskin CD4+ T cells were also observed to support HIV infection by both lab adapted and T/F viruses. NL4-3 92TH14-12 (R5) exhibited the most profound infection in foreskin lymphocytes. Importantly, the fusion inhibitor, maraviroc was most effective in blocking HIV infection against lymphocytes compared to myeloid cells. Noteworthy, there was also high individual variability among the different participants used. While some participants portrayed very high HIV infection, significantly increasing the standard deviation; there were some that remained uninfected.

IV. DISCUSSION

Understanding key players in HIV transmission, dissemination and sustenance is key in designing intervention strategies to help curtail its spread and persistence. Myeloid cells, if fully characterized and their role in HIV transmission understood, provide one such avenue, as they have been postulated to play a double-edged sword in HIV pathology. While myeloid cells are adapted to offer the first line of defense against invading pathogens including HIV, through various PRRs and host restriction mechanisms, they have also been shown amenable to hijacking by HIV to aid its own dissemination and propagation. Myeloid cells have additionally been shown to express low levels of CD4 and CCR5, and thus permissible to *cis* infection while displaying anti-cytopathic characteristics and therefore contributing to perpetual inflammation and immune exhaustion. Macrophages have particularly been reported to aid viral persistence as contributors of the viral reservoir and to thus, hinder the absolute success of anti-retroviral therapy. Understanding the molecular factors enabling viral entry and spread in myeloid cells is therefore key in designing future anti-viral strategies. More-so, using a relevant model is helpful in the identification of niche specific molecular markers. Therefore, a foreskin pluricellular cell suspension model was used in this study to help elucidate the composition, quantity, and characteristics of foreskin myeloid cells and to assess their subsequent interaction with HIV *ex vivo* in order to determine molecular markers at play.

Foreskin myeloid cells display mixed ontogeny and migration potential

The first objective of this study was to isolate and immunophenotype foreskin myeloid cells and thus, in its fulfilment, foreskin primary cells were isolated from 31 seronegative participants who were STI negative and characterized using multi-parameter flow cytometry. Two cell isolation methods were used, namely the migratory assay (crawl) and the non-migratory assay (liberase). The migration assay capitalizes on the innate ability of DCs to migrate to and from the lymph nodes for antigen presentation and T cell activation. This has in-fact, been one of the key features that have been used to distinguish DCs from macrophages that have otherwise been reported as a tissue resident population with limited migration potential as substantiated by tissue explant studies[169].

Interestingly, the leukointegrin, CD11c, has been rendered key in the activation and migration of granulocytes and its deletion shown to impair migration, antigen presentation as well as T cell activation[213]. In a separate study, activated, migratory LCs were also shown to upregulate the co-expression of $CD11c^{int\text{-}high}$, $HLA\text{-}DR^{hi}$ and CD80/86[214].

Migratory foreskin cells were therefore CD11c+CD14-, while non migratory cells were predominantly CD11c-CD14+. CD11c expression has additionally been shown to aid phagocytosis, cytokine production and although some studies have postulated LCs as CD11c-, others have reported CD11c to induce T cell proliferation by LCs[213]. This suggests that CD11c can also be used as a marker for maturity in DCs and LCs while also being used to identify the M1 macrophage phenotype due to its pro-inflammatory and cytokine induction properties[213].

The ubiquity of CD11c expression among cells of the myeloid lineage is also applicable to CD14 expression that, due to its role in pathogen clearance, has been referred to as a PRR[121]. More importantly, CD14 can be used to identify the origin and ontogeny of LCs. While monocytes, macrophages and monocyte derived myeloid cells (DCs, LCs and macrophages) are typically CD14+, self-renewing LCs that seed the epidermis from the yolk sac or fetal liver lack the expression of CD14[111]. Therefore, incorporating CD14 in the panel was instrumental in deciphering the parentage of foreskin LCs (although requiring supplementation with a wider panel of ontogeny markers inclusive of transcription factors), in addition to being used as a pan-myeloid marker. Owing to this, foreskin LCs were assessed for CD11c and CD14 expression and accordingly distinguished into the different subsets while "macrophage-like" cells were identified from an LC exclusionary gate inclusive of CD11c+CD14+, CD11c+CD14+ and CD14+CD11c-cells.

Notably, overall myeloid cells in their respective groupings into CD11c+, CD14+ and CD11c+CD14+ myeloid cells were only a fraction of the total foreskin epithelial cells. The foreskin, epidermis, similarly to all skin epithelia is encumbered with epithelial cells such as keratinocytes, fibroblasts and NK cells that have been suggested to cross-talk with immune cells such as LCs, thereby initiating the innate immune response [148].

Foreskin LCs only made up 1 % of the total live foreskin epidermal cell population, while macrophages were 10 %. The inverse has been reported using quantitative immunohistochemistry whereby, macrophages have been shown to only attribute 0.1 % - 2.7 % of the foreskin mucosa while LCs have been shown to range from 1 % - 15.6 % depending on age, ongoing or previous infection [216]. Both LCs and macrophages have been reported as more frequent in the foreskin compared to cervical mucosa [216]. While cervical mucosal macrophages have been reported as 2-fold less, LCs were 10-fold lower in comparison to the foreskin mucosa[32,69,216]. This was also observed when compared to paediatric foreskins, where the mean proportions of LCs were 5-fold higher than LCs isolated from the ectocervix of adult women [32,69,216]. Although it was not within the scope of this study to characterise lymphocytes, a mean frequency of 4.8 %, within the total isolated foreskin cells was observed. This was slightly higher than has been reported in other foreskin studies using immunohistochemistry, where memory CD4+ T cells have been shown to range from 0.4 % - 3.1% [216]. Similarly, to LCs and macrophages, the

ectocervix has been reported to harbour lower proportions of lymphocytes compared to the foreskin [216]. Vascular lymphocytes were not excluded in our study, and therefore, possibly measured.

Furthermore, the distribution of these cells has been shown to differ by foreskin compartment. The inner foreskin has been reported to have higher mean proportions of LCs (63.1 %) compared to the outer foreskin (52.8 %)[77,78,215,216]. This was also observed in this study, with particular reference to the CD11c+ LCs and the CD11c+CD14+ LCs that were both 2-times more frequent in the inner, compared to the outer foreskin. Additionally, the mean frequency of CD4+CCR5+ cells was higher in migratory LCs compared to non-migratory LCs in the foreskin, thereby corroborating with findings that migratory LCs are primary targets in vaginal HIV transmission, additionally disseminating to CD4+ T cells[69,170]. Unlike LCs, macrophages have not been shown to differ by foreskin compartment[216,217]. Likewise, there were no significant differences in the proportions of "M2-like" macrophages and "M1-lke" macrophages in the inner and outer foreskin.

Compared to the ectocervix, foreskin CD4+ T cells and LCs express higher levels of CCR5 [216]. The expression of CXCR4, although at lower levels, has also been reported as more highly expressed in foreskin LCs and CD4+ T cells than in cervico-vaginal counterparts[216]. CXCR4 expression was, however, not assessed in this study, although infection with NL4-3 X4 virus could be viewed as an indication of CXCR4 expression in foreskin CD4+ T cells and LCs as observed in this study. The foreskin, therefore, harbours higher proportions of HIV susceptible immune cells compared to cervico-vaginal samples reported in other studies[216]. This has been further substantiated by increased detection of HIV-1 DNA, in proportions 9 times higher in the foreskin compared to cervico-vaginal samples[32,69,216].

Foreskin Langerhans cells

Foreskin LCs were distinguishable into varied subsets inclusive of conventional/traditional LCs that were characterized as CD14-CD11c- and constituted the majority of the foreskin LC population. Other non-conventional LC subsets were inclusive of CD11c+CD14- LCs, CD14+CD11c- LCs, CD3+ LCs and the CD11c+CD14+ LCs. To further substantiate the role of CD11c in migration, CD11c+CD14- LCs were predominantly migratory and with high HLA-DR+CD80/86+ co-expression, similarly to CD11c+CD14+LCs. Meanwhile CD14+CD11c- LCs were predominantly non-migratory and portrayed the least frequency of CD80/86+HLA-DR+ cells among all LC subsets. Foreskin traditional LCs were also migratory, although without CD11c expression. CD11c expression can therefore not be used to determine the migration potential of traditional LCs whose migration has been shown, by other authors, to rely on CXCR4-CXCL12, CCR7 and the downregulation of E-cadherin[107,199].

This mixed heterogeneity of foreskin LCs could be attributed to ontogeny and function as alluded to above. LCs are reported to originate from dual precursors inclusive of (i) embryonic (fetal liver/yolk sac) precursors and (ii) bone-marrow derived circulatory monocytes[108]. Embryonic precursors seed the epidermis before birth, and differentiate into a population of self-renewing LCs (bona fide LCs) that persists throughout adulthood [107,108] while circulatory precursors seed the epithelium on a need basis (monocyte derived LCs or "LC-like" cells). Although both have been shown present under steady state conditions, monocyte derived LCs have been reported to increase during inflammation, ultra-violet injury, psoriasis or atopic dermatitis [107,108,125,218]. Unlike, yolk sac or fetal liver derived LCs; monocyte derived LCs lack self-renewal properties and are deemed short-lived as they are eventually replenished by the resident self-renewing LCs once inflammation has passed[107]. The foreskin is therefore likely to be populated with both monocyte derived LCs as well as self-renewing LCs, hence the different subsets that were identified[86,216].

It is important to decipher parentage in epithelial populations as it could give insight regarding ongoing or previous inflammatory conditions that could potentially exacerbate one's vulnerability to HIV infection. Importantly, the foreskin LC subsets that were productively infected with HIV were the CD14+ LCs and the CD14+CD11c+ LCs. Based on ontogeny, this suggests that it is the monocyte derived LCs and not bona-fide resident LCs that support HIV infection in the foreskin. To further substantiate this, HIV infected CD14+ LCs portrayed high expression levels of the CLR, DC-SIGN and IFN-1 inducible Siglec-1, that have been purported to lack in traditional LCs[72]. DC-SIGN was additionally identified as key in mediating the infection of foreskin CD14+ LCs and the CD11c+CD14+ LCs, without which there was no infection. Although DC-SIGN does not function as an HIV receptor, it has been shown in various studies to promote the efficiency with which HIV target cells take up the virus. Therefore, the role of DC-SIGN, while associated with *trans* infection, also concentrates virions on the surface of HIV target cells in a manner that culminates in *cis* infection as was observed in foreskin LC infection, whereby increment in the proportions of p24+ cells was used as proxy for productive infection.

Although there were no profound differences in the infectivity of different viruses in the infected LCs, CD14+ LCs portrayed the highest levels of p24+ expression when infected with transmitted founder Subtype C viruses, particularly CH198 (TF). Among the lab-adapted strains, infection of foreskin explants has been reportedly more pronounced with HIV-BaL (CCR5) than with HIV Lai (CXCR4)[29]. The same phenomenon was observed in our model, FSK cells were most permissive to infection with NL4-3 92TH14-12 (R5) and HIV-BaL while NL4-X4 infected cells decreased with time progression. Although the increment of p24+ cells with time progression, was used in this study as proxy for productive infection, the likelihood of productive infection culminating in cell lysis was not measured. It is, therefore, possible that a decrease in proportions of p24+ cells could be due to viral cytopathic

effect on infected cells indicative of productive infection. Future studies could address this measuring the RT activity in the culture supernatants to corelate with the cell-associated virus kinetics.

Additionally, NL4-3 X4 infection displayed high p24 detection in foreskin LCs at earlier time-points, and only decreased as time progressed. This was suggestive of HIV entry and possible accumulation of NL4-3 X4 virions in foreskin LCs followed by premature abrogation, and thus the decline in p24+ cells. This was in corroboration with the langerin mediated abrogation that's been reported in immature LCs [28].

While the maturation states of HIV infected LCs could not be measured, CD14+ LCs portrayed the least HLA-DR+CD80/86+ co-expression among all other LC subsets during Immunophenotyping. This was further substantiated by the predominantly non-migratory phenotype of these cells. Therefore, it can be postulated that CD14+ LCs may have conferred resistance against NL4-3 X4 in this regard, although further work needs to be done to confidently affirm this. While maturation has been shown to nullify langerin mediated resistance and to increase the susceptibility of mature LCs to infection[28,32], there are also other factors that been implicated to override this resistance.

Reportedly, transmitted founder viruses are resistant to LC mediated abrogation, portray IFN resistance and have also been shown to display more infectivity than lab-adapted strains in mature vaginal and skin LCs[28,32,219]. This potentially explains the susceptibility of foreskin LCs to transmitted founder virus infection and the higher enrichment in p24+ cells as time progressed when infected with these viruses. Any host restriction mechanisms potentially conferred by CD14+LCs and CD11c+CD14+ LCs were insufficient against transmitted founder viruses. Notably, HIV susceptibility is also governed by the type of tissue and location of susceptible cells. In other studies, foreskin tissue explants have been shown to display more R5 HIV permissiveness in comparison to cervical tissue explants due to the higher proportions CCR5+ cells in foreskin cells[29]. This could also explain the preferential permissiveness to transmitted founder and NL4-3 R5 viruses displayed by foreskin LCs.

LCs have always been described as the major MNP in the epidermis although there is an emergence of reports showing otherwise. Populations such as epidermal CD11c+ DCs[72] as well as the inflammatory dendritic epidermal cells (IDECs) are increasingly being described in epidermal tissues[218,220,221]. Both IDECs and the epidermal CD11c+ DCs have been distinguished from LCs by the lack of langerin and high expression of CD11c and the mannose receptor[72]. Moreover, epidermal CD11c+ LCs have also been identified as an HIV target cell in foreskin and abdominal tissues, with high CCR5 expression and capable of supporting HIV replication. Although a similar population was deciphered in this study, the foreskin CD11c+ LC subset portrayed low expression of CLRs inclusive of the mannose receptor, DC-SIGN as well as Siglec-1.

The co-expression of CD4 and CCR5 was additionally low in this subset, and as such there was no infection in the CD11c+ foreskin LCs, although p24 expression was observed at 18 hours. Although there may have been the possibility of a restrictive mechanism, the infection model did not incorporate a washing step following virus inoculation and thus potentially attributable to p24 detection. The foreskin epidermis therefore harbors a CD11c+ LC population, that is not infectable with HIV and thus, unique from the epidermal CD11c+ DCs described by other authors.

IDECs have additionally been differentiated from LCs by location. While bona-fide LCs reside in the upper epidermis, IDECs have been shown to reside in the lower epidermis alongside monocyte-derived LCs. Although there may be such stratification, the migration assay and the enzymatic digestion cell isolation protocols used in this study, were not designed to differentiate the different subsets according to location. This is especially because monocyte derived LCs have been shown to express low E-cadherin levels thus highly migratory and difficult to distinguish from activated traditional LCs that are also highly migratory. To better tell these apart, one would have to incorporate imaging.

The population that we identify as CD11c+CD14+ LCs closely resembles IDECs and epidermal CD11c+ DCs due to the high CD11c and MR expression. However, due to lack of CD14 co-expression and low langerin expression, IDECs and the epidermal CD11c+ DCs are distinct from the foreskin CD11c+CD14+ LCs which, similarly to CD14+CD11c- LCs, were also observed to support HIV replication. Noteworthy, this subset portrayed the highest proportions of CD4+CCR5+ during foreskin LC characterization. Although there are no reports of CD11c+CD14+ LCs, migratory CD11c+CD14+ DCs have been described and shown to co-express high levels of DC-SIGN and CD169 while effectively disseminating HIV to uninfected CD4+ T cells in both cervical and seminal studies[121,189,222]. Inclusion of markers such as CLEC9A, would help decipher if the foreskin CD11c+CD14+ LCs are a novel subset or a langerin+ version of the CD11c+CD14+ DCs.

Interestingly, we were also able to identify CD3+ LCs, that, similarly to the CD11c+CD14+ LCs, also portrayed high CD4+CCR5+ co-expression. There has been a surge of reports describing the emergence of mixed lineage populations[111,158,189,223]. Across various studies, three categories have been used to explain these populations which include i) technological artefacts of flow cytometry (doublets) ii) *in vivo* biological processes (trogocytosis, immunological synapses and heterokaryons) and iii) novel T-DC populations[187] (all described in more detail below). Noteworthy, we were able to identify CD3+ LCs in the granulocyte cells after lymphocyte exclusion and use of the singlet gate as shown in the gating strategies in the Results section. Therefore, the CD3+ LCs that we identify in the foreskin could have been due to either *in vivo* complexes that cannot be distinguished using flow cytometry alone without microscopy or they could indeed represent a novel population, an addition to the current T-DC

populations. Further studies need to be done to ascertain this, possibly through assessment of the TCR as has been done in the classification of other myeloid-lymphoid populations[159,161–163,187,224], as well as through gene expression analysis. Although CD3+ LCs have yet to be described, foreskin CD3+ LCs were non-migratory and co-expressed high levels of CLRs; especially DC-SIGN and Siglec-1.

Foreskin "Mϕ--like" cells

In comparison to the frequency of foreskin LCs, foreskin "Mϕ-like" populations were ten-fold higher in the foreskin epidermis and coincided with reports that have shown tissue resident Mϕ as constitutive of 10-15 % of the dermal population under quiescent conditions, typically predominated by the M2 phenotype[225]. Within the L-gate (CD11c/CD14), foreskin "Mϕ-like" cells were CD14+CD11c- and non-migratory, thus mirroring various reports that have shown CD14+ Mϕ as constitutive of 40-50 % of the tissue resident mononuclear phagocyte population (MNPs)[189]. Notably, these CD14+ Mϕ have been delineated from the CD14+CD11c+ DCs, shown to constitute 1/3 of the tissue resident CD14+ cells, by lack of DC-SIGN[189].

However, the foreskin CD14+CD11c- "Mϕ-like" cells interestingly portrayed high DC-SIGN expression whereas non-migratory CD14+CD11c+ cells were a minority constituting only < 1 %. DC-SIGN expression was thus, a characteristic of tissue resident "Mϕ-like" cells and was also used as part of the gating strategy to identify the "M2-like" macrophages. This was further supported by its lack or low expression in "M1-like" Mϕ that were migratory. Therefore, the foreskin was populated with "M2-like" Mϕ, that averaged 10% - 20 % of the isolated foreskin cells. This was ten-fold higher than the frequency of the "M1" phenotype, suggestive of an inflammatory micro-environment requiring inflammation resolution. M2 Mϕ serve a homeostatic and inflammatory resolution role which polarizes to the M1 phenotype in diseased tissue and inflammatory settings.

However, Mϕ polarization states are non-static and dependant on the micro-environment and although also possibly impacted by cell isolation techniques and reagents, the polarization states of isolated Mϕ can therefore be reflective of the inflammatory status of the specific tissue. Although to measure this, other authors have sought to determine the origin of the isolated issue-resident Mϕ. A high percentage of F4/80^{hi} self-renewing Mϕ has been postulated as representative of "normal" conditions while Mϕ likely derived from peripheral monocytes (F4/80^{lo}), are indicative of previous ablation of resident tissue Mϕ[226]. Notably, F4/80 is specific to murine macrophages, and foreskin assessment would require the human equivalents of these markers. This could be further and more confidently resolved by bioinformatic analyses. Such knowledge would be beneficial in providing a more refined assessment of the stability, origin and possibly; role of the tissue resident macrophages. In addition, this would help

decipher the extent to which monocyte derived macrophages replenish the tissue resident macrophages lost during severe inflammation. It is also still murky as to whether converted cells fully recapitulate the function of those they replenish and what the physiological impact is [227].

In HIV infection, it is the M2 Mϕ that have been shown more permissive to HIV infection, when compared to M1 Mϕ despite the higher expression levels of CD4 and CCR5 in the M1-phenotype[35,52,176]. This may be related to the higher expression levels of CLRs in the M2 phenotype such as DC-SIGN and the MR[35,52,61,176], although it then brings into question if all M2 Mϕ infection is productive. Limiting to this project was the inability to differentiate between VCC compartmentalized HIV from endocytosed virions. However, the introduction of maraviroc was seen to block HIV infection, suggesting that Mϕ infection engages co-receptor usage, and thus potentially *cis*. Further to this, foreskin "M2-like" Mϕ were permissive to HIV infection with the CCR5 using transmitted founder Subtype C CH198 virus, similarly to the CD14+ LCs.

In addition to the "M1-like" and "M2-like" Mϕ, we were also able to identify intermediates of these populations that were characterised by the simultaneous co-expression of M1 and M2 markers. However, these comprised a minute fraction of the foreskin Mϕ population (< 0.5 %) and while unidentifiable using the HIV infection panel in this study, other studies have identified them as predominant in the urethra of cART-suppressed individuals and additionally shown to harbour replication competent HIV, thereby serving as viral reservoirs[35]. In particular an M1/M2 transitionary macrophage subpopulation characterised as CD206+CD163-IL-1R+IL4R+, was identified to harbour HIV products such as VCCs, HIV RNA and R5 DNA in the absence of T cell co-localization. Importantly, these cells were seen to yield potent HIV upon reactivation[35].

CD3+ "Mϕ-like" cells

Similarly to LCs, we were also able to identify a subset of CD3+ "Mϕ-like" cells accounting for approximately 3 % of the foreskin epidermal cell population. Unlike, the CD3+ LCs that have yet to be described, CD3+ Mϕ have been identified in other studies[162,163]. In the past, the inclusion of lineage markers other than the lineage of interest has been for the purposes of "cleaning" and exclusion of contaminating cell-types, hence the creation and use of a dump channel and the singlet gate[187]. For this reason, non-conventional populations have not been detected nor extensively studied. Where they have been detected, it has been attributed to random cellular proximity as well as non-specific antibody staining. However, the inclusion of Fc-receptor blockers and reagents such as EDTA have been reported to retain these populations, thereby re-affirming them as "genuine" populations[187].

Immunological *in vivo* complexes

Physiologically, CD3+ T cells and APCs interact *in vivo* through immunological synapses that aid antigen presentation and T cell activation. As such, there have been suggestions that the detection of CD3 on myeloid cells be accounted to *in vivo* immune complexes that are inseparable during antibody staining and flow cytometry acquisition. Some scholars have reported the detection of CD14 expression and a selection of monocyte genes in sorted PBMC derived memory CD4+ T cells. SSC-A and FSC-A properties of these cells were reportedly identical to those of conventional lymphocytes although with a high detection of both T cell ILFA and APC ICAM[187]. ILFA is an adhesion molecule that's employed by T cells to engage with ICAM on APCs during the formation of an immunological synapse as deciphered by Dupont and Sattentau, 2020 and Burel, J. G. et al., 2019 in the images below[187,194].

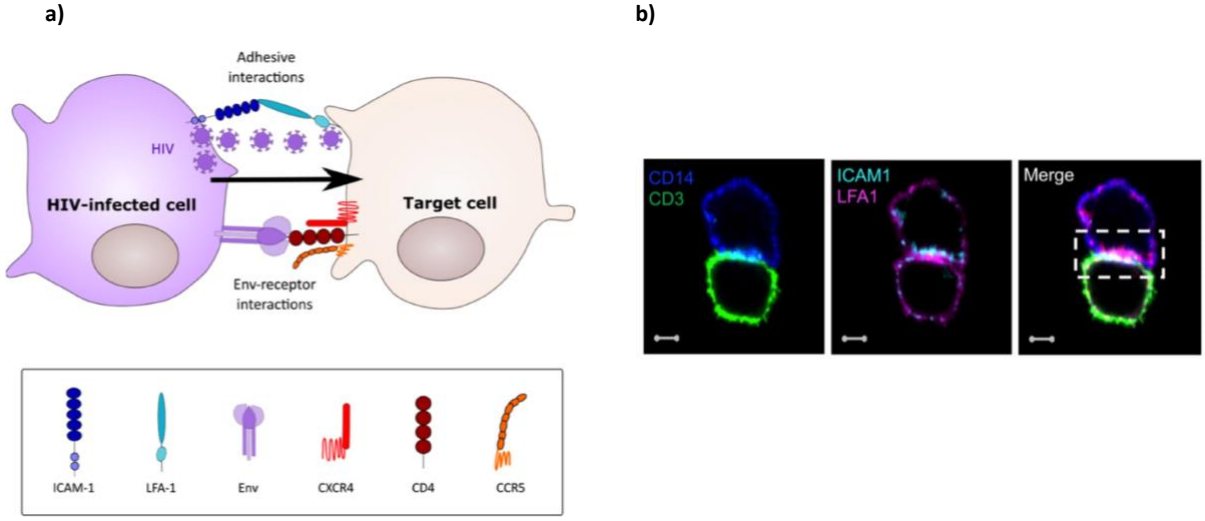

Figure 112. ***Prototypical virological synapse and an in vivo immunological synapse (immune complex) captured by microscopy. (a)*** *Immunological/virological synapse between a donor and a recipient cell interacting through adhesion molecules, ICAM and LFA-I (**b**) CD3+ T lymphocytes and CD14+ monocytes form in vivo immune complexes in PBMCs, through interactions of ICAM and LFA-I that are inseparable by flow cytometry. Images adapted from Dupont and Sattentau, 2020)[194] and Burel, J. G. et al. 2019 [187]*

While these were detected in PBMCs, there are not yet reports on their detection in isolated primary cells from tissue. The co-localization of CD3+ T cells and DCs has, however, been reported in HIV dissemination studies on explants[72,91]. Note, it has been postulated that the PBMCs' immune complexes originate either from the peripheral blood due to some unknown perturbations or migrate from tissue already formed. In that light, we were also able to detect this "ambiguous" cell population within the foreskin granulocyte fraction as illustrated in Figures 113 (a) – (e) below.

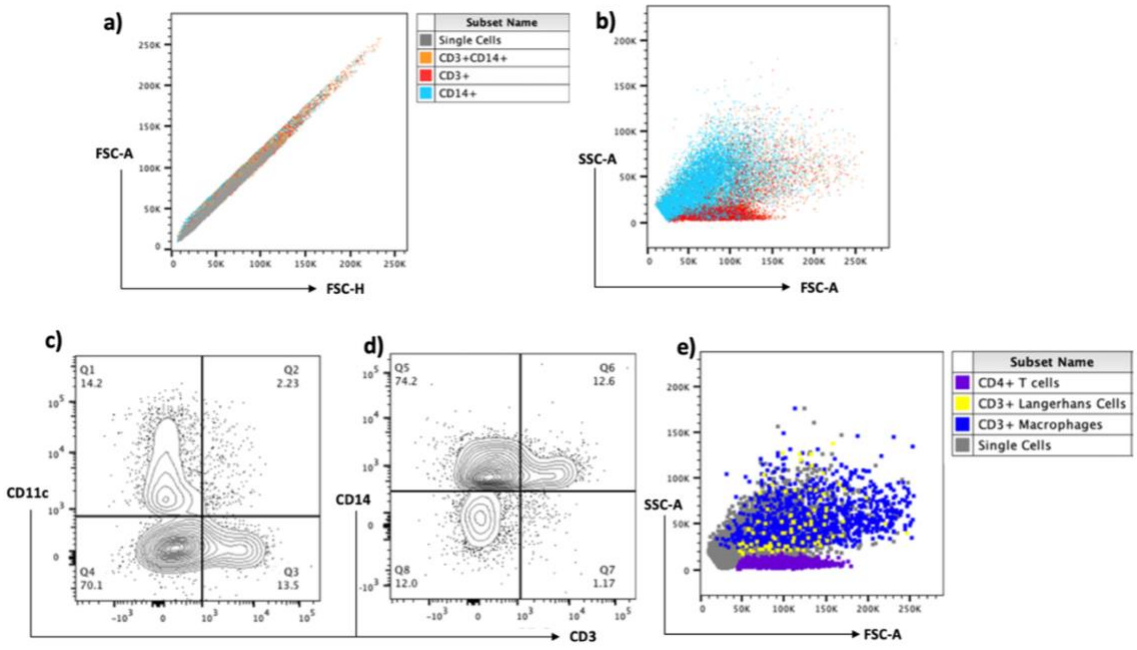

Figure 113. ***Cell populations expressing both T cell (CD3) and pan-myeloid surface markers (CD11c and CD14) exist in the live singlet cell population of migratory and non-migratory foreskin epithelial cells (a)*** *Gated on 'singlet total live cells' (grey), (i) CD3+CD14+ (orange), (ii) CD3+CD14- (red) and (iii) CD3-CD14+ (blue) cell populations were identified* ***(b)*** *Based on FSC and SSC parameters, CD3+CD14+ cells were dispersed within the granulocyte gate alongside the conventional CD3-CD14+ cells. CD3+CD14- cells were within their conventional lymphocyte gate.* ***(c)-(d)*** *Representative flow cytometry plots showing the identification of CD3+CD11c+ and CD3+CD14+ populations from the L gate (CD14+/-CD11c+/- gate) (E) CD3+ Langerhans cells and CD3+ macrophages were in the granulocyte gate while CD4+ T cells were strictly confined to the lymphocyte gate.*

Figure 113 (a) illustrates the occurrence of CD14+CD3+ cells (*orange*) in the singlet gate, and their forward and side scatter properties are shown in Figure 113 (b) where they are dispersed in the granulocyte gate alongside CD14+CD3- cells (*blue*). Both pan-myeloid markers, CD11c and CD14, were shown to be simultaneously co-expressed with CD3 in foreskin cells, although more frequent in CD14+ cells than in CD11c+ cells as shown in Figures 113 (c) and (d) respectively. Furthermore CD3+ LCs and "Mϕ-like" cells were also shown to retain the same SSC-A and FSC-A properties as those of conventional LCs and "Mϕ-like" cells as shown in Figure 113 (e).

CD3+ foreskin myeloid cells are therefore singlet gate cells that portray the size and granularity of myeloid cells while additionally co-expressing the lymphoid marker, CD3. As to what their nature is remains a mystery. However, cell-cell engagements are of utmost importance in HIV pathology, as they enable the formation of virological synapses that facilitate HIV spread[20,228]. *In vivo* APC-T cell

complexes have been suggested responsible for the identification of CD209+CD169+ DC/CD4+ T cell conjugates that have been identified as the cells responsible for early establishment in HIV entry in human tissue [22,23,25,194]. This phenomenon has specifically been described for human tissue derived migratory CD11c+CD14+ DCs which are responsible for dissemination in lymph nodes [29,222,229].

Spillage into the CD3 channel?

The CD3 anomaly was further assessed for technological artefacts by investigating potential spillage into the APC-Cy7 fluorochrome (CD3). Using the CD3 FMO control (*red*); foreskin LCs (*blue*) were assessed for CD3 detection as illustrated in Figure 114 below. While there was no CD3 background or detection in the CD3 FMO LCs, additional assays such as imaging are required for further validation in future studies.

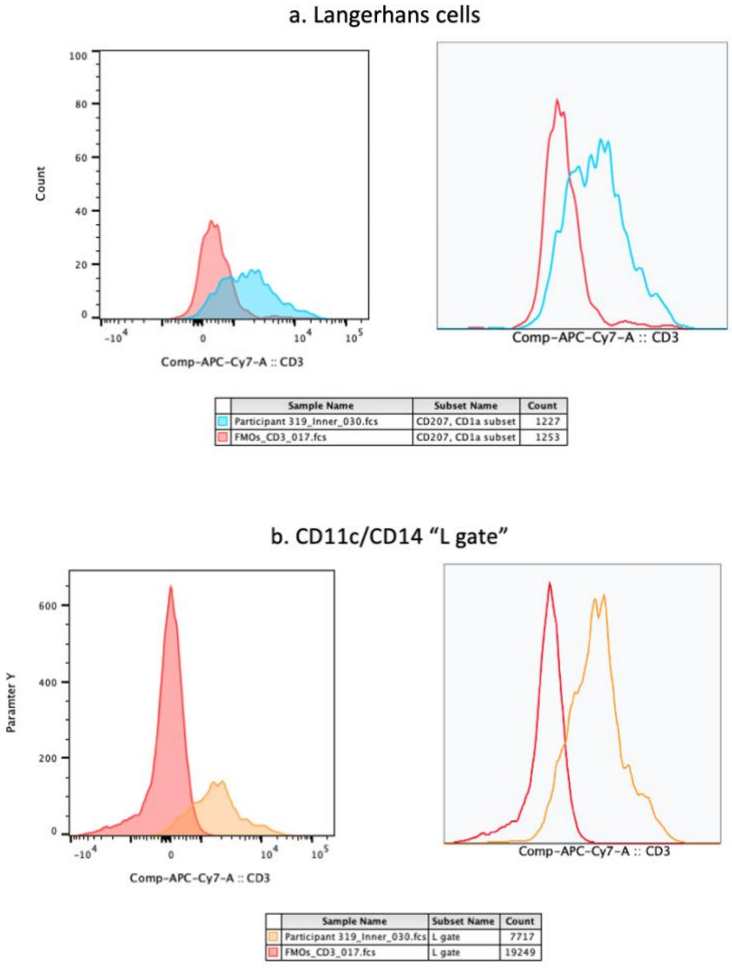

Figure 114. ***CD3 FMO and fully stained LCs and "macrophage-like" cells showing CD3 expression****. Population overlays of the* ***(a)*** *CD3 FMO LCs* ***(red)*** *and the fully stained LCs* ***(blue)*** *using the panel shown in Table 1****. (b)*** *CD3 FMO "macrophage-like cells (L gate)* ***(red)*** *and fully stained "macrophage-like" cells (orange). The CD3 FMO demonstrates lack of background/spillage from the other fluorochromes into the APC-Cy7 fluorochrome where CD3 expression was detected. Subset names and annotation colours are described on the tables (below graphs); fully stained LCs (blue), fully stained "macrophage-like" cells (orange) and CD3 FMOs (red).*

Heterokaryons

Heterokaryons, defined as multinucleate cells that contain genetically different nuclei arising from cell fusion or phagocytosis of other cells by antigen presenting cells (APCs), have also been implicated in attempts to explain the origins of CD3+ myeloid cells. Multinucleated Mϕ have been described *in vivo* as one of the leading causes of intracytoplasmic detection of markers such as CD3 and CD2 in Mϕ populations[22,174,230]. This has been substantiated *in vitro* by co-cultures of uninfected MDMs with HIV infected CD4+ T cells resulting in the detection of HIV proteins in CD3 "expressing" Mϕ[24,230]. As such, the detection of heterokaryons is particularly more profound in HIV infected Mϕ possibly due to the intrinsic role of Mϕ to phagocytose and clear HIV infected CD4+ T cells. Note, when a Mϕ fuses with an infected CD4+ T cell, the resultant heterokaryon cannot be distinguished by flow cytometry as to the nature of the infection. To resolve this, other studies have used the detection of TCR-γδ DNA to identify T cell derived (phagocytosed or infused) HIV. This would be distinguishable from the CD3+ macrophages that are increasingly emerging as new macrophage populations shown to delineate as either TCRαβ- or TCRαβ+. This is therefore recommended for future studies. Also, virions harboured inside VCCs take on two forms, i) cell free or ii) bound to DC-SIGN or CD169. This represents one of the ways through which non-lymphocyte proteins can end up being detected in lymphoid cells as we do in HIV infected foreskin T cells (data not shown).

Heterokaryons are also long lived similarly to macrophages and therefore, persist over extended periods of time. This is of concern in HIV infection because virus shedding from heterokaryons is reportedly higher than is witnessed from VCCs[22,24,25,173,230,231]. Furthermore, the introduction of fusion inhibitors has been shown to block the formation of heterokaryons therefore suggesting that their formation is dependent on the engagement of the envelope and HIV receptors thereby establishing them as a valid transmission mechanism[174]. However, this is only relevant to phagolysosomes of CCR5 infected T cells[23,174]. MDM engulfment of CXCR4 infected T cells were not seen to productively infect macrophages. The mechanisms through which this fusion is regulated are unclear. Macrophages retain the ability to fuse with infected T cells even in the presence of known efferocytosis inhibitors that typically block phagocytosis of CD4+ T cells, hence it is important to elucidate mechanisms underlying these uptake mechanisms[176]. More to this, host restriction, particularly by SAMHD1, is reportedly limited against HIV infected heterokaryons. Transfer of cyclin/CDK components from the merged cytoplasms is thought to block SAMHD1 activity[23]. The T cell nucleus is also purported to transcribe

HIV within the heterokaryon, in a way that enables it to bypass reverse transcription that would typically be imparted by SAMHD1 restriction[23]. Given this, it is important for us, to be able to elucidate the exact nature through which foreskin macrophages are interacting with HIV and CD3+CD4+ T cells. "M2-like" macrophages were the most predominant subpopulation in HIV infected cells and were also seen to co-express CD3. In addition, infected foreskin cells were intracellularly stained hence the possibility that intracytoplasmic CD3, if any, was also detected are high.

While heterokaryon formation is more extensively studied in macrophages; immature DCs have also been reported to fuse with infected CD4+ T cells in this manner[232]. The high frequencies of CD3+ LCs and CD3+ Mϕ in HIV infected foreskin cells could also be potentially arising in this manner. LCs have also been shown to present as multinucleated giant cells in varied pathologies [232]. With microscopy, we would be able to decipher the morphology of these CD3+ Langerhans cells and CD3+ Mϕ to determine if they are immune complexes, multinucleated cells, or a sub-population of HIV permissive myeloid cells that resembles the newly discovered CD3+ Mϕ.

Trogocytosis

Some authors have also attributed the occurrence of CD3+ myeloid cells to trogocytosis, a phenomenon that results in "cross-dressing" [233,234]. Cell re-programming or trans-differentiation has also been reported to attribute to mixed lineages, especially in its early stages[234]. However, for this to hold, it must be substantiated by the detection of clonal rearrangement of the TCR. This further cements the need for the TCR antibody in our panel for future studies and further elucidation of these phenotypes.

Pathology

Apart from proposed biological processes attributing to the occurrence of mixed-lineage phenotypes, CD3+ myeloid cells are associated with several disease pathologies, such as malaria and TB[162,163]. They have been shown to express chemokine receptors that effectively render them migratory[161,163] and were also observed to portray a time-dependant upregulation of CD3 subunits and TNF-alpha in BCG immunization[161]. This is suggestive of an antigen inducible expression of CD3 and a TNFR1 dependant recruitment of CD3+ macrophages to pathological sites. Proportions of CD3+ cells were also higher in HIV infected LCs and Mϕ, compared to uninfected cells although they were non-migratory.

Duality of CD169 during HIV infection

Another distinct Mϕ population, distinguished as neither M1 nor M2, but with high CD169 expression was identified. These were characterised as CD169+ Mϕ, and although reported as ubiquitously distributed in various tissues, only accounted for <1% of the foreskin Mϕ population. Studies on

ontogeny have attributed the derivation of CD169+ Mϕ to peripheral monocytes due to the low expression of F4/80[226]. Interestingly, foreskin LCs were also observed to portray CD169 expression, although at lower levels, possibly also due to monocyte derivation.

Similarly, to CLRs (CD206, CD209, CD207); CD169 also plays a dual role in HIV infection as it has been shown to facilitate HIV entry, while also reported to illicit a robust anti-viral immune response. CD169+ Mϕ are pro-inflammatory and much like the foreskin "M1-like" Mϕ, were also predominantly migratory. CD169+ Mϕ have also been shown to positively corelate with the virus specific clonal expansion of cytotoxic CD8+ T cells while also engaging the CD8+ DCs[235,236]. CD169+ macrophages, are thus IFN-1 inducible and implement antiviral activity through secretion of the same[64,139,159,237,238].

CD169 expression is protective against HIV infection of foreskin Macrophage-like cells and Langerhan's Cells

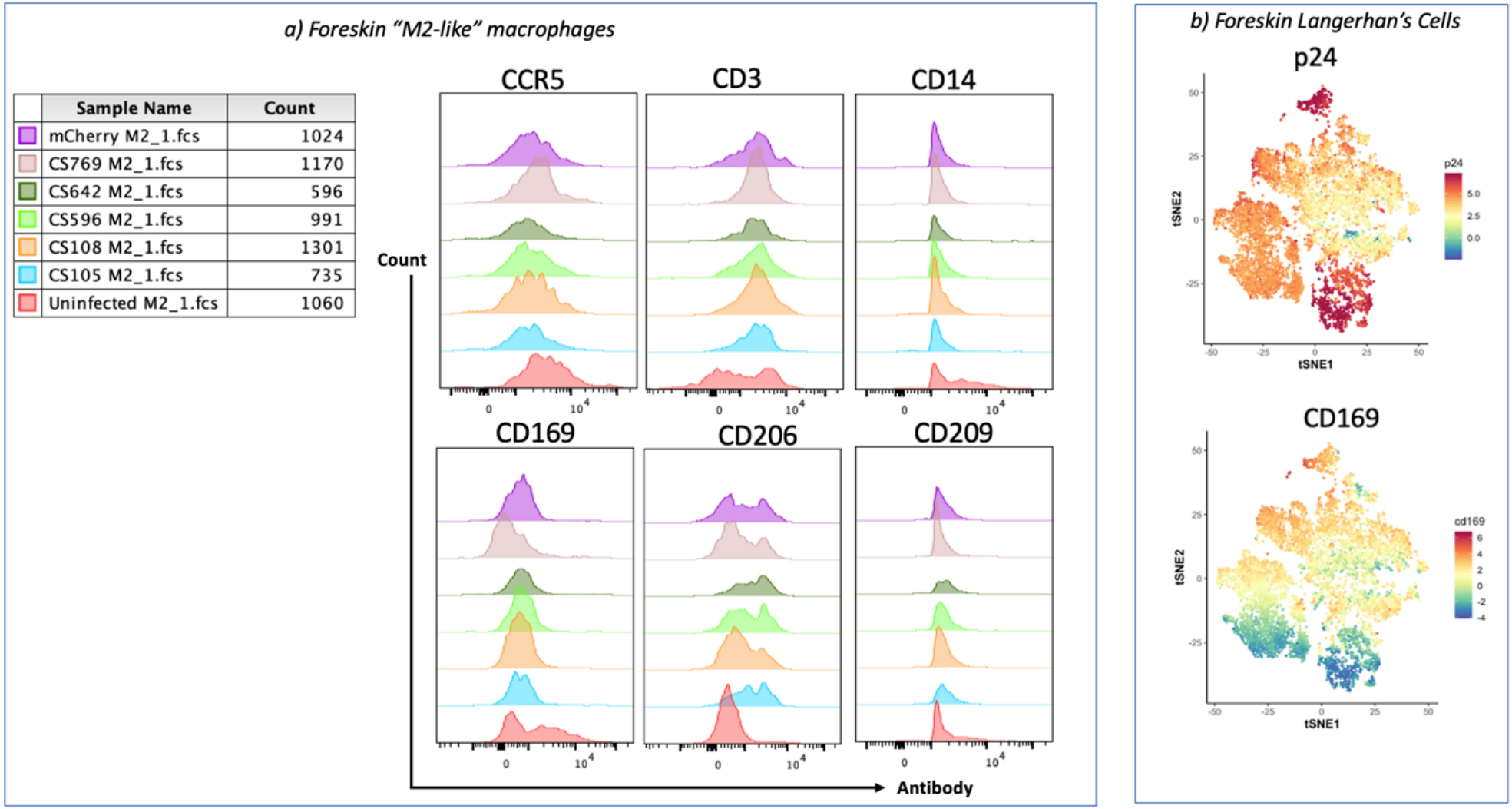

Figure 115. ***CD169 expressing foreskin "M2" macrophages and Langerhans cells are uninfectable with HIV****. (a) Histograms illustrating marker expression profile of concatenated foreskin "M2" macrophages infected with different viruses in comparison to uninfected "M2" macrophages; red (uninfected), purple (NL4-3 Bal), brown (Subtype C CH198), olive green (Subtype C CH167), lime (Subtype C ZM246F-10), orange (NL4-3 R5) and blue (NL4-3 X4). CD169+ macrophages were only present in uninfected macrophages. Infected "M2' macrophages are CD169- (b) tSNE plots from concatenated foreskin Langerhans Cells demonstrating that CD169- LCs co-express p24 (HIV infection)*

Consistent to this protective role, CD169 expression was observed to confer a protective role against HIV infection in both foreskin "M2-like" Mϕ and LCs as demonstrated in Figure 115 (a) and (b) above. It was the CD169- "M2-like" Mϕ that were infected across all viruses in Figure 115 (a), as was similarly observed for the p24hi LC clusters that were CD169- as described in Results and also shown in manually gated foreskin LCs in Figure 115 (b) below. Therefore, it possible that the anti-viral, HIV inhibitory role trumps the pre-disposing features of the CD169 molecule in foreskin primary cells or that HIV infection downregulates its expression.

However, CD169 has also been implied to induce prolonged and inadequate IFN-1 secretion related to an upregulation of PDL-1 and IL-10. Consequently, this has been shown to accelerate exhaustion of conventional cytotoxic CD8+ T cells, in a manner favourable to *in vivo* HIV persistence and longevity during chronic infection[239]. As described above, CD169 was also described key in mediating cell-cell spread and thus, the implication that CD169+ Mϕ also promote *trans* infection and possibly, *cis* infection although this observation was not made in the foreskin[122,123,240,241]. Therefore, on the flip side, the CD169 molecule recognizes and binds HIV, disseminates to CD4+ T cells, masks IFN-1 response, induces formation of VCCs, and confers subsequent VCC maintenance[114,121,123,240]. In line with this, silencing Siglec-1 reportedly blocks viral fusion and transmission via TNTs in MDMs[23,194].

Noteworthy, the role of CD169 in HIV infection has been studied in murine models and not much has been reported in human tissue, particularly foreskin mucosae. Therefore, CD169+ Mϕ may be imprinted with tissue and micro-environment specific attributes that govern their role in HIV infection and pathology. As such the determinants of the specific role assumed by human CD169+ Mϕ and/or LCs during HIV spread remains rudimentary and requires further elucidation.

Individual variability

The frequency of p24+ cells was highly variable in Langerhans cells isolated from foreskins of 17 different individuals as illustrated in Figures 116 (a)-(b). 10 of these exhibited statistically significant differences among each other as shown in Figure 116 (a). In particular, participant 37, was infectable with all viruses, exhibiting more profound HIV infection with lab adapted NL4-3 BaL (purple) and the Subtype C viruses as shown in Figure 116 (b). Meanwhile, participants 27, 28, 29 and 30 portrayed very minimal HIV infection and were significantly variable from Participant 37 as shown in Figure 116 (a).

Therefore, while some participants portrayed high p24 expression, others within the same experimental batch remained uninfected or portrayed minimal infection. This suggests the presence of other confounding factors outside of batch effects. Although the presence of STIs has been reported as pre-

disposing and to increase one's susceptivity to HIV infection[12,78,79,242], individuals portraying significant differences amongst each other did not differ according to STI status in this study. Note, all participants used for HIV challenge assays were negative for asymptotic STIs. Susceptibility to HIV infection is governed by several factors, some of which include, intrinsic replicative properties of the virus, immune evasion, modulatory cellular and effector molecules of the innate and adaptive immune response.

a) Different participants display significant individual variability

Estimate	Participant1	Participant2	p value	p < 0.05
Frequency of p24	20	28	0,04306252	TRUE
Frequency of p24	20	39	0,04682276	TRUE
Frequency of p24	26	28	0,00388833	TRUE
Frequency of p24	26	29	0,03563619	TRUE
Frequency of p24	26	30	0,01694851	TRUE
Frequency of p24	26	39	0,00817191	TRUE
Frequency of p24	27	39	0,03867413	TRUE
Frequency of p24	28	33	0,03794539	TRUE
Frequency of p24	28	37	0,0391903	TRUE
Frequency of p24	28	38	0,0040249	TRUE
Frequency of p24	29	38	0,02123984	TRUE
Frequency of p24	30	38	0,01004121	TRUE
Frequency of p24	33	39	0,03407921	TRUE
Frequency of p24	37	39	0,01819363	TRUE
Frequency of p24	38	39	0,00573897	TRUE

b) Differential susceptibility of different participants to different HIV viruses

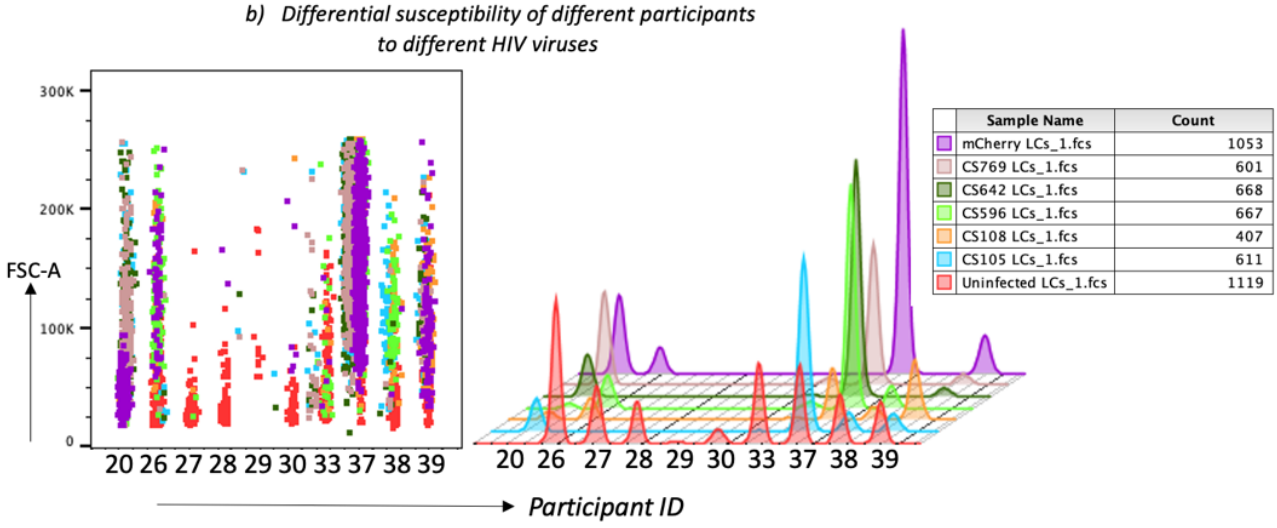

Figure 116. ***Differential participants display significantly varied levels of permissiveness to HIV infection.*** ***(a)*** *Table showing 10 participants that were significantly variable from each other* ***(b)*** *Flow cytometry plots and histograms showing the differential infection of 10 participants with different viruses; red (uninfected), purple (NL4-3 Bal), brown (Subtype C CH198), olive green (Subtype C CH167), lime (Subtype C ZM246F-10), orange (NL4-3 R5) and blue (NL4-3 X4).*

While all these are impactful, studies on differential progression to AIDS and elite controllers have also extensively reported on the impact of genetic variability on differential susceptivity among different individuals. Although beyond the scope of this study, there are numerous human allelic variants that have been identified and assessed for use as predictors of disease progression and as determinants of protection against HIV infection. CCR5Δ32 is one of the most studied, in both its recessive and dominant forms[243]. When recessive, it confers resistance to infection, through expression of non-functional, truncated CCR5. Dominant individuals have therefore been shown to portray delayed progression to AIDS. In African cohorts such as ours, the allelic variant A29S, has been identified to culminate in failure to bind RANTES, MIP-1β and MIP-1α which are CCR5 ligands[243]. It would therefore, be beneficial to assess individual variability to HIV susceptibility by conducting a larger study with genotyping. Variable cell surface expression levels of C-type lectins receptors also influence HIV susceptibility among different individuals. In particular, DC-SIGN polymorphism has been reported to influence HIV susceptibility, particularly in individuals with a 336C allele compared to those with 336T[243].

Using our flow cytometry data, we were able to identify discrepancies in marker expression among different individuals. As such, we sought to assess differential marker expression in individuals portraying high permissiveness to HIV infection in comparison to those that remained uninfected to determine likely determinants. Interestingly, similar expression profiles were observed for most markers used in this study (data not shown), except for the expression of CD169, CD11c and CD3. Individual participants (represented by different colours) were distinguishable when assessed for the expression of CD169 and CD11c as can be seen on the Uninfected LCs in Figure 117 (a) below.

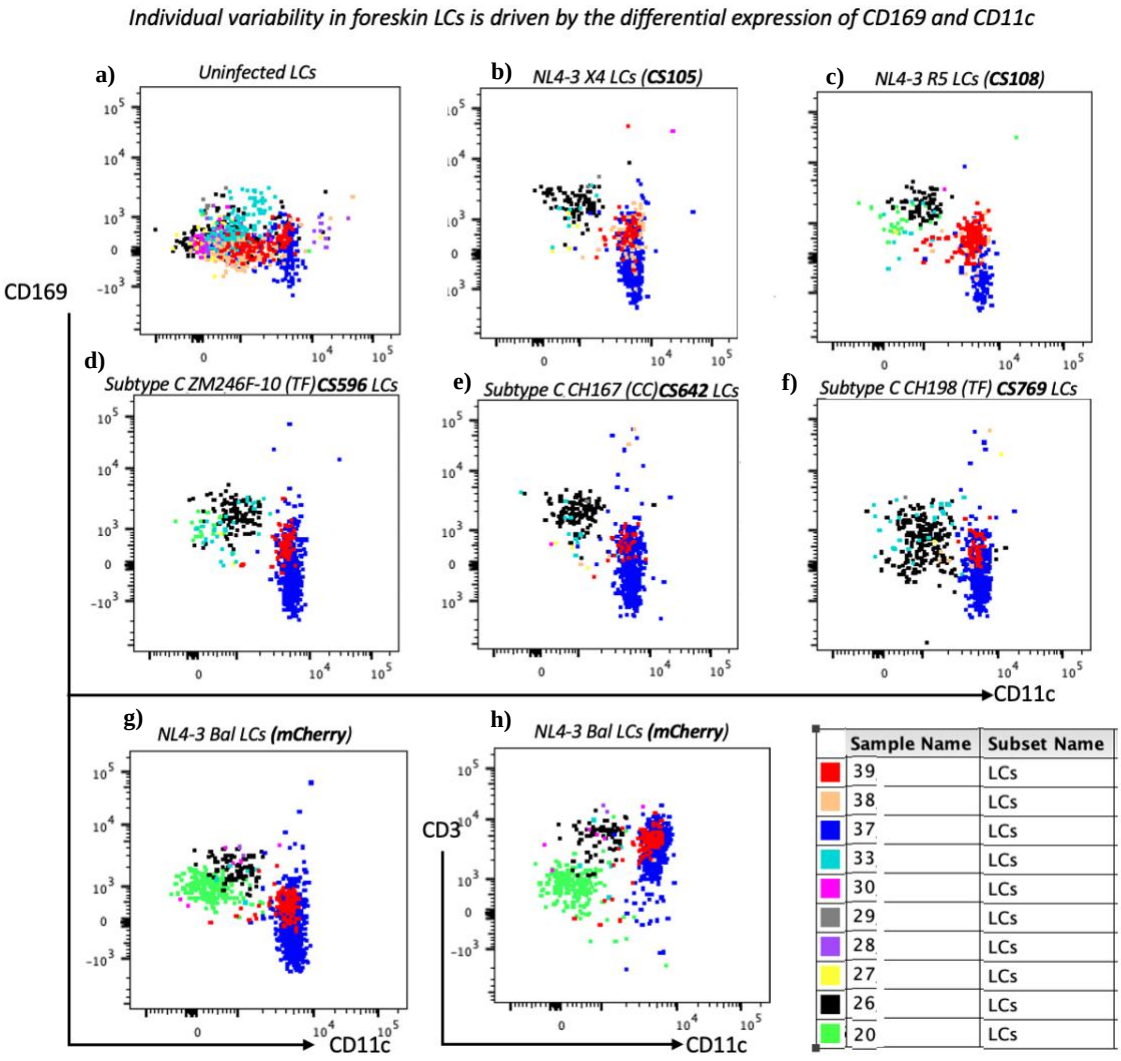

Figure 117. Different participants display differential expression of CD169 and CD11c which influence their susceptibility to HIV infection. Representative flow cytometry overlays illustrating that the significant differences observed for 10 participants (color coded) were driven by different expression levels of Siglec-1 and CD11c.

Participants shown to express CD169, especially participant 33 (*turquoise*), were uninfected and therefore not present on the virus plots as illustrated in Figures 117 (a) - (h). However, LCs isolated from participant 26 (*black*), seemingly upregulated CD169 and were infected with all viruses, contrary to the non-infection of CD169 co-expressing LCs described above. While these were additionally CD11c-; high CD11c expressing participants, such as participant 37 (*blue*) and 39 (*red*) predominated infected cells across all viruses. Note, CD11c was described above to positively corelate with activation and potentially the reason participants with higher CD11c co-expression were more susceptible. We acknowledge that there are more complex factors governing these differences, and therefore, cannot at this point make any conclusive remarks. To do this, our flow cytometry data would need to be supplemented with transcriptomic or genomic data of these participants. So we tentatively conclude

that individuals with CD169+ foreskin LCs, except Participant 26, display decreased susceptibility to HIV infection when compared with individuals whose LCs have low or no CD169 co-expression. To conclusively report on this, further interrogation would need to be conducted in future using a larger cohort. Furthermore, CD11c co-expression in addition to lack of CD169 expression was also deemed favourable to HIV infection. While this corroborates with the purported anti-viral effects of CD169 reported in various studies and described above, the proposed role of CD11c in migration and possible co-relation with maturity could potentially attribute to this increased susceptibility.

HIV infection of foreskin cells downregulates CD4 and HLA-DR expression

During HIV infection with different viruses, foreskin LCs and "macrophage-like" cells were observed to "lose" the expression of markers otherwise expressed in uninfected equivalents especially CD4 and HLA-DR as illustrated in Figure 118 below.

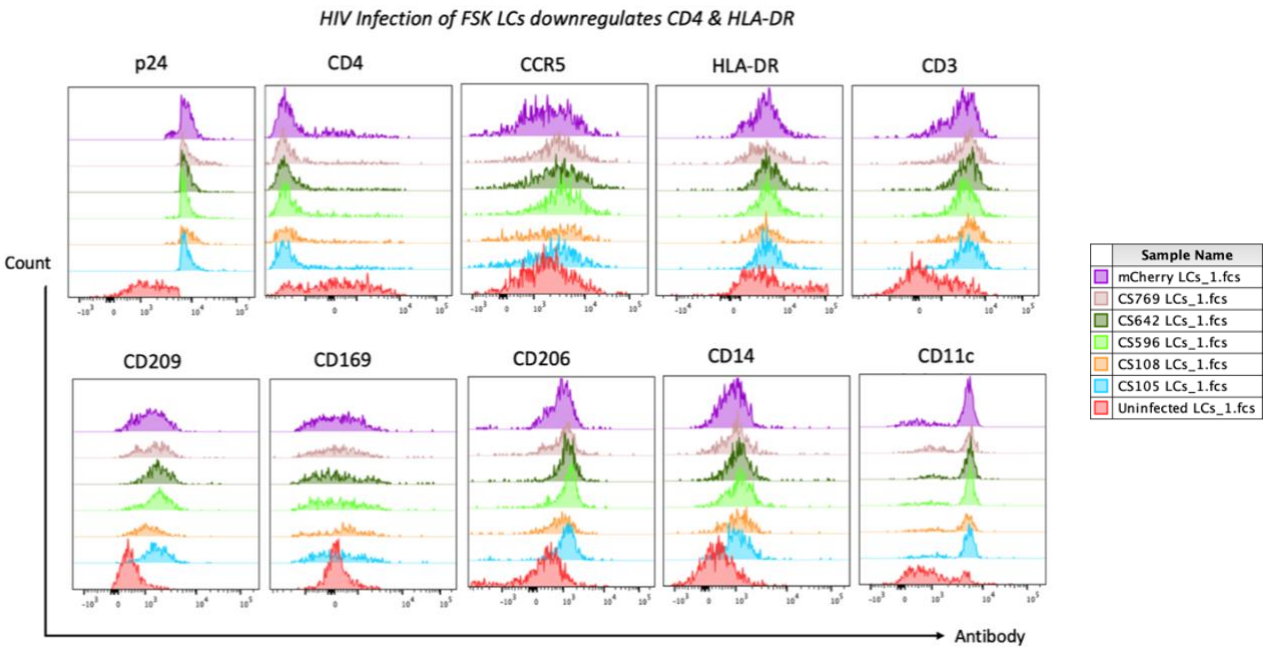

Figure 118.. HIV infection of foreskin LCs using different viruses downregulates the expression of CD4 and HLA-DR. Flow cytometry histograms displaying the infection of foreskin LCs with different viruses; red (uninfected), purple (NL4-3 Bal), brown (Subtype C CH198), olive green (Subtype C CH167), lime (Subtype C ZM246F-10), orange (NL4-3 R5) and blue (NL4-3 X4), and the impact on the expression of markers.

HIV executes this due to the interference of CD4 against envelope incorporation and generation of progeny virions[68,244]. To implement this, HIV uses the accessory proteins, nef and vpu to direct protein targets towards the trans-Golgi network, endosomes, or lysosomes for redistribution and/or degradation[68,244]. Nef facilitates an abnormal sorting of cell-surface proteins to lysosomes while

encouraging retention of these proteins within the trans-Golgi region. More specifically, nef hijacks endocytic machinery, AP-1 and AP-2 and redirects it towards endocytosis of the cell-surface expressed MHC I and CD4 respectively [68,244–246]. Therefore, CD4 and HLA-DR downregulation can be used as an indicator of HIV infection in HIV infection assays.

However, the downregulation of MHC-1 downregulation is less complete compared to the absolute downregulation of CD4 that is witnessed with HIV or IMCs carrying unmutated, intact Nef. Using IMCs with impaired nef expression, can result in incomplete CD4 downregulation that can consequently lead to increased susceptibility to antibody dependant cytotoxicity[246]. Cell exhaustion markers such as PD1can be used to correlate the effects of nef disturbance to immune evasion or lack thereof. IMCs used in this study were incorporated with GFP in the nef region. However, in comparison to the mCherry incorporated IMC, that was alternatively inserted into the LTR region, the downregulatory effects on both CD4 and HLA-DR were comparatively similar. Nef expression was therefore uninterrupted by GFP incorporation.

In addition, Nef and Vpu have also been implicated in re-organization of components of the immunological synapse and the TCR, resulting in the formation of the virological synapse[228,247]. Nef also implements putative induction of chemoattractants, such as MIP1 alpha and beta to facilitate more spread by attracting target CD4+ T cells towards infected macrophages[228,247].

ART protocol considerations are required for non-lymphoid HIV targets

Using the pluricellular cell suspension foreskin HIV infection model, we were able to show that foreskin LCs and "Mϕ-like" cells differentially support HIV infection with different viruses. We were also able to show that maraviroc effectively inhibits the *ex vivo* infection of foreskin lymphocytes. However, maraviroc inhibition was less impactful on myeloid cells, thereby suggesting that current ART protocols are more optimal and solely designed for CD4+ T cells without much consideration for other potential CD4+ HIV targets such as monocytes, Mϕs, DCs and LCs[248].

Of concern, especially in people living with HIV (PLWH), are the ART induced gene alterations resulting in the emergence of "new" myeloid cell subsets whose role and impact on the immune system is unknown. For instance, a DC (CD11c+ HLA-DR$^{int/hi}$CD14-CD3-CD19-CD56-) population has been identified that exhibits profound transcriptional changes when compared to its uninfected equivalents[248]. Reportedly, this population has been elucidated to harbour RNAs of non-surface expressed markers such as CD14 and to upregulate Mϕ markers such as CD163[248,249]. Numerous transcription factors and up-to 49 other genes are reportedly, irreversibly impacted in ART treated PLWH.

Some schools of thought have attributed these changes to immunological processes other than ART induced alterations, such as shedding of CD14 from CD11c+CD14+ macrophages, internalization of CD14 following LPS binding[249,250] or simply infiltration of CD14lo monocytes[250]. However, the non-response and restoration over the course of ART treatment is why this is a point of concern. Especially since some of these changes have been suggested to impact the immune surveillance abilities of the altered populations. In particular, changes in IFN secretion have been noted[248,251].

Evidently, ART is imposing an alteration on myeloid cell types whose impact remains ambiguous. There is a requirement for specificity for a broader range of HIV targets. We suggest that CD14+ LCs, CD11c+CD14+ LCs and "M2-like" Mϕ be considered in future ART development, as they have been shown to support productive infection in the foreskin. More importantly, the widespread use of pre-exposure prophylaxis (PrEP), calls for these ART-specific changes on myeloid cells to be further investigated and completely understood for the long-term impact.

V. STUDY LIMITATIONS & RECOMMENDATIONS

Owing to the diversity of foreskin myeloid cells, there is need to incorporate more markers that would elucidate further, the ontogeny of these cells as well cytokines to ascertain their effector roles. Cell sorting, single cell transcriptomic analyses and/or imaging would especially benefit the CD3+ myeloid cell mystery. Additionally, the TCR would also need to be factored into the characterisation panel. The different foreskin cell subsets were isolated and immunophenotyped according to foreskin compartment and migration or non-migration whereas the infection model was not discriminative according to either aspect. Elucidating LC and macrophage infectivity according to anatomical site (inner or outer foreskin) is recommended especially owing the higher CD4+CCR5+ proportions that were observed in the inner foreskin in this study. Moreover, the infection model was also not optimised to elucidate the distance and exact location of HIV susceptible cells with respect to the extracellular surface, a phenomenon that could inform the initial HIV-myeloid cell interactions. This could be addressed by imaging of infected foreskin tissue. Although p24 expression was validated as a proxy for HIV infection, using other confirmatory techniques such as RT-PCR would also be beneficial. The perceived restriction against NL4-3 X4 infection could also benefit from further validation through the identification and quantification of other chemokine receptors such as CXCR4 in foreskin myeloid cells, using a larger cohort and incorporation of gene expression analysis. The infection model was also limited by the decreased longevity of myeloid cells in cell culture conditions as evidenced by decreased proportions of uninfected cells with time progression. There is therefore a requirement to optimise further, the cell culture conditions to improve the viability and longevity of foreskin LC and macrophages post-isolation

while avoiding phenotype alterations. DC-SIGN blockers are also required to understand the indispensability of DC-SIGN mediation in foreskin infection, alongside anti-CD4 antibodies to further elaborate on the magnitude of *trans* infection and *cis* infection of foreskin LCs and macrophages.

Other limitations to this study were in relation to virus inocula and the use of p24 as a measure of HIV infection. While it has been shown in semen analysis studies that the physiologic virus titres range from <10 TCID50 to <300 TCID50, these titres were sub-optimal in this study[127]. Optimized infectious titres were therefore higher than the physiologically perceived titres. Furthermore, much of the *in vivo* infection has been purported to occur through cell-cell transmission as shown in Figure119[12] below although in this study, the virus inocula was cell free. However, the design of the infection model was optimal for cell-cell interactions to occur.

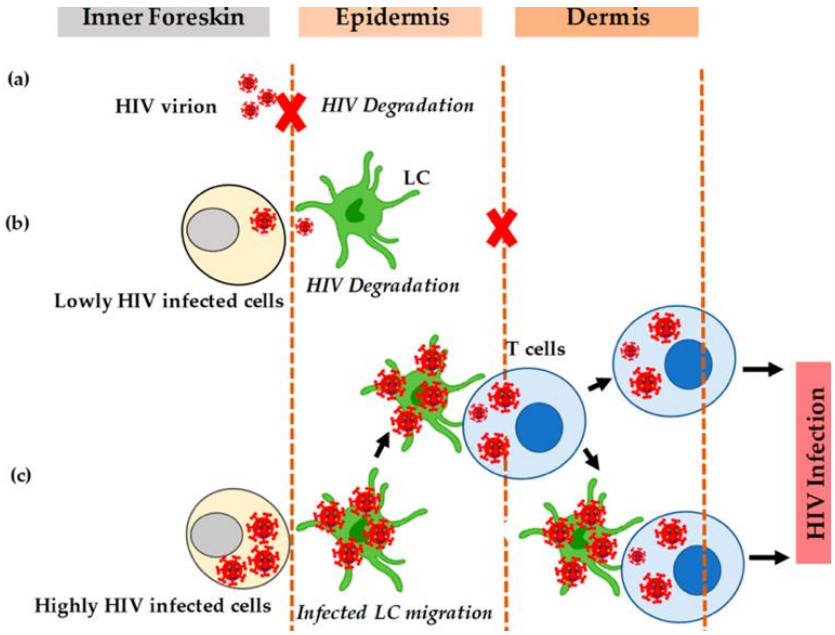

Figure 119. Cell-free vs Cell-Cell HIV transmission in the inner foreskin. The inner foreskin is exposed to different virus inocula during sexual intercourse, inclusive of cell free virions, lowly infected cells and highly infected cells. (a-b) Cell free virions and lowly infected cells are restricted and do not establish infection. (c) Cell-cell transmission using highly infected cells as inocula establishes HIV infection of Langerhans cells and the subsequent spread. Image adapted from Sharma et al., 2021: Circumcision as an Intervening Strategy against HIV Acquisition in the Male Genital Tract12

While using p24 antigen to measure HIV infection was robust, it is reportedly 5-fold lesser per unit of RT activity and RNA copy numbers when Subtype C viruses are assessed for infection[42]. As a result, this has been shown to lead to an underestimation of virus replication, and over-estimation of virus inocula when used in titre determination although the latter was conducted using relative light units (RLUs) and the Reed Muench method to curb this limitation[252,253]. Incorporation of RT assays is

however important in future experiments for the assessment of HIV replication in infected myeloid cells. Notably, small molecules were ultimately not included due to time constraints and will thus, be the main focus of upcoming work.

VI. CONCLUSION

The human foreskin is an immunological site laden with lymphoid and myeloid cells that are susceptible to HIV infection. Within the myeloid cell component, HIV susceptibility defined by CD4+CCR5+ co-expression and the presence of the C-type lectin receptor, DC-SIGN was measured. While all foreskin LCs were HLA-DR+, CD80/86 was differentially co-expressed among the different LC subsets in relation to migration. The frequency of CD80/86+ cells was 6.71 % less in non-migratory cells compared to migratory cells. Our hypothesis that spontaneously migrating cells from the foreskin are of an activated phenotype, and that tissue resident cells that remain bound, are less activated was validated. The most prevalent foreskin myeloid cell observed were the "M2-like" macrophages. We also observed a bi-fold downregulation of DC-SIGN in migratory cells as has been reported in other studies [113,133,134, 139].

In addition to the different activation states, we identified CD14- and CD14+ foreskin LCs. Studies on ontogeny have deciphered LCs to derive from two sets of precursors that could translate to the expression or lack of CD14 [101,102]. It has been reported that in the early stages of gestation (7 weeks), yolk sac derived HSCs seed the fetal liver and the epidermis, later differentiating into self-renewing precursors that subsequently give rise to LCs with self-renewal capabilities [101,102]. Such LCs would, therefore, be CD14- and thus, possibly the CD14- LCs that we observed to populate the foreskin epidermis. Infiltrating monocytes have also been reported to flood the epidermis during inflammation, subsequently differentiating into monocyte derived LCs, thereby giving rise to CD14+ LCs that were also observed in this study[107,108,125,218]. These findings will need further interrogation to better understand the ontogenic identity of foreskin CD14- and CD14+ LCs. The presence of transcription factors such as the F4/80 human homolog, EMR1[101,102], and other genes would elucidate this.

Traditional LCs are historically classified as CD14-CD11c-, possibly arising from the self-renewing precursors[101,102]. Self-renewal properties of such LCs would render them long-lived and, thus, potential cellular reservoir contributors if infected with HIV. It was, however, the unconventional LCs that were productively infected with HIV and unable to restrict HIV, contrary to the traditional LCs that have also been reported in other studies as capable of effective restriction against NL4-3-X4 infection[28,30]. Productively infected LCs were identified as the i) CD14+CD11c- LCs and the ii) CD14+CD11c+ LCs. Cervico-vaginal studies have reported on the infectivity of CD11c+CD14+ DCs with high DC-SIGN co-expression[29]. Similarly, to these reports, high DC-SIGN co-expression was also observed to drive

HIV susceptibility in foreskin LCs[29,33,34]. This was further corroborated by the lack of DC-SIGN expression in the non-infectable, traditional LC subset (CD11c-CD14-). We therefore show that DC-SIGN, previously show to increase HIV susceptibility in DCs, is also an important determinant in the HIV infection of foreskin LCs, and not the other CLRs such as the mannose receptor or Siglec-1.

Foreskin LCs that were productively infected with HIV, exhibited a "macrophage-like" phenotype owing to the co-expression of CD14 and predominant in non-migratory cells. The perceived monocyte derivation of CD14 co-expressing LCs could potentially inform previous or ongoing inflammation, that would exacerbate one's susceptibility to HIV infection as observed. Although there were no significant differences among the different virus strains, both CD14+CD11c- LCs and the CD14+CD11c+ LCs, exhibited similar trends whereby the frequency of NL4-3 X4 infected cells reduced with time progression, while the frequency of cells infected with transmitted founder, subtype C virus, CH198, increased with time. While this, may have been indicative of productive infection and lack thereof in NL4-3 X4 infection; it may also have been indicative of HIV induced cytopathic loss, thus productive infection. Future studies could incorporate measurement of RT activity in the supernatants of infected cells to assay for this.

"M2-like" macrophages were identified as the most frequent myeloid cell subset, while also being productively infected with HIV, similarly to CD3+ macrophages. The co-expression of CD3 in both LCs and macrophages was unexpected but corroborates reports of T-DCs and CD3+TCRαβ+/- macrophages in women with Chlamydia infections [162,163]. It has further been suggested in these reports that pro-inflammatory CD3+TCRαβ+ MDMs proliferate in pathogenic conditions such as tuberculosis (TB), and therefore potentially relevant in multiple other infections, as seen by their susceptibility to HIV infection in the foreskin[162,163]. While the exact role and mechanisms of the unconventional cells is unclear, their association with pathological conditions requires further elucidation and could be integral in strategizing intervention technologies against HIV infection.

The foreskin therefore harbours heterogenous populations of HIV susceptible cells whose location offers an opportunity for early intervention against HIV entry. Further characterisation of these cells would offer invaluable insights into understanding the pathobiology of HIV and inform the development of HIV interventions.

VII. PUBLICATION PLANS

Two publications, separated by cell-type, are expected to emanate from this study. The intended journal for these manuscripts is the Journal of Mucosal Immunology.

REFERENCES

1. WHO. World Health Organization: HIV/AIDS. *https://www.who.int/health-topics/hiv-aids/#tab=tab_1* (2021).
2. Hemelaar, J. *et al.* Global and regional molecular epidemiology of HIV-1, 1990–2015: a systematic review, global survey, and trend analysis. *Lancet Infect Dis* **19**, 143–155 (2019).
3. Zuma, K. *et al.* The HIV Epidemic in South Africa: Key Findings from 2017 National Population-Based Survey. *Int J Environ Res Public Health* **19**, 8125 (2022).
4. UNAIDS. *IN DANGER: UNAIDS Global AIDS Update 2022. Geneva: Joint United Nations Programme on HIV/ AIDS; 2022. Licence: CC BY-NC-SA 3.0 IGO*. (2022).
5. Gray, C. M. *et al.* Impact of chemokine C–C ligand 27, foreskin anatomy and sexually transmitted infections on HIV-1 target cell availability in adolescent South African males. *Mucosal Immunol* (2019) doi:10.1038/s41385-019-0209-6.
6. Anderson, D. J. & Pudney, J. Human Male Genital Tract Immunity. in *Mucosal Immunology* 2125–2140 (Elsevier, 2015). doi:10.1016/B978-0-12-415847-4.00109-9.
7. Anderson, D., Politch, J. A. & Pudney, J. HIV Infection and Immune Defense of the Penis. *American Journal of Reproductive Immunology* **65**, 220–229 (2011).
8. Prodger, J. L. *et al.* Foreskin T-cell subsets differ substantially from blood with respect to HIV co-receptor expression, inflammatory profile, and memory status. *Mucosal Immunol* **5**, 121–128 (2012).
9. Gray, R. H., Wawer, M. J., Polis, C. B., Kigozi, G. & Serwadda, D. Male circumcision and prevention of HIV and sexually transmitted infections. *Curr Infect Dis Rep* **10**, 121–127 (2008).
10. Morris, B. J. & Wamai, R. G. Biological basis for the protective effect conferred by male circumcision against HIV infection. *Int J STD AIDS* **23**, 153–159 (2012).
11. Jayathunge, P. H. M. *et al.* Male Circumcision and HIV Transmission; What Do We Know? *Open AIDS J* (2014) doi:10.2174/1874613601408010031.
12. Sharma, A. L., Hokello, J. & Tyagi, M. Circumcision as an Intervening Strategy against HIV Acquisition in the Male Genital Tract. *Pathogens* **10**, 806 (2021).
13. Loevinsohn, G. *et al.* Effectiveness of Voluntary Medical Male Circumcision for Human Immunodeficiency Virus Prevention in Rakai, Uganda. *Clinical Infectious Diseases* **73**, e1946–e1953 (2021).
14. Bailey, R. C. *et al.* Male circumcision for HIV prevention in young men in Kisumu, Kenya: a randomised controlled trial. *Lancet* (2007) doi:10.1016/S0140-6736(07)60312-2.
15. Dinh, M. H. *et al.* No difference in keratin thickness between inner and outer foreskins from elective male circumcisions in Rakai, Uganda. *PLoS One* (2012) doi:10.1371/journal.pone.0041271.
16. Prodger, J. L. & Kaul, R. The biology of how circumcision reduces HIV susceptibility: Broader implications for the prevention field. *AIDS Research and Therapy* Preprint at https://doi.org/10.1186/s12981-017-0167-6 (2017).
17. Szabo, R. & Short, R. How does male circumcision protect against HIV infection? *BMJ* (2000) doi:10.1136/bmj.320.7249.1592.
18. Guilliams, M. *et al.* Dendritic cells, monocytes and macrophages: a unified nomenclature based on ontogeny. *Nat Rev Immunol* **14**, 571–578 (2014).
19. Esra, R. T. *et al.* Does HIV exploit the inflammatory milieu of the male genital tract for successful infection? *Front Immunol* **7**, 1–9 (2016).
20. Geijtenbeek, T. B. H. *et al.* DC-SIGN, a Dendritic Cell–Specific HIV-1-Binding Protein that Enhances trans-Infection of T Cells. *Cell* **100**, 587–597 (2000).
21. Bermejo-Jambrina, M. *et al.* C-Type Lectin Receptors in Antiviral Immunity and Viral Escape. *Front Immunol* **9**, (2018).
22. Bracq, L., Xie, M., Benichou, S. & Bouchet, J. Mechanisms for Cell-to-Cell Transmission of HIV-1. *Front Immunol* **9**, (2018).
23. Xie, M. *et al.* Cell-to-Cell Spreading of HIV-1 in Myeloid Target Cells Escapes SAMHD1 Restriction. *mBio* **10**, (2019).
24. Bracq, L. *et al.* T Cell-Macrophage Fusion Triggers Multinucleated Giant Cell Formation for HIV-1 Spreading. *J Virol* **91**, (2017).
25. Leroy, H. *et al.* Virus-Mediated Cell-Cell Fusion. *Int J Mol Sci* **21**, 9644 (2020).
26. Geijtenbeek, T. B. H. & van Kooyk, Y. DC-SIGN: A novel HIV receptor on DCs that mediates HIV-1 transmission. *Current Topics in Microbiology and Immunology* Preprint at https://doi.org/10.1007/978-3-662-06508-2_2 (2003).

27. Rodriguez-Plata, M. T. *et al.* The infectious synapse formed between mature dendritic cells and CD4+T cells is independent of the presence of the HIV-1 envelope glycoprotein. *Retrovirology* **10**, 42 (2013).
28. Geijtenbeek, T. B. *et al.* Human immature Langerhans cells restrict CXCR4-using HIV-1 transmission. *Retrovirology* **11**, 52 (2014).
29. Cloherty, A. P. M. *et al.* Autophagy-enhancing drugs limit mucosal HIV-1 acquisition and suppress viral replication ex vivo. *Sci Rep* **11**, 4767 (2021).
30. van den Berg, L. M. *et al.* Caveolin-1 mediated uptake via langerin restricts HIV-1 infection in human Langerhans cells. *Retrovirology* **11**, 123 (2014).
31. Ribeiro, C. M. S. *et al.* Receptor usage dictates HIV-1 restriction by human TRIM5α in dendritic cell subsets. *Nature* **540**, 448–452 (2016).
32. van Teijlingen, N. H. *et al.* Immune activation of vaginal human Langerhans cells increases susceptibility to HIV-1 infection. *Sci Rep* **13**, 3283 (2023).
33. Nobile, C. *et al.* Covert Human Immunodeficiency Virus Replication in Dendritic Cells and in DC-SIGN-Expressing Cells Promotes Long-Term Transmission to Lymphocytes. *J Virol* **79**, 5386–5399 (2005).
34. Hertoghs, N., Pul, L. van & Geijtenbeek, T. B. Mucosal dendritic cells in HIV-1 susceptibility: a critical role for C-type lectin receptors. *Future Virol* **12**, 373–388 (2017).
35. Ganor, Y. *et al.* HIV-1 reservoirs in urethral macrophages of patients under suppressive antiretroviral therapy. *Nat Microbiol* **4**, 633–644 (2019).
36. Abraha, A. *et al.* CCR5- and CXCR4-tropic subtype C human immunodeficiency virus type 1 isolates have a lower level of pathogenic fitness than other dominant group M subtypes: implications for the epidemic. *J Virol* **83**, 5592–605 (2009).
37. Ball, S. C. *et al.* Comparing the ex vivo fitness of CCR5-tropic human immunodeficiency virus type 1 isolates of subtypes B and C. *J Virol* **77**, 1021–38 (2003).
38. Haaland, R. E. *et al.* Inflammatory Genital Infections Mitigate a Severe Genetic Bottleneck in Heterosexual Transmission of Subtype A and C HIV-1. *PLoS Pathog* **5**, e1000274 (2009).
39. Abrahams, M.-R. *et al.* Quantitating the Multiplicity of Infection with Human Immunodeficiency Virus Type 1 Subtype C Reveals a Non-Poisson Distribution of Transmitted Variants. *J Virol* **83**, 3556–3567 (2009).
40. Robertson, D. L. *et al.* HIV-1 Nomenclature Proposal. *Science (1979)* **288**, 55–55 (2000).
41. Bhoopat, L. *et al.* In Vivo Identification of Langerhans and Related Dendritic Cells Infected with HIV-1 Subtype E in Vaginal Mucosa of Asymptomatic Patients. *Modern Pathology* **14**, 1263–1269 (2001).
42. Parrish, N. F. *et al.* Phenotypic properties of transmitted founder HIV-1. *Proceedings of the National Academy of Sciences* **110**, 6626–6633 (2013).
43. Keele, B. F. *et al.* Identification and characterization of transmitted and early founder virus envelopes in primary HIV-1 infection. *Proceedings of the National Academy of Sciences* **105**, 7552–7557 (2008).
44. Salazar-Gonzalez, J. F. *et al.* Genetic identity, biological phenotype, and evolutionary pathways of transmitted/founder viruses in acute and early HIV-1 infection. *Journal of Experimental Medicine* **206**, 1273–1289 (2009).
45. Wilen, C. B., Tilton, J. C. & Doms, R. W. HIV: Cell binding and entry. *Cold Spring Harb Perspect Med* (2012) doi:10.1101/cshperspect.a006866.
46. Kirchhoff, F. HIV Life Cycle: Overview. in *Encyclopedia of AIDS* (2013). doi:10.1007/978-1-4614-9610-6_60-1.
47. Kariuki, S. M., Selhorst, P., Ariën, K. K. & Dorfman, J. R. The HIV-1 transmission bottleneck. *Retrovirology* Preprint at https://doi.org/10.1186/s12977-017-0343-8 (2017).
48. https://app.biorender.com/biorender-templates. Biorender.com. *Biorender.com* Preprint at (2022).
49. Azevedo-Pereira, J. M., Canhão, P., Calado, M., Santos-Costa, Q. & Barroca, P. Inhibition of HIV Replication by Host Cellular Factors. in *Trends in Basic and Therapeutic Options in HIV Infection - Towards a Functional Cure* (InTech, 2015). doi:10.5772/60795.
50. Salazar-Gonzalez, J. F. *et al.* Deciphering Human Immunodeficiency Virus Type 1 Transmission and Early Envelope Diversification by Single-Genome Amplification and Sequencing. *J Virol* **82**, 3952–3970 (2008).
51. Turville, S. G. *et al.* HIV gp120 receptors on human dendritic cells. *Blood* **98**, 2482–2488 (2001).
52. Lai, J. *et al.* Oligomerization of the Macrophage Mannose Receptor Enhances gp120-mediated Binding of HIV-1. *Journal of Biological Chemistry* **284**, 11027–11038 (2009).
53. Woodham, A. W. *et al.* Human Immunodeficiency Virus Immune Cell Receptors, Coreceptors, and Cofactors: Implications for Prevention and Treatment. *AIDS Patient Care STDS* **30**, 291–306 (2016).
54. Parra, J. *et al.* Clinical utility of maraviroc. *Clin Drug Investig* **31**, 527–542 (2011).
55. Soriano, V. Optimizing management of treatment-naïve and treatment-experienced HIV+ patients: the role of maraviroc. *HIV/AIDS - Research and Palliative Care* 51 (2010) doi:10.2147/HIV.S4977.
56. Belaunzarán-Zamudio, P. F. *et al.* Immunologic Effects of Maraviroc in HIV-Infected Patients with Severe CD4 Lymphopenia Starting Antiretroviral Therapy: A Sub-Study of the CADIRIS Trial. *Pathog Immun* (2017) doi:10.20411/pai.v2i2.181.

57. Shukla, E. & Chauhan, R. Host-HIV-1 Interactome: A Quest for Novel Therapeutic Intervention. *Cells* **8**, (2019).
58. Azzoni, L. *et al.* Pegylated Interferon Alfa-2a Monotherapy Results in Suppression of HIV Type 1 Replication and Decreased Cell-Associated HIV DNA Integration. *J Infect Dis* **207**, 213–222 (2013).
59. Herbein, G. & Varin, A. The macrophage in HIV-1 infection: From activation to deactivation? *Retrovirology* **7**, 33 (2010).
60. Veenhuis, R. T., Abreu, C. M., Shirk, E. N., Gama, L. & Clements, J. E. HIV replication and latency in monocytes and macrophages. *Semin Immunol* **51**, 101472 (2021).
61. Coleman, C. M. & Wu, L. HIV interactions with monocytes and dendritic cells: Viral latency and reservoirs. *Retrovirology* Preprint at https://doi.org/10.1186/1742-4690-6-51 (2009).
62. Maasdorp, E. & Okwundu, C. I. Raltegravir for the treatment of HIV infection in adults and children. *Cochrane Database of Systematic Reviews* (2017) doi:10.1002/14651858.CD011467.pub2.
63. Kityo, C. *et al.* Raltegravir-intensified initial antiretroviral therapy in advanced HIV disease in Africa: A randomised controlled trial. *PLoS Med* **15**, e1002706 (2018).
64. Honke, N. *et al.* Enforced viral replication activates adaptive immunity and is essential for the control of a cytopathic virus. *Nat Immunol* **13**, 51–57 (2012).
65. Buffalo, C. Z., Iwamoto, Y., Hurley, J. H. & Ren, X. How HIV Nef Proteins Hijack Membrane Traffic To Promote Infection. *J Virol* **93**, (2019).
66. Kwon, Y. *et al.* Structural basis of CD4 downregulation by HIV-1 Nef. *Nat Struct Mol Biol* **27**, 822–828 (2020).
67. Ren, X., Park, S. Y., Bonifacino, J. S. & Hurley, J. H. How HIV-1 Nef hijacks the AP-2 clathrin adaptor to downregulate CD4. *Elife* **3**, (2014).
68. Dirk, B. S. *et al.* HIV-1 Nef sequesters MHC-I intracellularly by targeting early stages of endocytosis and recycling. *Sci Rep* **6**, 37021 (2016).
69. Miller, C. J. & Shattock, R. J. Target cells in vaginal HIV transmission. *Microbes Infect* **5**, 59–67 (2003).
70. McCoombe, S. G. & Short, R. v. Potential HIV-1 target cells in the human penis. *AIDS* **20**, 1491–1495 (2006).
71. Kaul, R. *et al.* Inflammation and HIV Transmission in Sub-Saharan Africa. *Current HIV/AIDS Reports* Preprint at https://doi.org/10.1007/s11904-015-0269-5 (2015).
72. Bertram, K. M. *et al.* Identification of HIV transmitting CD11c+ human epidermal dendritic cells. *Nat Commun* **10**, 2759 (2019).
73. Dzomba, A., Tomita, A., Govender, K. & Tanser, F. Effects of Migration on Risky Sexual Behavior and HIV Acquisition in South Africa: A Systematic Review and Meta-analysis, 2000–2017. *AIDS Behav* **23**, 1396–1430 (2019).
74. Ochsenbauer, C. *et al.* Generation of Transmitted/Founder HIV-1 Infectious Molecular Clones and Characterization of Their Replication Capacity in CD4 T Lymphocytes and Monocyte-Derived Macrophages. *J Virol* (2012) doi:10.1128/JVI.06157-11.
75. Jakobsen, M. R., Olagnier, D. & Hiscott, J. Innate immune sensing of HIV-1 infection. *Current Opinion in HIV and AIDS* Preprint at https://doi.org/10.1097/COH.0000000000000129 (2015).
76. Liu, C. M. *et al.* Penile anaerobic dysbiosis as a risk factor for HIV infection. *mBio* (2017) doi:10.1128/mBio.00996-17.
77. Lemos, M. P. *et al.* The inner foreskin of healthy males at risk of HIV infection harbors epithelial CD4+ CCR5+ cells and has features of an inflamed epidermal barrier. *PLoS One* (2014) doi:10.1371/journal.pone.0108954.
78. Zhou, Z. *et al.* HIV-1 efficient entry in inner foreskin is mediated by elevated CCL5/RANTES that recruits T cells and fuels conjugate formation with Langerhans cells. *PLoS Pathog* (2011) doi:10.1371/journal.ppat.1002100.
79. Chigorimbo-Murefu, N. T. L. *et al.* A pilot study to show that asymptomatic sexually transmitted infections alter the foreskin epithelial proteome. *Front Microbiol* **13**, (2022).
80. de Jong, M. A. W. P., de Witte, L., Taylor, M. E. & Geijtenbeek, T. B. H. Herpes Simplex Virus Type 2 Enhances HIV-1 Susceptibility by Affecting Langerhans Cell Function. *The Journal of Immunology* **185**, 1633–1641 (2010).
81. Akira, S., Uematsu, S. & Takeuchi, O. Pathogen recognition and innate immunity. *Cell* Preprint at https://doi.org/10.1016/j.cell.2006.02.015 (2006).
82. Hespel, C. & Moser, M. Role of inflammatory dendritic cells in innate and adaptive immunity. *European Journal of Immunology* Preprint at https://doi.org/10.1002/eji.201242480 (2012).
83. Takeda, K., Kaisho, T. & Akira, S. Toll-Like Receptors. *Annu Rev Immunol* **21**, 335–376 (2003).
84. Macedo, A. B., Novis, C. L. & Bosque, A. Targeting Cellular and Tissue HIV Reservoirs With Toll-Like Receptor Agonists. *Front Immunol* **10**, (2019).
85. Crocker, P. R., Paulson, J. C. & Varki, A. Siglecs and their roles in the immune system. *Nat Rev Immunol* **7**, 255–266 (2007).
86. Merad, M., Ginhoux, F. & Collin, M. Origin, homeostasis and function of Langerhans cells and other langerin-expressing dendritic cells. *Nat Rev Immunol* **8**, 935–947 (2008).
87. Yanez, D. A., Lacher, R. K., Vidyarthi, A. & Colegio, O. R. The role of macrophages in skin homeostasis. *Pflugers Archiv European Journal of Physiology* Preprint at https://doi.org/10.1007/s00424-017-1953-7 (2017).

88. Kawamoto, H. & Minato, N. Myeloid cells. *International Journal of Biochemistry and Cell Biology* Preprint at https://doi.org/10.1016/j.biocel.2004.01.020 (2004).
89. Soilleux, E. J. Expression of DC-SIGN in human foreskin may facilitate sexual transmission of HIV. *J Clin Pathol* **57**, 77–78 (2004).
90. Real, F., Sennepin, A., Ganor, Y., Schmitt, A. & Bomsel, M. Live Imaging of HIV-1 Transfer across T Cell Virological Synapse to Epithelial Cells that Promotes Stromal Macrophage Infection. *Cell Rep* **23**, 1794–1805 (2018).
91. Zhou, Z. *et al.* The HIV-1 viral synapse signals human foreskin keratinocytes to secrete thymic stromal lymphopoietin facilitating HIV-1 foreskin entry. *Mucosal Immunol* (2018) doi:10.1038/mi.2017.23.
92. Ganor, Y. *et al.* Within 1 h, HIV-1 uses viral synapses to enter efficiently the inner, but not outer, foreskin mucosa and engages Langerhans–T cell conjugates. *Mucosal Immunol* **3**, 506–522 (2010).
93. Passmore, J.-A. S., Jaspan, H. B. & Masson, L. Genital inflammation, immune activation and risk of sexual HIV acquisition. *Curr Opin HIV AIDS* **11**, 156–162 (2016).
94. Masson, L. *et al.* Genital Inflammation and the Risk of HIV Acquisition in Women. *Clinical Infectious Diseases* (2015) doi:10.1093/cid/civ298.
95. Martín-Moreno, A. & Muñoz-Fernández, M. A. Dendritic Cells, the Double Agent in the War Against HIV-1. *Front Immunol* **10**, (2019).
96. Wu, L. & KewalRamani, V. N. Dendritic-cell interactions with HIV: infection and viral dissemination. *Nat Rev Immunol* **6**, 859–868 (2006).
97. Cabeza-Cabrerizo, M., Cardoso, A., Minutti, C. M., Pereira da Costa, M. & Reis e Sousa, C. Dendritic Cells Revisited. *Annu Rev Immunol* **39**, 131–166 (2021).
98. Palucka, K. & Banchereau, J. Cancer immunotherapy via dendritic cells. *Nat Rev Cancer* **12**, 265–277 (2012).
99. de Kleer, I., Willems, F., Lambrecht, B. & Goriely, S. Ontogeny of Myeloid Cells. *Front Immunol* **5**, (2014).
100. Rosado-Sánchez, I. *et al.* Increased Frequencies of Myeloid-Derived Suppressor Cells Precede Immunodiscordance in HIV-Infected Subjects. *Front Immunol* **11**, (2020).
101. Freitas-Lopes, M., Mafra, K., David, B., Carvalho-Gontijo, R. & Menezes, G. Differential Location and Distribution of Hepatic Immune Cells. *Cells* **6**, 48 (2017).
102. Wildes, T. J., DiVita Dean, B. & Flores, C. T. Myelopoiesis during Solid Cancers and Strategies for Immunotherapy. *Cells* **10**, 968 (2021).
103. Mehraj, V., Jenabian, M.-A., Vyboh, K. & Routy, J.-P. Immune Suppression by Myeloid Cells in HIV Infection: New Targets for Immunotherapy. *Open AIDS J* **8**, 66–78 (2014).
104. Rodrigues, P. F. *et al.* Distinct progenitor lineages contribute to the heterogeneity of plasmacytoid dendritic cells. *Nat Immunol* **19**, 711–722 (2018).
105. Bonaud, A., Lemos, J. P., Espéli, M. & Balabanian, K. Hematopoietic Multipotent Progenitors and Plasma Cells: Neighbors or Roommates in the Mouse Bone Marrow Ecosystem? *Front Immunol* **12**, (2021).
106. Ziegler-Heitbrock, L. *et al.* Nomenclature of monocytes and dendritic cells in blood. *Blood* **116**, e74–e80 (2010).
107. Seré, K. *et al.* Two Distinct Types of Langerhans Cells Populate the Skin during Steady State and Inflammation. *Immunity* **37**, 905–916 (2012).
108. Merad, M. *et al.* Langerhans cells renew in the skin throughout life under steady-state conditions. *Nat Immunol* **3**, 1135–1141 (2002).
109. Ziegler-Heitbrock, L. The CD14+ CD16+ blood monocytes: their role in infection and inflammation. *J Leukoc Biol* (2007) doi:10.1189/jlb.0806510.
110. Issa, F. Single-cell RNA-Seq reveals new types of human blood dendritic cells, monocytes, and progenitors. *Transplantation* **101**, 1955–1956 (2017).
111. Italiani, P. & Boraschi, D. From Monocytes to M1/M2 Macrophages: Phenotypical vs. Functional Differentiation. *Front Immunol* **5**, (2014).
112. Tsukamoto, T. Hematopoietic Stem/Progenitor Cells and the Pathogenesis of HIV/AIDS. *Front Cell Infect Microbiol* **10**, (2020).
113. Otsuka, M., Egawa, G. & Kabashima, K. Uncovering the Mysteries of Langerhans Cells, Inflammatory Dendritic Epidermal Cells, and Monocyte-Derived Langerhans Cell-Like Cells in the Epidermis. *Front Immunol* **9**, (2018).
114. Martinez-Pomares, L. & Gordon, S. CD169+ macrophages at the crossroads of antigen presentation. *Trends Immunol* **33**, 66–70 (2012).
115. Campana, S., de Pasquale, C., Carrega, P., Ferlazzo, G. & Bonaccorsi, I. Cross-dressing: an alternative mechanism for antigen presentation. *Immunol Lett* **168**, 349–354 (2015).
116. Bigley, V. *et al.* Langerin-expressing dendritic cells in human tissues are related to CD1c $^{+}$ dendritic cells and distinct from Langerhans cells and CD141 ^{high} XCR1 $^{+}$ dendritic cells. *J Leukoc Biol* **97**, 627–634 (2015).
117. Gazi, U. & Martinez-Pomares, L. Influence of the mannose receptor in host immune responses. *Immunobiology* Preprint at https://doi.org/10.1016/j.imbio.2008.11.004 (2009).
118. Stahl, P. D. & Ezekowitz, R. A. B. The mannose receptor is a pattern recognition receptor involved in host defense. *Curr Opin Immunol* (1998) doi:10.1016/S0952-7915(98)80031-9.

119. Varchetta, S. *et al.* Sialic acid-binding Ig-like lectin-7 interacts with HIV-1 gp120 and facilitates infection of CD4posT cells and macrophages. *Retrovirology* **10**, 154 (2013).
120. Pena-Cruz, V. *et al.* HIV-1 replicates and persists in vaginal epithelial dendritic cells. *Journal of Clinical Investigation* (2018) doi:10.1172/JCI98943.
121. Perez-Zsolt, D., Martinez-Picado, J. & Izquierdo-Useros, N. When Dendritic Cells Go Viral: The Role of Siglec-1 in Host Defense and Dissemination of Enveloped Viruses. *Viruses* **12**, 8 (2019).
122. Martinez-Picado, J. *et al.* Identification of Siglec-1 null individuals infected with HIV-1. *Nat Commun* **7**, 12412 (2016).
123. Pino, M. *et al.* HIV-1 immune activation induces Siglec-1 expression and enhances viral trans-infection in blood and tissue myeloid cells. *Retrovirology* **12**, 37 (2015).
124. Perez-Zsolt, D. *et al.* Dendritic Cells From the Cervical Mucosa Capture and Transfer HIV-1 via Siglec-1. *Front Immunol* **10**, (2019).
125. Iwamoto, K. *et al.* Langerhans and inflammatory dendritic epidermal cells in atopic dermatitis are tolerized toward TLR2 activation. *Allergy* **73**, 2205–2213 (2018).
126. Xue, J. *et al.* Transcriptome-Based Network Analysis Reveals a Spectrum Model of Human Macrophage Activation. *Immunity* **40**, 274–288 (2014).
127. Aggarwal, A., McAllery, S. & Turville, S. G. Revising the Role of Myeloid cells in HIV Pathogenesis. *Curr HIV/AIDS Rep* **10**, 3–11 (2013).
128. Ghoreishi, M. *et al.* Expansion of Antigen-Specific Regulatory T Cells with the Topical Vitamin D Analog Calcipotriol. *The Journal of Immunology* **182**, 6071–6078 (2009).
129. Montealegre, S. & van Endert, P. M. Endocytic Recycling of MHC Class I Molecules in Non-professional Antigen Presenting and Dendritic Cells. *Front Immunol* **9**, (2019).
130. van den Berg, L. M. *et al.* Langerhans Cell–Dendritic Cell Cross-Talk via Langerin and Hyaluronic Acid Mediates Antigen Transfer and Cross-Presentation of HIV-1. *The Journal of Immunology* **195**, 1763–1773 (2015).
131. STEINMAN, R. M. *et al.* Dendritic Cell Function *in Vivo* during the Steady State: A Role in Peripheral Tolerance. *Ann N Y Acad Sci* **987**, 15–25 (2003).
132. van Dinther, D. *et al.* Functional CD169 on Macrophages Mediates Interaction with Dendritic Cells for CD8+ T Cell Cross-Priming. *Cell Rep* **22**, 1484–1495 (2018).
133. Stingl, G. *et al.* Langerhans cells in HIV-1 infection. *J Am Acad Dermatol* **22**, 1210–1217 (1990).
134. Clayton, K., Vallejo, A. F., Davies, J., Sirvent, S. & Polak, M. E. Langerhans cells-programmed by the epidermis. *Frontiers in Immunology* Preprint at https://doi.org/10.3389/fimmu.2017.01676 (2017).
135. Fehervari, Z. HIV keeps DCs immature. *Nat Immunol* **16**, 590–590 (2015).
136. Adiko, A. C., Babdor, J., Gutiérrez-Martínez, E., Guermonprez, P. & Saveanu, L. Intracellular Transport Routes for MHC I and Their Relevance for Antigen Cross-Presentation. *Front Immunol* **6**, (2015).
137. Yao, Y., Xu, X.-H. & Jin, L. Macrophage Polarization in Physiological and Pathological Pregnancy. *Front Immunol* **10**, (2019).
138. Rodrigues, V., Ruffin, N., San-Roman, M. & Benaroch, P. Myeloid Cell Interaction with HIV: A Complex Relationship. *Front Immunol* **8**, (2017).
139. Affandi, A. J. *et al.* CD169 Defines Activated CD14+ Monocytes With Enhanced CD8+ T Cell Activation Capacity. *Front Immunol* **12**, (2021).
140. Davies, J. *et al.* An IRF1-IRF4 Toggle-Switch Controls Tolerogenic and Immunogenic Transcriptional Programming in Human Langerhans Cells. *Front Immunol* **12**, (2021).
141. Collin, M. & Bigley, V. Human dendritic cell subsets: an update. *Immunology* **154**, 3–20 (2018).
142. Bourdely, P. *et al.* Transcriptional and Functional Analysis of CD1c+ Human Dendritic Cells Identifies a CD163+ Subset Priming CD8+CD103+ T Cells. *Immunity* **53**, 335-352.e8 (2020).
143. Cytlak, U. *et al.* Differential IRF8 Transcription Factor Requirement Defines Two Pathways of Dendritic Cell Development in Humans. *Immunity* **53**, 353-370.e8 (2020).
144. Polak, M. E. & Singh, H. Tolerogenic and immunogenic states of Langerhans cells are orchestrated by epidermal signals acting on a core maturation gene module. *BioEssays* **43**, 2000182 (2021).
145. Fluitsma, D. *et al.* Langerin is a natural barrier to HIV-1 transmission by Langerhans cells. *Nat Med* **13**, 367–371 (2007).
146. Mc Dermott, R. *et al.* Birbeck Granules Are Subdomains of Endosomal Recycling Compartment in Human Epidermal Langerhans Cells, Which Form Where Langerin Accumulates. *Mol Biol Cell* **13**, 317–335 (2002).
147. Sirvent, S. *et al.* Genomic programming of IRF4-expressing human Langerhans cells. *Nat Commun* (2020) doi:10.1038/s41467-019-14125-x.
148. Chopin, M. *et al.* Langerhans cells are generated by two distinct PU.1-dependent transcriptional networks. *Journal of Experimental Medicine* **210**, 2967–2980 (2013).
149. Totsuka, T. *et al.* RANK-RANKL Signaling Pathway Is Critically Involved in the Function of CD4+CD25+ Regulatory T Cells in Chronic Colitis. *The Journal of Immunology* **182**, 6079–6087 (2009).

150. Smith, P. D. *et al.* Intestinal macrophages and response to microbial encroachment. *Mucosal Immunol* **4**, 31–42 (2011).
151. Barros, M. H. M., Hauck, F., Dreyer, J. H., Kempkes, B. & Niedobitek, G. Macrophage Polarisation: an Immunohistochemical Approach for Identifying M1 and M2 Macrophages. *PLoS One* **8**, e80908 (2013).
152. Hristodorov, D. *et al.* Targeting CD64 mediates elimination of M1 but not M2 macrophages in vitro and in cutaneous inflammation in mice and patient biopsies. *MAbs* **7**, 853–862 (2015).
153. Li, G. *et al.* The shift of macrophages toward M1 phenotype promotes aortic valvular calcification. *J Thorac Cardiovasc Surg* **153**, 1318-1327.e1 (2017).
154. Jaguin, M., Houlbert, N., Fardel, O. & Lecureur, V. Polarization profiles of human M-CSF-generated macrophages and comparison of M1-markers in classically activated macrophages from GM-CSF and M-CSF origin. *Cell Immunol* **281**, 51–61 (2013).
155. Poli, G. 160 Polarization of M1 and M2 macrophages and HIV infection. *JAIDS Journal of Acquired Immune Deficiency Syndromes* **51**, (2009).
156. Wang, Y., Smith, W., Hao, D., He, B. & Kong, L. M1 and M2 macrophage polarization and potentially therapeutic naturally occurring compounds. *Int Immunopharmacol* **70**, 459–466 (2019).
157. Rojas-Celis, V., Valiente-Echeverría, F., Soto-Rifo, R. & Toro-Ascuy, D. New Challenges of HIV-1 Infection: How HIV-1 Attacks and Resides in the Central Nervous System. *Cells* **8**, 1245 (2019).
158. ChÃ¡vez-GalÃ¡n, L., Olleros, M. L., Vesin, D. & Garcia, I. Much More than M1 and M2 Macrophages, There are also CD169+ and TCR+ Macrophages. *Front Immunol* **6**, (2015).
159. Grabowska, J., Lopez-Venegas, M. A., Affandi, A. J. & den Haan, J. M. M. CD169+ Macrophages Capture and Dendritic Cells Instruct: The Interplay of the Gatekeeper and the General of the Immune System. *Front Immunol* **9**, (2018).
160. Liu, Y., Xia, Y. & Qiu, C.-H. Functions of CD169 positive macrophages in human diseases (Review). *Biomed Rep* **14**, 26 (2020).
161. Ocaña-Guzmán, R. *et al.* Murine RAW Macrophages Are a Suitable Model to Study the CD3 Signaling in Myeloid Cells. *Cells* **11**, 1635 (2022).
162. Rodriguez-Cruz, A. *et al.* CD3+ Macrophages Deliver Proinflammatory Cytokines by a CD3- and Transmembrane TNF-Dependent Pathway and Are Increased at the BCG-Infection Site. *Front Immunol* **10**, (2019).
163. Ramon-Luing, L. A. *et al.* Mycobacterium tuberculosis H37Rv Strain Increases the Frequency of CD3+TCR+ Macrophages and Affects Their Phenotype, but Not Their Migration Ability. *Int J Mol Sci* **23**, 329 (2021).
164. Puellmann, K. *et al.* A variable immunoreceptor in a subpopulation of human neutrophils. *Proceedings of the National Academy of Sciences* **103**, 14441–14446 (2006).
165. Fuchs, T. *et al.* The macrophage-TCRαβ is a cholesterol-responsive combinatorial immune receptor and implicated in atherosclerosis. *Biochem Biophys Res Commun* **456**, 59–65 (2015).
166. Qualai, J. *et al.* Expression of CD11c Is Associated with Unconventional Activated T Cell Subsets with High Migratory Potential. *PLoS One* **11**, e0154253 (2016).
167. Kuka, M., Munitic, I. & Ashwell, J. D. Identification and characterization of polyclonal αβ-T cells with dendritic cell properties. *Nat Commun* **3**, 1223 (2012).
168. Fuchs, T. *et al.* A combinatorial αβ T cell receptor expressed by macrophages in the tumor microenvironment. *Immunobiology* **222**, 39–44 (2017).
169. Larson, R. S. & Springer, T. A. Structure and Function of Leukocyte Integrins. *Immunol Rev* **114**, 181–217 (1990).
170. Hladik, F. *et al.* Initial Events in Establishing Vaginal Entry and Infection by Human Immunodeficiency Virus Type-1. *Immunity* **26**, 257–270 (2007).
171. Chitrakar, A., Sanz, M., Maggirwar, S. B. & Soriano-Sarabia, N. HIV Latency in Myeloid Cells: Challenges for a Cure. *Pathogens* **11**, 611 (2022).
172. Clayton, K. L. *et al.* Resistance of HIV-infected macrophages to CD8+ T lymphocyte–mediated killing drives activation of the immune system. *Nat Immunol* **19**, 475–486 (2018).
173. Deneka, M., Pelchen-Matthews, A., Byland, R., Ruiz-Mateos, E. & Marsh, M. In macrophages, HIV-1 assembles into an intracellular plasma membrane domain containing the tetraspanins CD81, CD9, and CD53. *Journal of Cell Biology* **177**, 329–341 (2007).
174. Tan, J. & Sattentau, Q. J. The HIV-1-containing macrophage compartment: a perfect cellular niche? *Trends Microbiol* **21**, 405–412 (2013).
175. Marozsan, A. J. *et al.* Differences in the Fitness of Two Diverse Wild-Type Human Immunodeficiency Virus Type 1 Isolates Are Related to the Efficiency of Cell Binding and Entry. *J Virol* **79**, 7121–7134 (2005).
176. Baxter, A. E. *et al.* Macrophage infection via selective capture of HIV-1-infected CD4+ T cells. *Cell Host Microbe* **16**, 711–21 (2014).
177. Adan, A., Alizada, G., Kiraz, Y., Baran, Y. & Nalbant, A. Flow cytometry: basic principles and applications. *Crit Rev Biotechnol* **37**, 163–176 (2017).

178. Quintelier, K. *et al.* Analyzing high-dimensional cytometry data using FlowSOM. *Nat Protoc* **16**, 3775–3801 (2021).
179. van Gassen, S. *et al.* FlowSOM: Using self-organizing maps for visualization and interpretation of cytometry data. *Cytometry Part A* **87**, 636–645 (2015).
180. Dzanibe, S. *et al.* Stereotypic Expansion of T Regulatory and Th17 Cells during Infancy Is Disrupted by HIV Exposure and Gut Epithelial Damage. *The Journal of Immunology* **208**, 27–37 (2022).
181. Aasen, T. & Belmonte, J. C. I. Isolation and cultivation of human keratinocytes from skin or plucked hair for the generation of induced pluripotent stem cells. *Nat Protoc* **5**, 371–382 (2010).
182. Choi, M. *et al.* Establishment of Immortalized Primary Human Foreskin Keratinocytes and Their Application to Toxicity Assessment and Three Dimensional Skin Culture Construction. *Biomol Ther (Seoul)* **25**, 296–307 (2017).
183. Dasgupta, A. & Wahed, A. Laboratory Statistics and Quality Control. in *Clinical Chemistry, Immunology and Laboratory Quality Control* 47–66 (Elsevier, 2014). doi:10.1016/B978-0-12-407821-5.00004-8.
184. Farver, T. B. Concepts of Normality in Clinical Biochemistry. in *Clinical Biochemistry of Domestic Animals* 1–19 (Elsevier, 1997). doi:10.1016/B978-012396305-5/50002-6.
185. Lee, S. & Lee, D. K. What is the proper way to apply the multiple comparison test? *Korean J Anesthesiol* **71**, 353–360 (2018).
186. Thissen, D., Steinberg, L. & Kuang, D. Quick and Easy Implementation of the Benjamini-Hochberg Procedure for Controlling the False Positive Rate in Multiple Comparisons. *Journal of Educational and Behavioral Statistics* **27**, 77–83 (2002).
187. Burel, J. G. *et al.* Circulating T cell-monocyte complexes are markers of immune perturbations. *Elife* **8**, (2019).
188. Oakley, M. S. *et al.* TCRβ-expressing macrophages induced by a pathogenic murine malaria correlate with parasite burden and enhanced phagocytic activity. *PLoS One* **13**, e0201043 (2018).
189. Chorazeczewski, J. K. *et al.* TCRβ Combinatorial Immunoreceptor Expression by Neutrophils Correlates with Parasite Burden and Enhanced Phagocytosis during a Plasmodium berghei ANKA Malaria Infection. *Infect Immun* **86**, (2018).
190. Poli, G. Cell-to-cell vs. cell-free HIV-1 transmission from macrophages to CD4+ T lymphocytes. *AIDS* **27**, 2307–2308 (2013).
191. van den Berg, L. M. & Geijtenbeek, T. B. H. Antiviral immune responses by human langerhans cells and dendritic cells in HIV-1 infection. *Adv Exp Med Biol* (2013) doi:10.1007/978-1-4614-4433-6-2.
192. Yu, H. J., Reuter, M. A. & McDonald, D. HIV Traffics through a Specialized, Surface-Accessible Intracellular Compartment during trans-Infection of T Cells by Mature Dendritic Cells. *PLoS Pathog* **4**, e1000134 (2008).
193. Eugenin, E. A., Gaskill, P. J. & Berman, J. W. Tunneling nanotubes (TNT) are induced by HIV-infection of macrophages: A potential mechanism for intercellular HIV trafficking. *Cell Immunol* **254**, 142–148 (2009).
194. Dupont, M. *et al.* Tuberculosis-associated IFN-I induces Siglec-1 on tunneling nanotubes and favors HIV-1 spread in macrophages. *Elife* **9**, (2020).
195. Hertoghs, N. *et al.* SAMHD1 Degradation Enhances Active Suppression of Dendritic Cell Maturation by HIV-1. *The Journal of Immunology* **194**, 4431–4437 (2015).
196. Iyer, S. S. *et al.* Resistance to type 1 interferons is a major determinant of HIV-1 transmission fitness. *Proceedings of the National Academy of Sciences* **114**, (2017).
197. Gondim, M. V. P. *et al.* Heightened resistance to host type 1 interferons characterizes HIV-1 at transmission and after antiretroviral therapy interruption. *Sci Transl Med* **13**, (2021).
198. Hladik, F. & McElrath, M. J. Setting the stage: Host invasion by HIV. *Nature Reviews Immunology* Preprint at https://doi.org/10.1038/nri2302 (2008).
199. de Jong, M. A. W. P. *et al.* TNF-α and TLR agonists increase susceptibility to HIV-1 transmission by human Langerhans cells ex vivo. *Journal of Clinical Investigation* **118**, 3440–3452 (2008).
200. Salasc, F. *et al.* A novel, sensitive dual-indicator cell line for detection and quantification of inducible, replication-competent latent HIV-1 from reservoir cells. *Sci Rep* **9**, 19325 (2019).
201. Montano, M. Model systems. in *Translational Biology in Medicine* 9–33 (Elsevier, 2014). doi:10.1533/9781908818652.9.
202. Maher, D. M., Zhang, Z. Q., Schacker, T. W. & Southern, P. J. Ex vivo modeling of oral HIV transmission in human palatine tonsil. *Journal of Histochemistry and Cytochemistry* **53**, 631–642 (2005).
203. Graham, A. L. Naturalizing mouse models for immunology. *Nat Immunol* **22**, 111–117 (2021).
204. Balaguer, P., Boussioux, A.-M., Demirpence, E. & Nicolas, J.-C. Reporter cell lines are useful tools for monitoring biological activity of nuclear receptor ligands. *Luminescence* **16**, 153–158 (2001).
205. Gervaix, A. *et al.* A new reporter cell line to monitor HIV infection and drug susceptibility *in vitro*. *Proceedings of the National Academy of Sciences* **94**, 4653–4658 (1997).
206. DuBridge, R. B. *et al.* Analysis of mutation in human cells by using an Epstein-Barr virus shuttle system. *Mol Cell Biol* **7**, 379–387 (1987).
207. Botting, R. A. *et al.* Phenotypic and functional consequences of different isolation protocols on skin mononuclear phagocytes. *J Leukoc Biol* **101**, 1393–1403 (2017).

208. Painter, K. J. Modelling cell migration strategies in the extracellular matrix. *J Math Biol* **58**, 511 (2009).
209. Vacharaksa, A. *et al.* Oral keratinocytes support non-replicative infection and transfer of harbored HIV-1 to permissive cells. *Retrovirology* **5**, 66 (2008).
210. Pear, W. S., Nolan, G. P., Scott, M. L. & Baltimore, D. Production of high-titer helper-free retroviruses by transient transfection. *Proceedings of the National Academy of Sciences* **90**, 8392–8396 (1993).
211. Platt, E. J., Bilska, M., Kozak, S. L., Kabat, D. & Montefiori, D. C. Evidence that Ecotropic Murine Leukemia Virus Contamination in TZM-bl Cells Does Not Affect the Outcome of Neutralizing Antibody Assays with Human Immunodeficiency Virus Type 1. *J Virol* **83**, 8289–8292 (2009).
212. Pacheco, M. A. *et al.* Multiplicity of Infection and Disease Severity in Plasmodium vivax. *PLoS Negl Trop Dis* **10**, e0004355 (2016).
213. Capucha, T. *et al.* Distinct Murine Mucosal Langerhans Cell Subsets Develop from Pre-dendritic Cells and Monocytes. *Immunity* **43**, 369–381 (2015).
214. Poulin, L. F. *et al.* The dermis contains langerin+ dendritic cells that develop and function independently of epidermal Langerhans cells. *Journal of Experimental Medicine* **204**, 3119–3131 (2007).
215. Fischetti, L., Barry, S. M., Hope, T. J. & Shattock, R. J. HIV-1 infection of human penile explant tissue and protection by candidate microbicides. *Aids* **23**, 319–328 (2009).
216. Patterson, B. K. *et al.* Susceptibility to Human Immunodeficiency Virus-1 Infection of Human Foreskin and Cervical Tissue Grown in Explant Culture. *Am J Pathol* **161**, 867–873 (2002).
217. Liu, A. *et al.* Differential compartmentalization of HIV-targeting immune cells in inner and outer foreskin tissue. *PLoS One* **9**, e85176 (2014).
218. Yoshida, K. *et al.* Distinct behavior of human Langerhans cells and inflammatory dendritic epidermal cells at tight junctions in patients with atopic dermatitis. *Journal of Allergy and Clinical Immunology* **134**, 856–864 (2014).
219. Hertoghs, N. *et al.* Sexually transmitted founder HIV-1 viruses are relatively resistant to Langerhans cell-mediated restriction. *PLoS One* **14**, e0226651 (2019).
220. Wollenberg, A., Kraft, S., Hanau, D. & Bieber, T. Immunomorphological and Ultrastructural Characterization of Langerhans Cells and a Novel, Inflammatory Dendritic Epidermal Cell (IDEC) Population in Lesional Skin of Atopic Eczema. *Journal of Investigative Dermatology* **106**, 446–453 (1996).
221. Wollenberg, A., Haberstok, J., Teichmann, B., Wen, S.-P. & Bieber, T. Demonstration of the low-affinity IgE receptor FcεRII/CD23 in psoriatic epidermis: inflammatory dendritic epidermal cells (IDEC) but not Langerhans cells are the relevant CD1a-positive cell population. *Arch Dermatol Res* **290**, 517–521 (1998).
222. Trifonova, R. T., Bollman, B., Barteneva, N. S. & Lieberman, J. Myeloid Cells in Intact Human Cervical Explants Capture HIV and Can Transmit It to CD4 T Cells. *Front Immunol* **9**, (2018).
223. Guo, A.-L. *et al.* HIV-1-Specific CD11c+ CD8+ T Cells Display Low PD-1 Expression and Strong Anti-HIV-1 Activity. *Front Immunol* **12**, (2021).
224. Fuchs, T. *et al.* A second combinatorial immune receptor in monocytes/macrophages is based on the TCRγδ. *Immunobiology* **218**, 960–968 (2013).
225. Hiemstra, I. H. *et al.* The identification and developmental requirements of colonic CD169 $^{+}$ macrophages. *Immunology* **142**, 269–278 (2014).
226. Gautier, E. L. *et al.* Gene-expression profiles and transcriptional regulatory pathways that underlie the identity and diversity of mouse tissue macrophages. *Nat Immunol* **13**, 1118–1128 (2012).
227. Lastrucci, C. *et al.* Tuberculosis is associated with expansion of a motile, permissive and immunomodulatory CD16+ monocyte population via the IL-10/STAT3 axis. *Cell Res* **25**, 1333–1351 (2015).
228. Arhel, N. *et al.* The inability to disrupt the immunological synapse between infected human T cells and APCs distinguishes HIV-1 from most other primate lentiviruses. *Journal of Clinical Investigation* (2009) doi:10.1172/JCI38994.
229. Hladik, F. & Hope, T. J. HIV infection of the genital mucosa in women. *Current HIV/AIDS Reports* Preprint at https://doi.org/10.1007/s11904-009-0004-1 (2009).
230. Ono, A. & Freed, E. O. Cell-Type-Dependent Targeting of Human Immunodeficiency Virus Type 1 Assembly to the Plasma Membrane and the Multivesicular Body. *J Virol* **78**, 1552–1563 (2004).
231. Rosas-Taraco, A. G., Arce-Mendoza, A. Y., Caballero-Olín, G. & Salinas-Carmona, M. C. *Mycobacterium tuberculosis* Upregulates Coreceptors CCR5 and CXCR4 While HIV Modulates CD14 Favoring Concurrent Infection. *AIDS Res Hum Retroviruses* **22**, 45–51 (2006).
232. Xu, Z., Padmore, R., Faught, C., Duffet, L. & Burns, B. F. Langerhans cell sarcoma with an aberrant cytoplasmic CD3 expression. *Diagn Pathol* **7**, 128 (2012).
233. HoWangYin, K.-Y. *et al.* Proper Regrafting of Ig-Like Transcript 2 after Trogocytosis Allows a Functional Cell–Cell Transfer of Sensitivity. *The Journal of Immunology* **186**, 2210–2218 (2011).
234. Daubeuf, S., Lindorfer, M. A., Taylor, R. P., Joly, E. & Hudrisier, D. The Direction of Plasma Membrane Exchange between Lymphocytes and Accessory Cells by Trogocytosis Is Influenced by the Nature of the Accessory Cell. *The Journal of Immunology* **184**, 1897–1908 (2010).

235. Camara, A. *et al.* CD169 $^{+}$ macrophages in lymph node and spleen critically depend on dual RANK and LTbetaR signaling. *Proceedings of the National Academy of Sciences* **119**, (2022).
236. ELORANTA & ALM. Splenic Marginal Metallophilic Macrophages and Marginal Zone Macrophages are the Major Interferon-?/? Producers in Mice upon Intravenous Challenge with Herpes Simplex Virus. *Scand J Immunol* **49**, 391–394 (1999).
237. Klaas, M. *et al.* Sialoadhesin Promotes Rapid Proinflammatory and Type I IFN Responses to a Sialylated Pathogen, *Campylobacter jejuni*. *The Journal of Immunology* **189**, 2414–2422 (2012).
238. Shaabani, N. *et al.* CD169+ macrophages regulate PD-L1 expression via type I interferon and thereby prevent severe immunopathology after LCMV infection. *Cell Death Dis* **7**, e2446–e2446 (2016).
239. Jans, J. *et al.* Siglec-1 inhibits RSV-induced interferon gamma production by adult T cells in contrast to newborn T cells. *Eur J Immunol* **48**, 621–631 (2018).
240. Jobe, O., Kim, J. & Rao, M. The role of Siglec-1 in HIV-1/macrophage interaction. *Macrophage (Houst)* **3**, (2016).
241. Lama, J. & Planelles, V. Host factors influencing susceptibility to HIV infection and AIDS progression. *Retrovirology* **4**, 52 (2007).
242. Looker, K. J. *et al.* Effect of HSV-2 infection on subsequent HIV acquisition: an updated systematic review and meta-analysis. *Lancet Infect Dis* **17**, 1303–1316 (2017).
243. Martin, M. P. *et al.* Association of DC-SIGN Promoter Polymorphism with Increased Risk for Parenteral, but Not Mucosal, Acquisition of Human Immunodeficiency Virus Type 1 Infection. *J Virol* **78**, 14053–14056 (2004).
244. Pawlak, E. N., Dirk, B. S., Jacob, R. A., Johnson, A. L. & Dikeakos, J. D. The HIV-1 accessory proteins Nef and Vpu downregulate total and cell surface CD28 in CD4+ T cells. *Retrovirology* **15**, 6 (2018).
245. Swigut, T. Mechanism for down-regulation of CD28 by Nef. *EMBO J* **20**, 1593–1604 (2001).
246. Prévost, J. *et al.* Incomplete Downregulation of CD4 Expression Affects HIV-1 Env Conformation and Antibody-Dependent Cellular Cytotoxicity Responses. *J Virol* **92**, (2018).
247. Arhel, N. & Kirchhoff, F. Host proteins involved in HIV infection: New therapeutic targets. *Biochimica et Biophysica Acta - Molecular Basis of Disease* Preprint at https://doi.org/10.1016/j.bbadis.2009.12.003 (2010).
248. Murray, S. M., Zhang, Y., Douek, D. C. & Sekaly, R. P. Myeloid Cells Enriched for a Dendritic Cell Population From People Living With HIV Have Altered Gene Expression Not Restored by Antiretroviral Therapy. *Front Immunol* **11**, (2020).
249. Bazil, V. & Strominger, J. L. Shedding as a mechanism of down-modulation of CD14 on stimulated human monocytes. *J Immunol* **147**, 1567–74 (1991).
250. Labeta, M. O., Durieux, J.-J., Fernandez, N., Herrmann, R. & Ferrara, P. Release from a human monocyte-like cell line of two different soluble forms of the lipopolysaccharide receptor, CD14. *Eur J Immunol* **23**, 2144–2151 (1993).
251. Murray, E. J., Burden, F., Horscroft, N., Smith-Burchnell, C. & Westby, M. Knockdown of USP18 increases alpha 2a interferon signaling and induction of interferon-stimulating genes but does not increase antiviral activity in Huh7 cells. *Antimicrob Agents Chemother* (2011) doi:10.1128/AAC.00644-11.
252. Ramakrishnan, M. A. Determination of 50% endpoint titer using a simple formula. *World J Virol* **5**, 85 (2016).
253. Lei, C., Yang, J., Hu, J. & Sun, X. On the Calculation of TCID50 for Quantitation of Virus Infectivity. *Virol Sin* **36**, 141–144 (2021).

APPENDIX

A1. Gating strategy and Proportions of foreskin myeloid cell groups

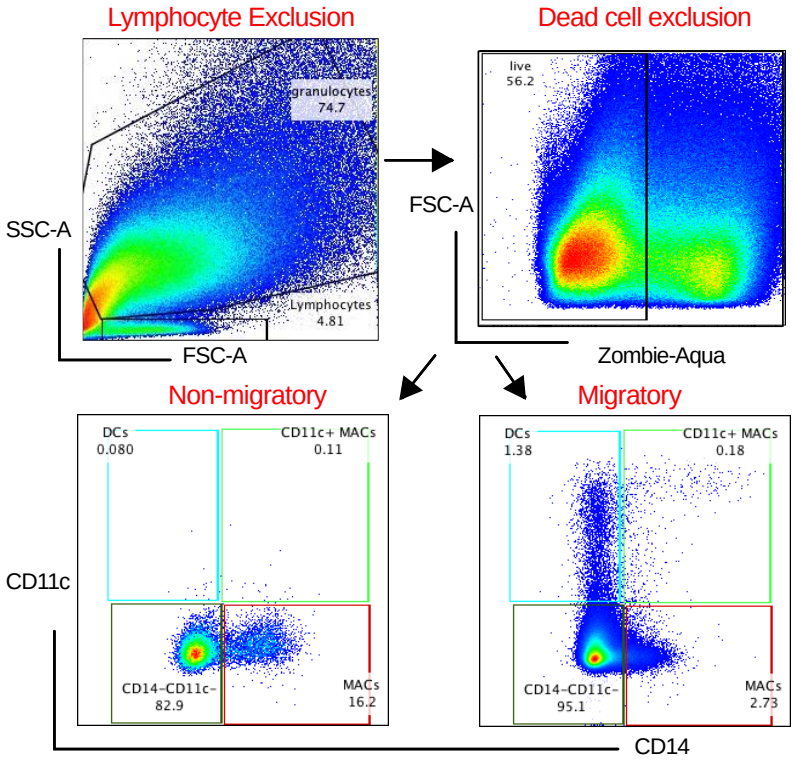

Figure A1. ***Gating strategy used to distinguish migratory and non-migratory myeloid cells.*** *Non-migratory foreskin myeloid cells are CD14+CD11c- while migratory myeloid cells are i) CD11c+CD14+, ii) CD11c+CD14- and CD11c-CD14+*

A2. Proportions of migratory and non-migratory LCs in the inner and outer foreskin

Compartment

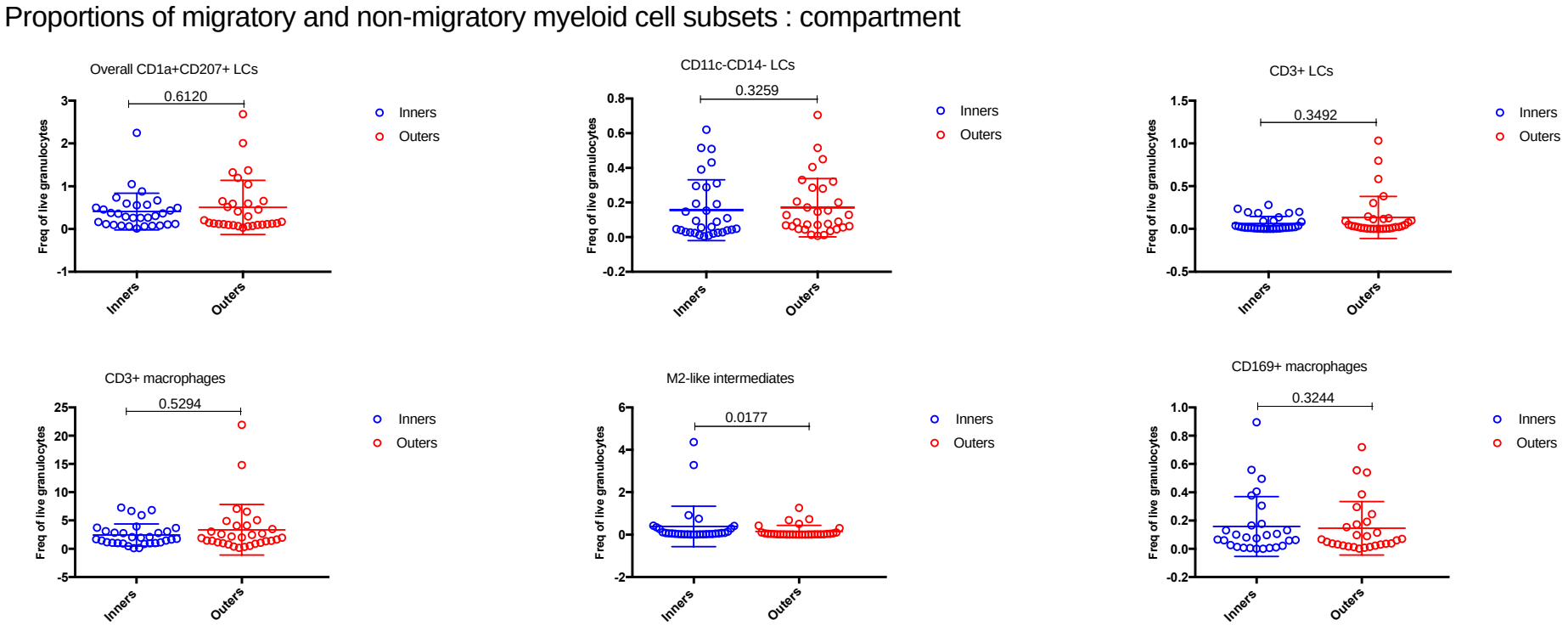

Figure A2. ***Proportions and distribution of migratory and non-migratory LCs in the inner and outer foreskin.*** *Proportions of LC by compartment and assay* ***(i)*** *Proportions of migratory vs non-migratory LCs* ***(ii)*** *Proportions of migratory and non-migratory LCs in the inner vs outer foreskin (n=31). Column Statistics were generated using the Shapiro Wilk test to test for Gaussian Distribution; non-parametric paired t-tests with the Wilcoxon test were used at 95 % CI of difference*

A3. Assay

Proportions of migratory and non-migratory myeloid cell subsets : assay

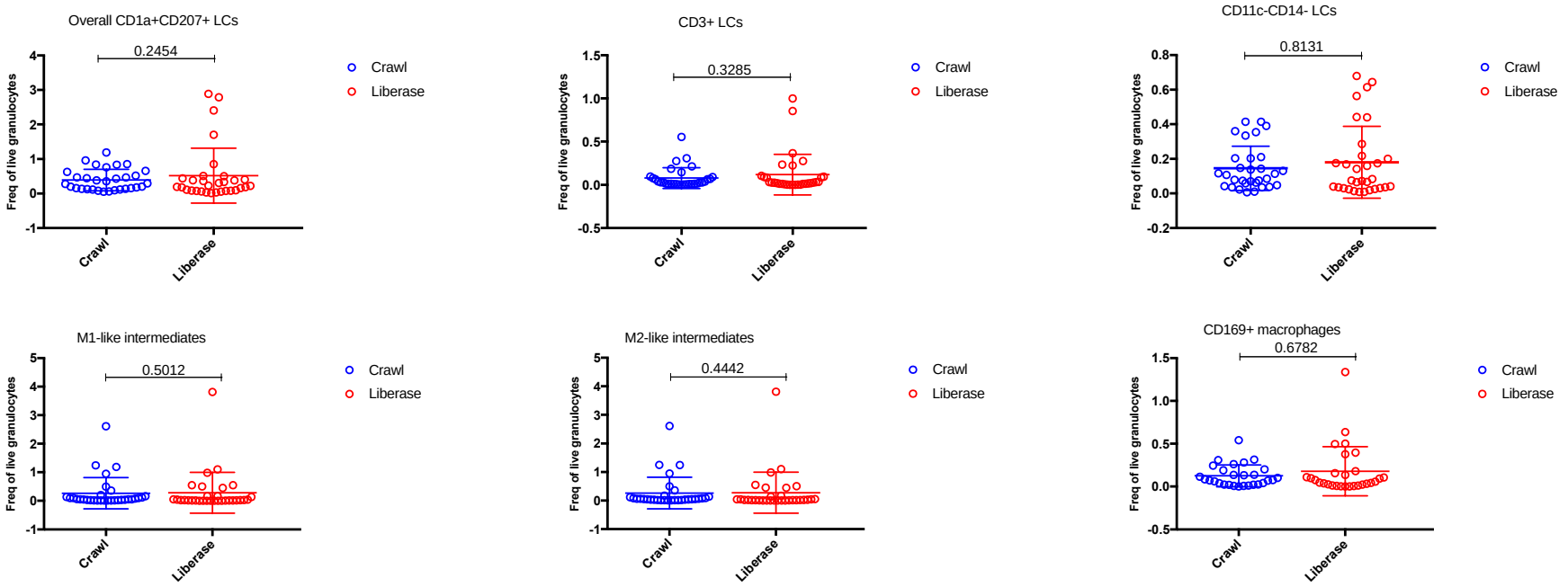

Figure A3. ***Proportions and distribution of migratory and non-migratory LCs in the inner and outer foreskin.*** *Proportions of LC by compartment and assay* ***(i)*** *Proportions of migratory vs non-migratory LCs* ***(ii)*** *Proportions of migratory and non-migratory LCs in the inner vs outer foreskin (n=31). Column Statistics were generated using the Shapiro Wilk test to test for Gaussian Distribution; non-parametric paired t-tests with the Wilcoxon test were used at 95 % CI of difference.*

A4. LC subsets: Quantification of CD4+CCR5+ in migratory and non-migratory I/O FS cells

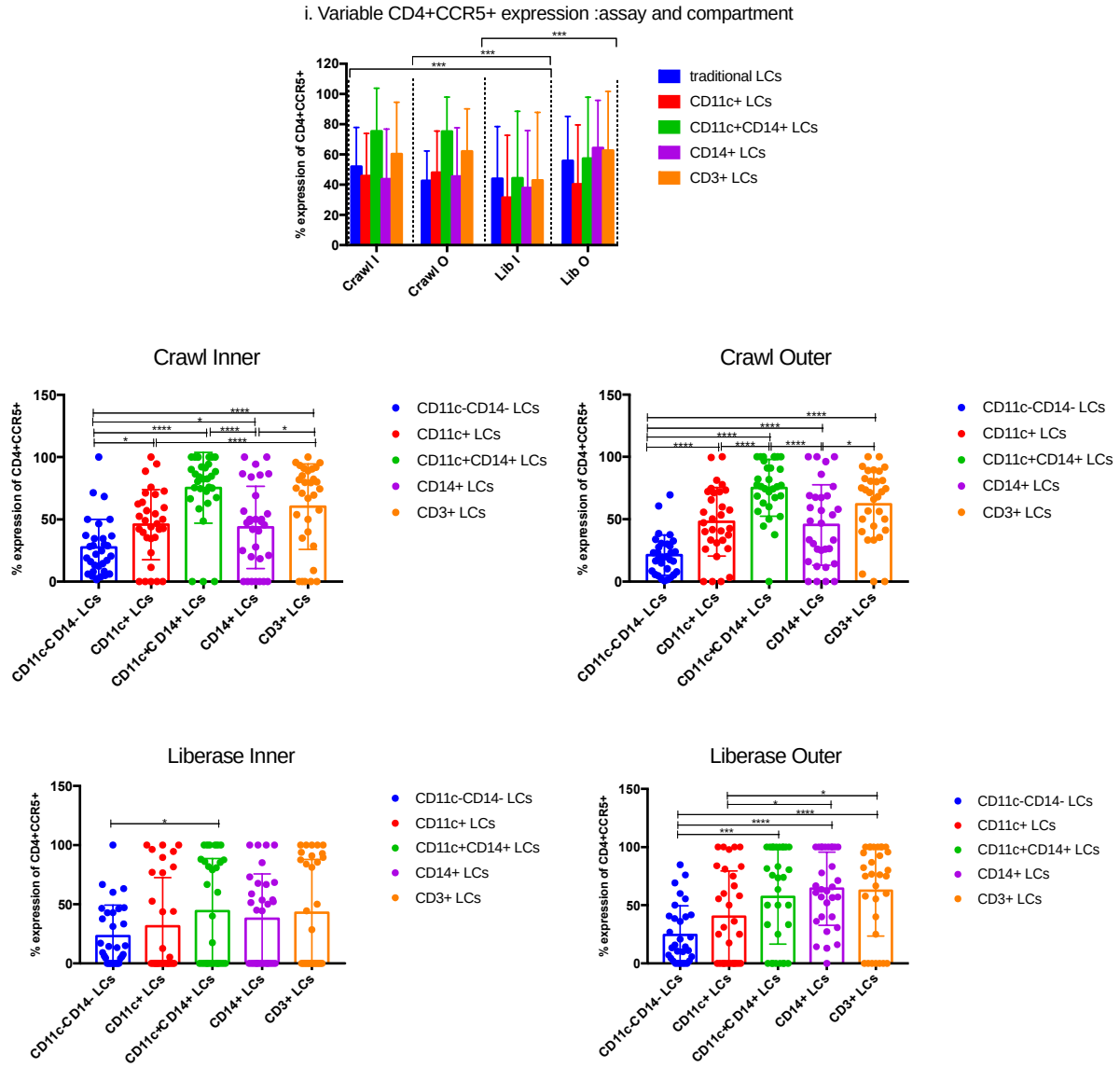

Figure A4. ***Proportions of markers of HIV susceptibility in migratory and non-migratory foreskin Langerhans Cells in the inner and outer foreskin.*** *Flow Cytometry quantification and measurement of HIV susceptibility in foreskin LCs.* ***(i)*** *Proportions of CD4+CCR5+ in migratory and non-migratory LC subsets in the inner and outer foreskin* ***(ii-v)*** *Proportions of CD4+CCR5+ in migratory and non-migratory foreskin LCs in the different foreskin compartments and isolation methods (n=31) Statistics were generated with two-way ANOVA using the Tukey's multiple comparisons test at 95 % CI of difference and adjusted p values. *p <0.05; **p < 0.01; ***p < 0.001; ****p < 0.0001*

A5. MDS plots: migratory LCs vs non-migratory LCs

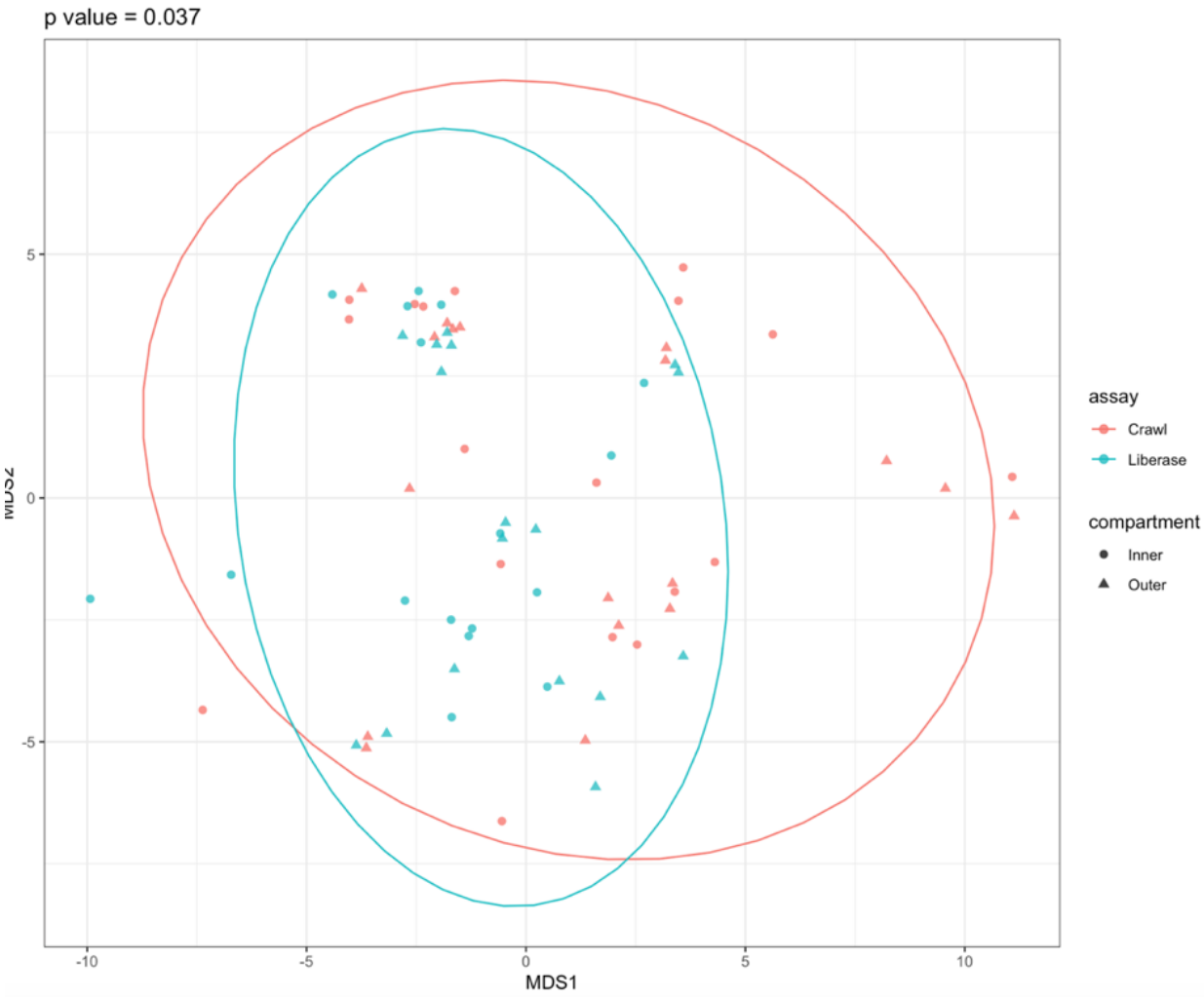

Figure A5. ***Multi-dimensional (MDS) plots showing differences between migratory and non-migratory LCs***

A6. Marker expression histograms per LC cluster

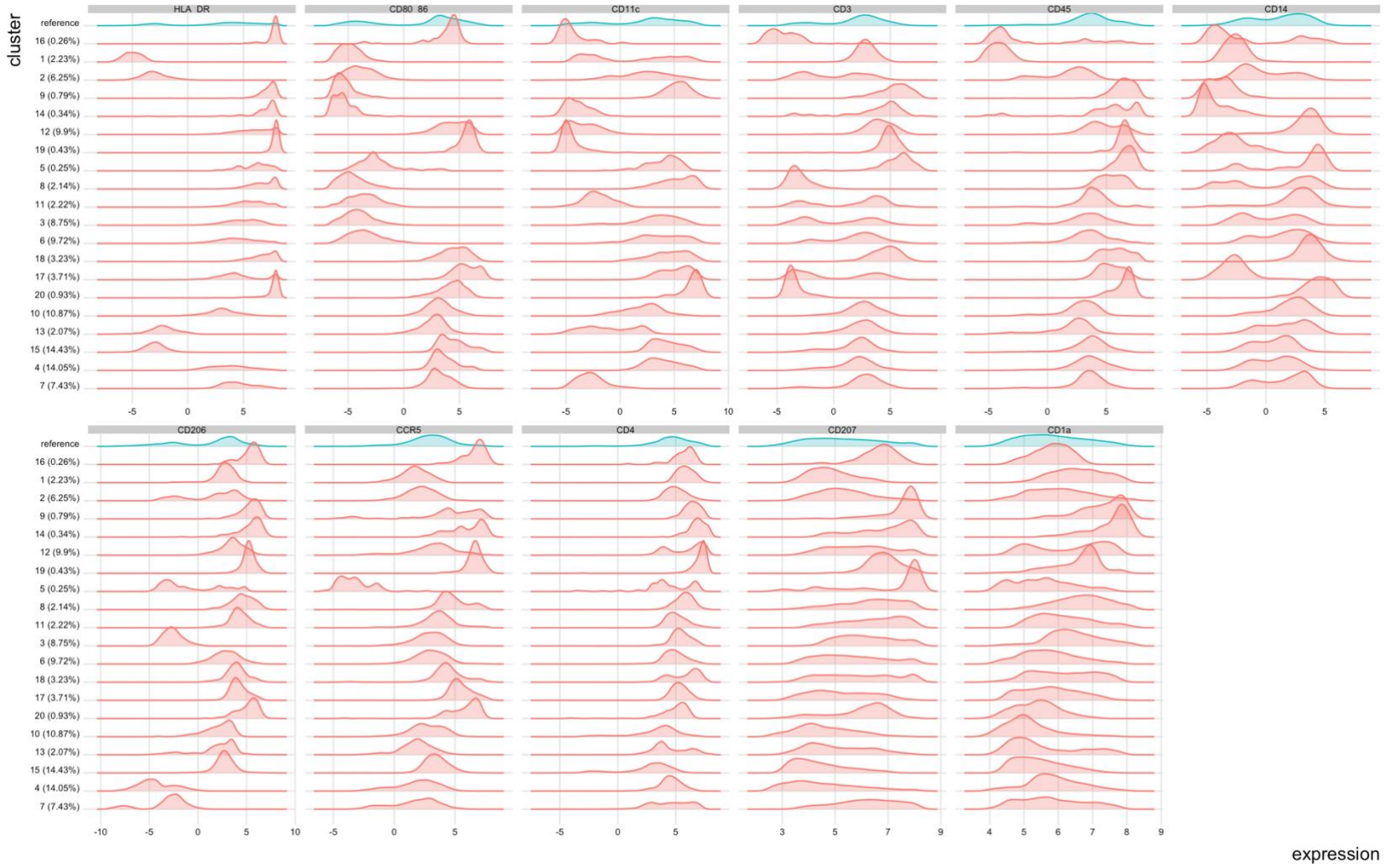

Figure A6. ***Marker expression profiles in 20 different LC clusters***

A7. tSNE plots: migratory vs non-migratory

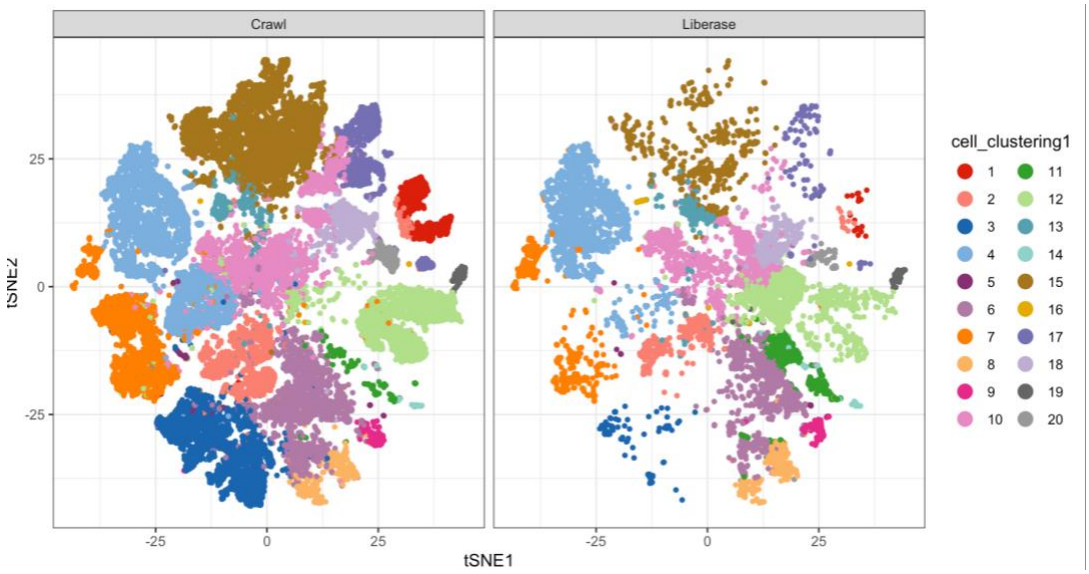

Figure A7. ***Determination of the different sub-populations within the concatenated migratory (Crawl)*** **vs** ***non-migratory (Liberase)*** **foreskin Langerhans Cells,** ***using colored tSNE plots generated by non-biased, computerised clustering.*** *tSNE plots demonstrating the different "Macrophage-like" subsets (clusters) shown in the plot as different colours and demarcated by migration potential (Crawl/Lib).*

A8. tSNE plots: inner vs outer

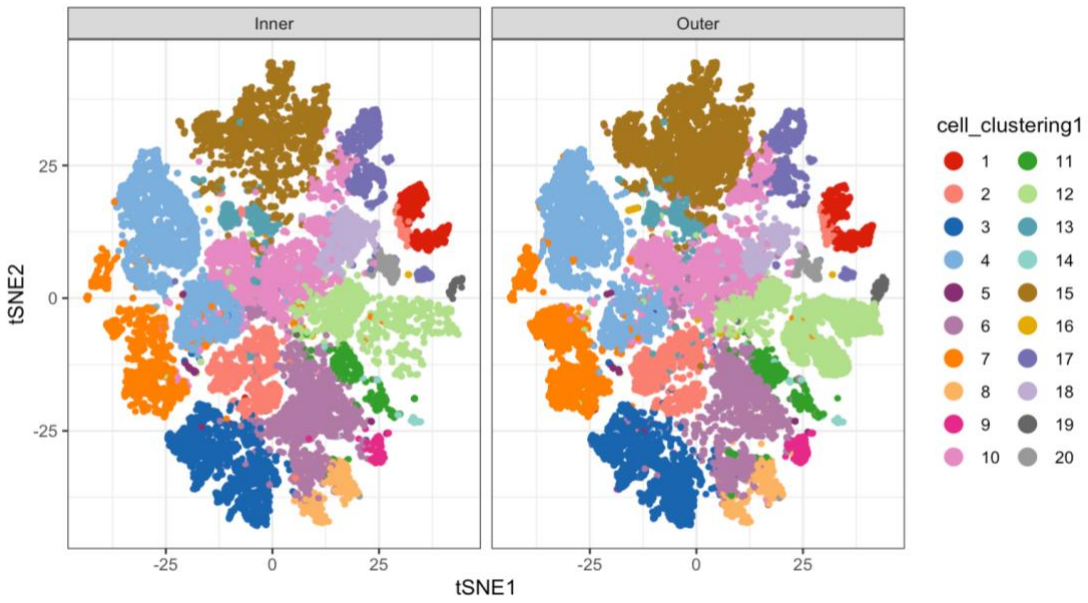

Figure A8. ***Determination of the different sub-populations within the concatenated foreskin Langerhans Cells, in the inner and outer foreskin using colored tSNE plots generated by non-biased, computerised clustering.*** *tSNE plots demonstrating the different "Macrophage-like" subsets (clusters) shown in the plot as different colours and demarcated by compartment(Inner/Outer)*

A9. PCA plots: LC clusters

Figure A9. ***Principal Component Analysis (PCA) plot demonstrating the phenotypic relationships and distances among the different LC clusters***

A10. UMAPs: migratory vs non-migratory LC clusters in the inner vs outer foreskin

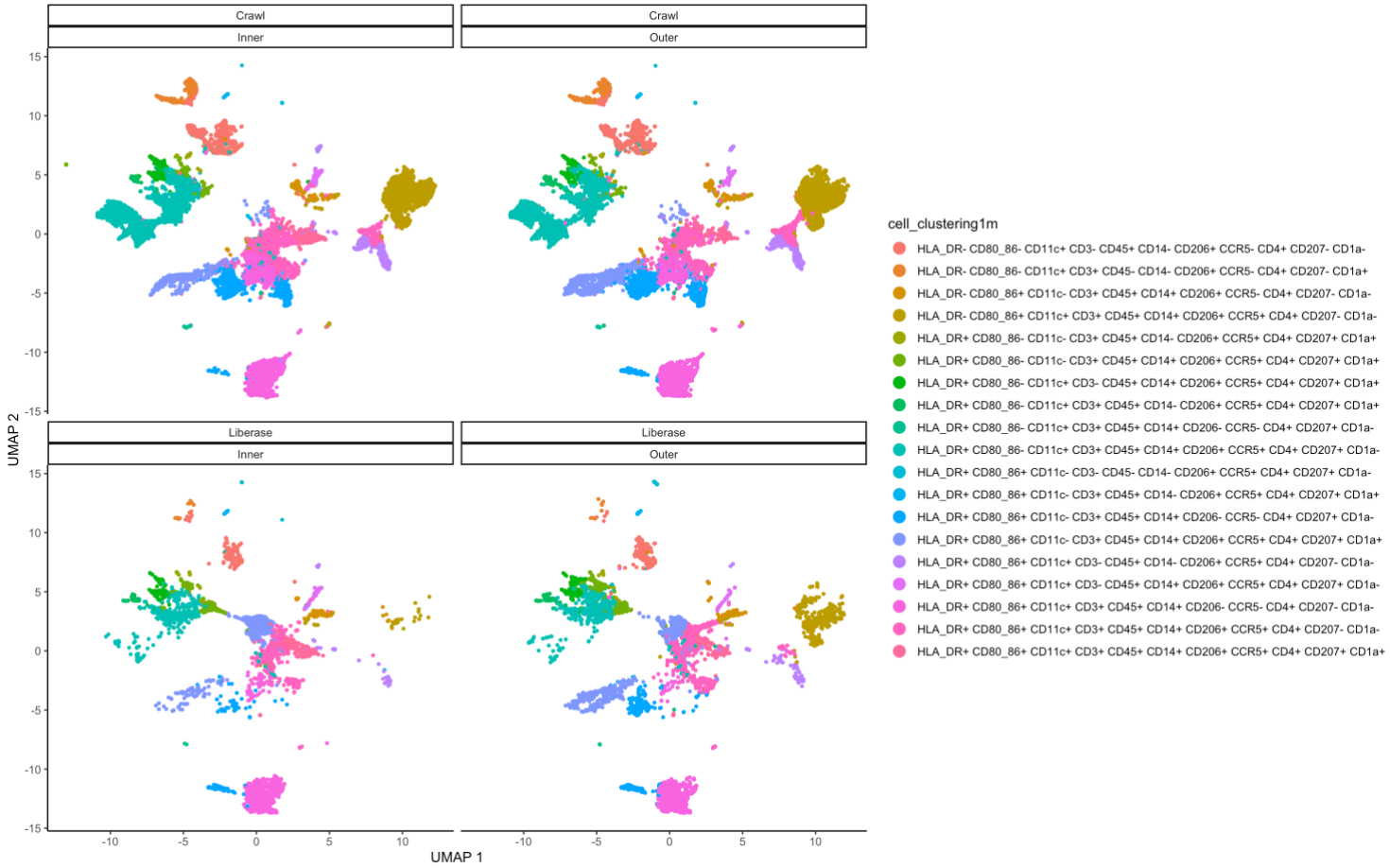

Figure A10. ***UMAPs demonstrating migratory and non-migratory foreskin LC clusters in the inner and outer foreskin***

A11. LC Cluster Abundance

Figure A11. ***Proportions of migratory and non-migratory LC clusters***

A12. LC Cluster QC plots

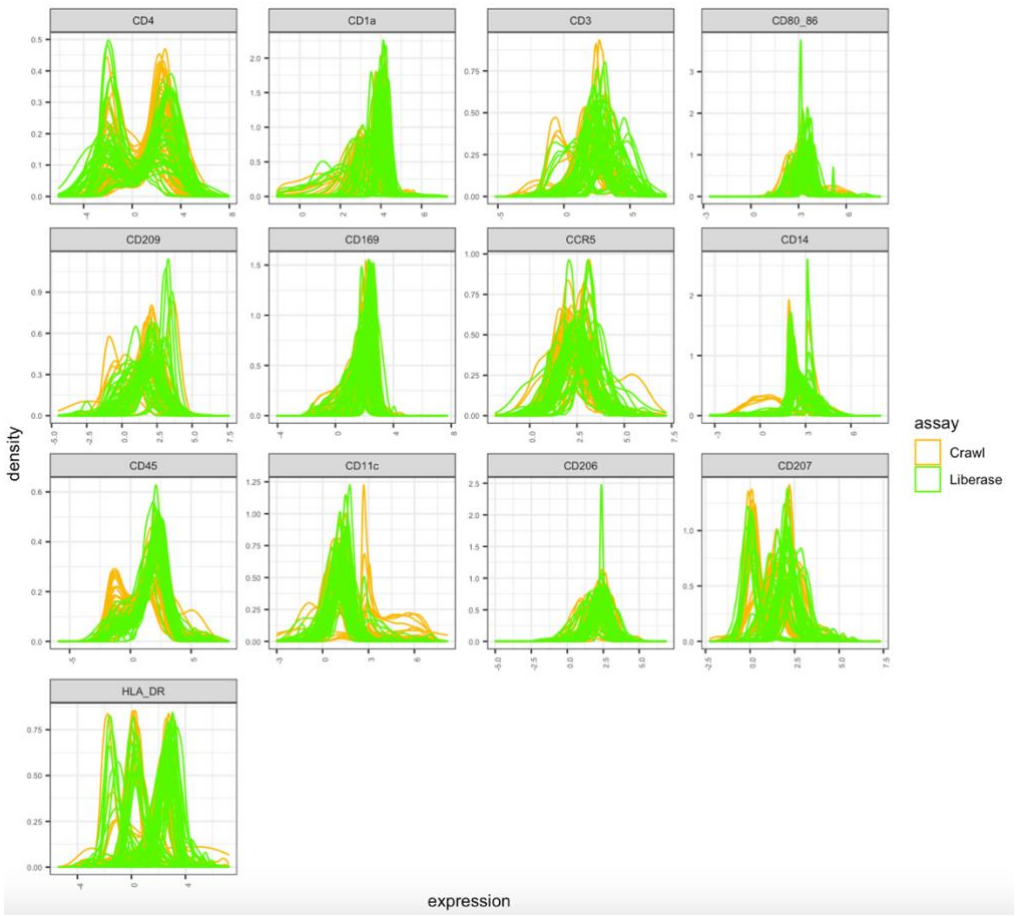

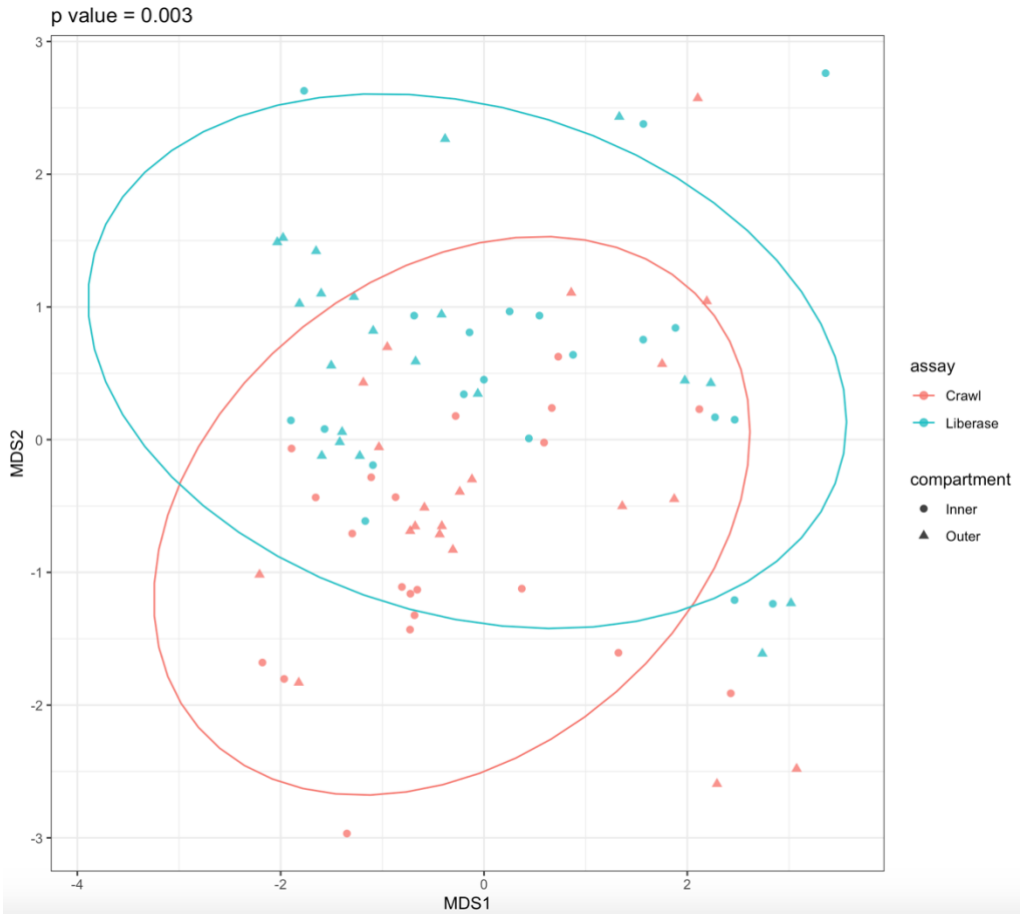

Figure A12. ***Marker expression profiles on concatenated foreskin "Macrophage-like" cells.Multi-dimensional (MDS) plots showing differences between migratory and non-migratory "macrophage-like" cells.*** *Migratory vs non-migratory "macrophage-like" cells*

A13. Non-Redundancy plot: “macrophage-like” cells

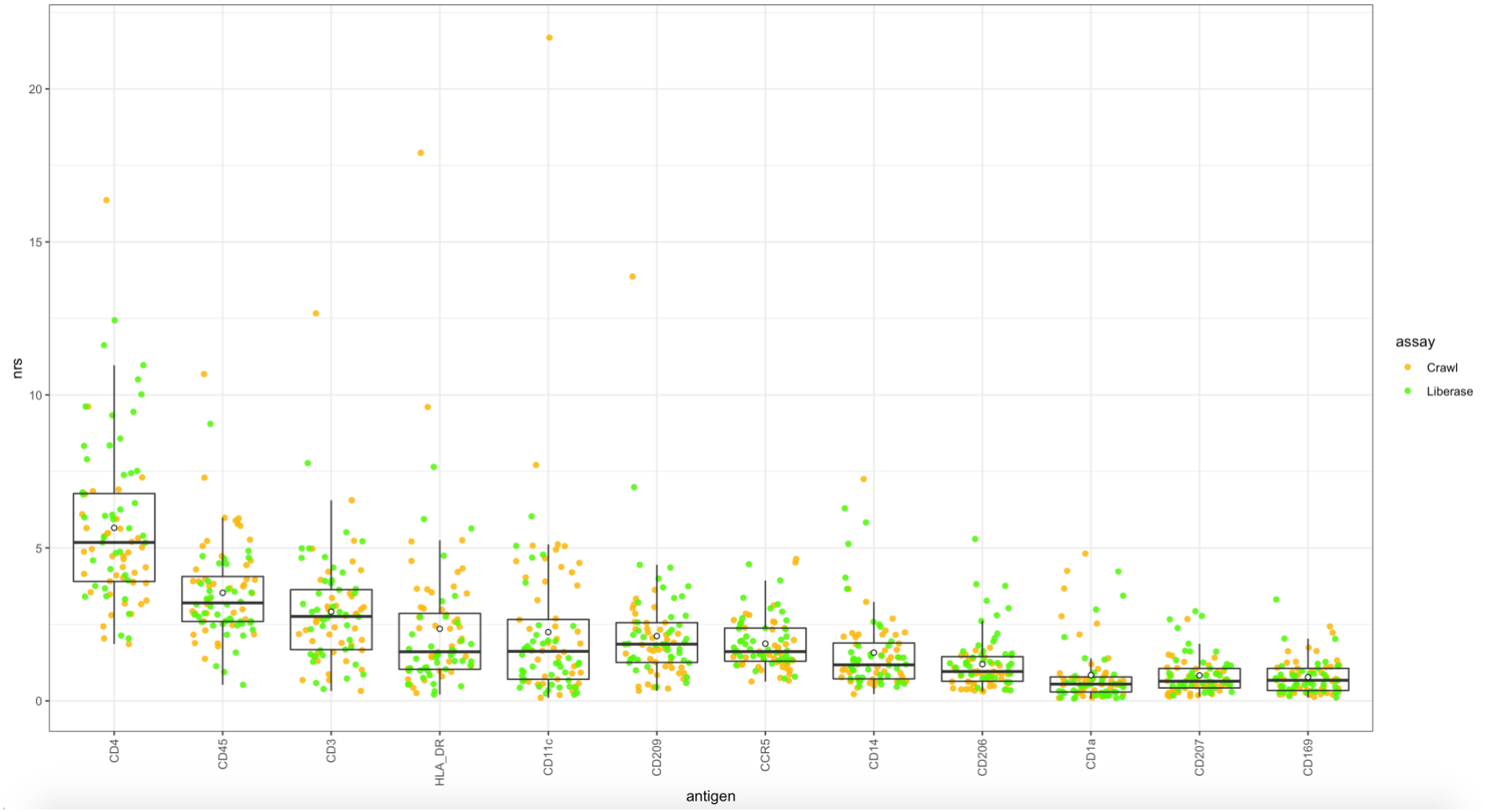

Figure A13. ***NRS plot showing the order of markers driving clustering.***

A14. Histograms: Marker expression per “macrophage-like” cluster

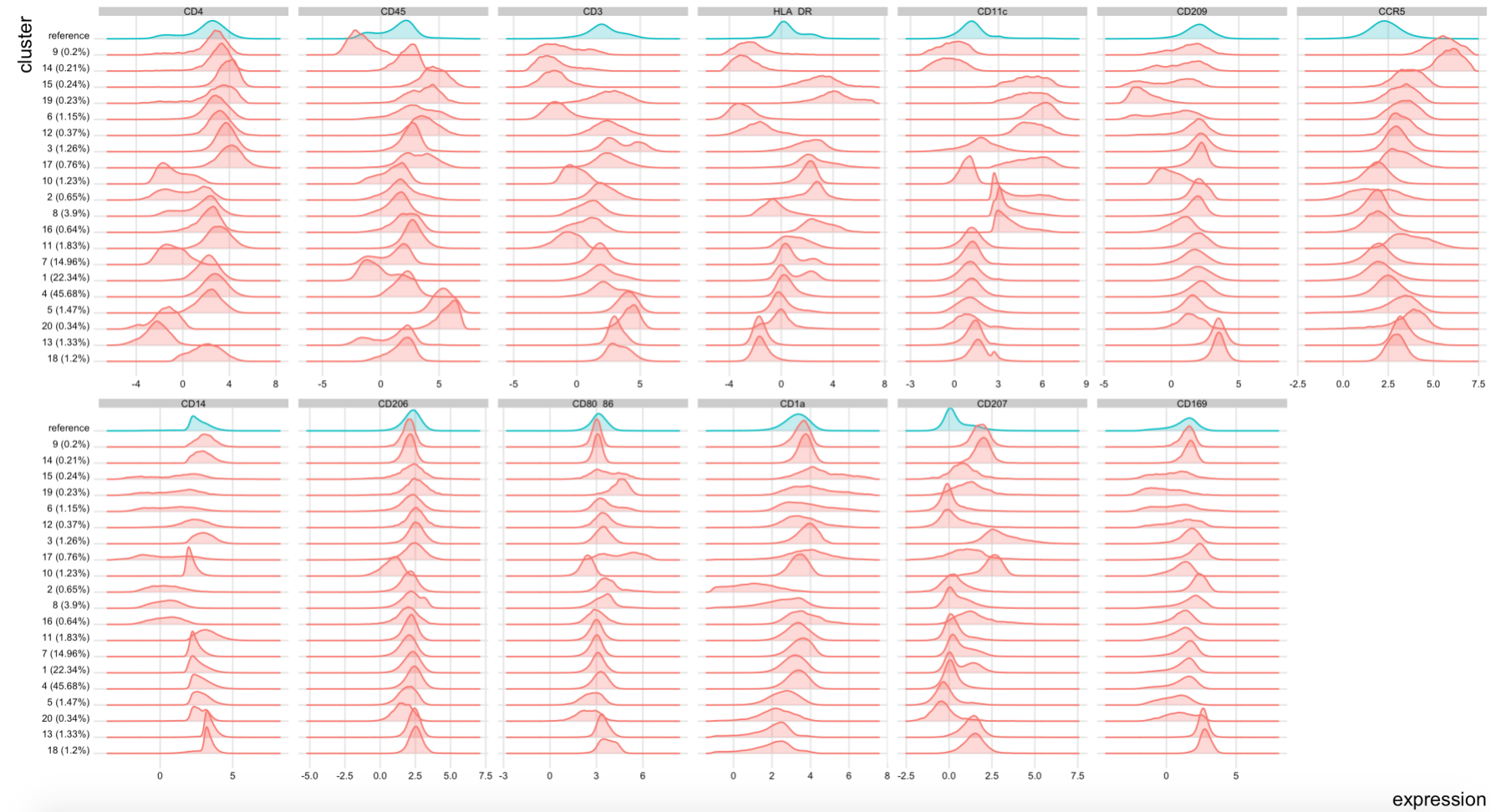

Figure A14. ***Marker expression profiles in 20 different “macrophage-like” clusters***

A15.PCA plot: “macrophage-like” clusters

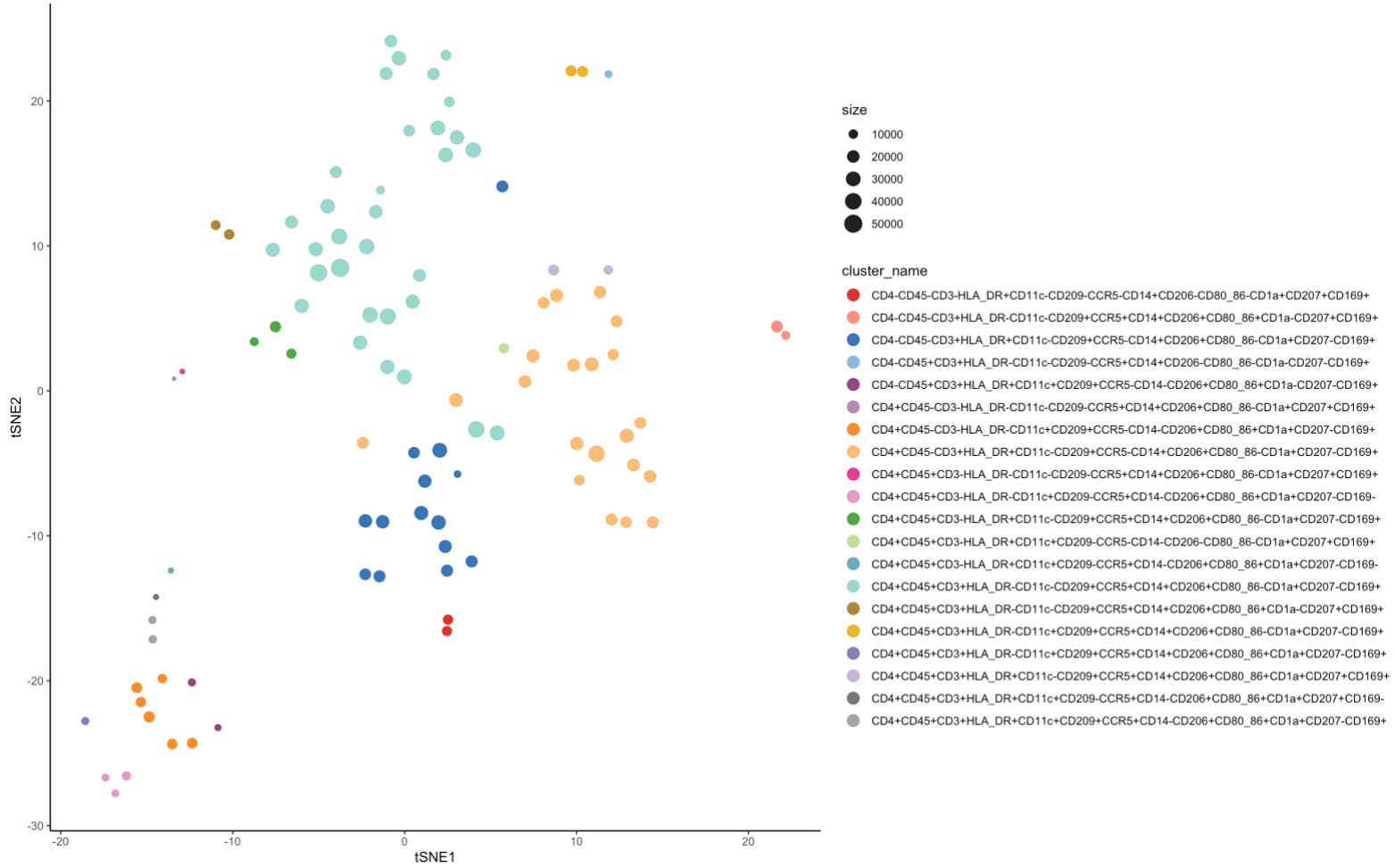

Figure A15. ***Principal Component Analysis (PCA) plot demonstrating the phenotypic relationships and distances among the different “macrophage-like” clusters***

A16. Abundance of migratory and non-migratory “macrophage-like” cells

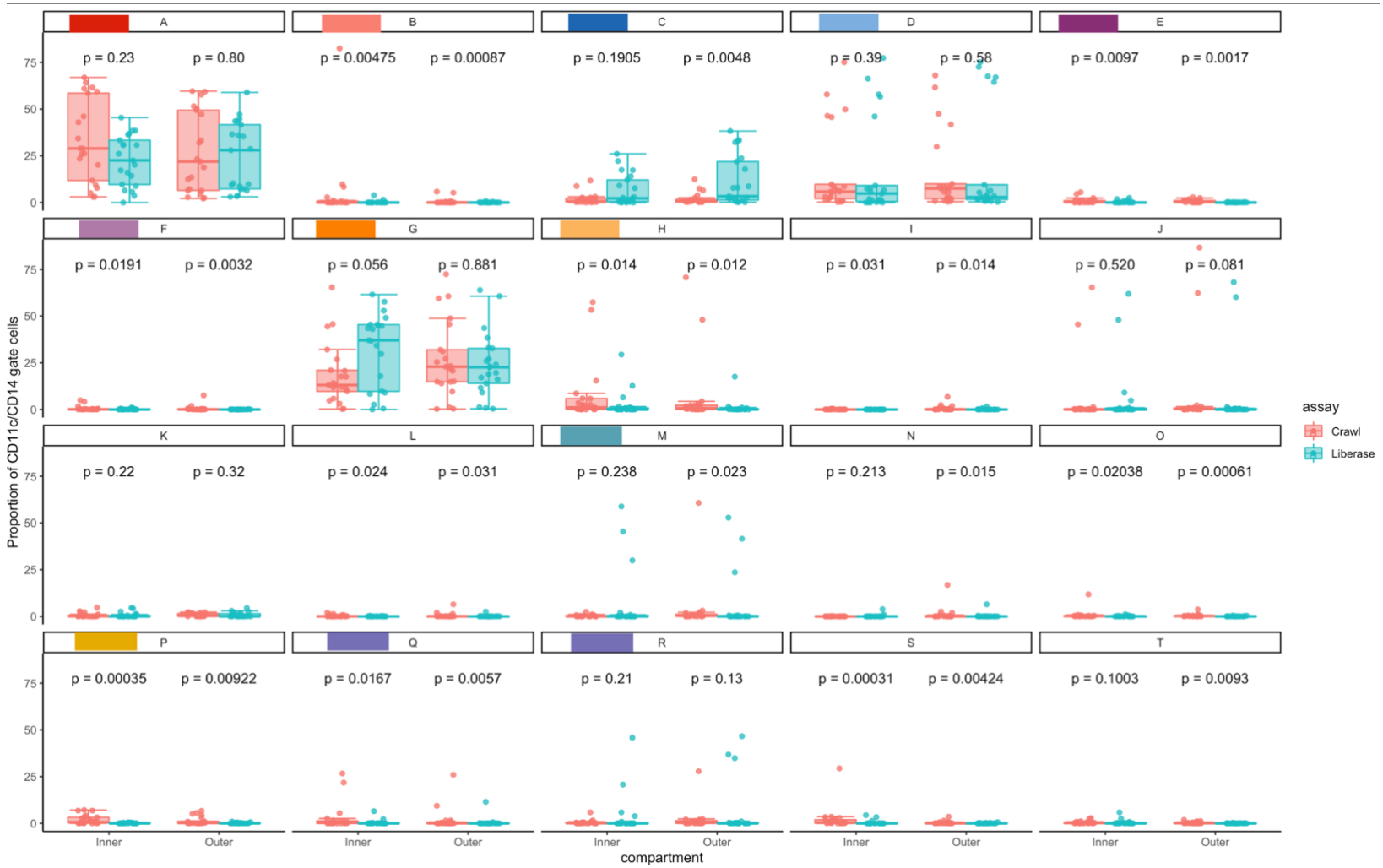

Figure A16. ***Proportions of migratory and non-migratory “macrophage-like” clusters***

Infection

A17. Optimization of Stimulation Conditions

Elimination of CD8+ cells

CD8 depletion and CD4 isolation

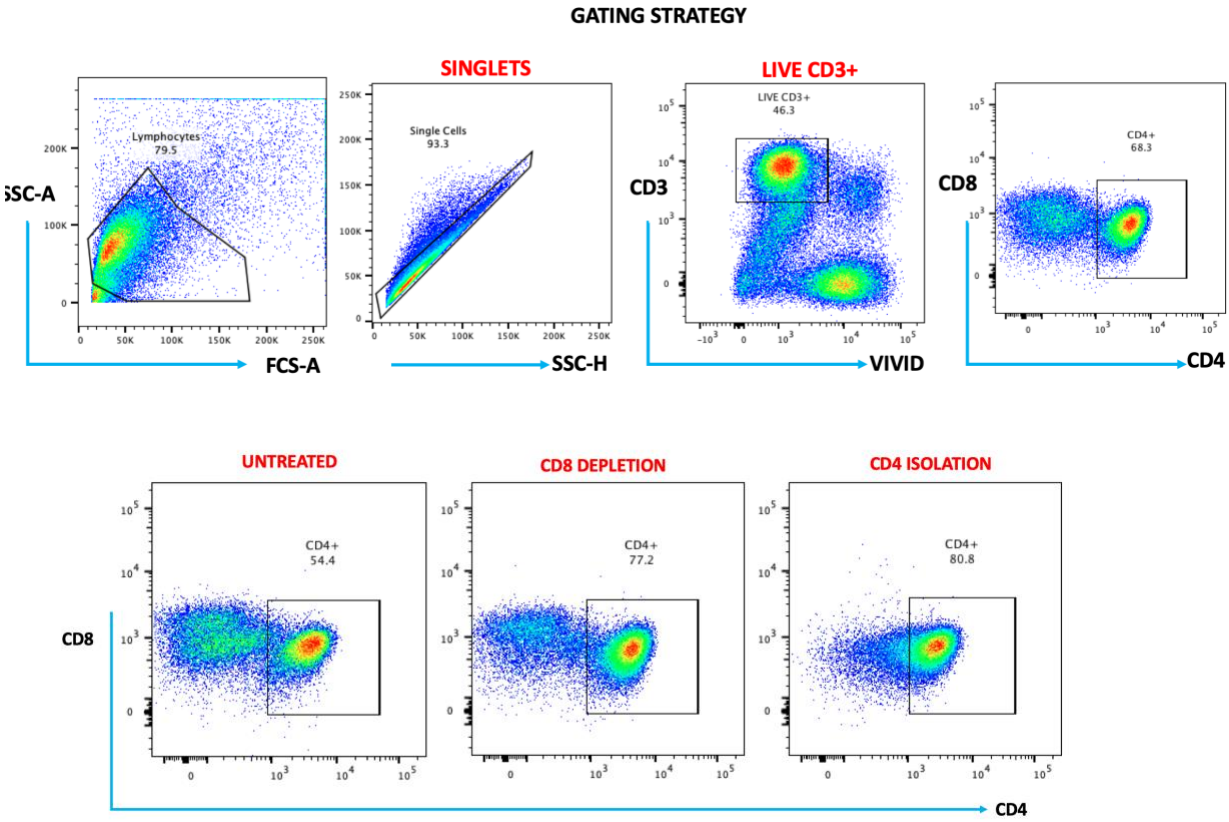

Figure A17. ***CD8 Depletion.*** *Flow plots illustrating PBMCs negatively isolated against CD8+ cells and positively isolated for CD4+ cells*

A18. PBMC Stimulation

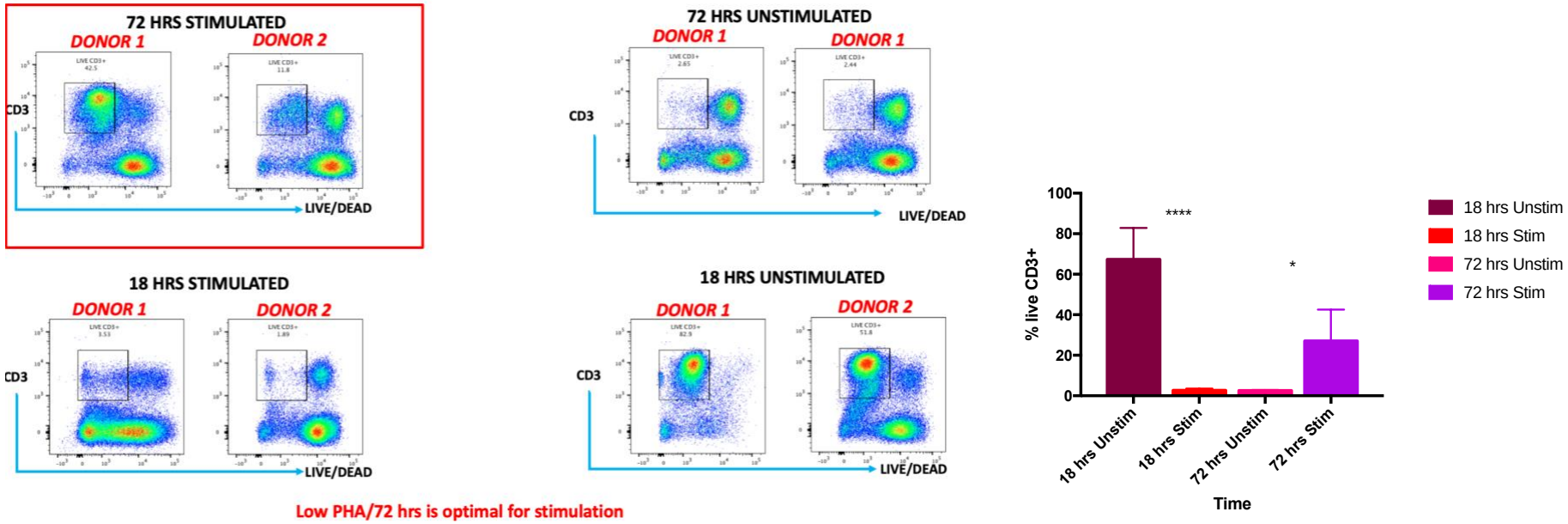

Figure A18. ***Optimisation of stimulation conditions for PBMC infection****. Representative flow cytometry plots showing PBMCs that were stimulated using low (0.5ug/ml) and high (15ug/ml) concentrations of PHA for 18 hours and 72 hours and analysed using flow cytometry. Optimal PBMC stimulation conditions were evaluated using different PHA concentrations at different time-points; 15ug/ml PHA for 18hrs and 0.5ug/ml PHA for 72hrs.*

A19. Determination of $TCID_{50}$, MOIs and incubation periods

Infection of stimulated CD8 depleted PBMCs with different M.O.Is at 24 hrs

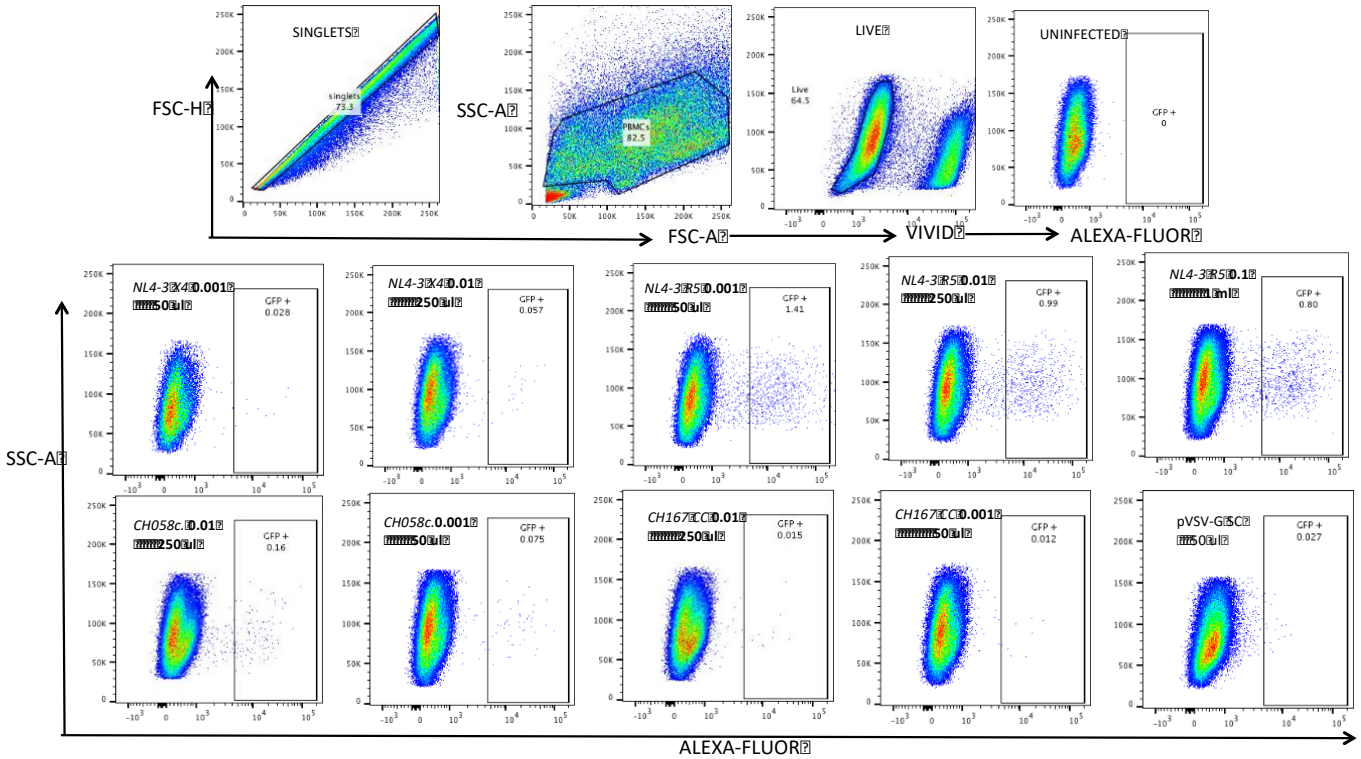

Figure A19. ***Assessment of optimal M.O.I and time-point for PBMC HIV Infection.*** *Representative flow cytometry plots showing proportions of HIV infected GFP+ and mCherry+ PBMCs infected using different* ***viruses*** *(CS108, CS105, CS377, CS642) as well as mCherry tagged (NL4-3-Bal and VSV-G) and different* ***MOIs*** *(0.1, 0.01 and 0.001) at 24 hrs and 72 hours. Statistics were generated using column statistic and non-parametric t-tests with the Wilcox test and exact p values.*

A20. Assessment of HIV inhibition in JLTR-5 cell line

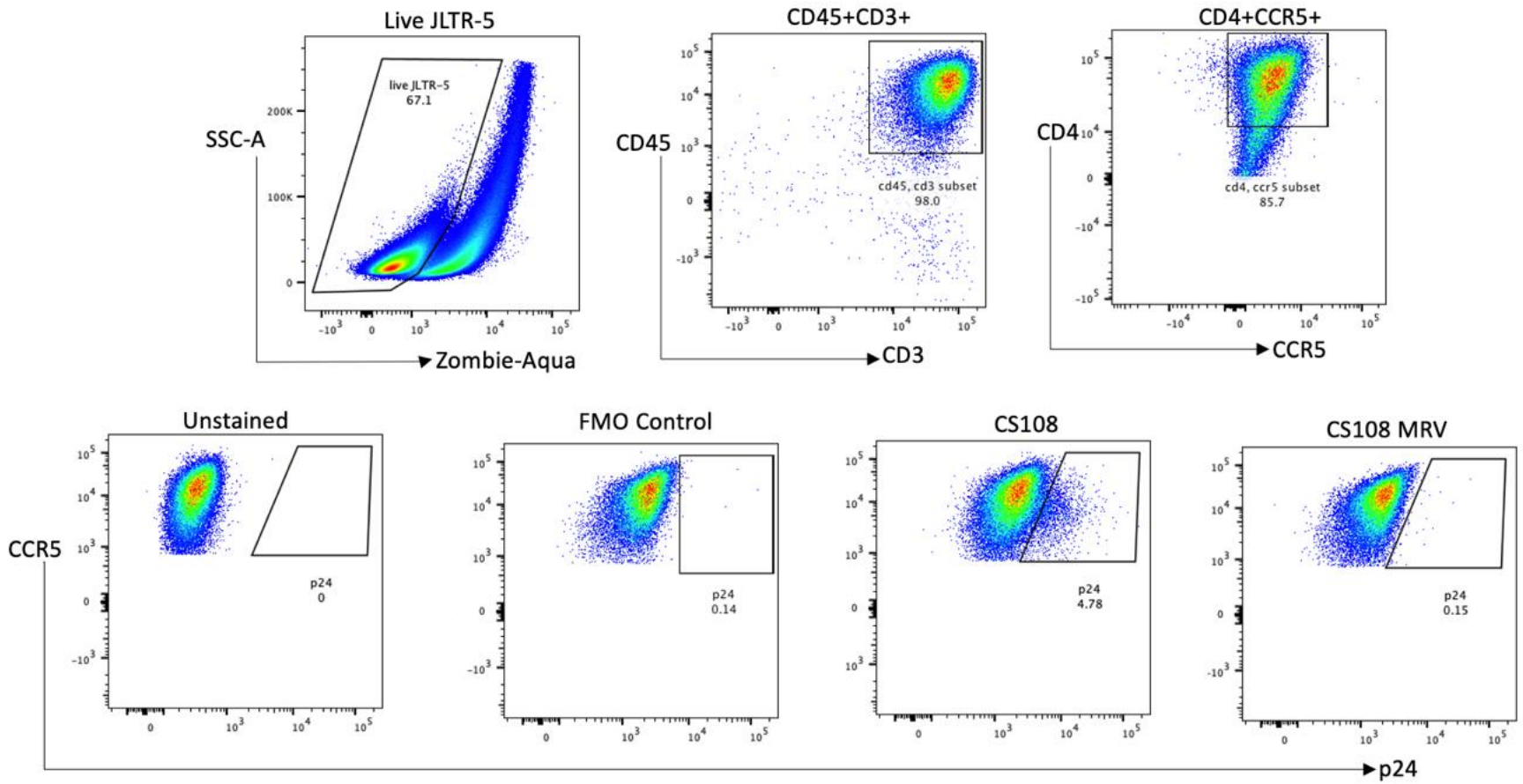

Figure A20. ***Optimisation of maraviroc inhibition against HIV infection of the JLTRG5 cell line.*** *Representative flow cytometry plots demonstrating Maraviroc inhibition against HIV infection of JLTR5 cells.*

A21. Infection of Cell lines

Representative flow cytometry plots

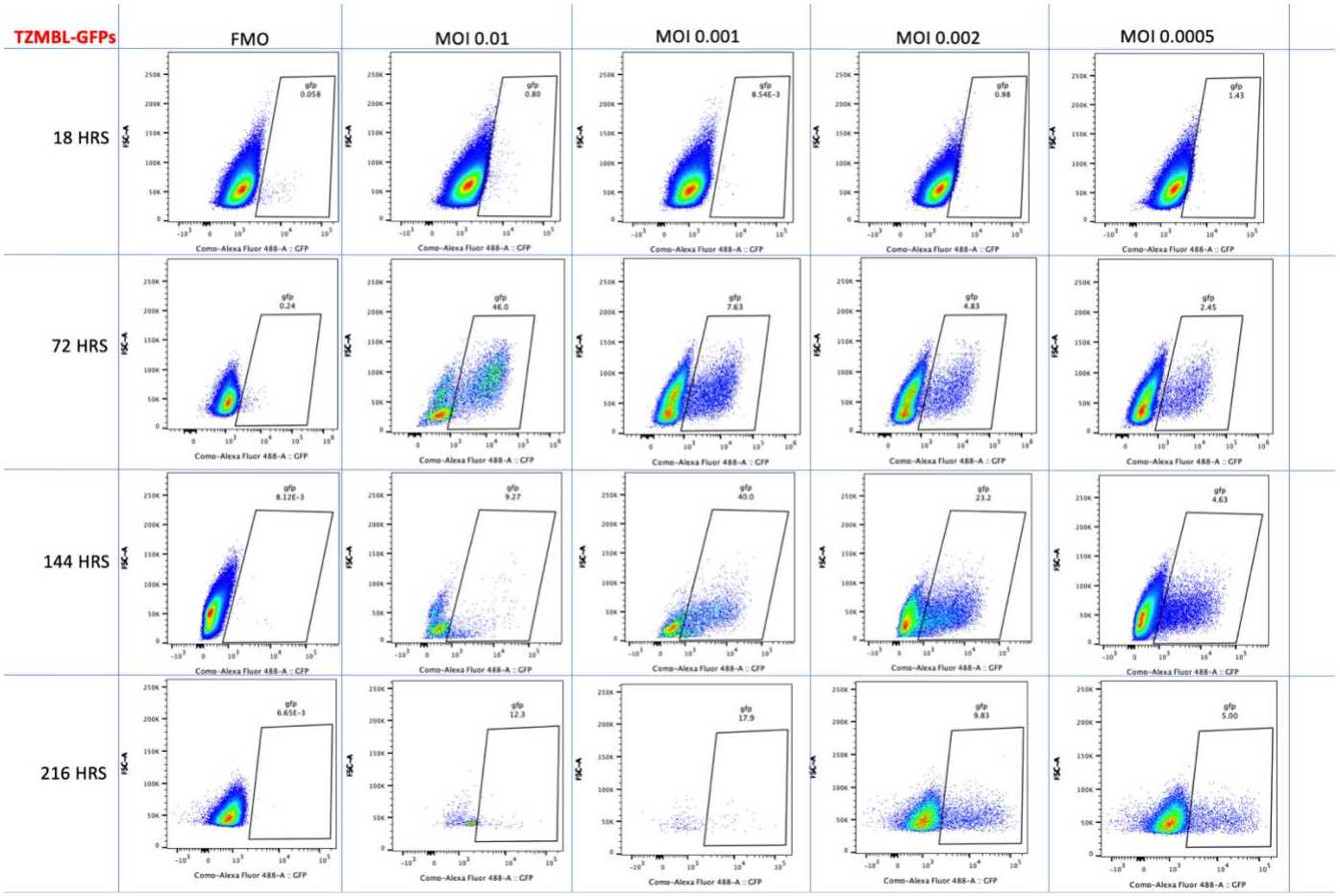

Figure A21. ***Optimisation of HIV infection and method validation in the TZM-GFP cell line.*** *TZM-GFPs were infected using CS108 at four different MOIs over 9 days.*

A22. Infection of foreskin cells

Evidence of HIV infection using drug inhibition

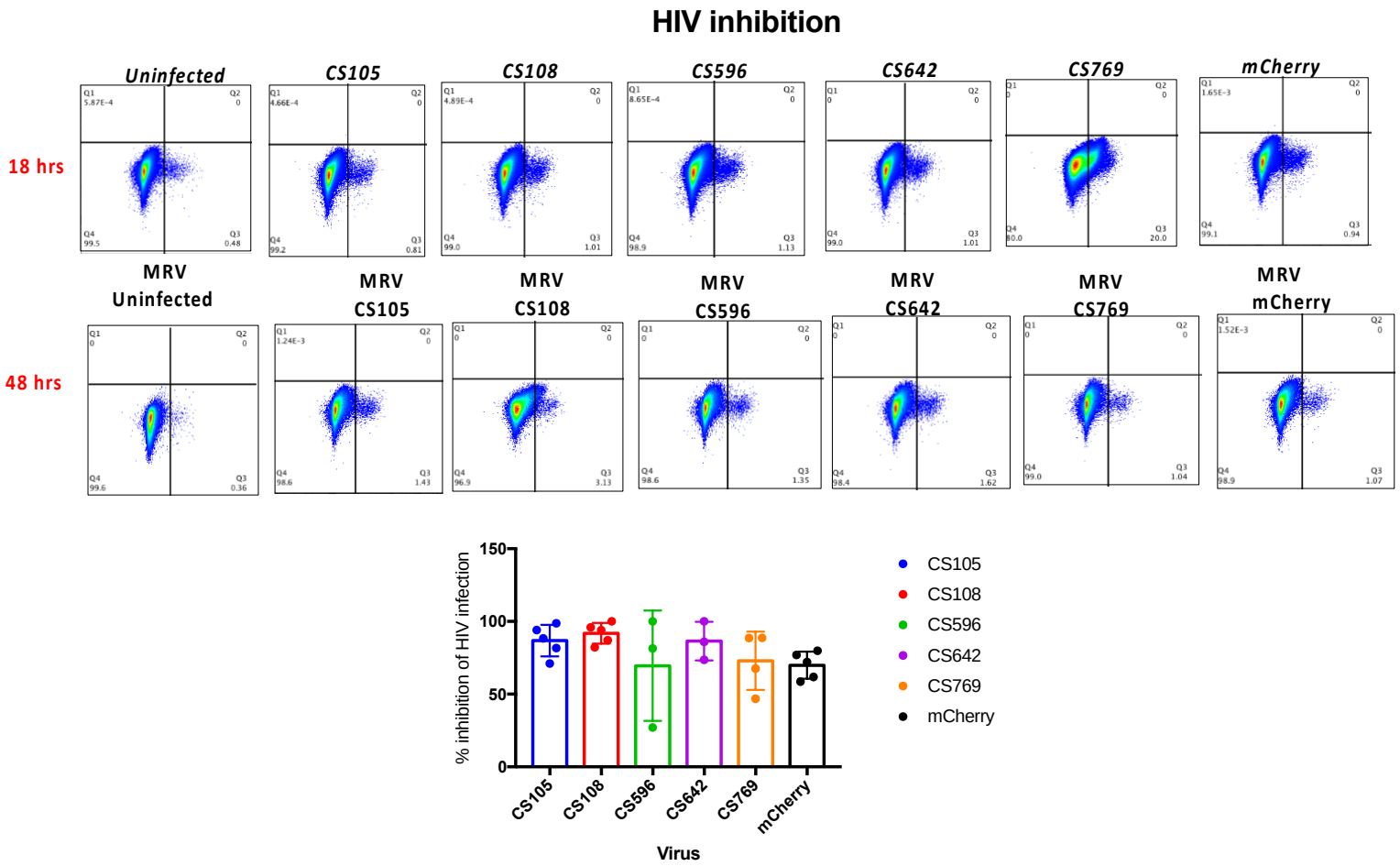

Figure A22. ***Inhibition of HIV infection of foreskin cells using maraviroc****. Representative flow cytometry plots demonstrating HIV inhibition against HIV infection of foreskin granulocytes. Foreskin lymphocytes and granulocytes (big cell gate) were differentially inhibited by maraviroc.*

A23. Representative flow cytometry plots Infection of foreskin cells at 18 hours vs 48 hours

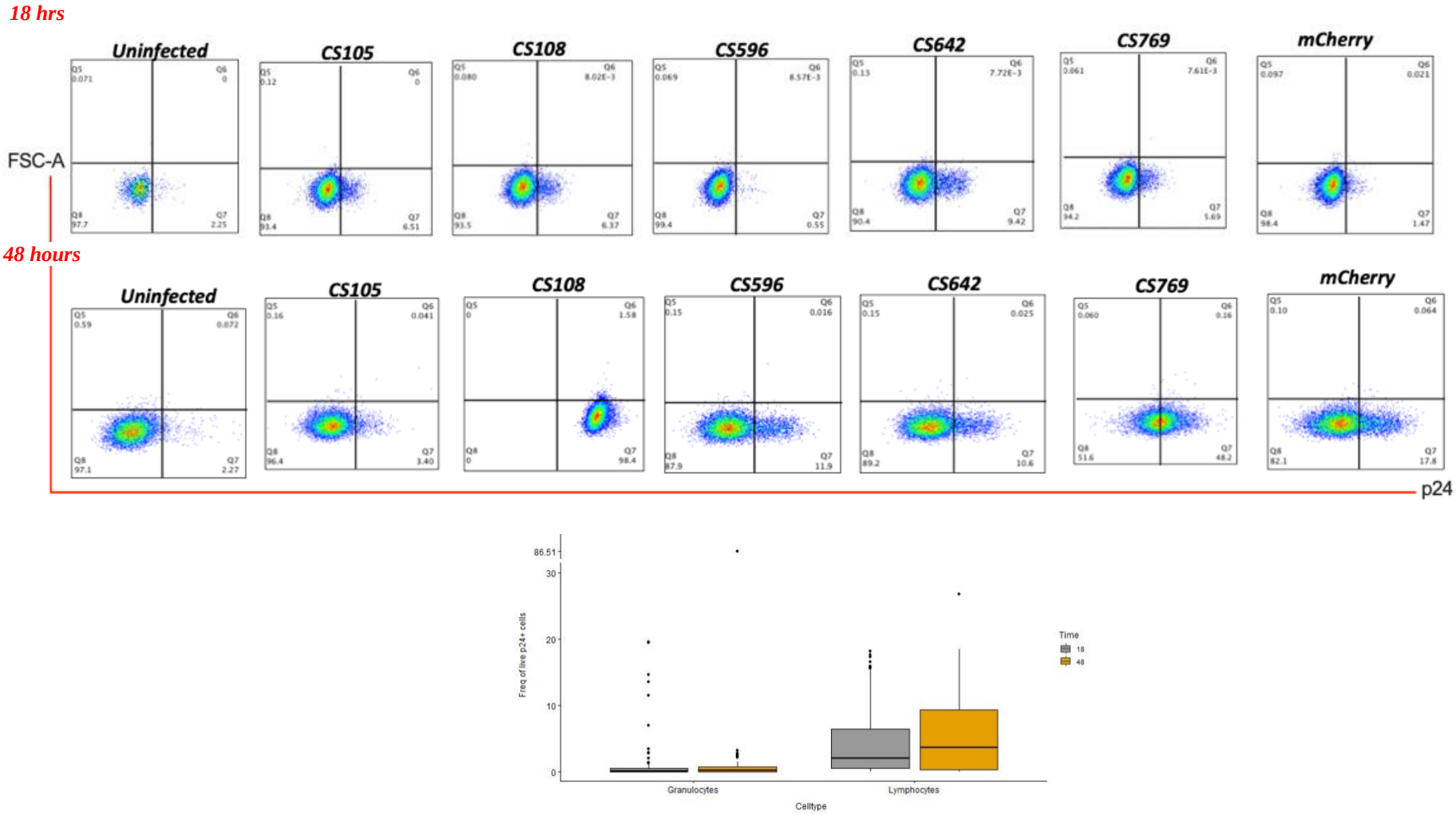

Figure A23. ***Proportions of HIV infected foreskin lymphocytes and granulocytes at 18 and 48 hours****. Foreskin lymphocytes and granulocytes (big cell gate), were infected using different viruses as assessed for infection using flow cytometry at 18 and 48 hours.*

A24. Tropism: foreskin lymphocytes and granulocytes

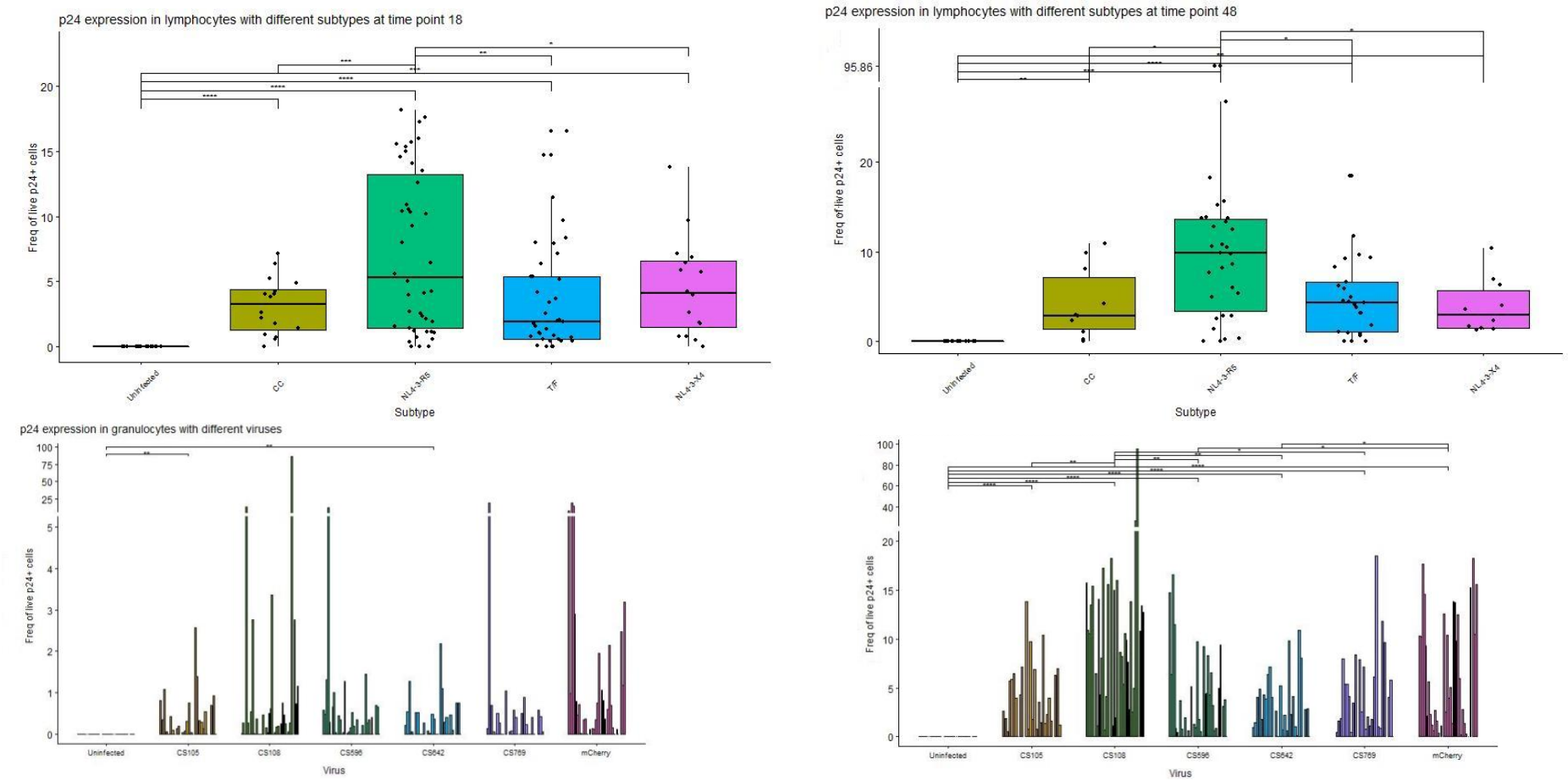

Figure A24. ***Differential infection of foreskin lymphocytes and granulocytes by different HIV strains at 18 and 48 hours.*** *Foreskin lymphocytes and granulocytes were differentially susceptible to varied HIV strains; X4-NL4 -3, R5-NL4-3, transmitted founder Subtype C (TF), chronic infection Subtype C (CC) (CS642), Subtype C CH198 (TF) (CS769). Flow cytometry was used to determine p24 expression which was used as a measure of HIV infection. Statistics were generated Kruskal Wallis using the Bonferroni test and adjusted p values*

A25. Tropism: foreskin lymphocytes and granulocytes

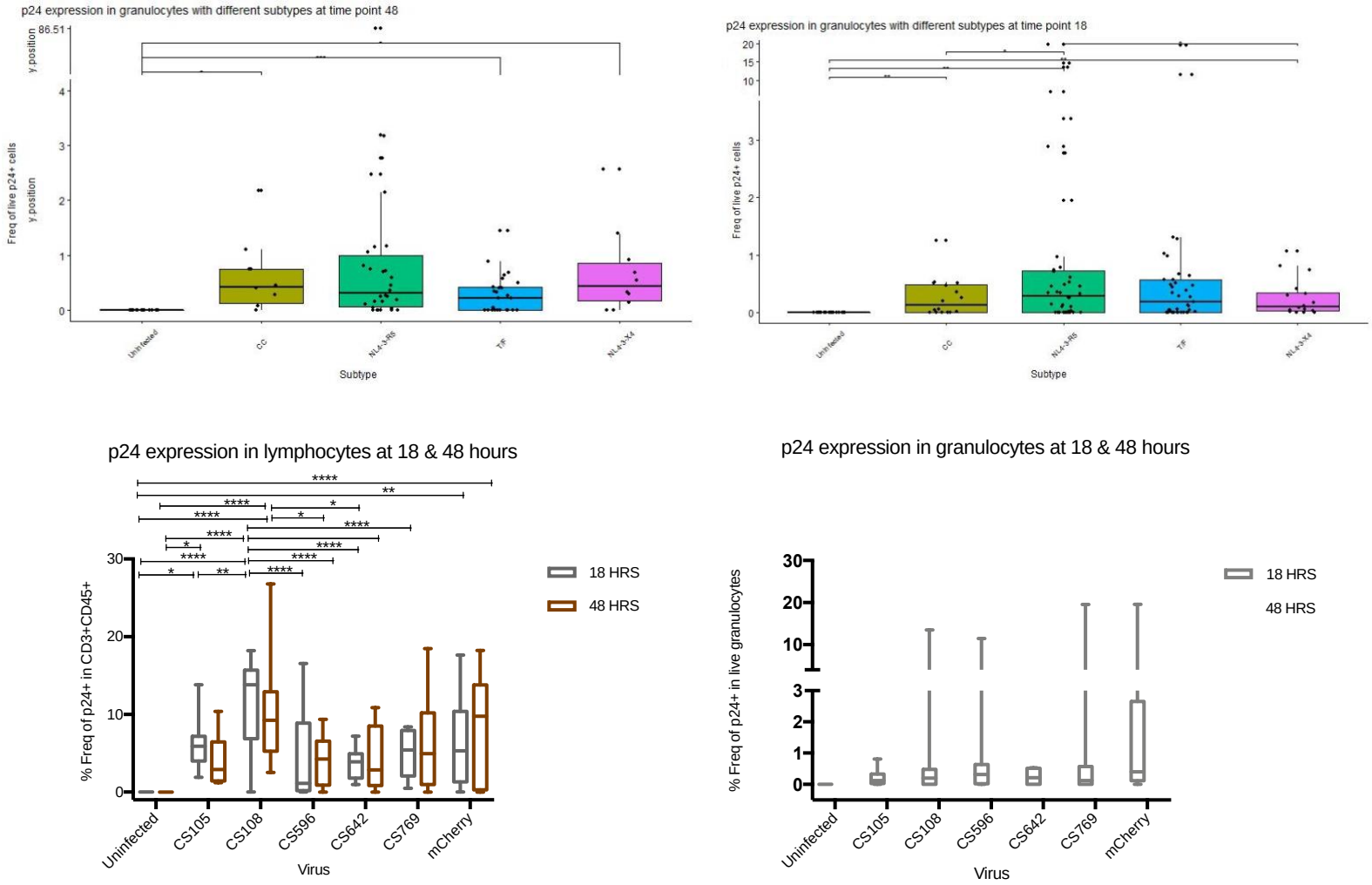

Figure A25. Proportions of HIV infected lymphocytes and granulocytes (without the outlier in CS108)

A26. HIV infection of specific granulocyte populations

Langerhans Cells

Proportions of HIV Infected LC subsets at 18 vs 48 hours

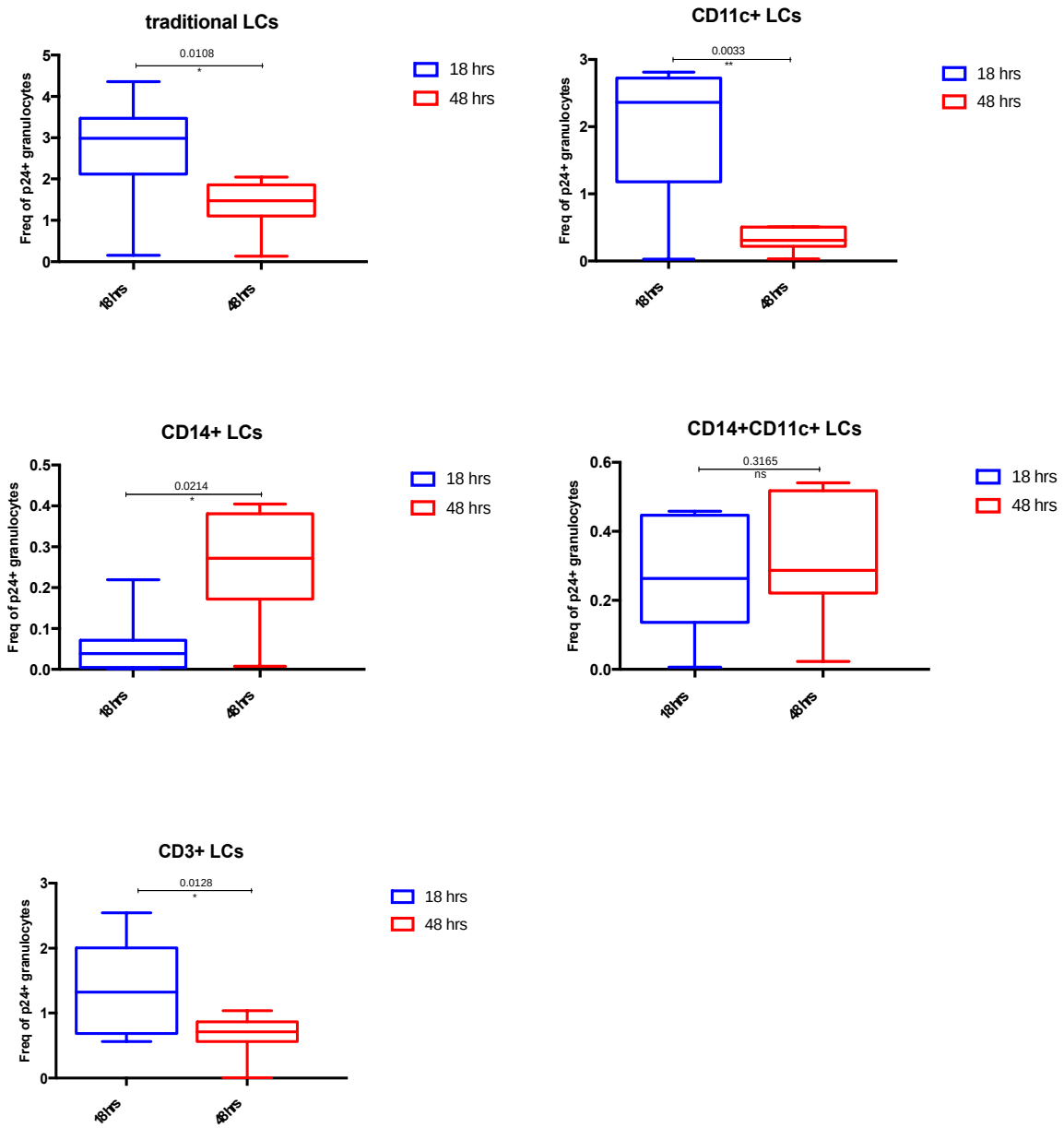

Figure A26. ***Proportions of HIV infected LC subsets at 18 and 48 hours.*** *The proportions of p24+CD14+ LCs and p24+CD14+CD11c+ LCs increased with time progression. All other subsets declined with time.*

A27. HIV infection unsupervised clustering

Optimization

LC marker expression profile per participant

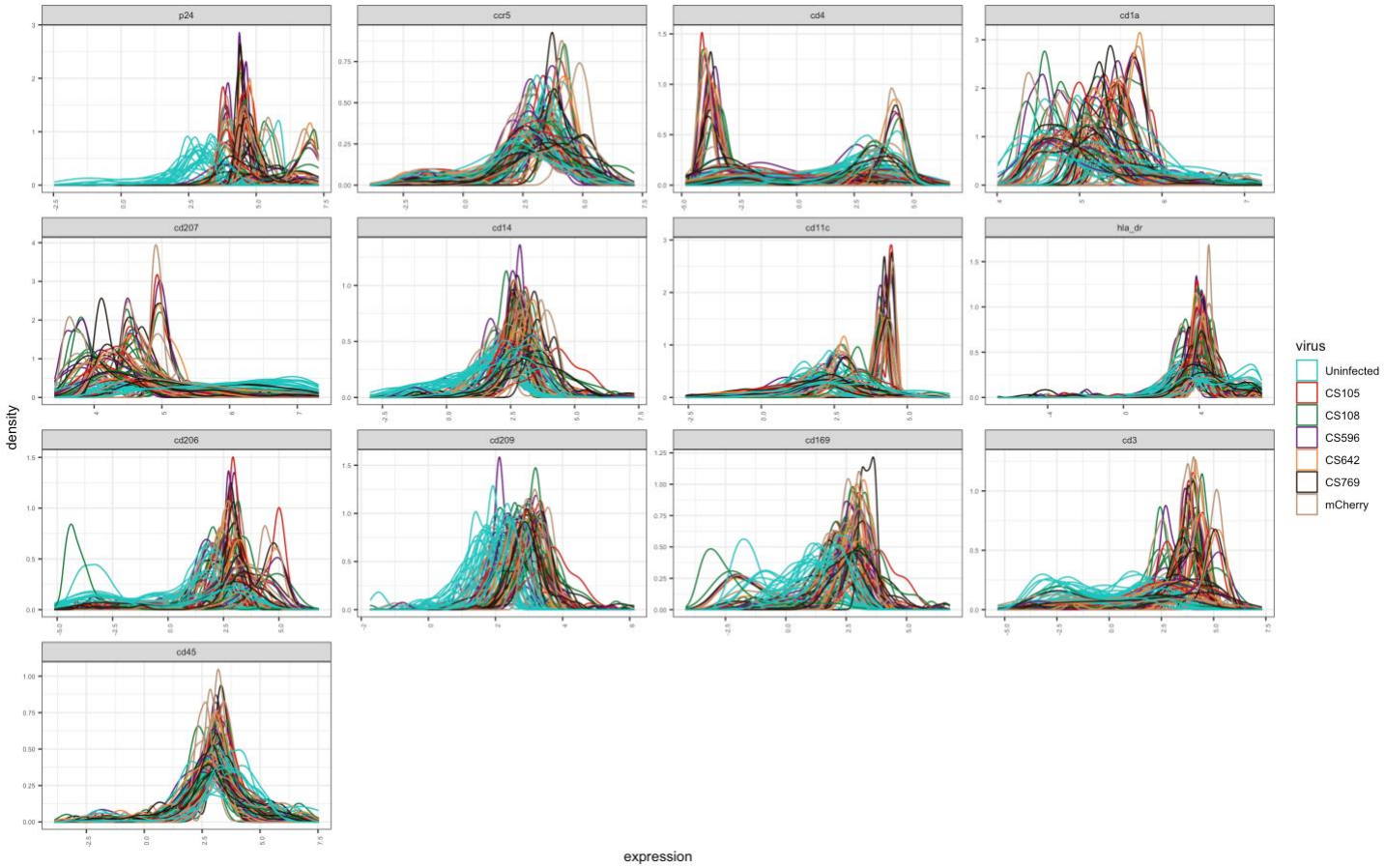

Figure A27. ***Marker Expression Profiles of Overall Concatenated HIV infected and uninfected LCs***

A28. Proportions of HIV infected foreskin LCs per participant

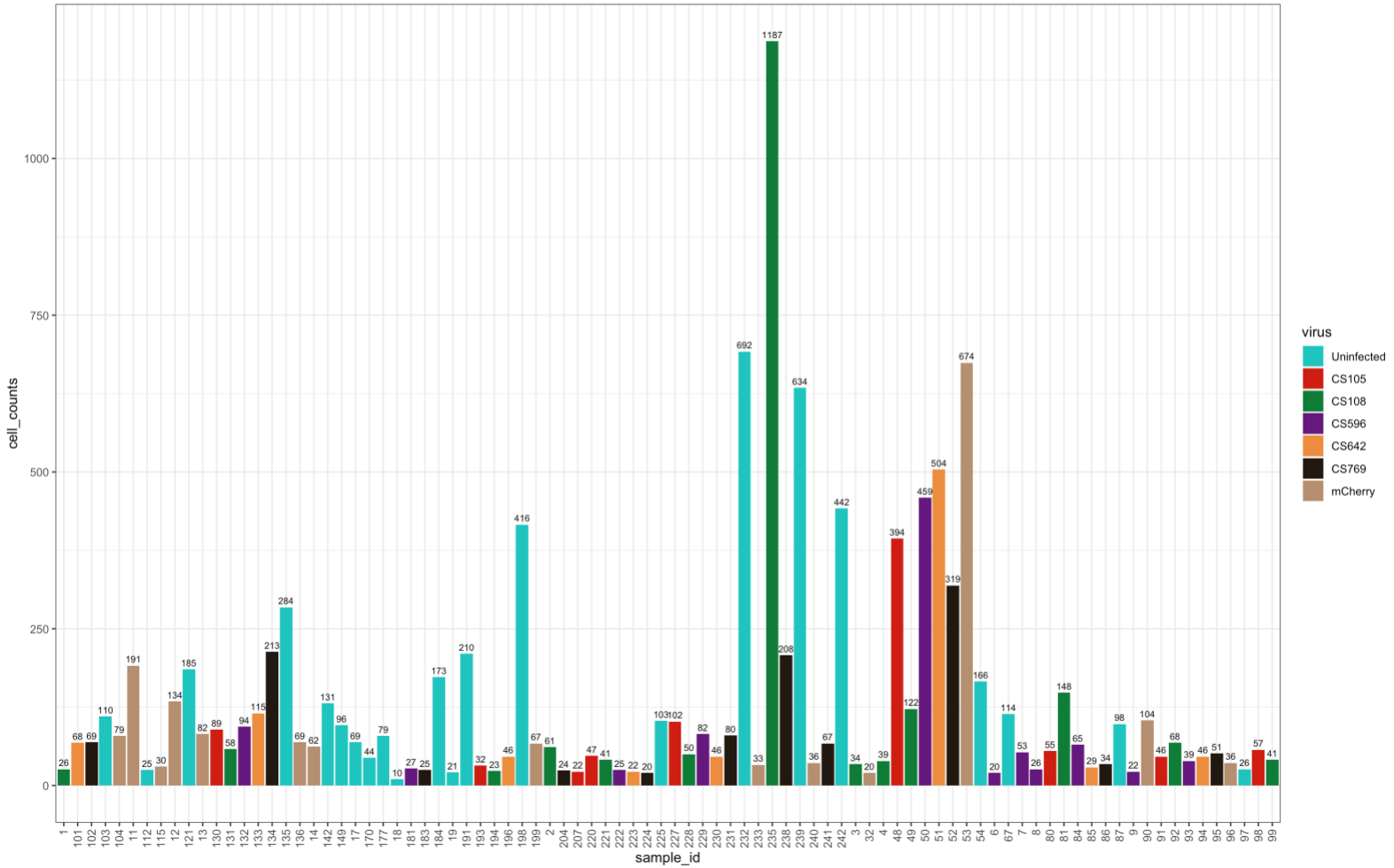

Figure A28. ***Cell Counts of the concatenated HIV Infected and Uninfected LCs***

A29.MDS plot

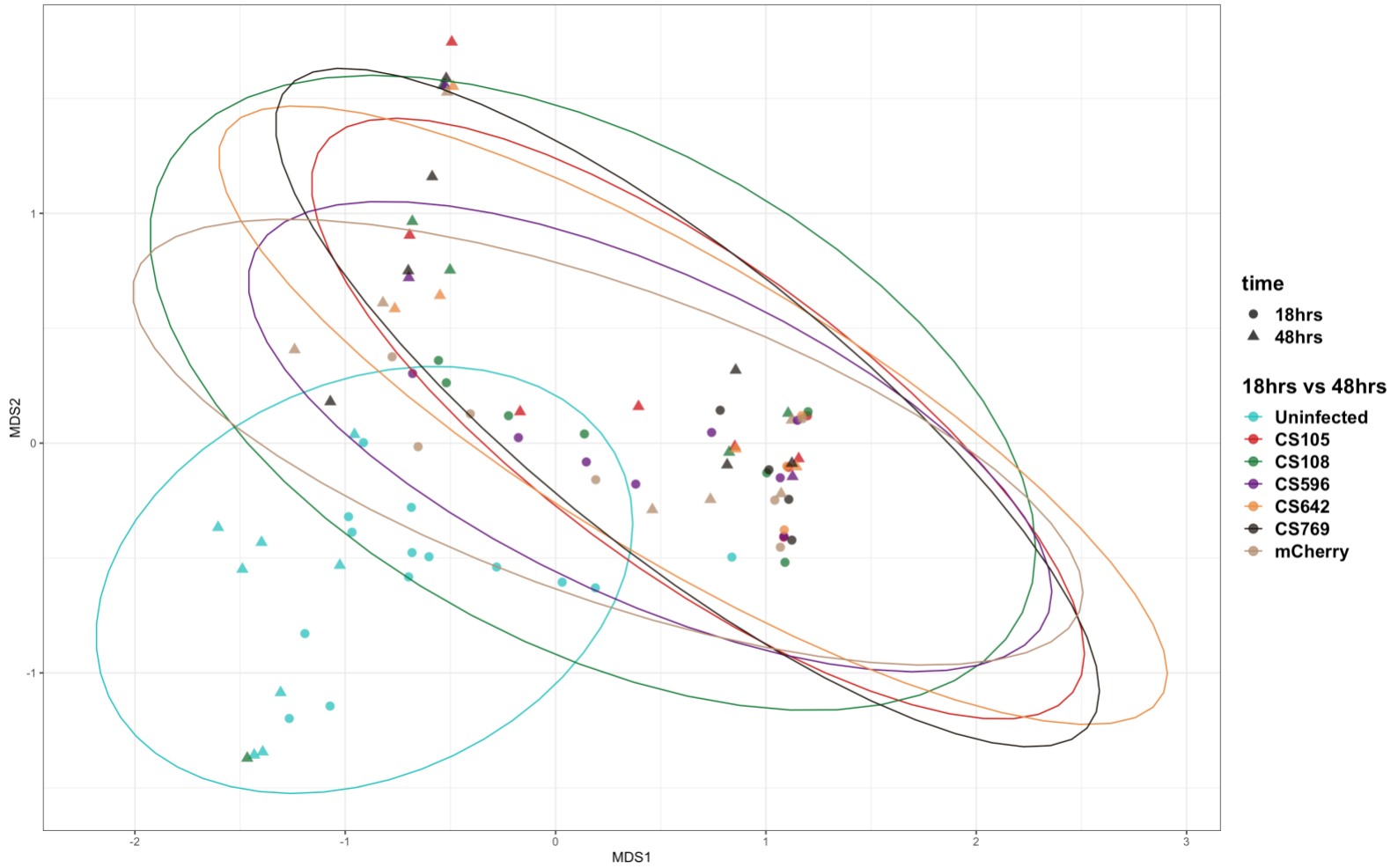

Figure A29. ***MDS plots showing differences between infected and uninfected concatenated LCs***

A30. Marker expression per cluster

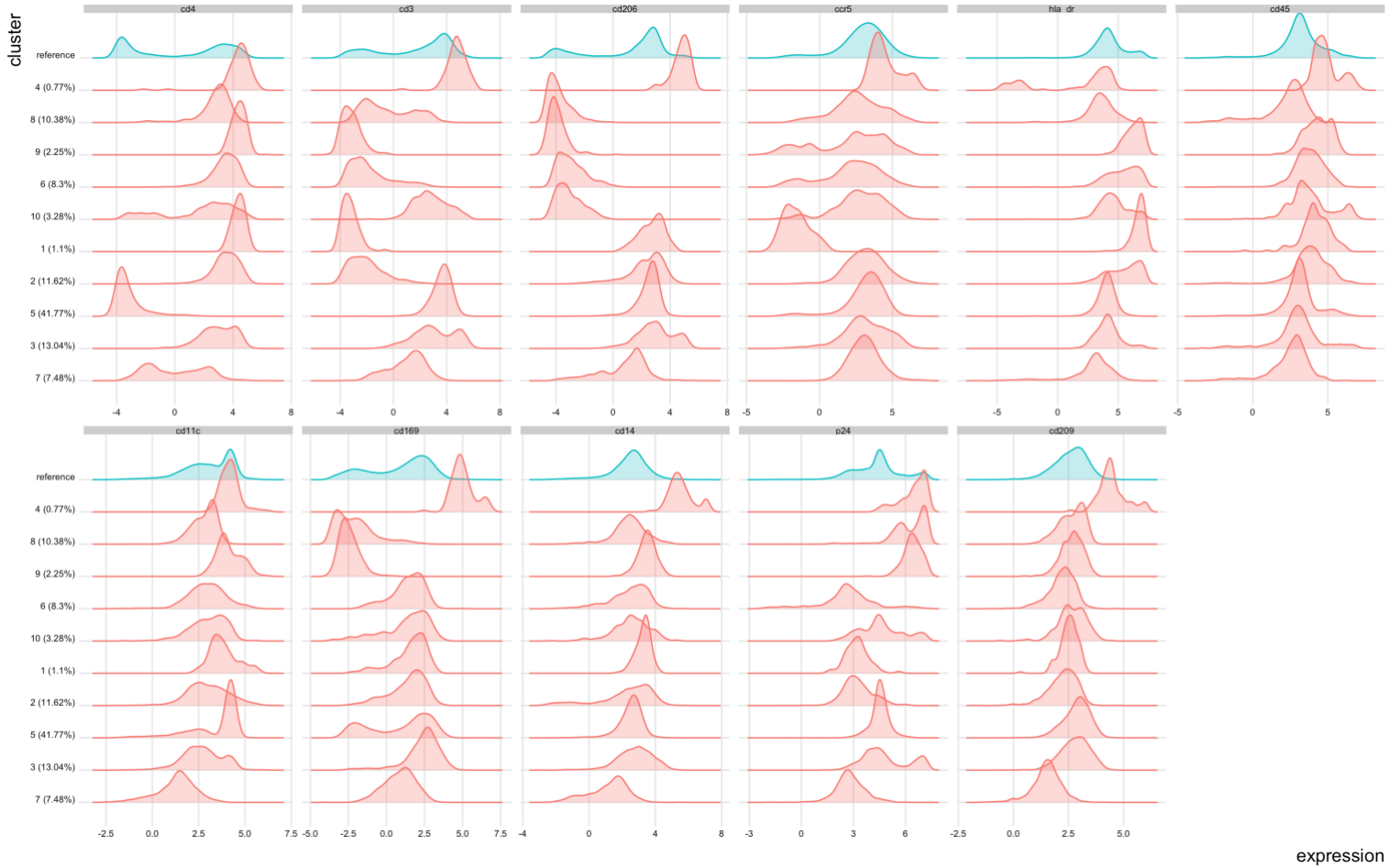

Figure A30. ***Marker Expression Profiles per LC cluster***

A31. tSNE plot displaying LC clusters per virus

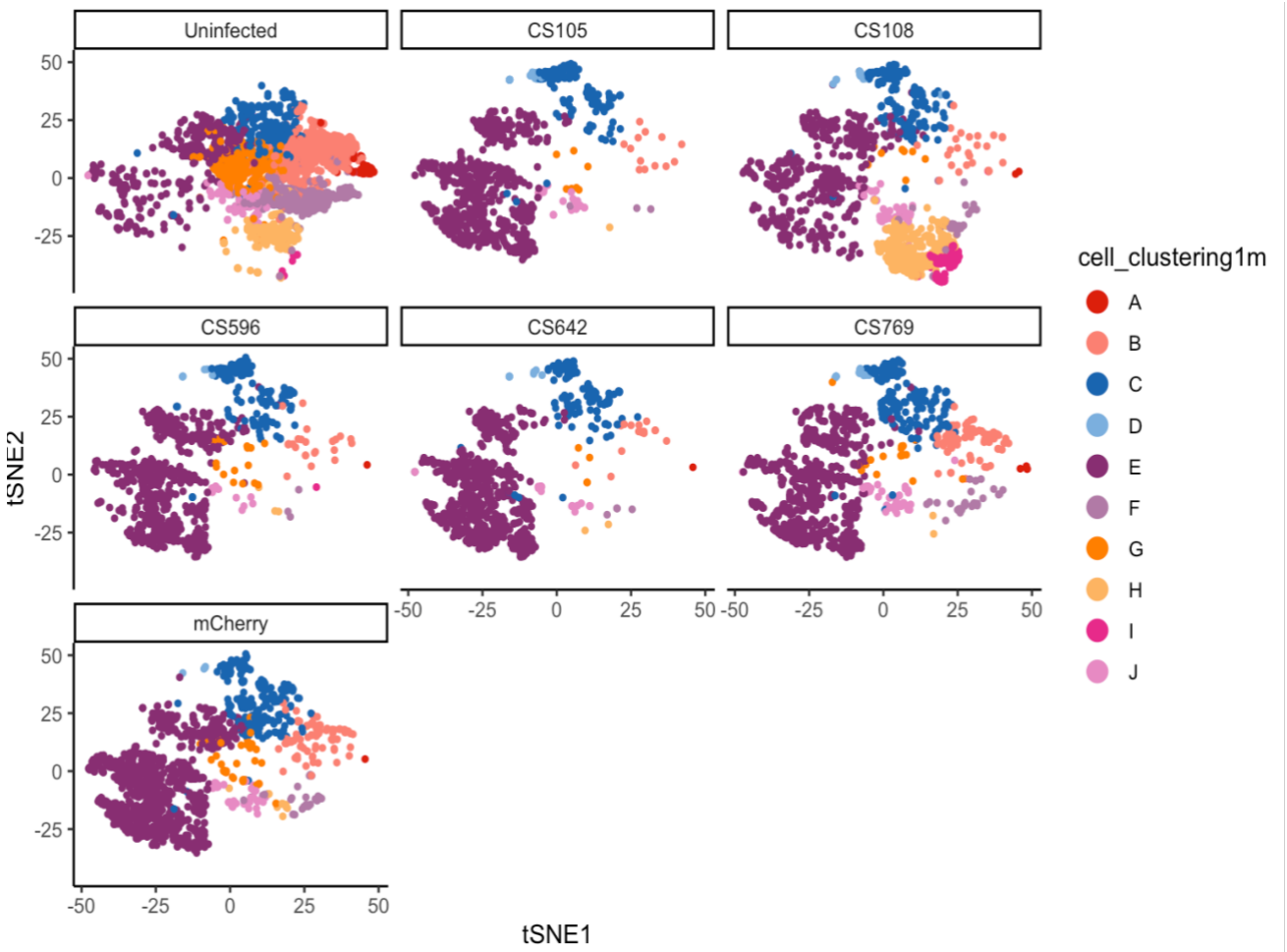

Figure A31. ***tSNE plots showing HIV Infected and uninfected LC clusters, by virus***

A32. PCA plot demonstrating phenotypic relationships among LC clusters

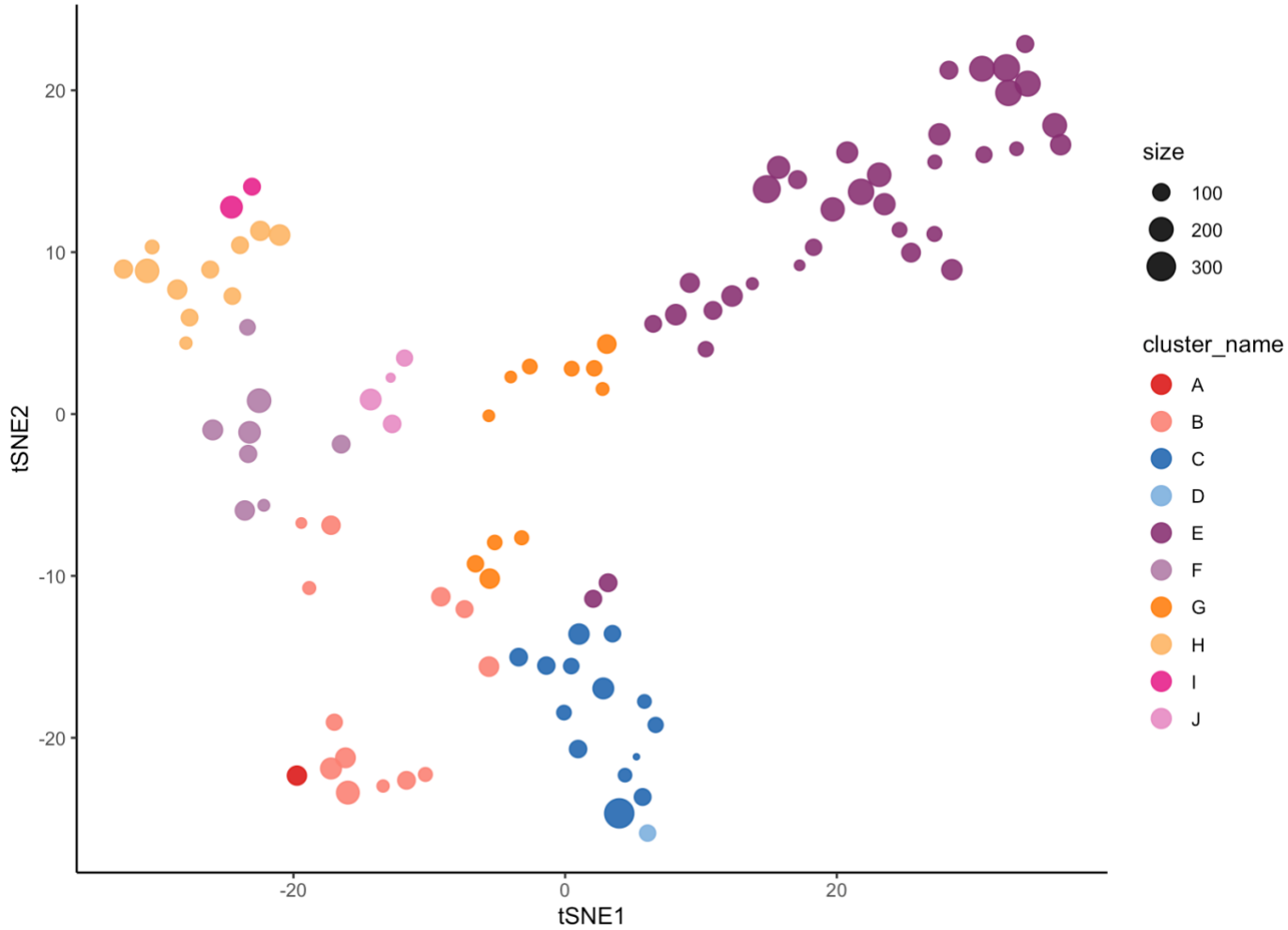

Figure A32. ***PCA plots showing phenotypic relationships among the different LC clusters***

A33. Proportions of the different LC clusters

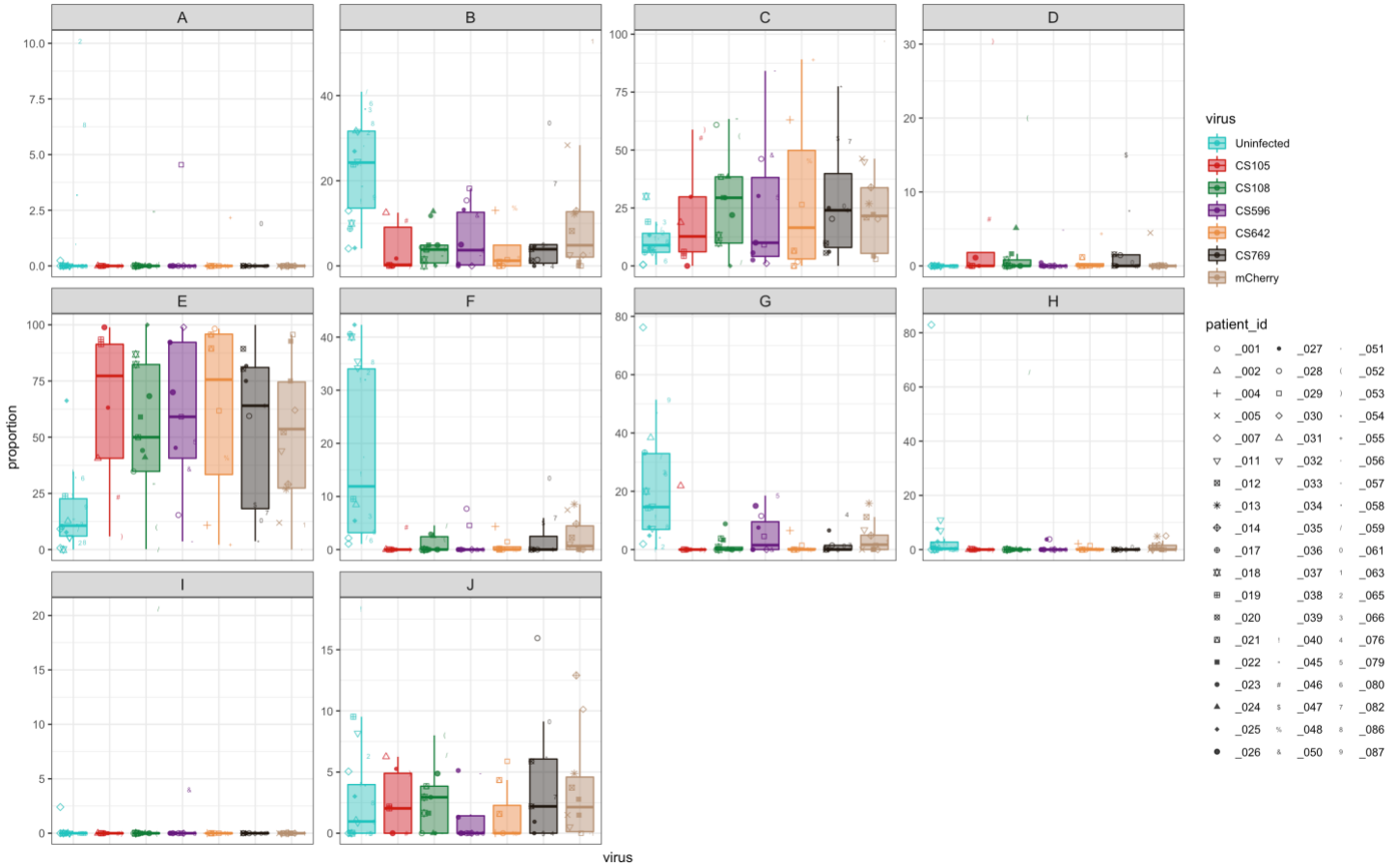

Figure A33. ***Proportions of the different LC clusters***

A34. Proportions of the different HIV infected and uninfected LC clusters at 18 and 48 hours

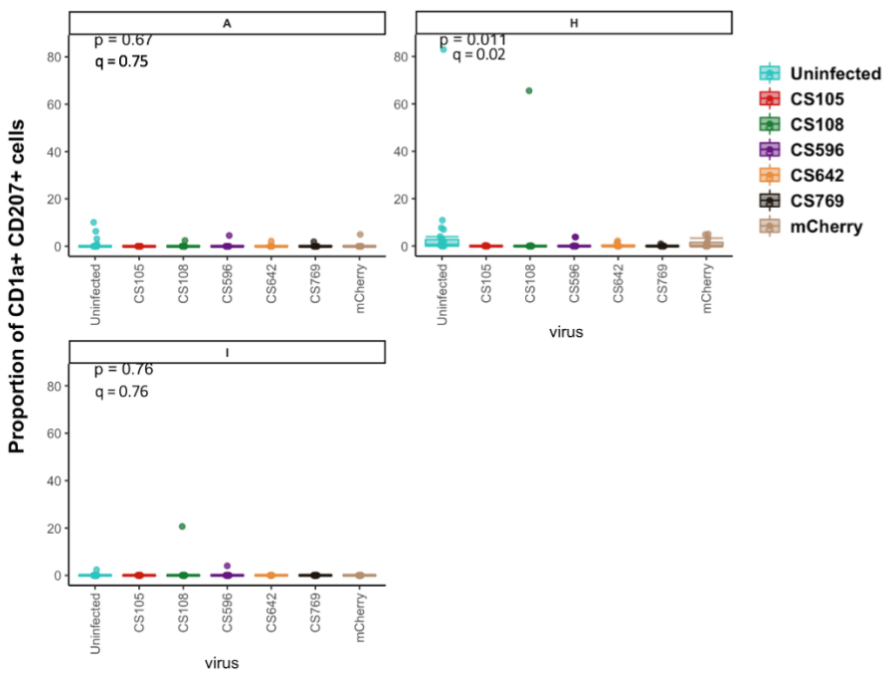

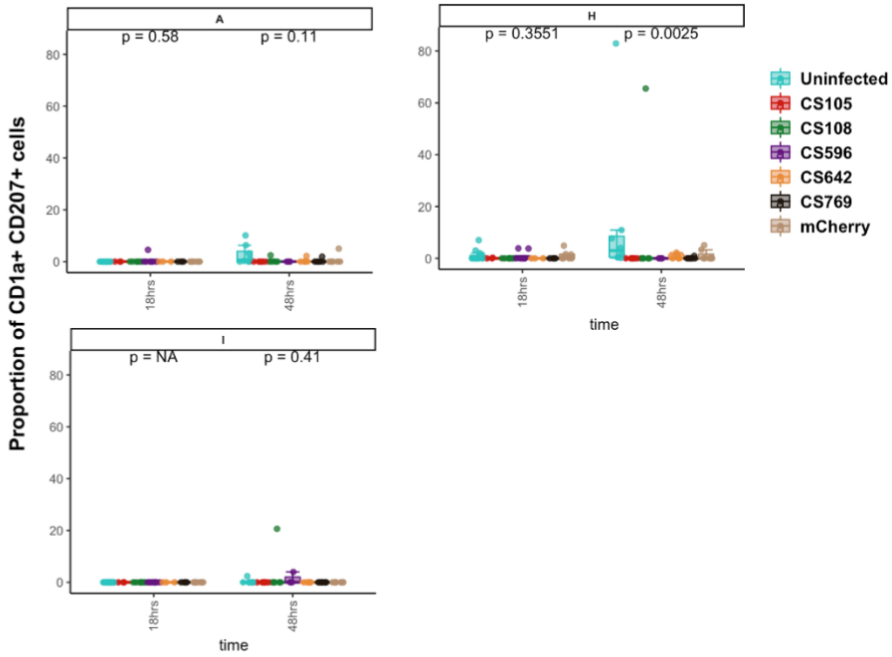

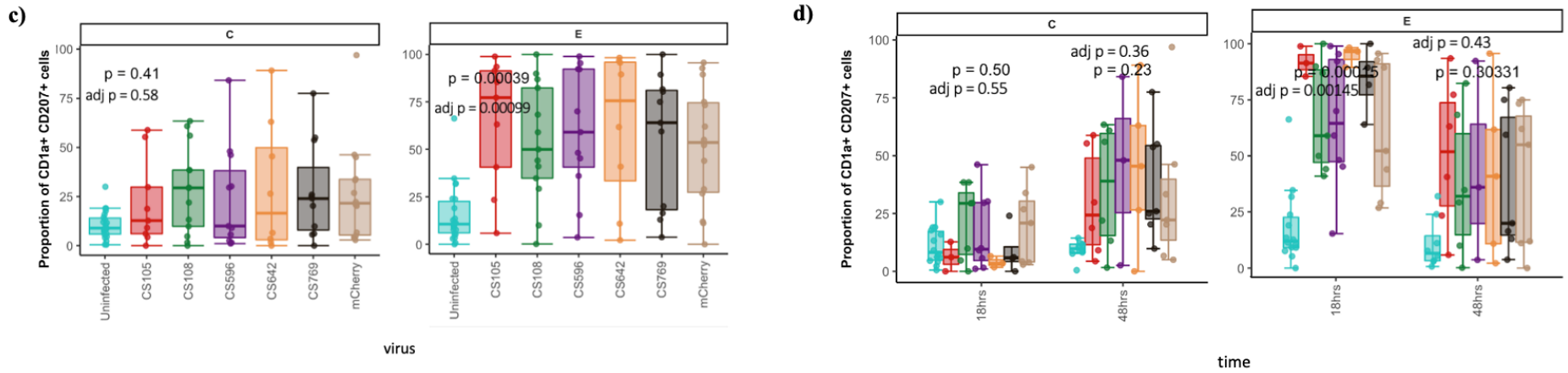

Figure A34. ***Proportions of the different HIV infected and uninfected LC clusters at 18 and 48 hours***

A35. HIV “Macrophage-like” cells – unsupervised clustering

Optimisation

Marker expression profiles per participant per virus

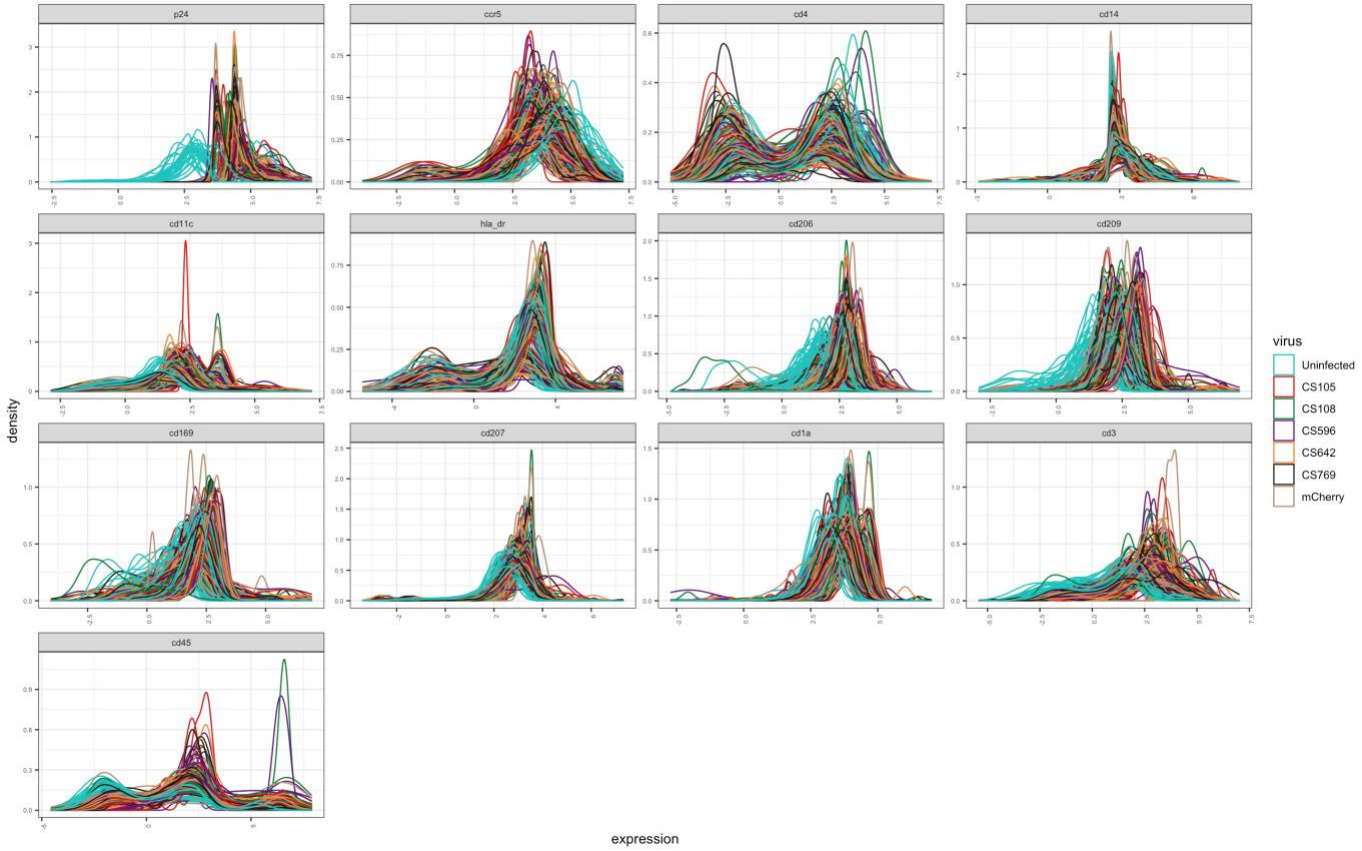

Figure A35. ***Marker Expression Profiles of the concatenated “macrophage-like” cells from the CD11c/CD14 gate***

A36. HIV infected “macrophage-like” cells - MDS plot

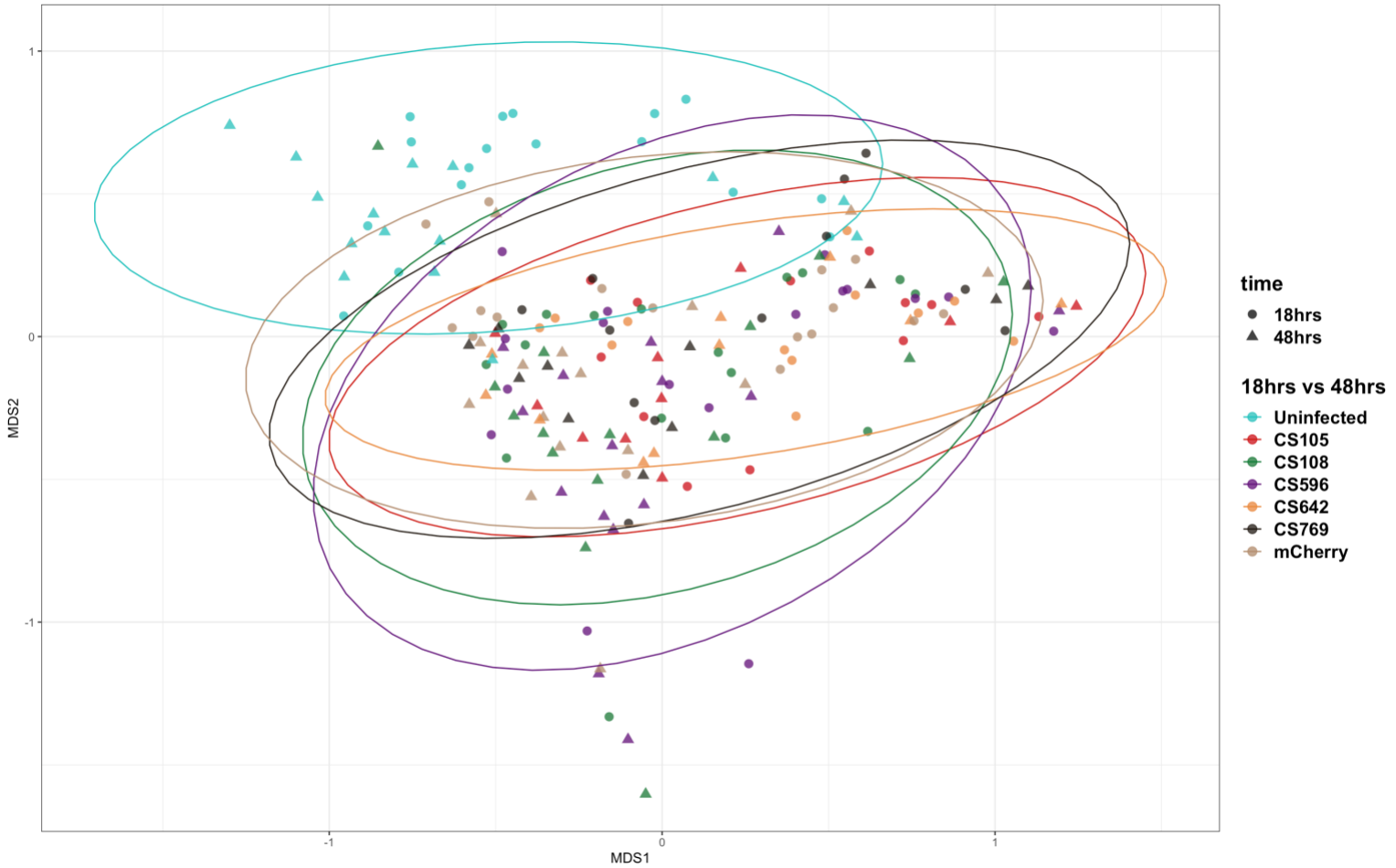

Figure A36. ***MDS plots portraying differences between the HIV infected and uninfected “macrophage-like” cells***

A37. Unsupervised Clustering: Marker expression profile per cluster

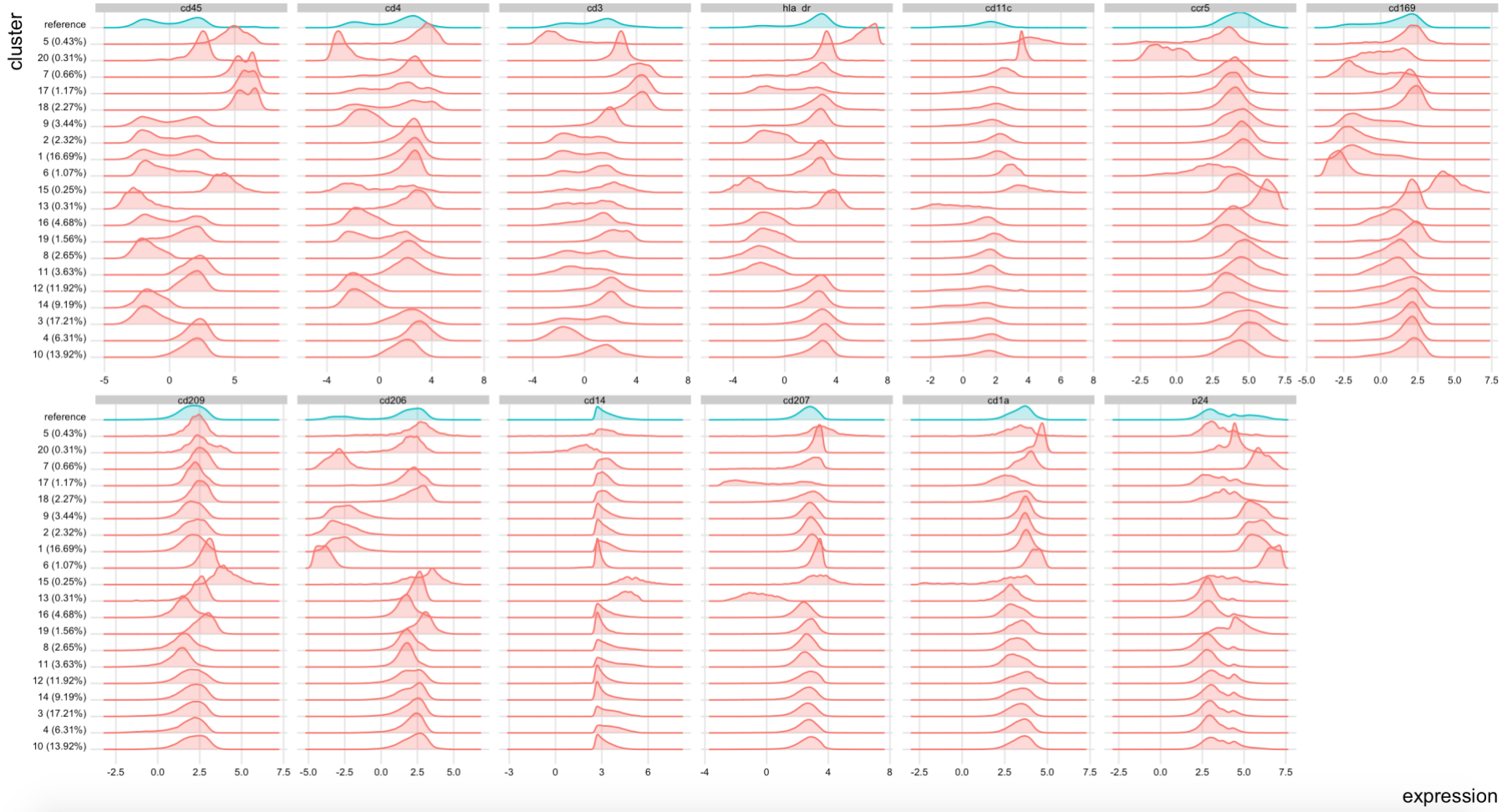

Figure 37. ***Marker Expression Profiles per Macrophage Cluster***

A38. tSNE plots displaying HIV infected and Uninfected “macrophage-like” clusters – by virus

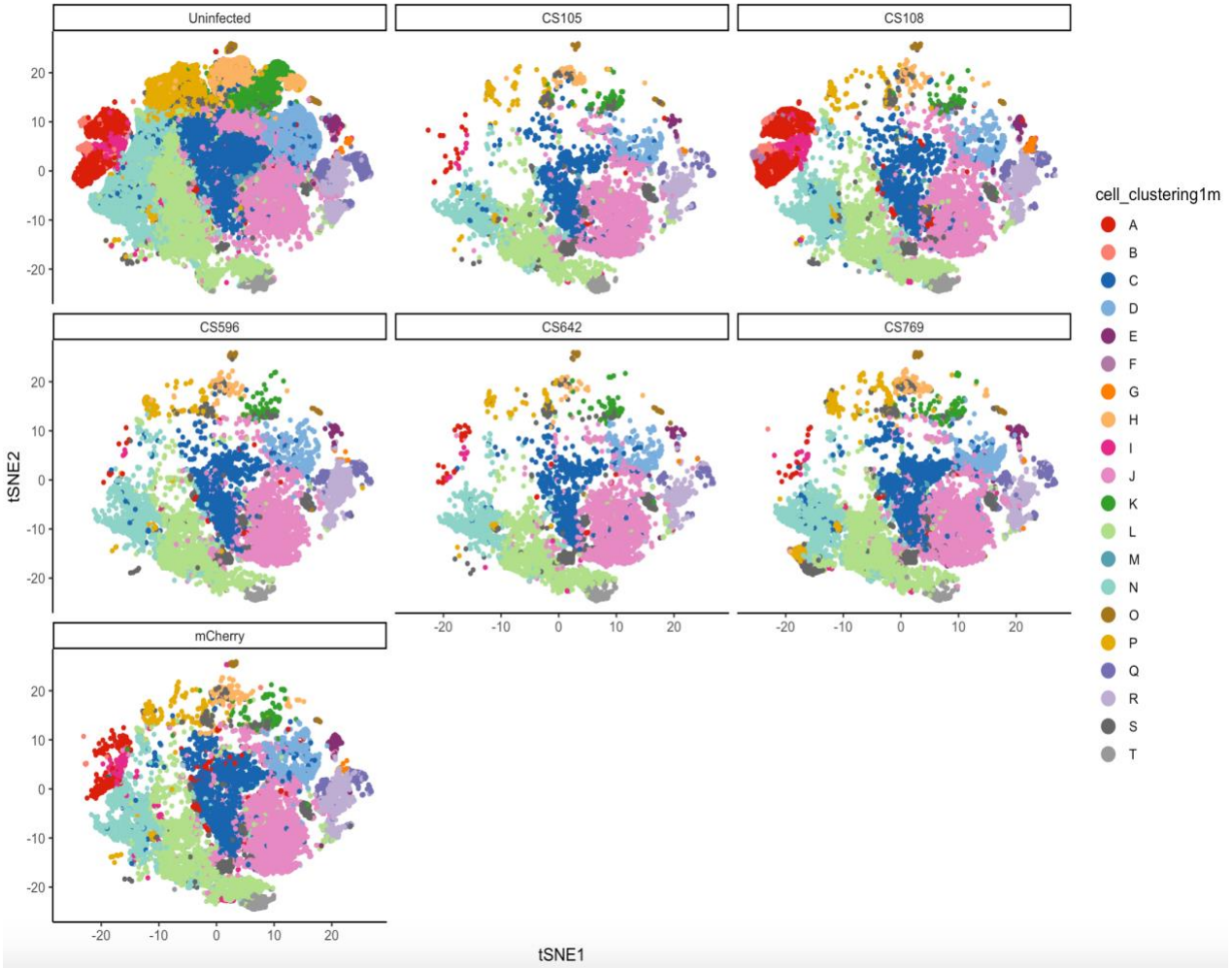

Figure A38. ***tSNE plots displaying HIV infected and Uninfected “macrophage-like” clusters – by virus***

A39. PCA plots displaying phenotypic relationships among the different “macrophage-like” clusters

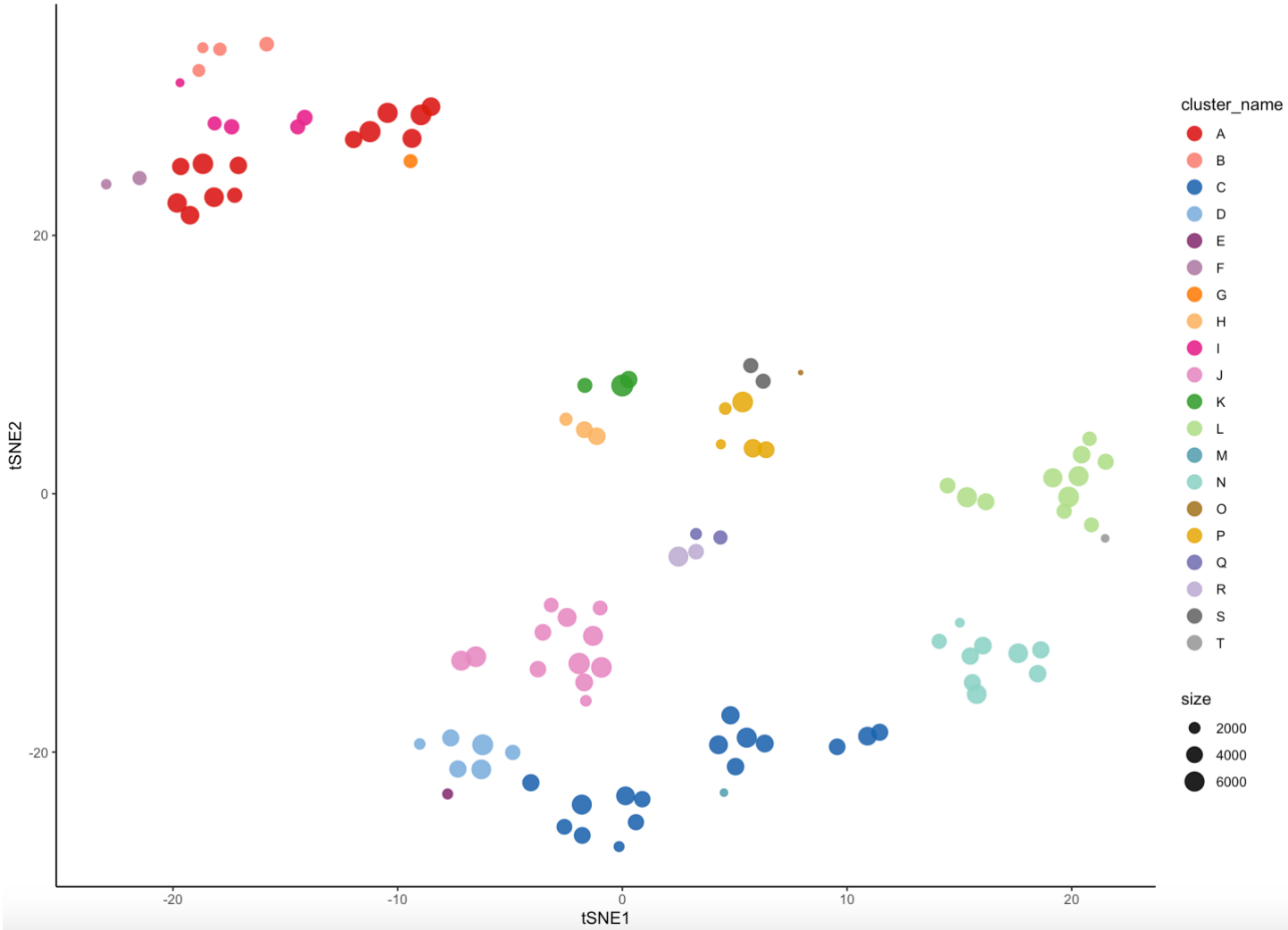

Figure A39. ***PCA plots displaying phenotypic relationships among the different “macrophage-like” clusters***

A40.Proportions of the different “macrophage-like” clusters

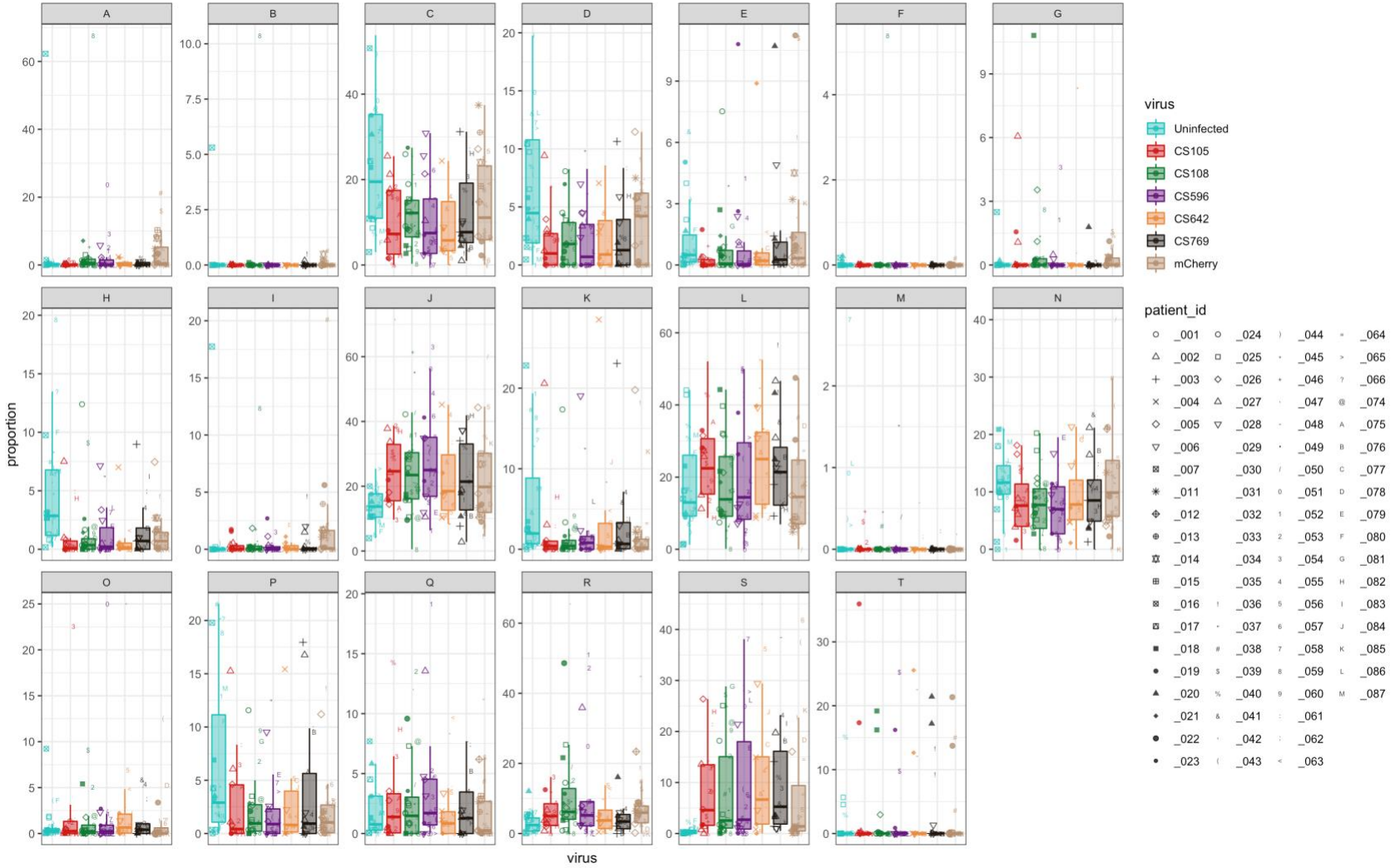

Figure A40. ***Differential abundance of the different “macrophage-like” clusters***

A41. Proportions of the different “macrophage-like” clusters

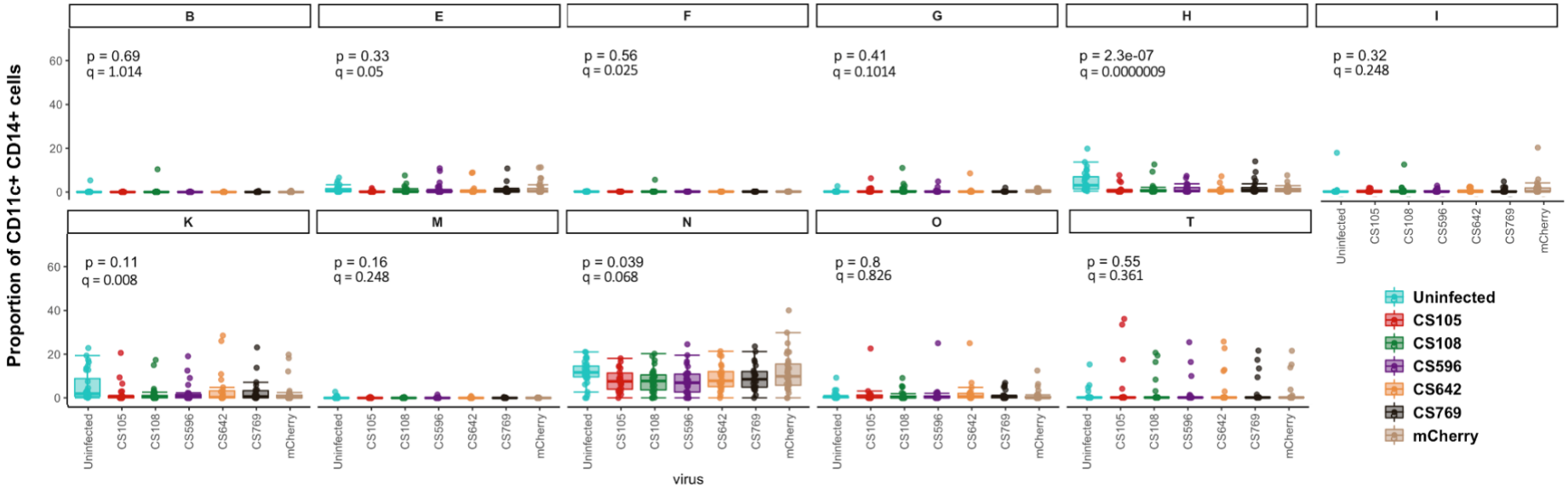

Figure A41. ***Proportions of the different “macrophage-like” clusters***

A42. Proportions of the different “macrophage-like” clusters at 18 and 48 hrs

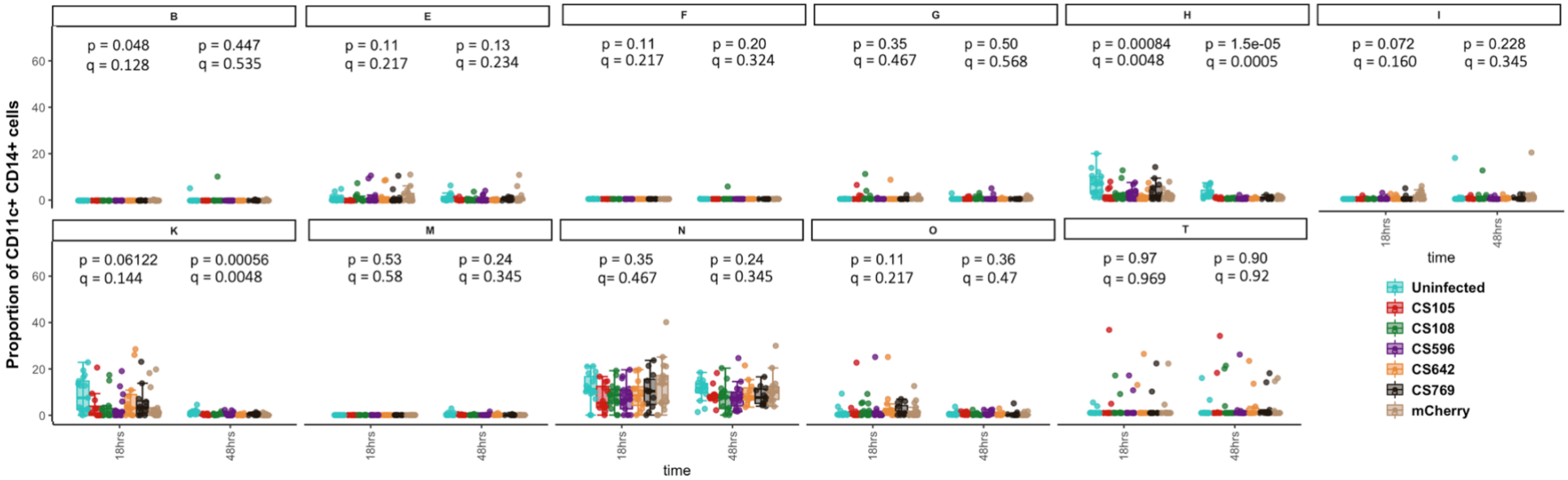

Figure A42 ***Proportions of the different “macrophage-like” clusters at 18 and 48 hrs***

Lymphocytes and granulocytes – marker MFIs (summary)

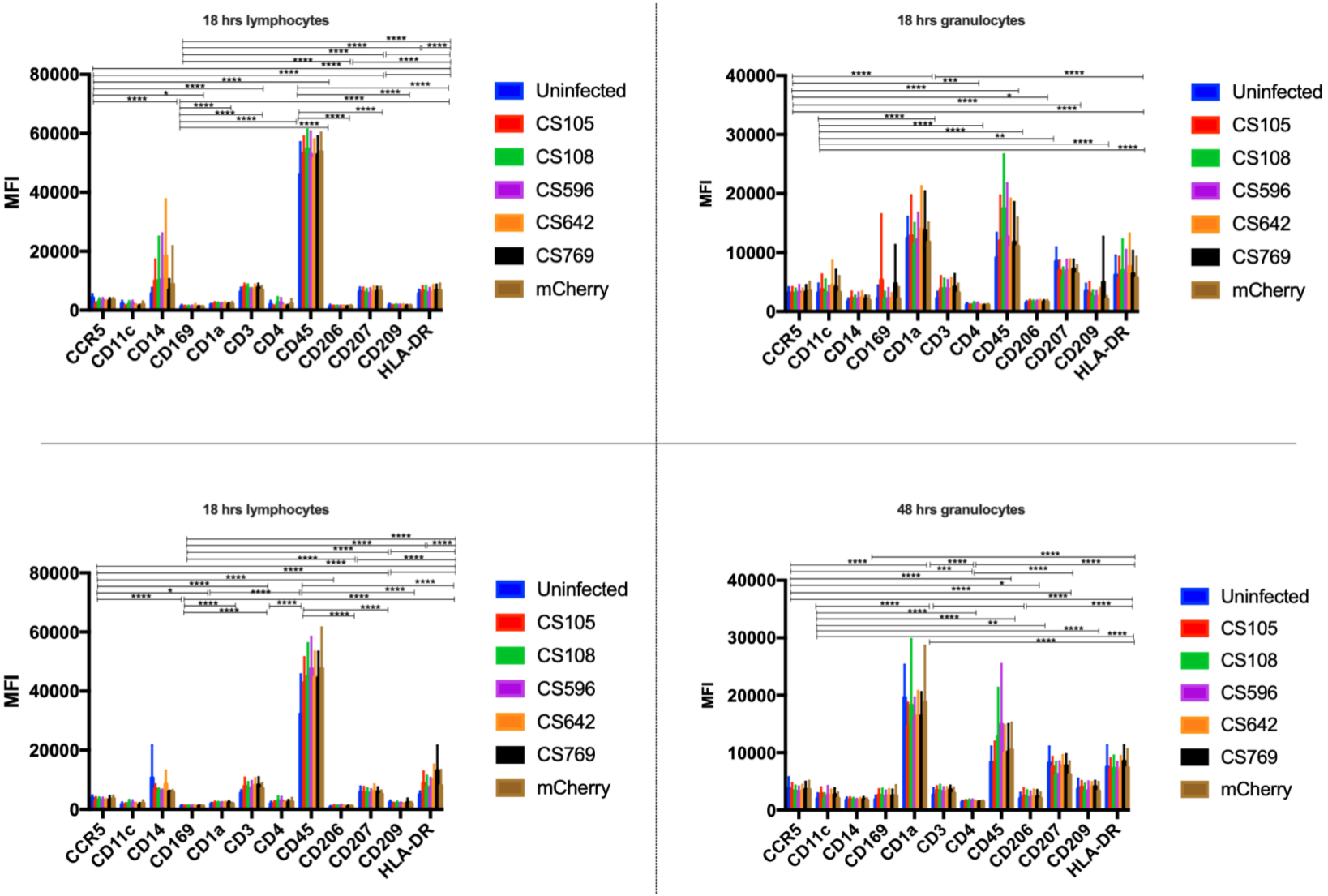

Figure A43 **. *Marker MFIs in foreskin lymphocytes and granulocyte***